Advanced Structured Materials

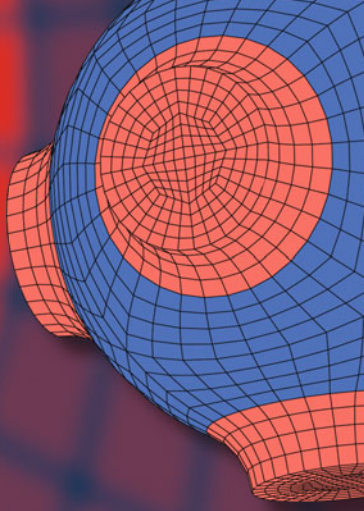

Vijay Kumar Thakur
Manju Kumari Thakur *Editors*

Eco-friendly Polymer Nanocomposites

Chemistry and Applications

Springer

Advanced Structured Materials

Volume 74

More information about this series at http://www.springer.com/series/8611

Vijay Kumar Thakur · Manju Kumari Thakur
Editors

Eco-friendly Polymer Nanocomposites

Chemistry and Applications

Springer

Editors
Vijay Kumar Thakur
Mechanical and Materials Engineering
Washington State University
Pullman, WA
USA

Manju Kumari Thakur
Division of Chemistry
Himachal Pradesh University
Shimla, Himachal Pradesh
India

ISSN 1869-8433 ISSN 1869-8441 (electronic)
Advanced Structured Materials
ISBN 978-81-322-2472-3 ISBN 978-81-322-2473-0 (eBook)
DOI 10.1007/978-81-322-2473-0

Library of Congress Control Number: 2015940723

Springer New Delhi Heidelberg New York Dordrecht London

Printed on acid-free paper

Springer (India) Pvt. Ltd. is part of Springer Science+Business Media (www.springer.com)

Dedicated to my parents and teachers who helped me become what I am today.

Vijay Kumar Thakur

Preface

Nanotechnology is the understanding and control of materials having dimensions roughly within the 1–100 nm range. The essence of nanotechnology is the ability to work at the molecular level, atom-by-atom, to create large structures with fundamentally new molecular organization. The ability to control and manipulate nanostructures will make it possible to exploit new physical, biological and chemical properties of systems that are intermediate in size, between single atoms, molecules and bulk materials. The term nanotechnology was introduced starting with the famous 1959 lecture by R.P. Feynman. The progress in nanotechnology has provided new insights into applications of well-known materials due to their exceptional properties owing to the nanoscale. As an example, nanocomposites based on polymer matrix and nanoscale fillers have appeared as good candidates in a broad range of applications. Such scenario can be credited to the use of new and multifunctional fillers that provide distinct and substantial features to the nanocomposites.

Recent trends in the nanocomposites field show the extensive use of biobased/environmental friendly materials as one of the component in these materials. Particular attention has been focused on the use of biodegradable polymer as matrix component in nanocomposite applications because of their widespread huge potential and advantages over other traditional synthetic materials. The use of natural polymers-based materials by humans is not new as these polymer materials have been used by people of earlier civilizations long back, many centuries ago. Among the biodegradable matrices of natural origin are, in particular, polysaccharides (starch, cellulose, pectin or chitin/chitosan); proteins (casein or gluten); and lipids (fatty acids, resins and waxes), which have the ability to form nanocomposite films that are non-toxic, and biocompatible and have the advantage of being able to be in contact with food products. Indeed, the nano-products play a dominant role in global manufacturing, and also in the not-so-distance future. Whereas new applications are being investigated every day in numerous areas, e.g. agriculture, lignocellulosic products, food, nano-reactive membranes for water purification, nanocatalysts for air purification, for water treatment, nanomaterials-based solar cells, as well as nano-coatings which are finding use in corrosion-

resistance, dirt repellence, water repellence, thermal insulation and anti-microbial to name a few. Eco-friendly polymer nanocomposites are such emerging nanostructure hybrid materials composed of environmental friendly components. Eco-friendly nanocomposites are becoming a subject of intensive research owing to their inherent properties such as non-toxicity, biocompatibility, biodegradability as well as improved structural and functional properties. Different research efforts all around the globe are continuing to improve the existing properties of these eco-friendly polymer nanocomposites. Researchers are collectively focusing their efforts to use the inherent advantages of eco-friendly materials for their targeted applications. Scientists in collaboration with industries are extensively developing new classes of eco-friendly polymer nanocomposites. Different kinds of sustainable materials can be obtained by exploration of such eco-friendly polymer nanocomposites.

This book is solely focused on "Eco-friendly Polymer Nanocomposites" and deals with the "Chemistry and Applications" aspects of these materials. Several critical issues and suggestions for future work are comprehensively discussed in this book with the hope that the book will provide deep insight into the state of art of "Eco-friendly Polymer Nanocomposites". We would like to thank the team at Springer for their invaluable help in the organisation of the editing process. Finally, we would like to thank our parents for their continuous encouragement and support.

Pullman, USA — Vijay Kumar Thakur
Shimla, India — Manju Kumari Thakur

Contents

About the Editors

Dr. Vijay Kumar Thakur Ph.D. has been working as Research Faculty (Staff Scientist) in the School of Mechanical and Materials Engineering at Washington State University, U.S.A, since September 2013. His former appointments include being a Research Scientist in Temasek Laboratories at Nanyang Technological University, Singapore, and a Visiting Research Fellow in the Department of Chemical and Materials Engineering at LHU-Taiwan. His research interests include the synthesis and processing of bio-based polymers, nanomaterials, polymer micro/nanocomposites, nanoelectronic materials, novel high dielectric constant materials, electrochromic materials for energy storage, green synthesis of nanomaterials and surface functionalization of polymers/nanomaterials. He did his post-doctorate in Materials Science at Iowa State University and his Ph.D. in Polymer Science (2009) at the National Institute of Technology. In his academic career, he has published more than 80 SCI journal research articles in the field of polymers/materials science and holds one United States patent. He has also published 15 books and 35 book chapters on the advanced state-of-the-art of polymers/materials science with numerous publishers. He is an editorial board member of several international journals and also is member of scientific bodies around the world. In addition to being on the editorial board of journals, he also serves as guest editor for the *Journal of Nanomaterials, International Journal of Polymer Science, Journal of Chemistry, and American Journal of Applied Chemistry*. vijayisu@hotmail.com

Dr. Manju Kumari Thakur M.Sc., M.Phil., Ph.D. has been working as an Assistant Professor of Chemistry at the Division of Chemistry, Government Degree College Sarkaghat Himachal Pradesh University—Shimla, INDIA since June 2010. She received her B.Sc. in Chemistry, Botany and Zoology; M.Sc., M.Phil. in Organic Chemistry and Ph.D. in Polymer Chemistry from the Chemistry Department at Himachal Pradesh University—Shimla, INDIA. She has rich experience in the field of organic chemistry, biopolymers, composites/nanocomposites, hydrogels, application of hydrogels in the removal of toxic heavy metal ions, drug delivery, etc. She has published more than 30 research papers in several international journals, co-authored one book and has also published 25 book chapters in the field of polymeric materials. shandilyamn@gmail.com

Eco-Friendly Polymer-Layered Silicate Nanocomposite–Preparation, Chemistry, Properties, and Applications

Raghavan Prasanth, Peter Samora Owuor, Ravi Shankar, Jarin Joyner, Suppanat Kosolwattana, Sujin P. Jose, Pei Dong, Vijay Kumar Thakur, Jung Hwi Cho and Manjusha Shelke

Abstract This chapter aims at exploring the revolutionary field of nanotechnology and some of its promising aspects in polymer nanocomposites in view of preparation, characterization, materials properties, and processing of polymer layered silicate nanocomposites. These materials are attracting considerable interest in polymer science research. Polymer layered silicate nanocomposites are an important class of hybrid, organic/inorganic materials with substantially improved mechanical, thermal, and thermomechanical properties in comparison to pristine polymers. In addition, they also show superior ultraviolet (UV) as well as chemical resistance and are widely being investigated for improving gas barrier and flame retardant properties. Hectorite and montmorillonite are among the most commonly used smectite-type layered silicates for the preparation of polymer–clay nanocomposites. Smectites are a valuable mineral class for industrial applications due to their high cation exchange capacities, surface area, surface reactivity, adsorptive properties, and, in the case of hectorite, high viscosity and transparency in solution. A wide range of polymer matrices are explored for the preparation of polymer–clay nanocomposites, however, this chapter deals with special emphasis on biodegradable polymers—cellulose and natural rubber. Also, the chapter describes the common synthetic techniques in producing polymeric layered silicate nanocomposites, its properties, and applications.

R. Prasanth (✉) · P.S. Owuor · J. Joyner · S. Kosolwattana · S.P. Jose
P. Dong · J.H. Cho · M. Shelke
Department of Materials Science and NanoEngineering, Rice University, 6100 Main, MS-325, Houston, TX 77005, USA
e-mail: prasanth.raghavan@rice.edu

R. Prasanth
Department of Mechanical Engineering and Materials Science, Rice University, 6100 Main, MS-321, Houston, TX 77005, USA

R. Shankar
Fujifilm Imaging Colorants, Inc, 233 Cherry Lane, New Castle, DE 19720, USA

V.K. Thakur
School of Mechanical and Materials Engineering, Washington State University, Pullman, WA 99164, USA

V.K. Thakur and M.K. Thakur (eds.), *Eco-friendly Polymer Nanocomposites*, Advanced Structured Materials 74, DOI 10.1007/978-81-322-2473-0_1

Keywords Polymer · Composite · Layered silicates · Clay modification · Biopolymer · Green composite · Polymer–clay nancomposite · Cellulose nanocomposite · Natural rubber–clay nanocomposite

Abbreviations

AFM	Atomic force microscope
AMPS	2-Acrylamido-2-methylpropane sulfonic acid
CA	Cellulose acetate
CAB	Cellulose acetate bioplastic
CB	Carbon black
CEC	Cation exchange capacity
CNBR	Carboxylatedacrylonitrile butadiene rubber
Cs30B	Cloisite 30B
Cs93A	Cloisite 93A
CTAB	Cetyltrimethylammoniumbromide
DNA	Deoxyribonucleic acid
DSC	Differential scanning calorimetry
e.g	Example
EA	Ethanolamine
EIC	English Indian Clay
ENR	Epoxidized natural rubber
EPDM	Ethylene-propylene thermoplastic rubber
EPDM-g-MAH	Maleatedethylene-propylene thermoplastic rubber
FHT	Sodiumfluorohectorite
HRTEM	High resolution transmission electron microscopy
IIR	Isobutylene–isoprene rubber
LDH	Layered double hydroxides clay
LS	Layered silicate
MFC	Microfibrillated cellulose
MMT	Montmorillonite
MMT-2M2HT	MMT modified with dimethyl dihydrogenated tallow
MMT-MT2EtOH	MMT modified with methyl tallow bis-2-hydroxyl quaternary ammonium
MMT-ODA	Octadecylamine
MMT-ODA	Primary amine
MMT-ODTMA	MMT modified with octadecyltrimethylamine
MMT-TMDA	Quaternary amine
Na-MMT	Sodium montmorillonite
NBR	Nitrile butadiene rubber
NMMO	N-methylmorpholine-N-oxide
NR	Natural rubber
OMLS	Organically modified layered silicate
OMMT	Organically modified clay
PANI	Polyaniline

phr	Parts per hundred rubber
PLA	Polylactic acid
PMMA	Poly(methylmethacrylate)
MMA	Methylmethacrylate
PNC's	Polymer nanocomposites
PP	Polypropylene
PUR	Polyurethane rubber
RNA	Ribonucleic acid
RTIL	Room temperature ionic liquid
SBR	Styrene butadiene-rubber
SEM	Scanning electron microscope
SNR	Synthetic natural rubber
TEM	Transmission electron microscope
TiO_2	Tin oxide
TO	Tetraoctadecylammoniumbromide
UMMT	Unmodified clay
US	United States
UV	Ultra-violet
XRD	X-ray diffraction
ZnO	Zinc oxide

Units

%	Percentage
°C	Degree celsius
A°	Angstrom
g mol^{-1}	Gram per mole
GPa	Giga pascal
H	Hour/Hours
J Kg^{-1}	Joule per kilogram
kHz	Kilohertz
kJ Kg^{-1}	Kilojoule per kilogram
MPa	Mega pascal
nD	Diffractive index
nm	Nanometer
W m^{-1} $°C^{-1}$	Watt per meter per degree Celsius
wt%	Weight percentage

1 Introduction

A polymer (the prefix *poly* referring to many and the suffix *mer* referring to units) is a macromolecule composed of many repeating subunits called monomer units. Polymers can be either naturally occurring or synthetic. The term 'polymer' derives

from the ancient Greek word πολύς (*polus*) and μέρος (*meros*). The term was coined in 1833 by Jöns Jacob Berzelius, a Swedish chemist considered to be one of the founders of modern chemistry. The modern concept of polymers as covalently bonded macromolecular structures was proposed in 1920 by Hermann Staudinger, a German chemist, who spent the next decade finding experimental evidence for this hypothesis. Natural polymers are made by living organisms, representing the macromolecular components of the cell. These compounds are also known as biopolymers or polymeric biomolecules and can be enumerated according to the monomeric units used and the structure:

(i) Polynucleotides or nucleic acids as DNA and RNA, which are long chain molecules composed of 13 or more nucleotide monomers. These polymers are responsible for the storage, transmission, and expression of genetic information.

(ii) Polypeptides or proteins are short chain polymers that play a fundamental role in the functionalization of various biological activities. Many proteins such as collagen, keratin, and fibroin serve as structural building blocks, while others, such as hemoglobin, act as transport agents in living organisms. Proteins can transmit information to distant parts of a living organism (proteichormones) as well as defend against foreign pathogens (antibodies). Another very important function accomplished by proteins is through the rule of the rate of metabolism reactions (enzymes).

(iii) Polysaccharides also known as glycans, are the form in which most natural carbohydrates occur. Polysaccharides are linear bonded polymeric carbohydrate structures that may contain various degrees of branching and are composed of monosaccharide units that are bound together by glycosidic linkages. This class of polymers acts as natural constituents (cellulose, chitin) as well as energy reserves (starch). Upon hydrolysis of glyosidic bonds, polysaccharides yield its constituent monosaccharides and/or oligosaccharides. Polysaccharides are heterogeneous, or homogeneous, containing slight modifications of the repeating unit. Depending on the structure, these macromolecules can have properties distinct from their monosaccharide building blocks. Linear polysaccharide compounds such as cellulose often pack together to form a rigid structure resulting in its insolubility in water; while glycans that are composed of branched forms (e.g., gum arabic) generally are soluble in water and make pastes. Polysaccharides composed of many molecules of one sugar or sugar derivative are called as homopolysaccharides (homoglycans) while those that consist of molecules of more than one sugar or sugar derivative are called heteropolysaccharides (heteroglycans). Homopolysaccharides composed of glucose include glycogen and starch, the storage carbohydrates of animals and plants respectively. Cellulose, another homopolysaccharide, is an important structural component of most plants. Preparations of dextran, another glucose homopolysaccharide found in slimes secreted by certain bacteria, are used as substitutes for blood plasma. Other homopolysaccharides include pentosans (composed of arabinose or xylose), which are found in plant

products and fructans (levans), which are found in roots and tubers such as the Jerusalem artichoke and dahlia. The repeating unit of chitin, a component of the outer skeleton of arthropods (e.g., insects, crustaceans, crab, etc.) is *N*-acetyl-D-glucosamine, a monosaccharide derived from glucose. The cell walls of most fungi are also chitin, while the shells of arthropods such as crabs and lobsters contain about 25 % chitin. This polysaccharide is also found in certain structures of annelid worms, mollusks, and other invertebrate groups (e.g., sea jellies, bryozoans, nematodes, and acanthocephalans). Most heteropolysaccharides contain only two different repeating units and are associated with proteins (glycoproteins such as gamma globulin from blood plasma, and acid mucopolysaccharides, which are widely distributed in animal tissues) or lipids (glycolipids; e.g., gangliosides in the central nervous system).

(iv) Natural rubber (NR) also called India rubber, or *caoutchouc* is a cross-linked polymer, which is composed of isoprene monomers that are joined together to make long hydrocarbon chains. NR is mostly utilized for its elastic properties. It is obtained from the coagulation of the latex product by more than two thousand species of plants, one of them being *Havea Brasiliensis*. Currently, rubber is harvested mainly in the form of latex, a sticky, milky colloid that suspends the rubber molecules. Latex is collecting as the exudate from the deep incisions made on the bark of the rubber tree. The rubber is collecting from the latex by a coagulation process. NR is used extensively in many applications either alone or in combination with other materials.

Because of their broad range and unique properties, polymers play an essential and ubiquitous role in modern everyday life. Many polymers also have unique physical properties, which include tensile strength, modulus, toughness, viscoelasticity, and a tendency to form glasses and semicrystalline structures rather than crystals. However, due to the inferior mechanical and thermal properties in comparison to metals, many of the polymeric materials have limited use in engineering applications and they can even easily form complex shapes. The mechanical, thermal, and degradation properties of virgin polymers can be improved by preparing its composite with reinforcing materials and cheapened by incorporating fillers. Composite materials are made from two or more chemically and physically different constituent phases separated by a distinct interface with significantly different physical or chemical properties, which when combined, produce a material with characteristics different from the individual components (matrix phase and dispersed phase). Hence in the composite, the different systems are combined judiciously to achieve a system with more useful structural or functional properties non-attainable by any of it's constituents material alone. Composite materials are becoming an essential part of today's industry due to advantages such as low weight, corrosion resistance, high fatigue strength, outstanding performance, faster assembly, and favorable cost compared to traditional materials. They are extensively used as materials in manufacturing of aircraft structures, electronic packaging to medical equipment, and spacecraft. The predominant useful composite materials used in our day-to-day life include wood, concrete, and ceramics. Surprisingly, the most important polymeric

composites are found in nature, thus being known as natural composites. The connective tissues in mammals belong to some of the most advanced polymer composites known to mankind. Within these composites, fibrous proteins that serve as the matrix while collagen serves as the reinforcement which functions as both as soft and hard connective tissue. Matrix phases are the primary phase having a continuous character and are usually more ductile and less hard. These matrices hold together the dispersed phase, which is another phase (reinforcing phase) that is embedded in the matrix in a discontinuous form.

In the composite, the individual components remain separate and distinct within the finished structure. In a polymer composite, when the resin systems are combined with reinforcing materials such as glass, carbon, aramid, fillers (such ceramic particles), nanoclay, carbon black (CB), carbon nanotubes, and fullerenes, the resulting polymer composite exhibit exceptional properties. Since polymer matrix composites combine a resin system and reinforcing fiber/filler particles, the properties of the resulting composite material will combine some resin properties with that of the fiber/fillers. In the composite materials, the resin matrix spreads the load applied to the composite between each of the individual fiber/filler particle and also protects the fibers from damage caused by abrasion and impact, which improve the load bearing capability of the composite. High strengths and stiffnesses, ease of fabricating complex shapes, high environmental resistance, all coupled with low densities, make the resultant composite superior to metals for many applications. The characteristic properties of polymer composites are (i) high specific strength, (ii) high specific stiffness, (iii) high fracture resistance, (iv) high abrasion resistance, (v) high impact resistance, (vi) high corrosion resistance, (vii) high fatigue resistance, and (h) low cost.

Based on the type of reinforcement used in the composite, these compounds are mainly classified as (i) particulate composites, (ii) fibrous composites, and (iii) laminate composites. The particulate composite can be either microcomposites (>100 nm) or polymer nanocomposites (≤100 nm). Within both micro- and nanocomposites, the dispersed phase is usually composed of ceramic or metal particles. Microcomposites are simply the dispersed particles on a micro scale while nanocomposites contain dispersed particles on a nanoscale. Fiber reinforced polymer (FRP) composites are comprised of a variety of short or continuous fibers bound together by an organic polymer matrix. Unlike micro- or nanocomposites, in which the reinforcement is used primarily to improve the fracture toughness, the reinforcement in a FRP composite provides high strength and stiffness. Fibrous composites can be further subdivided on the basis of biofibers or synthetic fibers. Biofiber composite can be again divided on whether its matrix is non-biodegradable or biodegradable (also known as green composites). Hybrid composites comprise of a combination of two or more types of fibers.

The major attractions of green composites are that they are eco-friendly, fully degradable as well as sustainable. The design and life cycle assessment of green composites have been exclusively dealt by Baillie [7]. Green composites may be used effectively in many applications such as mass-produced consumer products with short life cycles and products intended for one time or short time use before

disposal. The important biodegradable matrices are cellulose, NR, polysaccharides, starch, chitin, proteins, collagens/gelatin, lignin which are natural. Matrices such as polyamides, polyvinyl alcohol, polyvinyl acetate, polyglycolic acid, and polylactic acid are synthetic. Bio-based composites with their constituents derived from renewable resources are being developed, and its applications are extended to almost all the fields. The following section of the chapter deals with eco-friendly polymer nanocomposites, specifically cellulose clay nanocomposites and NR clay nanocomposites as well as their respective applications.

2 Polymer Nanocomposites

Polymer nanocomposites (PNCs) are a relatively new class of composites for which at least one dimension of the dispersed particles is in the range between 10 and 100 nm. Since the uniform dispersion of these nanoscopically sized grains, fibers, and particles produce an ultra large interfacial area per unit volume between the nanoelement and the host polymer, the properties of these nanosized materials are altered. These nanoelements are characterized by having very *high aspect ratios,* resulting in their effective dispersion in polymer matrices, which when combined with adequate interfacial adhesion between the filler and the polymer often have properties that are superior to conventional microcomposites. Due to these unique properties, these nanoparticles can account for the same effects at lower loadings than with conventional filler content in the composite, thereby achieving considerable *weight reduction.* As compared to neat resins or microcomposites, these nanocomposites have a number of significantly improved properties including tensile strength, modulus, heat distortion temperature, gas barrier properties, flame retardant properties, etc. This aspect of nanotechnology has potential in applications such as engineering plastics, polymer products, rubbers, adhesives, and coatings [13, 90]. Because of their uniqueness, polymer nanocomposites exhibit unexpected hybrid properties synergistically derived from two components. Among a variety of promising nanomaterials for preparing polymer composites inorganic clay minerals consisting of silicate layers are promising, and are called as *polymer–clay nanocomposites* [60, 80], often referred to as polymer layered silicate nanocomposites.

2.1 Polymer Layered Silicate Nanocomposites

The revival of interest in polymer layered silicate nanocomposites was stimulated by two major findings in the early 1990s. In the late 1980s, a novel polymer composite comprised of Nylon-6 interphased with small amounts of montmorillonite (MMT) was reported. This layered silicate clay composite was prepared at Toyota Central Research Labs in Japan who teamed up with Ube Industries Ltd. The small amounts of these aformentioned layered silicate loadings resulted in pronounced

improvements of thermal and mechanical properties [52]. Toyota subsequently used the material for timing belt covers and other "under the load" automotive applications, capitalizing on the material's heat resistance and dimensional stability. The second major finding, carried out by Vaia et al. [89]. They found that it was possible to melt-mix polymers with layered silicates without the use of organic solvents. The nanoclay interphased with the polymer greatly improved the mechanical properties of the Nylon with very small filler loadings (less than 50 %wt). The work was very significant, because the clay platelets, which are just 10 Å thick, were found to be well dispersed homogenously in the polymer matrix at the nanometer level. The incorporation of small amounts of layered silicate in the polymer matrix often exhibit remarkable improvement in the material's properties when compared with its virgin counterpart, or conventional micro- and macro composites. These improvements can include high moduli, increased strength and heat resistance, decreased gas permeability and flammability, and increased biodegradability. The prospect of dramatic weight savings and improvement in properties initiated research in the application of this technology to a wide variety of polymers, both thermoplastics and thermosets. Thus, over the past decade, polymer layered nanocomposites have been a hot topic of research among researchers from both academics as well as industry [2, 70].

3 Nanoclays–Structure, Properties, and Modifications

3.1 Layered Silicates

The layered silicate commonly used for preparing polymer layered silicate nanocomposites belongs to the same general family of 2:1 layered phyllosilicates [22]. Layered silicates have two types of structures: tetrahedral-substituted and octahedral substituted. Details regarding the structure and chemistry of these MMT (Fig. 1) and layered double hydroxides (LDH) (Fig. 2) silicates are provided in Table 1. The basic structure of phyllosilicates consists of layers made up of two tetrahedrally coordinated silicon atoms that are fused to an edge sharing octahedral sheet of either aluminum or magnesium hydroxide. Depending on the particular layered silicate, the layer thickness is around 1 nm, and the lateral dimensions of these layers may vary from 30 nm to several microns or larger, having aspect ratios in the range of 100–1500 [27]. The interconnected six-member rings of SiO_4^{-4} (Fig. 3) tetrahedra extend outwards into infinite sheets. Three oxygens are shared by each tetrahedra leading to a basic structure unit of $Si_2O_5^{-2}$. Furthermore, the majority of phyllosilicates contain hydroxide (OH^-) ions which are placed at the center of the six member ring forming $Si_2O_5(OH)^{-3}$. An octahedral coordination is achieved when other cations are bonded to SiO_4^{-4} sheets whereby sharing of OH^- ions and apical oxygen take place. Commonly occurring cations in 2:1 layered silicates are Mg^{+2}, Fe^{+2}, and Al^{+3}.

The octahedral layers can adopt two types of structures depending on the cations. Cations such as Al^{+3} forms a Gibbsite [$Al(OH)_3$] while cations with +2 oxidation states such as Fe^{+2} and Mg^{+2} lead to a Brunite structure $Mg(OH)_3$. In both structures,

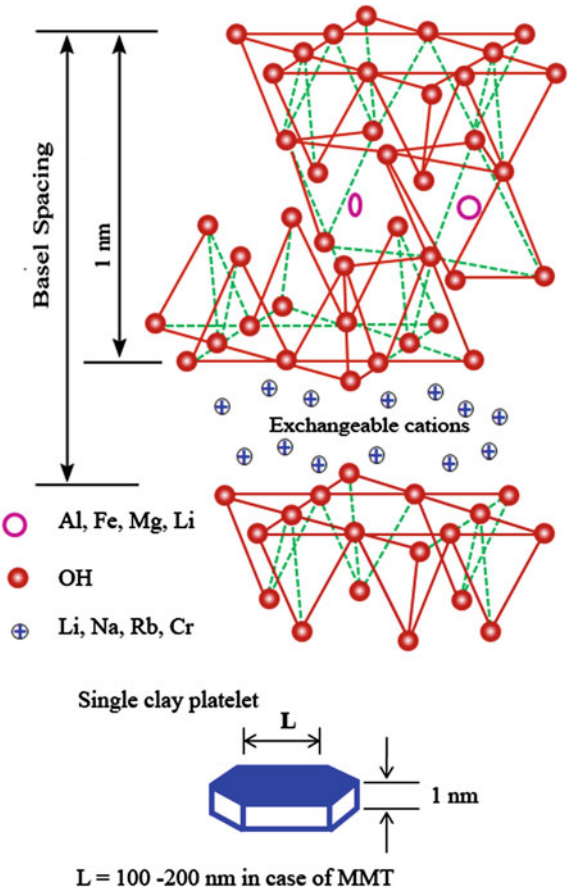

Fig. 1 Structure of montmorillonite layered silicate (MMT) [27]

all anions are OH^{-}. In brunite, the octahedral sites are all occupied while in Gibbsite, the 3rd cation site is occupied. When the phyllosilicates layers are stacked together, they lead to a formation of regular weak van der Waal gaps between the layers. These gaps are commonly referred to as gallery or interlayer [22]. Isomorphic substitution within the layers (for example, Al^{+3} replaced by Mg^{+2} / $Fe^{+2,}$ or Mg^{+2} replaced by Li^{+}) generates negative charges that are counterbalanced by alkali and alkaline earth cations situated inside the galleries. This type of layered silicate is characterized by a moderate surface charge known as the cation exchange capacity (CEC), and generally expressed as meq/100 g (milli-equivalents per 100 g). This charge is not locally constant with respect to location, but varies from layer to layer, and must be considered as an average value over the whole crystal. MMT, hectorite, and saponite are the most commonly used layered silicates. Among these, MMT is mainly used in polymer nanocomposites due to availability, high strength and stiffness, rigidity, impermeable properties [45], environmental friendliness, lower cost, and also the fact that its intercalation/exfoliation chemistry is well understood [25].

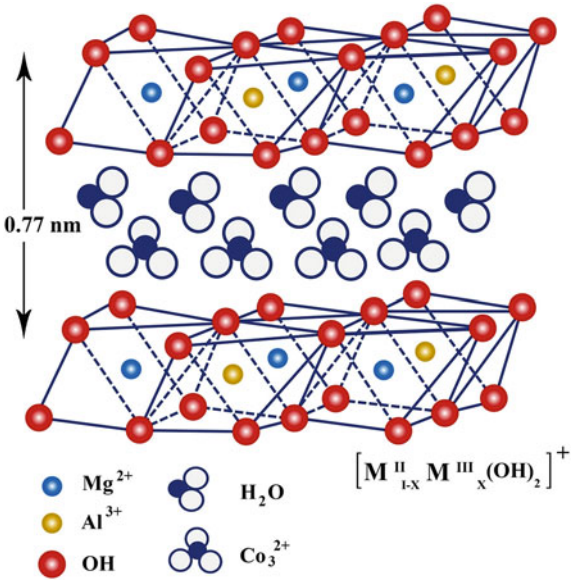

Fig. 2 Structure of layered double hydroxides silicate (LDH) [27]

Table 1 Chemical formula and characteristic parameter of commonly used 2:1 phyllosilicates

2:1 phyllosilicates	Chemical formula	CEC (mequiv/100 g)	Particle length (nm)
Montmorillonite	$M_x(Al_{4-x}Mg_x)Si_8O_{20}(OH)_4$	110	100–150
Hectorite	$M_x(Mg_{6-x}Li_x)Si_8O_{20}(OH)_4$	120	200–300
Saponite	$M_xMg_6(Si_{8-x}Al_x)$ $Si_8O_{20}(OH)_4$	86.6	50–60

M monovalent cation; *x* degree of isomorphous substitution (between 0.5 and 1.3)

3.2 Nanoclay Modifications

Two particular characteristics of layered silicates are generally considered for polymer layered clay nanocomposites. The first is the ability of the silicate particles to disperse into individual layers. The second characteristic is the ability to fine-tune their surface chemistry through ion exchange reactions via organic and inorganic cations. These two characteristics are, of course, interrelated since the degree of dispersion of layered silicates in a particular polymer matrix depends on the interlayer cation. The inter layer galleries of the pristine layered silicates usually contain hydrated inorganic cations such as Na^+, K^+, Ca^{+2} ions for balancing the charge of the oxide layers, which in turn leads to hydrophilicity in its pristine form [22, 25]. This respective property makes pristine layered silicates incompatible with a wide range of polymer types with the exception of polyvinyl alcohol and polyethylene oxide which are also hydrophilic in nature. Therefore, clays must often be chemically treated in order to make them organophilic. In these treatment processes,

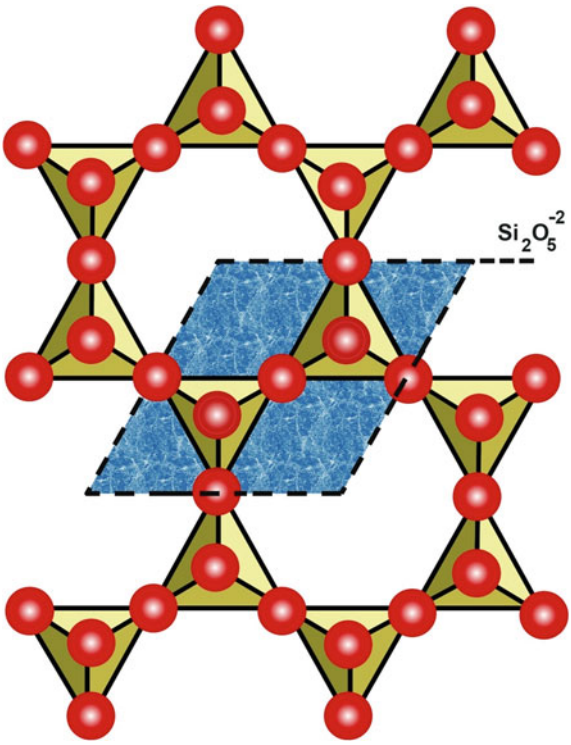

Fig. 3 Phyllosilicates basic structure consist of interconnected six member rings of SiO_4^{-4} (Image courtesy: Dr. Stephen A. Nelson)

the inter layer cations are readily ion-exchanged with a wide variety of positively charged species to make them more organophilic. This isomorphic substitution process is an integral part of these nanoclays for their use in making composites with polymers. The process involves the exchange of charges between phyllosilicate layers, e.g., Al^{+3} substituted by Mg^{+2} or Mg^{+2} by Li^{+2}. The process of ion exchange generates negative charges, which are counterbalanced by cations (mainly Na^{+} or Ca^{+2}) residing in the interlayer space making the clay organophilic, thereby compatible with hydrophobic (organophilic) polymers. In addition, the van der Waals forces between phillosilicate layers allow intercalation of polymers chains between them. When inorganic cations are exchanged by the organic cations, the yielded compound is referred to as an organically modified layered silicate (OMLS). The charges on the clay surface are generally expressed as the cation exchange capacity (CEC), which is the amount of exchangeable interlayer cations present between the surfaces. A high CEC leads to high levels of intercalation or exfoliation. For instance, MMT has a value ranging from 80 to 120 meq/100 g compared to only 3–5 meq/100 g making it difficult to disperse polymer molecules between layers of kaolinite [25].

Generally, ion exchange reactions are done by treating the clay with various cationic surfactants including primary, secondary, tertiary, and quaternary alky

$$Na^{+} + Clay + HO_2C\text{-}R\text{-}NH_3{}^{+}Cl^{-} \longrightarrow HO_2C\text{-}R\text{-}NH_3 + Clay + NaCl$$

Scheme 1 Rendering pristine clay organophilic [27]

ammonium [25, 27], alky phosphonium and sulfonium cations [45], or cations in various surfacants [22]. These cations in the organosilicate have a positive effect on the decreasing surface energy of the inorganic host and improve wetting characteristics of the polymer matrix. This in turn facilitates better adhesion between the clay with the polymer and in some cases can initiate the polymerization of monomers to improve the strength of the interface between the inorganic clay and polymer matrix [81]. One such example of rendering clay surfaces organophilic can be achieved by exchanging sodium ions in natural clay with unnatural amino acid derivatives such as 1, 2-aminododecanoic acid as shown in Scheme 1. Alkylammonium ions are the major cations used to modify MMT clay. Furthermore, it has been shown that surfactants with two alkyl tails result in better exfoliation and intercalation compared to those with one alkyl tail.

Recently, more surfactants have been researched extensively. For instance, Atai et al. [5] have used a proprietary surfactant called 2-acrylamido-2-methylpropane sulfonic acid (AMPS) which contains amido and sulfonic acids groups in its structure. It was postulated that exchange of Na^{+} and amido took place, thus providing reactive species that led to a better interfacial bond and improved properties of the poly(methylmethacrylate) (PMMA) composites compared to the pristine PMMA. Further comparison of Na-MMT (sodium montmorillonite) and organically modified montmorillonite (OMMT) clay using a transmission electron microscope (TEM), showed well-intercalated and exfoliated platelets in treated nanoclay compared to that of untreated clay. Functionalization of nanoclay has not been limited to organic surfactants only. An experiment was done to study the effect of water-soluble proteins as surfactants to the nanoclay [30]. It was observed that the presence of protein on MMT at all pH levels suggested electrostatic attraction and hydrogen bonding between MMT and proteins were taking place. This is a simple method to modify MMT, which can be used to manufacture bi-nanocomposite materials with improved mechanical properties. It is not only low cost method, but also utilizes biodegradable materials thereby making it environmentally friendly and mitigating the effect of pollution due to reliance on synthetic materials.

It has been observed that different surfactants have varying effects on the d-spacing of the nanoclay and many studies have been done on these phenomena. Concentration of the alky groups and chain length of the organic modifiers have been shown to increase the d-spacing of the phyllosicicate layers. In a study where three different organophilic surfactants were used (ethanolamine (EA), cetyltrimethyl ammoniumbromide (CTAB) and tetraoctadecylammoniumbromide (TO)), d-spacing was shown to increase differently according to the type of surfactant used leading to increase in the gap between the clay platelets. Better intercalation was obtained from the high concentration and long chain surfactant [105].

4 Polymer–Clay Nanocoposite Types, Chemistry, and Mechanism

4.1 Types of Nanocomposites

Low percentages of layered silicates that are properly dispersed throughout the polymer matrix create much higher surface area for polymer/filler interaction as compared to conventional composites. The complete dispersion of clay into the polymer or the strength of interfacial interactions between the polymer matrix and layered silicate (modified or not) involves reducing the micron size clay particles to nanosize and dispersing them throughout the polymeric resin. The dispersion of clay tactoids in a polymer matrix (there exists three different types of polymer layered silicate nanocomposites) are thermodynamically achievable as shown in Fig. 4. Depands on the extent of dispersion/intercalation the polymer-clay nanocomposites are categorized as:

(i) Non-intercalated nanocomposites: similar to the conventional microcomposite, where polymer is unable to intercalate between the silicate sheets/clay galleries. A phase-separated composite having a dispersed nano phase (Fig. 4a), however its properties stay in same range or slightly outperform compared to traditional mico- or macrocomposite composites.

(ii) Intercalated nanocomposites: nanocomposites in which the insertion of a polymer matrix into the layered silicate structure occurs in a crystallographically regular fashion, regardless of the clay to polymer ratio. In this structure, (Fig. 4b) a single extended polymer chain is intercalated between the silicate layers resulting in well-ordered multilayer morphology built up with alternating polymeric and inorganic layers. In other words, intercalated nanocomposites are normally interlayer by a few molecular layers of a polymer. Therefore, with respect to intercalations, the organic component is simply inserted between layers of clay such that interlayer spacing is expanded, but the layers still bear a well-defined spatial relationship to each other. Properties of the composites typically resemble those of ceramic materials. Apart from this morphology, flocculated nanocomposites structure is conceptually the same as intercalated nanocomposites may form. However, the silicate layers are sometimes flocculated due to hydroxylated edge–edge interactions of the silicate layers.

(iii) Exfoliated nanocomposites: nanocomposites in which the individual silicate layers completely separated out and are uniformly but randomly dispersed throughout the resin matrix (Fig. 4c) by an average distance, that depends on clay loading. In exfoliated nanocomposites, the clay layers do not bear a spatial relationship to each other. Usually, the clay content of an exfoliated nanocomposite is much lower than that of an intercalated nanocomposite. Most of the polymer layered silicate nanocomposites, however, are either partially intercalated, exfoliated, or a combination of these two structures.

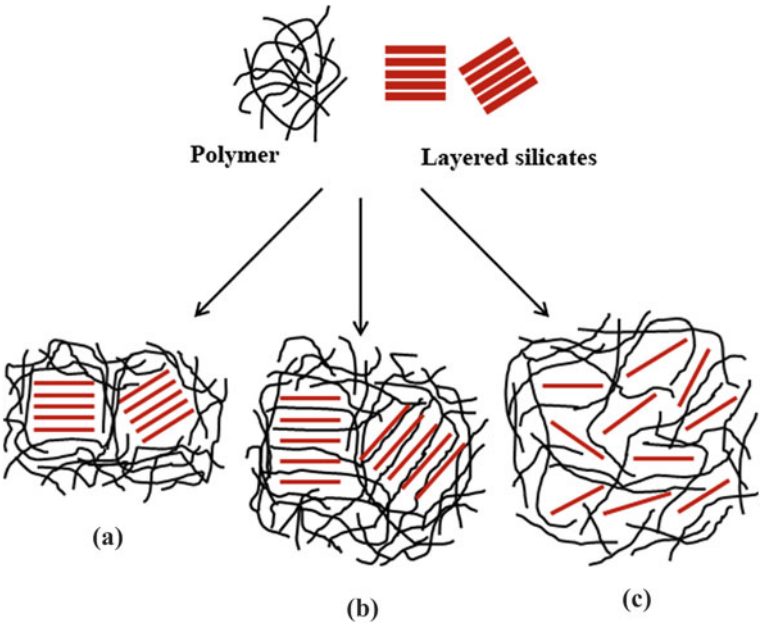

Fig. 4 Three different types of thermodynamically achievable polymer layered silicate nanocomposites; **a** phase separated microcomposite, **b** intercalated nanocomposite and **c** exfoliated nanocomposite

4.2 Chemistry and Mechanism

The need for lighter and stronger materials with high toughness has increased exponentially due to their demand in practically every industry resulting in extensive research for the fabrication of promising polymer layered silicate nanocomposites. Polymer nanocomposites are materials with ultrafine phase dimensions in the range of a few nanometers. These materials have emerged as an alternative to overcoming many engineering challenges in transportation, construction, and consumer applications [22]. Nanocomposites possess unique characteristics, which are far superior in quality compared to other composites or virgin materials. These characteristics include long-term durability, thermal and dimensional stability [98], fire retardation, and barrier properties against natural weathering [34, 98]. Furthermore, these materials offer a combination of stiffness, strength, and lightweight which make them suitable for critical engineering applications [22].

Dispersion of nanoclays into a polymer matrix are one of the most critical parameters in order to fabricate good quality end products with high mechanical, chemical, and physical properties. Fabrication method is closely related to the mixing methods employed to disperse the nanoclay into the polymer matrix, hence the selection of the mixing method will have a bearing on the final nanocomposite's properties. Various methods have been researched in order to achieve higher levels

of exfoliation and intercalation, e.g., sonication, two-roll mixing, magnetic stirring, mechanical mixing, melt blending etc. The twin screw extruder method increases the mechanical properties, i.e., thermal stability, storage modulus etc. [82], and glass the transition temperature [33]. This method produces nanocomposites with superior properties compared to internal mixers due to the high exfoliation achieved [74]. However, the combination of the two methods gives excellent exfoliation [71] and intercalation which in turn leads to a high tensile modulus, tensile strength, and unnotched impact strength [66]. The same trend is observed when all the other methods are used.

Figure 5 exhibits an idealized processing of polymer nanocomposites fabrication. As depicted in Fig. 5, the aim is to yield polymer chains between layers of nanoclay/clay galleries. To achieve this, (the nanoclay being hydrophilic) the nanoclay needs to be functionalized by various cations to facilitate compatibility with hydrophobic (organophilic) polymers. Selection of the surfactants plays a paramount role in achieving better interfacial bonds. For instance, the use of alkyl ammonium with additional tethering groups has shown different exfoliation or intercalation degrees. In one such study, the use of styryl and methacryl functionality showed extensive intercalation, which led to a shift in the basal plane. Furthermore, surfactants with methacryl-tethering groups facilitated diffusion of the PMMA molecules into the galleries of the nanoclay, promoting better exfoliation. The methacryl tethering groups, having similar chemical composition as methylmethacrylate (MMA) were cited as a reason. In addition, the unsaturated vinyl groups reacted further with MMA leading to higher exfoliation from both tethering groups [97]. This observation clearly demonstrated that compatibility between the surfactant and polymer monomer plays a significant role in the exfoliation and intercalation of the polymers into the nanoclay. Using different types of OMMT [46] such as Cloisite 30B (Cs30B) modified by dihyroxyethyl octadecyle methyl ammonium chloride, Cloisite 93A (Cs93A) modified by methylated dehydrogenated tallow ammonium, and Na-MMT showed varying levels of exfoliation or intercalation depending on the surface modification. Cs30B exhibits better compatibility with the polymer matrix in comparison with Cs93A. Its modifying structure contains two polar groups, making it a more polar cation than a nonpolar cation like Cs93A.

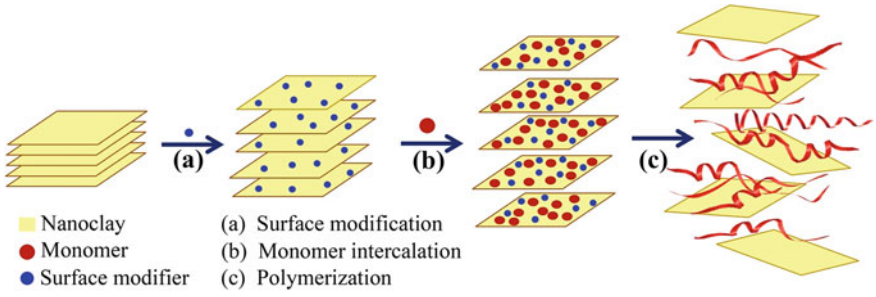

Fig. 5 Idealized process of nanocomposite fabrication using nanoclay. Images courtesy: Dr. Tie Lan

5 Nanocomposite Synthesis

Complete dispersion of clay tactoids in a monomer or polymer matrix involves three steps. The first is wetting the surface of clay tactoids by monomeric or polymeric molecules. This is followed by the subsequent intercalation of the monomer into the clay galleries. The third step is the exfoliation of clay layers. In polymer nanocomposites, these steps ensure incorporation of clay into the polymer matrix at the nano level. The different popular synthesis routes for preparing polymer-clay nanocomposites are discussed in the following sections.

5.1 Direct Intercalation

This method consists of spontaneous penetration of the polymer in the two-dimensional interlayer space by mixing the silicate and the polymer. A resulting polymer that is made by this method is polyethylene oxide. It's a simplest and economically cheap method, however one disadvantage of this method is the fact that most of the polymers are incompatible with the silicate making this method unsuitable.

5.2 In Situ Intercalative Polymerization

This method consists of the insertion of molecules or ions acting as monomers, which could be polymerized within the tetracrystalline region of the two-dimensional solid. The presence of transition metal ions as exchangeable cations is included in the structure of the layered solids to obtain the composites. This is the most successful approach to date, although it probably limits the ultimate applicability of these systems [81]. An example is that of polyamide 6-clay nanocomposite. In a typical synthesis, modified clay is dispersed in the monomer caprolactum, which is polymerized to form the polyamide 6-clay hybrid as an exfoliated composite. Complete exfoliation may be preceded by the intercalation of the monomer in the clay.

5.3 Ultrasound Irradiation

Ultrasound irradiation, as a new technology, has been widely used in chemical synthesis. When ultrasonic waves pass through a liquid medium, a large number of micro bubbles form, grow, and collapse in a very short time. This process, which occurs in a span of a few microseconds is called ultrasonic cavitation. These

ultrasonic cavitations can generate a local temperature as high as 5000 K, a local pressure as high as 500 atm, and a heating and cooling rate greater than 109 K/s. Therefore, ultrasound irradiation has been extensively applied in the dispersing, emulsifying, crushing, and activating of particles (e.g. polyaniline (PANI)/nano-SiO_2) [81].

5.4 Solution Polymerization

The layered silicate is exfoliated into single layers using a solvent in which the polymer (or a pre-polymer in the case of insoluble polymers such as polyimide) is soluble. It is well known that such layered silicates, owing to the weak forces that stack the layers together, can be easily dispersed in an adequate solvent. The polymer then adsorbs onto the delaminated sheets and when the solvent is evaporated (or the mixture precipitated), the sheets reassemble, sandwiching the polymer to form polymer-clay nanacomposite. The optimal case would involve an ordered multilayer structure [2]. Polar solvents can be used to synthesize intercalated polymer–clay nanocomposites [81]. The organoclay at first is dispersed in a nonpolar solvent such as toluene. Since alkylammonium treated clays swell considerably in nonpolar organic solvents forms gel structures. The polymer, dissolved in the solvent, is added to the solution and intercalates between the clay layers. The last step consists of removing the solvent by evaporation (e.g. polyurethane-clay nanocomposite or gelatin/MMT) [101].

5.5 Emulsion Polymerization

Emulsion polymerization is a new method to synthesize polymer nanocomposites. This synthesis is based on one step, which eliminates the environmental problems associated with the solution polymerization process and involves the addition of surfactants with unmodified silicate clay under stirring conditions. In order to begin this polymerization, a monomer is fed with an initiator and then proceeds under vigorous agitation conditions. The reaction mixture is then cooled to room temperature and the final product is obtained after filtration and washing several times with water followed by drying under reduced pressure e.g. PMMA/MMT [2].

5.6 Melt Blending (Compounding)

Intercalation with the aid of an extruder has been achieved by mixing the modified silicate with polymers in a melt [73]. An example is that of polypropylene (PP) nanocomposites, which are melted by compounding organophilic clays with

maleic anhydride grafted PP [23]. This layered silicate is mixed with the polymer matrix in the molten state. Under these conditions, if the layer surfaces are sufficiently compatible with the chosen polymer, the polymer can crawl into the interlayer space and form either an intercalated or exfoliated nanocomposite under these conditions. In this technique, no solvent is required hence it is environmentally friendly and not required any post processing like solvent evaporation or drying. Melt blending (compounding) depends on shear to help delaminate the clay and can be less effective than in-situ polymerization in producing an exfoliated nanocomposite.

6 Green Nanocomposites

There is currently a collective research effort in fabricating degradable materials to replace nondegradable materials, despite their superior advantages. Much energy is required to process these synthetic polymers and the fact that they are not degradable, poses a major environmental concern for current and future generations. There is also a concerted effort among scientists to find novel materials that are not petroleum based. In this search, it has been found that cellulose- and NR-based nanocomposites are very promising. Both cellulose and NR have many available sources and the fact that they are replenished seasonally within a short time makes them perfect candidates for natural composites with potential application in many industries. These include automobile, aerospace, consumer goods, and transportation industries.

6.1 Cellulose–Clay Nanocomposite

Cellulose derived composites have received much attention by researchers recently. This is attributed to their low density, biodegradability, low cost, high specific strength etc. Much research has focused in extracting the cellulose fiber and using it with either biopolymers or synthetic polymers to make a composite. It can be seen in recent studies that cellulose–clay nanocomposites have shown better properties compared to their counterparts [47, 75, 76, 103]. In addition, cellulose nanocomposite prepared with other nanoparticles also shown improved properties. Regenerated cellulose/TiO_2/ZnO nanocomposites showed excellent photocatalytic efficiency [36], and a decrease in cure time due to addition of cellulose nanosized materials, which is [35] an important parameter to those applications that require more time before the curing of resin. It has also been reported that superior thermal stability [21] increased storage modulus and crystallinity in polyamide [54] by addition of cellulose nanofibers. An improvement in mechanical strength was observed by addition of cellulose nanofibers into porous tissue [49]. However, the addition of cellulose led to an increase in the water uptake of the nanocomposite.

Furthermore, light transmittance of nanocomposites has shown an increase when cellulose nanofibers are added [53]. Nanocomposites fabricated from cellulose acetate powder modified with nanoclay showed an improvement in optimum mechanical properties with a 5 % compatibilizer loading. The better dispersion and exfoliation of clay (evaluated by TEM, XRD and atomic force microscopy (AFM)) in cellulose shows that these composites can be used as a replacement to non-biodegradable polymers [55, 56]. Park et al. [55, 56] also studied the effect of nanoclays on cellulose acetate bioplastic (CAB) and found that eco-friendly plasticizers like triethyl citrate varied in different amounts, while organically modified nanoclays maintained a constant weight at 5 %. Their results were in agreement with the literature that showed that intercalation and exfoliation of the clay is highly dependent on the amount of plasticizer in the matrix. Improvement in tensile strength, thermal stability, and modulus were achieved using a maximum of 20 % plasticizer. It was observed that percentage amount of plasticizer above 20 % resulted in the degradation in these properties. Preparation of transparent nano-fibrillated cellulose and nanoclay biohybrid films was done using high pressure homogenization methods [6]. Favorable exfoliation of the clay was recorded as well as inorganic content as high as 20 % was achieved without compromising the mechanical properties of the nanocomposites and its transparency. Addition of vermiculite improved the oxygen barrier of the hybrid film in high humidity environments. The high barrier property is an important characteristic because it can allow for packaging of oxygen-free organic electronics. Fabrication of cellulose/layered MMT nanocomposites was carried out by its precipitation from *N*-methylmorpholine-*N*-oxide (NMMO) in water [16]. Investigation on the extent of nanoclay dispersion showed more contact time is needed to yield a partial exfoliated morphology of the nanocomposites. The hybrid nanocomposites showed better thermal oxidative properties, which is important in the production of fire resistant materials. Nanoclays hinder the transfer of oxygen, heat, and degraded volatiles leading to high degradation temperatures of the final composite. Lower stability of cellulose at low temperatures is found to be due to the clay oxidizing and dehydrating the cellulose moieties. The use of various sequential mixing methods of triethyl citrate [57] in combination with maleic compatibilizers allowed these researchers to arrive at the optimum method leading to superior nanocomposites. The addition of compatibilizers accelerated the exfoliation of the clay in the matrix. In this case, the compatibilizer which is maleated, reacts with free OH^- groups in the clay structure and intercalates into the clay galleries, leading to a tensile strength and modulus improvement of 20 and 68 % respectively.

Glycerol triacetate, another glycerol plasticizer, has also been used with cellulose acetate and nanoclays to prepare nanocomposites [24]. Bio-based nanocomposites have been manufactured by melt intercalation of nanoclays with cellulose acetate (CA) in both presence and absence of a plasticizer. In the case where plasticizers were indeed present, they were varied up to 30 % together with OMMT and unmodified MMT clay (UMMT). UMMT clays can lead to poor exfoliation and intercalation compared to OMMT. The TEM studies found that less than 5 % unmodified clay led to an improvement in tensile strength and Young's modulus.

The interaction of cellulose acetate hydroxyl groups and free cations present in the clay galleries are cited as a possible cause for this observation. Elongation at the failure point remained constant. This was expected to drop as the addition of nanoclays normally lead to brittleness of the matrix.

Many studies have been done to improve the properties of nanocomposites from NR and cellulose. In one such study, in order to compare the thermal degradation of cellulose/clay nanocomposites and polyvinyl alcohol-starch-carboxymethyl [83] was carried out and, the results was shown that the addition of clay to the blend matrix led to high improvement in thermal stability in the films with the 5 % nanoclay giving the best results. Nanoclay was theorized to form a barrier which prevented mass and heat transfer. The high degradation of the matrix at high temperature was curtailed by clay layers allowing further reaction and thereby holding the degradation products for a longer time. One of the biggest hurdles faced by cellulose-based nanocomposites with respect to its application in fire retardants is the poor thermal stability of cellulose when exposed to high temperatures. There is a need to develop nanocomposites based in cellulose to exhibit better thermal stability at higher temperatures. The majority of current flame retardants in use are synthetic materials, some of them exhibiting toxicity and required high energy to produce. The use of layered silicate nanoclay has shown more promise to be used as better flame retardant. In addition, this composite is environmentally friendly and readily degradable. In his dissertation, Delhom [20] used various methods to achieve better exfoliation and intercalation of nanoclay in the cellulosic matrix. He used different solvents and pretreated clay using various techniques. Using NMMO as a solvent for cellulose and functionalized nanoclay, he optimized the degradation temperature by 45 °C. However, this resulted in a lower crystalline melt temperature of 15 °C.

An innovative method to prepare cellulose reinforced MMT nanocomposite films was developed by Mahmoudian et al. [44] and his colleagues using room temperature molten salts collectively known as room temperature ionic liquid (RTILS). This is an environmental friendly method where 1-butyl-3-methylimidazolium chloride is used as ionic medium. Cellulose and MMT are mixed separately with the ionic media. Cellulose can be magnetically stirred at approximately 85 °C for 4 h, while MMT is dispersed into the ionic media using a sonicator. The two solutions are later mixed together and stirred for a day at 85 °C to form a homogeneous MMT/cellulose composite in ionic media. The mixture was then vacuum degassed and casted on glass plates. There was an improvement in thermal stability and tensile strength until a clay loading of 8 % by weight of cellulose. The composite properties were decreased due to the aggregation of clays at higher content. Thus, this nanocomposite can be applied in packaging and membrane technology.

Extrusion is an important method in fabricating polymer composites commercially, and therefore has been well established and used widely in industry. This method was used by Bondeson [12] to study its effectiveness in producing nanocomposites reinforced by cellulose nanowhiskers. Two methodologies were adopted for the preparation of cellulose nanowhiskers; these include the hydrolysis of either sulfuric or hydrochloric acid. Furthermore, the nanowhiskers were either

dry mixed or freeze-dried prior to extrusion, and then compounded and extruded. To improve dispersion of the whiskers in cellulose acetate butyrate and polylactic acid (PLA), water and a surfactant were used. The results showed no improvement in thermal and mechanical properties in polylactic acid due to degradation and possibly poor dispersion of whiskers. However, on the other hand, there was an improvement in both thermal and mechanical properties in cellulose acetate butyrate. The possibility to make nanocomposites by pumping the cellulose nanowhiskers in an extruder with polymers was demonstrated. Contrary to the reduction of thermal and mechanical properties by using cellulose nanowhiskers, the use of cellulose nanofibers in polylactic acid was shown to lead to an improvement in tensile strength and modulus from 58 to 71 MPa and 2.9 to 3.6 GPa, respectively, and a great increase in the storage modulus and glass transition temperatures were observed by an addition of 5 wt% cellulose nanofibers [32]. Taking into consideration these extrusion methods that were used, it can be seen that different structures of the cellulose can lead to varied results.

6.2 Natural Rubber–Clay Nanocomposites

6.2.1 Natural Rubber

Natural Rubber (NR) is one of the most important elastomeric materials consumed in the industry, half of its total consumption being used for rubber products. It is harvested as latex from a class of plants growing in the tropics. Latex is the colloidal dispersion of rubber particles in an aqueous medium, which is collected by making an inclined cut on the bark of the rubber tree. This process is known as tapping. Nowadays, more than 95 % of NR is harvesting from Heveabrasiliensis which originates from South America, growing primarily in the rubber plantations of Indonesia, Malay Peninsula, Sri Lanka, and India. The field latex is concentrated by centrifugation, creaming, or electro-decantation for cost-effective transportation or making latex products such as condoms, balloons, gloves, or elastic threads, collectively called dipped rubber goods. For dry rubber products such as molded goods and tire manufacturing, the collected filed latex is strained and diluted with water and coagulated mostly by adding diluted acids (mostly diluted sulfuric acid or acetic acid) to cause destabilization of the colloid, which leads the agglomeration of the suspended rubber particles by sticking together within the latex called coagulation. The clumps or agglomerated rubber particles are separated and pressed between a series of plain rollers and grooved rollers to form thin sheets and then subsequently dried in air, smoke or sunlight before shipping to the processing plants. The average size of the rubber particles are 3 μm in size. The purified form of NR is chemically 100 % cis-polyisoprene. The molecular weight of the NR is normally in the range of 10^4–10^7 g mol^{-1} depending on the age of the rubber tree, weather, nature of the soil, rain fall, method of rubber isolation, etc. The molecular

Table 2 Properties of unvulcanized natural rubber

Properties	
Density (g cm^{-3})	0.91
Glass transition temperature (°C)	−70
Thermal conductivity (W m^{-1} $°C^{-1}$)	0.134
Heat of combustion (J Kg^{-1})	4.5×10^6
Equilibrium melting temperature (°C)	28
Heat of fusion of crystal (kJ kg^{-1})	64
Refracyive index (nD)	1.52
Dissipation factor(1 kHz)	2.4
Dielectric constant (1 kHz)	0.001–0.003
Dirt content (% by mass)	0.03
Volatile mass (% by mass)	0.50
Nitrogen (% by mass)	0.30
Ash (% by mass)	0.40
Initial plasticity number (P_0)	38
Plasticity retention index	78

weight distribution of rubber is relatively broad, which offers excellent processing behavior. Although it has high initial viscosity, it breaks down easily to a processable viscosity. The glass transition temperature (T_g) of this polymer is −70 °C and is subjected to a unique property known as stress-induced crystallization, the crystallization of the rubber molecules under strain. Table 2 shows the properties of the unvulcanized NR. The advantages of the use of NR include outstanding flexibility at use temperature, excellent mechanical strength, exceptional tear strength, good abrasion resistance, and low hysteresis (heat buildup under flexing). However, the aging properties of this material are poor. In addition, since it is of biological origin, NR is renewable, inexpensive, and creates no health hazard problems. The properties of the NR are improved by compounding or making composites with filler particles or reinforcements. By addition of reinforcing elements such as silica, clay, or CB and occlusion of rubber tremendously increase the tensile strength, wear and tear resistance, and modulus, but adversely affect the heat buildup.

6.2.2 Types of Clays for Rubber Nanocompoiste

Reinforcing of NR has been exclusively done by CB, but more environmental friendly nanoparticles are now being explored. Apart from silica or other ceramic fillers, different types of nanoclays are being used to reinforce the NR. Studies show that properties of the composite are greatly influenced by the type of nanoclay. For instance, the effect of two types of nanoclay such as MMT and LDH showed differing results due to the makeup of the nanoclays. As mentioned earlier, MMT is a cationinc clay while LDH is an anionic clay with the possible formula $[M^{II}_{x} M^{III}_{1-x}(OH)_2](A^{n-1})_{x/n}{*}yH_2O$ where M^{II} represent divalent metal ions, the M^{III}

representing trivalent metal ions. The x values range between 0.2 and 0.33 and in this case *y* is equal to 0.4.

It was shown that unmodified LDH leads to reduction in the cure rate of certain rubbers [19]. The interaction between MMT or LDH with rubber molecules is via hydrogen bonding of the nitrogen atom attached with thiourea, the cross-linking agent of the rubber molecules and electronegative oxygen in the clay layers. The anionic properties of LDH make it have high affinity for electron rich species leading to higher interaction with rubber. The cationic effect of the nanoclay improved the physical properties of the rubber, i.e., tensile, dynamical mechanical properties, etc. From this study, thermal stability can be improved by noting that LDH and CB always have a tendency to restrict crystallization of polychloroprene rubber, but not the case with OMMT.

6.2.3 Method of Preparation of Rubber–Clay Nanocomposite

Presently, there are four principal methods used for preparing rubber–clay nanocomposites: (i) melt mixing or compounding, (ii) in-situ polymerization, (iii) latex blending, and (iv) solution intercalation. Among these methods, melt intercalation and in-situ polymerization are considered as simple and commercially attractive approaches for preparing "rubber–clay nanocomposites." However, in-situ polymerization is not a possible method for preparing NR–clay nanocomposites as it is extracted as latex from the rubber tree. Latex blending is a promising method for the rubbers available in aqueous dispersions (e.g., NR or styrene butadiene rubber abbreviated as SBR) because in this case pristine layered silicates can be used [10, 11,72, 91, 93, 99]. The latex blending method is not possible for many synthetic rubbers due to non-availability of its latex form. Solution intercalation methods can be used for preparing rubber–clay nanocomposite of most of the elastomers, which is soluble in hydrocarbon solvents [31, 96]. However, melt intercalation has received much attention since it offers significant processing advantages that would greatly expand the easiness of commercial production of rubber–clay nanocomposites with conventional or slightly modified rubber processing machineries such as extruders, banbury mixer, or two-roll mills [94]. Also, melt compounding would be significantly more economical and simpler than in-situ polymerization minimizing capital costs because of its compatibility with existing industrial rubber processing equipment. Since there is no solvent or liquid medium required, melt processing is environmentally friendly, more economical, and avoids postprocessing such as solvent stripping or coagulation. In addition, it enhances the specificity for the intercalation of polymer, by eliminating the competing host-solvent and polymer-solvent interactions. Indeed most of the rubber–clay nanocomposites were prepared by melt blending technique. The melt processing method used for the preparation of rubber–clay nanocomposites is similar to that used for conventional polymer–clay nanocomposites. Therefore, nanocomposite production is swung downstream, giving end-use manufacturers many possibilities

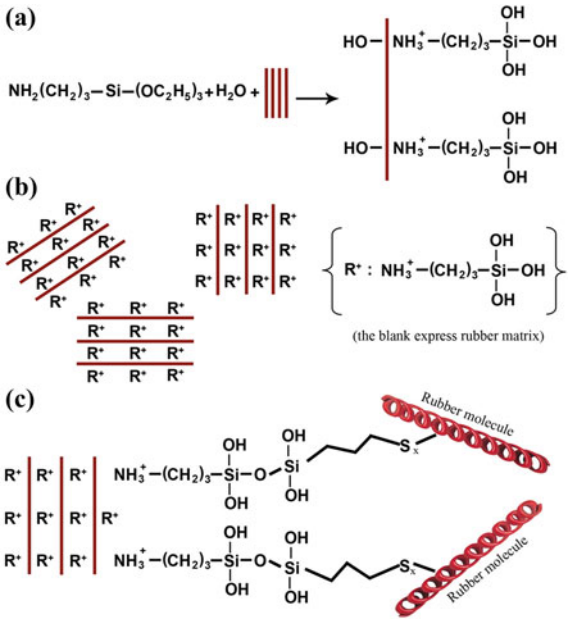

Scheme 2 Proposed schematic of modification mechanism with silane coupling agent: **a** cation exchange in clay suspension with 3-aminopropyltriethoxysilane (KH-550), **b** after co-coagulating, the sturucture of RCK flocculate, **c** after adding bis[3-(triethoxysilyl)propyl]tetrasulfide) (Si-69) and sulfur curing ingredients on a two-roll mill, and curing the compounds at 150 °C, the interaction among KH-550, Si-69 and rubber molecules in rubber-clay nanocomposite. (Adapted from Ref. 29)

with respect to final product specifications (e.g., selection of polymer grade, choice of organoclay, level of reinforcement, etc.).

6.2.4 Natural Rubber–Clay Nanocomposite (Dry Rubber Process)

Nanoclays are being researched as an alternative to CB, the principal reinforcing filler in rubber compounds. The biggest problem with nanoclays thus far has been dispersion into the NR to achieve the desired improvement. It is difficult to achieve exfoliation or intercalation of nanoclays into NR, because nanoclays have a tendency to agglomerate with increasing amount into rubber or polymer matrix. Various methods have been used to solve this problem. One promising method was reported by Mohan et al. [48] and his co-workers mentioned previously as the Banburry method. This is a two-stage method where in the first stage uncured rubbers with all additives are mixed in the mixer at 60 rpm at 145.8 °C. Once maturation is achieved at roughly 26 h, the nanoclay is then added at different amounts, until the desired amount is achieved. At this stage, mixing speed is reduced to 40 rpm and the temperature is around 100–110 °C. The mixture is then

allowed to reach maturity after 24 h. This is followed by sheeting the compounds using a two roll mill. The molds are steam heated at 148 °C at a pressure of 10 MPa. A two roll–roll mixer is then employed for the 3 % nanoclay in rubber. Results from XRD showed increase in d-spacing between the nanoclay, allowing rubber to enter into the clay galleries. Nanoclays also reduced curing time due to the reaction of the cationic ions of clay with rubber. Although nanoclay has been known to lead to brittleness of the matrix, the brittleness was only confirmed by transmission electron microscopcopy at 3 % nanoclay by weight of matrix. Increase in cross-linking of the nanoclay in rubber leads to increase in hardness and gas barrier properties. The thermal tests showed nanoclay/rubber having higher stabilities at high temperatures compared to pristine rubber.

Another dispersion method which shows promising results by providing highly dispersed nanocomposites with excellent interfacial bond strength was devised by Jia et al. [29]. This method, called the two-step method, employs the use of two silane coupling agents; 3-aminopropyl triethoxysilane (KH-550), and bis(triethoxysilylpropyl)tetrasulfide (Si-69). To generate hydroxyl groups, 3-aminopropyl triethoxysilane (KH550) is added to a mixture of water and clay in an in-situ organic modification. It was found that hydrolysis of Si-$(OR)_3$ leads to the production of hydroxyl groups. Bis(triethoxysilylpropyl)tetrasulfide is later added into the mixture of rubber and clay and mechanically blended by two-roll milling. In the vulcanization process, ethoxysilylpropyl groups from bis(triethoxysilylpropyl)tetrasulfide react with S-OH of the dispersed clay in rubber leading to a chemical bond between rubber and clay phases. This results in a strong interfacial bond which leads to high tensile strength, thermal stability, and high stresses at certain strains. Possible mechanisms for the reactions are shown in Scheme 2.

6.2.5 Hybrid Natural Rubber-Clay Nanocmoposite

In multi-component compounding, two or more different types of fillers are used, called hybrid compounds or hybrid structures. A hybrid structure combines the effect of different materials [17, 28, 50, 51, 87]. Recent investigations on composites having multi-component filler systems focus mainly on thermoplastic and thermoset polymers and are not so familiar with rubbery materials. In most of the applications, CB and the silica have been used together as a hybrid filler system to optimize the advantages and disadvantages of the individual filler system [69]. Among all the fillers, CB plays an important role in the rubber industry as reinforcing filler. By incorporation of CB into the rubber matrix, many of the desirable properties like dynamic mechanical properties, fracture behavior, tensile strength, tear strength, modulus, hardness, and abrasion resistance are increased, which make CB an ideal candidate as a reinforcing filler in NR compounds and has been extensively exploited in numerous rubber engineering products, hence it is known as universal reinforcing filler in rubber industry. Despite these advantages, CB is a product of petroleum processing and much energy is required in its production. In addition, it must be mentioned that it is a hazardous material. Compared to silica, the widely

used reinforcing filler for non-black rubber products, CB reinforced rubber has a higher modulus. In tire treads, silica provides lower rolling resistance at equal wear resistance and wet grip than CB. Like silica, nowadays the emergence of natural fillers, like nanoclays which is cheaper and friendly to the environment, have been utilized in rubber compounding along with CB to overcome certain negative aspects of CB include tire tread wear and tear. However, it is virtually impossible to completely eliminate CB from the NR composite for certain applications. For example, nanoclays do indeed improve the properties of NR, but not to the extent required for many end-use products such as tires, consumer goods, and/or automobiles.

6.2.6 Natural Rubber–Clay-Carbon Black Nanocomposite

An innovative approach to improving nanocomposite properties is to use a hybrid of two reinforcing fillers such as nanoclay and CB; one such study was conducted by Praveen et al. [62]. The study established that high improvement on vulcanizate properties of NR nanocomposite can be achieved by using the two fillers due to synergic effect of the different fillers. The study showed that even CB increases the gap between clay nanoplatelets, thereby contributing an appreciable increase in the strength of the resulting nanocomposites. Furthermore, there was a substantial increase in modulus attributed to the network structure of CB, which tends to restrict slippage of macromolecular chains. Improvement of glass transition temperature of the composites was due to decrease in interfacial slide and relaxation, which resulted in better intercalation of clay/CB with the rubber. The effect of hybrid nanoclay/CB, and the effect on its ratios on the curing kinetics, cross-linking behavior, and activation energy of NR [78, 77], mechanical and dynamic mechanical properties of the vulcanizate for application in truck tires [3], cut growth behavior and gas permeability were studied. The results showed that the hybrid filler has a pronounced effect on certain properties of the nanocomposites.

The influence of organically modified nanoclay-CB hybrid filler on the curing behavior of NR was studied by Janak Sapkota et al. [79]. Two types of modifications (dimethyl-dihydrogenated tallow alkyl ammonium salt and octadecylamine) of the clay was employed. The partial replacement of CB with nanoclays influences the curing behavior substantially, and the addition of the clay significantly decreases the activation energy of the networking system. Also, results show that quaternary ammonium modified clay compounds increased the curing rate and lowered the torque. The activation energy for initiating the cross-linking reaction is decreased with addition of clay and thus cross-linking tends to take place in an easier manner in the presence of the modified nanoclays. Dynamic mechanical tests performed under a strain sweep showed the Payne effect due to better dispersion of CB. In addition, Mooney viscosity results showed that the replacement of CB with modified nanoclay can help in the dispersion of fillers. Strong interactions between CB, nanoclay, and NR matrix were also found. In another study carried out by Anwendungen [3], the nanoclay was modified with stearic acid before adding it with CB and used unmodified organoclay as the baseline. The hybrid prepared with

modified clay had better reinforcing capability compared to the unmodified clay. It was further observed that hybrid nanoclay/CB had an effect of reducing fossil fuel resource use by almost 40 % for truck tires manufacturing, in addition to better performance in rolling resistance. In addition, when premixing with the organoclay, the stearic acid serves to swell the clay layers, allowing the rubber molecules to be intercalated into the gallery of the layered silicate. This process enhances the mechanical properties of the composites with low loading of CB without sacrificing other physical properties like tensile strength, modulus, hardness, and rebound resilience. In another study, [67] two types of nanoclays, calcined clay and devolite, were used and it was shown that 2 phr (parts per hundred rubber) of both types of clay can be replaced with 1 phr CB to maintain the same hardness value. There was also a decrease in curing and resilience of the composites when the clay/CB was lowered while torque, strength, and thermal aging resistance were improved. Calcined clay/CB also showed lower gas barrier properties and cure time but higher modulus, tear strength, cut tensile strength, and higher cross-link density. The addition of nanoclay/CB changes the crack growth from a simple lateral to a more oblique one resulting in its higher tensile strength.

6.2.7 Natural Rubber–Carbon Black-Silica-Clay Nanocomposite

Hybrid nanoparticles of CB, silica, and nanoclay have been utilized to study various properties of NR. The influence of nanoparticles on mechanical properties of the final composites was conducted by research groups such as Rattanasom et al. [68], while other researchers such as Lo and Chu [40] used the same kind of nanoparticles to study their effect on the environmental resistance of hard rubber. In the study by Rattanasom et al. [68] the nanoparticles were mechanically mixed at 50 rpm, followed by the use of a two-roll mixer and 10 end-roll before sheeting, and then finally carrying out a compression molding at 150 °C. It was observed that MMT filled NR vulcanizate shows higher values of hardness at lower content compared with the other filler particles; silica and/or CB which require a higher loading to achieve the same hardness. The comparison of the composite with equal loading of clay into NR exhibited higher values in tensile strength, compression, and modulus, but poor crack growth and heat buildup resistance. Scanning electron microscopy (SEM) showed better dispersion of CB in NR and higher cross-link density, which resulted in overall better mechanical properties. In the Lo and Chu [40] study, NR and additives were mixed in a mixing chamber at 20 rpm and compounded at 150 °C for 2 h. The optimum CB content in clay/CB-filled hard rubber samples was 45 phr when total filler content is either 105 or 120 phr. Environmental tests were carried out using laboratory electrolytic cleaning tank immersion setup. The CB showed better resistivity but unlike the previous study [68], it had improved hardness after immersion. The CB/silicate NR composite did not pass the electrolytic cleaning test due to dissolving of the silica in the testing process.

6.2.8 Natural Rubber–Clay Nanocomposites: Solution or Latex Route

Solution Route

NR clay nanocomposites using rubber solutions or latex have been successfully prepared and reported by many groups. Magaraphan et al. [43] studied the effect of different amine intercalants on the mechanical properties of NR clay nanocomposites prepared using the solution process. The composite was prepared by dissolving NR in toluene along with MMT modified with primary or quaternary intercalants bearing different hydrocarbon alkyl tails. The curing agents were then subsequently mixed with the composite. After drying, the mixture was homogenized on an open mill. It was found that the composite prepared with primary amine intercalants had better mechanical performance over its counterpart that was prepared with quaternary amine intercalants. Liang et al. [39] compared the effectiveness of melt and solution intercalation methods on the dispersing of organically modified clays. In another study, the structure and properties of rubber/organophilic MMT nanocomposites carried out by Lo´pez-Manchado et al. [41], MMT was modified (although it was intercalated initially) with octadecylamine (MMT-ODA). It was found that both methods delivered similar nanocomposite structures with intercalated and exfoliated nanoscale clay layers. The basal spacing of the clay was almost doubled for those dispersed into the composites due to the intercalation of rubber molecules into the clay galleries. However, the solution technique (toluene served as solvent) yielded a higher amount of bound rubber, improved the dynamic mechanical properties and enhanced the compression set hardness [41], and exhibited a higher aspect ratio (compared to the melt method). In addition, this technique also resulted in outstanding mechanical and gas barrier properties [39].

Because NR is highly nonpolar, a better method for uniform dispersion of the clay in the matrix needs to be developed. It has been reported that the use of an epoxidized natural rubber (ENR) as a compatibilizer can lead to better dispersion of clay into the rubber matrix. Rajasekar et al. [65] performed this experiment by preparing an ENR by solution mixing. The nanocomposites were mixed into SBR and sulfur was used as a curing agent. High resolution transmission electron microscopy (HRTEM) showed highly intercalated clay layers. Dynamic mechanical tests showed a highly improved storage modulus and lower damping characteristic as well as an improvement in the mechanical properties of the resulting composites.

Latex Route

In contrast with solution processing, the latex compounding method employs the use of water instead of organic solvents as a host medium. The latex is the colloidal suspension of submicron sized rubber particles in water. To prepare the nanocomposite, pristine clay or its suspension/dispersion in aqueous medium (slurry) can be added directly into the rubber latex. As discussed earlier, clays are strongly hydrophilic and thus easily adsorb water molecules, which is associated with an

expansion in its intergallery spacing. In other words, hydration decreases the attractive forces between the phyllosilicate layers, resulting in more exfoliation during stirring. After mixing the clay uniformly in the lattices, the compounded composite rubber latex was casted into a mold and left to dry. In this case, the rubber clay nanocomposite collected remains unvulcanized. The curatives can then be incorporated into the composite and molded into different products. In contrast, suitable rubber curatives, which can be dispersed in water, can also be mixed with the clay-containing rubber latex before casting and drying. This latter mentioned process is most suitable for dipped goods such as condoms or gloves where the former are dipped into the compounded rubber composite latex mixture. The mixture can then be dried in either air, or temperature controlled air ovens followed by curing at high temperature (above room temperature in air or in boiled water).

Varghese et al. [93] investigated the properties of NR layered silicate vulcanized nanocomposites with different clay types. These types included sodium bentonite (natural) and sodium fluorohectorite (FHT, a synthetic layered silicate) that were studied in conjunction with a non-layered inert filler (English India clay or commercial clay) as a reference material. The study found that FHT gave the highest mechanical performance and the lowest toluene swelling compared to inert non-layered clay or layered bentonite clay. This can be attributed to the high platelet aspect ratio, intercalation/exfoliation of the silicates due to its prominent water swelling ability of FHT, and the formation of a skeleton (house of cards) silicate network in the NR matrix. In another study by the same group, [92] polyurethane rubber (PUR) and prevulcanized NR latex were blended with a pristine synthetic layered clay, known as sodium fluorohectorite. They prepared films of nanocomposite structure with enhanced stiffness characteristics to study the morphology-dependent mechanical properties of layered silicates. Compared to NR, it was found that a higher degree of intercalation due to better compatibility of the layered silicate with PUR (thus being nano-reinforced) and has a pronounced reinforcing effect. The ultimate tensile strength as well as tear strength was strongly increased (more than three times) and a dramatic improvement was found in the moduli at different elongations. The property improvement was traced to a layered silicate (LS) skeleton-type (‘house of cards’) structuring in the corresponding nanocomposite. Fourier transform infrared spectroscopy (FTIR) and broadband dielectric analysis were adopted to examine the NR/LS, PUR/LS and NR/PUR/LS nanocomposites formed via the latex route [64, 63, 92]. It was found that the PUR chains, due to their polar character, facilitate the intercalation/exfoliation of the layered silicate. Further, LS was preferably located in the PUR phase in the blends, which exhibited excellent mechanical properties despite the incompatibility between NR and PUR.

Different structures of rubber clay nanocomposites were prepared by co-coagulation of latex with aqueous clay suspension to form NR–clay, SBR–clay, carboxylated acrylonitrile butadiene rubber (CNBR)-clay and nitrile butadiene rubber (NBR)–clay. The TEM and XRD were performed on the resulting nanocomposites [99]. In this method, an aqueous suspension of clay and rubber latex were mixed and stirred vigorously for a required time. The mixture is then co-coagulated in an electrolyte solution of dilute triethylenetetrammonium chloride

solution for NR and SBR, while a calcium chloride aqueous solution is used for NBR and CNBR. The mixture is later washed with water and oven dried at approximately 80 °C for 18 h. Vulcanization additives are then incorporated into the nanocomposite using a two-roll mill. The structural characterization performed on nanocomposites showed that the rubber molecules led to the separation of the clay into individual layers and/or silicate aggregates with thickness in the nanometer range with no intercalation of rubber into the clay galleries. This was mainly due to the competition between reaggregation of clay layers and latex particle separation during co-coagulation. Further results showed a higher aspect ratio and a higher glass T_g due to the increased network of rubber/clay nanocomposites in comparison with pristine rubber. In addition, it was also found that tensile strength was increased (by a factor of 6), and there was an observed decrease of almost 50 % of gas permeability when 20 phr clay was added to the rubber.

In an effort to understand the effects of different types of organically modified clay on NR, [42], a comparison study of methyltallow bis-2-hydroxyethyl ammonium-modified montmorillonite (MMT-TMDA) and MMT-ODA was carried out. For further comparison purposes, layered silicate sodium bentonite was also used in addition to un-layered clay. Results from XRD and TEM showed better dispersion of MMT-ODA clay and poor dispersion of un-layered clay. In addition, organically modified clays exhibited better mechanical properties such as tensile strength, compression set, resilience, hardness, and tear strength. The high interlayer distance between the layers of modified clay was cited as the reason for these improved properties. In another study, a conventional compounding method was used to prepare latex–clay nanocomposites [26]. This method is limited by the fact that, as the loading of the clay increases, there is a buildup of high viscosity, generating difficulty in nanoclay processing. The XRD results agreed with the literature where it was shown that the layered phyllosilicate was ordered or delaminated, which led to better intercalation but partial exfoliated structure. A study on the effect of clay on the transportation properties of the nanocomposite was conducted by measuring the sorption, permeation, and diffusion coefficient using toluene at 303 K. A tortuous path provided by nanoclay [33] resulted in a decrease in the coefficient of diffusion. Better gas barrier properties were recorded for oxygen molecules. This was observed even for lower loading of the clay into the rubber latex. There was also better compatibility of the clay and the rubber leading to the formation of elastomeric networks. Improvement of the nanocomposite properties by adding nanoclay in rubber highly depends on the exfoliation of phyllosilicate layers or intercalation of the rubber molecules into the clay galleries.

6.2.9 Effect of Clay on Microstructure

The effect of clay on the microstructure and morphology of NR network is a complex process. Much research has been conducted to study this effect in order to predict the final microstructure of rubber matrices after intercalation or exfoliation of the clay. For instance, Carretero-Gonza et al. [15] used dielectric spectroscopy

and wide angle XRD to study the effect of organically modified clay on NR microstructures. The introduction of nanoparticles into the NR led to a homogeneous and well-distributed structure. The homogeneous structure resulted in an early occurrence and increased crystallization under uniaxial deformation. The enhancement of the crystallization was brought about by the alignment of the nanoclay during stretching. Mobility of the clay into the natural matrix during crystallization led to a highly networked structure having cross-linked chemical chains. A shift in the tanδ curve showed that there was limited mobility of the NR matrix into the clay nanoparticles.

Changes in mechanical properties of non-vulcanized dialyzed NR by addition of nanoclay have been studied by performing uniaxial deformations. It was shown that non-rubber molecules contributed to the auto-reinforcement of the nanocomposites [72]. Nanocomposites prepared by aqueous dispersion of clay and latex mixing contained exfoliated clay with the presence of tactoids. It was expected that presence of tactoids in the matrix would lead to poor mechanical properties, but this hypothesis was not observed, possibly due to the alignment of clay.

Cellulose nanoparticles in the form of either whiskers or nanofibers have been used as reinforcement into natural fiber matrices in order to achieve high performance nanocomposites [1, 9, 95]. The following conclusions can be stated; addition of cellulose whiskers from waste bamboo led to increase in thermal stability, storage modulus, and decrease in elongation at failure [95]. A comparison between cellulose whiskers and micro-fibrillated cellulose, the latter performing better when used as reinforcement in NR. Presence of residual lignin and fatty acids on the micro-fibrillated cellulose promoted better adhesion resulting in high stiffness and tensile strength of the nanocomposites [9]. A reduction in solvent absorption and a decrease in the diffusion coefficient of nanocellulose NR composites were attributed to the presence of a double network of cellulose–cellulose and rubber–rubber [1]. Lastly, there was a decrease in viscosity as the nanocellulose content was increased.

7 Physical Properties of Natural Rubber-Clay Nanocomposite

7.1 Without Compatibilizer

Vu et al. [96] took the first effective effort in the preparation of rubber-nanoclay composites. In this initial study, different rubber–clay nanocomposites based on synthetic natural rubber (SNR) and ENR were prepared by both melt mixing and solution intercalation techniques. Either an OMMT or Na-MMT clay modified with alkyl ammonium cations by an ion exchange reaction to make the galleries more hydrophobic and thus more compatible with the nonpolar rubbers. XRD studies verified the intercalation of NR and ENR into the silicate interlayers and/or exfoliation of the silicate layers into the elastomer matrices. However, the surface morphology of the composite was not studied to visualize the clay dispersion and

exfoliation by SEM or TEM. The vulcanizates with organically modified clay exhibited better tensile properties due to the better polymer-filler interactions and weaker filler–filler interactions. Compared with silica fillers, the effect of the dynamic strain amplitude on the storage modulus with Na-MMT was higher, possibly due to a greater hydrodynamic reinforcement as a result of melt intercalation of the rubber in to the Na-MMT galleries. The storage modulus increased with epoxidation of NR and clay loading. This increase was attributed to the stronger rubber–filler interactions due to the higher degree of epoxidtion. The increase of the interfacial adhesion between the clay tactoids and the polymer matrix is remarkably improved due to the formation of partially intercalated structures with clay loading, hence the storage modulus was higher with clay loading [37]. Varghese et al. [92] and Modhusoodanan et al. [42] studied the properties of NR-clay nanocomposites prepared by melt mixing. In the Varghese et al. [92] study, NR–clay nanocomposites containing 10 phr of organoclay, found that the interlayer spacing of the rubber nanocpomposite was higher for clay modified with primary amine (MMT-ODA) than for one modified with quaternary amine (MMT-TMDA). In the study, the property improvements caused by the fillers were ranked as follows: organophilic clays > pristine synthetic layered silicate (sodium fluorohectorite) > pristine natural clay (purified sodium bentonite) > precipitated non-layered silica (used as a reference) (actually state the actual property improvement when listing these superlatives).

In a study carried out by Modhusoodanan et al. [42], the highest interlayer distance of 3 nm was observed for organoclay filled NR nanocomposites studied by XRD and TEM. The addition of organoclay into the NR decreased the cure time as well as the scorch time of the rubber compounds. However, the effect is not pronounced compared to NR gum compounds with bentonite and English Indian Clay (EIC). The organoclay filled compounds showed high Mooney viscosity revealing that intercalation occurred during mixing of the silicate into the rubber. The physical–mechanical properties such as tensile strength, modulus, hardness, abrasion resistance, and tear strength of NR improved in the presence of organoclays, even at low loading due to the exfoliation of the silicates, which caused an increase in surface area several fold, resulting in better interaction between the filler and rubber molecules. Carretero-Gonzalez et al. [15] reported that the presence of nanoclays introduce a dual crystallization mechanism due to the alignment of nanoparticles during stretching. The improved properties in NR–clay nanocomposites was also attributed to both the microstructural and morphological changes induced by nanoclay as well as to the nanoclay mobility in the NR matrix during crystallization. Usuki et al. [88] also reported that strong ionic interaction between polymer and silicate layers, which generate some crystallinity at the interface, is responsible for the effect of reinforcement. Carli et al. [14] revealed that silica can be replaced with a considerably low amount of organoclay with a reduction of filler content by 12.5 times without adversely affecting the mechanical properties of the final composite, even after aging. Yahaya et al. [102] found that NR–clay nanocomposites achieved a maximum value of tensile and tear strength with 6 phr of clay loading after which a fall was observed. The reduction in tensile strength of the modified, filled

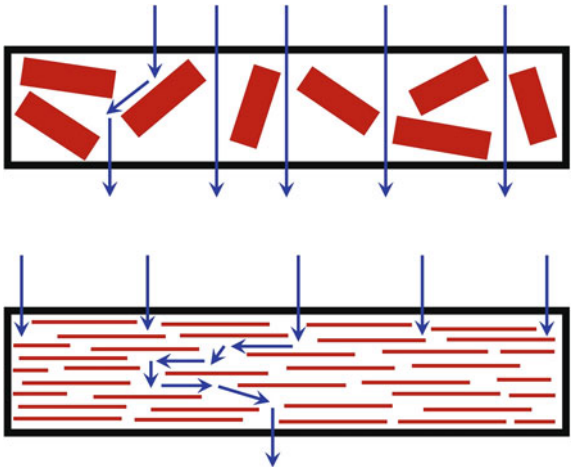

Fig. 6 Tortuous path formed by the interaction of clay

vulcanizates was above 6 and 8 phr for the unmodified vulcanizates. This can be attributed to the excess amount of filler particle or the result of physical contact between agglomerates [102]. The higher amount of agglomerates in high filler dosage composites played a role in obstructing molecular chain movement of the NR, thereby initiating failure under stress. The tensile and tear properties for the organomodified vulcanizates showed higher values than the unmodified filled nanocomposites, these properties increased linearly as a function of the organoclay loading. The enhancement on tensile and tear strength of the clay nanocomposite is mainly due to clay tethering and uniform dispersion of clay particles, which improved the interfacial properties between the filler and rubber molecules, inhibiting the stress concentration and leading to delayed crack propagation [58, 67].

It was reported that gas barrier properties [3, 4, 33, 39, 48, 67], swelling behavior, and flame retardant properties [3, 48] of the rubber composite are marginally enhanced by the incorporation of nanoclays. Yahaya et al. [102] observed that, sorption behavior of nanocomposites filled with 8 phr modified organoclay is better compared to unmodified clay in toluene at room temperature. The organomodified vulcanizates evidently possess silicates that are uniformly dispersed in the NR. This is in contrast to the unmodified filled NR which has poor dispersion of the clay layers, hence increased solvent uptake. Other studies also found that rate of solvent uptake decreased with the incorporation of the organoclays [3, 48, 59]. The trend can be attributed to the presence of the nanodispersed impermeable clay layers, which decreased the rate of transportation by increasing the average diffusion path length in the rubber matrix [59]. The gas barrier properties were also enhanced due to the improved tortuous path as shown in Fig. 6. The US patent, Barbee [8] claims an invention that relates to a polymer-clay nanocomposite having an improved gas permeability comprising a melt-processible matrix polymer, thereby incorporating a layered clay material intercalated with a mixture of at least two organic cations. The clays are believed to increase the barrier properties by

creating a tortuous path that retards the progress of gas molecules (i.e., gas diffusion) through the matrix resin as reported by Cheol et al. [18]. The organoclay platelets have an aspect ratio of 10,000:1 and significantly increase the path/travel distance for the gas molecules.

The thermal, flame retardant, and chemical stability properties of the nanocompoaiste were also improved by the incorporation of organosilicate layered clay into the rubber matrix [3, 48]. The flame retardant mechanism in clay nanocomposites involve a higher performance of carbonaceous silicate char, which builds up on surface during burning. This insulates the underlying material and slows the mass loss rate of decomposition products [100], which leads to higher thermal stability.

7.2 With Compatibilizer

The properties of NR-clay nanocmposites [4, 86] and a blend of NR/SBR-clay nanocompsoites [85] with compatibilizers were studied. Teh et al. [86] and Arroyo et al. [4] prepared NR-organoclay nanocomposites by melt compounding methods. In these studies, ENR25 and ENR50 (NR epoxidized with 25 and 50 mol% epoxy groups, respectively) were used as compatibilizers. Pristine MMT was modified with octadecyltrimethylamine and abbreviated as MMT-ODTMA. In the Teh et al. [86] study, the pristine MMT was modified with octadecyltrimethylamine and the amount of organoclay was fixed to only 2 phr while the amount of ENR was varied. NR/MMT-ODTMA showed mostly an intercalated structure of the organoclay and the best dispersion of organoclay in NR nanocomposites was achieved in the presence of ENR50. This observation was attributed to the incorporation of ENR50 in NR which facilitated the penetration of both molecules into the interlayer space of MMT. The rheological studies showed that organoclay filled NR vulcanizates have the lowest torque values, while the improvement of tensile strength, as well as the elongation at break and tear properties were considerably higher compared to CB and silica filled compounds.

Arroyo et al. [4] prepared the NR-clay nanocomposites by mixing the clay modified with two different modifiers, namely dimethyl dihydrogenated tallow (MMT-2M2HT) and methyl tallow bis-2-hydroxyl quaternary ammonium (MMT-MT2EtOH) and blended with ENR25 and ENR50. The exfoliated structure of the organoclay was observed in the presence of ENR due to its higher polarity, which favors the intercalation of long rubber chains in the interlayer space of clay. Because of the poor compatibility between the unmodified clay and hydrophobic rubber molecules, unmodified clay slightly changed the cure characteristics of NR and nevertheless, the optimum cure time was reduced steeply in the presence of the organoclay. Similar behavior was also observed in the case of CB, but the extent of decrement was smaller compared to the organoclay. NR filled with 10 phr of organoclay exhibited higher torque compared to the NR with 40 phr CB. This observation can be attributed to the higher cross-link density which was further confirmed by swelling and differential scanning calorimetry (DSC) experiments.

The mechanical properties of the composite with 10 phr organoclay are observed to be comparable with the compound with 40 phr CB.

Tavakoli et al. [85] prepared nanocomposites based on 70/30 blends of NR/SBR, and organoclays by melt-mixing processes. In the study, maleated-ethylene-propylene thermoplastic rubber (EPDM-*g*-MAH) and ENR50 were employed as compatibilizers. The morphological studies showed that the use of EPDM-*g*-MAH as a compatibilizer enhanced the clay nanolayer dispersion and their interaction with rubber phases more readily than ENR in the rubber matrix. Both XRD and TEM examinations verified that two rubber phases of the rubber blend compatibilized by both EPDM-g-MAH and ENR50 could be intercalated into the galleries of organoclay. These analytical techniques also showed that a high extent of clay intercalation/exfoliation could be obtained in these nanocomposites. Tavakoli et al. [85] also studied the effectiveness EPDM-g-MAH as an interfacial compatibilizer in enhancing the extent of interaction between NR matrix and organoclay nanolayers [84]. As in the earlier morphological studies carried out by Tavakoli et al. [85], the microstructural characterizations revealed that EPDM-*g*-MAH have more potential for separating and dispersing the clay nanoplatelets in the rubber matrix with better interface enhancement compared to ENR50. The pronounced compatibilizing effect of EPDM-g-MAH is attributed to the lower polarity, which leads to more affinity for the NR matrix to be diffused onto the galleries of organoclay. The uniform dispersion of orgnoclay nanolayers and better interfacial properties of the nanocomposite resulted in higher elasticity and physico–mechanical properties, which is verified with the unvulcanized NR/organoclay/EPDM-g-MAH nanocomposites in melt rheological measurements. The studies concluded that, compared to ENR as a compatibilizer, EPDM-*g*-MAH has greater potential for separating and dispersing the clay nanoplatelets in the polymer matix with better interface enhancement in the nanocomposite.

8 Applications of Green Polymer-Clay Nanocomposite

Nanocomposites based on polymeric matrices are showing promising success in various industries due to their excellent properties that include lightweight, low cost, and improved thermal, mechanical, electrical, optical, and gas barrier properties [67, 104]. The nanophase in the composite is superior compared to other conventional materials. With emphasis on biodegradability, much work is now focused to find fillers which are environmental friendly. Studies carried out by Abraham et al. [1] showed that they can be used in the critical industry of solvent membrane transportation where they have shown better flow properties and are also resistant to thermal degradation. The materials are able to provide a tortuous path to solvent flow and hence they can be tailored to only allow certain solvents though. This is an important parameter in rubber manufacturing where transportation of solvents should be minimized to enhance the durability of rubber tires. Nanoclays have been used to reinforce elastomers with an aim of lowering its flow properties as it can reduce the viscosity of the result composite better than conventional fillers. This allows for ease in processability of the reinforced

composites [19]. Cellulose whiskers and microfibrillated cellulose (MFC) have also been used to reinforce NR to improve the stiffness and reduce the solvent uptake of toluene and water. The whiskers and MFC increase the T_g of rubber which can allow the final nanocomposites to be used in slightly higher operating temperatures compared to their pristine composite counterparts [9, 95]. Currently, in order to increase mechanical properties of rubber tires, chemical cross-links as well as the addition of fine particles of CB or silica with minimum weight of 20–30 % are needed. This not only leads to an expensive rubber composite but also enviromental hazards, because the fillers are not environmentally friendly [15]. Functionalized nanoclays, e.g., MMT have shown that they can be used to replace expensive CB as reinforcement filler in vulcanized rubber in very low loading weights. The clay improves the aging of the rubber by prolonging its durability and it can increase the stiffness of the rubber tires greatly [104]. To improve the properties of thin films and fibers, nanoclay has been added with tremendous improvement. The most preferred method used was melt intercalation and electrospinning where fibers with improved mechanical properties were realized [25]. Superior properties, biocompatibility, and ease of fabrication, layered silicate clay reinforced nanocomposites have been used as dental adhesive reinforcing fillers compared to the established nondegradable fillers. Its durability to be used as a dental filler adhesive was shown through the fact that the shear bond was much superior for the nanoclay reinforced adhesive [5]. Nanoclay is also increasingly being used to modify bitumen in order to improve its properties. Jahromi et al. [27] and his colleagues showed that it can lead to high stability, high indirect tensile strength, resilient modulus, and superior performance compared to the unmodified bitumen under dynamic creep loading and low fatigue properties in low temperatures. The larger surface area and aspect ratios of the particles are responsible for these improvements. NR filled with nanoclays have also shown better improvement in fire resistance, hence the materials can be used as fire retardants, which are cheaper and less toxic than other conventional fire retardants such as fluorinated polymers [29]. Gas barrier properties are an important performance characteristic of rubber products due to their operation in highly compressed air in air springs, cure bladders, and tire inner-tubes. Nanoclays have shown better performance in the food and beverage industry as an enhancement in barrier properties of the composite. Isobutylene–isoprene rubber (IIR) reinforced with nanoclays can meet the high gas barrier requirements of industries like high-vacuum systems, aerospace, and aircraft where there are reduced gas permeability required standards [38]. The demands for better food packaging materials with improved gas barrier properties that satisfy the safety requirement have led researchers to turn to natural materials. Biopolymers are touted as the best materials for this revolution, however, their biggest hindrance is in their inherent permeability to vapor and gases, poor barrier to gases, and poor mechanical properties. Nano-reinforced materials are seen as the solution to this problem. Nanoclay-reinforced biopolymers have shown great promise in the food and packaging industry with enhanced barrier properties [45]. Nanoclay reinforced nanocomposites have also been used to improve the scratch resistant and adhesion properties of the composites as shown by Mohamadpour et al. [46] where there was a substantial improvement in these properties depending on the loading weight of the nanoclay.

9 Conclusion

In this chapter, various reinforcing routes for NR and cellulose-based nanocomposites have been explored. It is a well-researched area and much more work is still ongoing. A general observation showed that there is a vast improvement in mechanical, chemical, and physical properties of resulted nanocomposites due to addition of all the mentioned polymer reinforcing nanofillers. The improvement was noticed to highly depend on the weight of the nanoparticles in the NR polymer matrix. It was also observed that different types of nanoclays lead to varying improvement depending on the types of functionalization or surface modification. However, in general, functionalized nanoclays do indeed perform better. A major problem that still presents a challenge in the use of nanocellulose is through its hydrophilic nature, though there are some promising results from surface modification. It was also shown that small amounts of nanoclays can be used to provide the same or better quality compared to the considerable amount needed of CB to reinforce NR. Furthermore, hybrid cellulose/nanoclays also lead to high improvement of the final nanocomposites.

References

1. Abraham E, Thomas MS, John C, La Pothen, Shoseyov O, Thomas S (2013) Green nanocomposites of natural rubber/nanocellulose: membrane transport, rheological and thermal degradation characterisations. Ind Crops Prod 51:415–424. doi:10.1016/j.indcrop.2013.09.022
2. Alexander M, Dubois P (2000) Polymer nanocomposites: synthesis, characterization, and modeling. In: Krishnamoorti R, Vaia RA (eds) Oxford University Press, Oxford, 2001. (Mater Sci Eng 28:1–63)
3. Anwendungen RUND (2010) Synergistic effects of expanded nanoclay and carbon black on natural rubber compounds. Raw Mater Appl 7/8(August), pp 296–302
4. Arroyo M, Lopez-Manchado MA, Herrero B (2003) Organo-montmorillonite as substitute of carbon black in natural rubber compounds. Polymer 44(8): 2447–2453. doi: 10.1016/S0032-3861(03)00090-9
5. Atai M, Solhi L, Nodehi A, Mirabedini SM, Kasraei S, Akbari K, Babanzadeh S (2009) PMMA-grafted nanoclay as novel filler for dental adhesives. Dent Mater: Official Publ Acad Dent Mater 25(3):339–347. doi:10.1016/j.dental.2008.08.005
6. Aulin C, Salazar-Alvarez G, Lindström T (2012) High strength, flexible and transparent nanofibrillated cellulose-nanoclay biohybrid films with tunable oxygen and water vapor permeability. Nanoscale 4(20):6622–6628. doi:10.1039/c2nr31726e
7. Baillie C (2004) Green composites: Polymer composites and the environment, Elsevier, ISBN: 978-1-85573-739-6
8. Barbee RB (2000) US Patent 6,034,163, 07th March 2000
9. Bendahou A, Kaddami H, Dufresne A (2010) Investigation on the effect of cellulosic nanoparticles' morphology on the properties of natural rubber based nanocomposites. Eur Polym J 46(4):609–620. doi:10.1016/j.eurpolymj.2009.12.025
10. Bhowmick AK, Bhattacharya M, Mitra S (2010) Exfoliation of Nanolayer Assemblies for Improved Natural Rubber Properties: Methods and Theory. J Elastomers Plast 42:517–537. doi: 10.1177/0095244310383752

11. Bhowmick AK, Bhattacharya M, Mitra S, Dinesh Kumar K, Maji PK, Choudhury A, George JJ, Basak GC (2011) Morphology–property relationship in rubber-based nanocomposites: Some recent developments. Adv Polym Sci 239:1–83 ISBN: 978-3-642-19503-7, doi: 10.1007/12_2010_95
12. Bondeson D (2007) Biopolymer-based nanocomposites: processing and properties. Norwegian University of Science and Technology. http://www.diva-portal.org/smash/get/diva2:123559/FULLTEXT01.pdf
13. Brauer S (2004) Polymer nanocomposites. www.bccresearch.com/plastics/P234.html
14. Carli LN, Roncato CR, Zanchet A (2011) Characterization of natural rubber nanocomposites filled with organoclay as a substitute for silica obtained by the conventional two-roll mill method. Appl Clay Sci 52(1–2):56–61. doi: 10.1016/j.clay.2011.01.029
15. Carretero-gonza J, Retsos H, Verdejo R, Toki S, Hsiao BS, Giannelis EP, Lo MA (2008) Effect of nanoclay on natural rubber microstructure. Macromolecules 41(18):6763–6772. doi:10.1021/ma800893x
16. Cerruti P, Ambrogi V, Postiglione A, Rychlý J, Matisová-Rychlá L, Carfagna C (2008) Morphological and thermal properties of cellulose-montmorillonite nanocomposites. Biomacromolecules 9(11):3004–3013. doi:10.1021/bm8002946
17. Chand N, Gautam KKS (1994) Influence of Load on Abrasion Fly-ash Glass Fiber Reinforced Composites. J Mater Sci Lett 13(4):230–233. doi: 10.1007/BF00571759
18. Cheol KB, Blumstein A, Kumar J, Samuelson LA, Kim DW (2004) Barrier properties of ordered multilayer polymer nanocomposites, dekker encyclopedia of nanoscience and nanotechnology. Taylor and Francis, Abingdon, pp 213–224
19. Das A, Costa FR, Wagenknecht U, Heinrich G (2008) Nanocomposites based on chloroprene rubber: Effect of chemical nature and organic modification of nanoclay on the vulcanizate properties. Eur Polym J 44(11):3456–3465. doi:10.1016/j.eurpolymj.2008.08.025
20. Delhom C (2009) Development and thermal characterization of cellulose/clay nanocomposites. Louisiana State University. http://etd.lsu.edu/docs/available/etd-04032009-094316/unrestricted/Delhom-ETD-Final.pdf
21. Frone AN, Berlioz S, Chailan JF, Panaitescu DM (2013) Morphology and thermal properties of PLA-cellulose nanofibers composites. Carbohydr Polym 91(1):377–384. doi:10.1016/j.carbpol.2012.08.054
22. Giannees BEP (1996) Polymer layered silicate nanocomposites. Adv Mater 8(1):29–35. doi: 10.1002/adma.19960080104
23. Gopakumar TG, Lee JA, Kontopoulou M, Parent JS (2002) Polymer 43(1):5483–5491. doi. 10.1016/S0032-3861(02)00403-2
24. Hassan-Nejad M, Ganster J, Bohn A, Pinnow M, Volkert B (2009) Bio-based nanocomposites of cellulose acetate and nano-clay with superior mechanical properties. Macromol Symp 280(1):123–129. doi:10.1002/masy.200950614
25. Hegde RR (2009) Structure and properties of nanoclay reinforced polymer films, fibers and nonwovens. University of Tennessee. http://trace.tennessee.edu/utk_graddiss/39
26. Jacob A, Kurian P, Aprem AS (2008) Transport properties of natural rubber latex layered clay nanocomposites. J Appl Polym Sci 108:2623–2629. doi:10.1002/app
27. Jahromi SG, Andalibizade B, Vossough S (2010) Engineering properties of nanoclay modified asphalt concrete mixtures. Arabian J Sci Eng 35(1):89–103. http://ajse.kfupm.edu.sa/articles/351b-p.6.pdf
28. Jarvela PA, Jarvela PK (1996) Multicomponent compounding of polypropylene. J Mater Sci 31(14):3853–3860. ISSN 0022-2461, doi: 10.1007/BF00352802
29. Jia QX, Wu YP, Wang YQ, Lu M, Zhang LQ (2008) Enhanced interfacial interaction of rubber/clay nanocomposites by a novel two-step method. Compos Sci Technol 68(3–4):1050–1056. doi:10.1016/j.compscitech.2007.07.006
30. Jin M, Zhong Q (2013) Surface-coating montmorillonite nanoclay by water-soluble proteins extracted from hominy feed. J Food Eng 119(3):687–695. doi:10.1016/j.jfoodeng.2013.07.001
31. Joly S, Garnaud G, Ollitrault R, Bokobza L (2002) Organically modified layered silicates as reinforcing fillers for natural rubbers. Chem Mater 14:4202–4208. doi: 10.1021/cm020093e

32. Jonoobi M, Harun J, Mathew AP, Oksman K (2010) Mechanical properties of cellulose nanofiber (CNF) reinforced polylactic acid (PLA) prepared by twin screw extrusion. Compos Sci Technol 70(12):1742–1747. doi:10.1016/j.compscitech.2010.07.005
33. Kim J, Hu C, Woo R, Sham M (2005) Moisture barrier characteristics of organoclay?epoxy nanocomposites. Compos Sci Technol 65(5):805–813. doi:10.1016/j.compscitech.2004.10.014
34. Kornmann X, Lindberg H, Berglund LA (2001) Synthesis of epoxy–clay nanocomposites: influence of the nature of the clay on structure. Polymer 42(4):1303–1310. doi:10.1016/S0032-3861(00)00346-3
35. Kuo PY, Yan N, Sain M (2013) Influence of cellulose nanofibers on the curing behavior of epoxy/amine systems. Eur Polym J 49(12):3778–3787. doi:10.1016/j.eurpolymj.2013.08.022
36. Li C, Liu Q, Shu S, Xie Y, Zhao Y, Chen B, Dong W (2014) Preparation and characterization of regenerated cellulose/TiO_2/ZnO nanocomposites and its photocatalytic activity. Mater Lett 117:234–236. doi:10.1016/j.matlet.2013.12.009
37. Li J, Zhou C, Wang G, Zhao D (2003) Study on rheological behavior of polypropylene/clay nanocomposites. J Appl Polym Sci 89(13):3609–3617. doi: 10.1002/app.12643
38. Liang Y, Cao W, Li Z, Wang Y, Wu Y, Zhang L (2008) A new strategy to improve the gas barrier property of isobutylene–isoprene rubber/clay nanocomposites. Polym Test 27(3):270–276. doi:10.1016/j.polymertesting.2007.11.003
39. Liang Y, Wang Y, Wu Y, Lu Y, Zhang H, Zhang L (2005) Preparation and properties of isobutylene–isoprene rubber (IIR)/clay nanocomposites. Polym Test 24(1):12–17. doi:10.1016/j.polymertesting.2004.08.004
40. Lo H, Chu C (2011) Influence of clay, silicate and carbon black on the environmental resistance properties of hard rubber. Chin Steel Tech Rep 16(24):40–47. www.csc.com.tw/csc_e/ts/ena/publ.html
41. Lo'pez-Manchado MA, Herrero B, Arroyo M (2004) Organoclay-natural rubber nanocompositessynthesized by mechanical and solution mixing methods. Polym Int 53 (11):1766–1772. doi: 10.1002/pi.1573
42. Madhusoodanan KN, Varghese S (2006) Technological and processing properties of natural rubber layered silicate-nanocomposites by melt intercalation process. J Appl Polym Sci 102 (3):2537–2543. doi:10.1002/app.24680
43. Magaraphan R, Thaijaroen W, Lim-Ochakun R (2003) Structure and properties of natural rubber andmodified montmorillonitenanocomposites. Rubber Chem Technol 76(2):406–418. doi: rubberchemtechnol.org/doi/abs/10.5254/1.3547751
44. Mahmoudian S, Wahit MU, Ismail AF, Yussuf AA (2012) Preparation of regenerated cellulose/montmorillonite nanocomposite films via ionic liquids. Carbohydr Polym 88 (4):1251–1257. doi:10.1016/j.carbpol.2012.01.088
45. Majeed K, Jawaid M, Hassan A, Abu Bakar A, Abdul Khalil HPS, Salema AA, Inuwa I (2013) Potential materials for food packaging from nanoclay/natural fibres filled hybrid composites. Mater Des 46(1):391–410. doi:10.1016/j.matdes.2012.10.044
46. Mohamadpour S, Pourabbas B, Fabbri P (2011) Anti-scratch and adhesion properties of photo-curable polymer/clay nanocomposite coatings based on methacrylate monomers. Sci Iranica 18(3):765–771. doi:10.1016/j.scient.2011.06.001
47. Mohan TP, Kanny K (2011) Water barrier properties of nanoclay filled sisal fibre reinforced epoxy composites. Compos Part A: Appl Sci Manuf 42(4):385–393. doi:10.1016/j.compositesa.2010.12.010
48. Mohan TP, Kuriakose J, Kanny K (2011) Effect of nanoclay reinforcement on structure, thermal and mechanical properties of natural rubber–styrene butadine rubber (NR–SBR). J Ind Eng Chem 17(2):264–270. doi:10.1016/j.jiec.2011.02.019
49. Nasri-Nasrabadi B, Mehrasa M, Rafienia M, Bonakdar S, Behzad T, Gavanji S (2014) Porous starch/cellulose nanofibers composite prepared by salt leaching technique for tissue engineering. Carbohydr Polym 108:232–238. doi:10.1016/j.carbpol.2014.02.075
50. Nicotera I, Enotiadis A, Angjeli K, Coppola L, Gournis D (2012) Evaluation of smectite clays as nanofillers for the synthesis of nanocomposite polymer electrolytes for fuel cell applications. Int J Hydrogen Energy 37(7):6236–6245. doi:10.1016/j.ijhydene.2011.06.041

51. Nugay N, Erman B (2001) Property optimization in nitrile rubber composites via hybrid filler systems. J Appl Polym Sci 79:366–374. doi: 10.1002/1097-4628(20010110)
52. Okada A, Kawasumi M, Usuki A, Kojima Y, Kurauchi T, Kamigaito O (1990) Synthesis and properties of nylon-6/clayhybrids. In: Schaefer DW, Mark JE (eds) Polymer basedmolecular composites. MRS Symposium Proceedings, Pittsburgh, vol. 171, pp 45–50
53. Okahisa Y, Abe K, Nogi M, Nakagaito AN, Nakatani T, Yano H (2011) Effects of delignification in the production of plant-based cellulose nanofibers for optically transparent nanocomposites. Compos Sci Technol 71(10):1342–1347. doi:10.1016/j.compscitech.2011.05.006
54. Panaitescu DM, Frone AN, Nicolae C (2013) Micro- and nano-mechanical characterization of polyamide 11 and its composites containing cellulose nanofibers. Eur Polym J 49 (12):3857–3866. doi:10.1016/j.eurpolymj.2013.09.031
55. Park HM, Liang X, Mohanty AK, Misra M, Drzal LT (2004) Effect of compatibilizer on nanostructure of the biodegradable cellulose acetate/organoclay nanocomposites. Macromolecules 37(24):9076–9082. doi:10.1021/ma048958s
56. Park HM, Misra M, Drzal LT, Mohanty AK (2004) "Green" nanocomposites from cellulose acetate bioplastic and clay: effect of eco-friendly triethyl citrate plasticizer. Biomacromolecules 5(6):2281–2288. doi:10.1021/bm049690f
57. Park HM, Mohanty AK, Drzal LT, Lee E, Mielewski DF, Misra M (2006) Effect of sequential mixing and compounding conditions on cellulose acetate/layered silicate nanocomposites. J Polym Environ 14(1):27–35. doi:10.1007/s10924-005-8704-0
58. Pattanayak A, Jana SC (2005) Properties of bulk-polymerized thermoplastic polyurethane nanocomposites. Polymer 46:3394–3406. doi: 10.1016/j.polymer.2005.03.021
59. Peiyao L, Li W, Guojun S, Lanlan Y, Feng Q, Liangdong S (2008) Characterization of high performance exfoliated natural rubber/organoclay nanocomposites. J Appl Polym Sci 109 (6):3831–3838. doi:10.1002/app.28480
60. Pinnavia TJ, Beall G (eds) (2001) Polymer–clay nanocomposites, Wiley, New York. ISBN: 978-0-471-63700-4
61. Prasertsri S, Rattanasom N (2012) Fumed and precipitated silica reinforced natural rubber composites prepared from latex system: mechanical and dynamic properties. Polymer Testing 31(5):593–605. doi:10.1016/j.polymertesting.2012.03.003
62. Praveen S, Chattopadhyay PK, Albert P, Dalvi VG, Chakraborty BC, Chattopadhyay S (2009) Synergistic effect of carbon black and nanoclay fillers in styrene butadiene rubber matrix: Development of dual structure. Compos part A: Appl Sci Manuf 40(3):309–316. doi:10.1016/j.compositesa.2008.12.008
63. Psarras GC, Gatos KG, Karahaliou PK et al (2007) Relaxation phenomena in rubber/layered silicatenanocomposites. Express Polym Lett 1(1):837–845. doi:10.3144/expresspolymlett.2007.116
64. Psarras GC, Gatos KG, Karger-Kocsis J (2007) Dielectric properties of layered silicate reinforcednatural and polyurethane rubber nanocomposites. J Appl Polym Sci 106(2):1405–1411. doi:10.1002/app.26831
65. Rajasekar R, Heinrich G, Das A, Das CK (2009) Development of SBR-Nanoclay composites with epoxidized natural rubber as compatibilizer. J Nanotechnol 2009:1–5. doi:10.1155/2009/405153
66. Rajesh JJ (2012) Effect of injection molding parameters on nanofillers dispersion in masterbatch based PP-clay nanocomposites. Express Polym Lett 6(3):237–248. doi:10.3144/expresspolymlett.2012.26
67. Rattanasom N, Prasertsri S (2012) Mechanical properties, gas permeability and cut growth behaviour of natural rubber vulcanizates: Influence of clay types and clay/carbon black ratios. Polym Test 31(5):645–653. doi:10.1016/j.polymertesting.2012.04.001
68. Rattanasom N, Prasertsri S, Ruangritnumchai T (2009) Comparison of the mechanical properties at similar hardness level of natural rubber filled with various reinforcing-fillers. Polym Test 28(1):8–12. doi:10.1016/j.polymertesting.2008.08.004

69. Rattanasom N, Saowapark T, Deeprasertkul C (2007) Reinforcement of natural rubber with silica/carbon black hybrid filler. Polym Test 26(3):369–377. doi:10.1016/j.polymertesting.2006.12.003
70. Ray SS, Okamoto M (2003) Polymer/layered silicate nanocomposites: a review from preparation to processing. Prog Polym Sci 28(11):1539–1641 doi: 10.1016/j.progpolymsci.2003.08.002
71. Ren J, Huang Y, Liu Y, Tang X (2005) Preparation, characterization and properties of poly (vinyl chloride)/compatibilizer/organophilic-montmorillonite nanocomposites by melt intercalation. Polym Test 24(3):316–323. doi:10.1016/j.polymertesting.2004.11.004
72. Rezende CA, Bragança FC, Doi TR, Lee LT, Galembeck F, Boué F (2010) Natural rubber-clay nanocomposites: mechanical and structural properties. Polymer 51(16):3644–3652. doi:10.1016/j.polymer.2010.06.026
73. Riechert P (2001) Morphological stability of poly(propylene) nanocomposites. Macromol Rapid Commun 22(7):519–523. doi:10.1002/1521-3927(20010401)
74. Ryu SH, Chang YW (2005) Factors affecting the dispersion of montmorillonite in LLDPE nanocomposite. Polym Bull 55(5):385–392. doi:10.1007/s00289-005-0437-7
75. Saminathan K, Selvakumar P, Bhatnagar N (2008) Fracture studies of polypropylene/nanoclay composite. Part I: effect of loading rates on essential work of fracture. Polym Test 27(3):296–307. doi:10.1016/j.polymertesting.2007.11.008
76. Sancaktar E, Kuznicki J (2011) Nanocomposite adhesives: mechanical behavior with nanoclay. Int J Adhes Adhes 31(5):286–300. doi:10.1016/j.ijadhadh.2010.09.006
77. Sapkota J, Poikelispa M (2013) Influence of nanoclay-carbon black hybrid fillers on cure and properties of natural rubber compounds. Polym Eng Sci 53(3):615–622. doi:10.1002/pen
78. Sapkota J, Poikelispää M, Das A, Dierkes W, Vuorinen J (2012) Partial carbon black replacement by nanoclay for enhanced crosslinking. SPE Plastics Research Online pp 1–2. doi: 10.2417/spepro.004513
79. Sapkota J, Poikelispää M, Das A, Dierkes W, Vuorinen J (2013) Influence of nanoclaycarbon black hybrid fillers on cure and properties of natural rubber compounds. Polym Eng Sci 53 (3):615-622. doi:10.1002/pen.23297
80. Schadler LS (2003) Polymer-based and Polymer-filled Nanocomposites. In: Nanocomposite science and technology. Ajayan PM, Schadler LS, Braun PV (eds) Wiley VCH, New York, ISBN: 3-527-30359-6, pp. 77–144.
81. Schmidt H (1990) Polymer based molecular nanocomposites. In: Polymer based molecular momposites. Schaefer DW, Mark JE (eds) Material Research Society, Pittsburg. ISBN AD-A229 199, Vol. 171, pp. 57–63. http://www.dtic.mil/dtic/tr/fulltext/u2/a229199.pdf
82. Sridhar R, Narasimha Murthy HN, Pattar N, Vishnu Mahesh KR, Krishna M (2012) Parametric study of twin screw extrusion for dispersing MMT in vinylester using orthogonal array technique and grey relational analysis. Compos B Eng 43(2):599–608. doi:10.1016/j.compositesb.2011.08.025
83. Taghizadeh MT, Sabouri N (2013) Thermal degradation behavior of polyvinyl Alcohol/Starch/Carboxymethyl Cellulose/Clay Nanocomposites. Univers J Chem 1(2):21–29. doi:10.13189/ujc.2013.010202
84. Tavakoli M, Asghar Katbab A, Nazockdast H (2011) Effectiveness of maleic anhydride grafted EPDM rubber (EPDM-g-MAH) as compatibilizer in NR/organoclay nanocomposites prepared by melt compounding. J Macromol Sci Part B Phys 50(7):1270–1284. doi: 10.1080/00222348.2010.507439
85. Tavakoli M, Asghar Katbab A, Nazockdast H (2012) NR/SBR/organoclay nanocomposites: Effects of molecular interactions upon the clay microstructure and mechano-dynamic properties. J Appl Polym Sci 123(3):1853–1864. doi: 10.1002/app.34673
86. Teh PL, Ishak ZAM, Hashim AS, Karger-Kocsis J, Ishiaku US (2006) Physical properties of natural rubber/organoclay nanocomposites compatibilized with epoxidized natural rubber. J Appl Polym Sci 100(2):1083–1092. doi: 10.1002/app.23452
87. Uddin MF, Sun CT (2010) Improved dispersion and mechanical properties of hybrid nanocomposites. Compos Sci Tech 70(2):223–230 doi: 10.1016/j.compscitech.2009.09.017

88. Usuki A, Koiwai A, Kojima Y, Kawasumi M, Okada A, Kurauchi T, Kamigaito O (1995) . Interaction of nylon 6-clay surface and mechanical properties of nylon 6-clay hybrid. J Appl Polym Sci 55(1):119–123. doi: 10.1002/app.1995.070550113
89. Vaia RA, Ishii H, Giannelis EP (1993) Synthesis and properties of two-dimensional nanostructures by direct intercalation of polymer melts in layered silicates. Chem Mater 5 (12):1694–1696. doi: 10.1021/cm00036a004
90. Vaia RA (2002) Polymer nanocomposites open a new dimension for plastics and composites. AMPTIAC Q -A Look Inside Nanotechnol 6(1):17–24. www.dtic.mil/cgi-bin/GetTRDoc?AD=ADA436321
91. Valadares LF, Leite CAP, Galembeck F (2006) Preparation of natural rubber–montmorillonite nanocomposite in aqueous medium: evidence for polymer–platelet adhesion. Polymer 47(2):672–678. doi: 10.1016/j.polymer.2005.11.062
92. Varghese S, Gatos KG, Apostolov AA, Karger-Kocsis J (2004) Morphology and mechanical propertiesof layered silicate reinforced natural and polyurethane rubber blends produced by latex compounding. J Appl Polym Sci 92(1):543–551. doi: 10.1002/app.20036
93. Varghese S, Karger-Kocsis J (2003) Natural rubber-based nanocomposites by latex compounding with layered silicates. Polymer 44(17):4921–4927. doi: 10.1016/S0032-3861(03)00480-4
94. Varghese S, Karger-Kocsis J (2004) Melt-compounded natural rubber nanocomposites with pristine and organophilic layered silicates of natural and synthetic origin. J Appl Polym Sci 91(2):813–819. doi: 10.1002/app.13173
95. Visakh PM, Thomas S, Oksman K, Mathew AP (2012) Crosslinked natural rubber nanocomposites reinforced with cellulose whiskers isolated from bamboo waste: Processing and mechanical/thermal properties. Compos Part A: Appl Sci Manuf 43(4):735–741. doi:10.1016/j.compositesa.2011.12.015
96. Vu YT, Mark JE, Pham LH, Engelhardt M (2001) Clay nanolayer reinforcement of cis-1,4-polyisoprene and epoxidized natural rubber. J Appl Polym Sci 82(6):1391–1403. doi: 10.1002/app.1976
97. Wang M, Yu JH, Hsieh AJ, Rutledge GC (2010) Effect of tethering chemistry of cationic surfactants on clay exfoliation, electrospinning and diameter of PMMA/clay nanocomposite fibers. Polymer 51(26):6295–6302. doi:10.1016/j.polymer.2010.10.040
98. Woo R, Zhu H, Leung C, Kim J (2008) Environmental degradation of epoxy-organoclay nanocomposites due to UV exposure: Part II residual mechanical properties. Compos Sci Technol 68(9):2149–2155. doi:10.1016/j.compscitech.2008.03.020
99. Wu YP, Wang YQ, Zhang HF, Wang YZ, Yu DS, Zhang LQ, Yang J (2005) Rubber–pristine clay nanocomposites prepared by co-coagulating rubber latex and clay aqueous suspension. Compos Sci Technol 65(7–8):1195–1202. doi:10.1016/j.compscitech.2004.11.016
100. Xiong J, Liu Y, Yang X, Wang X (2004) Thermal and mechanical properties of polyurethane/montmorillonite nanocomposites based on a novel reactive modifier. Polym Degrad Stab 86(3):549–555. doi: 10.1016/j.polymdegradstab.2004.07.001
101. Xu R, Manias E, Snyder AJ, Runt (2003) Low permeability biomedical polyurethane nanocomposites J Biomed Res Part A 64 A(1):114–119. doi: 10.1002/jbm.a.10377
102. Yahaya LE, Adebowale KO, Menon ARR, Rugmini S, Olu-Owolabi BI, Chameswary J (2010) Natural rubber/organoclay nanocomposites: effect of filler dosage on the physicomechanical properties of vulcanizatesAfrican. J Pure Appl Chem 4(9):198–205
103. Yang W, Hu Y, Tai Q, Lu H, Song L, Yuen RKK (2011) Fire and mechanical performance of nanoclay reinforced glass-fiber/PBT composites containing aluminum hypophosphite particles. Compos Part A: Appl Sci Manuf 42(7):794–800. doi:10.1016/j.compositesa.2011.03.009
104. Yehia AA, Akelah AM, Rehab A, El-Sabbagh SH, El Nashar DE, Koriem AA (2012) Evaluation of clay hybrid nanocomposites of different chain length as reinforcing agent for natural and synthetic rubbers. Mater Des 33:11–19. doi:10.1016/j.matdes.2011.06.066
105. Zawrah MF, Khattab RM, Saad EM, Gado RA (2014) Effect of surfactant types and their concentration on the structural characteristics of nanoclay. Spectrochim Acta Part A Mol Biomol Spectrosc 122:616–623. doi:10.1016/j.saa.2013.11.076

Hydrogels Nanocomposites Based on Crystals, Whiskers and Fibrils Derived from Biopolymers

André R. Fajardo, Antonio G.B. Pereira and Edvani C. Muniz

Abstract The advent of nanotechnology has provided new insights of applications of well-known materials due to the exceptional properties owing to the nanoscale. As an example, nanocomposites based on polymer matrix and nanoscale fillers have appeared as good candidates in a broad range of applications. Such scenery can be credited to the use of new and multifunctional fillers that provide distinct and substantial features to the nanocomposites. Recent trends on the nanocomposites field show that crystalline biopolymers, such as cellulose, chitin, and starch, are an excellent source of fillers, especially nanocrystals like fibrils, whiskers, and platelets. The incorporation of such fillers in different matrices (e.g., crosslinked polymeric network) has demonstrated outstanding improvement of several properties, such as mechanical, water uptake capacity, thermal, optical, etc. Furthermore, crystals, fibrils and whiskers can induce desirable properties in the final materials (e.g., solute retention or release, crystallinity, biodegradability, biocompatibility, antibacterial activity, etc.). This chapter condenses the relevant works regarding the preparation of polysaccharide-based crystals, whiskers, and fibrils, their application in the development of hydrogel nanocomposites as well as the future trends of this area.

Keywords Nanocomposites · Hydrogels nanocomposites · Biopolymers · Crystals · Whiskers · Fibrils

A.R. Fajardo (✉)
Centro de Ciências Químicas, Farmacêuticas e de Alimentos (CCQFA), Federal University of Pelotas, Pelotas, RS P.O. Box 354, 96160-000, Brazil
e-mail: andre.fajardo@pq.cnpq.br

A.G.B. Pereira
Universidade Tecnológica Federal do Paraná (UTFPR), Estrada para Boa Esperança, Dois Vizinhos, PR 85660-000, Brazil

E.C. Muniz
Grupo de Materiais Poliméricos e Compósitos (GMPC), Maringá State University, Maringá, PR 87020-900, Brazil

V.K. Thakur and M.K. Thakur (eds.), *Eco-friendly Polymer Nanocomposites*, Advanced Structured Materials 74, DOI 10.1007/978-81-322-2473-0_2

1 Introduction

The first Industrial Revolution, at the end of eighteenth century, has triggered the development of technological research and the obtention of novel materials. The challenges today are focused on adapting the available technology to produce desirable responses from a material or a process with the minor onus (e.g., low cost and high efficiency). One of the most brilliant methods created to answer such condition is the nanotechnology. Nanotechnology, in general lines, is the science that treats the matter at the molecular level. It means that new materials; substances, and products are formulated in this field with atomic accuracy [97, 98]. The direct results are the obtention of a wide range of desirable properties and unlimited possible applications. For example, the materials prepared or obtained in nanosized scale (particles, aggregates, or agglomerates where at least or more than 50 % show size dimension between 1 to 100 nm) have been utilized in hundreds applications. Nanomaterials have been included in various commercial products (e.g., dentifrices, batteries, paints, clothes, etc.) in order to increase, modify or even create new features [18, 154, 155]. Several fields, such as medical, optics, electronic, biotechnology, energy, and environmental have benefited a lot from nanomaterials [18]. The association of different classes of materials, such as polymers (synthetic or natural), ceramics, and metals and nanosized fillers allows preparing high-performance nanocomposites materials [54, 141, 153]. The term nanocomposite defines a multiphase solid material with one of the phases in the nanosized dimension [165]. In other words, it is the combination of a solid bulk matrix and nanodimensional phases differing in properties due to dissimilarities in structure (morphological, chemical, and dimensional) and physicochemical features. As a consequence, the nanocomposite properties will markedly differ from the individual components. For instance, in mechanical terms, nanocomposites could present better performance than traditional composite materials due to the outstanding high aspect ratio presented by the nanomaterials (also known as "filler") incorporated into the bulk matrix [27, 68]. Another aspect is that the interface area between the matrix and the filler phase(s) is typically an order of magnitude greater than that for conventional composite materials.

Taking into account that nanosized fillers can be prepared/obtained from numerous organic (polymer) and inorganic (metals, oxides) sources [68, 82, 119, 155, 191, 199], they vary in relation to the size, chemical composition, shape, surface area, production cost, and toxicity. Crucial aspects that must be considered are the (bio)availability of the source and the toxicity and cost of chemicals involved in the preparation of the fillers. Biopolymers are quoted currently as potential candidates to extract fillers to form nanocomposites due to issues such as biodegradability, low cost, nontoxicity, relatively reactive surface, etc.

1.1 Biopolymers

Biopolymers are polymeric macromolecules produced by living organisms. Polysaccharides (e.g., cellulose, starch, and chitin), proteins and peptides, and nucleic acids (DNA and RNA) are examples of biopolymers [105, 108]. Some of them, such as cellulose and chitin, are the most abundant biopolymers on earth [166–170]. The main difference between the conventional polymers and biopolymers can be credited to their structure [181–183]. Repeating units form both polymer and biopolymers; however in most of the cases, biopolymers show a well-defined three-dimensional structure, while the conventional polymers do not [173–177]). The exact chemical composition and well-defined sequence in which the repeating units are organized are characteristic of the primary structure of the polymer. Many biopolymers show a complex structure, which defines biologic activity for instance [105]. Biopolymers can show very complex folding patterns, included secondary and tertiary structures, both based on the properties of the primary structure [163]. On the other hand, the conventional polymers, such as the synthetic ones, show a simple and random (stochastic) structure [19]. Therefore, such class of polymers shows a typical molar weight distribution, which is not observed for the biopolymers. However, a well-defined structure presented by biopolymers contributes to decreasing their range of molar weight distribution, which results in higher monodispersity. Such characteristic is contrasting with synthetic polymers, which can present high polydispersity [19].

Biopolymers have been extracted and purified for several finalities (food, commercial, industrial, etc.) and at the same time some of them are studied in different areas. These studies include the development/obtention of novel materials to replace the oil-based ones (e.g., synthetic polymers, elastomers, etc.), which show, in general, high-cost production, low availability, environmental problems, etc. [178–180]. The main drawback to replace the oil-based materials is to develop materials with similar, interesting properties. Several efforts in this sense have been done. The novel nanocomposites, especially those based on biopolymers, are suitable candidates to this challenge. Biopolymers have replaced synthetic polymers in some application and also have been associated to them, resulting in composites materials [101, 156, 204]. This last strategy is convenient and highly reliable to enhance or induce some specific properties (e.g., thermal, mechanic, absorbing, etc.) [9, 14]. The incorporation of biopolymers in synthetic polymeric matrices, generating a polymer blend, may improve biodegradability and biocompatibility [126, 136]. Such attractive profile has attracted the interest of several researchers, and as a consequence the number of manuscripts published in this field has grown considerably in the last years.

Currently, biopolymers are being used as a source of nanofillers to be included in distinct bulk matrices [74, 114]. For example, biopolymers with fibrous characteristics have been incorporated with exceptional success in thermoplastic resins as polyvinyl chloride or polyethylene [106]. Such reinforcing fibers lead to two significant improvements: lighter final material because the filler density is, in general,

lower than the matrix density; and the enhancement of mechanical properties [186]. Despite this favorable scenery, sometimes a good dispersion of biopolymer fillers in the polymeric matrix is not achieved. The fillers proceeding from biopolymers have hydrophilic features due to their polar functional groups (charge density), while the polymeric matrix is hydrophobic, as consequence of their nonpolar groups [96–99]. Innovative strategies to overcome this undesirable effect have been described by several authors. Among those strategies, the controlled chemical modification of the fillers surface has been performed, in order to increase the interfacial compatibility between the polymeric matrix and filler [104, 158].

The good results presented by the use of fibers and short coir fibers, as reinforcement fillers, have encouraged today their use to produce alternative low-cost composite materials for structural and nonstructural applications (i.e., automotive, packaging, and building applications, rubber technology, furniture and consumer goods) [12, 141, 152]. In the last decades, the fibers have received massive support from others nanomaterials, also proceeding from biopolymers, to form suitable composite materials [178–180]. Nanocrystals, nanofibrils, and nanowhiskers have been extensively used to prepare nanocomposites with excellent thermal, mechanical, barrier properties, and reactive surface compared with conventional materials and composites [34, 87, 100]. Outstanding data about these superior properties are related in the literature even when low levels of such nanomaterials are utilized. Additionally, promising researches show that the incorporation of nanomaterials like fibrils, crystals, and whiskers, increases the levels of recyclability, transparency, and low weight of the final composite materials [178–180]. All these desirable aspects, associated with all the above-mentioned advantages allow inferring that biopolymers are the most exciting and encouraging source for nanomaterials to act as fillers in composite materials.

2 Crystals, Whiskers and Fibrils Derived from Biopolymers

Biopolymers can be separated into three main classes according to the monomeric units that build their structure: polynucleotides (i.e., nucleic acids); polypeptides (i.e., short polymers based on amino acids); and polysaccharides. Polysaccharides are polymeric carbohydrate macromolecules composed of long chains of mono- or disaccharide units bound together by glycosidic linkages [105, 108]. In general, the hydrolysis of polysaccharides gives their mono-, di-, or oligosaccharides constituents units. From the structural aspect, polysaccharides range from linear to highly branched structures and their quite heterogeneous characteristics (with slight modification on the repeating units) can drive to crystalline or amorphous arrangements [56, 79]. Such modifications can promote even the insolubility of some polysaccharides in water. When all repeating units in a polysaccharide backbone are the same residue, it is classified as homopolysaccharide or

homoglycan; however when more than one residue are present they are called heteropolysaccharides or heteroglycans [56, 79]. The most important and abundant polysaccharides are starch, cellulose, chitin, and chitosan.

2.1 Starch

Starch, the energetic reserve of the most part of green plants, is probably the second most abundant polysaccharide next to cellulose in nature [117]. The word "starch" derives from sterchen, meaning to stiffen. Starch grains from the rhizomes of Typha (cattails, bulrushes) as flour have been identified from grinding stones in Europe dating back to 30,000 years ago [143]. Starch grains from sorghum were found on grindstones in caves in Ngalue, Mozambique dating up to 100,000 years ago. Pure extracted wheat starch paste was used in Ancient Egypt possibly to glue papyrus. The extraction of starch is first described in the history around AD 77–79. Romans used it also in cosmetic creams, to powder the hair and to thicken sauces. Persians and Indians used it to make dishes similar to gothumai wheat halva. Rice starch as surface treatment of paper was used in paper production in China, from AD 700 onwards.

All the potentialities of this useful polysaccharide have been explored for years by food industries and the technological fields. Starch presents very attractive properties such as good nutrition facts, natural abundance, nontoxicity, biocompatibility, and biodegradability. Nowadays, the primary sources of starch are the cereal and root crops (rice, maize, wheat, potato, and cassava). Starch is mainly composed of two homopolysaccharides: amylose and amylopectin [58, 107]. These homopolysaccharides have the same repeating units that are linked in linear and branched fashion [201].

Amylose is a linear homopolysaccharide composed of α-(1,4)-D-glucopyranosyl units, in which slightly branched points may occur. Due to its simpler polymeric structure, amylose has tendency to assemble into a regular pattern forming crystals. On the other hand, amylopectin is the highly branched component of starch formed mainly by D-glucopyranosyl units joined together through α-(1,4) linkages. However, 5–6 % of α-(1,6) linkages can be found at the branching points [16]. The high branching structure confers to amylopectin a molecular weight that is ca. 1000 times greater than those presented by amylose. Besides these two main components, starch could present in some particulate material (i.e., cell wall fragments) and surface and internal components (i.e., proteins, enzymes, lipids, amine, and nucleic acids) [8, 16].

Both homopolysaccharides that form starch has large number of hydroxyl groups on their backbones, which drive to a high number of hydrogen bonds. Such bonds keep the starch chains hold together in an ordered manner that results in crystalline regions alternated by less-ordered amorphous starch chains. The presence of the crystalline regions is also credited to the intertwining of amylopectin side-chains, which is affected by amylose distribution in the starch granules [125].

Depending on the botanical origin of starch, the amylose chains can occur in the granule as individual molecules (amorphous regions), randomly interspersed among or in bundles between amylopectin clusters (amorphous and crystalline regions). Additionally, amylose can occur co-crystallized with amylopectin chains. Depending on their X-ray diffraction pattern, reflecting long-range ordering in the granule, starches are categorized in three crystalline types (polymorphs) called A, B, and C [90]. Such characteristics allow developing very attractive nanomaterials from starch like starch nanocrystals, which are crystalline platelets, prepared by the acid or enzymatic hydrolysis of amorphous moieties of the starch backbone. Some studies showed that despite the influence of the botanical origin on the starch final properties, different sources could provide nanocrystals with similar size and crystallinity [88, 89]. The acid hydrolysis carried out in the amorphous moieties, composed majorly of amylose, results in particles with square-like morphology about 10 nm thick and 50-100 nm equivalent diameters. This morphology is predominant when the initial amylopectin content and A-type crystallinity increase. However, it is worthy to say that although the nanocrystals crystallinity is higher than that of their corresponding native starches, they are not fully crystalline [90].

Starch nanocrystals are currently applied in bio-based nanocomposites formulation, in order to improve the mechanical, thermal, swelling, and barrier properties of different polymeric matrices, especially those that fit the actual environmental concerns [69, 71, 96–99]. The inclusion of starch nanocrystals in the polymeric matrix has been done basically by: (i) mixing an aqueous suspension of starch nanocrystals and the polymer solution; (ii) vacuum degassing; (iii) water evaporation (casting process); and (iv) film formation [96–99]. Various works indicate that the starch nanocrystals content in the resultant composites ranged from 2 to 50 wt% [96–99]. Inside the polymeric matrix, the starch nanocrystals can form three-dimensional networks through hydrogen linkages between the starch nanoparticles cluster and also to favorable interactions between the matrix and filler. Such particulars promote miscibility and dispersion of the starch nanocrystals in the polymeric matrix. Additionally, the incorporation of starch nanocrystals into polymer matrices with some shortcomings (i.e., high cost, non-biodegradability, non-biocompatibility, etc.) should ameliorate them to some degree. Some works report the chemical modification of starch nanocrystals surface in order to enhance their use as filler materials in different synthetic or natural polymeric matrices [30, 87, 114]. The success of starch nanocrystals as filler can be credited to its intrinsic rigidity, morphology, strong interfacial interactions, ability to organize percolated networks, and simple preparation method.

2.2 Cellulose

Cellulose, the most abundant polysaccharide on earth, has been exhaustively studied as a source of fillers for developing novel nanocomposites. Cellulose was discovered in 1838 by the French chemist Anselme Payen, who isolated it from

plant material and determined its chemical formula. Payen also established the word "cellulose," derived from the latin word "*cella*" (from *celare* that means to hide;). It was used to denote a small compartment, such as the cell of a honeycomb or a storeroom. The diminutive of "*cella*" is *cellula*, which is a frequent prefix (*cellulo*) in English scientific words, and gives us cellulose, full of little cells. Hermann Staudinger determined the structure of cellulose in 1920 [78]. Kobayashi et al. chemically synthesized cellulose without the use of any biologically derived enzymes in 1992 [80].

Cellulose is composed of D-glucopyranose units held together by β-(1,4) glycosidic linkages, which contrasts with the α-(1,4) glycosidic linkages present in the most part of the polysaccharides. Cellulose presents linear chains, unlike starch, with average molar mass ranging from 104 to 106 g/mol, depending on the source. Such chains adopt an extended and stiff rod-like structure, aided by the equatorial conformation of the glycosidic units. Many properties of cellulose depend on its degree of polymerization. Cellulose from wood pulp, for example, has typical chain lengths between 300 to 1,700 glycosidic units; cotton and other plant fiber as well as bacterial cellulose have chain lengths ranging from 800 to 10,000 glycosidic units [78]. Chains with small lengths result from the breakdown of cellulose and are known as cellodextrins. In contrast to the long chain of cellulose, cellodextrins are typically soluble in water and organic solvents.

Cellulose is found in nature as a structural component in the primary cell wall of plants, algae, and bacteria [164]. In plants, the primary cell wall consists of three central regions, and each region has lignin, hemicellulose, and cellulose microfibrils (30–90 %, according to the source) as the principal components [149] (see Table 1). In plants, cellulose gives rigidity to the cells. It is estimated that 1012 tons of cellulose are photosynthesized every year [78].

As a natural polymer, cellulose is biodegradable, biocompatible, renewable, and affordable. Therefore, it has been used in many different fields including paper industry and fabrics [70], gunpowder and propellants [11] and food additives (anticaking agent, emulsifier, stabilizer, dispersing agent, thickener, and gelling agent) [17] for decades. More recently, cellulose found applications in the nanomaterials field [51] and in the production of bioethanol [24].

Table 1 Percentage of cellulose, hemicellulose, and lignin from different botanic sources [47]

Source	Cellulose (%)	Hemicellulose (%)	Lignin (%)
Wheat straw	35.80	26.80	16.70
Sweet sorghum	44.60	25.30	18.00
Alamo wood	48.80	17.30	27.70
Corn stover	36.40	22.60	16.60
Corn ears	38.50	32.80	18.70
Rice straw	35.62	11.96	15.38
Bean straw	30.64	23.14	9.35

Cellulose presents three hydroxyl groups in each sugar residue and, as a linear polymer, the interchains H-bond interactions occur at high level and, as a consequence, cellulose is found in nature as a highly crystalline polymer with crystallinity index as much as 80 % [131]. Differently to starch, cellulose is much more crystalline. Whereas, starch undergoes a crystalline to amorphous transition in water in the temperature range of 60–70 °C, cellulose undergoes the same transition in water close to 320 °C and high pressure. Cellulose possesses several different crystalline structures, which can be assigned to the location of hydrogen bonds between and within strands. Natural cellulose is denoted as cellulose I, with structures Iα and Iβ [121, 122]. These two structures have the same fiber repeating distance (1.043 nm for the repeat dimer interior to the crystal, 1.03 nm on the surface but differing displacements of the sheets) relative to one another. Cellulose produced by bacteria and algae is enriched in Iα while cellulose of higher plants consists mainly of Iβ. Cellulose from regenerated cellulose fibers is denoted as cellulose II. In this case, the structure shows an antiparallel arrangement of the strands and intermolecular and both intra and intersheet hydrogen bonding. The conversion of cellulose I to cellulose II is irreversible, suggesting that cellulose I is metastable and cellulose II is stable. With various chemical treatments, it is possible to produce the structures cellulose III and cellulose IV [135]. The high crystallinity renders cellulose insoluble in most common solvents, and therefore prevents many of its potential applications [6]. Water cannot penetrate crystalline cellulose but dry amorphous cellulose absorbs water becoming soft and flexible. Some of this water is nonfreezing, but most is just trapped. Less water is bound by direct hydrogen bonding if the cellulose has high crystallinity but some fibrous cellulose products can hold a considerable amount of water in the pores and its typically straw-like cavities; water-holding ability correlating well with the amorphous (surface area effect) and void fraction (that is, the porosity). The preparation of nanofibrils and nanowhiskers from cellulose, which are easily dispersed in water, is an interesting way to overcome the solubility restrictions [57]. Cellulose micro- and nanofibrils are substructural elements of cellulosic fibers that can be mechanically disintegrated from the cell wall matrix. Recent enzymatic or chemical pretreatments combined with mechanical disintegration process of the fibers produce stable and homogeneous nanofibrils, which show outstanding potential for many technological applications [74]. Noteworthy, the size and nature of these native cellulose nanofibrils make these structures amenable to the manufacture of robust thin films and bio-based nanocomposites [74, 203].

The most crystalline form of cellulose is the nanowhiskers, which are shorter than the nanofibrils. Cellulose nanowhiskers are isolated from microcrystalline cellulose using acid hydrolysis or sonication process [34]. So, it is usual to submit cellulose to a previous delignification process. Cotton, bamboo, and wood are the most usual sources of cellulose to produce nanowhiskers. As a result, nanowhiskers crystallinity and size dimension are dependent of the botanical source of cellulose and preparation method. In the last decade, several research groups have focused efforts on developing new methodologies to prepare cellulose nanowhiskers from different botanic sources. Additionally, a huge number of works have been

published in literature regarding the incorporation of cellulose nanowhiskers in polymeric and composites matrices [32, 160, 189]. Such enthusiasm is due to the innumerous advantages that cellulose nanowhiskers show in relation to the conventional inorganic nanosized materials. Simple methodology, low-cost cellulosic feedstock, and mechanical properties compared to those presented by the carbon nanotubes and inorganic nanofibers, fact that allows cellulose nanowhiskers to be a promising filler material.

2.3 Chitin and Chitosan

Further starch and cellulose, chitin and its derivative chitosan have been extensively utilized to prepare nanosized fillers [134]. Chitin was the first polysaccharide discovered and after cellulose is the second most abundant biopolymer in nature being found among the kingdoms of Fungi, Plantae (plants), and Animalia (animals). Some chitin sources are shown in Table 2.

Chitin (first called as *fungine*) was first isolated in 1811 by Henry Braconnot, a French scientist during his experiments with mushrooms had found an insoluble fraction in acid and bases on their cell walls. Afterward, on 1823 August Odier found the same compound in the cuticles of insects and called it chitin [76]. The word chitin derives from French "*chitine*" that in your turn is from the Greek "*khiton*" or "*chiton*", which means protection or wrapping. Although it had been found in 1811, the chitin structure was described only in 1929, almost one century after, by the Swiss chemistry, Albert Hofmann. Chitin is a linear polysaccharide formed by N-acetyl-D-glucosamine units hold together by β-(1,4) glycosidic linkages. In nature, it occurs as ordered crystalline microfibrils forming structural components in the exoskeleton of crustaceous, mollusks, and insects or in the cell walls of fungi and yeast [26, 146]. The chitin content in a living organism can vary from 3 to 40 % according to the specimen. Table 3 shows some data about the composition of different sources utilized to extract the chitin [83].

Table 2 Chitin main sources [146]

Sea animals	Insects	Microorganisms
Annelida	Scorpions	Green algae
Mollusca	Spiders	Yeast (β-type)
Coelenterata	Brachiopods	Fungi (cell walls)
Crustaceans	Ants	Mycelia penicillium
Lobster	Cockroaches	Brown algae
Crab	Beetles	Spores
Shrimp		Chytridiaceae
Krill		Blastocladiaceae
		Ascomydes

Table 3 Composition of different sources of chitin [83]

Source	Chitin (%)	$CaCO_3$ (%)	Proteins (%)	Lipids (%)
Crab	15–30	40–50	15	2–5
Shrimp	30–40	20–30	35	5–10
Krill	20–30	20–25	–	–
Squid pen	20–40	*Insignificant*	–	–
Clams	3–6	85–90	–	–
Insect	5–25	*Insignificant*	–	–
Fungi	10–25	*Insignificant*	5–10	5–10

*Values referent to the dry mass

The structure of chitin is comparable to cellulose because both polysaccharides have the same supporting function in the organism in which they are present. The difference between these two polysaccharides is the acetamide group attached at C2 carbon of the chitin.

Among several properties of chitin, its nontoxicity, biodegradability, and biocompatibility are the most relevant [146]. Due to these features, this polysaccharide has been widely used in biomedical and pharmacological applications. Chitin shows a rigid crystalline structure and depending on the source (crabs or shrimps, for instance) it can occur as two allomorphs, namely the α and β forms, which can be differentiated by infrared and solid-state NMR spectroscopy together with X-ray diffraction analysis [150]. Both α and β forms of chitin are insoluble in water or the usual organic solvents. Despite natural crystallinity variations, the insolubility is the major problem preventing further development of processing and uses of such a polysaccharide. Besides this limitation, the crystallinity of chitin allows preparing nanofibers from prawn shell by a simple grinding treatment after the removal of protein and minerals under neutral pH conditions. Chitin nanofibers are highly uniform and the width ranges from 10 to 20 nm [65].

Several derivatives are synthesized from chitin; among them the most important is chitosan. Despite the occurrence in nature of partially deacetylated chitin (with a small content of glucosamine units), chitosan is obtained by partial (or total) deacetylation of chitin in the solid-state under alkaline conditions (concentrated NaOH) or by enzymatic hydrolysis in the presence of chitin deacetylase [42, 146]. The main parameters that influence all the chitosan properties are the molecular weight and deacetylation degree [75]. Such parameters are straightly determined by the conditions used in the chitosan preparation. Chitosan is insoluble in water as chitin; however, its solubilization can be obtained at acidic conditions. At low pH, the amino groups of chitosan are protonated, which increases the electrostatic repulsion among the chains allowing their solvatation by water molecules [36]. In the solid state, chitosan is a semi-crystalline polysaccharide with many polymorphs according to the literature [20, 146]. Single crystals of chitosan have been obtained using fully deacetylated chitin of low molecular weight, for instance. Chitosan shows similarly as chitin, nontoxicity, biocompatibility, biodegradability, hemostatic potential, antibacterial and antitumoral activity, and good film-forming

properties [137]. Furthermore, the amino and hydroxyl groups of chitosan are placed in adjacent positions, which confer a chelating feature to this polysaccharide. The use of chitosan to formulate materials to remove metals, ionic compounds and dyes from contaminated wastewater is encouraged [28, 35].

For decades, both chitin and chitosan have been used to design the most sorts of materials for applications ranging from environmental treatments to tissue engineering [137, 146]. Recently, these polysaccharides have attracted attention as significant sources of nanosized fillers for innumerous polymeric matrices [30, 65, 114]. Nanofibrils and nanowhiskers can be prepared from chitin or chitosan by breaking down their structures in crystalline nanofragments [65, 114]. Such fillers can be obtained with specific shapes or self-assembling of basic building blocks due to chain cleavage, which occurs at random location. This forms rod-like or spindle-like particles that tend to align cooperatively and to develop rigid structures [94, 114]. A brief research in the literature shows that chitin and chitosan nanowhiskers have been used as reinforcing additives for high-performance environment-friendly biodegradable nanocomposite materials. For example, as biomedical composites for drug and gene delivery, nanoscaffolds in tissue engineering, nanostructures for medical and veterinary applications, cosmetic, and orthodontics [114, 118]; Zeng et al. 2012. According to the biological source of chitin and taking into account the methodology used to prepare chitosan, the resultant nanowhiskers can be use in antitumor application and immune-modulating activity [62, 114].

The next sections present the most popular methodologies that have been used to prepare nanosized fillers from cellulose and their main applications as well as the cut-edging technologies that are being developed.

3 Hydrogels Nanocomposites

Nature has found many different ways to overcome structural limitations during the history of evolution from early prokaryotes to the complex living systems that are found nowadays. This fact is supported by the knowledge of very rigid and tough natural materials, such as; the stiff exoskeleton that protects the fragile internal structures of arthropods [138], or the plant cell walls [124] that provide enough strength for giant trees from North America like sequoia (*sequoias sempervirens*) to grow as high as 115 meters or the bones that compose the internal skeleton of vertebrates from the tiny frog (*paedophryne amauensis*) of only 7.7 mm found in Papua New Guinea [147] to the extinct predator Tyrannosaurus Rex having ca. 13 m in length [61] and to the robust Blue whales (*balaenoptera musculus*) having incredible average size of 26 m [15]. Under detailed scrutiny, researchers have discovered that although composed of different substances, all these supporting materials (exoskeletons, bones, and plant cell walls) are naturally constructed based on the same principles. About them, the crystalline phases or mineralized particles are dispersed (or chemically bound) into a polymer matrix, and are considered nanocomposites [73, 145, 187]. The term nanocomposite was defined in earlier

sections, and it is considered as a multiphase material in which one of the phases has at least one of the dimensions ranging from 1 to 100 nm.

Understanding structure/properties relationship of such high-performance natural materials is a rational pathway to develop biologically inspired nanocomposites to the most diverse ends. Nature provides inestimable sorts of resources, and it is an excellent platform for nanomaterials. Taking into account healthy and environmental concerns that have risen in the last years from non-biodegradable synthetic polymers or the conventional inorganic fillers owing to the fact that many precursors are toxic and expensive [172], biopolymers such as cellulose, chitin, and starch are promising candidates for preparing crystalline biocompatible and biodegradable nanofillers that could replace the use of inorganic nanoparticles in some applications for preparing nanocomposites [41]. However, the reader should have in mind that polysaccharide nanocrystals have broader applications than replacing inorganic nanofillers as it is pointed out in this chapter.

More recently, there has been an increasingly interest in the development of hydrogel nanocomposites, in which the reinforcement phase is composed of polysaccharide nanocrystals since such nanofillers can improve mechanical, thermal, and optical properties [10, 132] as well as the water uptake response to external stimuli. Hydrogels are regarded as physically or chemically crosslinked polymeric chains capable of absorb and retain water and/or other aqueous fluids without dissolving, and are still considered one of the most important branches of the polymer science field. This status is supported by the fact that hydrogels may find application in ordinary utensils like a diaper [123] or soil conditioner beads for plants [120] as well as in more sophisticated technologies such as in drug delivery systems [81, 133], in gene delivery [93, 95], in tissue engineering [91], in separation science [205], in wound dressing [113], in sensors [184], among others. Reports focusing on the different aspects of development and application of hydrogel and hydrogel composites can be found in the scientific literature [2, 13, 23, 67, 84, 128, 148]. Therefore, this chapter condenses the most relevant works regarding the preparation of polysaccharide nanocrystals, their application in the development of hydrogel nanocomposites as well as the future trends of the area.

3.1 Based on Cellulose Nanocrystals

The recent development of nanotechnology has offered new possibilities of cellulose exploitation such as the preparation of cellulose nanoparticles; e.g., cellulose nanocrystals (CNC) and cellulose nanofibers (CNF), or both. A quick search at Web of Science © database under the topic “cellulose nanocrystals” revealed more than 1,000 published papers (164 paper only in the first half of 2014) illustrating the importance of such a topic in academia and industry.

Both CNC and CNF could be derived from botanical, animal, or bacterial cellulosic sources [45, 63, 190]. In general, the extraction of cellulose from the biomass may involve the use of organic solvents for removing waxes, alkali treatment

for removing hemicellulose, and other soluble polysaccharides followed by bleaching to eliminate lignin and polyphenols [109]. CNC are obtained by removing the amorphous phase, usually by acid hydrolysis in which H_2SO_4 is the most common acid, resulting in highly crystalline nanoparticles. On the other hand, CNF are obtained by different methodologies (e.g., mechanical disintegration, 2,2,6,6-tetramethylpiperidine-1-oxil radical-mediated oxidation, enzymatic hydrolysis, etc.) as a mixture or both crystalline and amorphous domains [64, 195]. CNC and CNF have been prepared by different sources and the most common are cotton [115], wood pulp [66], and tunicates (sea animals) [4]. However, many other sources have been reported as basis for preparing CNC and CNF such as sugarcane bagasse [171], algae [59], sisal fibers [157], banana plant [116], jute fibers [139], straw [142], and bamboo [188], among many others. CNC is derived as slender rods of few nanometers wide ($\sim$ 10-50 nm) and hundreds of nanometers long, but shorter than CNF, which can reach a few micrometers in length. It has been reported that CNC isolated from chardonnay grape skins presented as spherical nanoparticles (up to 100 nm) composed of a core-shell structure of self-assembled 50 nm long cellulose nanorods surrounded by cellulose nanofragments of less than 5 nm formed due to strong interfacial hydrogen bonds [102]. As the native cellulose fibrils dimensions and amount vary, the source and method of isolation have a substantial effect on the size of nanocrystals. For instance, cellulose nanocrystals from tunicates were found to have up to 2 μm in length and are significantly longer than those obtained from different sources such as cotton or wood pulp which may vary between 100 and 300 nm in length [4]. Table 4 shows dimensional aspects of CNC obtained by acid hydrolysis from various sources and exemplifies the effect of source and reaction conditions on nanocrystals size. Controlling reaction time and temperature are paramount to obtain consistent hydrolysis of amorphous regions or less-ordered chains without promoting damage to the crystalline phase.

CNC and CNF have been used in the preparation of nanocomposites in the most diverse fields. Many review papers referring to methodologies, issues involved for preparing CNC and CNF, chemical modification of nanocellulose and applications of both CNC and CNF can be found in the literature [21, 29, 31–33, 51, 63, 85, 86, 109, 158]. Therefore, the development and the chemical modification aspects of CNC and CNF are not discussed in details in this chapter, which will be devoted to the main features of hydrogel nanocomposites based on CNC and CNF as reinforcement.

CNC have been incorporated into hydrogels aiming at improved mechanical properties due to its low density, to its excellent axial and transverse elastic moduli (150 and 10–50 GPa, respectively) and to the ability of forming a network into the matrix through hydrogen bonding, also known as percolation effect. Han et al. [52, 53] prepared hydrogels based on poly(vinyl alcohol) and borax reinforced with nanocellulose. Alkaline (20 wt% NaOH, 4 h) pretreated wood fibers were acid hydrolyzed (64 wt% H_2SO_4, fiber-to-acid ratio of 1:20, 45 °C, 1 h) followed by high-pressure (207 MPa) homogenization (at a rate of 135 mL/min for five passes) to generate CNC (length: 149 ± 40 nm; width: 9 ± 2 nm; 66 % crystalline). CNF (length: 732 ± 208 nm; width: 21 ± 7 nm; 58 % crystalline) were prepared using all

Table 4 CNC obtained by acid hydrolysis from different botanic sources

Source	Methodology	Length (nm)	Width (nm)	Reference
Sisal fibers	Acid hydrolysis (40 min, 60 wt% H_2SO_4, 50 °C)	215 ± 67	5 ± 1.5	[157]
Sisal fibers	Acid hydrolysis (15 min, 65 wt% H_2SO_4, 60 °C)	250 ± 100	4 ± 1	[44]
Sisal fibers	Acid hydrolysis (50 min, 65 wt% H_2SO_4, 50 °C)	195	15	[1]
Sugarcane bagasse	Acid hydrolysis (30 min, 60 wt% H_2SO_4, 45 °C)	255 ± 55	4 ± 2	[171]
Sugarcane bagasse	Acid hydrolysis (180 min, 64 wt% H_2SO_4, 40 °C)	247 ± 32	10 ± 3	[159]
Sugarcane bagasse	Enzymatic hydrolysis followed by sonication	84–300	2–12	[25]
Cotton	Acid hydrolysis (300 min, 64 wt% H_2SO_4, 50 °C)	248	–	[37]
Cotton	Acid hydrolysis (45 min, 60 wt% H_2SO_4, 45 °C)	94 ± 31.6	21 ± 5.5	[194]
Alamo switchgrass	Acid hydrolysis (45 min, 60 wt% H_2SO_4, 45 °C)	148 ± 42.1	21 ± 4.3	
Maize Straw	Acid hydrolysis (150 min, 60 wt% H_2SO_4, 25 °C)	388 ± 43	19 ± 2	[142]
Banana plant	Acid hydrolysis (30 min, 11 M H_2SO_4, 50 °C)	466 ± 159	19 ± 6	[116]
	Acid hydrolysis (60 min, 11 M H_2SO_4, 50 °C)	441 ± 116	17 ± 5	
	Acid hydrolysis (90 min, 11 M H_2SO_4, 50 °C)	375 ± 100	13 ± 4	
	Acid hydrolysis (120 min, 11 M H_2SO_4, 50 °C)	361 ± 61	17 ± 4	
	Acid hydrolysis (180 min, 11 M H_2SO_4, 50 °C)	378 ± 66	17 ± 4	
	Acid hydrolysis (240 min, 11 M H_2SO_4, 50 °C)	319 ± 68	15 ± 4	

the same conditions for CNC, but at 48 wt% H2SO4. Nanocellulose-PVA-Borax hydrogels (2 wt% PVA; 0.4 wt% borax; 1 wt% CNC or CNF) were prepared by dissolving 0.1 g of borax in 1 wt% nanocellulose aqueous suspension followed by addition of 0.5 g of PVA. The reaction remained at 90 °C for 2 h and then cooled to room temperature. The incorporation of nanocellulose enhanced the compressive strength and viscoelasticity of the hybrid hydrogels. In this case, the crystalline nanocellulose can act as a multifunctional crosslinking agent acting both physically or chemically. It was demonstrated that crosslinking density, viscoelasticity, and stiffness of hydrogels were improved as the aspect ratio (length/width ratio) increased at a cost of loss of transparency (mean transparency of 51.0 % for CNC). The free-standing, high elasticity, and moldable hydrogels exhibited self-recovery under continuous step strain, and thermo-reversibility under temperature sweep have potential of applications including artificial muscles, bioactuators, soft machines, tissue scaffolds, and drug delivery devices.

McKee [110, 111] prepared thermo responsive hydrogels based on methylcellulose (Mn = 86 kg/mol, DS of 1.78) physically crosslinked by cellulose nanocrystals with tunable mechanical properties. CNC (dimensions not informed) were isolated from ground Whatman ashless filter paper by acid hydrolysis (64 wt%

H_2SO_4, 45 °C, 45 min). It was showed that the elastic modulus (G') of the viscoelastic solution at 20 °C could be tuned from 1 to 75 Pa by increasing the CNC concentration from 0 to 3.5 wt% at 1 wt% methylcellulose while at 60 °C the G' values varied from 110 to 900 Pa for the same increasing CNC concentration. Yang et al. [197, 198] also reported the reinforcement effect of cellulose nanocrystals from acid hydrolyzed (60 wt% H_2SO_4, 55 °C, 2 h) pulp fibers in acrylate-modified poly(ethylene glycol) hydrogels. Homogeneous composites were formed for CNC volume fraction lower than 1.5 %. At 1.2 v/v-% modulus, fracture stress, and fracture strain enhanced by a factor of 3.48, 5, and 3.28, respectively. Oscillatory shear data indicated the CNC—PEG nanocomposite hydrogels were more viscous than the neat PEG hydrogels and were efficient at energy dissipation due to the reversible interactions between CNC and PEG polymer chains.

Yang et al. [197, 198] investigated the relation of CNC aspect ratio and the mechanical behavior of nanocrystal/poly(acrylic acid) hydrogels. Acid hydrolyzed (55 wt% H_2SO_4, 50 °C, 2 h) microcrystalline cellulose and wood pulp generated CNC having aspect ratio (L/d) of 31 and 14, respectively. The fracture strength of hydrogels increased from 157 to 229 kPa as the aspect ratio of CNC increased from 14 to 22, and then the strength further increased to 254 kPa at L/d of 31. It was also demonstrated the polymer chains rearrange on the CNC surfaces according to the stretched state of hydrogel changing both pore size and pore wall during deformation.

Osorio-Madrazo et al. [129] demonstrated the reorganization of cellulose nanocrystals (width: 30 ± 12 nm; length: 200 nm to 4 μm), isolated from green algae *Cladophora sp* (50 wt% H_2SO_4, 40 °C, 8 h), into agarose hydrogels under tensile loading. In other words, uniaxial stretching under controlled humidity conditions induced anisotropy. The drying process was essential for specific filler/matrix interactions allowing a stress transference while stretching and promoting crystals alignment. This process would allow tuning the mechanical features of the hydrogel.

It has been reported that CNC played a role in the water absorption capacity of hydrogels. Spagnol et al. [160–162] prepared hydrogel composites composed of different polymeric matrices, e.g., chitosan-*graft*-poly(acrylic acid), starch-*graft*-poly(sodium acrylate), and poly(acrylamide-*co*-acrylate) reinforced with CNC isolated from cotton fibers by acid hydrolysis (36.5 % HCl, of 1/20 g/mL cellulose/HCl ratio, 45 °C, 1 h). It was showed that independently on polymer matrix, the addition of CNC up to 10 wt% substantially increases the water uptake due to the extra hydrophilic groups of cellobiose unit, but at higher concentrations the hydroxyl groups from CNC took place in the crosslinking reaction increasing the crosslinking density and, as a result, decreasing the absorption of water. Through surface response methodology and analysis of variance (ANOVA) it was demonstrated that CNC contributed 30 % to the swelling degree.

Mckee et al. [110, 111] prepared supramolecular stable and stiff hydrogel composites with healable features based on brush-modified cellulose nanocrystals crosslinked with soft polymeric chains by dynamic host–guest interactions using cucurbit[8]uril as supramolecular crosslinker. The hydrogels combined high storage

modulus, fast sol-gel transition (<6 s) and self-healing ability as fast as 30 s. Besides, the self-healing capacity was also observed for hydrogel samples aged for 4 months. This work suggests robust strategies to combine highly dynamic supramolecular interactions with mechanically active colloidal reinforcements for the preparation of the next generation of advanced materials from renewable resources.

Nanocellulose can present a chiral nematic phase in water, in which the CNC self-assemble in the helical configuration. If the helical pitches of nanocrystals assemble, have the same order of the visible light wavelength the system can exhibit photonic color. In this sense, Kelly et al. developed photonic hydrogels by controlling the polymerization condition to ensure the CNC nematic phase was preserved [72]. That was possible by previous evaporation-induced self-assembly (EISA) followed by UV-photo-polymerization. It was showed that any change in the helical pitch due to variations of external media (such as salt, pH, etc.) the reflected color of the hydrogel could be tuned.

CNC and CNF have been incorporated in hydrogels or other polymeric matrices seeking improvement of drug release behavior for delivery systems, swelling features, improved mechanical properties for materials with potential application in bone and tissue repair, and in the preparation of hydrophobic-absorbing matrix based on functionalized CNF aerogels, as summarized in a recent review paper [148].

3.2 Based on Chitin Nanocrystals

Chitin can be derived from innumerous sources, but from the commercial point of view, the most important are shrimp, lobster and crab shells, which are residue from food industry. Chemical [151], physical [77], enzymatic and microbiological [46] methodologies have been explored to isolate chitin. In general, the extraction process involves several steps for removing bound proteins, minerals, lipids, and pigments.

Chitin nanowhiskers (CtNW) and chitin nanofibers (CtNF) can be isolated by 2,2,6,6-tetramethylpiperidine-1-oxil radical-mediated oxidation (TEMPO-oxidation) surface cationization followed by mechanical disintegration and acid hydrolysis, [200]. Similarly, to the obtention of CNC, the acid hydrolysis of chitin is the most common procedure for isolating CtNW, and it is based on the faster hydrolysis kinetics of the amorphous phases. However, in the case of chitin, HCl is used instead of the H_2SO_4 used for cellulose. Although different reaction conditions have been reported (Table 5), the most used is 3 N HCl, for 90 min at boiling, as described elsewhere [130, 134], which in general, generates 50–300 nm long and 10–50 nm wide CtNW.

Similarly to CNC, the majority of applications described in the literature are employing CtNW as the reinforcement phase in the preparation of nanocomposites due to attractive features, e.g., derived from renewable sources, biodegradable, nontoxic, and excellent transversal and longitudinal moduli (15 and 150 GPa,

Table 5 CtNW and CtNF obtained by different reaction conditions [39, 40, 48, 55, 103, 144, 192, 193, 196]

Source	Methodology	Length (nm)	Width (nm)
Crab	Acid hydrolysis (HCl 3 N, 60 min)	50–300 (150)	10
Crab	Acid hydrolysis (HCl 3 N, 90 min)	100–600 (240)	4–40 (15)
Crab	Acid hydrolysis (HCl 3 N, 90 min)	100–650 (500 ± 50)	10–80 (50 ± 10)
Crab	Acid hydrolysis (HCl 3 N, 90 min)	200–500	5–20
Crab	Acid hydrolysis (HCl 3 N, 360 min)	255	31
Crab	TEMPO-oxidation	340	8
Crab	Surface cationization	250	6
Shrimp	Acid hydrolysis (HCl 3 N, 360 min)	230–970	31
Shrimp	Acid hydrolysis (HCl 3 N, 360 min)	180–820 (427)	43
Shrimp	Acid hydrolysis (HCl 3 N, 360 min)	110–975 (343)	46

respectively). CtNW have been introduced into polymeric films for reducing O_2 permeability [38], into fibers to improve mechanical properties [185], in lithium battery electrolytes for improved thermal and mechanical stability as well as ionic conductive [5], in membranes to enhance cell compatibility [60], among others.

CtNW have been far less studied than CNC and only a few papers report on the preparation of hydrogel nanocomposites based on CtNW as reinforcement. Even though, it has been shown significant effects on swelling capacity and drug release behavior caused by the incorporation of CtNW. Lin et al. [96] acid hydrolyzed (3 N HCl, 90 min, at boil) shrimp chitin to prepare 300–400 nm long and 10–20 nm wide CtNW to be further incorporated into alginate microspheres (900 ± 20 μm) hydrogels crosslinked by calcium ions. It was demonstrated the addition of 50 wt% CtNW increased the swelling capacity from 1.815 to 2.329 % due to the inhibition of crosslinking points caused by the presence of CtNW, which provided a less rigid matrix allowing more fluid (pH 7.4 phosphate buffer solution) intake. The presence of CtNW also promoted an increase in the encapsulation efficiency of theophylline from 33 % (standard hydrogel without CtNW) to 55 % at 50 wt% CtNW, which acted as a barrier to prevent drug leaking. Besides, CtNW-loaded microspheres showed sustained releasing profile, in which the drug releasing mechanism was found to occurs by diffusional transport (n = 0.419) contrasting the anomalous transport (n = 0.716) presented by the pristine alginate microspheres.

Hybrid hemicellulose-based hydrogels prepared by freeze (10 h, −20 °C)-thawing (1 h, 80 °C) cycles nanoreinforced with CtNW has been recently reported [49]. CtNW (length: 200 ± 10 nm; width: 40 ± 10 nm) were prepared by acid hydrolysis (3 N HCl, 90 min, 90 °C) and incorporated into hydrogels at different volume ratio (0–2) at the constant (1:1) hemicellulose/poly(vinyl alcohol ratio of 2 wt% solutions (each). The presence of CtNW (up to ratio 1:1:1) induced larger and more numerous porous to the hydrogel structure, while at higher concentration (e.g., 1:1:2) the result observed was opposite. The samples absorbed 10–20 g of water by gram of dry hydrogel, and statistically no significant effect on swelling

was verified by the introduction of CtNW. On the other hand, the mechanical features were dependent on CtNW loading, but no linear tendency with concentration was observed: e.g., at 0.5 CtNW the fracture stress was maximum (9.6 MPa), but at 0.75 CtNW the value was lower (8.1 MPa) than the standard (9.3 MPa). It was suggested the prepared samples present potential to be applied in the tissue engineering field.

CtNW has also been chemically bound to silane-modified magnetic nanoparticles for DNA extraction [22] from E. coli and S. aureus microorganisms. CtNW (dimensions not explicitly informed) were isolated by acid hydrolysis (3 N HCl, 3 h, 105 °C). The CtNW-Magnetic nanoparticles formed a stable colloidal suspension in both water and DMSO. Furthermore, the magnetic nanoparticles could be aligned by the application of a magnetic field. It was showed that the size of nanoparticles depends on the surface charges on CtNW, which are controlled by adjusting the pH of the media.

Araki et al. [7] reported chitosan hydrogels filled with CtNW (6–8 nm wide, 100–200 nm long, 3 N HCl, 3 h, at boil) using isocyanate hexamethylene-1,6-di-(aminocarboxysulfonate) (HDS) as crosslinker. The addition of CtNW promoted an increasing in the hydrogel stiffness as showed by the Young's modulus that changed from 2.53 kPa at 0 wt% CtNW to ~170 kPa at 13 wt% that represents about 67-folds increase. Similarly, the stress at break increased 41-fold for the same variation of composition. However, the improved mechanical properties were accompanied by a loss in the swelling capacity of ca. ten-folds, which was attributed to the suppression of chitosan chains mobility caused by the presence of the rigid CtNW.

3.3 Based on Starch Nanocrystals

Starch nanocrystals (SNC), unlike CNC and CtNW, are platelet-shaped nanoparticles with much shorter length of 20–40 nm, width of 15–30 nm, and a few nanometers of thickness [29, 87]. Preparation of SNC by acid hydrolysis of native starch has the time-consuming process, which can take up to 30 days, and the low yield as the major drawbacks. The choice of starch source, acid type and concentration, reaction conditions (temperature and time) and pretreatment (e.g., enzymatic, mechanical treatment, etc.) are paramount to reduce hydrolysis time and improve yield [88, 90]. Most reports on SNC preparation follows the procedure described by Angellier et al. [3], in which the hydrolysis is conducted using 3.16 M H_2SO_4 solution for 5 days at 40 °C.

Although SNC are much shorter and less crystalline (~45 %) than other polysaccharide nanocrystals (>90 %), the reinforcing effect due to the percolation of SNC into different polymeric matrix (natural rubber, polyurethane, starch, pullulan, PVA, among others) has been reported [43, 87, 112, 140]. SNC have also been studied as stabilizing agents in emulsions (also denoted as pickering emulsion) with potential applications in food, cosmetics and pharmaceuticals [50, 92, 93].

Up to date, only few works report on the incorporation of SNC into hydrogels. For instance, SNC (40–60 nm long, 15–30 nm wide) hydrolyzed (3.16 M H2SO4, 5 days, 40 °C) from pea starch were used to form hydrogel nanocomposites based on Ca^{+2}-crosslinked alginate polymer matrix [96–99]. The composites presented pH-dependent swelling behavior, where the fluid uptake at pH 1 and at 50 wt% SNC was less than 30 % whereas at pH 6.8 and 7.4 the swelling was higher than the noncomposite hydrogels reaching about 2000 %. The efficiency of theophylline encapsulation was 55 % in the composite contrasting the lower efficiency of only 34 % of the standard hydrogel. The releasing behavior of theophylline-loaded hydrogel nanocomposites microspheres was investigated under different pH conditions (1 and 7.4). It was showed the composite samples could sustain the release for a longer time, and the equilibrium was reached at ∼400 min, more than the double period observed for the noncomposite hydrogel. Besides, the mechanism by which the drug is released changed from anomalous transport (n = 0.716) to diffusional transport (0.424) with the addition of SNC. Therefore, SNC could prevent the drug release burst at the first minutes of releasing, allowing the composite to be applied as carriers for drug delivery systems.

Zhang et al. [202] prepared supramolecular hydrogel based on cyclodextrin inclusion filled with SNC with potential for injection-implantation drug delivery. SNC (10–20 nm wide, 40–70 nm long) were made by hydrolyzing pea starch in 3.16 M H_2SO_4 solution for 5 days at 40 °C. The presence of polysaccharide nanocrystals increased the stability of the hydrogel framework and inhibited the diffusion of bovine serum albumin, which served as a model protein drug in the nanocomposite hydrogels and showed prominent sustained release profiles. The shear-thinning property of the nanocomposite allows it to be applied as injectable material.

4 Conclusions and Future Trends

This chapter demonstrates that polysaccharide nanocrystals (PN) derived from well-known biopolymers such as cellulose, chitin, and starch can be versatile nanoparticles to be applied in different fields, especially in the preparation of hydrogel nanocomposites. Interestingly, by using nanotechnology one can take advantage from the same features that once prevented cellulose and chitin to be largely explored by industry (specially due to high crystallinity and lack of solubility in common solvents) to produce highly crystalline and high-performance rod-shaped nanoparticles (also called nanowhiskers, nanocrystals or nanofibrils). It also should be pointed out that such nanocrystals are excellent candidates to replace traditional inorganic fillers (metal oxides, noble metals, carbon, etc.) in the preparation of many nanocomposites. The natural abundance, renewability, low cost, biodegradability, biocompatibility, low density, and outstanding elastic modulus of such polymers, as well as the absence of expensive and toxic precursors, stimulate their use.

Although polysaccharide nanocrystals have been proved to be promising materials, some challenges are still to be overcome. For instance, most researches on PN are conduct by academic groups purely by scientific curiosity and commercial or industrial production of PN is restricted to a few companies and mostly to CNC.

So far, CNC have been more explored than CtNW or SNC in the preparation of hydrogel nanocomposites, but it has been demonstrated that any of those particles can strongly influence either the mechanical properties or swelling/release features of hydrogel composites.

More comprehensive studies on the concepts that drive the properties of such soft-hard combined composite hydrogels will broaden the understanding of structure–properties relationship allowing new materials and new applications.

References

1. Ahmad EEM, Luyt AS (2012) Morphology, thermal, and dynamic mechanical properties of poly(lactic acid)/sisal whisker nanocomposites. Polym Compo 33(6):1025–1032
2. Alarcon CDLH, Pennadam S, Alexander C (2005) Stimuli responsive polymers for biomedical applications. Chem Soc Rev 34(3):276–285
3. Angellier H, Choisnard L, Molina-Boisseau S, Ozil P, Dufresne A (2004) Optimization of the preparation of aqueous suspensions of waxy maize starch nanocrystals using a response surface methodology. Biomacromolecules 5(4):1545–1551
4. Anglès MN, Dufresne A (2000) Plasticized starch/tunicin whiskers nanocomposites. 1. Structural analysis. Macromolecules 33(22):8344–8353
5. Angulakhsmi N, Thomas S, Nair JR, Bongiovanni R, Gerbaldi C, Stephan AM (2013) Cycling profile of innovative nanochitin-incorporated poly (ethylene oxide) based electrolytes for lithium batteries. J Power Source 228:294–299
6. Araki J (2013) Electrostatic or steric?—preparations and characterizations of well-dispersed systems containing rod-like nanowhiskers of crystalline polysaccharides. Soft Matter 9 (16):4125–4141
7. Araki J, Yamanaka Y, Ohkawa K (2012) Chitin-chitosan nanocomposite gels: reinforcement of chitosan hydrogels with rod-like chitin nanowhiskers. Polym J 44(7):713–717
8. Araujo MA, Cunha AM, Mota M (2004) Enzymatic degradation of starch-based thermoplastic compounds used in protheses: Identification of the degradation products in solution. Biomaterials 25(13):2687–2693
9. Arora A, Padua GW (2010) Review: Nanocomposites in food packaging. J Food Sci 75(1): R43–R49
10. Azizi S, Ahmad MB, Hussein MZ, Ibrahim NA, Namvar F (2014) Prepararion and properties of poly(vinyl alcohol)/chitosan blend bionanocomposites reinforced with cellulose nanocrustais/ZnO-Ag. Int J Nanomed 9:1909–1917
11. Barbosa IVM, Merquior DA, Peixoto FC (2006) Estimation of kinetic and mass-transfer parameters for cellulose nitration. AIChE J 52(10):3549–3554
12. Bensadoun F, Kchit N, Billotte C, Bickerton S, Trochu F, Ruiz E (2011) A study of nanoclay reinforcement of biocomposites made by liquid composite molding. Int J Polym Sci
13. Berger J, Reist M, Mayer JM, Felt O, Peppas NA, Gurny R (2004) Structure and interactions in covalently and ionically crosslinked chitosan hydrogels for biomedical applications. Eur J Pharm Biopharm 57(1):19–34

14. Bhardwaj R, Mohanty AK (2007) Advances in the properties of polylactides based materials: a review. J Biobased Mater Bio 1(2):191–209
15. Branch TA, Abubaker EMN, Mkango S, Butterworth DS (2007) Separating southern blue whale subspecies based on length frequencies of sexually mature females. Mar Mammal Sci 23(4):803–833
16. Buléon A, Colonna P, Planchot V, Ball S (1998) Starch granules: Structure and biosynthesis. Int J Biol Macromol 23(2):85–112
17. Burdock GA (2007) Safety assessment of hydroxypropyl methylcellulose as a food ingredient. Food Chem Toxicol 45(12):2341–2351
18. Buzea C, Pacheco II, Robbie K (2007) Nanomaterials and nanoparticles: sources and toxicity. Biointerphases 2(4):MR17–MR71
19. Campbell IM (2003) Introduction to synthetic polymers. London, Oxford
20. Cartier N, Mazeau K, Domard A, Chanzy H (1992) Single-crystals of chitosan. Adv Chitin Chitosan, 155–164
21. Charreau H, Foresti ML, Vázquez A (2013) Nanocellulose patents trends: a comprehensive review on patents on cellulose nanocrystals, microfibrillated and bacterial cellulose. Recent Pat Nanotec 7(1):56–80
22. Chatrabhuti S, Chirachanchai S (2013) Single step coupling for multi-responsive water-based chitin/chitosan magnetic nanoparticles. Carbohydr Polym 97(2):441–450
23. Chawla P, Ranjan A, Pandey P, Chawla V (2014) Hydrogels: A journey from diapers to gene delivery. Mini-Rev Med Chem 14(2):160–173
24. Chen Y, Dong B, Qin W, Xiao D (2010) Xylose and cellulose fractionation from corncob with three different strategies and separate fermentation of them to bioethanol. Bioresour Technol 101(18):6994–6999
25. De Campos A, Correa A, Cannella D, De M Teixeira E, Marconcini J, Dufresne A, Mattoso LC, Cassland P, Sanadi A (2013) Obtaining nanofibers from curauá and sugarcane bagasse fibers using enzymatic hydrolysis followed by sonication. *Cellulose, 20*(3): 1491-1500
26. Dean J, Dixon B (1992) Advances in Chitin and Chitosan. Elsevier, London
27. Diez-Pascual AM, Naffakh M, Marco C, Ellis G, Gomez-Fatou MA (2012) High-performance nanocomposites based on polyetherketones. Prog Mater Sci 57(7):1106–1190
28. Ding P, Huang KL, Li GY, Zeng WW (2007) Mechanisms and kinetics of chelating reaction between novel chitosan derivatives and Zn(II). J Hazard Mater 146(1–2):58–64
29. Dufresne A (2008) Polysaccharide nano crystal reinforced nanocomposites. Canad J Chem 86(6):484–494
30. Dufresne A (2010) Processing of polymer nanocomposites reinforced with polysaccharide nanocrystals. Molecules 15(6):4111–4128
31. Dufresne A (2012) Processing of polymer nanocomposites reinforced with cellulose nanocrystals: a challenge. Int Polym Proc 27(5):557–564
32. Dugan JM, Gough JE, Eichhorn SJ (2013) Bacterial cellulose scaffolds and cellulose nanowhiskers for tissue engineering. Nanomedicine 8(2):287–298
33. Durán N, Lemes AP, Seabra AB (2012) Review of cellulose nanocrystals patents: preparation, composites and general applications. Recent Pat Nanotechnol 6:16–28
34. Eichhorn SJ (2011) Cellulose nanowhiskers: promising materials for advanced applications. Soft Matter 7(2):303–315
35. Fajardo AR, Lopes LC, Rubira AF, Muniz EC (2012) Development and application of chitosan/poly(vinyl alcohol) films for removal and recovery of Pb(II). Chem Eng J 183:253–260
36. Fajardo AR, Piai JF, Rubira AF, Muniz EC (2010) Time- and pH-dependent self-rearrangement of a swollen polymer network based on polyelectrolytes complexes of chitosan/chondroitin sulfate. Carbohydr Polym 80(3):934–943
37. Fan J-S, Li Y-H (2012) Maximizing the yield of nanocrystalline cellulose from cotton pulp fiber. Carbohydr Polym 88(4):1184–1188

38. Fan Y, Fukuzumi H, Saito T, Isogai A (2012) Comparative characterization of aqueous dispersions and cast films of different chitin nanowhiskers/nanofibers. Int J Biol Macromol 50(1):69–76
39. Fan Y, Saito T, Isogai A (2007) Chitin nanocrystals prepared by TEMPO-mediated oxidation of α-chitin. Biomacromolecules 9(1):192–198
40. Fan Y, Saito T, Isogai A (2010) Individual chitin nano-whiskers prepared from partially deacetylated α-chitin by fibril surface cationization. Carbohydr Polym 79(4):1046–1051
41. Faramarzi MA, Sadighi A (2013) Insights into biogenic and chemical production of inorganic nanomaterials and nanostructures. Adv Colloid Interface Sci 189:1–20
42. Felse PA, Panda T (1999) Studies on applications of chitin and its derivatives. Bioprocess Eng 20(6):505–512
43. Gao YJS, Zhao S, Liao SQ, Fang L, Wang ZF, Li LF (2014) Reinforcement of natural rubber latex film by starch nanocrystal. Appl Mech Mater 543–547:3886–3891
44. Garcia De Rodriguez NL, Thielemans W, Dufresne A (2006) Sisal cellulose whiskers reinforced polyvinyl acetate nanocomposites. Cellulose 13(3):261–270
45. George J, Ramana KV, Bawa AS, Siddaramaiah (2011) Bacterial cellulose nanocrystals exhibiting high thermal stability and their polymer nanocomposites. Int J Biol Macromol 48 (1):50–57
46. Ghorbel-Bellaaj O, Jellouli K, Younes I, Manni L, Ouled Salem M, Nasri M (2011) A solvent-stable metalloprotease produced by pseudomonas aeruginosa grown on shrimp shell waste and its application in chitin extraction. Appl Biochem Biotechnol 164(4):410–425
47. Gonzalez-Renteria SM, Soto-Cruz NO, Rutiaga-Quinones OM, Medrano-Roldan H, Rutiaga-Quinones JG, Lopez-Miranda J (2011) Optimization of the enzymatic hydrolysis process of four straw bean varieties. Rev Mex Ing Quim 10(1):17–28
48. Gopalan Nair K, Dufresne A (2003) Crab shell chitin whisker reinforced natural rubber nanocomposites. 1 process swelling behavior. Biomacromol 4(3):657–665
49. Guan Y, Zhang B, Bian J, Peng F, Sun R-C (2014) Nanoreinforced hemicellulose-based hydrogels prepared by freeze–thaw treatment. Cellulose 21(3):1709–1721
50. Haaj SB, Thielemans W, Magnin A, Boufi S (2014) Starch nanocrystal stabilized pickering emulsion polymerization for nanocomposites with improved performance. ACS Appl Mater Interface 6(11):8263–8273
51. Habibi Y, Lucia LA, Rojas OJ (2010) Cellulose nanocrystals: chemistry, self-assembly, and applications. Chem Rev 110(6):3479–3500
52. Han J, Lei T, Wu Q (2013) Facile preparation of mouldable polyvinyl alcohol-borax hydrogels reinforced by well-dispersed cellulose nanoparticles: physical, viscoelastic and mechanical properties. Cellulose 20(6):2947–2958
53. Han J, Lei T, Wu Q (2014) High-water-content mouldable polyvinyl alcohol-borax hydrogels reinforced by well-dispersed cellulose nanoparticles: dynamic rheological properties and hydrogel formation mechanism. Carbohydr Polym 102:306–316
54. Hanemann T, Szabo DV (2010) Polymer-nanoparticle composites: from synthesis to modern applications. Materials 3(6):3468–3517
55. Hariraksapitak P, Supaphol P (2010) Preparation and properties of α-chitin-whisker-reinforced hyaluronan–gelatin nanocomposite scaffolds. J Appl Polym Sci 117(6):3406–3418
56. Heinz TE (2005) Polysaccharides I. Springer, New York
57. Hon DNS (1994) Cellulose—a random-walk along its historical path. Cellulose 1(1):1–25
58. Hovgaard L, Brondsted H (1996) Current applications of polysaccharides in colon targeting. Crit Rev Ther Drug 13(3–4):185–223
59. Hua K, Carlsson DO, Alander E, Lindstrom T, Stromme M, Mihranyan A, Ferraz N (2014) Translational study between structure and biological response of nanocellulose from wood and green alga. RSC Adv 4(6):2892–2903
60. Huang Y, Zhang L, Yang J, Zhang X, Xu M (2013) Structure and properties of cellulose films reinforced by chitin whiskers. Macromol Mater Eng 298(3):303–310

61. Hutchinson JR, Bates KT, Molnar J, Allen V, Makovicky PJ (2011) A computational analysis of limb and body dimensions in *tyrannosaurus rex* with implications for locomotion, ontogeny, and growth. PLoS One 6(10):E26037
62. Ifuku S, Saimoto H (2012) Chitin nanofibers: preparations, modifications, and applications. Nanoscale 4(11):3308–3318
63. Isogai A (2013) Wood nanocelluloses: fundamentals and applications as new bio-based nanomaterials. J Wood Sci 59(6):449–459
64. Isogai A, Saito T, Fukuzumi H (2011) TEMPO-oxidized cellulose nanofibers. Nanoscale 3 (1):71–85
65. Jayakumar R, Menon D, Manzoor K, Nair SV, Tamura H (2010) Biomedical applications of chitin and chitosan based nanomaterials-a short review. Carbohydr Polym 82(2):227–232
66. Jin L, Wei Y, Xu Q, Yao W, Cheng Z (2014) Cellulose nanofibers prepared from TEMPO-oxidation of kraft pulp and its flocculation effect on kaolin clay. J Appl Polym Sci 131 (12):2345–2353
67. Kabiri K, Omidian H, Zohuriaan-Mehr MJ, Doroudiani S (2011) Superabsorbent hydrogel composites and nanocomposites: a review. Polym Composite 32(2):277–289
68. Kalia S, Dufresne A, Cherian BM, Kaith BS, Averous L, Njuguna J, Nassiopoulos E (2011) Cellulose-based bio- and nanocomposites: a review. Int J Polym Sci, ID 837875
69. Karimi S, Dufresne A, Tahir PM, Karimi A, Abdulkhani A (2014) Biodegradable starch-based composites: effect of micro and nanoreinforcements on composite properties. J Mater Sci 49(13):4513–4521
70. Karmazsin E (1987) Thermal-analysis in the cellulose, paper and textile-industry. Thermochim Acta 110:471–475
71. Kaushik A, Kumra J (2014) Morphology, thermal and barrier properties of green nanocomposites based on tps and cellulose nanocrystals. J Elastom Plast 46(3):284–299
72. Kelly JA, Shukaliak AM, Cheung CCY, Shopsowitz KE, Hamad WY, Maclachlan MJ (2013) Responsive photonic hydrogels based on nanocrystalline cellulose. Ang Chem Int Ed 52(34):8912–8916
73. Kerstens S, Decraemer WF, Verbelen J-P (2001) Cell walls at the plant surface behave mechanically like fiber-reinforced composite materials. Plant Physiol 127(2):381–385
74. Khalil H, Bhat AH, Yusra AFI (2012) Green composites from sustainable cellulose nanofibrils: a review. Carbohydr Polym 87(2):963–979
75. Khan TA, Peh KK, Chíng HS (2002) Reporting degree of deacetylation values of chitosan: The influence of analytical methods. J Pharm Pharm Sci 5(3):205–212
76. Khoushab F, Yamabhai M (2010) Chitin research revisited. Mar Drug 8(7):1988–2012
77. Kjartansson GT, Zivanovic S, Kristbergsson K, Weiss J (2006) Sonication-assisted extraction of chitin from north atlantic shrimps (pandalus borealis). J Agr Food Chem 54(16):5894–5902
78. Klemm D, Heublein B, Fink HP, Bohn A (2005) Cellulose: fascinating biopolymer and sustainable raw material. Angew Chem Int Ed 44(22):3358–3393
79. Klemm DE (2006) Polysaccharides II. Springer, New York
80. Kobayashi S, Kashiwa K, Shimada J, Kawasaki T, Shoda S (1992) Enzymatic polymerization—the 1st invitro synthesis of cellulose via nonbiosynthetic path catalyzed by cellulase. Macromol Symp 54–5:509–518
81. Kono H, Otaka F, Ozaki M (2014) Preparation and characterization of guar gum hydrogels as carrier materials for controlled protein drug delivery. Carbohydr Polym 111:830–840
82. Kuilla T, Bhadra S, Yao DH, Kim NH, Bose S, Lee JH (2010) Recent advances in graphene based polym composite. Prog Polym Sci 35(11):1350–1375
83. Kurita K (2006) Chitin and chitosan: Functional biopolymers from marine crustaceans. Mar Biotechnol 8(3):203–226
84. Laftah WA, Hashim S, Ibrahim AN (2011) Polymer hydrogels: a review. Polym Plast Technol 50(14):1475–1486

85. Lagerwall JPF, Schutz C, Salajkova M, Noh J, Hyun Park J, Scalia G, Bergstrom L (2014) Cellulose nanocrystal-based materials: from liquid crystal self-assembly and glass formation to multifunctional thin films. NPG Asia Mater 6:E80
86. Lam E, Male KB, Chong JH, Leung ACW, Luong JHT (2012) Applications of functionalized and nanoparticle-modified nanocrystalline cellulose. Trend Biotechnol 30(5):283–290
87. LeCorre D, Bras J, Dufresne A (2010) Starch nanoparticles: a review. Biomacromolecules 11 (5):1139–1153
88. LeCorre D, Bras J, Dufresne A (2011) Influence of botanic origin and amylose content on the morphology of starch nanocrystals. J Nanopart Res 13(12):7193–7208
89. LeCorre D, Vahanian E, Dufresne A, Bras J (2011) Enzymatic pretreatment for preparing starch nanocrystals. Biomacromolecules 13(1):132–137
90. LeCorre D, Bras J, Dufresne A (2012) Influence of native starch's properties on starch nanocrystals thermal properties. Carbohydr Polym 87(1):658–666
91. Lee KY, Mooney DJ (2001) Hydrogels for tissue engineering. Chem Rev 101(7):1869–1880
92. Li C, Li Y, Sun P, Yang C (2014) Starch nanocrystals as particle stabilisers of oil-in-water emulsions. J Sci Food Agr 94(9):1802–1807
93. Li C, Sun P, Yang C (2012) Emulsion stabilized by starch nanocrystals. Starch Stärke 64 (6):497–502
94. Li J, Revol JF, Naranjo E, Marchessault RH (1996) Effect of electrostatic interaction on phase separation behaviour of chitin crystallite suspensions. Int J Biol Macromol 18(3): 177–187
95. Li Y, Yang C, Khan M, Liu S, Hedrick JL, Yang Y-Y, Ee P-LR (2012) Nanostructured PEG-based hydrogels with tunable physical properties for gene delivery to human mesenchymal stem cells. Biomaterials 33(27):6533–6541
96. Lin N, Huang J, Chang PR, Anderson DP, Yu JH (2011) Preparation, modification, and application of starch nanocrystals in nanomaterials. a review. J Nanomater
97. Lin M-F, Thakur VK, Tan EJ, Lee PS (2011) Dopant induced hollow $BaTiO_3$ nanostructures for application in high performance capacitors. J Mater Chem 21:16500–16504
98. Lin M-F, Thakur VK, Tan EJ, Lee PS (2011) Surface functionalization of $BaTiO_3$ nanoparticles and improved electrical properties of $BaTiO_3$/polyvinylidene fluoride composite. RSC Adv 1:576–578
99. Lin N, Huang J, Chang PR, Feng L, Yu J (2011) Effect of polysaccharide nanocrystals on structure, properties, and drug release kinetics of alginate-based microspheres. Colloid Surf B 85(2):270–279
100. Ling SJ, Li CX, Adamcik J, Wang SH, Shao ZZ, Chen X, Mezzenga R (2014) Directed growth of silk nanofibrils on graphene and their hybrid nanocomposites. Acs Macro Lett 3 (2):146–152
101. Liu D, Zhang Y, Sun X, Chang PR (2014) Recent advances in bio-sourced polymeric carbohydrate/nanotube composites. J Appl Polym Sci 131(12)
102. Lu P, Hsieh Y-L (2012) Cellulose isolation and core–shell nanostructures of cellulose nanocrystals from chardonnay grape skins. Carbohydr Polym 87(4):2546–2553
103. Lu Y, Weng L, Zhang L (2004) Morphology and properties of soy protein isolate thermoplastics reinforced with chitin whiskers. Biomacromolecules 5(3):1046–1051
104. Ly B, Thielemans W, Dufresne A, Chaussy D, Belgacem MN (2008) Functionalization of cellulose fiber and their incorporation in renewable polymeric matrices. Compos Sci Technol 68:3193–3201
105. Magdy EE (2011) Biotechnology of biopolymers. Intechem, Rjeka, Croatia
106. Majeed K, Jawaid M, Hassan A, Abu Bakar A, Khalil H, Salema AA, Inuwa I (2013) Potential materials for food packaging from nanoclay/natural fibres filled hybrid composites. Mater Des 46:391–410
107. Malafaya PB, Elvira C, Gallardo A, San Roman J, Reis RL (2001) Porous starch-based drug delivery systems processed by a microwave route. J Biomater Sci Polym Ed 12(11): 1227–1241
108. Mano E (1989) Introdução à polímeros. Edgar Blucher, São Paulo

109. Mariano M, El Kissi N, Dufresne A (2014) Cellulose nanocrystals and related nanocomposites: review of some properties and challenges. J Polym Sci B Polym Phys 52 (12):791–806
110. Mckee JR, Appel EA, Seitsonen J, Kontturi E, Scherman OA, Ikkala O (2014) Healable, stable and stiff hydrogels: Combining conflicting properties using dynamic and selective three-component recognition with reinforcing cellulose nanorods. Adv Funct Mater 24 (18):2706–2713
111. Mckee JR, Hietala S, Seitsonen J, Laine J, Kontturi E, Ikkala O (2014) Thermoresponsive nanocellulose hydrogels with tunable mechanical properties. ACS Macro Lett 3(3):266–270
112. MéLé P, Angellier-Coussy HLN, Molina-Boisseau S, Dufresne A (2011) Reinforcing mechanisms of starch nanocrystals in a nonvulcanized natural rubber matrix. Biomacromolecules 12(5):1487–1493
113. Miguel SP, Ribeiro MP, Brancal H, Coutinho P, Correia IJ (2014) Thermoresponsive chitosan–agarose hydrogel for skin regeneration. Carbohydr Polym 111:366–373
114. Mincea M, Negrulescu A, Ostafe V (2012) Preparation, modification, and applications of chitin nanowhiskers: a review. Rev Adv Mater Sci 30(3):225–242
115. Morais JPS, Rosa MDF, De Souza Filho MDSM, Nascimento LD, Do Nascimento DM, Cassales AR (2013) Extraction and characterization of nanocellulose structures from raw cotton linter. Carbohydr Polym 91(1):229–235
116. Mueller S, Weder C, Foster EJ (2014) Isolation of cellulose nanocrystals from pseudostems of banana plants. RSC Adv 4(2):907–915
117. Murphy P, Mitchell JR, Starch (2000) Handbook of Hydrocolloids. Woodhead Publishing, UK
118. Muzzarelli RAA (2011) Biomedical exploitation of chitin and chitosan via mechano-chemical disassembly, electrospinning, dissolution in imidazolium ionic liquids, and supercritical drying. Mar Drug 9(9):1510–1533
119. Naffakh M, Diez-Pascual AM, Marco C, Ellis GJ, Gomez-Fatou MA (2013) Opportunities and challenges in the use of inorganic fullerene-like nanoparticles to produce advanced polymer nanocomposites. Prog Polym Sci 38(8):1163–1231
120. Narjary B, Aggarwal P (2014) Evaluation of soil physical quality under amendments and hydrogel applications in a soybean–wheat cropping system. Commun Soil Sci Plan 45 (9):1167–1180
121. Nishiyama Y, Langan P, Chanzy H (2002) Crystal structure and hydrogen-bonding system in cellulose 1 beta from synchrotron x-ray and neutron fiber diffraction. J Amer Chem Soc 124 (31):9074–9082
122. Nishiyama Y, Sugiyama J, Chanzy H, Langan P (2003) Crystal structure and hydrogen bonding system in cellulose 1(alpha), from synchrotron x-ray and neutron fiber diffraction. J Amer Chem Soc 125(47):14300–14306
123. Nizam El-Din HM (2012) Surface coating on cotton fabrics of new multilayer formulations based on superabsorbent hydrogels synthesized by gamma radiation designed for diapers. J Appl Polym Sci 125(S2):E180–E186
124. Northcote DH (1972) Chemistry of the plant cell wall. Annu Rev Plant Physiol 23(1):113–132
125. Oates CG (1997) Towards an understanding of starch granule structure and hydrolysis. Trend Food Sci Technol 8(11):375–382
126. Okamoto M, John B (2013) Synthetic biopolymer nanocomposites for tissue engineering scaffolds. Prog Polym Sci 38(10–11):1487–1503
127. Oksman K, Etang JA, Mathew AP, Jonoobi M (2011) Cellulose nanowhiskers separated from a bio-residue from wood bioethanol production. Biomass Bioenergy 35(1):146–152
128. Omidian H, Rocca JG, Park K (2005) Advances in superporous hydrogels. J Control Release 102(1):3–12
129. Osorio-Madrazo A, Eder M, Rueggeberg M, Pandey JK, Harrington MJ, Nishiyama Y, Putaux J-L, Rochas C, Burgert I (2012) Reorientation of cellulose nanowhiskers in agarose hydrogels under tensile loading. Biomacromolecules 13(3):850–856

130. Paillet M, Dufresne A (2001) Chitin whisker reinforced thermoplastic nanocomposites. Macromolecules 34(19):6527–6530
131. Park S, Baker JO, Himmel ME, Parilla PA, Johnson DK (2010) Cellulose crystallinity index: measurement techniques and their impact on interpreting cellulase performance. Biotechnol Biofuel 3
132. Peng BL, Dhar N, Liu HL, Tam KC (2011) Chemistry and application of nanocrystalline cellulose and its derivates: a nanotechnology perspective. Can J Chem Eng 9999:1–16
133. Peppas NA, Bures P, Leobandung W, Ichikawa H (2000) Hydrogels in pharmaceutical formulations. Eur J Pharm Biopharm 50(1):27–46
134. Pereira AGB, Muniz EC, Hsieh Y-L (2014) Chitosan-sheath and chitin-core nanowhiskers. Carbohydr Polym 107:158–166
135. Perez S, Samain D (2010) Structure and engineering of celluloses. Adv Carbohydr Chem Biochem 64(64):25–116
136. Phua YJ, Lau NS, Sudesh K, Chow WS, Ishak ZAM (2012) Biodegradability studies of poly (butylene succinate)/organo-montmorillonite nanocomposites under controlled compost soil conditions: Effects of clay loading and compatibiliser. Polym Degrad Stabil 97(8):1345–1354
137. Pillai CKS, Paul W, Sharma CP (2009) Chitin and chitosan polymers: Chemistry, solubility and fiber formation. Prog Polym Sci 34(7):641–678
138. Raabe D, Sachs C, Romano P (2005) The crustacean exoskeleton as an example of a structurally and mechanically graded biological nanocomposite material. Acta Mater 53 (15):4281–4292
139. Rahman MM, Afrin S, Haque P, Islam MM, Islam MS, Gafur MA (2014) Preparation and characterization of jute cellulose crystals-reinforced poly(l-lactic acid) biocomposite for biomedical applications. Int J Chem Eng 7
140. Rajisha KR, Maria HJ, Pothan LA, Ahmad Z, Thomas S (2014) Preparation and characterization of potato starch nanocrystal reinforced natural rubber nanocomposites. Int J Biol Macromol 67:147–153
141. Reddy MM, Vivekanandhan S, Misra M, Bhatia SK, Mohanty AK (2013) Biobased plastics and bionanocomposites: current status and future opportunities. Prog Polym Sci 38(10–11):1653–1689
142. Rehman N, De Miranda M, Rosa SL, Pimentel D, Nachtigall SB, Bica CD (2014) Cellulose and nanocellulose from maize straw: an insight on the crystal properties. J Polym Environ 22 (2):252–259
143. Revedin A, Aranguren B, Becattini R, Longo L, Marconi E, Lippi MM, Skakun N, Sinitsyn A, Spiridonova E, Svoboda J (2010) Thirty thousand-year-old evidence of plant food processing. P Natl Acda Sci USA 107(44):18815–18819
144. Revol JF, Marchessault RH (1993) In vitro chiral nematic ordering of chitin crystallites. Int J Biol Macromol 15(6):329–335
145. Rey C, Combes C, Drouet C, Glimcher MJ (2009) Bone mineral: update on chemical composition and structure. Osteoporosis Inter 20(6):1013–1021
146. Rinaudo M (2006) Chitin and chitosan: properties and applications. Prog Polym Sci 31 (7):603–632
147. Rittmeyer EN, Allison A, Gründler MC, Thompson DK, Austin CC (2012) Ecological guild evolution and the discovery of the world's smallest vertebrate. PLoS One 7(1):E29797
148. Rodrigues FHA, Spagnol C, Pereira AGB, Martins AF, Fajardo AR, Rubira AF, Muniz EC (2014) Superabsorbent hydrogel composites with a focus on hydrogels containing nanofibers or nanowhiskers of cellulose and chitin. J Appl Polym Sci 131(2):1323–1329
149. Rowell RM (2005) Handbook of wood chemistry and wood composites. CRC Press, Taylor and Francis, Boca Raton
150. Rudall KM, Kenching W (1973) Chitin system. Biol Rev Camb Philos Soc 48(4):597–605
151. Sagheer FAA, Al-Sughayer MA, Muslim S, Elsabee MZ (2009) Extraction and characterization of chitin and chitosan from marine sources in arabian gulf. Carbohydr Polym 77(2):410–419

152. Samir M, Alloin F, Dufresne A (2005) Review of recent research into cellulosic whiskers, their properties and their application in nanocomposite field. Biomacromolecules 6(2): 612–626
153. Singha AS, Thakur VK (2008) Effect of fibre loading on urea-formaldehyde matrix based green composites. Iran Polym J 17(11):861–873
154. Singha AS, Thakur VK (2010) Mechanical, morphological, and thermal characterization of compression-molded polymer biocomposites. Int J Polym Anal Ch 15(2):87–91
155. Singha AS, Thakur VK (2010) Synthesis, chacterization, and sutyd of pine needles reinforced polymer matrix based composites. J Rein Plast Comp 29(5):700–709
156. Sionkowska A (2011) Current research on the blends of natural and synthetic polymers as new biomaterials: review. Prog Polym Sci 36(9):1254–1276
157. Siqueira G, Bras J, Dufresne A (2008) Cellulose whiskers versus microfibrils: influence of the nature of the nanoparticle and its surface functionalization on the thermal and mechanical properties of nanocomposites. Biomacromolecules 10(2):425–432
158. Siqueira G, Bras J, Dufresne A (2010) Cellulosic bionanocomposites: a review of preparation, properties and applications. Polymers 2(4):728–765
159. Slavutsky AM, Bertuzzi MA (2014) Water barrier properties of starch films reinforced with cellulose nanocrystals obtained from sugarcane bagasse. Carbohydr Polym 110:53–61
160. Spagnol C, Rodrigues FHA, Neto AGVC, Pereira AGB, Fajardo AR, Radovanovic E, Rubira AF, Muniz EC (2012) Nanocomposites based on poly(acrylamide-co-acrylate) and cellulose nanowhiskers. Eur Polym J 48(3):454–463
161. Spagnol C, Rodrigues FA, Pereira AB, Fajardo A, Rubira A, Muniz E (2012) Superabsorbent hydrogel nanocomposites based on starch-g-poly(sodium acrylate) matrix filled with cellulose nanowhiskers. Cellulose 19(4):1225–1237
162. Spagnol C, Rodrigues FHA, Pereira AGB, Fajardo AR, Rubira AF, Muniz EC (2012) Superabsorbent hydrogel composite made of cellulose nanofibrils and chitosan-graft-poly (acrylic acid). Carbohydr Polym 87(3):2038–2045
163. Swift G (1994) Water-soluble polymers. Polym Degrad Stabil 45(2):215–231
164. Taylor NG (2008) Cellulose biosynthesis and deposition in higher plants. New Phytol 178 (2):239–252
165. Thakur VK, Yan J, Lin M-F et al (2012) Novel polymer nanocomposites from bioinspired green aqueous functionalization of BNNTs. Polym Chem 3:962–969
166. Thakur VK, Singha AS, Thakur MK (2012) Graft copolymerization of methyl acrylate onto cellulosic biofibers: synthesis, characterization and applications. J Polym Environ 20: 164–174
167. Thakur VK, Singha AS, Thakur MK (2012) Modification of Natural Biomass by Graft Copolymerization. Int J Polym Anal Charact 17:547–555
168. Thakur VK, Singha AS, Thakur MK (2012) Green composites from natural fibers: mechanical and chemical aging properties. Int J Polym Anal Charact 17:401–407
169. Thakur VK, Singha AS, Thakur MK (2012) In-air graft copolymerization of ethyl acrylate onto natural cellulosic polymers. Int J Polym Anal Charact 17:48–60
170. Thakur VK, Singha AS, Thakur MK (2012) Surface modification of natural polymers to impart low water absorbency. Int J Polym Anal Charact 17:133–143
171. Teixeira EDM, Bondancia TJ, Teodoro KBR, Corrêa AC, Marconcini JM, Mattoso LHC (2011) Sugarcane bagasse whiskers: extraction and characterizations. Ind Crop Prod 33 (1):63–66
172. Thakkar KN, Mhatre SS, Parik RY (2010) Biological synthesis of metallic nanoparticles. Nanomed Nanotech Biol Med 6:257–262
173. Thakur VK, Singha AS, Thakur MK (2013) Natural cellulosic polymers as potential reinforcement in composites: physicochemical and mechanical studies. Adv Polym Technol 32:E427–E435
174. Thakur VK, Singha AS, Thakur MK (2013) Fabrication and physico-chemical properties of high-performance pine needles/green polymer composites. Int J Polym Mater Polym Biomater 62:226–230

175. Thakur VK, Singha AS, Thakur MK (2013) Ecofriendly biocomposites from natural fibers: mechanical and weathering study. Int J Polym Anal Charact 18:64–72
176. Thakur VK, Thakur MK, Gupta RK (2013) Synthesis of lignocellulosic polymer with improved chemical resistance through free radical polymerization. Int J Biol Macromol 61:121–126
177. Thakur VK, Thakur MK, Gupta RK (2013) Development of functionalized cellulosic biopolymers by graft copolymerization. Int J Biol Macromol 62:44–51
178. Thakur VK, Singha AS, Mehta JK (2014) Renewable resource based green polymer composite: analysis and characterization. Int J Anal Ch 15(3):137–146
179. Thakur VK, Thakur MK, Gupta RK (2014) Graft copolmers of natural fibers for green composite. Carbohydr Polym 104(1):87–93
180. Thakur VK, Thakur MK, Reghavan P, Kessler MR (2014) Progress in green polymer from lignin of multifunctional application. ACS Sustain Chem Eng 2(5):1072–1092
181. Thakur VK, Thakur MK (2014) Recent advances in graft copolymerization and applications of chitosan: a review. ACS Sustain Chem Eng 2:2637–2652
182. Thakur VK, Thakur MK (2014) Recent trends in hydrogels based on psyllium polysaccharide: a review. J Clean Prod 82:1–15
183. Thakur VK, Thakur MK (2014) Processing and characterization of natural cellulose fibers/thermoset polymer composites. Carbohydr Polym 109:102–117
184. Tou ZQ, Koh TW, Chan CC (2014) Poly(Vinyl Alcohol) hydrogel based fiber interferometer sensor for heavy metal cations. Sensor Actuat B Chem 202:185–193
185. Uddin AJ, Fujie M, Sembo S, Gotoh Y (2012) Outstanding reinforcing effect of highly oriented chitin whiskers in PVA nanocomposites. Carbohydr Polym 87(1):799–805
186. Van De Velde K, Kiekens P (2002) Biopolymers: overview of several properties and consequences on their applications. Polym Test 21(4):433–442
187. Vincent JFV (2002) Arthropod cuticle: A natural composite shell system. Compos Part A Appl S 33(10):1311–1315
188. Visakh PM, Thomas S, Oksman K, Mathew AP (2012) Crosslinked natural rubber nanocomposites reinforced with cellulose whiskers isolated from bamboo waste: processing and mechanical/thermal properties. Compos Part-A Appl S 43(4):735–741
189. Wang DX, Yu J, Zhang JM, He JS, Zhang J (2013) Transparent bionanocomposites with improved properties from poly(propylene carbonate) (PPC) and cellulose nanowhiskers (Cnws). Compos Sci Technol 85:83–89
190. Wang H, Zhu E, Yang J, Zhou P, Sun D, Tang W (2012) Bacterial cellulose nanofiber-supported polyaniline nanocomposites with flake-shaped morphology as supercapacitor electrodes. J Phys Chem C 116(24):13013–13019
191. Wang Q, Zhu L (2011) Polymer nanocomposites for electrical energy storage. J Polym Sci Part B Polym Phys 49(20):1421–1429
192. Watthanaphanit A, Supaphol P, Tamura H, Tokura S, Rujiravanit R (2008) Fabrication, structure, and properties of chitin whisker-reinforced alginate nanocomposite fibers. J Appl Polym Sci 110(2):890–899
193. Wongpanit P, Sanchavanakit N, Pavasant P, Bunaprasert T, Tabata Y, Rujiravanit R (2007) Preparation and characterization of chitin whisker-reinforced silk fibroin nanocomposite sponges. Eur Polym J 43(10):4123–4135
194. Wu Q, Meng Y, Wang S, Li Y, Fu S, Ma L, Harper D (2014) Rheological behavior of cellulose nanocrystal suspension: influence of concentration and aspect ratio. J Appl Polym Sci 131(15):898–912
195. Xu X, Liu F, Jiang L, Zhu JY, Haagenson D, Wiesenborn DP (2013) Cellulose nanocrystals vs cellulose nanofibrils: a comparative study on their microstructures and effects as polymer reinforcing agents. ACS Appl Mater Interface s 5(8):2999–3009
196. Yamamoto Y, Nishimura T, Saito T, Kato T (2010) CaCO3/Chitin-whisker hybrids: formation of CaCO3 crystals in chitin-based liquid-crystalline Suspension. Polym J 42 (7):583–586

197. Yang J, Han C-R, Duan J-F, Xu F, Sun R-C (2013) Mechanical and viscoelastic properties of cellulose nanocrystals reinforced poly(ethylene glycol) nanocomposite hydrogels. ACS Appl Mater Interface 5(8):3199–3207
198. Yang J, Zhao J-J, Xu F, Sun R-C (2013) Revealing strong nanocomposite hydrogels reinforced by cellulose nanocrystals: insight into morphologies and interactions. ACS Appl Mater Interface 5(24):12960–12967
199. Zanetti M, Lomakin S, Camino G (2000) Polymer layered silicate nanocomposites. Macromol Mater Eng 279(6):1–9
200. Zeng J-B, He Y-S, Li S-L, Wang Y-Z (2011) Chitin whiskers: an overview. Biomacromolecules 13(1):1–11
201. Zhang JF, Sun XZ (2004) Mechanical properties of poly(lactic acid)/starch composites compatibilized by maleic anhydride. Biomacromolecules 5(4):1446–1451
202. Zhang X, Huang J, Chang PR, Li J, Chen Y, Wang D, Yu J, Chen J (2010) Structure and properties of polysaccharide nanocrystal-doped supramolecular hydrogels based on cyclodextrin inclusion. Polymer 51(19):4398–4407
203. Zhao JQ, He X, Wang YR, Zhang W, Zhang XX, Zhang XD, Deng YL, Lu CH (2014) Reinforcement of all-cellulose nanocomposite films using native cellulose nanofibrils. Carbohydr Polym 104:143–150
204. Zhao R, Torley P, Halley PJ (2008) Emerging biodegradable materials: starch- and protein-based bio-nanocomposites. J Mater Sci 43(9):3058–3071
205. Zheng S, Shin JY, Song SY, Yu SJ, Suh H, Kim I (2014) Hexafunctional poly(propylene glycol) based hydrogels for the removal of heavy metal ions. J Appl Polym Sci 131 (16):1987–1996

Fabrication, Property, and Application of Lignin-Based Nanocomposites

Xiaoying Wang, Guocheng Han, Zuguang Shen and Runcang Sun

Abstract Lignin, the second most abundant natural polymer, has shown its immense potential as sustainable resources for the synthesis of nanocomposites. This chapter reviewed recent developments related to lignin-based nanocomposites, including the fabrication, properties, and applications of nanocomposites based on lignin and its derivatives. We introduced nanocomposites combining physical and chemical properties of lignin and organic materials such as biopolymer and synthetic polymer, and we discussed lignin-based metallic nanocomposites with preferable property and catalytic performance. Furthermore, lignin-based carbonaceous nanocomposites exhibiting enhanced electrical properties were illustrated. Other lignin-based nanocomposites were also presented in this chapter.

Keywords Lignin · Polymer · Metallic · Carbonaceous · Nanocomposites

1 Introduction

Cellulose, hemicellulose, and lignin, the most common natural polymers from plants, are always one of the research emphases in eco-friendly polymer science and nanotechnology [113]. Materials and nanocomposites based on cellulose, hemicellulose, chitosan, and natural fibers have attracted interest of scientist during the recent years [97–99, 101], resulting in eco-friendly natural polymer-based composites with outstanding properties combination [94, 95, 100]. To make the best use

X. Wang · G. Han · Z. Shen · R. Sun (✉)
State Key Laboratory of Pulp and Paper Engineering, South China University of Technology, Guangzhou 510640, China
e-mail: ynsun@scut.edu.cn

R. Sun
China Beijing Key Laboratory of Lignocellulosic Chemistry, Beijing Forestry University, Beijing 100083, China

V.K. Thakur and M.K. Thakur (eds.), *Eco-friendly Polymer Nanocomposites*, Advanced Structured Materials 74, DOI 10.1007/978-81-322-2473-0_3

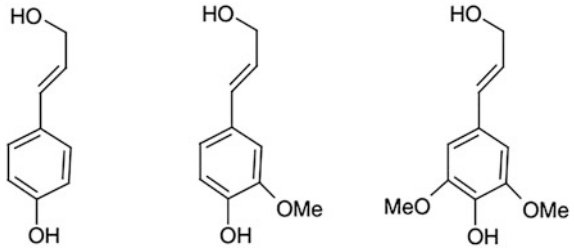

Fig. 1 Three monomer species of lignin: *p*-coumaryl alcohol, coniferyl alcohol, and sinapyl alcohol [81] (Reprinted with permission from John Wiley & Sons, Inc. Copyright (2009), Blackwell Publishing Ltd)

of plant fiber resource effectively and efficiently, lignin is drawing more and more attention in recent years.

The term "lignin", from the Latin word *lignum*, meaning "wood", is used by the Swiss botanist Candolle for the first time [30]. Lignin is next to cellulose the second largest natural polymer [33] as well as the largest aromatic polymer in nature [69].

The plant species determines the lignin composition and ratio. Studies of lignin structure reveal that lignin is a natural polymeric compound made of dehydrogenative polymerization of three monomer species, namely p-coumaryl alcohol, coniferyl alcohol, and sinapyl alcohol (Fig. 1). Furthermore, lignin can be divided into hard wood lignin, soft wood lignin, and grass lignin, depending on the structural units of lignin from various kinds of plants [2, 88]. Since the structure of lignin is so complicated that people are still on the way to figure it out, there is no exact molecular structure of lignin.

The amounts and proportions of main functional reactive groups such as hydroxyl, methoxyl, carboxyl, and carbonyl groups in lignin vary from the plant species and extraction processes applied [32]. Several commercial lignins based on different procedures of extraction and isolation results in wide range of molecular masses and diverse chemical and physical functionalities, making them available for various applications [30].

Currently, the lignin or lignin-derived products all over the world has exceeded 50 million tons per year [12]. However, the majority of lignin is used as fuels or other low-value applications such as activated carbon, dispersants, and adhesive agents [33]. As it is estimated that about one-third of all carbon in nature can be attributed to lignin [37], lignin is a promising sustainable resource which can provide us ample chances to develop high technology or high-value applications in future. Additionally, from the viewpoint of the complexity of lignin structure and reactivity, it is reasonable to prepare high-value polymer materials with lignin as raw resource [102]. Many studies have drawn attention to the fabrication and application of lignin-based nanocomposites, opening new directions and ways for the further studies of lignin and even other biomass resource.

In this chapter, we reviewed the fabrication, properties, and applications of nanocomposites based on lignin and its derivatives, including lignin-biopolymer

nanocomposites, lignin-synthetic polymer nanocomposites, lignin-based metallic nanocomposites, lignin-based carbonaceous material nanocomposites, and so on.

2 Lignin-Biopolymer Nanocomposites

Natural biopolymer-based nanocomposites have received great attention due to their outstanding properties: renewable origin, low cost, facile processability, high specific strength, lower density than inorganic-reinforce composites, energy saving, and recycling possibility [52, 83].

2.1 Lignin-Polysaccharides Nanocomposites

In recent years, eco-friendly nanocomposite films based on biopolymers have been used for membrane productions [79]. Cellulose and lignins are two potential natural materials that can prepare nanocomposites films with considerable properties [38]. Cellulose films have received widespread attention as nanocomposite films with high-performance and have little influence on environment [77]. Owing to their thermoplastic character, cellulosic ester is one of major commercial cellulose derivatives for preparing organic membranes. However, some of these cellulose films have several disadvantages such as low mechanical strength as well as poor resistance to oxidation [6]. To overcome these limits and enhance the compatibility, from the chemical viewpoint, it is advantageous to use lignin as fillers of cellulose derivatives.

Nevárez et al. prepared biopolymer-based nanocomposite films using cellulose triacetate (CTA) as polymer matrix and lignin as filler [79]. Organosolv, hydrolytic, and kraft lignin particles were incorporated with CTA. Vapor-induced phase separation was used in fabricating the self-supported films, during which the temperature and relative humidity were controlled. Among the three raw lignins studied, nanocomposites films based on acetylated organosolv lignin was the best, and acetylation of lignin provided substantial improvement in homogeneity.

Using the same vapor-induced phase separation method, Nevárez et al. prepared another nanocomposite films from propionated lignin and CTA [80]. The kind of CTA-lignin nanocomposite has impact on film performances, while propionation of lignin was higher, the wettability and fluxes of nanocomposites were lower. The prepared nanocomposite films were used to purify groundwater containing high concentrations of F, Ca, As, Na, and Mg as filter. The nanocomposites film can filter 15–35 % of anions, 12–42 % of monovalent cations and 27–54 % of divalent cations, respectively.

Ago et al. reported a defect-free electrospun nanofibers and thin films in lignin/poly (vinyl alcohol) aqueous dispersions, using the cellulose nanocrystals (CNCs) as reinforcing solid phase [4]. As shown in Fig. 2, on the surface of as-prepared nanocomposites film, it can be observed that the amounts of CNCs increased when increase the loading, and the increase approximately followed a simple mixing rule.

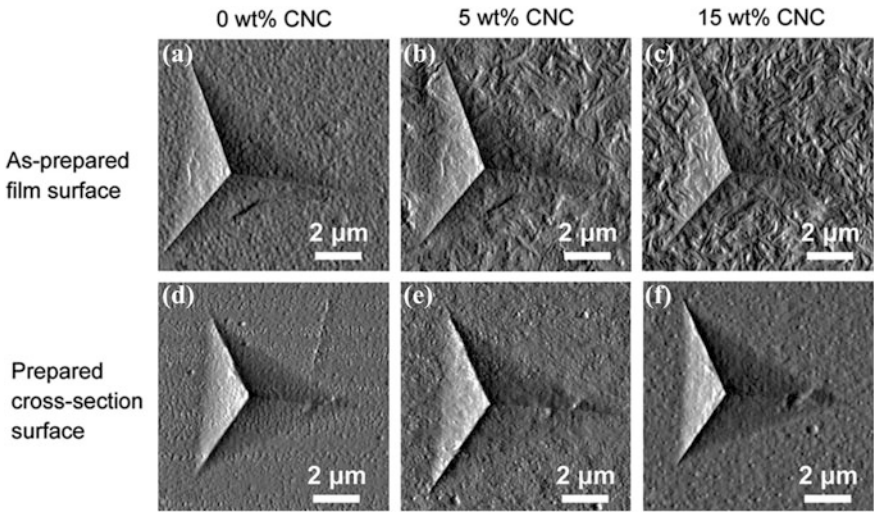

Fig. 2 AFM images of residual 9.5 mN indent impressions in 75:25 lignin:PVA spin-coated films on the as-prepared film surface (**a**–**c**) and the surface prepared in cross section (**d**–**f**) with 0 wt% CNCs (**a**, **d**), 5 wt% CNCs (**b**, **e**) and 15 wt% CNCs (**c**, **f**) (Reprinted with permission from Ago et al. [4]. Copyright (2013), American Chemical Society)

For nanoindents in cross section, the spin-coated cross section was more closely related to electrospun fiber mat than as-prepared film surface. The addition of CNCs further improved interaction of molecules and showed the ability to stabilize the nanocomposites against water absorption.

Hambardzumyan and co-workers prepared nanocomposite coatings based on synthetic/fractionated lignin and CNCs without chemical modification or functionalization of the raw materials [38]. There were nodules of lignin dispersed in the matrix of cellulose, which make films smooth and homogeneous. Noteworthily, the specific surface area of CNCs increases with the introduction of nanoparticles, and as a result, the lignin molecules could be better dispersed throughout the nanocomposite film. These nanocomposite coatings exhibited high transmittance in the range of visible spectrum, high-performance optical properties, as well as a high blocking in the UV spectrum under proper weight ratio of lignin to CNC.

Chitosan, another abundant polysaccharide with good biocompatibility biodegradability and multiple functionalities, has been widely studied in many fields such as water treatment, biosensors, and tissue engineering [55]. Chen and co-workers prepared biodegradable composite films based on lignin and chitosan with various compositions via a casting/solvent evaporation method [14]. As a result of strong interfacial interaction, well dispersed lignin/chitosan solution was obtained when the lignin content below 20 wt%. Therefore, the tensile strength, storage modulus, thermostability, as well as glass transition temperature of lignin/chitosan nanocomposite film improved largely by the addition of lignin, showing the potential as packaging films or wound dressings.

2.2 Other Lignin-Biopolymer Nanocomposites

Proteins are some macromolecules make up of amino acid residues chains. As readily available and relatively low-cost biopolymer, soy protein has been studied as a potential renewable source from a perspective of materials science [109]. Soy protein can be made into plastics, possessing good biodegradability but poor flexibility [112, 114], so three-dimensional structural lignin can be used as a plasticizer to improve the stability of soy protein plastics, meanwhile maintaining high tensile strength. Chen et al. prepared soy protein isolate (SPI)/hydroxypropyl alkaline lignin (HPL) nanocomposite plastic sheets, by adding a few glutaraldehyde as compatibilizer in the mixture of SPI and HPL solution [15]. The dimension of HPL-domain in SPI/HPL nanocomposites was about 50 nm when HPL content lower than 6 wt%, indicating a high interfacial activity. Comparing with the SPI sheets, the prepared nanocomposite sheets with 6 wt% HPL and 3.3 wt% glutaraldehyde had an enhanced tensile strength of 23.1 MPa. Lignin had the tendency to form supermolecular structures because of strong intermolecular and intramolecular interactions as well as polyfunctionality, so the dispersion of small HPL particles in SPI matrix effectively blended SPI and HPL in the solution state.

Jiang et al. prepared natural rubber/lignin nanocomposites from lignin-cationic polyelectrolyte colloids and rubber latex via co-precipitation method [47]. Self-assembly technology was employed to obtain colloidal lignin-poly (diallyldimethylammonium chloride) complexes (LPCs) through ion–ion interactions, cation-π and π–π interactions. The lignin particles were stable in aqueous solution with an average particle size less than 100 nm. LPCs accelerated the vulcanization of natural rubber/LPCs nanocomposites. Furthermore, LPCs were homogenously distributed in matrix of natural rubber, leading to improvement in mechanical properties, thermal- and thermo-oxidative stability of the prepared natural rubber/LPCs nanocomposites.

3 Lignin-Synthetic Polymer Nanocomposites

In the past century, various synthetic polymers in different forms (plastics, fibers, and synthetic rubbers) have been developed for all sorts of utilization, such as packaging materials, construction materials, and medical devices [112]. Although the continual pollution of environment caused by nondegradable synthetic polymer wastes has driven a rapid development of biodegradable polymers, the latter are still far from becoming substitutes for conventional synthetic polymer materials because of poor processability, high hydrophilicity, and so on [112]. As a result, combining advantages of synthetic polymers and biodegradable polymers such as lignin has become a wise strategy to balance social demands and ecological request, especially using nanotechnology to obtain remarkable enhanced performance [35, 45, 68].

3.1 Lignin-PLA Nanocomposites

Poly (lactic acid) (PLA) is a thermoplastic, high-strength, high-modulus aliphatic polymer derived from corn or potato starch, tapioca roots, beet, sugarcane, lactose, and other renewable resources [31]. PLA is considered to be the most promising biodegradable material because of its excellent biodegradability and biocompatibility [112].

Chung et al. fabricated lignin-PLA composites using a solvent-free method with catalyst [16]. Briefly, ring-opening polymerization along with the organic catalyst triazabicyclodecene was employed to graft PLA onto unmodified lignin directly. As lignin could absorb UV light, the PLA-lignin films with a low amount of lignin-g-PLA (0.9 wt%) blocked half of UV-A, almost all UV-B and UV-C, exhibiting excellent UV light barrier properties. And with proper chain length of PLA, it was found the elasticity modulus of the lignin-g-PLA composites synergistically strengthened.

Zhu et al. prepared a spherical lignin/PLA adsorbent via solvent evaporation method and investigated the effects of dispersed phase contents, PLA concentration and ratio of PLA to lignin on the diameter and mechanical strength of the PLA/lignin nanocomposite adsorbent spheres [115]. Owning to the three-dimensional structure of lignin, the as-prepared nanocomposite adsorbent had porous structure, and significantly increased mechanical strength.

In Thunga's work, butyration modified lignin (B-lignin) was successfully melt-processed into fine fibers and blended with PLA for conversion to carbon fibers [103]. The chemical modification of raw lignin included forming of ester functional groups via butyration to replace polar hydroxyl groups (–OH), which enhanced the miscibility of lignin with PLA. Fine fibers with diameters on the nanoscale extending from the cross-sectional surface can be seen clearly. The B-lignin/PLA 75/25 may be the desirable composition for future carbon fiber production due to overall high compatibility, storage modulus, and lignin content (therefore, higher carbon yields in the carbonized fibers). The fibers with 75 and 50 wt% of B-lignin showed cylindrical fiber structures, so the PLA phases stabilized the integrity of the fiber for the subsequent carbonization.

3.2 Lignin-Polyaniline Derivatives Nanocomposites

Since there is a large amount of O-containing functional groups on the three-dimensional structure of lignin [1], it has been widely used in removal of heavy metal ions such as Pb [37], Cu [53], Co [56, 59], and Cr [10] from wastewater.

Since the discovery of high electrical conductivity in 1980s, polyaniline (PANI) has attracted great attention of scientists due to its rich chemical and other attractive properties [42]. Moreover, PANI molecules contain large amounts of the amino, which can adsorb metal ions well though complexation [48], ion exchange [40], or

redox reaction [65]. As a result, lignin-polyaniline nanocomposite is convinced to be a kind of low-cost and effective materials for metal ion adsorption and many other industrial fields.

In Lü's work [58], one-step polymerization of aniline with lignosulfonate (LS) was employed to prepare hollow nanospheres. The uniform-shaped hollow nanospheres with average diameter of 100–200 nm were obtained under optimal condition (polymerization temperature at 25 °C, polymerization time of 1–12 h, 18 wt% of LS, molar ratio of oxidant and aniline was 1:1). The sulfonic groups with negative charge on LS acted as an external stabilizing agent, which resulted in the high stability, controllable size, and optimizable electroconductivity of the PANI-LS hollow nanospheres.

He et al. prepared polyaniline-(enzyme-hydrolyzed lignin) (lignin-PANI) nanocomposites via an in situ polymerization from aniline by using enzyme-hydrolyzed lignin (EHL) as a dispersant [39]. It was found that the content of EHL played an important role in the structure and properties of the lignin-PANI nanocomposites. Nanocomposite particles with 70 nm on average could be obtained when the EHL content was 10 wt%. The silver ions adsorption capacity of the lignin-PANI nanocomposites showed a maximal adsorption capacity of 565.4 mg/g. After adsorption, silver nanobelts with length of 1 cm, width of 0.22–4.38 μm and thickness of 219–311 nm were achieved onto the lignin-PANI nanocomposite.

Noteworthily, compared with PANI, PANI derivatives have more advantages such as their ease of fabrication, optimizable electrical properties, good stability, particularly the enhancement of processability [66]. Lü et al. synthesized well-sized distributed lignin-poly (*N*-methylaniline) (lignin-PNMA) nanocomposites with mean size of 68 nm using *N*-methylaniline and enzyme-hydrolyzed lignin via the chemical oxidative polymerization method [57]. The lignin-PNMA nanocomposites showed impressed Ag^+ adsorption property as compared to PMMA and enzyme-hydrolyzed lignin alone. The saturated capacity of the nanocomposites was up to 1556.8 mg/g; eventually, silver nanoparticles could be obtained through a redox reaction and ion-exchange between lignin–PNMA nanocomposites and Ag^+, as shown in Fig. 3.

Lü and co-workers [56, 59] prepared poly (*N*-butylaniline)-lignosulfonate (PBA-LS) nanospheres with electroconductive property under a mild condition, using in situ polymerization of *N*-butylaniline without stirring. During the polymerization, lignosulfonate (LS) was added as dispersant and dopant. The as-prepared PBA-LS nanospheres exhibited an enhanced electroconductive property (0.109 S/cm), higher than that of poly (*N*-butylaniline) (0.0751 S/cm). Moreover, it is found that under the initial ion concentration of 50 mmol/L, the maximum adsorption capacity of Ag^+ on PBA-LS nanospheres reached 815.0 mg/g. It was proposed that according to its simulated pseudo-second-order adsorption kinetics, chemical adsorption was the major adsorption principle of Ag^+ onto the PBA-LS nanospheres. The oxygen-, sulfur-, and nitrogen-containing groups on the spherical PBA-LS nanocomposites may be beneficial for the adsorption of reactive Ag^+ [23].

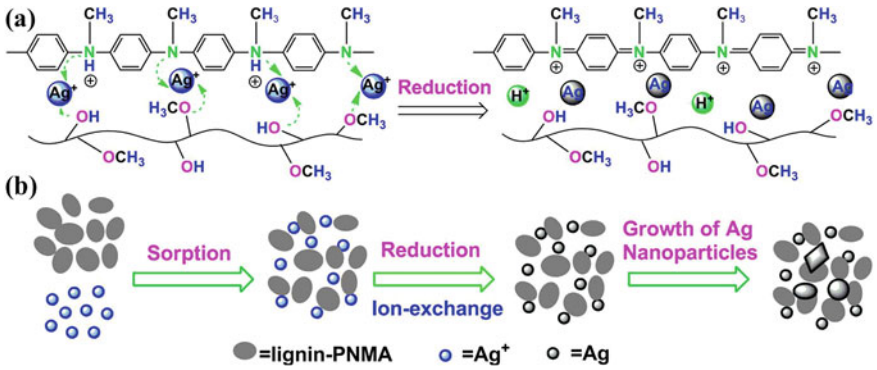

Fig. 3 Possible adsorption mechanism of Ag^+ on lignin-PNMA nanocomposites (Reprinted with permission from Lü et al. [57]. Copyright (2014), American Chemical Society)

3.3 Other Lignin-Synthetic Polymer Nanocomposites

As a synthetic biostable polymer with low tendency to degrade in various environment, polyethylene (PE) is the largest produced and consumed polyolefin in its diverse grades convertible to a broad variety of commodities including flexible and semi-flexible plastic items [28]. Lignin is a polar network polymer with low density and low abrasive features, which make it viable as organic filler to replace inorganic fillers. The use of plastics filled with lignin has great potential in the design and production of eco-compatible plastic products. In Samal's work, formulations of low-cost biodegradable PE/lignin hybrid polymeric nanocomposites were prepared using ethylene/vinyl acetate (EVA) copolymer as compatibilizer and a transition metal salt as biodegradation promoter [92]. The incorporation of the pro-oxidant/pro-degradant additive improved the oxidation process of the full carbon continuous matrix of bio-based hybrid nanocomposites. This low-cost material is of potential interest for the production of plastic items with a controlled service life in the application fields such as personal care products, packaging, agricultural mulch films and disposable items.

An alternative strategy to obtain polymer nanocomposites with high filler content is based on the concept of "one-component" hybrid materials, which means that the nanocomposite materials are synthesized by the assembly of polymer-grafted particles [105]. Hilburg et al. illustrated the application of atom transfer radical polymerization (ATRP) in fabricating thermoplastic "one-component" nanocomposites that based on polystyrene (PS) and poly (methyl methacrylate) (PMMA) grafted kraft lignin [43]. Tensile testing showed a decreased modulus but enhanced toughness of all nanocomposites as compared to homopolymers, and the ultimate elongation of PMMA-grafted nanocomposites was nearly twice as large as the PS grafts at high-graft density. Toughness values of both types of grafted nanocomposites were more than 10 times larger than that of the corresponding kraft-lignin/polymer blend system, indicating the potential of ATRP as the substrate

for the "one component" nanocomposite approach toward more sustainable polymeric materials. As a result, hermoplastic polymers grafted lignin could be a promising material that offers unique mechanical properties compared with many other inorganic nanoparticles based nanocomposites.

It has been reported that lignin-poly (vinyl alcohol) (PVA) blend composites can be used to form miscible homogeneous systems, in which lignin contributed to high mechanic strength and biodegradable polymer PVA provided high hydrophilicity and good chemical stability. The formation of strong intermolecular interaction between lignin and PVA enhanced the material performance [27, 54]. Li et al. synthesized PVA/quaternized lignin (QL) nanocomposite absorbent from PVA and modified lignin crosslinked by glutaraldehyde for NO_3^- removal from aqueous solution [62]. A large amount of connected holes was observed on the nanocomposite absorbent, revealing a highly developed network structure. The absorbent exhibited improvement in mechanical strength through combination of PVA and modified lignin, as well as the crosslinkage of glutaraldehyde. Lignin first became highly reactive after phenolation, and then aminated by monomeric quaternary ammonium groups. The surface area of PVA/QL absorbent became much more intensive after crosslinkage, as well as more active functional groups for NO_3^- absorption. Therefore, charge neutrality action and adsorption bridging action may have significant impact on the adsorption of PVA/QL. The PVA/QL showed a maximal adsorption capacity of 5.75 mg/g for NO_3^-, which was better than that of pure lignin, crosslinked lignin, and crosslinked quaternized lignin.

Milczarek and Inganas prepared polymer cathodes in lignin derivatives solutions by oxidation of pyrrole to polypyrrole via electrochemistry method [75]. The proton and electron during redox cycle processes were storaged and exchanged on the quinone group within lignin; therefore, within the prepared interpenetrating polypyrrole/lignin composite (Ppy(Lig)), there was combination of charge storage in lignin and polypyrrole. They proposed that the anion insertion followed by the proton release was the possible reason for the redox activity in the composite electrode. Comparison of the capacitance per mass and the charge capacity between Ppy(Lig) and those for polypyrrole/carbon composites showed that Ppy(Lig) electrode exhibited higher capacitance and charge density of than most of those electrodes. Furthermore, the phenolic groups in lignosulfonates varies widely, indicating that the performance of Ppy(Lig) composite is optimizable using processed lignins with different loading, charge densities, and there is a possibility to improve charge capacity.

4 Lignin-Based Metallic Nanocomposites

On account of their distinct physical and chemical properties, metal-containing nanomaterials, particularly polymer-based nanomaterials, have drawn intense attention at present, revealing tremendous possibility for useful applications [106].

In order to meet the new potential commercial chances to fabricate functional metallic nanomaterials, it is important to follow the principles of green chemistry to minimize consumption of reactant and production of by-products [17]. Structurally, there are many hydroxyl groups on lignin molecule that show both aliphatic and aromatic behaviors as surfactants [24], and there are also several functional groups that can be easily oxidized and used for reduction of high-valent metal ions to the zero-valent state as reducing agents for reduction. Actually, studies on lignin as reducing agent and stabilizer for the materials synthesis have been increasing continually, particularly for the synthesis of nanomaterial [11].

Furthermore, there are several important advantages while using lignin for the synthesis of nanoparticles: first, the experiments can be conducted under mild conditions, during which organic solvent is evitable; second, it is a facile synthesis process; lastly, lignin is a green reducing and stabilizing agents with wide accessibility, thus other expensive chemical additives can be avoided [18].

4.1 Lignin-Based Precious Metal Nanocomposites

Precious metal elements usually contains the gold, silver, and platinum group metals including Iridium, Osmium, Platinum, Palladium, Ruthenium, and Rhodium, which are resistant to corrosion and oxidation in moist air. The electrochemical sensors or high-efficient catalysts based on precious metal nanoparticle materials have been widely reported [44, 61, 71, 86].

Buoro et al. prepared lignin–Au NP-modified carbon paste electrodes (CPME) by adsorbing lignin or oxidized lignin contained composites onto graphite [11]. The lignin-reduced gold nanoparticles were incorporated in oxidized lignin/graphite nanocomposites to increase the conductivity of these nanomaterials. The as-prepared Au/graphite/oxidized lignin nanocomposite showed enhanced electrochemical characteristics. The better CPME was fabricated using the nanocomposite consisting of 2.5 % oxidized lignin and 0.2 % gold. It can be seen that the CPME acted as a catalyst toward the oxidation of reducing agents such as dopamine, ascorbic acid, and oxidation agents such as nitrite and iodate under a range of positive potential.

Coccia and co-workers synthesized Pt and Pd nanoparticle (NP) via a one-pot green method at mild temperature (80 °C), during which two lignin derivatives were used as both reducing and stabilizing agents in aqueous solution under aerobic conditions [17]. The Pd NPs were spherical, with diameters of 16–20 nm, larger and more uniform than those of Pt NPs. It is found that lignin actively participates in the reduction process of the precious metal nanoparticles as defined amounts of lignin were degraded into the typical product vanillin. The lignin–Pd NP nanocomposites were used in the aerobic oxidation of alcohols and the $NaBH_4$ reduction of 4-nitrophenol as catalyst. Both lignin–Pt and lignin–Pd NPs nanocomposites had excellent performance in catalyzing the reduction reaction, meanwhile only the lignin–Pt NP catalyst showed effectiveness in the aerobic oxidation reaction.

Ruiz-Rosas et al. synthesized Pt-contained lignin fibers via electrospinning method in solution of lignin/ethanol/platinum acetyl acetonate [90]. By increasing the carbonization temperature, the carbon and surface platinum proportion increased, and the oxygen content of the fibers decreased, meanwhile a higher ordered structure was obtained. Lignin-based/Pt carbon fibers had very smooth surface with no defects, and the introduction of Pt on the lignin-based carbon fibers led to a slight reduction to the oxidation resistance.

According to Coccia et al., water-soluble lignin and lignosulfonate samples were employed in the preparation of Pd NPs under definitely green experimental conditions, serving as reducing and stabilizing agents [18]. The spherical Pd NPs exhibited a diameter of 8–14 nm (lignin) and 16–20 nm (lignosulfonate), and the as-prepared nanoparticle composites showed a remarkable stability under aerobic conditions and ambient temperature that no significant changes were observed after 1 month. The lignin–Pd NPs nanocomposite was served as catalyst in carbon–carbon coupling reactions such as Suzuki and Heck reactions at mild conditions. The lignin-based Pd NP nanocomposites catalyst was found to be reusable after repeating the procedure, with a conversion of 30 % and a yield of 23 %.

Johnston and Nilsson employed lignin-containing cellulose fibers to synthesis nanogold (Au NP) and nanosilver (Ag NP) composites with antimicrobial properties [49]. The prepared Au NPs and Ag NPs were bound directly onto the unbleached lignin-containing fibers. Lignin played an essential role as crosslinker, so no external crosslinker was needed. The lignin-containing cellulose fibers were immersed in the Au and Ag ions solutions, on and within which with associated lignin there was redox reduction of Au^{3+} and Ag^{+} into Au NPs and Ag NPs, respectively, while the reduction process did not happen on the fibers without lignin. The Au NP composite fibers and especially the Ag NP composite fibers exhibited effective antimicrobial activity against *Staphlococcus aureus* microbes. Moreover, as the Au NPs and Ag NPs were chemically bound to the nanocomposite fibers (as shown in Fig. 4), they did not wash off and present any adverse environmental effects.

4.2 Other Lignin-Based Metallic Nanocomposites

Since the last century, transition metals and the metallic compounds exhibit various properties such as optical properties [29], electronic properties [20], catalytic properties [19], magnetic properties [8], and biomedical properties [9].

Layer-by-layer (LBL) self-assembly technology is a powerful and efficient method to process metallic nanoparticles into thin films on certain size and shape of substrates [21, 25, 96]. In the LBL technique, ultrathin films are formed by assembling nanoparticles and polyelectrolytes onto specific solid substrates from their liquid solutions, and main features of the thin films are fully tunable by external deposition parameters [72, 84, 85]. Lignin is a kind of natural anionic

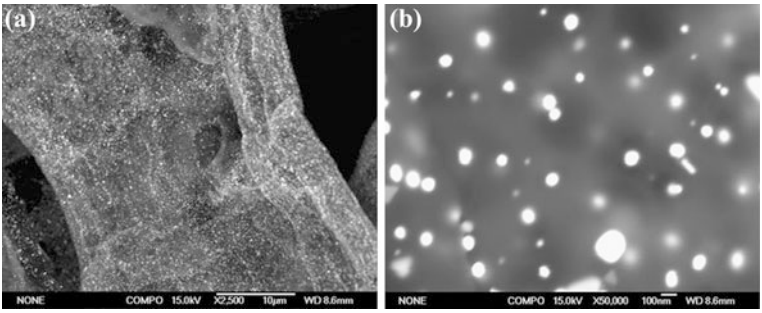

Fig. 4 SEM images of the lignin-cellulose/Au NP composite fibers, showing the Au NPs on the fiber surface [49] (Reprinted with permission from Springer Science+Business Media. Copyright (2012), Springer)

polyelectrolytes [73], and it is a promising material for LBL self-assembly as building block due to its accessibility and low cost.

Based on LBL self-assembly technology, there have been some success in the fabrication of TiO_2 films by assembling TiO_2 and synthetic polyelectrolytes on solid substrate [82, 104]. Li and co-workers used the LBL self-assembly technology to prepare photocatalytic multilayer nanocomposite films based on TiO_2 NPs and lignosulfonates (LS) on quartz slides, as seen in Fig. 5 [63]. It was found that during the LBL deposition process, the intensities of Ti and S peaks increased, and a highly reproducible step-by-step multilayer growth process on the quartz slides was observed. TiO_2 NPs completely covered on the quartz slide and formed a 10-bilayer multilayer film. The photocatalytic properties of the TiO_2/LS multilayer nanocomposite films showed an increasing degradation efficiency of methyl orange with the increasing amount of TiO_2 layers, and the contaminant molecule could diffuse into inner layer of nanocomposite films with no limit. Moreover, the TiO_2/LS multilayer nanocomposite films exhibited excellent photocatalytic decomposition

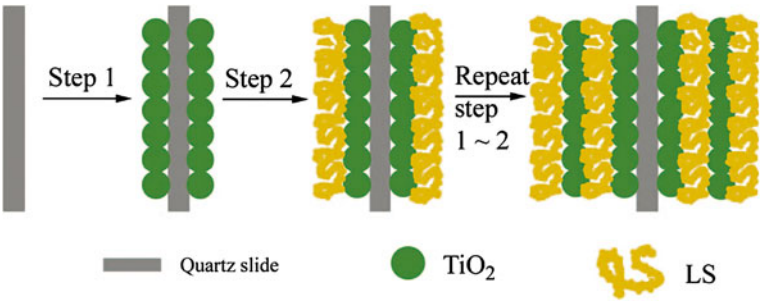

Fig. 5 Schematic preparation process of the TiO2/LS multilayer nanocomposite films [63] (Reprinted with permission from John Wiley & Sons, Inc. Copyright (2012), SIOC, CAS, Shanghai, & WILEY-VCH Verlag GmbH & Co. KGaA, Weinheim)

ability of bacteria, while the increasing number of bilayers resulted in an increasing decomposition degree of bacteria (*Escherichia coil*).

Owing to its abundant availability, nontoxicity, reusability, high photosensitivity, excellent chemical stability, and large excitation binding energy at room temperature, ZnO has been widely studied as an efficient metal oxide semiconductor photocatalyst since it was found [51, 108]. Wang et al. prepared nanocrystalline ZnO by using lignosite (LS) from low-price resources of lignin as surfactant, template, and nucleating promoter, in order to cut down the synthesis cost [107]. Flower cluster-like ZnO nanoparticle photocatalysts doped with different amounts of LS were obtained by liquid-phase precipitation. Doping of LS significantly improved the surface state of ZnO, changed the morphology of ZnO, and increased the specific surface area with more hydroxyl groups, which was helpful to obtain petal-like ZnO. The photocatalysts had good crystallinity and a small crystal size when the calcination temperature was 300 °C. When the doping amount of LS was 2 g, smaller band gap width and much higher photocatalytic activity of the petal-like ZnO nanoparticle photocatalysts were obtained than the pure ZnO. The high photocatalytic performance of ZnO–LS nanocomposites for the methyl orange degradation was attributed to the increasing surface hydroxyl groups and crystallinity.

Spinel ferrites are special minerals with high electrical resistivity, large dielectric loss, and low eddy current, especially in low frequency range. It is reported that Fe (II)-mixed spinel ferrites can be replaced by other divalent metal cations such as Co (II) [5]. In cobalt ferrite, hole and electron hopping can be responded in regions of both high and low conductivity [50]. Alcantara et al. successfully produced ultrathin nanocomposite films for chemical sensing by employing the LBL technology to assembly $CoFe_2O_4$ nanoparticles (np-$CoFe_2O_4$) (as shown in Fig. 6), combining with different polyelectrolytes: doped polyaniline (PANI), poly-3,4-ethylenedioxy thiophene: polystyrene sulfonic acid (PEDOT:PSS), and sulfonated lignin (SL) [5]. By immersing a solid substrate alternately into dispersion of nanoparticles and polyelectrolyte solutions, the content of $CoFe_2O_4$ nanoparticles within the nanocomposites increased. The nanocomposites showed typical $CoFe_2O_4$ nanoparticles with unique spherical morphology and dense package while surrounded by SL and other two polyelectrolytes. The PANI/SL/np-$CoFe_2O_4$/SL nanocomposite films presented low electrical conductivity because of the presence of np-$CoFe_2O_4$. Furthermore, as np-$CoFe_2O_4$ processes enhanced interfacial area and electrical insulating property, the nanocomposite films became much more sensitive to the ions in solution, while compared to the films only made of polyelectrolytes.

Among the electrode materials, NiO is regarded as a promising one due to its low cost, usability, and good pseudo-capacitive behavior [67]. The composite materials have got enhanced electrical conductivity and mechanical strength when there are more and more applications of active materials such as metal oxide/carbon. Chen and co-workers demonstrated the fabrication of NiO nanoparticles with high dispersity, which were embedded in mesoporous carbon (MPC) frameworks derived from lignin via self-assembly technology [13]. Lignin was used as a carbon precursor through polymerizing with formaldehyde or glutaraldehyde.

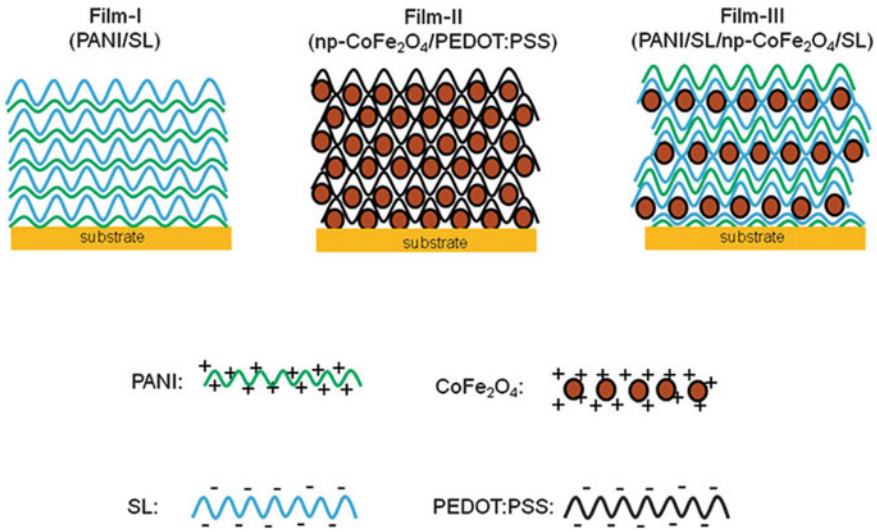

Fig. 6 Schematic diagram of different architectures of the nanocomposite films [5] (Copyright (2013), with permission from Royal Society of Chemistry)

Self-assembly was performed by evaporating the solvent of the liquid crystalline mesophases containing of nickel nitrate hydrate and lignin derivatives, which resulted in NiO/MPC nanocomposites under the N_2 atmosphere at 600 °C. The resulting NiO/MPC had excellent performance as supercapacitor electrode with higher specific capacitance, enhanced rate capability, and cycle stability, which can be ascribed to the unique mesoporous structures derived from lignin.

The rare earth phosphates are well-known materials due to their wide applications in high-performance luminescent devices, heat-resistant materials, catalysts, magnets, and so on [26]. Among those materials, $CePO_4$ has been extensively used in heat-resistant, tribology, and ceramic materials. It is reported that $CePO_4$/Carbon core-shell nanorods have been synthesized by the hydrothermal method, using glucose and $CePO_4$ as raw materials [70]. Li et al. synthesized lignin-based carbon/$CePO_4$ nanocomposites with previously extracted lignin and $CePO_4$, $NaH_2PO_4{\cdot}2H_2O$, or $Ce(NO_3)_3{\cdot}6H_2O$ by the solvothermal method [64]. The solvothermal method employed was beneficial for the carbonization of lignin as well as the preparation of $CePO_4$ and carbon, because it provided a high temperature and pressure environment. By using one-third of the $CePO_4$ precipitate with the lignin, carbon/$CePO_4$ nanocomposites were fabricated with spherical and congregated fiber-like shapes. With increasing $CePO_4$ concentration, the lignin-based carbon/$CePO_4$ nanocomposite spheres had a decreasing size and a smooth surface, while the concentration of $NaH_2PO_4{\cdot}2H_2O$ and $Ce(NO_3)_3{\cdot}6H_2O$ also had a significant impact on the microstructure and shape of carbon/$CePO_4$ nanocomposites. The obtained lignin-based carbon/$CePO_4$ nanocomposite with outstanding

photoluminescence property indicated that it has immense potential as a promising material for luminescent devices.

Nenkova et al. developed an economy method to fabricate copper sulfide lignocellulose nanocomposites, transferring waste water containing of lower concentration and quantities of Cu^{2+} and S^{2-} into nanomaterials with improved electroconductivity and microwave absorption ability [78]. Copper sulfide is an additive that can improve electroconductivity of polymers, and the corresponding materials usually possess microwave absorption properties. The copper sulfide in nanoscale combined with the lignocellulose matrix as a net and led to a better property. Two reduction systems with three components ($CuSO_4 \cdot 5H_2O$, $Na_2S_2O_3 \cdot 5H_2O$, and glyoxal) or two components ($CuSO_4 \cdot 5H_2O$ and $Na_2S_2O_3 \cdot 5H_2O$) were developed to optimize the preparation of the nanocomposites, in which the modification system with two components was better. The investigation of the combination mechanisms between copper sulfides and the lignocellulose matrix confirmed that the copper ions were coordinating with the hydroxyl in the aromatic nucleus of the lignin macromolecule.

5 Lignin-Based Carbonaceous Nanocomposites

For years, scientists have spent time on researching and developing innovative carbon-based materials. Besides a large amount of carbon nanotubes, nanorods, spheroids, fibers, there are fullerenes, graphene, and other carbonaceous nanocomposites [7]. To overcome poor solubility of carbon materials, it is an attractive way to surface-functionalize carbon materials with polyelectrolytes, especially natural poly-phenolic biopolymers such as lignin. Lignin can be extended to carbon nanotubes and other nanostructured carbons due to its adsorption capability. Furthermore, the nanocomposite was found to have promising electrocatalytic properties and convincing electrochemical activities [74].

5.1 Lignin-Based Carbon Nanotubes Nanocomposites

Milczarek and Nowicki reported a detailed study of the microstructural, spectral, and electrochemical properties of the surface-functionalized multiwall carbon nanotubes (MWNTs) with kraft lignin (KL), as shown in Fig. 7 [76]. It was found that the effective adsorption of lignin molecule on the surface of MWNTs led to an increasing oxygen content of the nanocomposites, as well as the spectral characteristic of highly oxidized polyphenol compounds. The modified MWNTs can be dispersed easily in aqueous (0.1 M ammonia) and organic (DMSO) solutions due to the presence of KL. Uniform cast made of the functionalized MWNTs suspensions was deposited on the gold electrode surface, and the electrode showed not only persistent electrochemical activities under various pH range, but also excellent

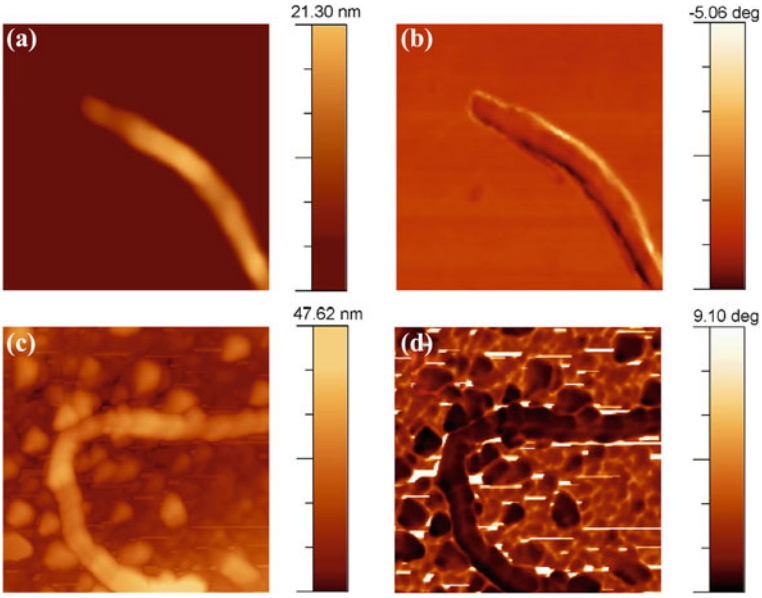

Fig. 7 AFM images of individual unmodified carbon nanotube (**a**) and (**c**) and KL-functionalized carbon nanotube (**b**) and (**d**). Images (**a**) and (**b**) are topographic and images (**c**) and (**d**) are phase contrast images. Image size ~0.6 mm × 0.6 μm in all cases [76] (Copyright (2013), with permission from Elsevier)

charge storage properties ascribed to both the pseudocapacitance of the quinone groups derived from lignin and the electrical double layer capacitance of the MWNTs. As a result, the lignin adsorbed on the MWNTs was used for charge storage due to its reversible redox activity. Compared with the unmodified ones, lignin-modified carbon nanotubes provided more than 100 % enhancement in the capacitance.

Dong and Shen synthesized a novel PANI with organic solvent-solubility and high electrical conductivity by a new method [22]. In the first step, a noncovalent approach was initially developed to self-assemble MWNTs-LsCa nanocomposites using calcium lignosulfonate (LsCa) to functionalize MWNTs. After that, the MWNT-LsCa nanocomposites were employed as template, on the surface of which the anilinium monomers were directly alignment aligned to initialize the polymerization of PANI. The noncovalent method to modify the MWNTs avoided their agglomeration effectively and allowed them doped in PANI at the molecular level. The PANI chains wrapped on the MWNTs-LsCa nanocomposites played an important role in the improvement of crystal orientation. The novel PANI/MWNTs–LsCa nanocomposites exhibited high conductivity (55.43 S/cm) as well as good solubility.

According to Rudnitskaya and co-workers [89], hardwood lignin and softwood lignin obtained from pulping process were used in fabricating via copolymerization

method. Then 0.72 % (w/w) was added into the obtained lignin-based copolymers in order to increase their electrical conductivity for sensor applications. It is found that both the π-electron delocalization and electrical conductivity are enhanced because that doped MWCNTs interacted with lignin with the copolymer matrix. As a result, all solid-state chemical sensors are easy to prepare due to the high conductivity of the MWNTs-doped lignin-polyurethanes materials. The characteristics of sensor are reproducible attributed to the maintaining of stable chemical properties as well as low leaching of the membrane components. In particular, the organosolv lignin and lignosulfonate-based sensors exhibited a high sensitivity toward hexavalent chromium in acidic media. The MWNTs-doped lignin-polyurethanes conducting nanocomposites were believed to be the Cr(VI)-sensitive potentiometric sensors with great promise.

5.2 Other Lignin-Based Carbon Nanocomposites

Lai and co-workers prepared mechanically flexible mats consisting of electrospun carbon nanofibers (ECNFs) by electrospinning aqueous mixtures of alkali lignin and polyvinyl alcohol (PVA), followed by stabilization in air and carbonization in inert environment [60]. The ECNFs well retained the overall morphologies of their precursors (neat PVA nanofibers and lignin/PVA composite nanofibers), and showed about 30 % reduction of fiber diameters. With the higher amount of lignin in the precursor nanofibers, the resulting ECNFs had the smaller average pore size, higher specific surface area, and larger pore volume, as shown in Fig. 8. The ECNFs (70/30), which was derived from the composite nanofibers with 70 wt% of lignin, had an average fiber diameter of about 100 nm and the BET specific surface area of 583 m^2/g. The lignin-based ECNF mats (particularly the ECNFs (70/30) mats) performed very well as free-standing and/or binder-free electrode materials for supercapacitors. The ECNFs (70/30) mats had the highest gravimetric capacitance of 64 F/g at the current density of 400 mA/g and 50 F/g at 2000 mA/g. Furthermore, the gravimetric capacitance was merely reduced by about 10 % after 6000 cycles of charge/discharge, indicating that the ECNFs (70/30) electrode was electrochemically stable and durable. The ECNF mats made from alkali lignin was innovative and sustainable electrode materials for flexible high-performance supercapacitors.

He et al. prepared carbon micro/nanospheres (C_{PAN} and C_{PNA}) containing of nitrogen and oxygen based on lignosulfonate/polyaniline and lignosulfonate/poly (*N*-ethylaniline) composite spheres via direct pyrolysis at 700 °C, as shown in Fig. 9 [41]. The two types of lignin-derived composite spheres were fabricated by in situ polymerization of lignosulfonate with aniline and *N*-ethylaniline, respectively. Different electrochemical performances were observed on the two carbon nanospheres ascribed to the different functional groups and structures. Compared to C_{PNA} microspheres, the C_{PAN} nanospheres with better electrochemical properties were promising materials of lithium-ion battery anodes, exhibiting a first discharge

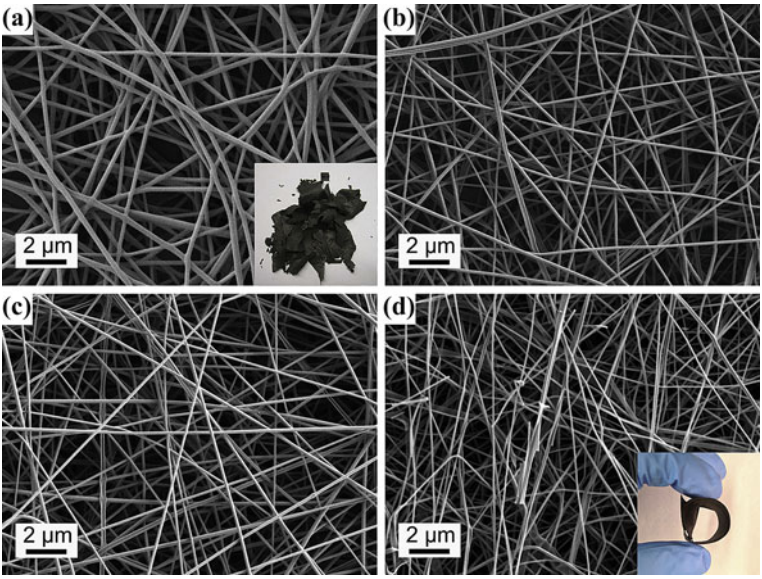

Fig. 8 SEM images of different ECNF mats: **a** ECNFs (PVA) mat, the inset showing that the mat was brittle; **b** ECNFs (30/70) mat, **c** ECNFs (50/50) mat, and **d** ECNFs (70/30) mat, the inset showing that the mat was flexible [60] (Copyright (2014), with permission from Elsevier)

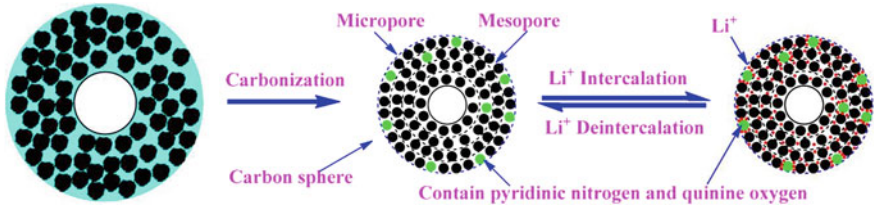

Fig. 9 Possible mechanism of lithium-ion intercalation and deintercalation for the C_{PAN} and C_{PNA} spheres (Reprinted with permission from He et al. [41]. Copyright (2013), American Chemical Society)

capacity of 1450, 1094, and 770 mAh/g and a first charge capacity of 707, 698, and 446 mAh/g at a current density of 60, 100, and 200 mA/g, respectively, indicating the potential of the low-cost C_{PAN} carbon nanospheres as high-performance lithium-ion battery anode materials.

Xu and co-workers reported a co-electrospinning method to produce lignin and cellulose nanofibrils (CNFs)-based porous core-shell carbon fibers by controlled carbonization [111]. The shell of the fiber was formed by lignin while its electrospinability increased after the addition of Polyacrylonitrile. CNFs were surface acetylated and a homogenous dispersion was obtained by dispersing CNFs in silicon oil, followed by electrospinning the porous core. Then carbonization was

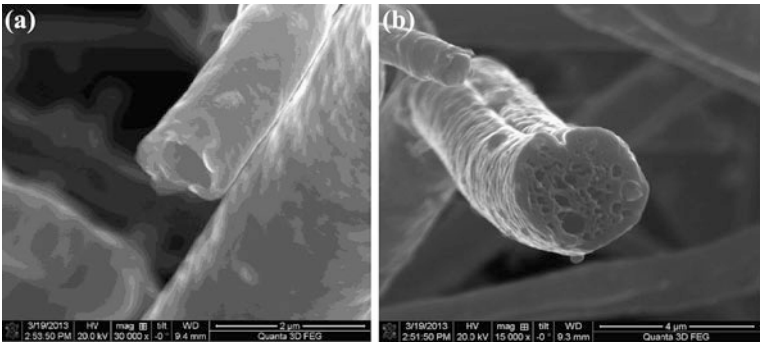

Fig. 10 SEM images of lignin/PAN hollow carbon fiber (**a**) and CNFs-lignin/PAN core-shell carbon fiber (**b**) [111] (Copyright (2013), with permission from Elsevier)

conducted to obtain hollow and core-shell carbon fibers and no obvious changes occurred on the fiber structure, as shown in Fig. 10. The two novel carbon fibers, especially the porous core-shell one, exhibited larger porosity and surface area while compared with any other conventional solid fibers, which made it easier for the fibers to interact variously with their surrounding environments. Therefore, the performance of the fibers can be potentially enhanced in some advanced applications such as gas sensing and adsorption, energy storage, catalysis, and environmental remediation.

6 Other Lignin-Based Nanocomposites

Lignin-based nanocomposites have been studied all around the world. Besides the combination between lignin and polymers, metallic materials and carbonaceous materials, nanocomposites based on lignin and silicate clays, molecular sieves, layered double hydroxide, inorganic acid, etc., have also been investigated.

Guigo et al. elaborated the fabrication of a novel nanocomposite based on lignin, silicate clays, and natural fibers by shear mixing them in a twin-screw extruder [36]. In situ dispersion of the three components in the shear mixture was under investigation in order to improve their mechanical and thermal properties. Sepiolite or organophilic montmorillonite (Org-MMT) were incorporated by melt processing to prepare these two silicate lignin/clays/natural fiber nanocomposites. The inorganic sepiolite clays were partial delaminated under the shear mixing into the system. Moreover, while using Org-MMT, the silicate layers was interacted well with the lignin matrix into good nanoscale dispersion, result in the forming of passive protective barriers.

Sevastyanova et al. prepared lignin-based nanocomposites and nanofibers by mechanical mixing organosolv lignin/organoclay mixtures, followed by melt intercalation [93]. Two types of organic montmorillonite clays modified by different

ammonium cations were employed to produce lignin intercalation compounds with different hydrophobicity. When compared to initial lignin, the glass transition temperature for both nanocomposites increased, indicating that the organoclays were well interacted with the lignin macromolecules. It is also found that both the tensile strength and melt processability increased substantially in the intercalated nanocomposites.

According to Jairam's research, a lignin–clay nanohybrid was fabricated based on the saponite clay modified lignin, which was recovered from a biorefinery waste stream. The lignin–clay nanohybrid was wrapped by polystyrene butyl acrylate (PSBA) copolymer shell via one-step miniemulsion polymerization in order to form stable composite latex [46]. Approximately 30 wt% of lignin was first modified by epoxypropyl trimethylammonium chloride to obtain cationic lignin, which was beneficial for the swelling and intercalation of clays. The premodification process had a significant impact on the exfoliation of clay plates to improve the latex stability. As a result the exfoliated lignin–clay nanohybrid wrapped by the PSBA droplets could be stable latex. When the content of lignin–clay nanohybrid was 5.3 %, nanocomposites exhibited a remarkable enhancement in tensile strength, and a 42 % decrease in oxygen permeability as well as about 50 °C increase in degradation temperature while compared with pure PSBA film.

Saad and Hawari described a novel of lignin-grafted SBA-15 nanocomposite, of which the lignin was silylated with triethoxychlorosilane followed by treatment with nanostructured silica [91]. The decrease intensity of three diffraction planes in lignin-SBA-15 nanocomposites revealed that there was big difference between the silica walls and the open pores of lignin-SBA-15 nanocomposites. The specific surface area of lignin-SBA-15 nanocomposites decreased drastically as a result of the lignin coating on SBA-15. The grafting of lignin to SBA-15 made little changes in its morphology. The lower specific surface area and unique thermal stability of the newly synthesized lignin-based nanocomposite made it available in several industrial applications such as removal of various contaminants from water.

Privas et al. demonstrated the combination of lignosulfonate modified layered double hydroxide (LDH/LS) with thermoplastic starch, which was regarded as a facile method to obtain the nanoscale LDH with homogeneous dispersion [87]. Under the LDH/LS concentration of 1–4 wt%, the LDH was almost reaching completely exfoliation. When incorporating with starch, LDH/LS composite was used in slurry form to avoid the formation of aggregates. The LDH/LS-starch nanocomposites were mixed in different concentrations of ethylene/butyl acrylate/maleic anhydride terpolymer. When the loading of LDH/LS-starch nanocomposites was 20 wt%, the processability and mechanical properties of the terpolymer remained and the oxygen barrier property was improved, indicating the terpolymer was partially bio-based.

Xiao et al. synthesized lignin-LDH nanocomposites by in situ method, followed by the preparation of styrene-butadiene rubber (SBR)/lignin-LDH composites via melt compounding method [110]. The crystalline LDH was obtained and the lignin-LDH nanocomposites were well dispersed in SBR matrix. Compared to LDH/SBR composites, lignin-LDH/SBR exhibited a significant improvement in hardness,

300 % modulus, tensile strength, and elongation at break. Furthermore, The lignin-LDH/SBR showed a decrease in thermal degradation temperature at 10 % weight loss (T_{10}), whereas T_{50} increased drastically than that of LDH/SBR, indicating that the lignin-LDH/SBR nanocomposites were promising filler for rubber.

Admassie and co-workers reported the electrochemical synthesis of a ternary system consisting of polypyrrole, lignosulfonate, and phosphomolybdic acid ($H_3PMo_{12}O_{40}{\cdot}nH_2O$) for electrochemical capacitors [3]. A simple one-step strategy was used to synthesize the ternary composite supercapacitor electrode via simultaneous electrochemical deposition, followed by characterization by electrochemical methods. The ternary composite system showed the highest specific capacitance and charge storage capacities than the values reported before, from 477 to 682 F/g (at a discharge current of 1 A/g) and from 69 to 128 mAh/g, respectively. The cycling stability of the ternary composite further enhanced after the addition of phosphomolybdic acid.

Grance et al. reported the fabrication of lignin-CNSL-formol magnetic nanocomposites as novel petroleum absorbents [34]. The nanocomposite was prepared from lignin, cashew nutshell liquid (CNSL), and formaldehyde through bulk polycondensation, as well as the addition of magnetite nanoparticles. The density of lignin-based nanocomposites was lower than water, which is easy for them to float. Nanocomposite containing 3.3 vol. % of magnetite showed oil removal capability equal to (11.2 ± 0.5) g/g. These lignin-based nanocomposites also exhibited an excellent cure degree of (94 ± 5) %, allowing their promising utilization in oil recovery processes.

7 Conclusions

This chapter reviewed the recent progress in synthesis methods, properties, and applications of different kinds of lignin-based nanocomposites. Lignin-based polymer nanocomposites (lignin-based biopolymer or synthetic polymer nanocomposites), lignin-based metallic nanocomposites, lignin-based carbonaceous nanocomposites, etc., have attracted considerable interest since they can be used in various fields like food, packaging, engineering, detection, energy, and so on. With the continual concern about the scarcity of petroleum and petroleum-based chemicals, and the increasing appeals for saving resources, biomass is one of the vital resources that will play an important role in future economies. Lignin, with its huge available volume, unique structure, and properties, is well placed to act this role. For the outstanding properties, there will be an attractive prospect for lignin in nanotechnology.

References

1. Adhikari BB, Gurung M, Alam S, Tolnai B, Inoue K (2013) Kraft mill lignin—A potential source of bio-adsorbents for gold recovery from acidic chloride solution. Chem Eng J 231:190–197
2. Adler E (1977) Lignin chemistry—past, present and future. Wood Sci Technol 11:169–218
3. Admassie S, Elfwing A, Jager EWH, Bao Q, Inganas O (2014) A renewable biopolymer cathode with multivalent metal ions for enhanced charge storage. J Mater Chem A 2:1974–1979
4. Ago M, Jakes JE, Rojas OJ (2013) Thermomechanical properties of lignin-based electrospun nanofibers and films reinforced with cellulose nanocrystals: A dynamic mechanical and nanoindentation study. ACS Appl Mater Interfaces 5:11768–11776
5. Alcantara GB, Paterno LG, Fonseca FJ, Pereira-da-Silva MA, Morais PC, Soler MAG (2013) Dielectric properties of cobalt ferrite nanoparticles in ultrathin nanocomposite films. Phys Chem Chem Phys 15:19853–19861
6. Arthanareeswaran G, Thanikaivelan P, Srinivasn K, Mohan D, Rajendran M (2004) Synthesis, characterization and thermal studies on cellulose acetate membranes with additive. Eur Polym J 40:2153–2159
7. Bazargan A, Yan Y, Hui CW, McKay G (2013) A review: synthesis of carbon-based nano and micro materials by high temperature and high pressure. Ind Eng Chem Res 52:12689–12702
8. Bedanta S, Kleemann W (2009) Supermagnetism. J Phys D Appl Phys 42:013001
9. Benyettou F, Lalatonne Y, Chebbi I, Di Benedetto M, Serfaty JM, Lecouvey M, Motte L (2011) A multimodal magnetic resonance imaging nanoplatform for cancer theranostics. Phys Chem Chem Phys 13:10020–10027
10. Brdar M, Sciban M, Takaci A, Dosenovic T (2012) Comparison of two and three parameters adsorption isotherm for Cr(VI) onto Kraft lignin. Chem Eng J 183:108–111
11. Buoro RM, Bacil RP, da Silva RP, da Silva LCC, Lima AWO, Cosentino IC, Serrano SHP (2013) Lignin-AuNp modified carbon paste electrodes-preparation, characterization, and applications. Electrochim Acta 96:191–198
12. Carrott P, Ribeiro Carrott M (2007) Lignin–from natural adsorbent to activated carbon: A review. Bioresour Technol 98:2301–2312
13. Chen F, Zhou W, Yao H, Fan P, Yang J, Fei Z, Zhong M (2013) Self-assembly of NiO nanoparticles in lignin-derived mesoporous carbons for supercapacitor applications. Green Chem 15:3057–3063
14. Chen L, Tang CY, Ning NY, Wang CY, Fu Q, Zhang Q (2009) Preparation and properties of chitosan/lignin composite films. Chin J Polym Sci 27:739–746
15. Chen P, Zhang LN, Peng SP, Liao B (2006) Effects of nanoscale hydroxypropyl lignin on properties of soy protein plastics. J Appl Polym Sci 101:334–341
16. Chung YL, Olsson JV, Li RJ, Frank CW, Waymouth RM, Billington SL, Sattely ES (2013) A renewable lignin-lactide copolymer and application in biobased composites. ACS Sustainable Chem Eng 1:1231–1238
17. Coccia F, Tonucci L, Bosco D, Bressan M, d'Alessandro N (2012) One-pot synthesis of lignin-stabilised platinum and palladium nanoparticles and their catalytic behaviour in oxidation and reduction reactions. Green Chem 14:1073–1078
18. Coccia F, Tonucci L, d'Alessandro N, D'Ambrosio P, Bressan M (2013) Palladium nanoparticles, stabilized by lignin, as catalyst for cross-coupling reactions in water. Inorg Chim Acta 399:12–18
19. Cokoja M, Bruckmeier C, Rieger B, Herrmann WA, Kühn FE (2011) Transformation of carbon dioxide with homogeneous transition-metal catalysts: A molecular solution to a global challenge? Angew Chem Int Ed 50:8510–8537
20. Cox PA (2010) Transition metal oxides: an introduction to their electronic structure and properties. Oxford University Press

21. Decher G, Hong JD (1991) Buildup of ultrathin multilayer films by a self-assembly process, 1 consecutive adsorption of anionic and cationic bipolar amphiphiles on charged surfaces, Makromolekulare Chemie Macromolecular Symposia. Wiley Online Library
22. Dong JQ, Shen Q (2009) Enhancement in solubility and conductivity of polyaniline with lignosulfonate modified carbon nanotube. J Polym Sci, Part B: Polym Phys 47:2036–2046
23. Donia AM, Atia AA, Elwakeel KZ (2007) Recovery of gold (III) and silver (I) on a chemically modified chitosan with magnetic properties. Hydrometallurgy 87:197–206
24. El Mansouri NE, Salvadó J (2007) Analytical methods for determining functional groups in various technical lignins. Ind Crop Prod 26:116–124
25. Elbakry A, Zaky A, Liebl R, Rachel R, Goepferich A, Breunig M (2009) Layer-by-layer assembled gold nanoparticles for siRNA delivery. Nano Lett 9:2059–2064
26. Feldmann C, Justel T, Ronda CR, Schmidt PJ (2003) Inorganic luminescent materials: 100 years of research and application. Adv Funct Mater 13:511–516
27. Fernandes D, Winkler Hechenleitner A, Job A, Radovanocic E, Gómez Pineda E (2006) Thermal and photochemical stability of poly (vinyl alcohol)/modified lignin blends. Polym Degrad Stab 91:1192–1201
28. Galli P, Vecellio G (2004) Polyolefins: The most promising large-volume materials for the 21st century. J Polym Sci, Part A: Polym Chem 42:396–415
29. Gao F, Wang Y, Shi D, Zhang J, Wang M, Jing X, Humphry-Baker R, Wang P, Zakeeruddin SM, Grätzel M (2008) Enhance the optical absorptivity of nanocrystalline TiO_2 film with high molar extinction coefficient ruthenium sensitizers for high performance dye-sensitized solar cells. J Am Chem Soc 130:10720–10728
30. Garcia Calvo-Flores F, Dobado JA (2010) Lignin as renewable raw material. Chemsuschem 3:1227–1235
31. Garlotta D (2001) A literature review of poly (lactic acid). J Polym Environ 9:63–84
32. Gosselink R, Abächerli A, Semke H, Malherbe R, Käuper P, Nadif A, Van Dam J (2004) Analytical protocols for characterisation of sulphur-free lignin. Ind Crop Prod 19:271–281
33. Gosselink R, De Jong E, Guran B, Abächerli A (2004) Co-ordination network for lignin—standardisation, production and applications adapted to market requirements (EUROLIGNIN). Ind Crop Prod 20:121–129
34. Grance EGO, Souza FG, Varela A, Pereira ED, Oliveira GE, Rodrigues CHM (2012) New petroleum absorbers based on lignin-CNSL-formol magnetic nanocomposites. J Appl Polym Sci 126:E304–E311
35. Graupner N (2008) Application of lignin as natural adhesion promoter in cotton fibre-reinforced poly (lactic acid)(PLA) composites. J Mater Sci 43:5222–5229
36. Guigo N, Vincent L, Mija A, Naegele H, Sbirrazzuoli N (2009) Innovative green nanocomposites based on silicate clays/lignin/natural fibres. Compos Sci Technol 69:1979–1984
37. Guo X, Zhang S, Shan XQ (2008) Adsorption of metal ions on lignin. J Hazard Mater 151:134–142
38. Hambardzumyan A, Foulon L, Chabbert B, Aguie-Beghin V (2012) Natural organic UV-absorbent coatings based on cellulose and lignin: designed effects on spectroscopic properties. Biomacromolecules 13:4081–4088
39. He LH, Lin TT, Ling YH, Wu HJ, Lu QF (2013a) Preparation of polyaniline-lignin nanocomposites and their reducing adsorption for silver ions. Acta Polym Sin:320–326
40. He ZW, Lü QF, Zhang JY (2011) Facile preparation of hierarchical polyaniline-lignin composite with a reactive silver-ion adsorbability. ACS Appl Mater Interfaces 4:369–374
41. He ZW, Yang J, Lu QF, Lin Q (2013) Effect of Structure on the Electrochemical Performance of Nitrogen- and Oxygen-Containing Carbon Micro/Nanospheres Prepared from Lignin-Based Composites. ACS Sustainable Chem Eng 1:334–340
42. Heeger AJ (2001) Nobel Lecture: Semiconducting and metallic polymers: The fourth generation of polymeric materials. Rev Mod Phys 73:681–700

43. Hilburg SL, Elder AN, Chung H, Ferebee RL, Bockstaller MR, Washburn NR (2014) A universal route towards thermoplastic lignin composites with improved mechanical properties. Polymer 55:995–1003
44. Huang HX, Chen SX, Yuan CE (2008) Platinum nanoparticles supported on activated carbon fiber as catalyst for methanol oxidation. J Power Sources 175:166–174
45. Ishizu K, Tsubaki K, Mori A, Uchida S (2003) Architecture of nanostructured polymers. Prog Polym Sci 28:27–54
46. Jairam S, Tong ZH, Wang LT, Welt B (2013) Encapsulation of a biobased lignin-saponite nanohybrid into polystyrene co-Butyl acrylate (PSBA) latex via miniemulsion polymerization. ACS Sustainable Chem Eng 1:1630–1637
47. Jiang C, He H, Jiang H, Ma L, Jia DM (2013) Nano-lignin filled natural rubber composites: Preparation and characterization. Express Polym Lett 7:480–493
48. Jiang N, Xu Y, Dai Y, Luo W, Dai L (2012) Polyaniline nanofibers assembled on alginate microsphere for Cu^{2+} and Pb^{2+} uptake. J Hazard Mater 215:17–24
49. Johnston JH, Nilsson T (2012) Nanogold and nanosilver composites with lignin-containing cellulose fibres. J Mater Sci 47:1103–1112
50. Jonker G (1959) Analysis of the semiconducting properties of cobalt ferrite. J Phys Chem Solids 9:165–175
51. Khodja AA, Sehili T, Pilichowski JF, Boule P (2001) Photocatalytic degradation of 2-phenylphenol on TiO_2 and ZnO in aqueous suspensions. J Photochem Photobiol, A 141:231–239
52. Kiziltas A, Gardner DJ, Han Y, Yang HS (2011) Thermal properties of microcrystalline cellulose-filled PET–PTT blend polymer composites. J Therm Anal Calorim 103:163–170
53. Kriaa A, Hamdi N, Srasra E (2010) Removal of Cu (II) from water pollutant with Tunisian activated lignin prepared by phosphoric acid activation. Desalination 250:179–187
54. Kubo S, Kadla JF (2003) The formation of strong intermolecular interactions in immiscible blends of poly (vinyl alcohol)(PVA) and lignin. Biomacromolecules 4:561–567
55. Kumar M (2000) A review of chitin and chitosan applications. React Funct Polym 46:1–27
56. Lü QF, Huang ZK, Liu B, Cheng X (2012) Preparation and heavy metal ions biosorption of graft copolymers from enzymatic hydrolysis lignin and amino acids. Bioresour Technol 104:111–118
57. Lü QF, Luo JJ, Lin TT, Zhang YZ (2014) Novel lignin-poly(N-methylaniline) composite sorbent for silver ion removal and recovery. ACS Sustainable Chem Eng 2:465–471
58. Lü QF, Wang C, Cheng X (2010) One-step preparation of conductive polyaniline-lignosulfonate composite hollow nanospheres. Microchim Acta 169:233–239
59. Lü QF, Zhang JY, He ZW (2012) Controlled preparation and reactive silver-ion sorption of electrically conductive poly (N-butylaniline)–lignosulfonate composite nanospheres. Chem - Eur J 18:16571–16579
60. Lai C, Zhou Z, Zhang L, Wang X, Zhou Q, Zhao Y, Wang Y, Wu XF, Zhu Z, Fong H (2014) Free-standing and mechanically flexible mats consisting of electrospun carbon nanofibers made from a natural product of alkali lignin as binder-free electrodes for high-performance supercapacitors. J Power Sources 247:134–141
61. Lee Y, Park TG (2011) Facile fabrication of branched gold nanoparticles by reductive hydroxyphenol derivatives. Langmuir 27:2965–2971
62. Li H, Fu SY, Peng LC, Zhan HY (2012) Photocatalytic nanocomposite films fabricated by layer-by-layer self-assembly of TiO_2 nanoparticles and lignosulfonates. Chin J Chem 30:1605–1610
63. Li H, Liu H, Fu S, Zhan H (2011) Surface hydrophobicity modification of cellulose fibers by layer-by-layer self-assembly of lignosulfonates. BioResources 6:1681–1695
64. Li SM, Sun SL, Ma MG, Dong YY, Fu LH, Sun RC, Xu F (2013) Lignin-based carbon/$CePO_4$ nanocomposites: Solvothermal fabrication, characterization, thermal stability, and luminescence. BioResources 8:4155–4170
65. Li X, Don Q, Huang M (2008) Highly effective sorption of heavy metal ions on polyaniline and its composites. Prog Chem 20:227–232

66. Li XG, Zhou HJ, Huang MR (2004) Synthesis and properties of processable conducting copolymers from N-ethylaniline with aniline. J Polym Sci, Part A: Polym Chem 42:6109–6124
67. Liu J, Jiang J, Bosman M, Fan HJ (2012) Three-dimensional tubular arrays of MnO_2-NiO nanoflakes with high areal pseudocapacitance. J Mater Chem 22:2419–2426
68. Liu T, Burger C, Chu B (2003) Nanofabrication in polymer matrices. Prog Polym Sci 28:5–26
69. Lora JH, Glasser WG (2002) Recent industrial applications of lignin: a sustainable alternative to nonrenewable materials. J Polym Environ 10:39–48
70. Ma MG, Zhu JF, Sun RC, Zhu YJ (2009) Hydrothermal synthesis and characterization of $CePO_4$/C core-shell nanorods. Mater Lett 63:2513–2515
71. Mahmoud M, Saira F, El-Sayed M (2010) Experimental evidence for the nanocage effect in catalysis with hollow nanoparticles. Nano Lett 10:3764–3769
72. Marangoni VS, Martins MVA, Souza JA, Oliveira ON Jr, Zucolotto V, Crespilho FN (2012) The processing of polyelectrolyte-covered magnetite nanoparticles in the form of nanostructured thin films. J Nanopart Res 14:1–10
73. Maximova N, Osterberg M, Laine J, Stenius P (2004) The wetting properties and morphology of lignin adsorbed on cellulose fibres and mica. Colloids Surf A 239:65–75
74. Milczarek G (2010) Kraft lignin as dispersing agent for carbon nanotubes. J Electroanal Chem 638:178–181
75. Milczarek G, Inganas O (2012) Renewable cathode materials from biopolymer/conjugated polymer Interpenetrating networks. Science 335:1468–1471
76. Milczarek G, Nowicki M (2013) Carbon nanotubes/kraft lignin composite: characterization and charge storage properties. Mater Res Bull 48:4032–4038
77. Moon RJ, Martini A, Nairn J, Simonsen J, Youngblood J (2011) Cellulose nanomaterials review: structure, properties and nanocomposites. Chem Soc Rev 40:3941–3994
78. Nenkova S, Velev P, Dragnevska M, Nikolova D, Dimitrov K (2011) Lignocellulose nanocomposite containing copper sulfide. BioResources 6:2356–2365
79. Nevarez LAM, Casarrubias LB, Celzard A, Fierro V, Munoz VT, Davila AC, Lubian JRT, Sanchez GG (2011) Biopolymer-based nanocomposites: effect of lignin acetylation in cellulose triacetate films. Sci Technol Adv Mater 12:045006
80. Nevarez LAM, Casarrubias LB, Canto OS, Celzard A, Fierro V, Gomez RI, Sanchez GG (2011) Biopolymers-based nanocomposites: Membranes from propionated lignin and cellulose for water purification. Carbohydr Polym 86:732–741
81. Notley SM, Norgren M (2009) Lignin: Functional biomaterial with potential in surface chemistry and nanoscience. John Wiley & Sons Ltd, The nanoscience and technology of renewable biomaterials
82. Ogawa T, Ding B, Sone Y, Shiratori S (2007) Super-hydrophobic surfaces of layer-by-layer structured film-coated electrospun nanofibrous membranes. Nanotechnology 18:165607
83. Oksman K, Mathew A, Bondeson D, Kvien I (2006) Manufacturing process of cellulose whiskers/polylactic acid nanocomposites. Compos Sci Technol 66:2776–2784
84. Paterno LG, Soler MA, Fonseca FJ, Sinnecker JP, Sinnecker EH, Lima EC, Novak MA, Morais PC (2009) Layer-by-layer assembly of bifunctional nanofilms: Surface-functionalized maghemite hosted in polyaniline. J Phys Chem C 113:5087–5095
85. Pichon BP, Louet P, Felix O, Drillon M, Begin-Colin S, Decher G (2011) Magnetotunable hybrid films of stratified iron oxide nanoparticles assembled by the layer-by-layer technique. Chem Mater 23:3668–3675
86. Pradhan N, Pal A, Pal T (2002) Silver nanoparticle catalyzed reduction of aromatic nitro compounds. Colloids Surf A 196:247–257
87. Privas E, Leroux F, Navard P (2013) Preparation and properties of blends composed of lignosulfonated layered double hydroxide/plasticized starch and thermoplastics. Carbohydr Polym 96:91–100
88. Roberts JC (1996) The chemistry of paper. The Royal Society of Chemisty

89. Rudnitskaya A, Evtuguin DV, Costa LC, Graca MPF, Fernandes AJS, Correia MRP, Gomes MTSR, Oliveira JABP (2013) Potentiometric chemical sensors from lignin-poly(propylene oxide) copolymers doped by carbon nanotubes. Analyst 138:501–508
90. Ruiz-Rosas R, Bedia J, Lallave M, Loscertales IG, Barrero A, Rodriguez-Mirasol J, Cordero T (2010) The production of submicron diameter carbon fibers by the electrospinning of lignin. Carbon 48:696–705
91. Saad R, Hawari J (2013) Grafting of lignin onto nanostructured silica SBA-15: preparation and characterization. J Porous Mat 20:227–233
92. Samal SK, Fernandes E, Corti A, Chiellini E (2014) Bio-based polyethylene–lignin composites containing a pro-oxidant/pro-degradant additive: Preparation and characterization. J Polym Environ 22:58–68
93. Sevastyanova O, Qin W, Kadla JF (2010) Effect of nanofillers as reinforcement agents for lignin composite fibers. J Appl Polym Sci 117:2877–2881
94. Singha AS, Thakur VK (2010) Mechanical, morphological, and thermal characterization of compression-molded polymer biocomposites. Int J Polym Anal Charact 15:87–97
95. Singha AS, Thakur VK, Mehta IK, Shama A, Khanna AJ, Rana RK, Rana AK (2009) Surface-modified hibiscus sabdariffa fibers: Physicochemical, thermal, and morphological properties evaluation. Int J Polym Anal Charact 14:695–711
96. Soler MA, Paterno LG, Morais PC (2012) Layer-by-layer assembly of magnetic nanostructures. J Nanofluids 1:101–119
97. Thakur VK, Thakur MK (2014) Processing and characterization of natural cellulose fibers/thermoset polymer composites. Carbohydr Polym 109:102–117
98. Thakur VK, Thakur MK (2014) Recent trends in hydrogels based on psyllium polysaccharide: A review. J Cleaner Prod 82:1–15
99. Thakur VK, Thakur MK (2014) Recent Advances in Graft Copolymerization and Applications of Chitosan: A Review. ACS Sustainable Chem Eng 2:2637–2652
100. Thakur VK, Singha AS, Misra BN (2011) Graft copolymerization of methyl methacrylate onto cellulosic biofibers. J Appl Polym Sci 122:532–544
101. Thakur VK, Thakur MK, Gupta RK (2014) Review: Raw natural fiber-based polymer composites. Int J Polym Anal Charact 19:256–271
102. Thakur VK, Thakur MK, Raghavan P, Kessler MR (2014) Progress in green polymer composites from lignin for multifunctional applications: A review. ACS Sustain Chem Eng 2:1072–1092
103. Thunga M, Chen K, Grewell D, Kessler MR (2014) Bio-renewable precursor fibers from lignin/polylactide blends for conversion to carbon fibers. Carbon 68:159–166
104. Uğur ŞS, Sarıışık M, Aktaş AH (2011) Nano-TiO_2 based multilayer film deposition on cotton fabrics for UV-protection. Fibers Polym 12:190–196
105. Von Werne T, Patten TE (1999) Preparation of structurally well-defined polymer-nanoparticle hybrids with controlled/living radical polymerizations. J Am Chem Soc 121:7409–7410
106. Wang L, Brazis P, Rocci M, Kannewurf CR, Kanatzidis MG (1998) Alpha-RuCl3: A new host for polymer intercalation. Lamellar polymer/alpha-$RuCl_3$ nanocomposites, in: Laine RM, Sanchez C, Brinker CJ, Giannelis E (Eds.), Mater Res Soc Symp P 519:257–264
107. Wang X, Xie W, Hao C, Zhang P, Fu X, Si N (2013) Liquid phase synthesis of flower cluster-like ZnO via lignosite template and its photocatalytic property. Acta Metall Sin 49:1098–1104
108. Wang Y, Li X, Lu G, Quan X, Chen G (2008) Highly oriented 1-D ZnO nanorod arrays on zinc foil: direct growth from substrate, optical properties and photocatalytic activities. J Phys Chem C 112:7332–7336
109. Wu Q, Zhang L (2001) Properties and structure of soy protein isolate-ethylene glycol sheets obtained by compression molding. Ind Eng Chem Res 40:1879–1883
110. Xiao S, Feng J, Zhu J, Wang X, Yi C, Su S (2013) Preparation and characterization of lignin-layered double hydroxide/styrene-butadiene rubber composites. Journal of Appl Polym Sci 130:1308–1312

111. Xu X, Zhou J, Jiang L, Lubineau G, Chen Y, Wu XF, Piere R (2013) Porous core-shell carbon fibers derived from lignin and cellulose nanofibrils. Mater Lett 109:175–178
112. Yang KK, Wang XL, Wang YZ (2007) Progress in nanocomposite of biodegradable polymer. J Ind Eng Chem 13:485–500
113. Zhang JM, Zhang J (2010) Advanced functional materials based on cellulose. Acta Polym Sin:1376–1398
114. Zhong ZK, Sun XZS (2001) Properties of soy protein isolate/polycaprolactone blends compatibilized by methylene diphenyl diisocyanate. Polymer 42:6961–6969
115. Zhu H, Lin X, Zhuo X, Zhang C (2011) Preparation and characterization of spherical lignin/polylactide composite adsorbent. Adv Mater Res 221:640–643

Nanocellulose and Its Application for Shape-Memory Materials

Shiyu Fu and Chen Tian

Abstract Nanocellulose (NC) has been attracting a great deal of interest as promising candidates for bionanocomposite due to their appealing intrinsic properties, such as low density, high surface area, and mechanical strength. In view of countless publications on nanocellulose composites already, this chapter concentrates on application of nanocellulose for reinforcing shape-memory composites. Shape-memory composites enable high-recovery stress levels and various functions due to their different components. The shape-memory behavior is also dependent on the size, shape, and concentration of the fillers. The effect of nanocellulose in these composites is determined by different shape-memory switches and interactions between nanocellulose and matrices. A challenge of using NC in shape-memory composites is the lack of compatibility between hydrophobic matrices and hydrophilic NCs. Various chemical modification methods have been explored to address this hurdle. In this chapter, we summarized the effect of nanocellulose on the deformation mechanism of shape-memory materials, with a particular focus on thermo- and water-sensitive switches. The application of shape-memory composites based on nanocellulose is also discussed.

Keywords Nanocellulose · Shape-memory materials · Nanocomposites

1 Introduction

Cellulose is the most abundant terrestrial organic polymer in nature. It is obtained from different natural resources depending upon the applications [103–107]. Its multifunctionality based on the chemical structure and hierarchical design is now newly being appreciated [117–120]. Cellulose exists naturally as crystalline and

S. Fu (✉) · C. Tian
State Key Laboratory of Pulp and Paper Engineering, South China University of Technology, Guangzhou, China
e-mail: shyfu@scut.edu.cn

V.K. Thakur and M.K. Thakur (eds.), *Eco-friendly Polymer Nanocomposites*, Advanced Structured Materials 74, DOI 10.1007/978-81-322-2473-0_4

amorphous configurations within plant, animal, and bacterial systems [113–116]. Moreover, cellulose is a high molecular and crystalline polymer with well-defined molecular and supramolecular structure [103, 104]. The crystalline domains in natural cellulose achieve irreducible packing, which is in the order of several nanometers in dimension [77]. Without question, plants ostensibly remain as a huge reservoir for the ultimate production of such "nanocrystalline" cellulose.

Nanocelluloses are a class of supramolecular structures that display diameters on the order of tens of nanometers and may be categorized as nanofibrillated cellulose (NFC), cellulose nanocrystals (CNCs), or bacterial cellulose (BC) [53]. NCs have been serenaded by researchers for numerous potential applications within the paper industry, electronics, cosmetics, and the biomedical arena [85]. Several of their most salient features are the large attendant surface area, extremely high crystallinity, and preternaturally high stiffness. These highly attractive properties imbue nanocelluloses with the peculiar attraction of being an excellent candidate for the effective reinforcement of composites, especially when applied at low levels (<5 wt%) [15, 129].

Although publication activities on nanocellulose grow quickly in recent years, application of nanocellulose in polymer reinforcement is still a relatively new research field, especially for shape-memory polymers. Shape-memory polymers (SMP) are defined as smart materials that can be deformed and fixed in a temporary shape. This temporary shape remains until a suitable external stimulus appears and induces the recovery of the original, permanent shape. SMP is intrinsically sensitive to the ambient environment, including temperature, pH values, absorbed gas molecules and optical wavelength. Therefore, SMPs have attracted research interest on both academia and industries [55, 72, 134]. However, the type of shape-memory responsiveness to external stimuli is limited by the polymer segments. Thus, physical combination with a reinforcing material to form two-phase copolymers is an effective way to enhance the flexibility of SMPs to respond to external stimuli.

Among various reinforcing materials, bio-based nanocellulose with a high rigidity has been widely used as a reinforcing agent in SMP matrix. Improvements of thermal and mechanical properties have been reported with a low content of cellulose nanoparticles (about 1–2 wt%) [33, 131]. Another useful effect of NCs in SMPs is their high density of hydroxyl groups, leading to a novel type of water-sensitive SMP nanocomposite. Therefore, recent researches of NCs in shape-memory materials were focused on their reinforcing effect and new ambient responsive switches, such as water-triggered rapid shape-recovery nanocomposites [66, 142].

However, the hydrophilic nature of NCs often results in poor compatibility within hydrophobic polymer matrices [30]. Furthermore, the strong hydrogen bonds formed during drying lead to irreversible agglomeration of NCs. Therefore, reliable and effective dispersion of NCs in hydrophobic matrices or in a nonpolar solvent is nearly impossible [95]. A key strategy for overcoming these latter challenges is the installation of hydrophobic moieties or so called polymer "brushes" on the surface,

which result in an improvement in both the modulus and strength of the final nanocomposites [38, 77]. These modification methods of NCs include etherification, esterification, silylation, oxidation, and polymer grafting.

In this chapter, we review the properties and applications of nanocellulose in shape-memory nanocomposites. First, we introduce the nanocellulose isolation, inherent properties, and their modification. Then, we discuss the shape-memory effects of SMPs, especially for thermal- and water-sensitive shape-memory polyurethanes. Finally, the key role of nanocellulose when used in the shape deformation and recovery processes is emphasized.

2 Isolation, Structure, and Properties of Nanocellulose

Native cellulose consists of a hierarchical structure of macroscopic fibers. This hierarchical structure is composed by smaller and mechanically stronger cellulose fibrils. The lateral dimension of these fibrils is typically of the order of a few nanometers, depending on the source of the cellulose. These nanofibrils interact strongly by the combined actions of crystallization, biopolymerization, and spinning, to form the natural cellulose fibers [108]. According to these morphological characters, cellulose fibers can be isolated to nanometric fragments using different treatment methods.

In quintessence, the principal reason to use NCs in composites is the high stiffness of cellulose crystals. This property can be further enhanced by reducing the amount of amorphous parts in natural cellulose and breaking down their hierarchical structure into individualized nanofibers of high crystallinity. It is possible to obtain a fibrous form of the material (CNCs or NFCs) with different aspect ratio (length/diameter). The reinforcing capabilities of the obtained nanocelluloses are potentially suitable for composite materials.

2.1 Isolation of Nanocellulose

As already mentioned, natural cellulose fibers can be dissociated into nanometric fragments by breaking down the hierarchical structure into individualized nanofibers. Generally, the production of natural cellulosic fibers in nanoscale elements requires acid hydrolysis or intensive mechanical treatment. However, chemical treatments or enzymatic hydrolysis may be utilized prior to acid hydrolysis or mechanical fibrillation [40, 83]. The polymerization degree, morphology, and aspect ratio of obtained NCs may vary with the used raw materials and isolation techniques [110].

2.1.1 Acid Hydrolysis

The main process for the isolation of NCs from native cellulosic fiber is based on acid hydrolysis. During the hydrolysis process, paracrystalline and amorphous regions of cellulose are preferentially hydrolyzed. Meanwhile, the crystalline regions, which are higher resistant to acid attack, remain intact and obtain rod-like CNCs [92].

In the structure of natural cellulosic fibers, chains appearing in the amorphous regions are stochastically arranged, leading to a lower density of these regions. Thus, the amorphous domains are more susceptible to acid attack. The hydrogen ions of acid can penetrate into the cellulose chains in these regions and promote the hydrolytic cleavage of the glycosidic bonds. The cleavage finally releases individual nanocrystallites [130]. Acid hydrolysis of natural cellulosic fiber induces a rapid decrease in the degree of polymerization (DP) due to the degradation of amorphous regions [39]. After acid hydrolysis, the amorphous domains are hydrolyzed and the remained crystalline regions generate homogeneous crystallites nanocellulose. These hydrolysis processes have been actually confirmed by electron microscopy [99], X-ray crystal diffraction [136], small-angle X-ray diffraction, and neutron diffraction analyses [82]. Meanwhile, a wide distribution of DPs is typically observed for different cellulose sources, resulting in a high polydispersity in the molecular weight of acid-hydrolyzed NCs.

Nanocellulose obtained, when using sulfuric acid, allows some sulfuric acid groups to randomly distribute on the surface of cellulose, thus, inducing a negative electrostatic repulsion between nanoparticles [28]. The repulsion is favorable for the dispersibility of NCs in the suspension. Jiang et al. [50] reported that due to the reaction of sulfuric acid with hydroxyl groups in cellulose molecules, charged sulfate half-esters covered on the surfaces of NCs, initiate repulsive forces between the crystallites and enhance the separation of nanocellulose crystallites.

Current methods for the isolation of CNCs are using 65 wt% sulfuric acid [87]. However, the reaction temperature can range from ambient temperature to 70 °C and the corresponding hydrolysis time can be varied from 30 min to overnight. Bondeson et al. [11] optimized the hydrolysis conditions by a response surface methodology. It was demonstrated that with a sulfuric acid concentration of 63.5 % (w/w) and a hydrolysis time of approximately 2 h, NCs with a yield of 30 % were obtained. The length of obtained NCs was between 200 and 400 nm and the width was <10 nm. They also reported that prolongation of the hydrolysis time induced a decrease of nanocellulose length and an increase of surface charge. CNCs are prepared by the hydrolysis of cotton linter with sulfuric acid. The obtained CNCs were rod-like, with a broad middle and two tapered ends. The nanorods averaged 20 nm in width and 200 nm in length (average of 100 CNC images), which were well dispersed with few aggregates. AFM image of the obtained CNCs is shown in Fig. 1.

Although sulfuric acid hydrolysis promotes dispersion of obtained NCs in water, the introduction of ionized sulfate groups compromises the thermostability of NCs. Thus, substitutes including hydrochloric and phosphoric hydrobromic acids have been extensively used to substitute for sulfuric acids. For hydrochloric acid

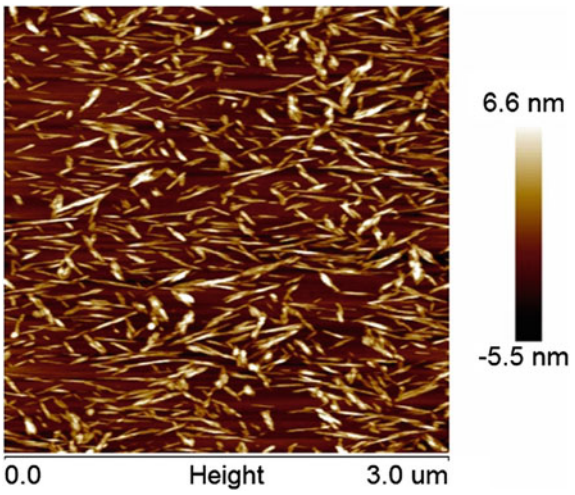

Fig. 1 AFM image of CNCs obtained by sulfuric acid hydrolysis (Raw materials: cotton linter, measured with Veeco Picoforce II)

catalyzed hydrolysis, the acid concentration is usually between 2.5 and 4 N with a reflux temperature, and the reaction time will vary depending on the source of the cellulosic material. However, the dispersing ability of NCs obtained by hydrochloric acid is limited, causing aggregation of NCs in aqueous suspensions [2]. In order to obtain nanocellulose with excellent dispersibility and fewer sulfate groups, a combining treatment using hydrochloric acid hydrolysis with sulfuric acid has been studied to control sulfate moieties on nanocellulose surfaces [3]. This treatment can generate spherical NCs instead of rod-like nanocellulose. These spherical NCs exhibit better thermal stability because of the fewer sulfate groups on their surfaces [126].

2.1.2 Mechanical Treatments

The production of NCs through fibrillation of cellulose fibers needs intensive mechanical treatment. Extensive separation of natural fibers into NCs can be achieved if conventional refining and homogenization methods are applied [128]. Cellulosic fibers are disintegrated into small fibrils by mechanical action, with lengths of micron scale and widths ranging from 10 to a few hundred nanometers. The resulting nanocellulose suspensions display gel-like characteristics in water.

For the refining treatment, the cellulose fibers are subjected to repeated cyclic stresses by being forced through a gap between stator disks and rotors in a disk refiner. This mechanical treatment causes irreversible changes in the fibers and increases their bonding potential by transforming their morphology and size [80]. Generally, the refining process is usually carried out prior to homogenization because of the gradual peeling of the external cell wall layers and the exposing of the S2 layer during the refining. This peeling process results in external fibrillation of fibers and loosens the fiber wall, which is conducive to the subsequent

homogenization treatment [81]. Another strategy to break up cellulose fibers into nanosized c structures is homogenization, which involves passing the fibers through a spring-loaded valve assembly at very high pressure. The valve opens and closes in rapid alternation, resulting in that the fibers are subjected to a large pressure drop with impact and shearing forces [80]. López-Rubio et al. [65] reported the mechanical diminution process, using a microfluidizer for the homogenization step. Such mechanical dispersion leads to nanostructures of cellulose fibers with diameters ranging from 20 to 100 nm and lengths of several tens of micrometers. Iwamoto et al. [46] reported the preparation of NFCs using homogenizing with cycles of 15 cycles, while further treatment of 30 cycles did not improve the fibrillation. This observation was in accordance with Malainine et al. [68], who achieved nanoscaled cellulose fibrils by applying 15 cycles through a homogenizer operated at 500 bars.

Except for the above-mentioned technologies, other methods of mechanical treatments including high-speed blending [122], cryocrushing [20], and steam explosion [51] are also developed. However, they are still in an early stage and far from being widely used.

Although mechanical treatments can produce nanoscaled cellulose fibrils, the major drawback is the high energy consumption accompanied with the mechanical disintegration [32]. In order to decrease the energy consumption, certain pretreatments including alkalization and oxidation are applied before mechanical treatments. Alkaline treatment of cellulose fibers can decompose the lignin structure and help to separate the structural linkages between lignin and carbohydrates. However, in order to obtain the intact nanofibers, alkali treatment conditions need to be carefully controlled to avoid excessive cellulose degradation. Alkali hydrolysis needs to be limited on the fiber surface only [126]. Saito et al. reported that 2,2,6,6-tetramethyl piperidine-1-oxyl (TEMPO) radicals could be used for oxidation of cellulose materials before mechanical treatment. TEMPO-mediated oxidation introduces carboxylate and aldehyde groups into solid native celluloses under mild aqueous conditions [94]. The initial fibrous morphology of natural cellulose is mostly unchanged after the TEMPO-mediated oxidation. The oxidation occurs only at the surface of the cellulose fibrils, making the fibrils negatively charged. These negative charges promote repulsion of the fibers, thus easing the subsequent mechanical treatments. NFCs were prepared with TEMPO-mediated oxidation followed by homogenization. The obtained NFCs formed network structures when they are made into films, whose TEM images are shown in Fig. 2.

2.1.3 Enzymatic Treatment

Analogously to the acid hydrolysis treatments, cellulase enzymes are expected to attack the amorphous regions of cellulosic materials and isolate NCs. The degradation processes involve a series of cellulases. Recently, a novel method to study the enzymatic dynamics was applied and demonstrated the obvious difference in time required to hydrolyze crystalline and amorphous films of cellulose [133]. Such

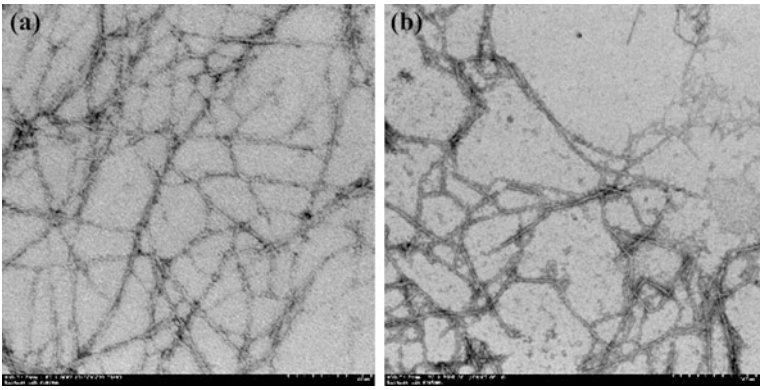

Fig. 2 TEM images of NFCs obtained by TEMPO-mediated oxidation and homogenization using different wood pulp. **a** Eucalyptus: **b** Pine

difference enables the separation of amorphous and crystalline components of the cell wall. Moreover, NCs prepared from enzymatic treatment show a more favorable structure than those produced by strong acid hydrolysis. Cellulose fibers subjected to low enzyme concentration (0.02 %) are successfully disintegrated while their molecular weight and fiber length are well remained. According to the above principle, Henriksson et al. [40] and Pääkkö et al. [83] found that endoglucanase treatment facilitates the disintegration of cellulosic wood fiber pulp into cellulose nanofibers. Janardhnan and Sain [49] reported that nanocellulose obtained by enzymatic treatment followed by high-shear refining exhibited a narrow particle size range.

2.2 Structure and Properties of Nanocellulose

Since isolated from natural cellulose fiber, some properties of NCs are similar to native cellulose, such as naturally renewable, biodegradable, and biocompatible. Moreover, NCs are supramolecular materials with nanoscaled structure. Thus, they exhibit some unique properties like high aspect ratios, high crystallinity, and high mechanical strength.

2.2.1 Morphology and Geometrical Dimensions

The morphology and geometrical dimensions (diameter (D), length (L), thickness (T), and aspect ratio (L/D)) of NCs always vary due to the different sources and isolation methods. The precise morphological characteristics can be studied by light scattering techniques or microscopy, including polarized and depolarized dynamic light scattering (DLS, DDLS), small-angle neutron scattering (SANS), transmission

electron microscope (TEM), atomic force microscope (AFM), and scanning electron microscope (SEM) [25, 75, 112]. NCs with rod-like morphology are generally isolated from botanic sources, with length and diameter ranging from 100 to 700 nm, and from 5 to 30 nm, respectively. Bacterial cellulose obtained from microorganism exhibits diameters from 5 to 50 nm, and lengths ranging from 100 nm to several mm [31]. A combination of mild enzymatic hydrolysis and high mechanical shearing forces can produce NFC [40]. These nanofibrils are consisted of individual nanoparticles with a length ranging from hundreds of nm to several mm, and a lateral dimension around 5 nm. Generally, NFCs tend to aggregate, leading to the dimensions range from 10 to 30 nm, or more. According to diameters and lengths, the aspect ratios of CNCs and NFCs are both large, providing a critical length for stress transfer in nanocomposites from the matrix to the reinforcing phase. This property is favorable for the potential reinforcing capabilities of NCs when used in nanocomposite materials.

2.2.2 Stiffness and Crystalline Characters

The crystalline structure of nanocellulose depends on the ordered packing of the raw cellulose chains. Theoretically, the crystallinity (ratio between the mass of crystalline regions and the total mass of nanocrystals) of nanocellulose should be 100 %, but the presence of the amorphous regions in nanocellulose may result in a lower degree of crystallinity. Like natural cellulose, the crystal structure of nanocellulose is constituted by amorphous and crystalline domains. The degree of crystallinity depends on their origin and on the isolation method. Actually, CNCs obtained from acid hydrolysis exhibit higher crystallinity (up to 90 %) compared with natural cellulose, due to the decomposition of amorphous regions during the hydrolysis process. However, the crystallinity of NFCs is lower than CNCs. Repeated passes through a grinder during mechanical treatment cause a reduction in the degree of polymerization of cellulose nanofibers, resulting in an increase in crystallinity and thermal expansion. Such changes of crystal structure lead to a decrease in the mechanical properties when using NFCs as reinforcement in nanocomposites [47].

Because of the high crystallinity, NCs exhibit prominent mechanical properties with high stiffness. Elastic modulus of NCs has been reported from 120 to 220 GP, using the technique of X-ray diffraction (XRD) [26]. Subsequently, more methods have been used to calculate and confirm the elastic modulus of NCs. Raman spectroscopy technique is widely utilized to calculate the elastic modulus of native cellulose crystals from cotton and tunicate, yielding values of 105 GPa [93], and 143 GPa [109], respectively. In another work, the modulus of tunicate cellulose nanocrystals of around 150.7 GPa was obtained, when using AFM bending stiffness approach as shown in Fig. 3 [48].

A modulus of 40–60 GPa is usually found for natural cellulose fibers, while the value potentially increases to 80 GPa for single cells [24] and then to a range of 100–140 GPa for NFCs and CNCs [43]. Such high strength of NCs obtained from

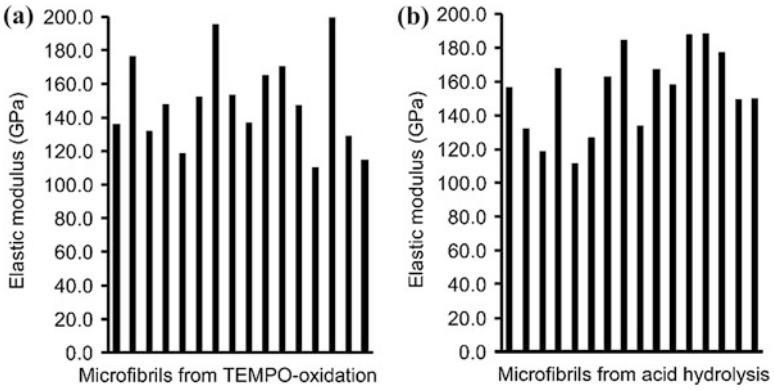

Fig. 3 Elastic moduli of the microfibrils prepared by **a** TEMPO oxidation and **b** acid hydrolysis of tunicate cellulose. (Reprinted with permission from Ref. [48], Copyright © 2009, American Chemical Society)

different origins is a desirable property for a reinforcement phase in nanocomposites. The desire is to enhance stress transfer and then improve the final composite modulus. Nevertheless, such reinforcing effects can only be obtained from NCs with a high aspect ratio. Only NCs with aspect ratios higher than 50 guarantee an efficient reinforcement effect.

2.2.3 Active Hydroxyl Groups for Functionalization

NCs possess a reactive surface covered with a large amount of active hydroxyl groups, which can facilitate forming of hydrogen bonds between the polymer matrices and nanocellulose filler. Moreover, hydroxyl groups on the surface modify the NCs via a chemical reaction strategy. These groups also promote the dispersibility of NCs in polar solvents. However, the accessibility of hydroxyl groups connecting with different carbon bonds may vary. For example, CNC is universally assumed that the covalent hydroxyls conjunct to the primary hydroxyl group (C_6–OH) possess the most accessibility, while the other two hydroxyl groups in the cellulose unit do less.

Owing to their strongly interacting surface hydroxyl groups, NCs have a significant tendency to self-association [61]. This is a very desirable feature for the formation of percolating architectures between NCs and a host polymer matrix. The prominent reinforcement observed for cellulose nanocomposites can be ascribed to the formation of rigid percolating network in which stress transfer can be facilitated by hydrogen bonding among the nanocrystals. It was reported that tunicate whiskers used as reinforcing phase in the polymer systems can both enhance the thermomechanical property and reduce the water sensitivity, while still keeping the biodegradability of the nanocomposite. This behavior may be caused by the strong interactions of hydrogen bonds between cellulose whiskers, which induce a rigid

network [64]. However, the excess intra- and intermolecular hydrogen bonds can also cause nanocellulose aggregation and limit the mechanical reinforcing. Therefore, these aggregations need to be avoided during the production of nanocomposites.

2.2.4 Dispersibility of NCs in Different Solvents

The dispersion state of NCs in aqueous and organic solvents determines significantly their properties and applications. However, the hydrophilic nature of NCs often results in poor compatibility within hydrophobic polymer matrices. Furthermore, the strong hydrogen bonds formed during drying lead to irreversible agglomeration of NCs. In aqueous suspensions, due to the hydrophilic nature and high surface area, NCs tend to aggregate because of their strong interparticle hydrogen bonding. As already mentioned, when sulfuric acid is used for acid hydrolysis, negatively charged surface acid groups (OSO_3^-/H^+) will be introduced on the surface of NCs promoting a perfectly homogeneous dispersion. However, the partial substitution of surface hydroxyl groups by sulfate groups decreases the accessibility of surface hydroxyl groups, which will give an adverse effect to the formation of percolating network in nanocomposites and will reduce the reactivity for chemical modification [82]. Thus, desulfation method should be applied to recover the surface of nanocellulose with hydroxyl groups. Huang et al. proposed a treatment based on the addition of ammonia (0.5–1 wt%) to form electrostatic conjunction between positive charge of NH_4^+ and negative charge OSO_3^-, reducing the effect of sulfate groups in the application of nanocellulose [62].

Except for water suspension, good dispersion of NCs can be achieved in a hydrogen-bond-forming solvent, when self-interactions are "switched off" by competitive dispersing. Nanocellulose can also be dispersed in dimethylsulfoxide (DMSO), dimethylformamide (DMF), and *N*-methyl pyrrolidine (NMP) without any surface modifications [70, 96, 124]. Berg and coworkers have reported that stable suspensions of tunicate nanowhiskers with negatively charged sulfate groups, commonly produced by hydrolysis of the native cellulose, can be prepared in NMP [124], *N,N*-dimethyl formamide (DMF) [96], m-cresol [124], and formic acid [124] by freeze-drying of aqueous suspensions and re-dispersion of the obtaining aerogel in the organic solvent [124]. The obtained images and results were shown in Fig. 4 and Table 1. Viet showed similar cellulose nanowhisker dispersing in polar organic solvents using nanocelluloses obtained from cotton [125]. However, NCs without surface charges, prepared by hydrochloric acid hydrolysis, do not disperse well in aprotic solvents (DMSO, DMF, NMP).

The excellent dispersibility of NCs in water attracts attentions in the area of preparing hydrophilic composites. However, most of the polymer matrices, especially SMPs dissolve better in organic solvents compared with water suspensions. In order to improve the dispersibility of NCs in organic media, several "solubilizing methods" have been explored, including chemical modification [4] and the use of surfactants [64]. These methods can tune the surface energy of NCs to improve their compatibility, especially when dispersed in nonpolar solvents and combined with

Fig. 4 Photographs of dispersions of SO_4-TW viewed through cross-polarizers at 5.0 mg/mL. From *left* to *right* as-prepared in water, freeze-dried, and re-dispersed in water, DMF, DMSO, *N*-methyl pyrrolidone, formic acid, and m-cresol. (Reprinted with permission from Ref. [124], Copyright © 2007, American Chemical Society)

Table 1 Overview of the dispersability of lyophilized tunicate whiskers in polar solvents

Solvent	SO_4-TW	HCl-TW
Water	++[a]	–
N,N-dimethyl formamide	+	–
Dimethyl sulfoxide	+	–
N-methyl pyrrolidone	++	–
Formic acid	++	++
m-cresol	++	++

(Reprinted with permission from Ref. [124], Copyright © 2007, American Chemical Society)

[a]Dispersability was examined at a concentration of 1 mg/mL using birefringence as an indicator. ++ Dispersed after 6 h or less of sonication. + Dispersed after 24 h (72 h in the case of *N,N*-dimethyl formamide) of sonication at ca. 60 °C. – Did not disperse

hydrophobic matrices. For instance, after adding surfactants, the suspensions of cotton and tunicate cellulose nanocrystals were stable in toluene and cyclohexane solvents [41]. Good dispersibility of these suspensions could be evidenced by using TEM images. The surfactant method has been proven to be an effective and simple way to stabilize NCs in organic suspensions.

3 Chemical Modification of Nanocellulose

The application of NCs in hydrophobic SMPs is limited due to their hydrophilicity. Thus, the compatibility of NCs with hydrophobic or nonpolar matrices needs to be improved by chemical modifications. The main challenge for the chemical

modification of NCs is to change the surface structure only, while the original morphology and crystal integrity of NCs maintain intact. Due to the different accessibilities of hydroxyl groups at the surface, different chemical modifications including noncovalent modification, etherification, esterification, silylation, oxidation, and polymer grafting can be attempted on the NCs.

Noncovalent surface modifications of NCs are typically performed via adsorption of surfactants, oppositely charged entities, and polyelectrolytes. The surfactant molecules form a thin layer about 15 Å at the surface of NCs. These surfactant-coated NCs dispersed well in nonpolar solvents [12]. Zhou et al. [141] introduced a new way of noncovalent modification based on the adsorption of saccharide-based amphiphilic block copolymers. Xyloglucan oligosaccharide-poly (ethylene glycol)-polystyrene triblock copolymer was adsorbed onto the surface of CNCs. The resulting nanocellulose showed excellent dispersion abilities in nonpolar solvents. Lee et al. [56] also used an entirely bio-derived polylactic acid (PLLA)-carbohydrate copolymer to modify BNC. They used polylactide carbohydrate copolymer (RP1) as a compatibilizer. The carbohydrate-based tail showed strong interaction with BNC surface through hydrogen bonding, thus improving the compatibility of BNC with PLA matrix. SEM images of PLLA, PLLA with RP1 (5 wt%), and RP1 on single BC nanofibers are illustrated in Fig. 5.

Except for noncovalent surface modifications, modification of hydroxyl groups through esterification is also widely implemented. Among the esterification reactions, acetylation is the most widely studied. It is focused on adding a mixture of acetic acid and acetic anhydride in the presence of a catalyst such as perchloric or sulfuric acid. Homogeneous and heterogeneous acetylation of NCs has been studied by Chanzy and Sassi by using acetic anhydride in acetic acid [97]. Ultrastructural study of NCs after acetylation showed that the reaction was performed by a reduction of the crystal diameters, while the length of NCs was hardly affected. An environmentally friendly acetylation of NCs was recently reported by Yuan et al. [140], using alkyenyl succinic anhydride (ASA) emulsions as a template. The resulting derivative conferred the acylated NCs a highly hydrophobic character, leading to easy dispersing of modified NCs in solvents with different polarities.

Another mechanism to stabilize the NC suspensions based on a partial silylation has been recently proposed. The introduced alkyl molecules include *n*-butyl, *n*-octyl, *n*-dodecyl, and isopropyl [35], which are randomly distributed at the nanocellulose surface. Their content is directly dependent on the degree of surface substitution (DS). It has been demonstrated that with DS between 0.6 and 1, NCs could disperse in solvents of low polarity, leading to stable suspensions with intact morphological properties. A coupling of NCs with *N*-octadecyl isocyanate via a bulk reaction has also been reported [102]. The modification enhanced dispersibility of NCs in organic medium. The compatibility of modified NCs with polycaprolactone (PCL) was also improved, leading to a melioration of the ductility and stiffness of resultant nanocomposites.

Surface-initiated polymerization has been used extensively to graft polymers onto the surface of macroscopic cellulose fibers. Grafting of the polymeric chains have also been reported on the surface of NCs, using the grafting from [78] and

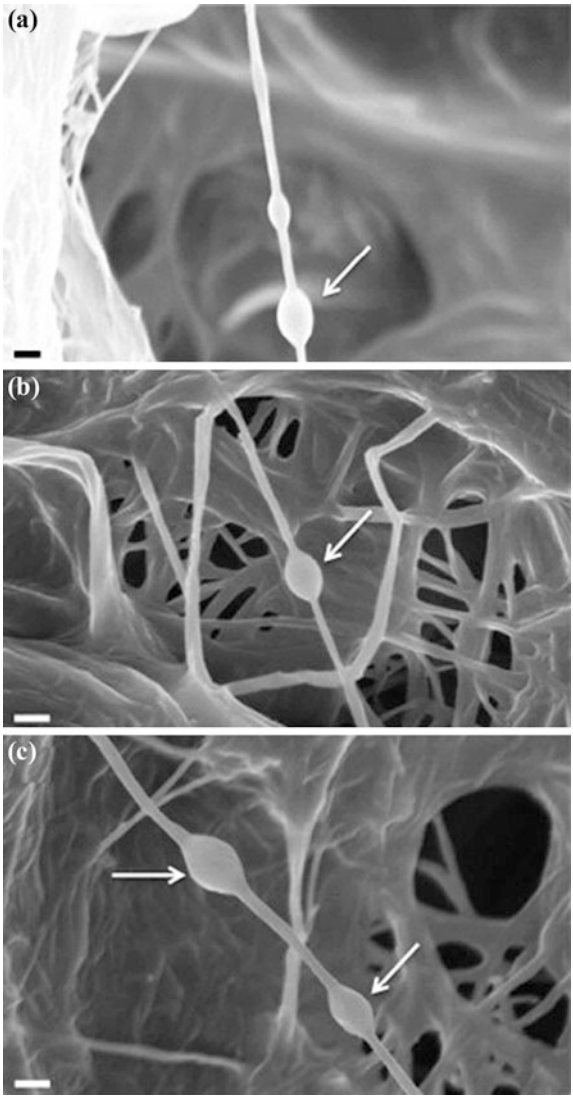

Fig. 5 Typical example of SEM images showing a polymer droplet on a single BC nanofiber, where the polymer is **a** PLLA, **b** PLLA and RP1 (5 wt%) and **c** RP1. The *arrow* indicates the polymer droplet on a single BC nanofiber. The scale bar represents 200 nm. (Reprinted with permission from Ref. [56], under the terms of the Creative Commons Attribution License (CC BY))

grafting onto [36] techniques. For instance, grafting of PCL on the surface of CNCs can be performed in toluene using stannous octoate ($Sn(Oct)_2$) as the catalyst [37]. A final PCL content of 85 wt% in the modified CNCs was reported. The PCL-grafted CNCs were subsequently shown to be a more obvious reinforcement to the mechanical properties of PCL–CNC composites compared with unmodified CNCs. Moreover, Habibi also reported that better compatibility can be obtained when the grafted chains and the polymer matrix are the same, due to the co-continuous phase forming between nanocellulose and the matrix [37]. Moreover, PCL is a significant component for the synthesis of shape-memory polyurethane

(SMPU). Therefore, PCL-grafted nanocellulose is a perfect choice for reinforcing the PCL-based SMPU. The formation of a continuous interphase between the nanocellulose phase and polymer matrix phase can improve their interfacial adhesion and promote the dispersibility of NCs in SMPU.

Another technique for the grafting of NCs with polymeric chains is the surface-initiated atom transfer radical polymerization (SI-ATRP). Yi et al. published the first report of using SI-ATRP to grow polymer brushes from the surface of CNCs [139]. 2-bromo-2-methylpropionyl bromide (Br-MPBr) was used as the initiating agent. The polymerization of styrene, 6-[4-(4-methoxyphenylazo) phenoxy] hexyl methacrylate (MMAZO) or *N,N*-dimethylaminoethyl methacrylate (DMAEMA) was then carried out in the presence of Cu(I)Br. The resulting modified CNCs exhibited thermally sensitive liquid crystalline behavior and could be applied in producing thermally sensitive shape-memory nanocomposites. Morandi et al. [78] studied the reaction conditions for the grafting using 2-bromoisobutyryl bromide as an initiator, followed by a series of polymerizations of polystyrene. A maximum surface modification of initiator content of up to 70 % was achieved, while the polystyrene content reached 22 wt%. The surface properties of modified NCs were controllable by tailoring the grafting density and the polymer chain length.

4 Application of NCs in Shape-Memory Materials

Shape-memory polymers are a series of "smart" materials which have various types of molecular architectures designed for different function. With the addition of NCs, new shape-memory materials can be manufactured for extensive fields of applications. In recent years, NCs have been widely used to enhance the hydrogen bonding density in SMPs, leading to improvements of mechanical and thermal properties of the nanocomposites. Moreover, the role of NCs in shape-memory materials may be classified as reinforcement and "switches" due to the different shape-memory effects of the SMPs.

4.1 Shape-Memory Effects (SME) of SMPs

When exposed to ambient stimuli, SMPs can achieve a temporary strain fixing. The temporary deformation can recover to the original shape through various physical methods with the potentially large extensibility derived from the intrinsic elasticity of polymeric networks. This alternation of deformation and recovery is caused by the "shape-memory effect" (SME) of the SMPs. From a macroscopic viewpoint, SME in polymers can be graphically depicted using the dynamic mechanical analyzer (DMA) which measured tensile elongation versus tensile stress and temperature [88]. Other important parameters for describing the shape-memory properties are the strain fixity rate (R_f) and strain recovery rate (R_r). R_f stands for the

ability of the switch segments to fix the mechanical deformation, whereas R_r quantifies the ability of SMPs to memorize their permanent shape [88].In general, SME is not linked to any intrinsic material property, but it depends on a combination of suitable molecular polymer network and a certain programming process. Therefore, a polymer with network structure for SMPs requires network points (netpoints) and molecular switch segments. Cross-linked polymers (covalently or physically) are elastic to large strains above either T_m (crystalline cases) or T_g (amorphous cases) of the bulk material. When $T > T_{crit}$ (T_m, T_g or other), chain segments between cross-link points of the polymer can deform quite freely and tend to being twisted randomly, leading to a "superelasticity" effect of polymer networks [89]. Based on this principle, SMPs can be typically categorized into two main types: thermally and athermally induced SMEs according to the different stimuli.

4.1.1 Thermally Induced SMEs

Thermoresponsive SMP is the most prominent class of SMPs studied in recent years. The corresponding SME originates from a phase transformation, associating with a change in volume [42, 123]. Various thermomechanical and viscoelastic models have been studied to illuminate the viscoelastic deformation with the shape-memory behavior [10, 63].

A thermoresponsive SMP can be thermally actuated by increasing the environment temperature above its thermal transition (T_{trans}) through direct or indirect heating. Thermally induced SMPs consist two different phases: the glassy state and the amorphous state. Their deformation properties are dependent on the transition of polymer chains from the glassy state to the rubber-elastic state. In the glassy state, movements of the polymer segments at original shape are frozen. When the thermal activation increases, the transition to the rubber-elastic state occurs, leading to the increasing flexibility of chain rotation around the segment bonds. This situation enables the chains to form one of the possible and equivalent structures without disentangling significantly. This conformation is entropically favored and much more probable than a stretched conformation, causing compact random coils in the majority of the macromolecules.

Thermally induced SMPs can be stabilized in the deforming state in a temperature range relevant to the particular application. This shape-memory functionality can be reached by using the network chains of the polymer as a kind of molecular switch. Thus, the flexibility of the segments is a function of the temperature. Various types of thermal transitions are suitable according to the switch segments, including glass transition (T_g), melting transition (T_m), and liquid-crystalline phase transition (T_{LC}). For the thermal transition of T_g, transformation of polymer chains occurs from the glassy to the elastic state during the recovery process, providing sufficient flexibility for the return of switch segments to the random coil formation [121]. In the case of T_m, crystallization induced by strain of the switching segment can be initiated by cooling down the SMP which has been stretched above T_{trans}. In general, the crystallites obtained with this transition temperature are adequate to fix

the temporary shape, although the crystallization is incomplete and a certain amount of the chains remains amorphous. When the polymer is heating above T_{trans}, the crystallites melt and the switch segments return to the random coil-like structures. In the recovery steps, crystallites formed prevent the segments from immediately reforming to the coil-like structure, and the permanent shape is spontaneously recovered by the netpoint transformation. The permanent shape of shape-memory networks is stabilized by the covalent netpoints, whereas the permanent shape of shape-memory thermoplasts is fixed by the phase with the highest thermal transition (T_{perm}). The process of thermally induced SME is shown in Fig. 6.

The SMEs of thermoresponsive SMPs can be quantified by cyclic, thermomechanical investigations. A single cycle includes deforming the test piece and recovering to its permanent shape. Results obtained from such a measurement are usually presented in a strain–stress (ε-σ) curve. Different effects during the shape-memory process result in changes of the curve, especially when the distorted sample is cooled down. These effects cause different expansion coefficient of the stretched material at temperatures above and below T_{trans}, as a result of entropy elasticity. Volume changes also arise from crystallization in the case of T_{trans} reaching a melting point.

According to the different switching segments including physical cross-links of physical intermolecular interactions and chemical cross-links of covalent bonds, thermal-responsive SMPs can be classified into two different categories: thermoplastic SMPs and thermosetting SMPs [55, 60]. For the thermoplastic SMPs, the formation of a phase-segregated morphology in the molecular conformation is the fundamental mechanism of the thermally induced SME. One phase in the polymers provides the physical cross-links and another phase acts as a molecular switch [57]. For the thermosetting SMPs, chemically interconnected structures are possessed by covalently cross-linked bonds, determining the original shape of SMPs. Their switching segments are generally the network chains between netpoints, with the thermal transition of the polymer segments using as the shape-memory switch. Their chemical, thermal, mechanical properties and SMEs are determined by the type and length of network chains, the cross-linking density, as well as the reaction conditions, and curing times.

Due to the accurate and adjustable response to thermal stimuli, thermal-responsive SMPs can be widely used in different areas including smart

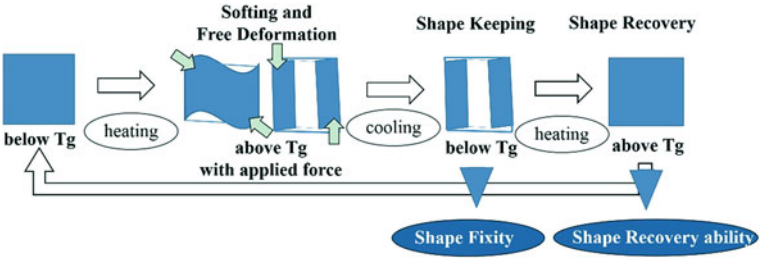

Fig. 6 Shape-memory process of thermally induced SMPs

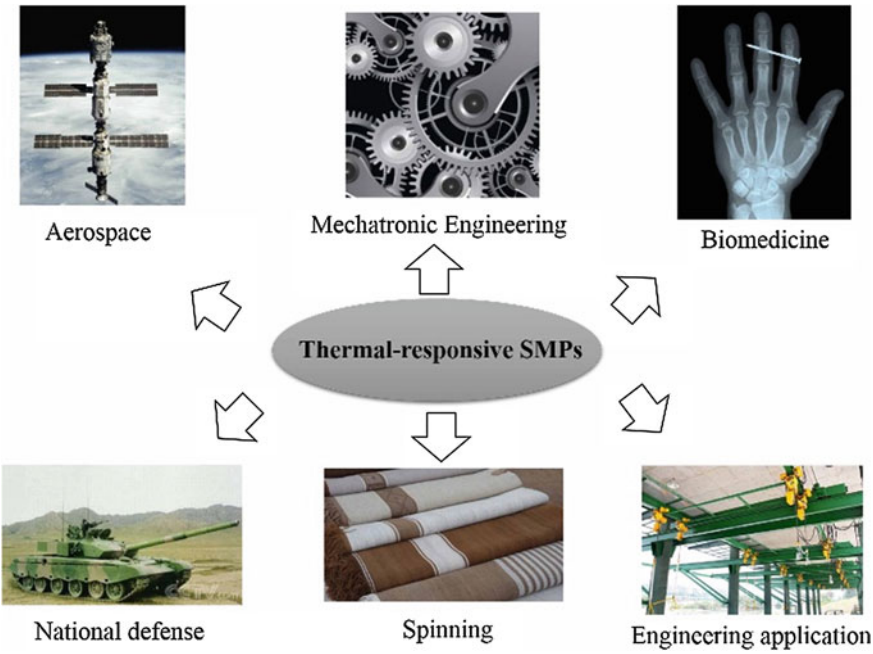

Fig. 7 Applications of thermal-responsive SMPs in different areas

textiles, biomedicine, automobile actuators, and self-healing composite systems, [27, 73] as shown in Fig. 7. Another utilization of thermal-responsive SMPs is cardiovascular stenting [137]. Due to their thermal responsiveness, the stent of SMPs can be activated at body temperature, resulting in a natural deployment without any auxiliary devices.

4.1.2 Athermally Induced SMEs

Athermally induced SMEs are caused by afebrile stimuli including light, electricity, magnetism, and solution-triggered actuation [58, 69, 76]. Wu et al. [132] reported a biodegradable light-sensitive SMP consisting of block polyurethanes and pendant cinnamamide moieties. This SMP was sensitive to nonheating-based light stimulus, whereas the shape fixity and activation were only 20–55 % and 60–120 min, respectively. Schmidt et al. [98] incorporated superparamagnetic nanoparticles of ferriferrous oxide into a thermoresponsive SMP. The magnetite nanoparticles with content between 2 and 12 wt% in the thermosetting SMP served as nanoantennas for magnetic heating. In the DMA test, the rectangular strip was deformed to a helix temporary shape at 70 °C and recovered to the original straight shape in 20 s with the application of an alternating electric field.

Recently, athermally induced SME caused by solution-sensitive SMP system has been widely discussed, especially for water-triggered actuation. The mechanism of the solution-induced SME is the plasticizing effect of solution molecule on polymeric materials. This effect can increase the flexibility of the polymer macromolecular chains and reduce the transition temperature of SMPs until shape recovery occurs [67]. It is well known that phase transition of polymeric materials often accompanies with great changes in physical properties. The solution-responsive SME is based on such a change of a large decrease in modulus. Meanwhile, this mechanism involves interactions between the polymeric macromolecules and micromolecules of the absorbed solution [59]. Physical swelling of polymers is another effective method to cause solution-responsive SMEs. The swelling effect can be triggered by the interaction between polymer macromolecules and solvent molecules, leading to an increase of the flexibility of polymer chains and a decrease in T_g. Toluene solvent can be selected as the trigger of a styrene-based SME due to its intensive swelling effect on the shape-memory polymer. After swelling, the flexibility of the macromolecular chains significantly increases, leading to a decrease of the transition temperature. Thus, the solvent-induced shape recovery occurs at a lower temperature [45].

Different from the organic solvent, water-induced SME can be performed by using hydrophilic polymers as soft domains of SMPs. Incorporation with hydrophilic polyols such as PEG allows the potential for shape-recovery process triggered by water. Moreover, an advantage of this method is the low melting temperature of the hard domain ($\sim$110 °C) amenable to thermal processing, but high enough for shape-recovery triggering [52]. Another method to obtain water-active SME is using a hydrophilic ingredient to synthesize shape-memory composite, such as nanocellulose and chitosan. For instance, the shape-memory composite containing carbon black (CB) decreased their moisture sensitivity [138]. During the water-driven shape-memory process of a CB/SMPU composite, a straight CB/SMPU wire was bended into a circular shape and fixed in a dry state. After being immersed in water for about 2 h at room temperature, the circular shape recovered most of its original shape. Chen et al. [21] reported a water-sensitive biodegradable film made of chitosan cross-linked PEG-400. The raw materials used in the preparation of the developed film are relatively hydrophilic. The self-expansion processes of the polymeric immersed in PBS solution were shown in Fig. 8. The degradable material is proposed to be used for local drug delivery or as an alternative to metallic stents.

4.2 Shape-Memory Polyurethane (SMPU)

SMPU is one of the most extensively studied thermoresponsive SMPs. It is commonly known as multiblock or block copolymers. Polyurethane is synthesized by the reaction of low molecular weight polyols with diisocyanates and diols (chain extender). During the synthesis, polyols terminated with hydroxyl ends are reacted

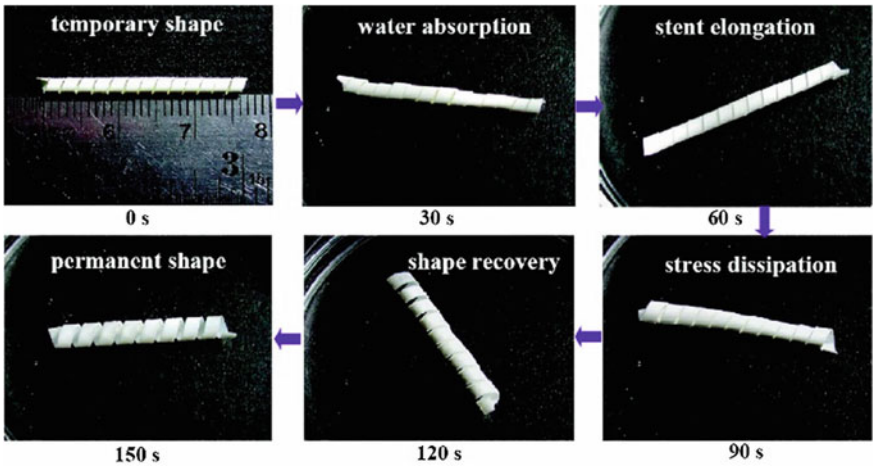

Fig. 8 Photographs of the time courses of self-expansion of the polymeric (CS/glycerol/PEO400) stent, immersed in PBS solution, stimulated by hydration. (Reprinted with permission from Ref. [21], Copyright © 2007, American Chemical Society)

with the diisocyanates and diols, in order to form a urethane linkage [86]. The semicrystalline hard segments of polyurethane are formed with the aromatic or aliphatic diisocyanate through the molecular interactions between the urethane linkages by hydrogen bonding, while the soft segments are made up of polyols groups, as the switching segment. The permanent shape of SMPU is maintained by the physical cross-linking of the hard segments, while the shape-memory behavior is attributed to the T_{trans} of the soft segments. Moreover, T_{trans} of SMPU can either be represented by T_g, as the soft segment being completely amorphous, or by T_m, as the soft segment being able to crystallize. The type and length of segments dramatically affect the properties of PUs [70]. The common soft segments uses for SMPU are made up of an amorphous polyol, including polyester and/or polyether. Many studies have been discussed about poly(tetramethylene glycol) (PTMG) used as the soft segment with various combinations of diisocyanates, such as 1,4-phenyldiisocyanate (PDI), 4,4′-diphenylmethane diisocyanate (MDI), as well as chain extenders of ethylenediamine (ED) and 1,4-butanediol (BD) [22]. The contents of hard segments and the length of soft segments have been reported to strongly influence the properties of SMPU, especially with respect to the recovery rate, shape fixity, and recovery speed. In general, hard-segment content should be between 35 and 40 wt%, in order to generate a shape-memory effect. Meanwhile, the soft segment length influences the overall hard-segment content, since the hard-segment content increases with decrease of polyol molecular weight. Chun et al. [23] reported the synthesis of SMPU with PTMG as soft segments. Molecular weight distribution of PTMG influenced the SME of obtained material. The results showed that a bimodal molecular weight distribution of soft segment can achieve a higher recovery rate and increased shape retention. Wang et al. [127] prepared

PLA-based SMP in a similar approach (diol route) and evaluated the mechanical and shape-memory properties. It was reported that SMPU with PLA as soft segment displayed better shape-recovery behavior under a small deformation and responded more rapidly to the thermal stimuli.

Except for the physical cross-link, chemical cross-linked polyurethanes were also synthesized by using excess diisocyanate or cross-linkers like trimethylol propane and glycerin. Xu et al. [135] synthesized hybrid PU with Si–O–Si cross-linker. The linkages acted as the netpoints of SMPU, as well as inorganic fillers for reinforcement. Buckley et al. [13] synthesized a novel thermosetting SMPU using 1,1,1-trimethylol propane as a cross-linker. Both of the recovery temperature and recovery rate increased due to introduction of the cross-linking.

Due to the excellent thermoresponsive SME, different structures and shape-memory properties, the application areas of SMPU are various. Baer et al. [8] studied the effect of processing parameters on the thermomechanical properties of SMPUs. It was obvious that when cooled at different rates, a significant variation in rubbery modulus occurred. Such thermomechanical properties of these materials are suitable for various medical applications. Another highlighted application of SMPU is the shape-memory composites. Different fillers give SMPU various types of stimuli responsibilities, as well as the reinforcing effect. Koerner et al. [54] studied polyurethanes reinforced with carbon nanotubes (CNTs) or CB of similar size. They discovered that both of the nanocomposites exhibited increasing shape fixity. Meanwhile, the CNT-reinforced SMPU showed almost 100 % shape recovery compared to CB- reinforced SMPU with a limited shape recovery of 30 %. Park et al. [84] synthesized Celite/SMPU composites using Celite as a cross-linker. The Celite was incorporated with polyurethane during the middle step of the polymerization. The addition of Celite improved the mechanical and shape-memory properties of SMPUs, with an optimized Celite content of 0.2 wt%.

4.3 Nanocellulose/Shape-Memory Polymer (NC/SMP) Nanocomposites

In general, SMPs exhibit lower strength and stiffness, limiting their use for many advanced applications. Thus, the incorporation of reinforcing fillers with SMP matrices has been investigated to improve their mechanical properties. Moreover, the addition of fillers can produce new “switches” and diversify the applications of SMPs, depending on their supermolecule structures [34]. As discussed above, NCs exhibit prominent mechanical properties with high elasticity modulus, due to their high crystallinity and stiffness, which make them suitable for the reinforcement of SMPs. Moreover, because of the substantial hydroxyls on the surface, hydrogen bonds can be easily formed between NCs and SMP matrices, resulting in new ambient responsive SMEs, especially for water-induced shape-memory

nanocomposites. The macroscopic behavior of NC-contained shape-memory materials depends on the volume fraction, specific behavior and the microstructure of each phase, as well as the interfacial properties between NCs and SMPs. In general, mechanical properties of NC/SMP nanocomposites can be affected by parameters including the geometrical aspect ratio, the processing method, and the resulting competition interactions between NCs and SMPs. The evaluation of resulting interactions among these parameters between NCs and matrices determines the differences of mechanical properties and SMEs in final materials.

4.3.1 Processing Methods of NC/SMP Nanocomposites

For shape-memory nanocomposites using NCs combined with SMPs, several challenges are widely studied, including the separation efficient of NCs, compatibilization of NCs with the matrices, and development of suitable methods for processing the NC/SMP nanocomposites [102]. The processing methods present the possibility of the formation of a continuous network and determine the final properties of the nanocomposites. These methods for manufacturing of NC/SMP nanocomposites include extrusion, hot pressing, and evaporation. The treatments cause changes in the orientation and interaction of NCs. Breakage of the fillers occurs and the aspect ratio also changes. These transformations ultimately affect the final mechanical properties of NC/SMP materials. For this reason, these processing methods are classified in an ascending order of their reinforcement efficiency: extrusion < hot pressing < evaporation, associated to the orientation and probable breakage of nanocellulose during processing [79]. In this way, aqueous and solvent solution casting via evaporation is the most effective method of preparing NC/SMPs nanocomposites. During slow water evaporation, the rearrangement of nanocellulose molecules occurs because of Brownian motions in the suspension or solution. Thus, the nanoparticles have enough time to interact and connect, forming a continuous network as the basis of their reinforcing effect. Moreover, due to the hydrophilic character of NCs, the polar aprotic solvents such as DMF was used to successfully redisperse the freeze-dried NCs, which formed NC/SMP materials without altering the formation of the percolating cellulosic network responsible for their high mechanical properties [100]. Conversely, during the freeze-drying/hot-pressing process, NCs arranged in the suspension are first frozen. During the hot-pressing stage, the melt viscosity of polymer matrices strongly limited the rearrangement of NCs, leading to a poor compatibilization of NCs with SMP matrices. Auad et al. [5] successfully incorporated NCs into SMPU using a suspension casting method. A small amount of well-dispersed NCs improved the stiffness of SMP dramatically, with no obvious decrease of shape-memory properties. Rueda et al. [91] mixed CNCs with SMPU in DMF and obtained films with a thickness of 0.1 mm by solvent casting procedure followed by a pressure–temperature cycle at 80 °C. It was found

that CNCs were effectively dispersed in the segmented SMPU matrix due to the favorable matrix–nanocrystals interactions through hydrogen bonding, with an enhancement of stiffness and stability versus temperature of the nanocomposites.

During the process of preparing NC/SMP materials, NCs can disperse well in a hydrophilic matrix or polar solvent because of the substantial surface hydroxyls. However, many of the SMPs are hydrophobic polymers and their solvent systems are nonpolar. This incompatibility causes aggregation of NCs in some SMP matrices and results in the decrease of reinforcement and switch effects. In order to extend the application of NCs in such matrices, modification is an effective pre-processing method for the synthesis of NC/SMP nanocomposites. As mentioned above, modification of NCs will change their surface properties and make them more hydrophobic, which improve their compatibility with low polarity matrices. Moreover, the modified NCs can obtain a variety of new characteristics depending on the modification monomers, and improve their flexibility to the ambient stimulus of NC/SMP nanocomposites. Cellulose whisker-reinforced waterborne SMPU nanocomposites were synthesized using in situ polymerization followed by a casting/evaporation technique [15]. The grafted chains formed a crystalline structure on the surface of the nanoparticles, inducing the cocrystallization with the matrix. Furthermore, this cocrystallization induced the formation of a co-continuous phase between the CNCs and SMPU matrix, which significantly enhanced the interfacial adhesion, leading to a highly improved mechanical strength of the NC/SMP nanocomposites. Rueda et al. [90] prepared isocyanate-rich CNCs by coupling CNCs with 1,6-hexamethylene diisocyanate (HDI) and incorporated them into segmented SMPU using the casting evaporation technique. Modified CNCs dispersed in the polyurethane and interacted with the matrix hard phase, promoting physical association with hard segments. DMA analysis shown in Fig. 9 illustrated that this association enhanced stiffness and dimensional stability of obtained CN/SMP nanocomposites, although decreased their shape-memory effect. NC/SMP nanocomposites obtained by incorporating polyaniline-grafted CNCs SMPU, with a content of 4–10 wt%, exhibited conductivity-induced shape-memory effects. They also showed a stepwise change in thermal, rheological, and electrical properties, the maintenance of shape responsiveness of the nanocomposites [7].

4.3.2 Thermally Induced NC/SMP Nanocomposites

Segmented polyurethane is one of the most widely thermal-responsive SMPs used for shape-memory composites. One paramount condition for preparing NC/SMPU nanocomposites with an obvious reinforcement is obtaining a good dispersion system. Meanwhile, based on the good dispersion of the NCs in a polyurethane network, hydroxyl groups on the surfaces of NCs interact with polar segments of PU, causing a strong interfacial adhesion which is necessary for nanocomposites [5, 131].

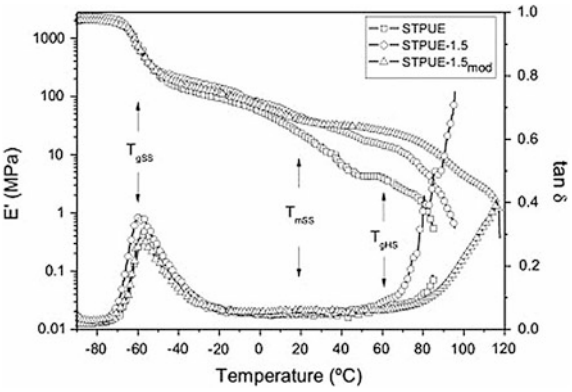

Fig. 9 Storage modulus and loss factor versus temperature for polyurethane and polyurethane nanocomposites containing 1.5 wt% of unmodified and modified CNC. (Reprinted with permission from Ref. [90], Copyright © 2011 Elsevier Ltd. All rights reserved)

Thermomechanical and Crystalline Properties of the NC/SMP Nanocomposites

The thermal behavior and crystalline properties of the NC/SMPU materials are significantly affected by the loading of NCs. Thermal properties of the NC/SMPU can be determined by DSC thermograms. Actually, a small amount of NCs in thermal-responsive SMPU can cause a measurable shift of melting temperature of the soft segments toward elevated temperatures, with an alterant melting enthalpy of the soft segments. These results were ascribed to the anchoring effect of NCs acting as a nucleation agent for the crystallization of the soft segments in segmented polyurethane. The perfection of the crystal structures led to a higher melting temperature of soft segments in the NC/SMPU nanocomposites [6]. Another effect of incorporating NCs in SMPU is the disappearance of the melting peak of hard segments, caused by the interactions between the NCs and the hard segments [74]. These interactions decrease hydrogen bonds between NCs and connect the hard segments together, preventing the hard segments from ordering and forming hard domains. Moreover, thermal transitions of the nanocomposites are related to the microphase separation of soft segments from hard segments. SMPU matrices and their nanocomposites exhibit the same temperature transitions and endotherms, demonstrating that the melting temperature endotherm and melting enthalpies are clearly associated to the soft and hard segments of SMPU.

The storage modulus (E′) and loss factor (tan δ) as a function of temperature can be determined from DMA tests. The two parameters are also considered as characteristic parameters to describe the thermomechanical properties of NC/SMPU nanocomposites. In the region of lower temperatures, the storage modulus slightly decreased with temperature but still remained basically constant, due to the restrictions of molecular motions to vibration and short-range rotation. As the

temperature increased, the storage modulus showed a significant decrease, corresponding to the main relaxation process of the soft phase in the matrix of NC/SMPU nanocomposites. However, a broadening in the loss factor can be observed when content of NCs increased, which is associated to the molecular mobility of amorphous macromolecular chains affected by the presence of NCs. Some authors found that NCs caused reduced molecular mobility of the polyurethane matrix [29]. This effect can be evidenced by a sharp decrease in tan δ height and peak area, indicating that the SMPU molecule fractions participated in the Tg decreases with the increase of cellulose content. Above the temperature corresponding to the melting range of the soft segment, NC/SMPU nanocomposites showed an improvement in storage modulus because of effective dispersion of NCs, as well as the filler–matrix interactions, which enhanced the crystallinity of hard segment. These interactions also decreased the molecular mobility and promoted rigidity of nanocomposites, as observed by DSC. However, the excessive high nanocellulose content up to 30 wt% leads to a lack of cohesion between amorphous and crystalline hard domains in SMPU, resulting in the decrease of stability upon temperatures and changes of thermomechanical behavior.

Reinforcement of NCs and SMEs of NC/SMP Nanocomposites

NC/SMPU can be prepared to allow the introduction of the NCs during the synthesis of PU (SMPU1), to covalently attach to the polymer, or after the synthesis (SMPU1*), where only strong physical interactions form. In both cases, improvement of tensile modulus of obtained NC/SMPU nanocomposites can be observed. Auad et al. prepared nanocomposites using NCs with contents from 0.1 to 1 wt% and segmented SMPU. Compared to pure PUs, the Young's modulus of obtained nanocomposites increased whereas the deformation at break decreases [6]. Cao et al. [14] also prepared nanocomposites from 30 % NCs and waterborne SMPU. The Young's modulus and tensile strength increased from 0.5 to 344 MPa and 4.3 to 14.9 MPa, respectively, while the elongation at break decreased from 1086 to 189 %. Addition of nanocellulose has two effects on the tensile properties of SMPU. One is increasing the modulus of PU. The other is the nanoparticles interfering with formation of the hard segments and causing a decrease in modulus. Tensile properties of the obtained NC/SMPU nanocomposites are depended on the balance between these two effects [6].

Incorporation of NCs also impacts the elongation at break of SMPU, with a decrease of elongation at break by adding NCs. Strong interactions between fillers and matrices restrict the motion of the matrix, causing a reduction in elongation at break. In general, with a low content of NCs (1 $\sim$ 2 %), disruption of the hard segments of SMPU matrices can assist higher elongation of the soft segments, resulting in the increase in elongation at break as compared to other nanocomposites. In this case, elongation of NC/SMP nanocomposites can be maintained greater than 800 %. On the other hand, although the ultimate elongation is reduced,

Table 2 Shape-memory properties of the SPU 2000-series

HS (%)	Cellulose (wt%)	R_f	R_r	R_r (N)
First cycle				
39	0	84.6	71.2	
32	0	62.9	80.6	
23	0	53.8	90.7	
23	1[a]	79.3	82.1	
Second cycle				
39	0	67.9	71.2	100
32	0	61.8	79.9	99.3
23	0	55.8	88.2	97.1
23	1[a]	80.9	80.2	97.6
Third cycle				
39	0	81.6	71.2	100
32	0	70.5	79.0	98.8
23	0	51.3	85.6	97.1
23	1[a]	78.2	80.0	99.8

(Reprinted with permission from Ref. [6], Copyright © 2009 Wiley Periodicals, Inc)

[a]Cellulose incorporated after reaction

it is obvious that the sample can reach nine times more than the initial length before breaking, which is still a high elongation.

The effect of covalent bonds forming between NCs and SMPU on the shape-memory behavior was also arrestingly studied. Maria et al. reported that the neat SMPU and SMPU1* exhibited excellent shape-memory behavior, while the NC reinforced SMPU1 does not have this capability [6]. In the case of SMPU1*, only physical interactions between the polymer and NCs are formed, which does not affect the microphase separation of shape-memory polyurethane. Shape-memory properties of NC-reinforced SMPU1* were shown in Table 2. However, for SMPU1, NCs are covalently bonded to the matrix. This covalent bond interfered with the formation of the hard domains, which are responsible for fixing the original shape, leading to the erase of the shape-memory property of the nanocomposites. From these results, it can be obtained that the NCs should be added to already synthesized SMPU matrices, if the shape-memory properties are needed to be maintained.

4.3.3 Water-Response NC/SMP Nanocomposites

A water-sensitive SMP system with athermally induced shape-memory effect consists of NCs and thermoplastic polyurethane [142]. The SME of this system can be attributed to the reversible formation and disruption of the nanocellulose percolation network, in which stress transfer is promoted by hydrogen bonding between NCs [16]. When the nanocomposite is exposed to water, hydrogen bonds

between NCs are weakened by the presence of water molecules. This effect allows an easy deformation of the nanocomposite into a temporary shape. The shape is fixed by the subsequent drying step, in which the chain mobility is limited by the re-formed hydrogen-bonded three-dimensional network of NCs. In the next recovery stage, the spontaneous shape recovery is triggered by water due to decoupling of the nanocellulose network. These changes of the microstructure indicate that chemomechanical response of water-sensitive shape-memory composites is a result of disruption of the filler–filler interactions of NCs other than the plasticization of the shape-memory matrix.

In view of the outstanding dispersibility of sulfate-modified cellulose whiskers in water, Capadona et al. [17] explored whether water could act as a chemical regulator for the filler–filler interactions using the cellulose/EO-EPI nanocomposites, which were inspired by the architecture and function of the sea cucumber dermis. After immersing into the deionized water for some time, all compositions of the nanocomposites exhibited modest aqueous swelling ($\sim$30 % v/v), indicating that water is the main uptake governed by the matrix polymer with only minor variations due to nanocellulose content. The tensile storage moduli for water swollen cellulose/EO-EPI nanocomposites were measured by DMA analysis. A pronounced reduction of E′ can be observed compared with the dry nanocomposites. The greatest mechanical contrast occurs in the case of the composite with the highest nanocellulose content up to 19 % v/v. At the same time, swelling of the nanocomposite with water results in a significant decrease of the tensile strength as well as an increase of the elongation at break. The stiffness reduction of the nanocomposites could be due to the decoupling of the stress-transferring rigid network of NCs upon the introduction of water molecules as a competitive hydrogen bonding agent. Agreed with the proposed mechanism, the switching is fully reversible since the nanocomposites recovered to their original stiffness upon drying.

Inspired by the sea cucumber dermis, a variety of shape-memory nanocomposites with a percolating network of NCs have been easily fabricated by mixing NCs and SMPs in a hydrogen-bond-forming solvent. During this progress, self-interactions of NCs through hydrogen bonds of surface hydroxyls are “switched off” by competitive hydrogen bonding with the solvent [18, 111]. When the solvent is evaporated, the interactions between the NCs are “switched on” and assembled into a percolating network. This structure and strong interactions between NCs maximize the stress transfer and the overall modulus. The mechanical properties of such nanocomposites can be altered by the immersion and removal of water, which acts as chemical stimuli and changes the hydrogen bonds between the shape-memory matrix and NCs [101]. Mendez et al. [71] reported new water-sensitive mechanically adaptive nanocomposites by introducing rigid cotton cellulose nanowhiskers into SMPU matrix. They found that the level of reinforcement was determined by the CNW content and followed the Halpin–Kardos model below the percolation limit of ~7 % v/v. Whereas, when the content was above ~7 % v/v, the reinforcement of CNW was adhered to the percolation model. When exposed to water, the materials with a CNW content of 20 % v/v swelled slightly and showed a decrease of E′ from 1 GPa to 144 MPa. The mechanically

adaptive property and a high elasticity of the wet nanocomposites are the basis for SME induced by water.

Zhu et al. [142] synthesized CNW/SMPU nanocomposites mentioned above and designed programming protocols including cyclic wetting and drying to evaluate the shape-memory effect of the nanocomposites. During the cyclic processes, R_f is maintained from cycle 1 to cycle 5 and increased with the increase of nanocellulose content. This improvement in shape fixity suggested that the high content of whiskers significantly enhanced the fixity ability of shape-memory nanocompsites. In contrast, the high fraction of elastomer network in the SMPU matrix favored good shape recovery with a low content of whiskers. The decrease of R_r from 90.5 to 53.6 % with the increase of the CNW fraction in cycle two illustrated that the reduction of the elastomer fraction in the CNW/SMPUs led to a more irreversible strain in the first tensile cycle.

The chemomechanical adaptability of NCs in the polymer matrix broadens their applications from reinforcement to smart or stimulus-responsive materials. Such rapidly switchable water-sensitive shape-memory nanocomposites are thought to have considerable application potential, especially for biomedical applications desiring slow, water diffusion-driven mechanical changes as well as thermally activated adaptability [44]. The nanocomposites may also be useful for consumer applications such as, self-propelled and artificial fishing lures.

4.3.4 Other NC/SMP Materials and Multi-material Systems

According to the shape-memory mechanisms summarized above, SMEs can be obtained by constructing composites triggered not only by heat, but also by electricity, light, magnetic fields, infrared radiation, and moisture or chemical solvents. The utilization of nanocellulose will add reinforcement and new switches to the existing framework according to the cellulose properties for novel SMEs. Thus, the nanocellulose-contained shape-memory materials are often synthesized by physical mixing of elastomers as a matrix and NCs as a switch. NCs after chemical modification can also create novel SMEs. The use of nanocellulose has provided many new shape-memory materials for wide areas of applications.

Casado et al. [19] reported composite films based on SMPUs and nanocellulose–polyaniline particles. They found that when the concentration of nanofillers was maintained under 5 wt% in the composite, the mechanical and shape-memory properties were not negatively affected with the addition, or even slightly improved. In particular, the addition of NCs led to an increase in the tensile modulus without affecting the elongation at break, indicating that the filler was acting as a classical reinforcement in this system instead of forming a percolating network. Meanwhile, the electrical conductivity of nanocellulose–polyaniline particles was higher than that of the neat PANI particles. However, the resulting composites did not achieve the conduction levels shown by the fibers. Also, the composites performed in the

range of semi conducting materials, probably because the electrical percolation of fibers through the matrix was not reached.

Aoki et al. [1] demonstrated SME of cellulose acetate derivatives by the modification with cross-linkable mercapto groups. In this system, the on–off switching of the materials was achieved by redox treatments. The shape-memory behavior through adequate redox treatments was due to the reversible, cross-linking association and dissociation between mercapto groups. However, the recovery time required for these films was long up to 96 h. Meanwhile, SME of the material progressively receded with repeated redox treatments.

Bai et al. [9] prepared a novel SMP by grafting microcrystalline cellulose with PCL, and then cross-linked with 4,4-methylenediphenyl diisocyanate (MDI). With a wide broad Tg, the material exhibited good dual-, triple-, quadruple-, and even quintuple-shape-memory effects. In this novel polymer, microcrystalline cellulose is used as the reversible phase for the SME. Moreover, due to the reinforcement of microcrystalline cellulose, the material exhibited outstanding mechanical properties. The tensile modulus and tensile strength could reach 273 and 467 MPa, respectively, with an elongation at break of 479 %, which were superior to many other PCL-based SMPs.

5 Conclusions

Nanocellulose is a reawaked novel material made from natural cellulose, the most abundant natural polymer available in nature. Due to the intrinsic low density, high surface area, and mechanical strength, nanocellulose can improve the final properties of composites in thermal stability, mechanical properties, toughness, barrier, and biological protection, which can extend the application of nanocellulose in medicine, biotechnology, power industry, and especially, intelligent nanomaterials. Ascribed to their nanostructure, nanocelluloses also exhibit a favorable dispersibility in polar solvents and high accessibility of surface hydroxyl groups so that nanocelluloses are suitable for chemical modification and application in nanocomposites.

One of the attractive applications of nanocellulose is its function in shape-memory materials, which are a series of macromolecule materials with various types of molecular architectures specifically designed. Consisted with the component and molecular conformation, shape-memory polymers could respond to a variety of ambient stimuli, such as heat, light, electricity, and water. Among these shape-memory materials, the thermally reduced shape-memory is one of the most widely studied. One of the typical thermally reduced SMPs is segmented polyurethane, which can transform into a temporary deformation and return to the original shape upon different temperatures. While nanocelluloses are applied in this shape-memory material it can serve as reinforcing agents and switches. The reinforcement of nanocellulose for SMP is obvious with the increase of tensile modulus

due to its high rigidity. Meanwhile, the substantial amount of surface hydroxyls enable nanocellulose to act as the switch of water-sensitive shape-memory materials.

Utilization of nanocelluloses in shape-memory materials leads to a novel material with structure transformation from original polymers, and nanocomposites with new and more SMEs. Such new materials are forecasted to have considerable application potentials in biomedicine, aerospace, sensors, and tissue reconstruction.

References

1. Aoki D, Teramoto Y, Nishio Y (2007) SH-containing cellulose acetate derivatives: preparation and characterization as a shape memory recovery material. Biomacromolecules 8:3749–3757
2. Araki J, Wada M, Kuga S, Okano T (1998) Flow properties of microcrystalline cellulose suspension prepared by acid treatment of native cellulose. Colloids Surf A 142:75–82
3. Araki J, Wada M, Kuga S, Okano T (1999) Influence of surface charge on viscosity behavior of cellulose microcrystal suspension. J Wood Sci 45:258–261
4. Araki J, Wada M, Kuga S (2001) Steric stabilization of a cellulose microcrystal suspension by poly (ethylene glycol) grafting. Langmuir 17(21–27):128
5. Auad ML, Contos VS, Nutt S, Aranguren MI, Marcovich NE (2008) Characterization of nanocellulose-reinforced shape memory polyurethanes. Polym Int 57:651–659
6. Auad ML, Mosiewicki MA, Richardson T, Aranguren MI, Marcovich NE (2010) Nanocomposites made from cellulose nanocrystals and tailored segmented polyurethanes. J Appl Polym Sci 115:1215–1225
7. Auad ML, Richardson T, Orts WJ, Medeiros ES, Mattoso LHC, Mosiewicki MA, Marcovich NE, Aranguren MI (2011) Polyaniline-modified cellulose nanofibrils as reinforcement of a smart polyurethane. Polym Int 60:743–750
8. Baer G, Wilson TS, Mathews DL, Maitland DJ (2007) Shape-memory behavior of thermally stimulated polyurethane for medical applications. J Appl Polym Sci 103:3882–3892
9. Bai Y, Zhang X, Wang Q, Wang T (2014) Shape memory property of microcrystalline cellulose–poly(e-caprolactone) polymer network with broad transition temperature. J Mater Sci 49:2252–2262
10. Beloshenko VA, Varyukhin VN, Voznyak YV (2005) Electrical properties of carbon-containing epoxy compositions under shape memory effect realization. Compos A: Appl Sci Manuf 36:65–70
11. Bondeson D, Kvien I, Oksman K (2006) ACS symposium series, vol 938. American Chemical Society, Washington, DC
12. Bonini C, Heux L, Cavaille J-Y, Lindner P, Dewhurst C, Terech P (2002) Rodlike cellulose whiskers coated with surfactant: a small-angle neutron scattering characterization. Langmuir 18:3311–3314
13. Buckley CP, Prisacariu C, Caraculacu A (2007) Novel triol-crosslinked polyurethanes and their thermorheological characterization as shape-memory materials. Polymer 48:1388–1396
14. Cao X, Dong H, Li CM (2007) New nanocomposite materials reinforced with flax cellulose nanocrystals in waterborne polyurethane. Biomacromolecules 8:899–904
15. Cao XD, Habibi Y, Lucia LA (2009) One-pot polymerization, surface grafting, and processing of waterborne polyurethane-cellulose nano crystal nanocomposites. J Mater Chem 19:7137-7145-7137

16. Capadona JR, Van Den Berg O, Capadona LA, Schroeter M, Rowan SJ, Tyler DJ, Weder C (2007) A versatile approach for the processing of polymer nanocomposites with self-assembled nanofibre templates. Nat Nanotech 2:765–769
17. Capadona JR, Shanmuganathan K, Tyler DJ, Rowan SJ, Weder C (2008) Stimuli-responsive polymer nanocomposites inspired by the sea cucumber dermis. Science 1370–1374
18. Capadona JR, Shanmuganathan K, Triftschuh S, Seidel S, Rowan SJ, Weder C (2009) Polymer nanocomposites with nanowhiskers isolated from microcrystalline cellulose. Biomacromolecules 10:712–716
19. Casado UM, Quintanilla RM, Aranguren MI, Marcovich NE (2012) Composite films based on shape memory polyurethanes and nanostructured polyaniline or cellulose–polyaniline particles. Synth Met 162:1654–1664
20. Chakraborty A, Sain M, Kortschot M (2005) Cellulose microfibrils: a novel method of preparation using high shear refining and cryocrushing. Holzforschung 59:102–107
21. Chen MC, Tsai HW, Chang Y, Lai WY, Mi FL, Liu CT (2007) Rapidly self expandable polymeric stents with a shape-memory property. Biomacromolecules 8:2774–2780
22. Chun BC, Cho TK, Chung YC (2006) Enhanced mechanical and shape memory properties of polyurethane block copolymers chainextended by ethylene diamine. Eur Polym J 42:3367–3373
23. Chun BC, Cho TK, Chung YC (2007) Blocking of soft segments with different chain lengths and its impact on the shape memory property of polyurethane copolymer. J Appl Polym Sci 103:1435–1441
24. Davies GC, Bruce DM (1998) Effect of environmental relative humidity and damage on the tensile properties of flax and nettle fibers. Text Res J 68:623–629
25. De Souza Lima MM, Wong JT, Paillet M, Borsali R, Pecora R (2003) Translational and rotational dynamics of rodlike cellulose whiskers. Langmuir 19:24–29
26. Diddens I, Murphy B, Krisch M, Muller M (2008) Anisotropic elastic properties of cellulose measured using inelastic X-ray scattering. Macromolecules 41:9755–9759
27. Dietsch B, Tong T (2007) A review-features and benefits of shape memory polymers (SMPs). J Adv Mater 39:3–12
28. Dong XM, Revol JF, Gray DG (1998) Effect of microcrystallite preparation conditions on the formation of colloid crystals of cellulose. Cellulose 5:19–32
29. Dufresne A (2000) Dynamic mechanical analysis of the interphase in bacterial polyester/cellulose whiskers natural composites. Compos Interfaces 7:53–67
30. Dufresne A (2003) Interfacial phenomena in nanocomposites based on polysaccharide nanocrystals. Compos Interfaces 10:369–387
31. Dufresne A (2011) Preparation of cellulose nanocomposite, in interface engineering of natural fiber composites for maximum performance. In: Zaferiropoulos NE (ed) Woodhead Publishing in Materials, Philadelphia, USA, Chapter 3:82–116
32. Eriksen O, Syverud K, Gregersen O (2008) The use of microfibrillated cellulose produced from kraft pulp as strength enhancer in TMP paper. Nordic Pulp Pap Res J 23:299–304
33. Fereidoonnia M, Barmar M, Barikani M (2009) Influence of a reactive organoclay on polymerization and properties of polyurethane nanocomposites. Polym Plast Technol Eng 48:90–96
34. Gall K, Dunn ML, Liu Y, Finch D, Lake M, Munshi NA (2002) Shape memory polymer nanocomposites. Acta Mater 50:5115–5126
35. Goussé C, Chanzy H, Excoffier G, Soubeyrand L, Fleury E (2002) Stable suspensions of partially silylated cellulose whiskers dispersed in organic solvents. Polymer 43:2645–2651
36. Habibi Y, Dufresne A (2008) Highly filled bionanocomposites from functionalized polysaccharide nanocrystals. Biomacromolecules 9:1974–1980
37. Habibi Y, Goffin A-L, Schiltz N (2008) Bionanocomposites based on poly(ε-caprolactone)-grafted cellulose nanocrystals by ring-opening polymerization. J Mater Chem 18:5002–5010
38. Habibi Y, Lucia LA, Rojas OJ (2010) Cellulose nanocrystals: chemistry, self-Assembly, and applications. Chem Rev 110:3479–3500

39. Håkansson H, Ahlgren P (2005) Acid hydrolysis of some industrial pulps: effect of hydrolysis conditions and raw material. Cellulose 12:177–183
40. Henriksson M, Henriksson G, Berglund LA, Lindstro MT (2007) An environmentally friendly method for enzymeassisted preparation of microfibrillated cellulose (MFC) nanofibers. Eur Polym J 43:3434–3441
41. Heux L, Chauve G, Bonini C (2000) Nonflocculating and chiral-nematic self-ordering of cellulose microcrystals suspensions in nonpolar Solvents. Langmuir 16:8210–8212
42. Hornbogen E (2006) Comparison of shape memory metals and polymers. Adv Eng Mater 8:101–106
43. Hsieh Y-C, Yano H, Nogi M, Eichhorn SJ (2008) An estimation of the Young's modulus of bacterial cellulose filaments. Cellulose 15:507–513
44. Huang, WM, Yang B, Zhao Y, Ding ZJ (2010) Thermo-moisture responsive polyurethane shape-memory polymer and composites: a review. Mater Chem 20:3367–3381 [99]
45. Hudgin DE (2000) Rubber elasticity. Marcel Dekker Inc, New York, pp 123–153
46. Iwamoto S, Nakagaito AN, Yano H, Nogi M (2005) Optically transparent composites reinforced with plant fiber-based nanofibers. Appl Phys A-Mater Sci Process 81:1109–1112
47. Iwamoto S, Nakagaito AN, Yano H (2007) Nano-fibrillation of pulp fibers for the processing of transparent nanocomposites. Appl Phys A 89:461–466
48. Iwamoto S, Kai W, Isogai A, Iwata T (2009) Elastic modulus of single cellulose microfibrils from tunicate measured by atomic force microscopy. Biomacromolecules 10:2571–2576
49. Janardhnan S, Sain M (2006) Isolation of cellulose microfibrils-An enzymathic approach. Bioresources 1:176–188
50. Jiang F, Esker AR, Roman M (2010) Acid-catalyzed and solvolyticde desulfation of H_2SO_4-hydrolyzed cellulose nanocrystals. Langmuir 26:17919–17925
51. Kaushik A, Singh M (2011) Isolation and characterization of cellulose nanofibrils from wheat straw using steam explosion coupled with high shear homogenization. Carbohydr Res 346:76–85
52. Kim B-S, Mather PT (2006) Amphiphilic telechelics with polyhedral oligosilsesquioxane (POSS) end-groups: dilute solution viscometry. Polymer 47:6202–6207
53. Klemm D, Heublein B, Fink H-P, Bohn A (2005) Cellulose: fascinating biopolymer and sustainable raw material. Angew Chem Int Ed 44:3358–3393
54. Koerner H, Price G, Pearce NA, Alexander M, Vaia R (2004) Remotely actuated polymer nanocomposites-tress-recovery of carbon-nanotube-filled thermoplastic elastomers. Nature Mater 3:115–120
55. Liu C, Qin H, Mather PT (2007) Review of progress in shape-memory polymers. J Mater Chem 17:1543–1558
56. Lee K-Y, Tang M, Williams CK, Bismarck A (2012) Carbohydrate derived copoly (lactide) as the compatibilizer for bacterial cellulose reinforced polylactide nanocomposites. Compos Sci Technol 72:1646–1650
57. Lendlein A, Kelch S (2002) Shape-memory polymers. Angew Chem-Int Ed 41:2034–2057
58. Lendlein A, Jiang H, Junger O, Langer R (2005) Light-induced shape memory polymers. Nature 434:879–882
59. Leng JS, Lv HB, Liu YJ, Du SY (2008) Comment on water-driven programable polyurethane shape memory polymer: demonstration and mechanism. Appl Phys Lett 92:206105
60. Leng JS, Lv HB, Liu YJ, Huang WM, Du SY (2009) Shape memory polymers -a class of novel smart material. MRS Bull LLC 34:848–855
61. Lima MMD, Borsali R (2004) Cellulose microcrystals: structure, properties, and applications. Macromol Rapid Commun 25:771–787
62. Lin N, Chen G, Huang J, Dufresne A, Chang PR (2009) Effects of polymer-grafted natural nanocrystals on the structure and mechanical properties of poly(lactic acid): a case of cellulose whisker-graft-polycaprolactone. J Appl Polym Sci 113:3417–3425
63. Liu Y, Gall K, Dunn ML, Greenberg AR (2006) Thermomechanics of shape memory polymers: uniaxial experiments and constitutive modeling. J Diani Int J Plast 22:279–313

64. Ljungberg N, Bonini C, Bortolussi F, Boisson C, Heux L, Cavaille Y (2005) New nanocomposite materials reinforced with cellulose whiskers in atactic polypropylene: effect of surface and dispersion characteristics. Biomacromolecules 6:2732–2739
65. López-Rubio A, Lagaron JM, Ankerfors M, Lindström T, Nordqvist D, Mattozzi A, Hedenqvist MS (2007) Enhanced film forming and film properties of amylopectin using micro-fibrillated cellulose. Carbohydr Polym 68:718–727
66. Luo HS, Hu JL, Zhu Y (2011) Polymeric shape memory nano-composites with heterogeneous-twin-switches. Macromol Chem Phys 212:1981–1986
67. Lv HB, Liu YJ, Zhang DX, Leng JS, Du SY (2008) Solution-responsive shape-memory polymer driven by forming hydrogen bonding. Adv Mater Res 47–50:258–261
68. Malainine ME, Mahrouz M, Dufresne A (2005) Thermoplastic nanocomposites based on cellulose microfibrils from Opuntia ficus-indica parenchyma cell. Compos Sci Technol 65:1520–1526
69. Maitland DJ, Metzger MF, Schumann D, Lee A, Wilson TS (2002) Photothermal properties of shape memory polymer microactuators for treating stroke. Lasers Surg Med 30:1–11
70. Marcovich NE, Auad ML, Bellesi NE, Nutt SR, Aranguren MI (2006) Cellulose micro/nanocrystals reinforced polyurethane. J Mater Res 21:870–881
71. Mendez J, Annamalai PK, Eichhorn SJ, Rusli R, Rowan SJE, Foster J, Weder C (2011) Bioinspired mechanically adaptive polymer nanocomposites with ater-activated shape-memory effect. Macromolecules 44:6827–6835
72. Meng H, Hu JL (2010) A brief review of stimulus-active polymers responsive to thermal, light, magnetic, electric, and water/solvent stimuli. J Intell Mater Syst Struct 21:859–885
73. Metcalfe A, Desfaits AC, Salazkin I, Yahia LH, Sokolowski WM, Raymond J (2003) Cold hibernated elastic memory foams for endovascular interventions. Biomaterials 24:491–497
74. Meyabadi TF, Sadeghi GMM, Dadashian F, Asl HEZ (2013) From cellulosic waste to nanocomposites. Part 2: synthesis and characterization of polyurethane/cellulose nanocomposites. J Mater Sci 48:7283–7293
75. Miller AF, Donald AM (2003) Imaging of anisotropic cellulose suspensions using environmental scanning electron microscopy. Biomacromolecules 4:510–517
76. Monkman GJ (2000) Advances in shape memory polymer actuation. Mechatronics 10:489–498
77. Moon RJ, Marini A, Nairn J, Simonsen J, Youngblood J (2011) Cellulose nanomaterials review: structure, properties and nanocomposites. Chem Soc Rev 40:3941–3994
78. Morandi G, Heath L, Thielemans W (2009) Cellulose nanocrystals grafted with polystyrene chains through surface-initiated atom transfer radical polymerization (SI-ATRP). Langmuir 25:8280–8286
79. Morin A, Dufresne A (2002) Nanocomposites of chitin whiskers from Riftia tubes and poly (caprolactone). Macromolecules 35:2190–2199
80. Nakagaito AN, Yano H (2004) The effect of morphological changes from pulp fiber towards nano-scale fibrillated cellulose on the mechanical properties of high-strength plant fiber based composites. Appl Phys A-Mater Sci Process 78:547–552
81. Nakagaito AN, Yano H (2005) Novel high-strength biocomposites based on microfibrillated cellulose having nanoorder- unit web-like network structure. Appl Phys A-Mater Sci Process 80:155–159
82. Nishiyama Y, Kim UJ, Kim DY, Katsumata KS, May RP, Langan P (2003) Periodic disorder along ramie cellulose microfibrils. Biomacromolecules 4:1013–1017
83. Pääkkö M, Ankerfors M, Kosonen H, Nykanen A, Ahola S, Osterberg M, Ruokolainen J, Laine J, Larsson PT, kkala O, Lindström T (2007) Enzymatic hydrolysis combined with mechanical shearing and high-pressure homogenization for nanoscale cellulose fbrils and strong gels. Biomacromolecules 8:1934–1941
84. Park JS, Chung YC, Lee SD, Cho JW, Chun BC (2008) Shape memory effects of polyurethane block copolymers cross-linked by celite. Fibers Polym 9:661–666

85. Qua EH, Hornsby PR, Sharma HSS, Lyons G, McCall RD (2009) Preparation and characterization of poly (vinyl alcohol) nanocomposites made from cellulose nanofibers. J Appl Polym Sci 113:2238–2247
86. Rehab A, Akelah A, Agag T, Shalaby N (2007) Polyurethane-nanocomposite materials via in situ polymerization into organoclay interlayers. Polym Adv Technol 18:463–471
87. Revol JF, Bradford H, Giasson J, Marchessault RH, Gray DG (1992) Helicoidal self-ordering of cellulose microfibrils in aqueous suspension. Int J Biol Macromol 14:170–172
88. Rousseau IA, Mather PT (2003) Shape memory effect exhibited by smectic-c liquid crystalline elastomers. J Am Chem Soc 125:15300–15301
89. Rubinstein M, Colby RH (2003) Polymer Physics. Oxford University Press, New York
90. Rueda L, Fernández d'Arlas B, Zhou Q, Berglund LA, Corcuera MA, Mondragon I, Eceiza A (2011) Isocyanate-rich cellulose nanocrystals and their selective insertion in elastomeric polyurethane. Compos Sci Technol 71:1953–1960
91. Rueda L, Saralegui A, Fernández d'Arlas B, Zhou Q, Berglund LA, Corcuera MA, Mondragon I, Eceiza A (2013) Cellulose nanocrystals/polyurethane nanocomposites. Study from the viewpoint of microphase separated structure. Carbohydr Polym 92:751–757
92. Ruiz MM, Cavaille JY, Dufresne A, Gerard JF, Graillat C (2000) Processing and characterization of new thermoset nanocomposites based on cellulose whiskers. Compos Interface 7:117–131
93. Rusli R, Eichhorn SJ (2008) Determination of the stiffness of cellulose nanowhiskers and the fiber-matrix interface in a nanocomposite using Raman spectroscopy. Appl Phys Lett 93:033111
94. Saito T, Kimura S, Nishiyama Y, Isogai A (2007) Cellulose nanofibers prepared by TEMPO-mediated oxidation of native cellulose. Biomacromolecules 8:2485–2491
95. Samir M, Alloin F, Dufresne A (2005) Review of recent research intocellulosic whiskers, their properties and their application innanocomposite field. Biomacromolecules 6:612–626
96. Samir M, Alloin F, Sanchez JY, El Kissi N, Dufresne A (2004) Preparation of cellulose whiskers reinforced nanocomposites from an organic medium suspension. Macromolecules 37:1386–1393
97. Sassi J-F, Chanzy H (1995) Ultrastructural aspects of the acetylation of cellulose. Cellulose 2:111–127
98. Schmidt AM (2006) Electromagnetic activation of shape memory polymer networks containing magnetic nanoparticles. Macromol Rapid Commun 27:1168–1172
99. Schurz J, John K (1975) Long periods in native and regenerated celluloses. Cellul Chem Technol 9:493
100. Shanmuganathan K, Capadona JR, Rowan SJ, Weder C (2010) Bio-inspired mechanically-adaptive nanocomposites derived from cotton cellulose whiskers. J Mater Chem 20:180–186
101. Shanmuganathan K, Capadona JR, Rowan SJ, Weder C (2010) Stimuli-responsive mechanically adaptive polymer nanocomposites. ACS Appl Mater Inter 2:165–174
102. Siqueira G, Bras J, Dufresne A (2009) Cellulose whiskers versus microfibrils: influence of the nature of the nanoparticle and its surface functionalization on the thermal and mechanical properties of nanocomposites. Biomacromolecules 10:425–432
103. Singha AS, Thakur VK (2009) Fabrication and characterization of *H. sabdariffa* fiber-reinforced green polymer composites. Polym-Plast Technol Eng 48:482–487
104. Singha AS, Thakur VK (2009) Fabrication and characterization of *S. cilliare* fibre reinforced polymer composites. Bull Mater Sci 32:49–58
105. Singha AS, Thakur VK (2009) Physical, chemical and mechanical properties of *Hibiscus sabdariffa* fiber/polymer composite. Int J Polym Mater 58:217–228
106. Singha AS, Thakur VK (2009) Grewia optiva fiber reinforced novel, low cost polymer composites. J Chem 6:71–76
107. Singha AS, Thakur VK (2009) Synthesis, characterization and analysis of *Hibiscus Sabdariffa* Fibre reinforced polymer matrix based composites. Polym Polym Compos 17:189–194

108. Somerville C (2006) Cellulose synthesis in higher plants. Annu Rev Cell Dev Biol 22:53–78
109. Sturcova A, Davies GR, Eichhorn SJ (2005) Elastic modulus and stress-transfer properties of tunicate cellulose whiskers. Biomacromolecules 6:1055–1061
110. Svagan AJ, Samir MASA, Berglund LA (2008) Biomimetic foams of high mechanical performance based on nanostructured cell walls reinforced by native cellulose nanofibrils. Adv Mater 20:1263–1269
111. Tang LM, Weder C (2010) Cellulose whisker/epoxy resin nanocomposites. ACS Appl Mater Interfaces 2:1073–1080
112. Terech P, Chazeau L, Cavaille JY (1999) A small-angle scattering study of cellulose whiskers in aqueous suspensions. Macromolecules 32:1872–1875
113. Thakur VK, Thakur MK, Gupta RK (2013) Development of functionalized cellulosic biopolymers by graft copolymerization. Int J Biol Macromol 62:44–51
114. Thakur VK, Singha AS, Thakur MK (2013) Fabrication and Physico-Chemical Properties of High-Performance Pine Needles/Green Polymer Composites. Int J Polym Mater Polym Biomater 62:226–230
115. Thakur VK, Singha AS, Thakur MK (2013) Ecofriendly biocomposites from natural fibers: mechanical and weathering study. Int J Polym Anal Charact 18:64–72
116. Thakur VK, Thakur MK, Gupta RK (2013) Synthesis of lignocellulosic polymer with improved chemical resistance through free radical polymerization. Int J Biol Macromol 61:121–126
117. Thakur VK, Thakur MK (2014) Processing and characterization of natural cellulose fibers/thermoset polymer composites. Carbohydr Polym 109:102–117
118. Thakur VK, Thakur MK, Gupta RK (2014) Review: raw natural fiber-based polymer composites. Int J Polym Anal Charact 19:256–271
119. Thakur VK, Grewell D, Thunga M, Kessler MR (2014) Novel composites from eco-friendly soy flour/SBS triblock copolymer. Macromol Mater Eng 299:953–958
120. Thakur VK, Thakur MK, Raghavan P, Kessler MR (2014) Progress in green polymer composites from lignin for multifunctional applications: a review. ACS Sustain Chem Eng 2:1072–1092
121. Tobushi H, Hayashi S, Kojima S (1992) Mechanical-properties of shape memory polymer of polyurethane series—(basic characteristics of stress-strain-temperature relationship. Jap Soc Mech Engrs Int J 35:296–302
122. Uetani K, Yano H (2010) Nanofibrillation of wood pulp using a high-speed blender. Biomacromolecules 12:348–353
123. Uo M, Watari F, Yokoyama A, Matsumo H (2001) Tissue reaction around metal implants observed by X-ray scanning analytical microscopy. Biomaterials 22:677–685
124. van den Berg O, Capadona JR, Weder C (2007) Preparation of homogeneous dispersions of tunicate cellulose whiskers in organic solvents. Biomacromolecules 8:1353–1357
125. Viet D, Beck-Candanedo S, Gray DG (2007) Dispersion of cellulose nanocrystals in polar organic solvents. Cellulose 14:109–113
126. Wang B, Sain M (2007) Dispersion of soybean stock-based nanofibre in a plastic matrix. Polym Int 56:538–546
127. Wang WS, Ping P, Chen X, Jing X (2006) Polylactide-based polyurethane and its shape-memory behavior. Eur Polym J 42:1240–1249
128. Wang B, Sain M, Oksman K (2007) Study of structural morphology of hemp fiber from the micro to the nanoscale. Applie Compos Mater 14:89–103
129. Wang YX, Tian HF, Zhang LN (2010) Role of starch nanocrystals and cellulose whiskers in synergistic reinforcement of waterborne polyurethane. Carbohydr Polym 80:665–671
130. Wise LE, Murphy M, d'Addiecco AA (1946) Chlorite holocellulose, its fractionnation and bearing on summative wood analysis and on studies on the hemicelluloses. Paper Trade J 122:35–43
131. Wu Q, Henriksson M, Liu X, Berglund LA (2007) A high strength nanocomposite based on microcrystalline cellulose and polyurethane. Biomacromolecules 8:3688–3692

132. Wu L, Jin C, Sun X (2010) Synthesis, properties, and light-induced shape memory effect of multiblock polyesterurethanes containing biodegradable segments and pendant cinnamamide groups. Biomacromolecules 12:235–241
133. Xavier T, Orlando JR, Randall SD (2008) Enzymatic kinetics of cellulose hydrolysis: A QCM-D study. Langmuir 24:3880–3887
134. Xie T (2010) Tunable polymer multi-shape memory effect. Nature 464:267–270
135. Xu J, Shi W, Pang W (2006) Synthesis and shape memory effects of Si-O-Si cross-linked hybrid polyurethanes. Polymer 47:457–465
136. Yachi T, Hayashi J, Takai M, Shimizu YJ (1983) Supermolecular structure of cellulose: stepwise decrease in LODP and particle size of cellulose hydrolyzed after chemical treatment. Appl Polym Sci: Appl Polym Symp 37:325
137. Yakacki CM, Shandas R, Lanning C, Rech B, Eckstein A, Gall K (2007) Unconstrained recovery characterization of shape-memory polymer networks for cardiovascular applications. Biomaterials 28:2255–2263
138. Yang B, Huang WM, Li C, Li L, Chor JH (2005) Qualitative separation of the effects of carbon nano-powder and moisture on the glass transition temperature of polyurethane shape memory polymer. Scripta Mater 53:105–107
139. Yi J, Xu Q, Zhang X, Zhang H (2008) Chiral-nematic self-ordering of rod-like cellulose nanocrystals grafted with poly(styrene) in both thermotropic and lyotropic states. Polymer 49:4406–4412
140. Yuan H, Nishiyama Y, Wada M, Kuga S (2006) Surface acylation of cellulose whiskers by drying aqueous emulsion. Biomacromolecules 7:696–700
141. Zhou Q, Brumer H, Teeri TT (2009) Self-organization of cellulose nanocrystals adsorbed with xyloglucan oligosaccharide-poly (ethylene glycol)-p-Polystyrene triblock copolymer. Macromolecules 42:5430–5432
142. Zhu Y, Hu JL, Luo HS, Young RJ, Deng LB, Zhang S (2012) Rapidly switchable water-sensitive shape-memory cellulose/elastomernano-composites. Soft Matter 8:2509–2517

Nanotechnologies for Production of High Performance Cellulosic Paper

Altaf H. Basta and Houssni El-Saied

Abstract Recently, nano-products play a dominant role in global manufacturing, and still in the not-so-distance future. Whereas new applications are being investigated everyday in many areas, e.g., agriculture, lignocellulosic products, food, nano-reactive membranes for water purification, nano-catalysts for air-purification, for water treatment, nanomaterials-based solar cells, as well as nano-coatings which are finding use in corrosion-resistance, dirt repellency, water repellency, thermal insulation, and antimicrobial applications. This paper reviews recent researches on utilizing nano-tech materials in production of high performance paper sheets. The highlight on our suggestions for production process of safety paper sheets from heterocyclic nanoparticles is also reported.

Keywords Cellulosic paper · Nanotechnology · Special paper · High performance paper sheets

1 General Introduction

Nanotechnology is the understanding and control of matters having dimensions roughly within the 1–100 nm range. Nanotechnology was introduced starting with the famous 1959 lecture by R.P. Feynman. It was suggested to name the nanometer scale the *Feynman* (Φnman) *scale* after Feynman's great contributions to nanotechnology (1 *Feynman* [Φ] = 10^{-9} *meter* = 10^{-3} *Micron* [μ] = 10 *Angstrom*s [Å]). The essence of nanotechnology is the ability to work at the molecular level, atom-by-atom, to create large structures with fundamentally new molecular organization. The ability to control and manipulate nanostructures will make it possible to exploit new physical, biological, and chemical properties of systems that are intermediate in size, between single atoms, molecules, and bulk materials [1–4].

A.H. Basta (✉) · H. El-Saied
Cellulose and Paper Department, National Research Centre, Dokki 12622, Cairo, Egypt
e-mail: Altaf_Basta2004@yahoo.com; Altaf_Basta@hotmail.com

V.K. Thakur and M.K. Thakur (eds.), *Eco-friendly Polymer Nanocomposites*,
Advanced Structured Materials 74, DOI 10.1007/978-81-322-2473-0_5

Various nanoparticle (NP)-based therapeutic platforms, including liposomes [5, 6] polymeric micelles [7, 8], quantum dots [9, 10], Au/Si/polymer shells [11, 12], and dendrimers [13, 14] have been established.

Nanotechnology has the potential of revolutionizing materials design for many applications, e.g., biomedicine [15, 16], agro-food sector [17, 18], water and wastewater treatments [19], building materials [20], textile and paper and lignocellulosic composites [21, 22], and solar PV cell [23].

The implications of nanotechnology for the paper industry range from wet-end chemistry, fabrics, and roll cover materials to adhesives as well as pigments [24]. The environmental benefits come from reduced process water consumption, e.g., via improved wet-end chemistry, nanofiltration, and water-less coating, while energy efficiency can be increased in addition to the improvements resulting from decreased water usage by minimized production losses through the application of new materials and better sensor technology [25].

Fully green nanotechnology is the ideal case of green nanotechnology, and it means all the input and output components (materials) involved in fully green nanotechnology should be environmentally safe (e.g., polysaccharides and natural cellulose fibers). Recently, cellulosic nanomaterials, e.g., nanocellulose (NC), microfibrillated cellulose, and electrospun cellulose nanofibers, have attracted the attention of researchers due to their distinctive optical properties, highly crystalline structure, and high surface area [26]. NC can be used for many applications such as optical devices [27], regenerative medicine [28], automotive applications [29], and so on. NCC suspensions can be used to form films having potential applications as ink pigments and optically variable films for security papers, since the optical properties cannot be reproduced by printing or photocopying [30]. Moreover, oxidized NC and its microparticulate system is used in TMP newsprint manufacture [31].

The answers to the question of why nanotechnology is important [32] are: (a) Less space, faster, less material, and less energy, (b) Novel properties and phenomena and (c) Most efficient length scale for manufacturing, therefore one important application of nanomaterial; [inorganic, organic, and/or natural fibers (NC)] is focused in production of high performance paper sheets [33–38]. Many techniques have been developed for protecting the documents to prevent counterfeiting or fraudulent use. Techniques such as holograms on credit cards and magnetic coding on various articles have been in use for some time [39, 40]. Fluorescent nanoparticles [41] and Fe_3O_4 nanoparticles [42] were also used as successful methods for anti-counterfeiting applications and documents' identification (safety paper).

This chapter looks at the current role of nanotechnology in production of high performance paper sheets. The highlight is on our published articles [43–45] for synthesis of fluorescence-active pyridinecarbonitriles as security marker for safety paper, and the fluorescence behavior of these heterocyclic compounds in nanoparticles form are also reported.

2 Scope Survey of Nanoparticles in Paper Manufacturing

2.1 Nanomaterials Containing Cellulosic Paper Sheets

The papermaking process includes steps of preparing the paper composition, wet beating, forming of wet sheet, pressing, drying, calendering, and probable surface finishing—printing, dyeing, coating, etc. [46]. During production of paper or board products there is often a desire to add nanomaterials either to furnish of paper, board, to the surface of the formed paper, or board product. The nanomaterials are often added to reduce production cost and/or improve properties such as printing properties of the finished paper or board product. Beating (pulping) regards the important step of papermaking required to obtain strong paper; Ioelovich [38] reported his trial to improve the paper properties via incorporating organic and inorganic nanomaterials in beated pulp composition. Organic nanocellulose consists of rod-like particles 150–200 × 20–40 nm having increased crystallinity, specific surface, and hydrophility. Dispersion of inorganic nano-chalk contains ellipsoidal particles of size 100–150 nm having relative low hydrohpility. He showed that introducing cellulose nanoparticles leads to sharp increase in paper density and strength. In contrast to this result, inorganic nanoparticles of chalk have negligible effect on properties of the final paper due to low bonding ability between inorganic particles and organic cellulose fibers.

The problem of working with dispersions or slurries comprising nanopartides is that they are not stable and the nanopartides easily form aggregates that are not as reactive as nanopartides in free form. Furthermore, dispersions comprising nanomaterial often have a problem with dusting and it could also be hazardous to handle the dispersions comprising nanopartides since they are being adsorbed by the skin. Dried dispersions comprising microfibrillated cellulose often also have problems with dusting. Heiskanen et al. [34, 35] invented the solution process that in an efficient and safe way is able to produce a stable dispersion comprising nanoparticles. The invented process for producing dispersion comprises microfibrillated cellulose and nanoparticles (e.g., bentonite, titanium dioxide, zinc oxide, silver, copper oxide, iron oxide, silica, calcium carbonate, such as nanoprecipitated calcium carbonate (PCC) and/or carbon nanotubes), wherein the nanoparticles are added to the slurry and treated by mechanical disintegration. Thus a dispersion comprising microfibrillated cellulose is formed in which the nanoparticles are absorbed onto the surface of the microfibrillated cellulose and/or into the microfibrillated cellulose. This invented process possibly to produces a much more stable dispersion at the same time as the dispersion also has other improved properties, such as decreased dusting problems. Mechanical disintegration is preferably done in a pressure homogenizator. It has been shown that by using a pressure homogenizator it is possible to produce microfibrillated cellulose with more open areas and at the same time disparate the nanoparticles of dispersion in an efficient way.

Other inorganic nanoparticles that have gained interest, especially in paper production from wood fibers and to a lesser degree in pulp production, are, e.g., Al_2O_3

ZnO, SiO_2, $CaCO_3$, and silanes. These have been applied for pulp production formulation, for paper and board with microfibrillated cellulose, in research for wear resistance and wet strength, and on paper surface among others [33, 35, 47, 48].

The process for improving the wet strength of a paper product and to a paper product with improved wet strength was also invented [33]. In accordance with the invention, pigments of less than 200 nm in size are used as filler in the paper product.

Direct synthesis of gold nanocatalysts on TEMPO-oxidized pulp paper containing aldehyde groups was investigated by Azetsu et al. [49]. The produced AuNPs on TEMPO-oxidized paper composites showed catalytic activity toward the aqueous reduction of 4-NP to 4-AP. Optically transparent nanofibril paper was also developed as a matrix for solar cells [50], and paper-like AuNPs catalysts composed of pulp fibers and zinc oxides [51].

Moreover, the benefit was nanoparticle-containing paper sheets in production oil and grease resistant paper and paper board [52]. This type of paper was produced via applying a homogeneous aqueous dispersion of fluorochemical surface-modified nanoparticles to a cellulosic substrate to form a treated cellulosic substrate, and subsequently drying the treated cellulosic substrate to form an oil repellent cellulosic material. Fluoro chemicals that can be used to modify the nanoparticles include fluoroalkylsilanes, ionic fluorochemicals, or fluorinated polyacrylate obtained by seeded emulsion polymerization of fluorinated acrylates on the nanoparticles. Paper, paperboard, and cellulose fiber articles that have been modified by the disclosed processes have improved oil and grease resistance properties. Another benefit investigated was that nanoparticles prevent the spread of microbial infections and provide safe paper product. The investigators studied the antibacterial activities of zinc oxide nanoparticle coated paper and the results showed a significant decrease in bacteria counts after 24 h [53]. Besides zinc oxide nanoparticles, silver nanoparticles, which possess strong antibacterial properties have also been loaded on filter paper for antibacterial purposes [54]. But one major problem for zinc oxide, silver nanoparticles and other metal-based materials is their toxicity to healthy cells (and the environment) due to generation of reactive oxygen species [55, 56]. These materials may result in severe health problems when such coated paper products are used for food wrapping or clinical applications. To decrease this drawback, selenium nanoparticles were used to coated paper towels. This approach of application of nanoparticles leads to increased eradication of bacteria in a wider range of clinical environments and in the food industry, thus improving human health [57].

In this subject of utilizing the nanoscale materials in production of precious application paper products, the previous literature showed both inorganic and natural fibers—(organic) nanoparticles are used individually or in combinations. Therefore, in further sections we present some of the literature work on the methods of production of nanoparticles, and their characteristics.

2.2 Production Methods of Nanoscale Materials

There are two fundamental approaches to fabricating nanomaterials [58]. The "bottom-up" approach represents the concept of constructing a nanomaterial from basic building blocks, i.e., atoms or molecules. This approach illustrates the possibility of creating materials with exactly the properties desired. The second approach, the "top-down" method, involves restructuring a bulk material in order to create a nanostructure.

Traditional nanoparticles (NPs) fabricated using bottom-up techniques are limited to spheres, partly due to the lack of fabrication technology to control the shape. Bottom-up techniques greatly involving self-assembly and aggregation of NPs depend on various factors, such as its thermodynamic energy minima and entropy limitations or factors affecting molecular self-assembly [59]. The energy-minimized stable structures thus produced tend to be spherical, because spheres have the least surface per unit volume and, thus, minimize the interfacial energies. The advancement of techniques involved in nanofabrication has enabled the development and production of various nonspherical NPs.

2.2.1 Methods of Production Nanoscale Inorganic Materials

Nano-size inorganic pigment is of potential technological interest especially as a filler application to reinforce materials in the nanocomposite. They are normally produced by chemical or mechanical methods. Chemical methods are generally based on intercalation and exfoliation. The preparation of tailored talc nanoparticles by mechanical milling has been undergoing investigation. In most cases, mechanical milling, especially in a high intensity ball milling device such as a planetary mill, causes delaminating in the initial stages followed by destruction of the structure and subsequent amorphization associated with reaggregation of fine particles. The comminuting process and microstructural evolution of talc during milling are influenced by the type of impulsive stress applied, which can either be of shock or shear [60]. The impulsive stress caused by the balls mainly depends on the mill rotational speed. Furthermore, for the milled layer silicate minerals where shear stress is dominant, highly anisotropic layers with a relatively preserved structure were obtained, while amorphous fine particles often result from milling with the shock-type stress [61]. Aside from these, other parameters such as grinding environment, addition of milling aids, and variation in the grinding media have been shown to play a role.

The particle size and morphology of nano-talc are relevant to its technological application since it has been reported that particles with well-preserved crystal structures and high geometrical anisotropic properties are promising fillers in polymer nanocomposites. These features can significantly decrease the percolation threshold and improve the mechanical and thermal properties compared to other inorganic nanoscale fillers such as calcium carbonate [62]. It is therefore interesting

to explore the processing routes based on plastic deformation, where an increase in the surface area is obtained and the crystal structure is preserved. Sonication process provides reduction in particle size while preserving the crystal structure; therefore this process appears more suitable in the production of talc nanosheets. In addition, talc does not need high stress deformation. This process is also believed to reduce other deformation mechanisms, which require a high stress level for activation and can induce larger crystal disordering.

Acid medium sonication reported also a method for preparation of low density talc nanosheets [63]. This method is carried out to produce talc nanosheets with a high aspect ratio and a relatively perfect crystal structure, which hasthe potential to be scaled-up to the industrial level.

Gas phase synthesis through the pyrolysis of organometallic precursors is reported as the method for industrial synthesis of commercially available nanopowder of mean size of 6–100 nm. This method runs without vacuum and gives a relative high productivity of laboratory equipment [64].

Spray techniques are simple, one-step methods suitable for manufacturing of a broad range of powders with controlled properties for specialty applications. These methods include but are not limited to spray drying (SD), mainly for producing pharmaceuticals and food powders. Three types of spray techniques are reported; Spray pyrolysis (SP) for fabricating nonagglomerated monodispersed fine and unltrafine ceramic powders; flame spray pyrolysis (FSP) for preparation of ceramic and complex nanoparticles, and melt atomization (MA), mostly for the production of metal powders. The other spray methods include spray freeze drying (SFD) and emulsion combustion method (ECM) [65].

2.2.2 Methods of Production Nanocelluloses (NC)

The word “nanocellulose” generally refers to cellulosic materials with one dimension in the nanometer range. The production of NC is generally carried out in two steps. The first stage consists of pretreatment of the raw material to obtain “purified” individual cellulosic fibers that can be further processed. Depending on the source of the raw material, different pretreatments are applied. The second stage (generally called “fibrillation”) concerns the transformation of the individual cellulosic fibers into microfibrils, MFCs or NCCs. The main processes typically used for this transformation are mechanical treatment [66–68], [69]; [70–72], acid hydrolysis [73–75] and enzymatic hydrolysis [76–78], which can be used separately or combined. The steam explosion process is another efficient pretreatment method for converting lignocellulosic biomass with that of separating nanofibers [79, 80].

The procedures production of CNs consists of the following steps: and also illustrated in Scheme 1 [79];

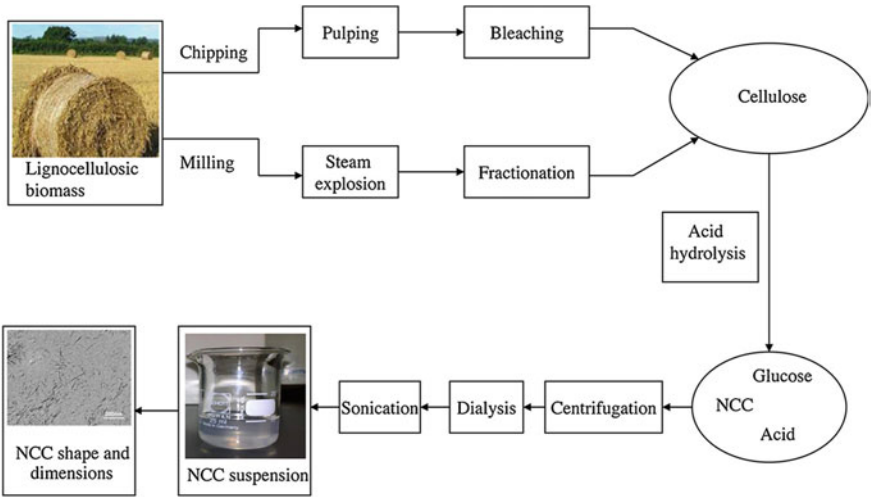

Scheme 1 Main steps needed to prepare NC from lignocellulosic biomass

(1) Strong acid hydrolysis of pure cellulosic material under strictly controlled conditions of temperature, time, agitation, and with control of other conditions such as nature and concentration of the acid and the acid to cellulose ratio;
(2) Dilution with water to stop reaction and repeated washing with successive centrifugation;
(3) Extensive dialysis against distilled water to fully remove free acid molecules;
(4) Mechanical treatment, usually sonication, to disperse the nanocrystals as a uniform stable suspension;
(5) Eventual concentration and drying of the suspension to yield solid NCC.

While, according to Gong et al. [81], the production of two types of nanocellulose from wood was carried out via extraction of α- cellulose followed by preparation of NC. They summarized these stages in the following schemes (Scheme 2a, b).

2.3 Characterization Techniques for Nanomaterials

Various techniques for characterization have been used extensively in nanomaterials research [82–85]). The commonly used powerful techniques are wide-angle X-ray diffraction (WAXD), small-angle X-ray scattering (SAXS), scanning electron microscopy (SEM), and transmission electron microscopy (TEM) [82, 86].

For SEM, it provides images of surface features associated with a sample. However, there are two other microscopies, scanning probe microscopy (SPM) and scanning tunneling microscopy (STM), which are indispensable in nanotube (CNT)

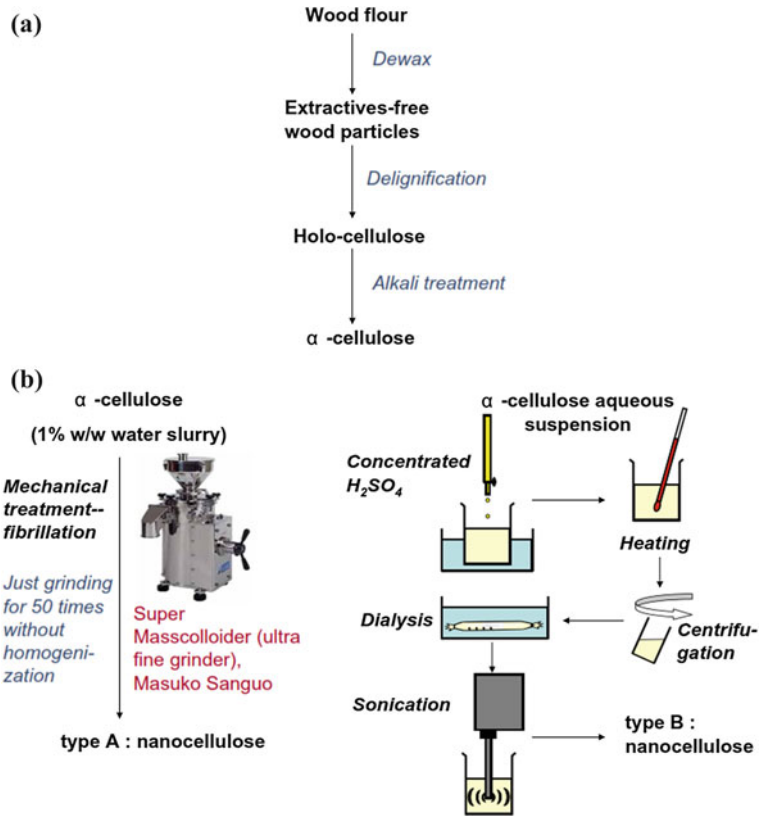

Scheme 2 **a** Preparation of cellulose from softwood flour, **b** Preparation of two kinds of nanocellulose

research [86]. The SPM uses the interaction between a sharp tip and a surface to obtain an image. In STM, a sharp conducting tip is held sufficiently close to a surface (typically about 0.5 nm), such that electrons can 'tunnel' across the gap [87]. This method provides surface structural and electronic information at atomic level. The invention of the STM inspired the development of other 'scanning probe' microscopes, such as the atomic force microscope (AFM) [88]. The AFM uses a sharp tip to scan across the sample.

The WAXD is also the most commonly used to probe the nanomaterial structure [89, 90], and occasionally to study the kinetics of the polymer melt intercalation [91]. In layered silicate nanocomposite systems, a fully exfoliated system is characterized by the absence of intensity peaks in WAXD pattern, e.g., in the range $1.5 \leq 2\theta \leq 10°$, which corresponds to a d-spacing of at least 6 nm [92]. Therefore, a WAXD pattern concerning the mechanism of nanocomposite formation and their structure are tentative issues for making any conclusion.

On the other hand, TEM allows a qualitative understanding of the internal structure, spatial distribution of the various phases, and views of the defective

Table 1 Characteristics of nanomaterials

Characteristics	N cell	N chalk
Particle length, run	150–200	–
Particle width or Diameter 11 m	20-40	100–150
Cry stall inity, %	75–80	90–100
Specific weight, g/cm^3	1.55–1.60	2.65–2.70
WRV, %	300–320	18–20
WVS, %	7−9	0.5–0.7

structure through direct visualization, in some cases of individual atoms. Therefore, TEM complements WAXD data [93]. Small-angle X-ray scattering (SAXS) is typically used to observe structures of the order of 10 in the range of 0° or 0.5°–5°. The TEM, AFM, and SEM are also required to characterize nanoparticle, carbon nanofiber dispersion, or distribution. However, X-ray diffraction has found relatively limited success in CNT research [94].

For thermal characterization and to study the cure behavior (typically for thermo-set resin systems), the commonly used techniques are differential scanning calorimeter (DSC), thermogravimetric analysis (TGA), thermomechanical analysis (TMA), Fourier-transform infrared (FTIR), dynamic modulus analysis (DMA), rheometer, etc. The next section will discuss the structure, properties, processing, and manufacturing of different PNCs with relevant applications.

Additional tests are required for the case of nano-organic materials (nanocellulose), e.g., degree of polymerization and strength. It has been reported that the degree of polymerization (DP) is strongly correlated with the aspect ratio of the nanofibers, and also with their length to determine the DP of MFC. Generally, use of a viscosity method with a cupriethylene diamine solution, based on ISO Standard 5351 [95], is made The average degree of polymerization of MFC samples is calculated from the viscosity using the Mark–Houwink equation.

For example, SEM investigations examined by Ioelovich [38] showed that particles of nanocellulose (NC) have rod-like shape, 150–200 nm long and 20–40 nm wide in average. Method of LLS also gave average length about 200 nm for cellulose nanoparticles. In contrast to NC, particles of nano-chalk have ellipsoidal shape of average diameter of 100–150 nm. Moreover, he reported some characteristics of the organic and inorganic nanoparticles, as in Table 1.

3 Fluorescence-Active Pyridinecarbonitriles as Security Marker in Safety Paper Production and Its Nanoparticle Characteristics

Due to the importance of security markers for preparing safety documents (e.g., cultural property, passports, government documents, banknotes, etc.), for protection from falsifications of original property, and when the basic requirement for secret

dyes is the photoluminescence emission which allows the marking signs to be observed with the help of a special pocket, the objective of this part was to present our published articles [43–45]; for synthesis the fluorescence-active pyridinecarbonitriles as security marker for safety paper, and the fluorescence behavior of these heterocyclic compounds in nanparticles were also reported.

3.1 Synthesis of Fluorescence Active Pyridinedicarbonitriles and Studying Their Application in Functional Paper (41, 42)

3.1.1 Objective

In out first published article [43] we reported the synthesis of 2-alkoxy-3-pyridinecarbonitrile derivatives of considerable fluorescence properties. This allowed their application to paper sheets prepared from nonwood fibrous material (bagasse pulp) affording special type of paper (security paper). In the second published article [44], our attempt was to improve the fluorescence behavior of a variety of pyridine derivatives. This was carried out via synthesis heterocyclic compounds possessing both the aforementioned functional groups, i.e., amino and alkoxy groups oriented *o*- and *o*'-positions of the pyridine nucleus and neighboring to nitrile functions. These heterocyclic compounds gathering the whole functional moieties are responsible for fluorescence properties in a sole structure system. Application of representative fluorescence active prepared heterocyclic compounds to various types of papers was also considered not only for evaluating the fluorescence properties of the produced paper but also to study the physical and mechanical properties of treated papers, attempting to obtain a novel type of safety paper sheets from nonwood fibrous pulps (sugarcane bagasse waste in blend with cotton linters).

3.1.2 Materials and Methods

Synthesis and Characterization of Fluorescence Materials

The starting compounds 1a, b were prepared according to the previously reported procedures [43, 94]. In a general procedure, a mixture of equimolar amounts of 1a–c and malononitrile 2 (10 mmol) in the corresponding alcohol (25 ml) containing sodium (~ 21 mmol) was stirred at room temperature (20–25 °C) for the appropriate time. The separated solid was collected, washed in water, and crystallized from a suitable solvent affording the corresponding 3a–h (Scheme 3).

Melting points are uncorrected and recorded on an Electrothermal 9100 digital melting point apparatus. IR spectra (KBr disks) were recorded on a Nexus 670 FT-IR spectrophotometer. UV spectra were recorded on a JASCO UV/Visible V-570

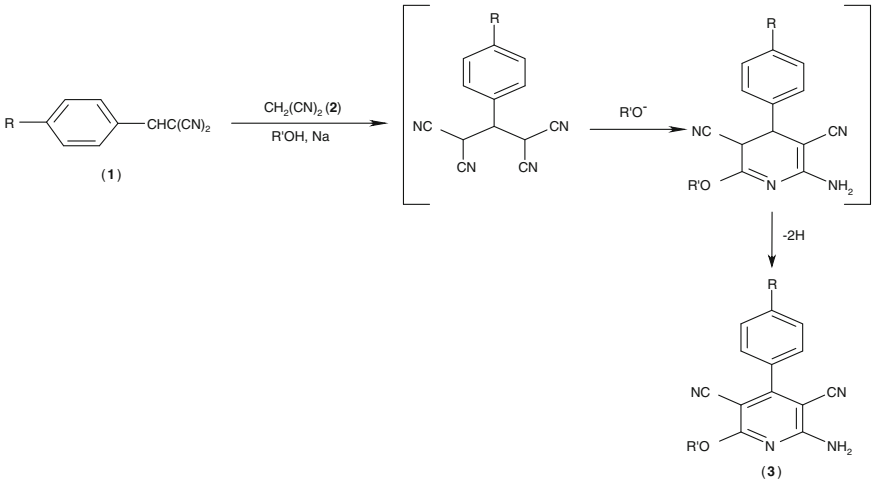

1a, R = 1-piperidinyl

1b, R = 4-morpholinyl

1c, R = 4-methyl-1-piperazinyl

3a, R = 1-piperidinyl, R' = CH_3

3b, R = 4-morpholinyl, R' = CH_3

3c, R = 1-piperidinyl, R' = C_2H_5

3d, R = 4-morpholinyl, R' = C_2H_5

3e, R = 4-methyl-1-piperazinyl, R' = C_2H_5

3f, R = 1-piperidinyl, R' = $CH_3(CH_2)_2$

3g, R = 4-morpholinyl, R' = $CH_3(CH_2)_2$

3h, R = 4-morpholinyl, R' = $CH_3(CH_2)_3$

Scheme 3 Synthesis route of fluorescence active pyridinedicarbonitriles

spectrophotometer. Fluorescence spectra were recorded on a JASCO spectrofluorometer (Xenon 150 Watt arc lamp; excitation and emission slit band width 5 nm each), the quantum yield was determined according to Morries et al. [96]. ^{1}H-NMR spectra were recorded on a Varian MERCURY 300 MHz spectrometer. ^{13}C-NMR spectra were recorded on a Jeol AS-500 (^{13}C: 125 MHz) spectrometer. Mass spectra were recorded on a Hewlett Packard model MS 5988 spectrometer (EI, 70 eV).

2-Amino-6-methoxy-4-[4-(4-morpholinyl)phenyl]-3,5-pyridinedicarbonitrile (**3b**).

Reaction time 24 h, almost colorless crystals from *N,N'*-dimethylformamide, mp 297–298 °C, yield 51 %. IR: $\nu_{max.}$/cm^{-1} 3433, 3324, 3220 (NH_2), 2214 (C≡N), 1656, 1586 (C=N, C=C). ^{1}H-NMR (DMSO-d_6): δ 3.25 (t, 4H, morpholinyl 2 NCH_2, J = 5.1 Hz), 3.75 (t, 4H, morpholinyl 2 OCH_2, J = 5.1 Hz), 3.96 (s, 3H, OCH_3), 7.07 (d, 2H, arom. H, J = 9.0 Hz), 7.41 (d, 2H, arom. H, J = 8.7 Hz), 7.83 (br. s, 2H, NH_2). MS: *m/z* (%) 335 (100). Anal. for $C_{18}H_{17}N_5O_2$ (335.36): Calcd., C 64.46, H 5.11, N 20.89; Found: C 64.62, H 5.19, N 21.13 %.

2-Amino-6-ethoxy-4-[4-(1-piperidinyl)phenyl]-3,5-pyridinedicarbonitrile (**3c**).

Reaction time 24 h, pale yellow crystals from *n*-butanol, mp 246–248 °C, yield 46 %. IR: $\nu_{max.}/cm^{-1}$ 3431, 3343, 3234 (NH_2), 2212 (C≡N), 1640, 1605 (C=N, C=C). ^{1}H-NMR ($CDCl_3$): δ 1.34 (t, 3H, CH_3, J = 7.2 Hz), 1.50–1.64 (m, 6H, piperidinyl 3 CH_2), 3.24 (t, 4H, piperidinyl 2 NCH_2, J = 5.7 Hz), 4.37 (q, 2H, OCH_2CH_3, J = 7.2 Hz), 5.46 (s, 2H, NH_2), 6.93 (d, 2H, arom. H, J = 8.1 Hz), 7.40 (d, 2H, arom. H, J = 9.0 Hz). MS: *m/z* (%) 347 (100). Anal. for $C_{20}H_{21}N_5O$ (347.41): Calcd., C 69.14, H 6.09, N 20.16; Found: C 68.91, H 5.90, N 20.38 %.

2-Amino-6-ethoxy-4-[4-(4-morpholinyl)phenyl]-3,5-pyridinedicarbonitrile (**3d**).

Reaction time 24 h, almost colorless crystals from *n*-butanol, mp 234–236 °C, yield 40 %. IR: $\nu_{max.}/cm^{-1}$ 3492, 3371 (NH_2), 2223, 2211 (C≡N), 1617, 1574 (C=N, C=C). ^{1}H-NMR ($CDCl_3$): δ 1.35 (t, 3H, CH_3, J = 7.2 Hz), 3.21 (t, 4H, morpholinyl 2 NCH_2, J = 4.8 Hz), 3.80 (t, 4H, morpholinyl 2 OCH_2, J = 4.8 Hz), 4.38 (q, 2H, OCH_2CH_3, J = 7.2 Hz), 5.48 (s, 2H, NH_2), 6.94 (d, 2H, arom. H, J = 8.7 Hz), 7.43 (d, 2H, arom. H, J = 8.7 Hz). MS: *m/z* (%) 349 (100). Anal. for $C_{19}H_{19}N_5O_2$ (349.38): Calcd., C 65.31, H 5.48, N 20.05; Found: C 65.27, H 5.38, N 20.23 %.

2-Amino-6-ethoxy-4-[4-(4-methyl-1-piperazinyl)phenyl]-3,5-pyridinedicarbonitrile (**3e**).

Reaction time 24 h, pale yellow crystals from *n*-butanol, mp 212–214 °C, yield 39 %. IR: $\nu_{max.}/cm^{-1}$ 3393 (NH_2), 2214 (C≡N), 1655, 1609 (C=N, C=C). ^{1}H-NMR ($CDCl_3$): δ 1.44 (t, 3H, OCH_2CH_3, J = 6.9 Hz), 2.41 (s, 3H, NCH_3), 2.64 (t, 4H, piperazinyl 2 NCH_2, J = 4.8 Hz), 3.39 (t, 4H, piperazinyl 2 NCH_2, J = 4.8 Hz), 4.46 (q, 2H, OCH_2CH_3, J = 6.9 Hz), 5.61 (s, 2H, NH_2), 6.99 (d, 2H, arom. H, J = 9.0 Hz), 7.50 (d, 2H, arom. H, J = 8.7 Hz). Anal. for $C_{20}H_{22}N_6O$ (362.43): Calcd., C 66.27, H 6.12, N 23.19; Found: C 66.01, H 5.95, N 23.26 %.

2-Amino-4-[4-(1-piperidinyl)phenyl]-6-propoxy-3,5-pyridinedicarbonitrile (**3f**).

Reaction time 48 h, pale yellow crystals from methanol, mp 227–229 °C, yield 39 %. IR: $\nu_{max.}/cm^{-1}$ 3438, 3339, 3230 (NH_2), 2214 (C≡N), 1637, 1605 (C=N, C=C). ^{1}H-NMR ($CDCl_3$): δ 1.05 (t, 3H, CH_3, J = 7.2 Hz), 1.65–1.88 (m, 8H, piperidinyl 3 CH_2 + CH_3CH_2), 3.34 (t, 4H, piperidinyl 2 NCH_2, J = 4.8 Hz), 4.36 (t, 2H, OCH_2, J = 6.6 Hz), 5.56 (s, 2H, NH_2), 7.06 (br. s, 2H, arom. H), 7.50 (d, 2H, arom. H, J = 8.7 Hz). MS: *m/z* (%) 361 (100). Anal. for $C_{21}H_{23}N_5O$ (361.43): Calcd., C 69.78, H 6.41, N 19.38; Found: C 69.96, H 6.55, N 19.54 %.

2-Amino-4-[4-(4-morpholinyl)phenyl]-6-propoxy-3,5-pyridinedicarbonitrile (**3 g**).

Reaction time 24 h, pale yellow crystals from methanol, mp 239–241 °C, yield 36 %. IR: $\nu_{max.}/cm^{-1}$ 3466, 3286, 3175 (NH_2), 2210 (C≡N), 1625, 1581 (C=N, C=C). ^{1}H-NMR ($CDCl_3$): δ 1.06 (t, 3H, CH_3, J = 7.2 Hz), 1.85 (sextet, 2H, CH_3CH_2, J = 7.2 Hz), 3.31 (t, 4H, morpholinyl 2 NCH_2, J = 4.8 Hz), 3.90 (t, 4H, morpholinyl 2 OCH_2, J = 4.8 Hz), 4.37 (t, 2H, OCH_2, J = 6.6 Hz), 5.59 (s, 2H, NH_2), 7.04 (d, 2H, arom. H, J = 8.7 Hz), 7.53 (d, 2H, arom. H, J = 9.0 Hz). MS: *m/z* (%) 363 (100). Anal. for $C_{20}H_{21}N_5O_2$ (363.41): Calcd., C 66.10, H 5.83, N 19.27; Found: C 66.31, H 6.02, N 19.51 %.

2-Amino-6-butoxy-4-[4-(4-morpholinyl)phenyl]-3,5-pyridinedicarbonitrile (**3 h**).

Reaction time 24 h, yellow crystals from methanol, mp 192–193 °C, yield 34 %. IR: $\nu_{max.}/cm^{-1}$ 3436, 3311, 3210 (NH_2), 2210 (C≡N), 1636, 1611 (C=N, C=C).

^{1}H-NMR (DMSO-d_6): δ 0.99 (t, 3H, CH_3, J = 7.5 Hz), 1.52 (sextet, 2H, CH_3CH_2, J = 7.5 Hz), 1.80 (quintet, 2H, OCH_2CH_2, J = 6.6 Hz), 3.30 (t, 4H, morpholinyl 2 NCH_2, J = 5.1 Hz), 3.89 (t, 4H, morpholinyl 2 OCH_2, J = 5.1 Hz), 4.41 (t, 2H, OCH_2, J = 6.6 Hz), 5.58 (s, 2H, NH_2), 7.02 (d, 2H, arom. H, J = 9.0 Hz), 7.52 (d, 2H, arom. H, J = 9.0 Hz). MS: *m/z* (%) 377 (100). Anal. for $C_{21}H_{23}N_5O_2$ (377.43): Calcd., C 66.82, H 6.14, N 18.56; Found: C 67.01, H 6.32, N 18.33 %.

Paper Sheets Formation and Tests

Bleached bagasse pulp (kindly supplied by Edfo Paper Mill-Upper Egypt) and cotton linters (supplied from Kafr El-Tawar Mill-Egypt) were used as a base furnish to prepare paper sheets. Both bleached bagasse and cotton linters were separately beaten to 50 SR^o (degree of schopper-Riegler), using a valley beater at 2 % consistency. From both types of pulps, sheets of 100 % cotton linters (CL), 100 % bleached bagasse pulp (B) and 75 % CL + 25 % B were prepared according to Tappi Standard method.

The prepared hand-sheets were sprayed with three promising fluorescence compounds **(3c**, **d**, **h)**, dissolved in $CHCl_3$ in 0.1 % (wt/vol), using automatic atomizer to achieve high degree of homogeneity distribution over one phase of sheet (0.25 g/m^2). The samples were conditioned at 20 °C and 50 % RH (ISO 187 [97]).

Strength properties, e.g., tensile, tear, and burst indices of paper samples were measured before and after treatment, according to Standard procedure [98]. While the fluorescence behavior was determined using a JASCO spectrofluorometer and surface ultraviolet examination was carried out using docucenter$^{(R)}$ 4500, Spectral Analysis System (Projectina, Swiss).

3.1.3 Results and Discussion

Chemistry of Heterocyclic Compounds

Reaction of arylidenemalononitriles **1a–c** with malononitrile **(2)** in the appropriate alcohol (namely, methanol, ethanol, *n*-propanol, *n*-butanol) containing sufficient amount of sodium, for production of the needed sodium alkoxide in the reaction medium, afforded directly the corresponding 6-alkoxy-4-aryl-2-amino-3,5-pyridinedicarbonitriles **3a–h**. The reaction Scheme 1" was assumed to take place via malononitrile nucleophilic attack at the β-carbon of unsaturated system of **1** under the effect of used basic conditions. Then, due to alkoxide nucleophilic attack at one of the intermediate nitrile groups, it led to cyclization to the corresponding pyridine nucleus with subsequent dehydrogenation giving finally 3,5-pyridinedicarbonitriles **3**.

Structure of the prepared compounds **3a–h** was deduced through spectroscopic (IR, ^{1}HNMR, MS) and elemental analyses data. The IR spectra of **3** reveal the presence of amino stretching vibration bands at v = 3505–3175 cm^{-1} in addition to the nitrile stretching bands at 2223–2209 cm^{-1}. ^1H NMR spectra exhibit the

alkoxide group (singlet at δ = 3.96 assignable for the methoxy function in case of **3a**, **b**; triplet and quartet signals at δ = 1.34–1.44, 4.37–4.46 assignable for the methyl and methylene protons of ethoxy function in case of **3c–e** triplet, sextet, and triplet signals at δ = 1.05–1.06, 1.65–1.88, 4.36–4.37 assignable for methyl and two methylene protons of propoxy function in case of **3f**, **g** and triplet, sextet, quintet, and triplet signals at δ = 0.99, 1.52, 1.80, 4.41 assignable for the methyl and three methylene protons of butoxy function, respectively). Mass spectra of **3b–d**, **f–h** exhibit the parent ion peaks as base peaks.

Absorption and Fluorescence Properties of the Prepared Compounds

The absorption and fluorescence properties of the prepared 3,5-pyridinedicarbonitriles **3c–h** were determined in chloroform [43, 99, 100]. Due to the high insolubility of compounds **3a**, **b**, the study of their absorbance, excitation, and emission was ignored. From the obtained data (Table 2 and Fig. 1) it is obvious that all the prepared 3,5-pyridinedicarbonitriles **3c–h** exhibit two main excitation bands at λ = 244.5–276, 327.5–330 nm corresponding to two UV absorption maxima at λ = 275–277, 327–330 nm. However, only one emission band was observed at λ = 404.5–443 nm at any of the observed excitation bands.

All the investigated pyridinedicarbonitriles show promising fluorescence properties with considerable quantum yield. It has been noticed that the substituent attached to the phenyl group at the 4-position of pyridinecarbonitriles affect greatly the observed quantum yield (ϕ_s) values. Morpholinyl residues always associate with enhanced quantum yield values comparable with piperidinyl and methylpiperazinyl functions, as exhibited in compounds **3c–e** (ϕ_s = 0.639, 0.826, 0.131, respectively); also, **3f** and **3g** (ϕ_s = 0.568, 0.810, respectively). It has also been noticed that the type of alkoxy group attached to the 6-position of pyridinedicarbonitriles may affect the observed quantum yield values. The best results were obtained when the ethoxy function was used comparable with propoxy residue as exhibited in pairs **3c**, **f** (ϕ_s = 0.639, 0.568, respectively) and **3d**, **g** (ϕ_s = 0.826, 0.810, respectively).

Eventually, the prepared heterocyclics **3d**, **g** and **3h** could be recognized as good candidates for application in the present study due to their remarkable fluorescence properties.

Evaluation of Papermaking

The fluorescence and mechanical properties of surface treated paper sheets made from cotton linters and sugarcane bagasse pulp, individual or in blend, using the above candidate fluorescence compounds (**3c**, **d**, **h**), are shown also in Table 2 and Fig. 2.

In order to investigate the fluorescence character, we measured the emission spectra and intensity of the emission band in paper samples using excitation wavelength $\lambda_{327–330}$ nm. The measurement of quantum yield of treated paper sheets

Table 2 Absorption, excitation, and emission spectral properties of the prepared compounds in chloroform and fluorescence measurements of paper sheets

Fluorescence	Fluorescence measurements of compounds in $CHCl_3$					Fluorescence measurements of treated paper sheets			
Compounds	Absorption		Excitation	Emission	ϕ_s	Type of	Excitation	Emission	Intensity
	λ_{max} (nm)	ε_{max}	λ_{max} (nm)	λ_{max} (nm)		Substrate	λ_{max} (nm)	λ_{max} (nm)	X 10^3
3c	275	21,401	273	440	0.639	Cotton Linters (CL) Bagasse pulp (BP) CL + BP	271(sh), 329, 375	462	8.45
	328	14,564	328.5[a]				272, 331, 374	452.5	1.88
	361	13,240	371.5				276, 331, 374	453	1.43
3d	277	21,016	244.5	430	0.826	Cotton Linters (CL) Bagasse pulp (BP) CL + BP	271(sh), 330 367	432.5	1.11
	327	19,264	327.5[a] 361[b]				275, 330, 369	438.5	2.68
							275, 330, 368	439	1.86
3e	277	21,484	276	404.5	0.131				
	328	18,744	328[a]						
3f	275	21,349	276	443	0.568				
	330	14,540	330[a]						
	361	12,694	372						
3g	277	21,632	274.5	429.5	0.810				
	328	19,968	327.5[a] 364[b]						
3h	277	21,201	275	431	0.814	Cotton Linters (CL) Bagasse pulp (BP) CL + BP	271(sh), 327, 375	420	2.2
	328	19,104	328[a] 361[b]				272, 330, 374	428	2.87
							271, 329, 370	438	3.04

[a]Wavelength at which quantum yield of the tested compound (ϕ_s) was measured relative to quinine sulfate, which was used as a reference standard
[b]Shoulder

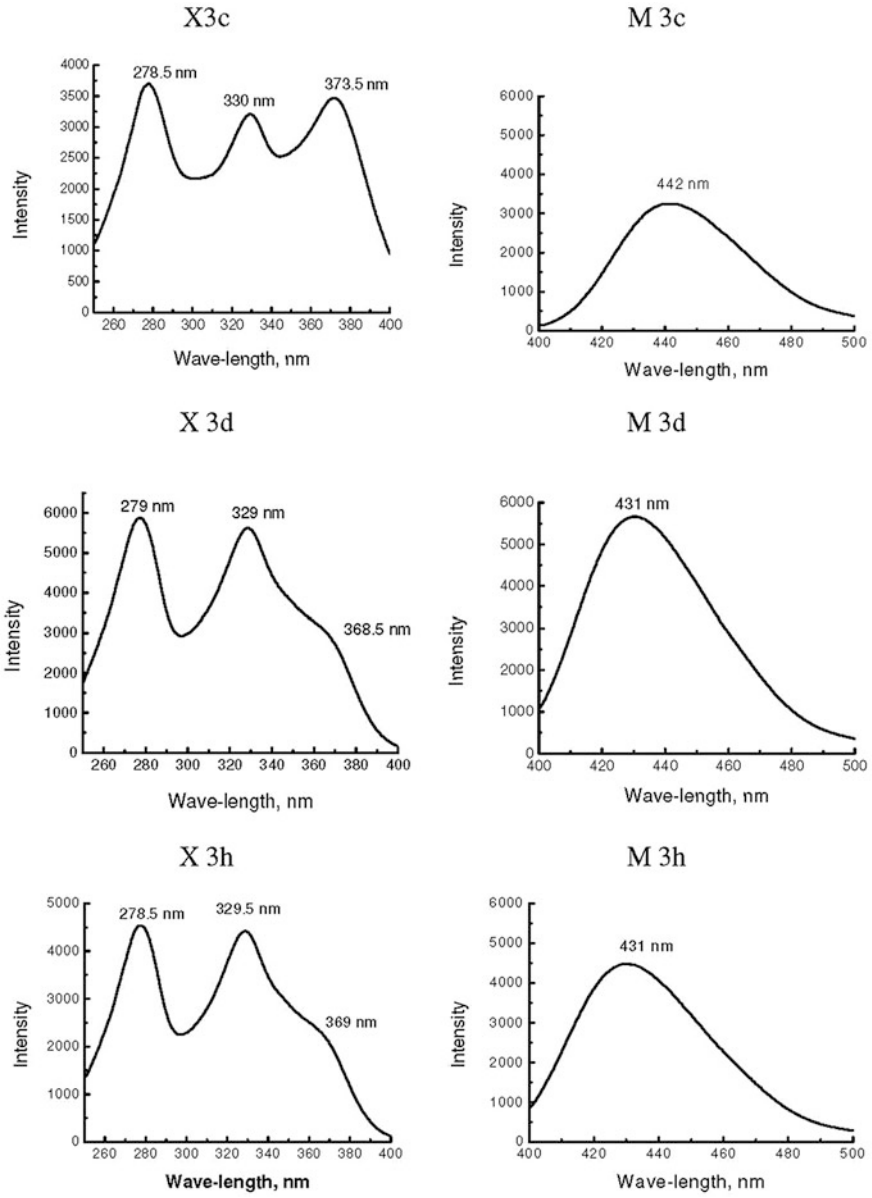

Fig. 1 Influence of candidate fluorescence compounds on the mechanical properties of paper sheets produced

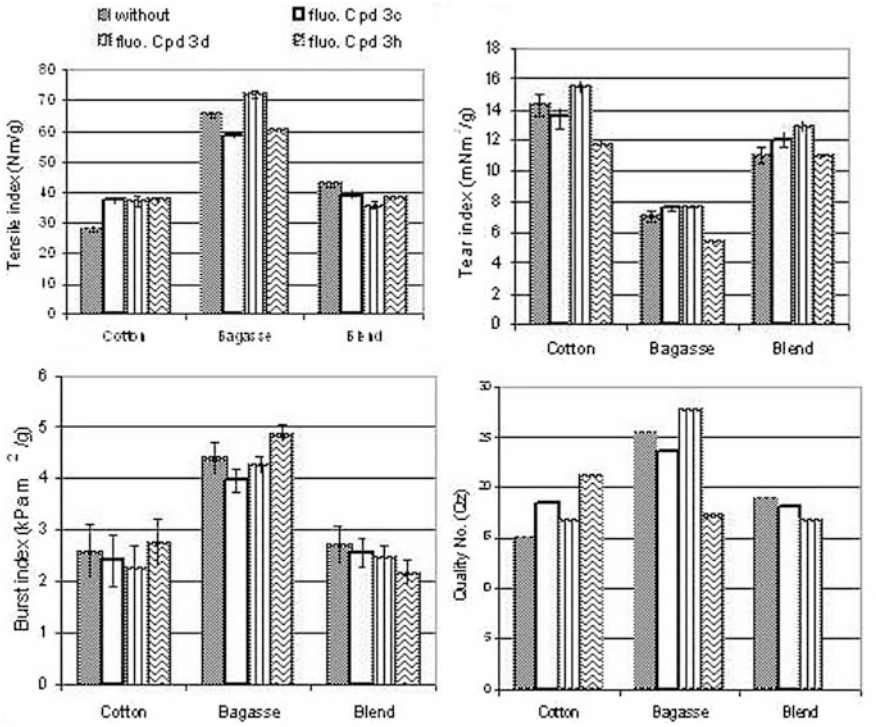

Fig. 2 Influence of candidate fluorescence compounds on the mechanical propertied of paper sheets produced

relative to quinine sulfate treated sheet is not possible due to the deterioration effect of quinine sulfate in sulfuric acid solution on substrates of paper sheets. Table 2 shows that the position of emission bands of paper treated with morpholinyl-containing fluorescence compounds (**3d**, **3h**) were shifted to shorter wavelength compared to that treated with piperidinyl-containing compound (**3c**). Substituting the ethoxide group, in o'-position of pyridine (cpd. **3d**), by butoxide (cpd. **3h**) leads to shift the emission band to shorter wavelength. This is ascribed to probable formation of hydrogen bonds between the lone-pair electron of oxygen in the long alkyl chain with the hydroxyl groups containing paper pulp. This may affect the functional moieties responsible for fluorescence properties (6-alkoxy-2-amino-4-aryl-pyridine functional groups). The presence of butoxide group instead of ethoxide may enhance the interaction of fluorescence compounds with pulp fibers and weaken the fiber–fiber bonding. As can be seen, changing the type of substrate of paper sheets is accompanied by changing the position of emission band. The relatively long shift and consequent increases in intensity of emission band were noticed for paper sheet made from bagasse pulp, using cpd **3c**.

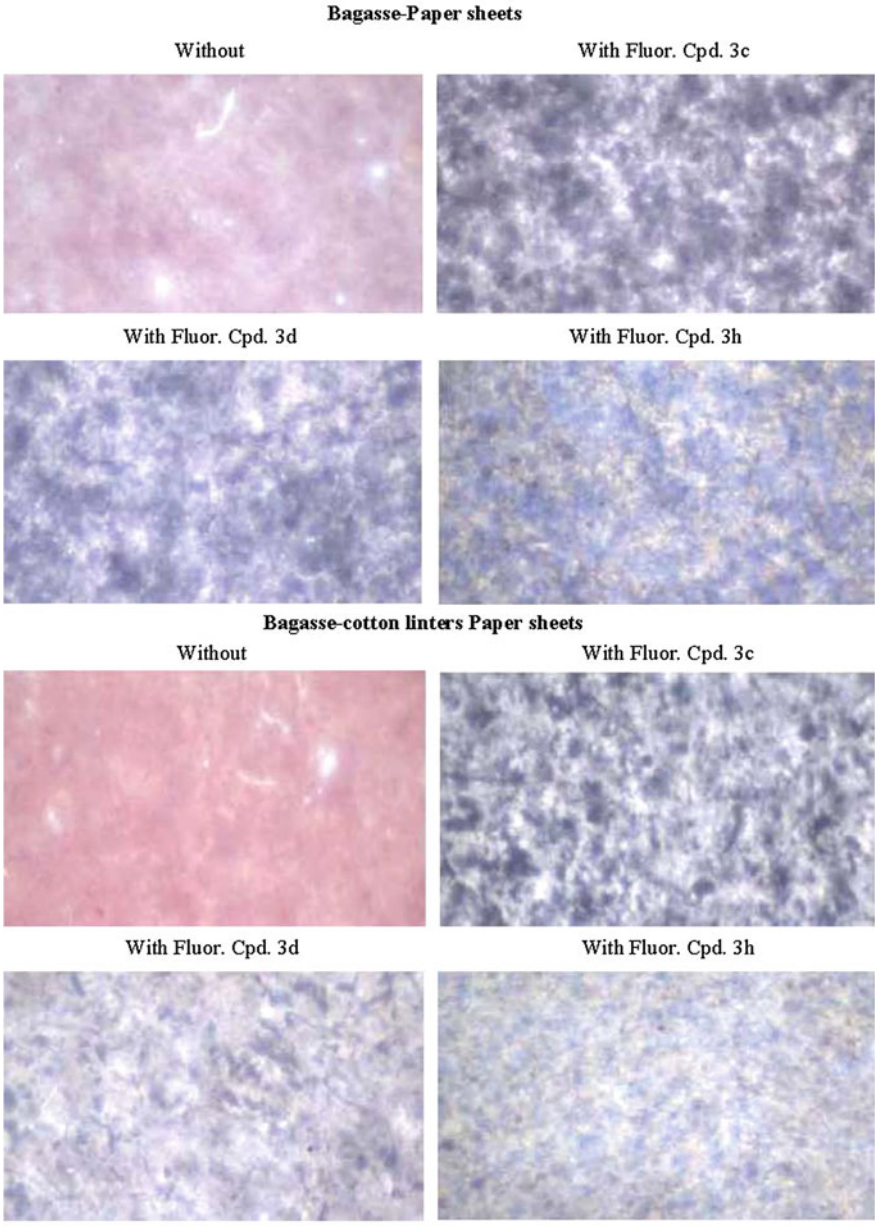

Fig. 3 UV photos of paper sheets treated with candidates Fluorescence compounds

For the mechanical properties, the histograms in Fig. 2 show that treating the paper sheets made from cotton linters with investigated fluorescence compounds, in addition to providing paper samples fluorescence character also improve the

breaking length and quality number, Q_z (refers to the trend of all strength properties) [101]. However, the reverse trend is observed in case of bagasse pulp containing paper sheets. As can be seen, there is a good relation between the fluorescence band intensity and the decrease in strength properties of paper sheets. Whereas treating with piperidinyl group containing fluorescence compound (**3c**) achieves relatively high improvement in strength properties of paper sheets from cotton linters, or reduces the deterioration effect of applied compounds on paper sheets from bagasse pulp cotton linter blend. It is interesting to note that this type of paper sheet is characterized by relatively high strength properties than that made from conventional cellulosic substrate (cotton-based fibers).

For UV-examination, Fig. 3 shows that fluorescence compounds sprayed on bagasse paper sheets provide more intense UV radiation than those prepared from blend of bagasse with cotton linter. It is that fluorescence radiation reflected from application of fluorescence compounds on surface of paper sheets were in the blue-violet region. The highest intensity was observed for compound **3d** followed by compound **3h** and compound **3c**. This observation is related to the quantum yield of the investigated fluorescence compounds in chloroform solutions, where the quantum yields (ϕ's) of compound **3d**, **h** and **3c** were 0.826, 0.814 and 0.639, respectively.

3.2 Preparation and Optical Properties of 2-Amino-6-Ethoxy-4-[4-(4-Morpholinyl)Phenyl]-3,5-Pyridinedicarbonitrile Fluorescent Nanoparticles: A Security Marker for Paper Documents (Mauro et al. 2012) [39]

3.2.1 Objective

The success of our investigated 2-amino-6-ethoxy-4-[4-(4-morpholinyl)phenyl]-3,5-pyridinedicarbonitrile (AEMP), had high quantum number (ϕ_s = 0.826/Quinin sulfate), to be used as a security marker in paper documents (Sect. 3.1, [44]), motivate us to examine its behavior as fluorescence nanoparticles [45]. This study depends on the knowledge and studies dealing the nano- and microcrystals of organic molecules that show size-dependent tunable photoluminescence with broad excitation spectra, which allows for simultaneous excitation of several particle sizes at a single wavelength [102]. Therefore, the objective of this section was to present our published article dealing with the behavior of AEMP as new fluorescence organic nanoparticles. The advantage of this material besides its high fluorescence quantum yield also has a long lifetime.

3.2.2 Experimental Methods

Synthesis of AEMP Molecules and Nanoparticles

AEMP fluorescence organic compound was synthesized via Scheme 1, Cpd. 3d (R = 4-morpholinyl, 3, R = 4-morpholinyl, R′ = $C_2H_{5)}$, which was prepared according to the previously reported procedure [43, 94]. While AEMP nanoparticles were prepared using the reprecipitation method [103–106], using water as a nonsolvent. 40, 100, or 200 μl of acetone solutions of AEMP (1 mM) were injected into 10 ml of de-ionized and 0.2 μm filtered water at room temperature using suitable pipettes. Some of the samples were prepared by magnetic stirring at 300 rotations per minute (rpm) in water during solution injection. Other samples were prepared in water under ultrasonic sonication with different times and process conditions. Water ultrasonic sonication was induced using a 20 kHz, 50 W, Vibra-Cell ultrasonic processor (Sonics & Materials, Inc., USA) connected to a titanium horn to radiate the ultrasonic energy to the liquid.

After injection AEMP molecules began to aggregate and dispersions of AEMP nanoparticles in water were obtained which exhibited an off-white turbidity due to light scattering of the nanoparticles. Homogeneous uniform dispersion state was maintained for more than 6 months.

Morphology of AEMP Nanoparticles

The size distribution of the obtained nanoparticles was checked in situ using Dynamic Light Scattering (DLS) method. DLS measurements were performed using an ALV-5000 system (ALV, Langen, Germany) equipped with a He–Ne laser operating at 632.8 nm. The scattering angle was fixed at 90°. The morphology of the nanoparticles after evaporation of water was observed using a variable pressure scanning electron microscope SEM-VP EVO 50 XVP (Carl-Zeiss Electron Microscopy Group) and a Nanosurf Mobile S atomic force microscope (AFM) with nanometric resolution in tapping mode [107]. The amplitude image referring to the z-distance variation of cantilever pedestal and the phase image where the contrast refers to the spatial variation of the phase of vibrating cantilever were recorded simultaneously on the investigated surface area. While the first is a good replica of the surface topography, the phase contrast imaging mode can indicate variations in composition, friction, viscoelasticity, adhesion, or hardness in heterogeneous samples surface.

Absorption and Photoluminescence Spectra

Optical measurements were carried out using home assembled experimental setups. Optical absorption of the AEMP nanoparticles dispersed in water was measured in the 250–600 nm wavelength range using a continuous-wave Deuterium lamp

monochromatized by a 30 cm focal length monochromator (Acton) as light source. Due to the fact that AEMP nanoparticles exhibit strong fluorescence, detection was realized using another 30 cm focal length monochromator (Acton), coupled to a preamplified UV-enhanced Si photodetector, scanning at the same wavelength of the light source monochromator. Deuterium lamp was mechanically chopped allowing lock-in detection. Quartz cuvette with 1 cm optical path length was used to house the water suspension. All absorption measurements were normalized to water filled quartz cuvette.

A Xenon flash lamp, monochromatized by a 12.5 cm focal length Oriel monochromator, was used as the excitation source for emission spectra measurements. The AEMP nanoparticles dispersed in water were housed in a 1 mm-thick quartz cuvette and a front-surface excitation and collection geometry was used. Luminescent emission was detected by an Avantes 2048 UV/VIS spectrophotometer synchronized with 5 s flashes, then background subtracted at every flash, and finally accumulated until a reasonable signal-to-noise ratio was achieved.

3.2.3 Results and Discussion

Production and Morphology of AEMP Nanoparticles

The process conditions used to obtain the AEMP nanoparticles are reported in Table 3. Four sets of samples were produced to compare nanoparticles produced by magnetic stirring to those produced using sonication. For the case of using sonication process, several preparation processes were performed, e.g., times (samples s5–s8), sonication powers (samples s10–s12), and amount of AEMP macromolecules solutions (samples s13–s16).

Table 3 Preparation conditions used to obtain the AEMP nanoparticles

Sample label	Method of preparation	Amount of AEMP solution (µl)	Process time (min)	Intensity
s1	Stirring	100	30	300 rpm
s3	Stirring	40	30	300 rpm
s5	Sonication	100	10	25 W
s6	Sonication	100	30	25 W
s7	Sonication	100	45	25 W
s8	Sonication	100	60	25 W
s10	Sonication	100	30	12.5 W
s4	Sonication	100	30	25 W
s12	Sonication	100	30	37.5 W
s13	Sonication	40	30	12.5 W
s16	Sonication	200	30	12.5 W

Figure 4 shows number-weighted radii distribution $P^*_N(R_h)$ (not normalized) as function of the hydrodynamic radius (R_h) of the AEMP nanoparticles dispersed in water, resulted from DLS measurements using the CONTIN method [108].

In the first experiment (Panel A), it was shown that by decreasing the amount of AEMP solution used during the reprecipitation process, from 100 to 40 μl, the distribution peaks at lower radius were from 268 to 156 nm, and the peak amplitude

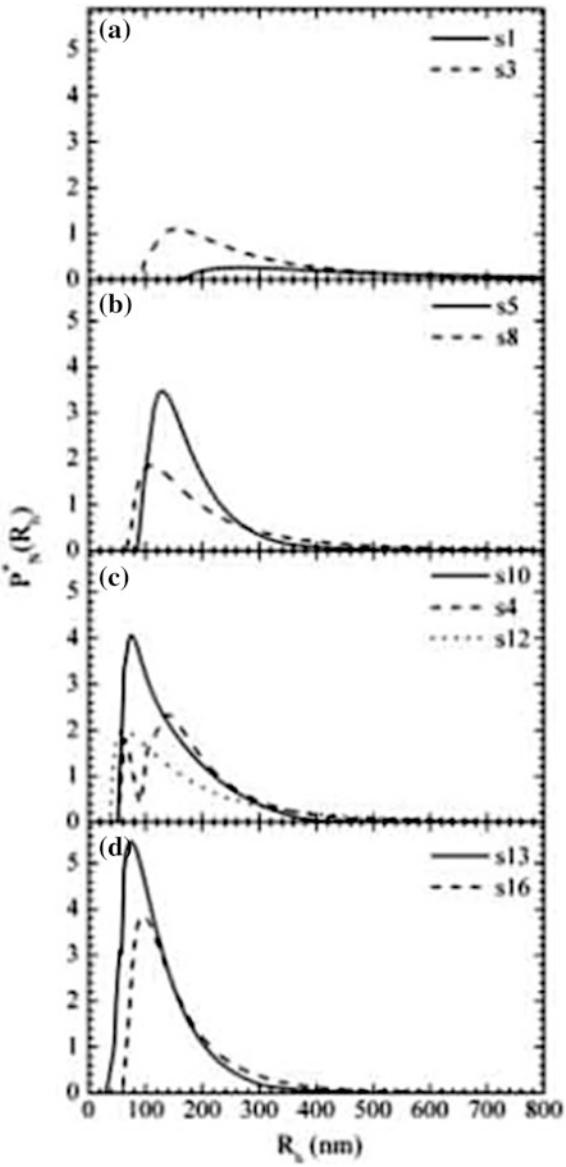

Fig. 4 Number-weighted radii distribution $P^*_N(R_h)$ (not normalized) in function of the hydrodynamic radius (R_h)

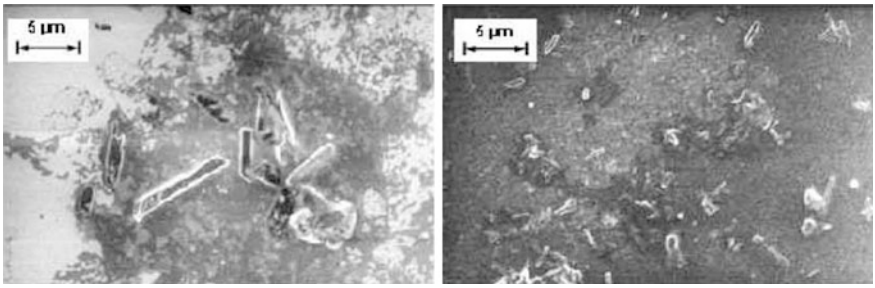

Fig. 5 VP-SEM images of dried droplets of s1 (*left*) and s3 (*right*) nanoparticles suspension

increases due to decreasing of the nanoparticles volumes [108] while the distribution width is lowered. However, both distributions are characterized by a long tail of large size, with not negligible values for $R_h > 500$ nm. This result can be interpreted as due to particles clustering or due to formation of large single particles. VP-SEM observations of dried droplets of nanoparticles suspension provide evidence of the second hypothesis (Fig. 5): Large single parallelepiped-shaped widespread particles, with dimensions up to $\sim 1 \times 8$ and $\sim 0.5 \times 2$ µm were found for s1 and s3 samples respectively. Schematizing the nanocrystals as rods of length L and diameter R, R_h can be expressed as $R_h^3 = (3LR^2)/4$, which gives $R_h \sim 1.8$ µm and 0.72 µm for samples s1 and s3, respectively, which explain the bigger size population indicated by the $P_N^*(R_h)$ distribution.

In a second experiment (Fig. 3, Panel B), nanoparticles were produced as function of the sonication time, it is shown the number-weighted radii distribution $P_N^*(R_h)$ (not normalized) of s5 and s8 AEMP nanoparticles, dispersed in water, as recovered from DLS measurements as described previously. In this case, even by using the smallest process time of 10 min, the distribution peaks at 131 nm, a value smaller than that of the nanoparticles produced using magnetic stirring, such as s1 or s3 samples. In addition, by increasing the process time from 10 to 60 min the distribution peak position shifts to smaller values down to 109 nm, even if a broadening toward higher sizes is observed.

In a third experiment (Fig. 4, Panel C), where the effect of the sonication power was studied ($P_N^*(R_h)$ distribution of the s10, s4, and s12 AEMP nanoparticles), it is shown that t is the lower sonication power of 12.5 W with distribution is peaked at 75 nm. By increasing the sonication power to 25 W (sample s4) a double peak distribution is found with maxima at 139 and 62 nm and a decreasing of the number of produced particles is observed. In case of higher sonication power of 37.5 W, as used for samples s12, it is still observed a single peak distribution peaked at 62 nm. Higher sonication powers could be accounted for AEMP macromolecules degradation thus limiting the final number of nanoparticles obtained in the process. Indeed AFM measurements on s12 sample, (Fig. 6), show particles approximately

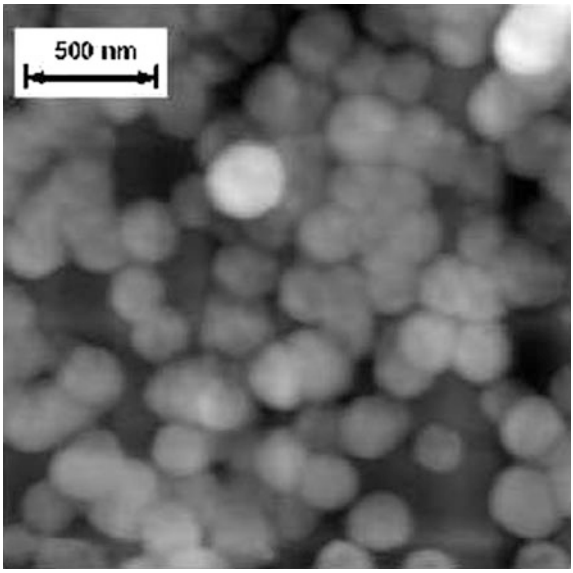

Fig. 6 AFM topographic image of nanoclusters observed on dried droplets of sample s12. Ellipsoidal object with average dimensions of 200 × 25 nm are found in this scanning field

ellipsoidal in shape, with size of about 200 nm across and 25 nm in height, which cover the observed area of 2 × 2 μm homogeneously. The shape of these particles is quite different from the parallelepiped-shaped ones, as observed in all other samples. VP-SEM measurements reinforced this conclusion by observation of very few crystalline objects, while large unshaped structures were observed. Indeed the volume of these ellipsoidal nanoparticles observed on dried droplets of nanoparticles suspension is equivalent to spherical object of 63 nm in radius in excellent agreement with peak at 62 nm of the number-weighted radii distribution P_N^* of the nanoparticles dispersed in water. This observation leads to the conclusion that the higher sonication power of 37.5 W has modified the AEMP macromolecules, perhaps by production of free radicals, therewith inhibiting ordering and leaving unshaped and probably amorphous aggregates as a final effect. In case of sample s4, the P^*_N weaker peak at 62 nm could be also explained by the presence of such unshaped aggregates in water suspension even at 25 W sonication power and their presence could also influence the P_N^* of s8 sample, which was produced by using 25 W for a long sonication time as 60 min.

Following these conclusions and because nanoparticles of smaller sizes were also obtained at low sonication power conditions, in final experiments it has been studied the effect of AEMP solution amount at the lower sonication power of 12.5 W. In Fig. 3 (Panel D) it is shown the number-weighted radii distribution $P_N(R_h)$ of the s13 and s16 AEMP nanoparticles dispersed in water. In this case, the increasing in amount of AEMP solution from 40 to 200 μl shifts the distribution peak from 75 to 96 nm without significantly increasing the distribution width.

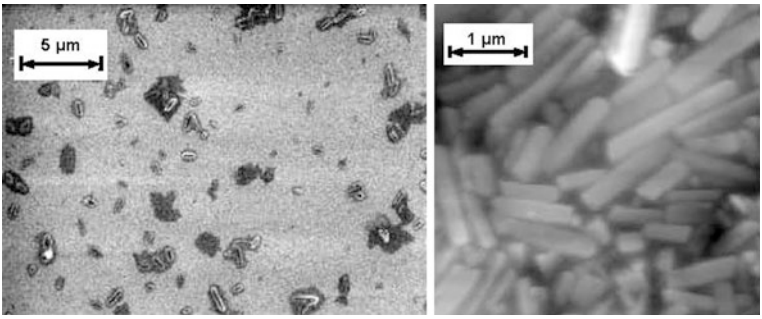

Fig. 7 VP-SEM image (*right*) and AFM topographic image (*left*) of parallelepiped-shaped AEMP nanoparticles observed on a dried droplet of sample s13

In particular, no relevant differences are observed by changing the amount of AEMP solution from 100 µl (sample s10) to 200 µl (sample s16).

VP-SEM and AFM topography images of sample s13 (Fig. 7) show well in evidence the parallelepiped-shaped nanoparticles similar to those already observed in sample s1 and s3 using VP-SEM (see Fig. 5). In case of sample s13 sizes ranges from the instrument resolution limit to approximately 1000 × 200 nm. Also, in this case by schematizing the nanocrystals as rods of length L and diameter R, an upper $R_h \sim 300$ nm value is found in good agreement with the P^*_N recovered by using LS.

Absorption and Photoluminescence Spectra

UV-Visible absorption spectra of AEMP/acetone solution and nanoparticles samples s3, s5, and s13 in water suspension are shown in Fig. 8. Data below a wavelength of 310 nm are not shown due to strong absorption of acetone that peaked at 280 nm and to absorption of residual acetone present in water, which peaked at 262 nm [109]. In case of AEMP/acetone solution (4.0×10^{-6} mol L^{-1}), the absorption spectrum shows one principal peak at 330 nm and a low energy tail with a shoulder at approximately 350–360 nm. Absorption spectra of AEMP molecules in chloroform (UV-transparent medium) show the existence of two more peaks at 238 and 275 nm. These high energy peaks could be attributed to phenyl ring [102, 110], while the low energy features to the n-$\prod^*$, $\prod$-$\prod^*$ and eventually n-$\prod^*$ transition of pyridine nuclei of AEMP molecules.

In case of s3, s5, and s13 AEMP nanoparticles two absorption peaks are evident (Fig. 8): one at approximately 350 nm and another at approximately 400 nm. Both peaks are observed in nanoparticles prepared by simple stirring and by stirring and sonication. The integrals of the absorption curves are proportional to the value of the integral $\int P^*_N(R_h)dR_h$, namely to the overall number of AEMP particles produced during reprecipitation processes.

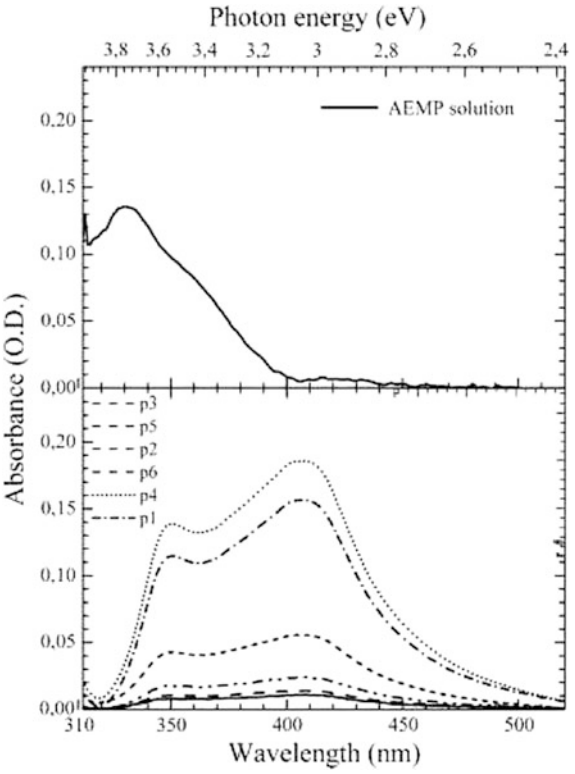

Fig. 8 UV-visible absorption spectra of AEMP solution in acetone and AEMP nanoparticles of samples in water suspension

The fluorescence excitation spectra of s3 and s13 AEMP nanoparticles and AEMP monomers in the diluted acetone solution, displayed in Fig. 8, allow us to shed more light on the energy levels involved in the optical absorption transitions. In case of AEMP monomers, the excitation spectrum collected at a wavelength of 465 nm confirms the presence of peaks at 330 and 350 nm; however, a new strong peak at 380 nm is highlighted where the absorption spectrum showed a tail. In this way the AEMP molecules in solution show a complex ultraviolet absorption with 2 peaks in the high energy side due to phenyl ring, and 3 peaks in the low energy side. We assign these 3 peaks at 330 nm (3.76 eV), 350 nm (3.54 eV) and 380 nm (3.26 eV) to, respectively, the n-$\prod$*, $\prod$-$\prod$* and n-$\prod$* transitions of pyridine nuclei of AEMP molecules.

In case of nanoparticles of samples s3 and s13, the excitation spectra collected at wavelength of 485 nm show the same features as the absorption spectra, namely two peaks at 340 and 400 nm whose positions do not seem to be dependent on nanoparticle sizes. Interestingly, the intensity ratio between the 400 to 340 nm peak, $I_{400/340}$, increases from $I_{400/340}$ (s13) = 1.11 to $I_{400/340}$ (s3) = 1.51 as nanoparticles size increases, while the minimum between peaks remains constant in intensity.

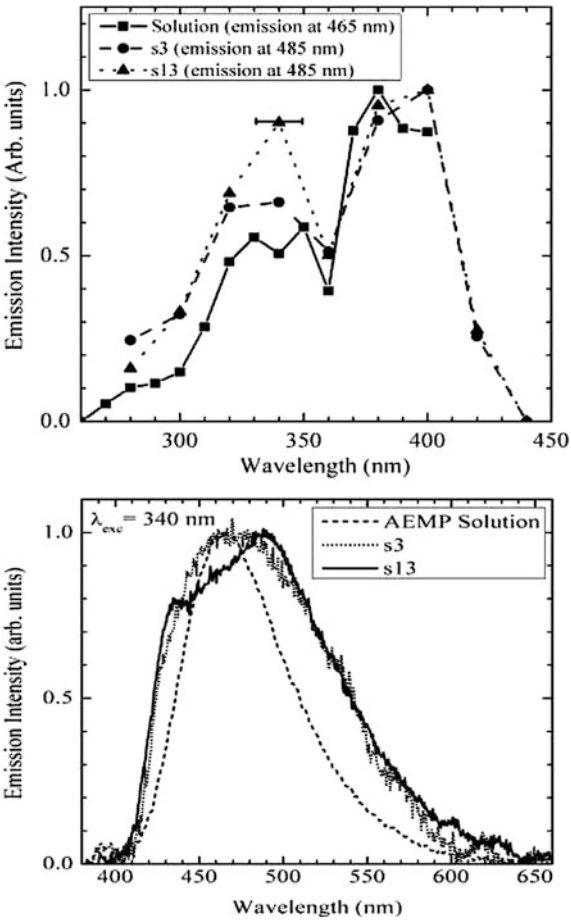

Fig. 9 Fluorescence excitation and emission spectra of AEMP solution in acetone and *s3* and *s13* nanoparticles dispersed in water

There are significant differences between the luminescence emission spectra of AEMP molecules solution and AEMP nanoparticles (Fig. 9). All these spectra are excited at 340 nm (3.65 eV), however, no evident changes in the shape of the solution and nanoparticles' emission spectra are observed as the pump energy changes from 280 to 400 nm (4.43 to 3.1 eV). AEMP solution emission is an asymmetric peak with maximum at 465 nm and the low energy tail (defined as the energy at which the intensity is >5 % of the peak intensity) extends to 575 nm (2.16 eV). This is compared with that of AEMP nanoparticles that show a size-dependent behavior: in case of sample s3 (maximum of $P_N^*(R_h)$ at $R_h = 156$ nm) a broader emission centered at 470 is observed while in case of sample s13 (maximum of $P_N^*(R_h)$ at $R_h = 75$ nm) appear to be clearly split into two peaks at 430 (2.88 eV) and 490 (2.53 eV) nm.

To interpret the absorption and emission data of pyridine nuclei it is possible to use an energy state diagram as shown in Fig. 9. The ground electronic state of pyridine nuclei of AEMP molecules is a spin-singlet and is labeled S_0. The high intensity absorption of Fig. 8 is the signature of spin-allowed singlet-singlet transitions. The high energy absorption n-$\prod$* type at 3.76 eV (330 nm) is assigned to direct S_0 to S_2 transition; the intermediate absorption $\prod$-$\prod$*, type at 3.54 eV (350 nm) to S_0 to S_1 transition; while the low energy feature at 3.26 eV (380 nm), weak in the absorption spectrum but well evident in the excitation spectrum of monomers, to the charge transfer n-$\prod$* transition from S_0 to CT.

In case of AEMP nanoparticles the n-$\prod$*, $\prod$-$\prod$* and n-$\prod$* transitions of pyridine nuclei of AEMP molecules shift to longer wavelength and, at the same time, a broadening and an overlapping of absorption peaks, evident even in the excitation spectra, is observed. Low energy S_0-CT transition appears to be the dominant feature of the absorption spectra and its maximum shifts from 380 in AEMP solution to 400 nm (energy differences of 0.16 eV). This behavior is in agreement with previous study of optical properties of organic nanoparticles where it was observed that CT transition grow significantly in intensity when molecules condense in nanoparticles and its intensity increases with nanoparticles size, as obtained in our case for $I_{400/340}$. Concerning S_0-S_1 and S_0-S_2 transitions, they appear to be superimposed and only one maximum at 350 is observed in absorption spectra (at 340 in excitation spectra). It is observed that absorption peaks' position is not dependent on the size of nanoparticles within the range of sizes studied in this work.

In case of emission spectra, by exciting from 280 (4.43 eV) to 400 nm (3.1 eV) and by varying the AEMP molecules concentration from 10^{-3} to 4.0×10^{-6} mol L^{-1}, only one emission peak is always observed for AEMP monomers in acetone solution. This result, together with the high intensity of the CT peak in excitation spectrum, allows us to state that the emission of AEMP monomers in solution can be assigned directly to a transition from the lower energy excited state CT to the ground state S_0. In case of excitation to higher energy levels S_1 and S_2, energy transfer to the CT occurs, followed by emission and decay to the ground S_0 state.

Even in case of AEMP nanoparticles emission spectra show the same shape by exciting from 280 (4.43 eV) to 400 nm (3.1 eV). However, the shape of emission spectra is dependent on the nanoparticles sizes. In case of s3 sample the shape shows only one peak red-shifted to 470 nm (energy difference 0.03 eV) with respect to the value of dilute solution. In addition, emission appears to be broader, and this could be explained by admitting some anharmonicity in the CT potential induced upon crystallinization and subsequent exciton delocalization, or additional vibrational modes of AEMP in the solid state. In case of sample s13 a new shoulder at 430 nm appears (2.88 eV). The appearance of this high energy peak as soon as

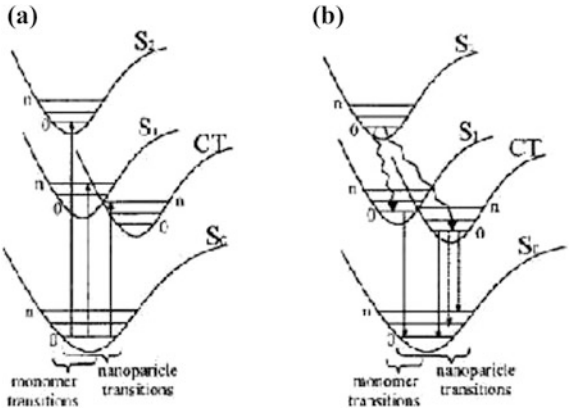

Fig. 10 Energy state diagram for **a** absorption and **b** emission transitions proposed for AEMP molecules

nanoparticles dimension decrease has been already observed in case of organic nanoparticles [7] and it has been assigned to be a transition from S_1 to S_0.

Moreover, the shape of each nanoparticle emission spectrum in Fig. 10 does not change as the excitation energy is varied between the energy difference between S_0-S_1 (corresponding to excitation directly into S_1) and S_0-CT (corresponding to excitation into the CT state). This indicates that, in AEMP nanoparticles, S_1 and CT are in equilibrium at room temperature and the probability of the emission transition S_1-S_0 increases with decreasing nanoparticle size.

To explain the size dependence of optical properties of organic nanoparticles, which differs from the so-called "quantum confinement effect" observed in metallic or semiconductor nanoparticles less than 10 nm in size, two explanations have been suggested: (a) the increasing of surface area causes lattice softening, and therefore the Coulombic interaction energies between molecules become smaller, leading to a wider band gap; (b) or electric field effect of surrounding media through the surface of nanoparticles.

Due to the possible application as a security marker of documents, fluorescence properties of AEMP nanoparticles have been also tested after deposition on solid substrates. Specific amounts of water suspension of nanoparticles have been centrifuged and the supernatant solution removed to increase the nanoparticles concentration by a factor of 10. Droplets of the concentrated water suspensions of nanoparticles were dried on optical glass or cotton cellulose paper substrates. Fluorescence spectra of AEMP nanoparticles after deposition on glass and paper substrates are shown in Fig. 11. While for glass substrate, the photo-luminescence spectra appear similar to that of AEMP particles in water suspension, on paper substrate the low energy tail extends more toward lower energy. This effect could be due to a resonant energy transfer from cellulose to nanoparticles due to the strong interaction between AEMP and cellulose [43].

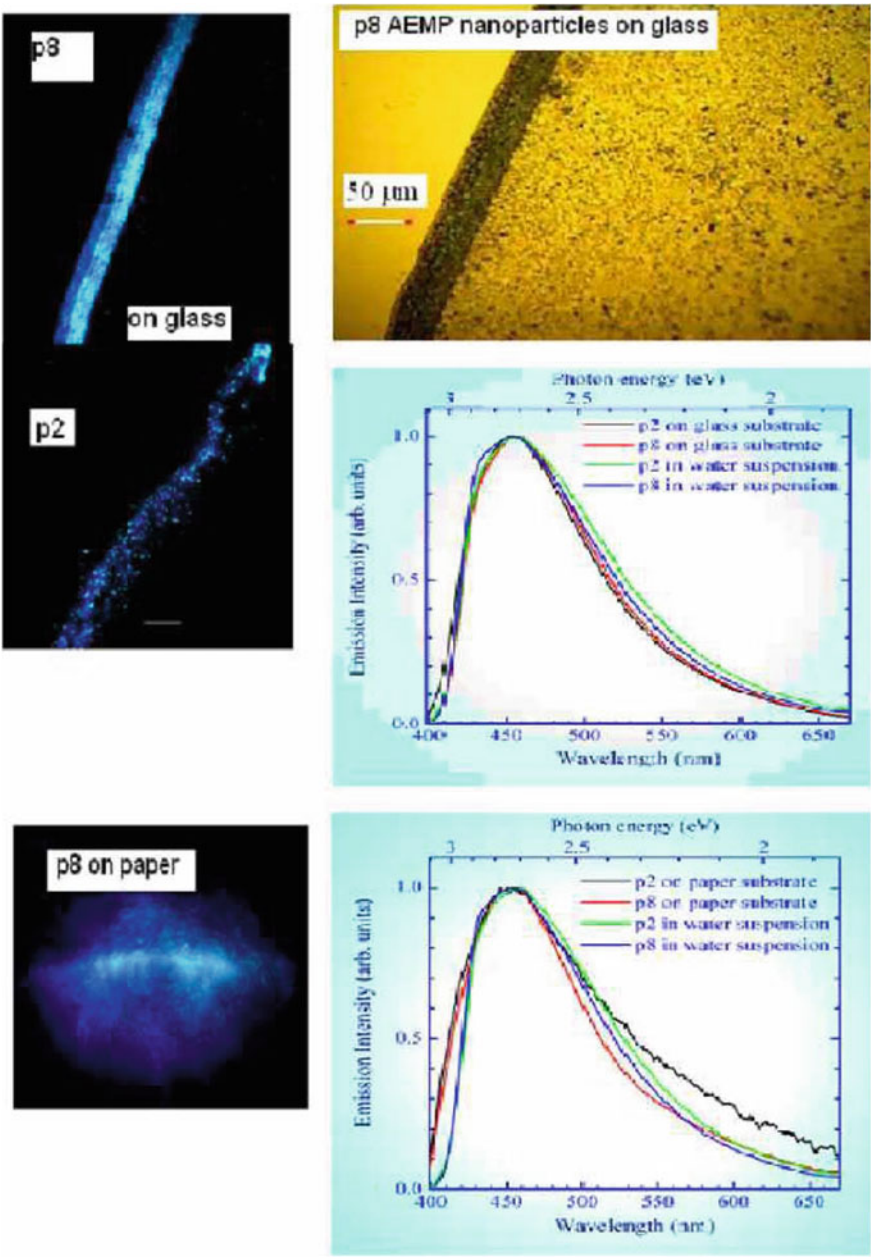

Fig. 11 Fluorescence spectra of AEMP nanoparticles after deposition on glass and paper substrates

4 Conclusions and Future Prospective

It is possible to prepare safety paper based on synthesize novel 6-alkoxy-2-amino-3,5-pyridinedicarbonitriles. These organic fluorescence materials have more than one functional moiety responsible for fluorescence property. The fluorescence quantum yield (ϕ_s) of these active compounds, relative to the fluorescence quantum yield of quinine sulfate, is reached at $\sim$0.83. The successful application of these fluorescence active compounds in the production of functionalized paper sheets, from bagasse pulp cotton linter blend is demonstrated. This type of paper sheet is characterized by relatively high strength properties than that made from conventional cellulosic substrate (cotton-based fibers).

The study also demonstrated the successful production of novel heterocyclic-based nanoparticles compounds (active azines) by the reprecipitation method. The preparation of nanoparticles with 2-amino-6-ethoxy-4-[4-(4-morpholinyl)phenyl]-3,5-pyridinedicarbonitrile (AEMP) component material results in a well-defined, controllable product. Sonication method has been demonstrated to give smaller nanoparticles sizes than magnetic stirring process. Studying the optical properties of this novel organic nanoparticles, especially the fluorescence properties, could help seriously in developing newly applicable secret dyes used for different types of safety paper as well as other related fields of applications. Further studies were performed and in preparation as article dealing with the application of AEMP nanoparticles for paper substrates. Moreover, the safety performance (unfalsifiable safety) of the treated paper toward mechanical and chemical erasure was evaluated.

5 Acknowledgment

The authors wish to thank the Egyptian Ministry for Scientific Research and Italian Foreign Ministry for supporting our presented articles Refs. [37, 98] through the Egypt–Italy collaborating program FY 2008–2010.

Also, the authors acknowledge the valuable contribution of Dr. A.S. Girgis (Professor in Pesticide Chemistry Department, National Research Centre), Dr. M. Missori (Dr. in Istituto dei Sistemi Complessi, Consiglio Nazionale delle Ricerche, Rome, Italy) and Dr. M. De Spirito (Professor in the Istituto di Fisica, Università Cattolica del Sacro Cuore, Rome, Italy), and their staff for kind help in practical achievement and preparing the published articles Refs. [37, 39, 98].

References

1. Ali Mansoori G (2002) Nanotechnology: the emerging cutting-edge technology UN-APCTT. Tech Monit 10:53–59 (Special Issue)
2. Lin M-F, Thakur VK, Tan EJ, Lee PS (2011) Dopant induced hollow $BaTiO_3$ nanostructures for application in high performance capacitors. J Mater Chem 21:16500–16504

3. Lin M-F, Thakur VK, Tan EJ, Lee PS (2011) Surface functionalization of $BaTiO_3$ nanoparticles and improved electrical properties of $BaTiO_3$/polyvinylidene fluoride composite. RSC Adv 1:576–578
4. Thakur VK, Yan J, Lin M-F et al (2012) Novel polymer nanocomposites from bioinspired green aqueous functionalization of BNNTs. Polym Chem 3:962–969
5. Sharma G, Anabousi S, Ehrhardt C, Ravi Kumar MN (2006) Liposomes as targeted drug delivery systems in the treatment of breast cancer. J Drug Target 14(5):301–310
6. Samad A, Sultana Y, Aqil M (2007) Liposomal drug delivery systems: an update review. Curr Drug Deliv 4(4):297–305
7. Sutton D, Nasongkla N, Blanco E, Gao J (2007) Functionalized micellar systems for cancer targeted drug delivery. Pharm Res 24(6):1029–1046
8. Torchilin VP (2004) Targeted polymeric micelles for delivery of poorly soluble drugs. Cell Mol Life Sci 61(19–20):2549–2559
9. Gao X, Yang L, Petros JA, Marshall FF, Simons JW, Nie S (2005) In vivo molecular and cellular imaging with quantum dots. Curr Opin Biotechnol 16(1):63–72 [PubMed: 15722017]
10. Smith AM, Ruan G, Rhyner MN, Nie S (2006) Engineering luminescent quantum dots for in vivo molecular and cellular imaging. Ann Biomed Eng 34(1):3–14
11. Koenig S, Chechik V (2006) Shell cross-linked Au nanoparticles. Langmuir 22(11):5168–5173 [PubMed: 16700609]
12. Lou X, Wang C, He L (2007) Core-shell Au nanoparticle formation with DNA-polymer hybrid coatings using aqueous ATR. Biomacromolecules 8(5):1385–1390
13. Duncan R, Izzo L (2005) Dendrimer biocompatibility and toxicity. Adv Drug Deliv Rev 57 (15):2215–2237 [PubMed: 16297497]
14. Najlah M, D'Emanuele A (2006) Crossing cellular barriers using dendrimer nanotechnologies. Curr Opin Pharmacol 6(5):522–527
15. Navalakhe RM, Nandedkar TD (2007) Application of nanotechnology in cancer: A review. Int J Bioformatics Res Appl 8(1/2):112–125
16. Silva GA (2004) Introduction to nanotechnology and Its application to medicine. Surge Neuro 61:216
17. Garcia M, Forbe T, Gonzalez E (2010) Potential applications of nanotechnology in the agro-food sector. Ciência e Tecnologia de Alimentos, Campinas 30(3):573–581, July.-set. 201
18. Weiss J, Takhistov P, McClements J (2006) Functional materials in food nanotechnology. J Food Sci 71(9):R107–R116
19. Qu X, Alvarez PJJ, Li Q (2013) Applications of nanotechnology in water and wastewater treatment. Water Res 47:3931–3946
20. Saurav (2012)/International Journal of Engineering Research and Applications (IJERA) ISSN: 2248–9622 www.ijera.com 2 (5):1077–1082
21. Joshi M, Bhattacharyya A, Wazed Ali S (2008) Characterization techniques for nanotechnology applications in textiles. Indian J Fiber Text 33:304–317
22. Shen J, Song Z, Qian X, Yang F, Kong F (2010) Nanofillers for papermaking wet end applications. BioResources 5(3):1328–1331
23. Sethi VK, Pandey M, Shukla P (2011) Use of nanotechnology in solar PV cell. Int J Chem Eng Appl 2(2):77–80
24. Procter AR (2002) Nanotechnology: it's in your future. Pulp Pap Can. 103(5):9
25. Puurunen K, Vasara P (2007) Opportunities for utilising nanotechnology in reaching near-zero emissions in the paper industry. J Clean Prod 15(13–14):1287–1294
26. Bai W, Holbery J, Li KC (2009) A technique for production of nanocrystalline cellulose with a narrow size distribution. Cellulose 16(3):455–465
27. Revol JF, Godbout L and Gray DG (1998) Solid self-assembled films of cellulose with chiral nematic order and optically variable properties, J Pulp Pap Sci 24(5):146–149
28. Fleming K, Gray DG, Matthews S (2001) Cellulose crystallites. Chem Eur J 7(9):1831–1835
29. Dahlke B, Larbig H, Scherzer HD, Poltrock R (1998) Natural fiber reinforced foams based on renewable resources for automotive interior applications. J Cell Plast 34:361–379

30. Pan J, Hamad W, Straus SK (2010) Parameters affecting the chiral nematic phase of nanocrystalline cellulose films. Macromolecules 43:3851–3858
31. Xu QH, Li WG, Cheng ZL, Yang G, Qin MH (2014) TEMPO/NaBr/NaClO- mediated surface oxidation of nanocrystalline cellulose and its microparticulate retention system. with cationic polyacrylamide. BioResources 9(1):994–1006
32. Moon RJ, Frihart CR, Wegner TW (2006) Nanotechnology applications in the forest products industry. For Prod J 56:4–10
33. Haakana S, Sinisalo L, Solismaa P, Sipilä M (2013) Process for improving wet strength and paper product with improved wet strength, WO 2008003827 A1 20080110
34. Heiskanen I, Axrup L, Norborg M-A, Knoeoes I (2013) Process for producing dispersion comprising nanoparticles and a dispersion produced according to the process, SE 1150997 A1 20130427
35. Heiskanen I, Axrup L, Norborg M-A, Knoos I (May 2013) Process for producing a dispersion comprising nanoparticles and a dispersion produced according to the process, Publisher No. WO2013061266 A1
36. Henriksson M (2008) Cellulose nano-paper structures and high toughness. Biomol 9:1579–1585
37. Hubbe MA (2006) Bonding between cellulosic fibers in the absence and presence of dry-strength agents. Bioresources 1(2):281–318
38. Ioelovich M (2010) Structure and properties nano-particles used in paper compositions. XXI TECNICELPA Conference and Exhibition/VI CIADICYP 2010. Lisbon, Portugal, 12–15 October 2010
39. Hogberg G (1976) Identity card having radioactive isotope of short half-life US Patent. 39, 59, 630
40. Stevenson NR, Dawson MJ, Heflinger L (2004) Use of isotopes to provide information to an article US Patent, 6, 750, 756 B2
41. Hendrick E, Frey M, Herz E, Wiesner U (2010) Cellulose acetate fibers with fluorescing nanoparticles for anti-counterfeiting and pH-sensing applications. J Eng Fibers Fabr 5(1):21–30
42. Small AC, Johnston JH (2009) Novel hybridmaterials of magnetic nanoparticles and cellulose fibers. J Colloid Interface Sci 331(1):122–126
43. Basta AH, Girgis AS, El-Saied H (2002) Fluorescence behavior of new 3pyridinecarbonitrile containing compounds and their application in security paper. Dyes Pigm 54(1):1–10
44. Basta AH, Girgis AS, El-Saied H, Mohamed MA (2011) Synthesis of fluorescence active pyridinedicarbonitriles and studying their application in functional paper. Mat Lett 65 (11):1713–1718
45. Missori M, De Spirito M, Ferrari L, Selci S, Gnoli A, Arcovito G, Girgis AS, El- Saied H, and Basta AH (2012) Preparation and optical properties of 2-Amino-6-ethoxy-4-[4-(4-morpholinyl)phenyl]-3,5 pyridinedicarbonitrile nanoparticles: a security marker for paper documents. NanoParticle Research J. 14:649, 1-12
46. Casey JP (1981) Pulp and paper chemistry and chemical technology 3. Interscience Publishers, New York, p 1914
47. Luna MN, Severiano PO, Gutierrez AJ, Pamanes BR, De Haene RGJ, Gomez CJ (2013) Hydrophobic paper or cardboard with self-assembled nanoparticles and a method for the production there of". WO 2013154414(A1):20131017
48. Talma AG, De Jong AJ, Brujin S, Baltussen JJM, Van Lare CEJ, Reedjk MF (2009) A process to make a clay comprising charge-balancing organic ions, clays thus obtained, and nanocomposite materials comprising the same, MX 2010006865 A 20101005
49. Azetsu A, Koga H, Yuan L-Y, Kitaoka T (2013) Direct synthesis of gold nano catalysts on TEMPO-oxidized pulp paper containing aldehyde groups. BioResources 8(3):3706–3717
50. Nogi M, Iwamoto S, Nakagaito AN, Yano H (2009) Optically transparent nanofiber paper. Adv Mater 21(6):1595–1598
51. Miura S, Kitaoka T (2011) In situ synthesis of gold nanoparticles on zinc oxides preloaded into a cellulosic paper matrix for catalytic applications. BioResources 6(4):4990–5000

52. Johnston JW, Suwanee GA, Townsend DF, Grayson, GA, Hagiopol C, Lilburn GA, Talbert LD, Ruffner C.G, Kingston TN (2014) Paper with higher oil repellency, Publisher No.: US 2014/0106165 A1 April 17
53. Ghule K, Ghule AV, Chen BJ, Ling LC (2006) Preparation and characterization of ZnO nanoparticles coated paper and its antibacterial activity study. Green Chem 8(12):1034–1041
54. Tankhiwale R, Bajpai SK (2009) Graft copolymerization onto cellulose-based filter paper and its further development as silver nanoparticles loaded antibacterial food-packing material. Colloids Surf B 69(2):164–168
55. Foldbjerg R, Olesen P, Hougaard M, Dang DA, Hoffman HJ, Autrup H (2009) PVP-coated silver nanoparticles and silver ions induce reactive oxygen species, apoptosis and necrosis in THP-1 monocytes. Toxicol Lett 190(2):156–162
56. Xia T, Kovochich M, Liong M et al (2008) Comparison of the mechanism of toxicity of zinc oxide and cerium oxide nanoparticles based on dissolution and oxidative stress properties. ACS Nano 2(10):2121–2134
57. Wang Q (2013) Short communication: inhibiting biofilm formation on paper towels through the use of selenium nanoparticles coatings. Int J Nanomedicine 8:407–411
58. Lane R, Craig B, Babcock W (2002) Material ease: materials engineering with nature's building blocks. Amptiac Q 6(1):31e6
59. LiuY, Tan J, Thomas A, Ou-Yang D, Muzykantov VR (2012) The shape of things to come: importance of design in nanotechnology for drug delivery. Ther Deliv. Author manuscript; available in PMC 2012, 3(2):181–194
60. Curulli A, Valentini F, Padeletti G, Viticoli M, Caschera D, Palleschi G (2005) Development of new generation of stable biosensors. Sens Actuators B: Chem 111–112:441–449
61. Vittori Antisari M, Montone A, Jovic N, Piscopiello E, Alvani C, Polloni L (2006) Low energy pure shear milling: a method for the preparation of graphite nano-sheets. Scr Mater 55:1047
62. Perez-Rodrıguez JL, Wiewiora A, Ramirez-Valle V, Duran A, Perez Maqueda LA (2007) Antiferromagnetic exchange interaction of Cr^{3+} dimer in acid erothro chloride $[(NH_3)_5CrOHCr(NH_3)_4(H_2O)]Cl_5{\cdot}H_2O$ and $LaAlO_3{:}Cr^{3+}$ molecules. J Phy Chem Solids 68:1225–1229
63. Jamil NH, Palaniandy S (2010) Acid medium sonication: a method for the preparation of low density talc nano-sheets. Powder Technol 200:87–90
64. Kauppinen (2006) Synthesis of nanoparticles by the gas phase decomposition of iron pentacarbonyl in the carbon monoxide atmosphere//Phys.-Chem. Kinetics in the Gas Dynamics. 4. 9 on-line at: www.chemphys.edu.ru/pdf/2006–07-18-001.pdf (in Russian)
65. Eslamian M, Shekarriz M (2009) Recent advances in nanoparticle preparation by spray and microemulsion methods. Recent Pat Nanotechnol 3:99–115
66. Dufresne A, Dupeyre D, Vignon MR (2000) Cellulose microfibrils tuber cells: processing and characterization of starch-cellulose microfibrilposites. J Appl Polym Sci 76:2080–2092
67. Iwamoto S, Nakagaito AN, Yano H (2007) Nano-fibrillation of pulp fibers for the processing of transparent nanocomposites. Appl Phys A 89:461–466
68. Saito T, Nishiyama Y, Putaux JL, Vignon M, Isogai A (2006) Homogeneous suspensions of individualized microfibrils from TEMPO-catalyzed oxidation of native cellulose. BioMacromol 7:1687–1691
69. Wang S, Cheng Q (2009) A novel process to isolate fibrils from cellulose fibers by high-intensity ultrasonication, Part 1: Process optimization. J Appl Polym Sci 113:1270–1275
70. Siró I, Plackett D (2010) Microfibrillated cellulose and new nanocomposite materials: Areview. Cellulose 17:459–494
71. Hamada H, Bousfield WD (2010) Nano-fibrillated cellulose as agent to improve print quality of synthetic fiber sheets. Nano-fibrillated cellulose as a coating agent to improve print quality of synthetic fiber sheets. In Presented at the TAPPI 11th advanced coating fundamentals symposium Munich, Germany
72. Mishra SP, Manent AS, Chabot B, Daneault C (2012) Production of nanocellulose from native cellulose-various options utilizing ultrasound. BioResources 7(1):422–436

73. Beck-Candanedo S, Roman M, Gray DG (2005) Effect of reaction conditions on the properties and behaviour of wood cellulose nanocrystal suspensions. Biomacromol 6:1048–1054
74. Elazzouzi-Hafraoui S, Nishiyama Y, Putaux J, Heux L, Dubrueil F, Rochas C (2008) The shape and size distribution of crystalline nanoparticles prepared by acid hydrolysis of native cellulose. Biomacromol 9:57–65
75. Favier V, Canova GR, Cavaille JY, Chanzy H, Dufresne A, Gauthier C (1995) Nanocomposites materials from latex and cellulose whiskers. Polym Adv Technol 6:351–355
76. Henriksson M, Henriksson G, Berglund LA, Lindström T (2007) An environmentally friendly method for enzyme-assisted preparation of microfibrillated. Eur Polym J 43:3434–3441
77. Höcker (1995) Enzyme treatments for wool and cotton. Rev Prog Color Rel Topics 25:57–70
78. Pääkkö M, Ankerfors M, Kosonen H, Nykanen A, Ahola S, Osterberg et al. (2007) Enzymatic hydrolysis combined with mechanical shearinghigh-pressure homogenization for nanoscale cellulose fibrils and strong. Biomacromolecules 8:1934–1941
79. Brinchi L, Cotana F, Fortunati E, Kenny JM (2013) Production of nanocrystalline cellulose from lignocellulosic biomass: technology and applications. Carbohyd Polym 94:154–169
80. Cherian BM, Leao AL, de Souza SF, Thomas S, Pothan LA, Kottaisamy M (2010) Isolation of nanocellulose from pineapple leaf fibres by steam explosion. Carbohyd Polym 81:720–725
81. Gong G, Mathew AP, Oksman K (2009) Preparation of nano cellulose with high aspect ratio from wood. Fokusomradet Materialvetenskap 4:e konferensen om maerialforskning pa LTU
82. Alexandre M, Dubois P (2000) Polymer-layered silicate nanocomposites: preparation, properties and uses of a new class of materials. Mater Sci Eng Rep 28:1–63 (Reproduced in part with permission from Elsevier 2006)
83. Thakur VK, Vennerberg D, Kessler MR (2014) Green aqueous surface modification of polypropylene for novel polymer nanocomposites. ACS Appl Mater Interfaces 6:9349–9356
84. Thakur VK, Vennerberg D, Madbouly SA, Kessler MR (2014) Bio-inspired green surface functionalization of PMMA for multifunctional capacitors. RSC Adv 4:6677–6684
85. Thakur VK, Thakur MK, Raghavan P, Kessler MR (2014) Progress in green polymer composites from lignin for multifunctional applications: a review. ACS Sustain Chem Eng 2:1072–1092
86. Meyyappan M (ed.) (2004) Carbon nanotubes, science and application. CRC (Reproduced in part with permission from Taylor & Francis, USA, 2006)
87. Giannelis EP (1996) Polymer layered silicates nanocomposites. Adv Mater 8:29–35
88. The Royal Society and the Royal Academy of Engineering (2004) Nanoscience and nanotechnologies (Reproduced in part with permission 2005)
89. Reichert P, Kressler J, Thomann R, Mulhaupt R, Stoppelmann G (1998) Nanocomposites based on a synthetic layer silicate and polyamide-12. Acta Polym 49(2–3):116–123
90. Yano K, Usuki A (1993) Synthesis and properties of polyimide-clay hybrid. J Polym Sci Part A: Polym Chem 31:2493–2498
91. Yano K, Usuki A, Okada A, Kurauchi T (1991) Synthesis and properties of polyimideclay hybrid. Polym Prep (Jpn) 32(1):65
92. Park JH, Jana S (2003) Mechanism of exfoliation of nanoclay particles in epoxy-clay nanocomposites. Macromolecules 36:2758–2768 (Reproduced in part with permission from American Chemical Society-2006)
93. Chen TK, Tien YI, Wei KH (1999) Synthesis and characterization of novel Segmented Polyurethane/Clay Nanocomposites via Poly (ε-caprolactone)/Clay. J Polym Sci Part A: Poly. Chem 37(13):2225–2233
94. Mishriky N, Asaad FM, Ibrahim YA, Girgis AS (1994) New pyridine- carbonitriles from fluoro arylpropenones. Recl Trav Chim Pays-Bas 113:35–39
95. ISO 5351(2010) Specifies a method which yields a number that is an estimate of the limiting viscosity number of pulp in a dilute cupri-ethylenediamine (CED) solution
96. Morris JV, Mahaney MA, Huber JR (1976) Fluorescence quantum yield determinations: 9,10-diphenylanthracene as a reference standard in different solvents. J Phys Chem 80:969–974

97. ISO 187 (1990) (E) Paper, board and pulps- Standard atmosphere for conditioning and testing and procedure for monitoring the atmosphere and conditioning of samples. This standard has been reviewed and then confirmed in 2013
98. Institute Method No. 428 (1951) Institute of paper chemistry. Appleton, Wisconsin, Jan (1951)
99. Girgis AS, Kalmouch A, Hosni HM (2004) Synthesis of novel 3-pyridinecarbonitriles with amino acid function and their fluorescence properties. Amino Acids 26:139–146
100. Jachak MN, Bagul SM, Ghotekar BK, Toche RB (2009) Synthesis and study of the fluorescent behavior of 3-pyridinecarbonitriles. Monatsh Chem 140(6):655–662
101. Basta AH (1998) Preparation, characterization and properties of paper sheets made from chemically modified wood pulp treated with metal salts. Int J Polym Mat 42(1–2):1–26
102. Fu H-B, Yao J-N (2001) Size effects on the optical properties of organic nanoparticles. J Am Chem Soc 123(7):1434–1439
103. Bertorelle F, Lavabre D, Fery-Forgues, S (2003) Dendrimer-tuned formation of luminescent organic microcrystals. J Am Chem Soc 125(20):6244–6253
104. Hitoshi Kasai HK, Okada S, Oikawa H, Matsuda H, Nakanishi H (1996) Size-dependent colors and luminescences of organic microcrystals. Jpn J Appl Phys 35 (Part 2, No. 2B): L221–L223
105. Kasai H, Oikawa H, Okada S, Matsuda H, Minami N, Kakuta A, Ono K, Mukoh A, Nakanishi H (1992) A novel preparation method of organic microcrystals. Jpn J Appl Phys 31 (Part 2, No. 8A): p. L1132–L1134
106. Nakanishi H, Katagi H (1998) Microcrystals of polydiacetylene derivatives and their linear and nonlinear optical properties. Supramol Sci 5(3–4):289–295
107. Delia Gazzoli SDR, Ferraris G, Valigi M, Ferrari L, Selci S (2008) Morphological and textural characterization of vanadium oxide supported on zirconia by ionic exchange. Appl Surf Sci 255:2012–2019
108. Maulucci GDS, Arcovito M, Boffi G, Castellano F, Congiu A, Giuseppe B (2005) Particle size distribution in DMPC vesicles solutions undergoing different sonication times. Biophys J 88(5):3545–3550
109. Feigenbrugel V et al (2005) Near-UV molar absorptivities of acetone, alachlor, metolachlor, diazinon and dichlorvos in aqueous solution. J Photo chem Photobiol A: Chem 174(1):76–81
110. Engert JM, Dick B (1996) The UV absorption spectrum of the phenyl radical isolated in solid argon. Appl Phys B: Lasers Opt 63(5):531–535

A Review on Bionanocomposites Based on Chitosan and Its Derivatives for Biomedical Applications

Ibrahim M. El-Sherbiny and Nancy M. El-Baz

Abstract Bionanocomposites are emerging nanostructure hybrid materials composed of natural polymers and inorganic solids. Bionanocomposites became a subject of intensive research owing to their inherent properties such as nontoxicity, biocompatibility, biodegradability as well as their improved structural and functional properties. Among these bionanocomposites, chitosan-based nanocomposites have attracted a great deal of attention especially in biomedical field. Globally, chitosan is the second most bountiful natural polymer following cellulose. Chitosan is a biocompatible and biodegradable polymer possessing unique structural, chemical, and biological properties. The last decade has witnessed enormous multidisciplinary research focused on improving the properties of chitosan and its derivatives. As a result, several chitosan-based nanocomposites with enhanced physical and chemical properties have been developed in eco-friendly and cost-effective manner. This chapter provides an overview on different aspects of chitosan including its properties and modifications, and focuses on chitosan-based nanocomposites. Important biomedical applications of chitosan-based nanocomposites are also discussed in this chapter including tissue engineering, wound healing, tissue regeneration, drug delivery, and biosensors.

Keywords Chitosan · Chitosan derivatives · Nanocomposites · Tissue engineering · Wound healing · Drug delivery · Biosensors

I.M. El-Sherbiny (✉) · N.M. El-Baz
Center for Materials Science, University of Science and Technology (UST),
Zewail City of Science and Technology, 6th October City, Giza, Egypt
e-mail: ielsherbiny@zewailcity.edu.eg

N.M. El-Baz
e-mail: nelbaz@zewailcity.edu.eg

V.K. Thakur and M.K. Thakur (eds.), *Eco-friendly Polymer Nanocomposites*,
Advanced Structured Materials 74, DOI 10.1007/978-81-322-2473-0_6

1 Introduction

Chitin is the most abundant natural polysaccharides after cellulose. Chitin is very cheap material and is readily available considering its millions of tons harvested annually. Chitin, poly-(1-4)-*N*-acetyl-glucosamine, has three forms known as α, β, γ, with ordered crystalline microfibrils forming the structure components in the cell wall of fungi and yeast. Chitin also presents in the exoskeleton of various insects and arthropods such as crabs and shrimps. Chitosan is the most important derivatives of chitin; it is linear semi-synthetic polysaccharides, consists of β-(1 → 4) glycosidic linkages, which are identical to cellulose structure [20]. Chitosan is obtained by deacetylation of chitin (Fig. 1). Deacetylation process of chitin is commonly performed under alkaline conditions using either sodium/potassium hydroxide solutions or mixtures of anhydrous hydrazine and hydrazine sulfate. Moreover, deacetylation of chitin can be performed via enzymatic hydrolysis in the presence of chitin deacetylase. The structure and properties of chitosan such as molecular weight (MW), degree of deacetylation (DD), and glucosamine content are varied depending on the chitin origin and the used deacetylation method [37, 38, 72].

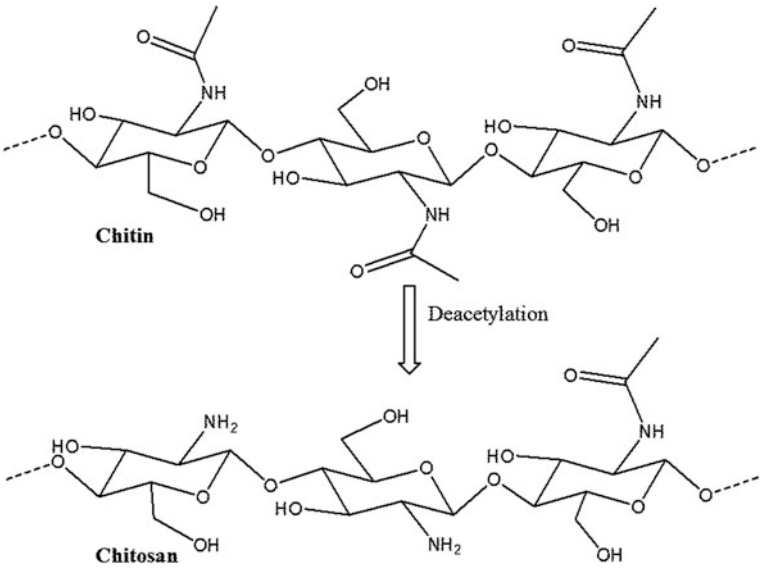

Fig. 1 Deacetylation of chitin into chitosan. Adapted with modification from Ref. [38]

1.1 Properties of Chitosan

1.1.1 Physicochemical Properties

The commercially available chitosan is classified based on its MW and DD into two different grades, namely high and low molecular weights. High molecular weight of chitosan ranged between 190 and 375 kDa with DD > 75 %, while low molecular weight ranged between 20 and 190 kDa with DD < 75 % [20]. The structure of chitosan is varied along with changing the proportions of *N*-acetyl-d-glucosamine, d-glucosamine residues, and MW. The chitosan structure is of a great importance as it significantly influences its physicochemical properties. It was well-known that chitosan of linear unbranched structure exhibits an excellent viscosity. Because the viscosity of chitosan significantly influences its properties especially the biological properties and degradation, the effect of different parameters such as MW, DD, and temperature on viscosity have been extensively explored. It was also found that the viscosity of chitosan is changed along with changing the deacetylation conditions. Therefore, the deacetylation conditions should be precisely controlled during the preparation process. The degradation rate of chitosan is also dependent on DD and the distribution and arrangement of acetyl groups. It was revealed that degradation rate of chitosan is found to be inversely proportional with DD. Studies revealed that high DD chitosan exhibits very low degradation rate, while low DD chitosan exhibits faster degradation rate [20, 86].

Chitosan comprises three reactive sites; one amino group and two hydroxyl groups in each glucosidic residue. The amino group of chitosan is very important because it is pH sensitive, which is responsible for cationic nature of chitosan as well as governs different physicochemical properties of chitosan such as solubility and biological properties [92]. As shown in (Fig. 2), the solubility of chitosan is dependent on the pH-sensitive amino groups, which have pKa of 6.3. At low pH, amino groups become protonated allowing chitosan to dissolve forming soluble cationic polysaccharides. Above pH 6, amino group is deprotonated rendering chitosan insoluble. The soluble/insoluble transition takes place at pKa value around 6–6.5 (Fig. 2) [20, 50, 86]. In addition to pH, the solubility of chitosan is also dependent on the used deacetylation method, ionic strength, and distribution of acetyl group along the chain. Recently, water-soluble chitosan was obtained in the presence of glycerol-2-phosphate. Stable chitosan solution was obtained at pH 7

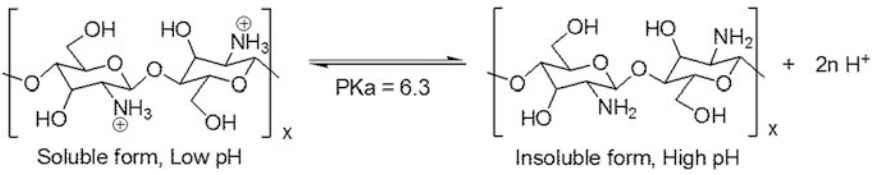

Fig. 2 Schematic illustration of the solubility of chitosan

and room temperature, while gel was formed upon heating to around 40 °C. The sol–gel transition was partially reversible based on the gelation temperature and experimental conditions. One successful example of chitosan gel has been clinically used for cartilage repair is chitosan–glycerol phosphate gel, which is exemplified in the market by BST-CarGel® [86]. The amino groups also provide a reactive site allowing ease functionalization of chitosan, for example, amino groups facilitates the adsorption and/or chelation of metal cations. The ease functionalization of chitosan allows altering and tailoring its properties such as cationic nature and acidic solubility. For instance, by sulfating the amino group of chitosan, chitosan became anionic, water soluble, and acquired anticoagulant property [50, 73].

1.1.2 Biological Properties

Chitosan is approved by FDA for wound dressing and dietary applications in Japan, Italy, and Finland. Indeed, chitosan is being a focus of various research areas owing to its inherent biological properties. Several studies confirmed that chitosan is a biodegradable, biocompatible, and nontoxic polymer [20, 45]. Recent studies also demonstrated that chitosan itself as well as its derivatives have potent biological properties such as antibacterial, antifungal, anti-inflammatory, and antitumor [37, 120].

Chitosan biocompatibility, the ability of chitosan to safely interact with living cells without evoking the immune system was heavily *in vitro* and in vivo studied [58]. Several *in vitro* and *in vivo* studies revealed that the biocompatibility ranking of chitosan and its derivatives in descending order was methylpyrrolidinone chitosan > chitosan lactate > glycol chitosan > chitosan glutamate > chitosan HCl, respectively. *In vitro* studies conducted to assess the biocompatibility of methylpyrrolidinone chitosan and chitosan HCl on fibroblast cells showed that methylpyrrolidinone chitosan caused 35 % reduction in cell viability, while chitosan HCl caused 70–80 % reduction in cell viability [86]. It was also found that DD of chitosan is directly proportional with its biocompatibility, where increasing DD, increases chitosan's compatibility owing to the presence of free amino groups which allow the interaction between the chitosan and cells. The solvent effect on the biocompatibility of chitosan was also examined by preparing chitosan films using different acidic solvents such as acetic acid and lactic acid. It was reported that chitosan prepared in acetic acid caused skin irritation, while chitosan prepared in lactic acid showed no skin irritation or toxicity [86, 131].

In addition to biocompatibility, chitosan biodegradability, the ability of chitosan to break down into monomers was also extensively investigated in vitro and in vivo. Biodegradability is the key property of chitosan because biodegradability of chitosan determines its metabolic fate; therefore, it should be fully explored and understood. The biodegradation rate of chitosan is often determined based on the intended application. For example, in tissue engineering applications, the biodegradation rate should be slow to maintain its structure and mechanical integrity until the tissue is formed, while in drug delivery applications, the biodegradation rate of chitosan should be relatively faster, but in a controlled manner to guarantee the

continuous release of payload drug. Studies demonstrated that the biodegradation rate of chitosan is inversely proportional with DD. It was reported that high DD chitosan exhibits very low degradation rate induces negligible inflammatory response, while low DD chitosan exhibits faster degradation rate induces acute inflammatory response due to the accumulation of amino saccharides producing inflammatory response and toxicity [20, 86]. The biodegradation rate of chitosan is also dependent on its MW. It was revealed that chitosan of MW ranged between 30,000 and 40,000 Da was eliminated by renal clearance [44]. However, above this MW, chitosan was first degraded either by enzymatic degradation (i.e., lysozyme or microflora in the colon) or chemical degradation (i.e., acid catalyze degradation in stomach), prior to renal clearance. Lysozyme is the primary enzyme responsible for chitosan digestion. The enzymatic degradation is initiated by biofouling, accumulation of proteins and cells on a foreign substance leading to immune system recognition and subsequent elimination. This is followed by penetration of water and lysozyme into chitosan structure leading to chitosan swelling. Afterwards, lysozyme breaks β-(1 → 4) glycosidic linkages of chitosan forming chito-oligomers and *N*-acetyl-D-glucosamine residues, which are eventually eliminated by renal clearance. On the contrary, chemical degradation refers to acidic hydrolysis. In fact, there are a few clinical data regarding chemical degradation of chitosan *in vivo*. The current clinical data revealed that chitosan is accumulated in liver and kidney and its elimination is mainly dependent on MW [44, 86, 119].

In addition to the unique biocompatibility and biodegradability properties of chitosan, several studies revealed that chitosan has an extraordinary antibacterial activity against broad spectrum of bacteria [25, 120]. The antibacterial activity of chitosan was ascribed to its cationic nature, which allows the interaction between chitosan and negatively charged lipid and proteins embedded in the bacterial cell wall. The attraction between opposite charges facilitates chitosan adsorption on bacterial cell wall resulting in compromising its function followed by diffusion into cell membrane. Chitosan diffusion into cell membrane leads to the expansion and disturbance of cell membrane permeability which eventually causes leakage of cytoplasmic components and bacterial death. Other *in vitro* studies also were conducted to verify the antibacterial activity of chitosan and emphasized that chitosan antibacterial action might also be ascribed to its DNA binding ability. It was reported that once chitosan enter the nuclei of bacteria, it binds with DNA and inhibits mRNA synthesis [46].

Recently, clinical studies proved that chitosan demonstrated an anti-inflammatory activity. Anti-inflammatory is an immune response against foreign bodies such as pathogen, toxic chemicals, and physical injury. There are two types of inflammation; acute and chronic inflammation. Acute inflammation is a short-term response mediated by leukocytes at the damaged region to induce tissue repair, while chronic inflammation is a long-term pathological response inducing tissue damage by matrix metalloproteinase (MMPs). Basically, it was well-known that chronic inflammation is related to various diseases such as hepatitis, arthritis, gastritis, and colitis. The nuclear factor kappa B (NF-B) plays a main role in regulating genes encoding proinflammatory κ cytokines, adhesion molecules, and cyclooxygenase-2 (COX-2).

Nonsteroidal anti-inflammatory drugs (NSAIDs) are the conventional treatment of many inflammation diseases. However, NSAIDs induces severe gastric, renal, and hepatic side effects. *In vitro* and *in vivo* studies confirmed that chitosan partially inhibits the secretion of IL-8 and TNF from mast cells, and reduces the inflammatory response [69]. Besides the anti-inflammatory activity of chitosan, studies demonstrated chitosan does not induce gastric side effects due to the presence of free amino groups which can neutralize the gastric acid creating a protective layer over the stomach and thus allowing the use of chitosan for the treatment of peptic ulcer. In addition, the use of chitosan in preventing and treating rheumatic arthritis has been also studied. It was found that chitosan possesses anti-inflammatory activity as well as can aid in repairing the connective tissue. The main reason behind the repairability of chitosan is the acid hydrolysis, which converts chitosan into glucosamine monosaccharides, the structural units of proteoglycans present in connective tissue and cartilage [86, 120].

More recently, chitosan derivative, chitoligosaccharides have received great deal of attention due to its unique anticancer activity against different cancers. The exact mechanism behind the antitumor activity of chitoligosaccharides is still unknown. However, there is a speculated mechanism stated that chitoligosaccharides trigger lymphocytes factors resulting in elevating T cells differentiation and proliferation. As a result, the activity of T cells increases and induces further tumor inhibitory effect. To identify the relation between the chitoligosaccharides' charge properties and its antitumor activity, chitoligosaccharides of different charge densities and types have been studied on three different cancer cell lines: HeLa, Hep3B, and SW480. The *in vitro* studies showed that highly charged chitoligosaccharides significantly reduce the viability of cancer cells regardless of their charge type, compared to the poor charged chitoligosaccharides [69, 119, 120].

1.2 Chitosan Limitations

Besides the distinctive properties of chitosan, it can be easy processed into different forms to suit different biomedical applications. For instance, chitosan can be used to prepare films, fibers, and sponge. Chitosan solution is prepared under acidic conditions and then processed under different conditions such as casting for films, spinning for fibers, and lyophilized for sponge. Finally, chitosan is precipitated via immersing in alkaline solution followed by purification and drying [86]. Beyond the ease preparation and distinctive properties of chitosan, it suffers from many limitations, which rise many safety issues regarding its biomedical use. These limitations include low solubility at physiological pH, 7.4, low thermal stability, low ductility, poor mechanical properties, and higher swelling degree in aqueous solutions owing to their pH sensitivity and high hydrophilic nature. The following section points out different modification approaches developed to overcome chitosan limitations including development of chitosan derivatives, composites, and nanocomposites [93].

2 Modifications of Chitosan

2.1 Chitosan Derivatives

Chitosan derivatives were commonly produced via chemical modification of chitosan chain either by adding a specific group to its reactive sites, such as amino group or hydroxyl groups, or by grafting polymer(s) onto its backbone. The chemical modification techniques (Fig. 3) of chitosan include quaternization, acylation, thiolation [113,115], and carboxymethylation [67, 93].

Among these different chemical modification techniques, quaternization is considered the most simple and straightforward technique. Quaternization refers to a reaction that occurs between chitosan and either methyl iodide or ethyl iodide under basic conditions. Quaternized chitosan derivatives have many advantages over other chitosan derivatives including increased aqueous solubility, maintained solubility over a wide pH range, improved mucoadhesive property, and controlled cationic character, and pH dependency. Due to the advantages of quaternization,

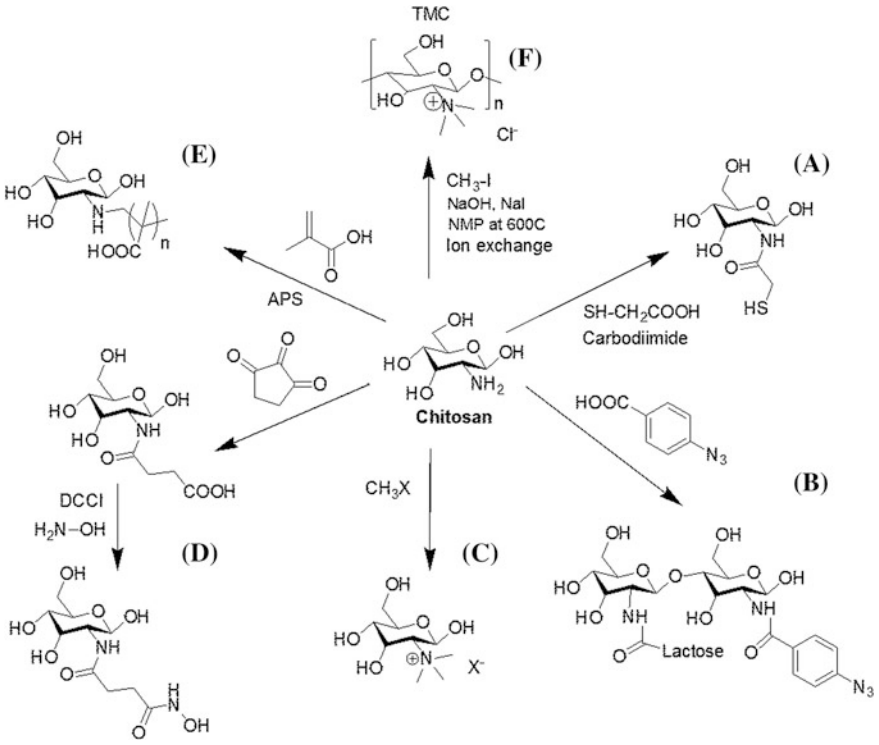

Fig. 3 Chemical modification techniques of chitosan: (*A*) thiolation; (*B*) azylation; (*C*) methylation; (*D*)*N*-succinylation, (*E*) copolymerization, and (*F*) schematic illustration of TMC synthesis. Available in Ref. [92]

researcher developed various quaternized chitosan derivatives. The most common quaternized chitosan derivative is N,N,*N*-trimethyl chitosan chloride (TMC) [53]. TMC is frequently used for different drug delivery applications owing to its mucoadhesive property and solubility. Moreover, TMC was proven to have a potent antibacterial activity over a wide pH range [82, 93]. TMC was synthesized via two step reactions (Fig. 3F); the first step involves the reaction of chitosan with methyl iodide in the presence of sodium hydroxide at 60 °C. The second step includes the substitution of iodide ion by chloride via an ion exchange process [84]. In an attempt to develop TMC with enhanced mucoadhesive property, Varkouhi et al. [53] developed thiol-bearing TMC. The addition of thiol to TMC causes a further enhancement in the mucoadhesive property due to the presence of thiol group, which facilitates the formation of disulfide bond with mucin proteins embedded in cell membrane [53].

Carboxylic acid–chitosan derivative is another derivative of chitosan. By modifying chitosan with carboxylic acid, it showed an enhanced transfection efficiency compared to pure chitosan. Despite the enhanced transfection efficiency of carboxylic acid-bearing chitosan [113], it was revealed that carboxylic acid–chitosan derivative exhibits weak DNA-binding ability. To optimize the transfection efficiency of carboxylic acid–chitosan derivative, it was modified with cationic polymer chains. In another study, secondary and tertiary amines were introduced to carboxylic acid–chitosan forming a carboxylic acid–imidazole–chitosan via one step synthesis process mediated by 1-ethyl-3-(3-dimethylaminopropyl) carbodiimide (EDC)[24]. The carboxylic acid–imidazole–chitosan demonstrated higher transfection efficiency than carboxylic acid–chitosan [81, 93].

One of the most important derivatives of chitosan is carboxymethyl chitosan (CMC). CMC is extensively used in biomedical applications such as tissue engineering, drug delivery, and cosmetic field owing to its unique properties. CMC is nontoxic, anionic, amphotheric, and water soluble at basic pH. The carboxylation can be performed either at the amino or hydroxyl groups of the chitosan. Based on the carboxymethyl substitution position, these derivatives are classified into O-CMC, N-CMC, and N, O-CMC. N-CMC is obtained upon reacting with glycoxylic acid followed by reducing with sodium cyanoborohydride (Fig. 4A). O-CMC is obtained by reacting chitosan with monochloroacetic acid using isopropyl alcohol as a solvent (Fig. 4B). On the other hand, N, O-CMC is synthesized by carboxymethylation of chitosan using monochloroacetic acid in alkaline medium (Fig. 4C) [38].

Graft copolymerization is another method used to create chitosan derivatives with complicated and tailored properties. Grafting in polymer chemistry is defined as a reaction that involves connecting two or more species of blocks to a macromolecule chain as side chains, producing a new polymer composite with different properties compared to the parent polymer. Different grafting techniques (Fig. 5) have been developed and used for modifying chitosan such as grafting initiated by free radicals, radiation-induced grafting, and enzymatic grafting [30, 86, 93, 132]. Chitosan was grafted with acrylic acid as a possible mean to create a hydrophilic and mucoadhesive chitosan derivative. Polymerization of acrylic acid onto chitosan was ascribed to the inter- and intramolecular bonding between carboxyl groups of

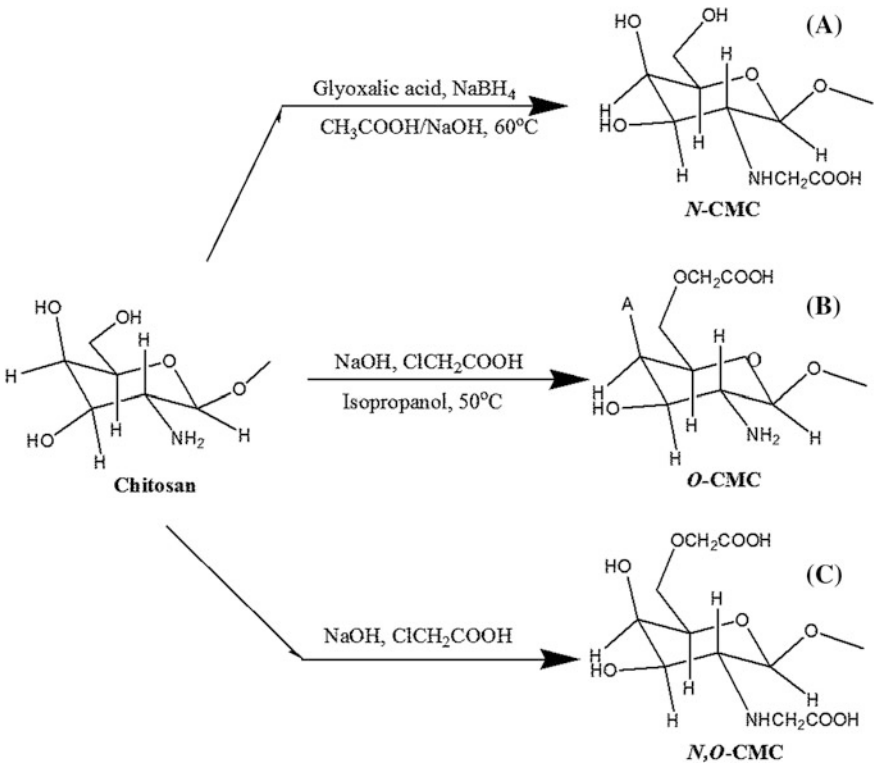

Fig. 4 Schematic illustration showing the synthesis of N-CMC (*A*), O-CMC (*B*), and N-CMC (*C*) from chitosan. Adapted with modification from Ref. [38]

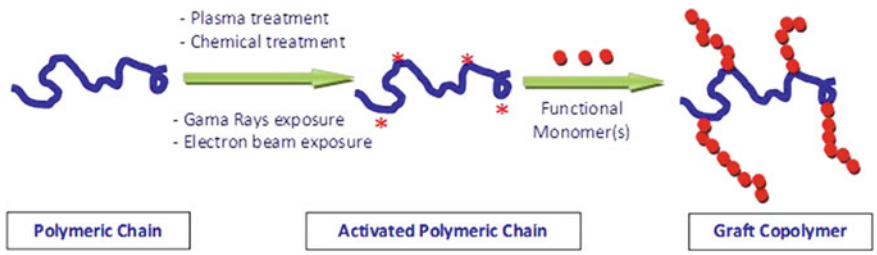

Fig. 5 Grafting copolymerization

poly (acrylic acid) and amino group of chitosan. Shantha et al. [90] successfully synthesized poly (acrylic acid)-g-chitosan using ceric ion as initiator [90]. Jere et al. [40] modified chitosan with low MW poly (ethylene imine) (PEI) chains forming PEI-g-chitosan copolymer. The PEI-g-chitosan copolymer showed superior transfection efficiency compared to pure chitosan. The PEI-g-chitosan copolymer was synthesized via two steps; the first step includes the reaction of chitosan with

potassium periodate in an acetate buffer resulting in glucosamine ring opening forming two aldehyde groups. Second step involves the reaction of the two aldehyde groups with the pendant primary amine of PEI oligomers resulting in forming an imine that was converted into amine after being reduced with $NaBH_4$ [40]. This reaction was minimized in one step synthesis process by using carbonyldiimidazole as coupling agent. Noh et al. [53] also grafted poly (L-arginine) (PLR) chains onto chitosan through forming an amide bond between carboxyl group of PLR and amino group of chitosan [53].

In an attempt to qualify chitosan for sensors applications, PANI-g-chitosan was developed using ammonium persulphate as an initiator under acidic conditions. The grafting of polyaniline (PANI) renders chitosan electrically conductive with good pH switching properties. The acquired electrically conductive property was found to be dependent on the pH and the grafting extent. Other studies also demonstrated that chitosan-g-PANI is an appealing sensing electrode for early diagnosis of breast cancer owing to its ability to hydride with DNA resulting in a change in the electric current that is electrochemically detected [53, 78, 92, 121].

PEGylated chitosan is another reasonably well-explored chitosan derivative. PEG is FDA-approved polymer for pharmaceutical products such as injectable biotechnology products. The importance of PEG relies on its stealth characteristic, which prolonged the drug circulation half-life. The stealth effect of PEG is a result of its hydrophilic nature, which forms a hydration layer preventing biofouling and thus preventing immune recognition and elimination. The PEG grafting onto chitosan is carried out on the amino group via grafting techniques. Chitosan is commonly modified with methoxylated PEGs (mPEGs), which has free hydroxyl group that binds to amino group of chitosan. The chitosan-g-PEG can be also obtained using different modified PEG polymers such as α-methoxy-poly (ethylene glycol)-ω-aldehyde), and α-methoxy-poly (ethylene glycol)-ω-carboxy). The PEGylated chitosan offers many advantages over other chitosan derivatives especially in the biomedical applications. These advantages include enhanced biocompatibility, prolonged circulation half-life as well as a good solubility over a wide pH ranges (1–11) depending on the degree of substitution (DS). The *in vivo* studies demonstrated that PEGylated chitosan can escape the immune system, renal clearance, and enzymatic degradation resulting in prolonged drug bioavailability. Such stealth effect of PEG has gained considerable attention in various drug delivery applications. Although PEG seems to be advantageous for various pharmaceutical applications, the nonbiodegradability of PEG rises many safety issues that should be thoroughly addressed by further toxicological studies [20, 67].

2.2 Chitosan Composites

Over the past two decades, development of polymeric composites has become a focus of research in terms of the scientific, technological, and commercial values [105–109]. The physical modification is the simplest way to create novel polymeric

composites. The physical modification such as polymer blending is performed by mixing two or more polymers resulting in a formation of composite possessing combined properties of the used polymers. Polymer blending has become the most attractive technique for creating different polymer composites because it is a simple, rapid and cost-effective technique, produces polymer composite with enhanced chemical, physical, mechanical, morphological, and biological properties. In addition, blending is able to create a polymer composite with tailored properties to fulfill requirement of different applications simply by altering the composition of starting polymers [2]. For example, various chitosan composites obtained by blending chitosan with one or two hydrophilic polymers such as poly (vinyl alcohol) (PVA), poly (vinyl pyrrolidone) (PVP), and poly (ethylene oxide) (PEO) to qualify their use for biomedical applications such as oral drug delivery systems. To study the interaction between chitosan and other polymers, various characterizations such as differential scanning calorimetry (DSC), Fourier transform infrared (FTIR) spectroscopy, thermogravimetric (TGA) analysis, and dynamic mechanical thermal analysis (DMA) have been proposed. Characteristic studies showed that chitosan forms miscible blend with PEO and PVP, while with PVA, chitosan only interacts when its concentration in the blend exceeds 50 % [116].

Park and Kim [69] successfully synthesized and studied the properties and interaction of PVA/chitosan blending film prepared in different acidic solvents such as citric acid, acetic acid, lactic acid, and malic acid. The study revealed that the acidic solvent initiates molecular interactions between the two polymers permitting the formation of PVA/chitosan blend with intermediate properties of both polymers including enhanced mechanical and barrier properties [69, 79]. The poly lactic acid (PLA)/chitosan blend has been also prepared by blend method. The key challenge of forming such a blend was the incompatibility between hydrophilic chitosan and hydrophobic PLA [87]. To overcome this issue, Chouwatat et al. [14] prepared a hydrophobic chitosan via mechanically blending aqueous chitosan with sodium dioctylsulfosuccinate. As a result, the hydrophobic chitosan can be easily blended with different hydrophobic polymers such as PLA to form new chitosan composites [14].

2.3 Chitosan-Based Nanocomposites

In the recent years, nanotechnology has become recognized as one of the most appealing area for technology development [55, 56]. Nanotechnology is a science of manipulating materials at nanoscale ranging from 1 to 100 nm. Nanomaterials such as nanoparticles, nanotubes, nanorods, nanofibers, nanosheets, etc., are the building block of nanotechnology. Nanomaterials exhibit attractive properties compared to their bulk counterparts owing to their large surface area to volume ratio. The large surface area of nanomaterials is attributed to the presence of large number of atoms on the nanomaterials' surfaces rendering them more reactive and acquires novel properties [99–101]. Stemming from the nanotechnology revolution, bionanocomposite comes onto the scenes as an alternative biomaterial possessing

improved characteristics for biomedical applications [20, 47, 92]. Bionanocomposite defined as a composite made up of natural biopolymers and inorganic solids with at least one dimension at nanoscale. Bionanocomposite attains superior properties compared to regular composites due to the vast increase in surface area to volume ratio [19]. Several synthesis techniques have been used to develop nanocomposites such as film casting, freeze-drying, layer-by-layer assembly, and electrospinning [103]. Due to the promising physicochemical and biological characteristics of bionanocomposites, chitosan-based nanocomposites have gained considerable attention in various biomedical applications such as tissue engineering, tissue regeneration, drug delivery, and biosensors [20, 31, 37].

Among different techniques, the most common and simplest technique used to create chitosan nanocomposite is cross-linking. There are two types of cross-linking; physical and chemical cross-linking. Both types of cross-linking were utilized to develop chitosan-based nanocomposite using a suitable cross-linker. The cross-linker is a compound that can form links between the polymer chains. Physical cross-linking takes place when polymer chains are linked via ionic or polyelectrolyte interactions, while chemical cross-linking occurs when polymer chains are cross-linked via intermolecular covalent linkages [6, 9, 86]. The commonly used physical cross-linkers are pentasodium tripolyphosphate (TPP) and sodium alginate. TPP was used to prepare different chitosan micro/nanoparticles and nanocomposites such as exotoxin–chitosan microparticles and 5-flurouracil–chitosan–g–PNVCL nanoparticle composites [85, 97]. Sodium alginate is also frequently used as polyelectrolyte cross-linker for formulating different chitosan nanoparticles and hydrogel nanocomposites [5]. On the other hand, the commonly used chemical cross-linkers are glutaraldehyde, genipin, and dextran sulfate. Chitosan is easily cross-linked with glutaraldehyde due to the presence of aldehyde groups, which bind to the amino groups of chitosan through formation of Schiff's base [9]. Several glutaraldehyde cross-linked chitosan nanocomposites such as polyvinyl pyrrolidone (PVP)-chitosan, and chitosan–polyvinyl alcohol (PVA) composites were formulated for drug delivery applications [17, 53]. Moreover, a pH-sensitive PVP/chitosan composite has been synthesized by employing a glutaraldehyde as a cross-linking agent, forming semi-interpenetrating polymer network. The pH-sensitive PVP/chitosan hydrogel was widely used in many biomedical applications such as controlled drug delivery system and tissue engineering [9, 92]. Despite the ease of preparation of glutaraldehyde cross-linked chitosan composites and nanocomposites, toxicity issue of glutaraldehyde is being a great concern that limits its use especially in biomedical applications [86].

To overcome the toxicity of glutaraldehyde and simultaneously form a stable cross-linked chitosan, genipin, a natural material, was used instead as a cross-linker for chitosan-based composites. The cross-linking between genipin and chitosan results in a formation of blue gel. The interaction of genipin and chitosan was ascribed to the nucleophilic attack by the chitosan's amino group on the olefinic carbon atom of genipin leading to dihydropyran ring opening, followed by the formation of a secondary amide and a heterocyclic amino linkage, eventually

forming genipin-cross-linked chitosan [41, 61]. Several forms of genipin-cross-linked chitosan composites were prepared including genipin cross-linked chitosan microspheres, O-CMC-alginate hydrogels, and chitosan–alginate beads [6]. Liu and Kim synthesized novel nanocomposites that consist of genipin-cross-linked chitosan/PEG/zinc oxide (ZnO)/silver (Ag) nanoparticles. The physiochemical properties of the nanocomposites were investigated by infrared analysis, X-ray diffraction and scanning electron microscopy, and was reported that the nanocomposite exhibits a pH-sensitive swelling property and enhanced mechanical property [54].

In an attempt to obtain chitosan with an ultimate mechanical property and thermal stability, different nano-sized reinforcements such as carbon nanotubes, organic and inorganic nanoparticles were incorporated with chitosan [125]. Wang et al. [117] prepared multiwall carbon nanotubes (MWCNTs)/chitosan nanocomposites using a simple solution–evaporation method. The nanocomposites were fully investigated by field emission scanning electron microscopy (SEM), bright field transmission electron microscopy (TEM), optical microscopy (OM), wide-angle X-ray diffraction (XRD), and tensile and nanoindentation tests. The results revealed that the MWNTs were evenly dispersed in the chitosan matrix. The tensile and nanoindentation tests demonstrated that the tensile modulus and strength of the nanocomposites containing 0.8 wt% of MWNTs were significantly enhanced by 93 and 99 % [117]. Yang et al. [53] also prepared graphene oxide (GO)–chitosan nanocomposite via self assembly in aqueous media. It was found that GO/chitosan nanocomposites showed enhanced mechanical and thermal properties [53]. Zuo et al. [134] also chemically functionalized chitosan with graphene oxide (GO) forming GO/chitosan nanocomposites (Fig. 6) via amide linkage formed between the carboxylic groups of GO and the amino groups of chitosan. This nanocomposite also showed an improved tensile strength by 2.5 folds as well as exhibited higher glass transition temperature and thermal stability compared to pure chitosan [134]. Ma et al. [57] developed PVA/GO/chitosan nanocomposite and studied its structure and physicochemical properties. The mechanical studies showed that the nanocomposite has tensile strength of 71.21 Mpa. The increase in the tensile strength was ascribed to the uniform dispersion of GO sheet in the chitosan matrix as well as the strong interfacial interaction between polymers and GO [57]. Archana et al. [7] also fabricated nanocomposite made up of poly(*N*-vinylpyrrolidone) (PVP)/titanium dioxide (TiO_2) nanoparticles/chitosan and studied its mechanical properties. The mechanical studies showed that the strength of nanocomposite increased upon the addition of TiO_2 nanoparticles. Moreover, the biocompatibility of PVP/TiO_2/chitosan nanocomposite was examined on fibroblast cells and has shown an excellent biocompatibility toward fibroblasts [7]. Chrissafis et al. [16] developed silica nanoparticles (SiO_2)/chitosan nanocomposites. The FTIR measurements confirmed that there is an interaction between hydroxyl group of SiO_2 nanoparticles and chitosan. Moreover, it was reported that the mechanical and thermal properties of nanocomposite increased along with increasing the content of SiO_2 nanoparticles [16].

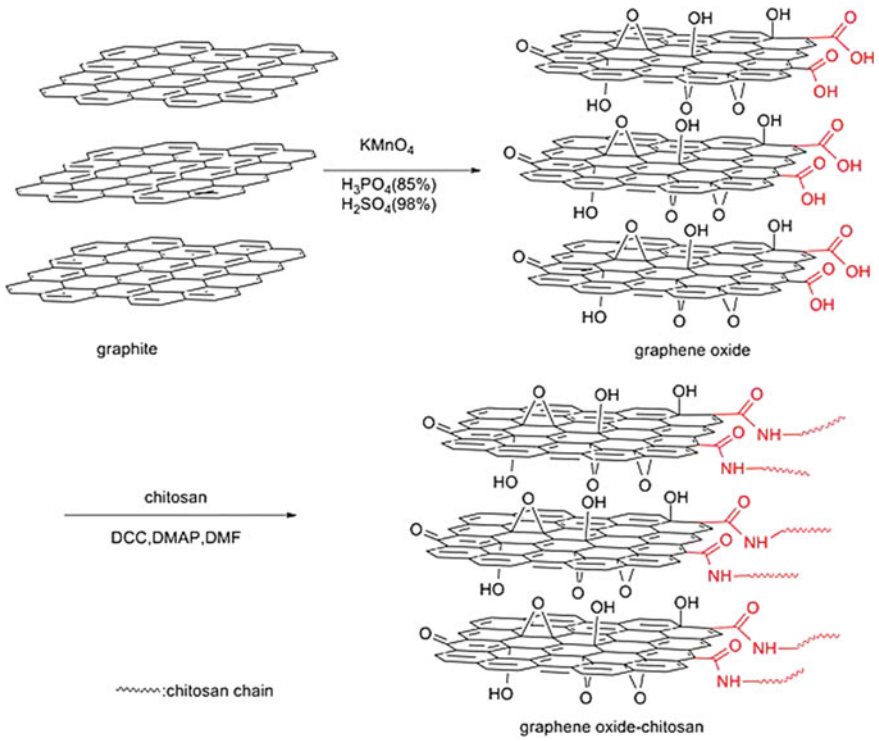

Fig. 6 Schematic illustration describes the synthesis process of GO/chitosan nanocomposite. Adapted from Ref. [134]

3 Biomedical Applications of Chitosan-Based Nanocomposites

Over the last years, a significant body of research has focused on the development of safe and efficient biomaterials based on chitosan for various biomedical applications such as tissue engineering, wound healing, drug delivery, and biosensors. Researchers heavily investigated potential biomedical applications based on chitosan in the form of nanocomposite with particular attention to its enhanced physicochemical and biological properties [20, 50, 74]. This section outlines the common biomedical applications of chitosan-based nanocomposites with particular focus on their related biological properties.

3.1 Tissue Engineering

Tissue engineering field has gained much attention of researchers from multiple disciplines aiming to create an artificial organ/tissue which structurally and

functionally resembles human body's organ/tissue [102–104]. In other words, tissue engineering is aiming to repair, replace, maintain, and improve the function of damaged organ/tissue. Tissue regeneration encompasses three major components: active cells, scaffold, and bioreactor. As shown in (Fig. 7a), tissue engineering process includes (1) seeding cells, (2) supporting and regulating cell growth with the aid of scaffold, (3) using inducers and signaling molecules, and (4) maintaining and enhancing cell growth ability and mass transport using bioreactor [52].

For cells to proliferate and organize themselves to form a new tissue, they require a continuous flow of signals from the surrounding environment to fulfill specific genetic programs essential for cell growth and tissue formation. The

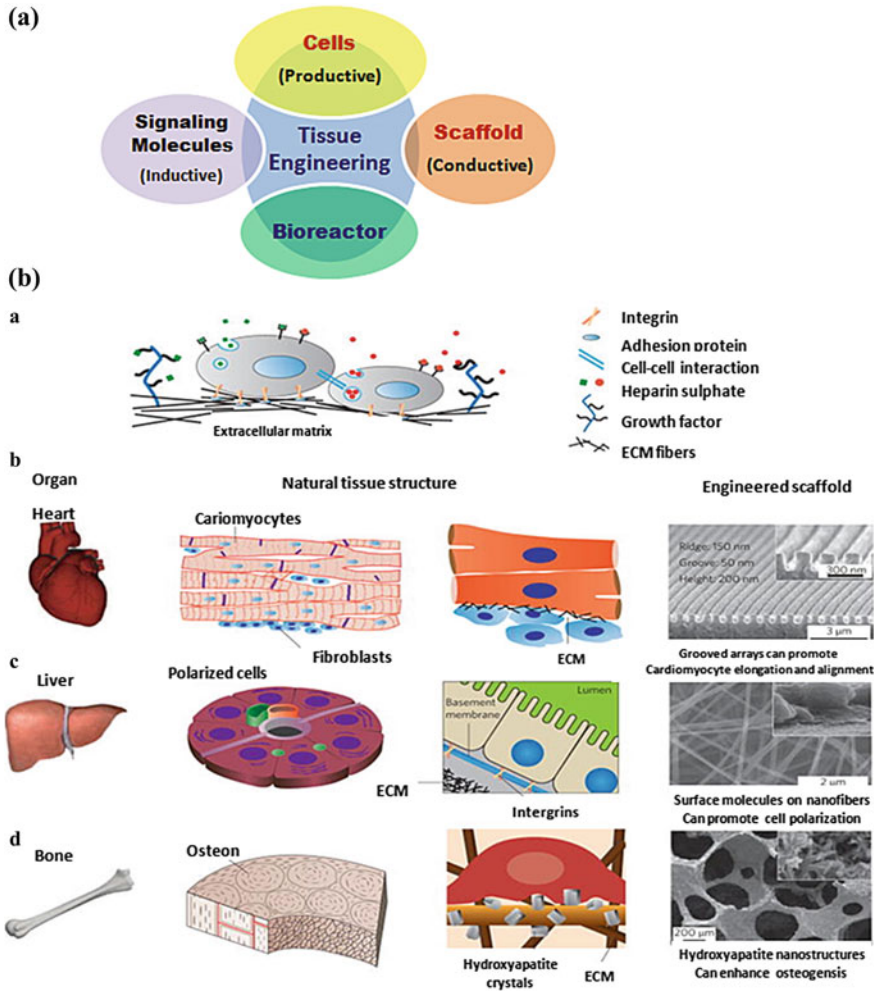

Fig. 7 **a** Basic components of tissue engineering and **b** The information provided to cells by the extracellular matrix (ECM). Adapted after modification from Ref. [24]

extracellular matrix (ECM) containing cell surface receptors, is responsible for cell–cell communications through receiving and responding to the extracellular signals (Fig. 7b). Consequently, ECM is considered as a key factor in tissue engineering. Scaffold-based tissue engineering is a promising approach based on using 3D porous matrix that behaves as a temporary ECM to support cell adhesion and growth, and finally degrades gradually after the formation of new tissue. ECM is composed of different molecules such as collagen, elastic fibers, glycosoaminoglycans (GAG), proteoglycans, and adhesive glycoproteins [80]. Therefore, to form an ideal tissue engineering scaffold that mimics ECM; the scaffold should fulfill certain fundamental requirements. First, the scaffold should be made of nontoxic, biocompatible, biodegradable materials to promote cell adhesion, proliferation, migration, and differentiation. The biodegradability rate is of a great importance as it should meet the growth rate of new tissue/organ. Secondly, scaffold should have a high surface area and porosity with a definite pore size distribution. Third, scaffold must have a reasonable structural integrity and mechanical properties to avoid pore collapsing during tissue formation [37, 124].

The nontoxicity, biocompatibility, and biodegradability of chitosan and its derivatives render them promising biomaterials for tissue engineering scaffold applications. Chitosan is degraded *in vivo* by enzymatic, lysozyme, hydrolysis into biocompatible oligosaccharides of variable length via targeting the chitosan's acetylated group. The degradation rate of chitosan plays a significant role in tissue engineering because it is essential for the scaffold to maintain its structure integrity and the mechanical strength until the tissue regeneration is completed. Depending on targeted engineered tissue, chitosan type that exhibits the appropriate degradation rate should be chosen. It was well-documented that chitosan degradation rate is inversely proportional to its DD. Therefore, high DD chitosan exhibits slow degradation rate that may last for several months, while low DD chitosan degrades rapidly. So, in case of long-term tissue engineering process such as tissue engineering of skeletal, high DD chitosan that exhibits slow degradation rate is chosen to be used as a scaffold [45, 91]. The pore morphology and orientations of chitosan-based scaffold also play important roles in tissue engineering. It was reported that the pore morphology and orientations of chitosan-based scaffold influence its mechanical properties. One study showed that porous chitosan scaffold exhibits low elastic moduli (0.1–0.5 MPa) in comparison with nonporous chitosan scaffold (5–7 MPa). The porous scaffold showed a stress–strain curve similar to composite materials with two distinct regions: a low modulus region at low strains and a transition to a two and three fold greater modulus at high strains. The tensile strengths of these porous scaffolds were ranged between 30 and 60 kPa [59]. Chitosan scaffold can be also synthesized in a form of interconnected porous structures either via lyophilizing chitosan solution or internal bubbling process. The internal bubbling process is a process where calcium carbonate ($CaCO_3$) is mixed with chitosan solution forming chitosan-$CaCO_3$ gel with a specific shape by using a mold [15]. The interconnected porous structure is very promising since many cells can be seeded, migrated inside, and proliferated. Studies also revealed that the porosity and pore morphology of a scaffold also influence angiogenesis process,

a natural process of new blood vessels and capillaries formation from the preexisted blood vessels, which is essential in aiding and supporting tissue development and optimization [59]. Taken together, regulating the scaffold porosity and degradation rate are considered key factors for controlling cellular proliferation rate and organization within the engineered tissue/organ.

In addition, chitosan possesses mucoadhesive property allowing the formation of molecular adhesive force between positively charged chitosan and negatively charged mucosal surfaces via electrostatic interaction. The mucoadhesive property of chitosan could be ascribed to (1) strong charges, (2) strong hydrogen bonding group, (3) chain flexibility, and (4) high molecular weight [123]. The cationic nature of chitosan also permits pH-dependent electrostatic interactions between chitosan and anionic charged molecules such as GAG and proteoglycans. Both molecules, GAG and proteoglycans, are of a great significance in tissue engineering owing to their binding affinity to many cytokines and growth factors such as heparin and heparin sulfate. Therefore, scaffold composed of GAG–chitosan complex could serve in retaining and concentrating growth factors secreted by seeding cells [45]. Nishikawa et al. [64] emphasized that structure of chitosan is closely similar to GAG structure, which consists of long chain, unbranched, repeated disaccharide units. The similarity in structure between both chitosan and GAG plays an important role in modulating cell morphology, differentiation, and function [64, 65]. The broad spectrum antibacterial activity of chitosan is another significant property boosting its use in tissue engineering. Aimin et al. [4] showed that chitosan inhibits osteomyelitis infection experimentally induced by *S. aureus* in rabbits [4].

Several chitosan-based nanocomposites scaffold have been developed aiming to create a scaffold with ideal properties for tissue engineering. Sultana et al. [94] also prepared three-dimensional (3D) porous scaffold composed of hydroxyapatite (HA) nanoparticles/chitosan nanocomposites for bone tissue engineering. The morphology and porosity of the scaffold were characterized by SEM and EDX spectroscopy. The results revealed that prepared scaffold exhibits high porosity and has interconnected pores within the micro-range. HA nanoparticles were found to be homogenously dispersed in the chitosan matrix [94]. Depan et al. [23] also synthesized a novel scaffold that consists of grafted chitosan-based nanocomposites for bone tissue engineering. The scaffold was synthesized by grafting chitosan with propylene oxide to form hydroxypropylated chitosan followed by linking with ethylene glycol functionalized nanohydroxyapatite forming organic/inorganic network structure. Different properties of the prepared nanoscaffold such as swelling, mechanical, and physicochemical properties were studied in comparison with pure chitosan scaffold. Studies revealed that the prepared nanoscaffold exhibits greater modulus, controlled swelling properties, reduced water absorption, but same water retention ability like pure chitosan scaffold [23]. Recently, bioactive glass ceramic (BGC)/chitosan nanoscaffold has been developed and studied for bone engineering and regeneration. BGC is a group of osteoconductive silicate-based materials used for bone repair. BGC was first developed by Hench and was used as biomaterial for bone repair. BCG is currently utilized in orthopedics and dentistry due to its

potential binding ability to soft and hard tissues. Recently, nano-BGC has been produced by sol–gel technique and showed an enhanced cell-material interaction compared to its microphase counterpart [32, 37]. Peter et al. [53] synthesized macroporous nBGC/chitosan scaffold with pore size ranging from 150 to 500 μm. *In vitro* studies conducted on osteoblast-like cells (MG-63) showed that the macroporous nBGC/chitosan scaffold supports cell adhesion, spreading, and proliferation [71]. More recently, much focus has been on creating bioactive scaffold such as scaffold incorporating delivery vehicles for growth factors or cells (Fig. 8) [24]. Rajam et al. [77] fabricated dual function collagen/chitosan nanoscaffold incorporated with chitosan nanoparticles for tissue engineering and drug delivery. The scaffold has 3D macroporous structure incorporated with chitosan nanoparticles encapsulating two growth factors; epidermal and fibroblast growth factors. The role of chitosan nanoparticles is to provide a control release of the growth factors to promote cellular signaling and growth. Results obtained from *in vitro* studies including MTT assay, flow cytometry, and SEM reported that the co-delivery of both epidermal and fibroblast growth factors greatly enhanced the cellular viability, activity, and growth [77].

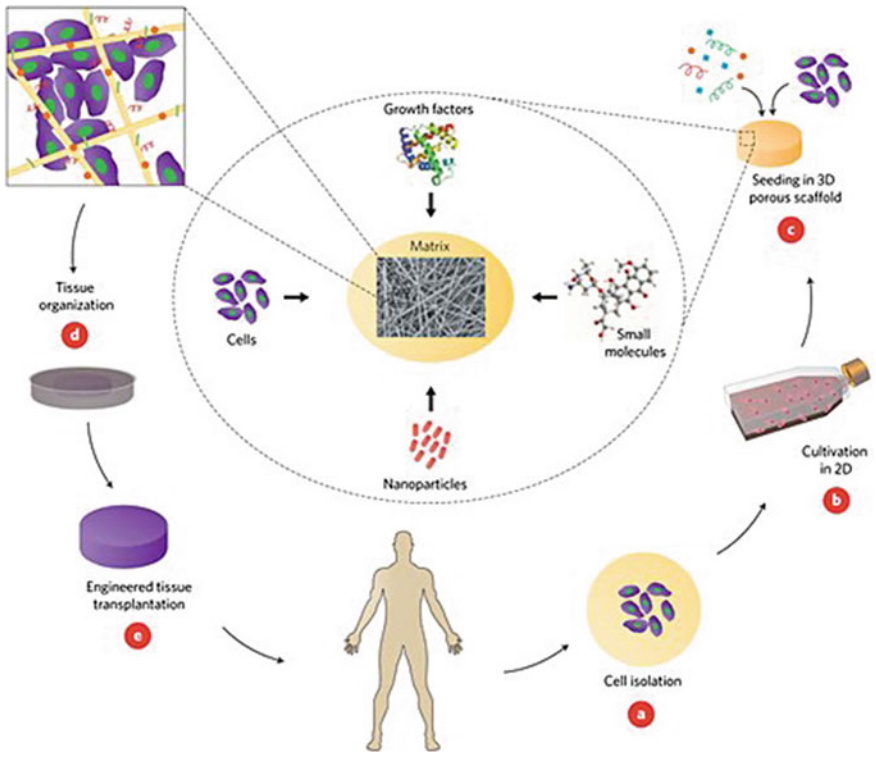

Fig. 8 Bioactive scaffold for tissue engineering. Adapted from Ref. [24]

Nanofibrous scaffold has also received much attention in tissue engineering applications because it mimics the fibrous structure of human native ECM and thus supports cells and allows their growth into the required artificial tissue [10, 37, 105]. Chitosan nanofibers scaffold were mainly produced via electrospinning, a process of utilizing the electric charge to produce, complex and three dimensional (3D) fibers either at micro- or nanoscale. Shalumon et al. [88] prepared water soluble PVA/CMC blend nanofibers scaffold, with concentration of 7 % CMC and 8 % PVA. Afterwards, these nanofibers were converted from water soluble to insoluble via cross-linking with glutaraldehyde vapors followed by thermal treatment. The prepared nanofibrous scaffold were *in vitro* tested on human mesenchymal stem cells (hMSCs). Results obtained from the *in vitro* studies showed that nanofibrous CMC/PVA scaffold allows cell attachment and growth [88]. Thien et al. [110] developed HA/chitosan nanofibrous scaffold for bone tissue engineering. Characterization studies demonstrated that Hydroxyapatite (HA)/chitosan nanofibrous scaffold showed an adequate mechanical strength required for bone repair and regeneration due to the presence of HA. The biocompatibility of chitosan/HA nanofibrous scaffold was *in vitro* investigated on rat osteosarcoma cell lines (UMR). Biocompatibility test showed that HA nanofibrous/chitosan scaffold has an excellent biocompatibility and enhanced osteoblasts proliferation and differentiation compared to chitosan nanofibers, film and HA/chitosan film. The enhanced osteoblasts proliferation and differentiation is a result of the presence of HA, a major bone component, which enhances the osteoblasts proliferation and mineralization [110].

3.2 Wound Dressing

The skin, the largest organ of the body, with an average surface area of 1.8 m^2 and an average weight of 11 kg, is very complicated organ serving many important functions such as homeostasis and protection against microbial pathogens, and chemical damage. Any physical disturbance of the skin structural integrity is defined as skin wound. Because the skin is responsible for the integral homeostatic body functions, a complicated wound healing process is launched by the body aiming at restoring and repairing the integrity and function of injured skin. Wound healing is a natural biological process occurring via three precisely programmed phases; inflammation, proliferation, and remodeling [22].

For promoting a proper wound healing, injured skin should be immediately covered to prevent microorganisms' invasion and accelerate healing process. Wound dressing is commonly used for promoting wound healing and treatment. The aims of wound dressing are (1) bleeding inhibition, (2) wound protection from the surrounding irritants, and (3) avoid water and electrolyte disturbance. Wound dressing are categorized into three main classes: biologic, synthetic, and biologic–synthetic. Biologic dressing such as alloskin and pigskin are frequently used in the clinic. However, they both suffer from many drawbacks including limited supplies,

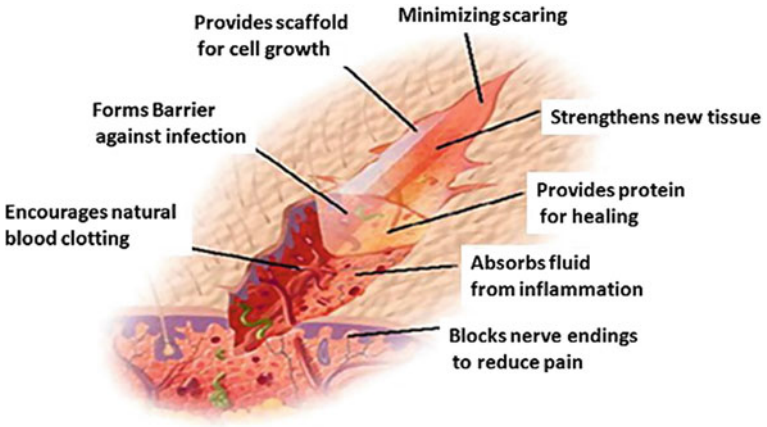

Fig. 9 Schematic illustration for the required properties of wound dressing biomaterial. Adapted from Ref. [39]

high immunogenicity, poor adhesives, and contamination susceptibility. On the contrary, synthetic dressing has a long shelf life, low immunogenicity, and negligible risk of contamination. Biologic–synthetic dressing is bilayer consisting of a combination of both synthetic polymer and biological materials. As illustrated in (Fig. 9), an ideal wound dressing should fulfill certain requirements; (1) form a protective barrier against microorganisms (2) maintain moist environment at wound interface, (3) allow gaseous exchange, (4) get rid of excess exudates, and (5) be non-toxic, non-allergic, non-adherent, and removable without causing trauma. Moreover, ideal wound dressing should be made from commercially available biomaterials possessing antimicrobial and wound healing properties that can be easily processed [37, 39].

In 1980, first dermal skin membrane was designed and composed of collagen and glycosoaminoglycans and was *in vitro* studied on human epidermal keratinocytes. The membrane was found to be suitable for epidermal keratinocytes growth and histologically resembled the skin. In 1981, Yannas and his research group [126] developed a bilayer artificial skin made up of a silicon membrane and a collagen sponge layer containing glycosoaminoglycans [126]. Recently, developing novel wound dressing with accelerating wound repairability using natural biomaterials such as chitosan became the main concern for many researchers. Chitosan seems as a promising material for wound dressing applications because it is composed of glucosamine and *N*-acetyl glucosamine units linked by β-1,4-glycosidic linkages, where *N*-acetyl glucosamine is the main components of skin and is essential for scar tissue repair. Chitosan has a positive charge surface which effectively induces and supports cell growth and is capable of promoting healing process at molecular, cellular, and systemic levels. Moreover, chitosan exhibits many biological properties suiting wound healing applications including good biocompatibility,

biodegradability, and nontoxicity as well as possesses a board spectrum of antimicrobial activity [18, 37, 39].

Several studies have been conducted to assess the host tissue response and wound healing potential of different chitosan-based scaffolds and implants. Studies revealed that chitosan-based materials promote a typical healing with formation of normal granulation tissue along with inducing accelerated angiogenesis, while only producing a minimal immune response with few or no fibrous encapsulation. Okamoto et al. [66] reported that chitosan affected all wound healing stages *in vivo*. The *in vivo* studies demonstrated that chitosan induces the proliferation of fibroblasts and controls the migration of immune cells such as neutrophils and macrophages resulting in enhanced repair process such as fibroplasias and re-epithelialization. In addition, chitosan showed distinctive hemostatic properties during the inflammatory phase that are different from the normal clotting cascades [66]. Kosaka et al. [48] also revealed that the cell-binding and cell-activation properties of chitosan are the main reasons behind its potential ability in wound healing applications as well as tissue engineering [48]. Collectively, the chitosan properties are favorable for promoting rapid dermal regeneration and accelerating wound healing and hence chitosan can suit different applications ranging from simple wound covering to complicated artificial skin regeneration [27, 91].

Focusing on the potential chitosan-based wound dressing applications, different chitosan nanocomposites were proposed and developed aiming to achieve an ideal wound dressing that provide an optimal protective barrier, accelerate wound repair, and achieve synergic antimicrobial activity [45]. Archana et al. [7] prepared and characterized PVP/TiO_2/chitosan nanocomposites for wound healing applications. FTIR and TGA results obtained confirmed the formation of nanocomposite with enhanced mechanical strength. Results also revealed that the strength of nanocomposite increased upon the addition of TiO_2 nanoparticles. *In vitro* and *in vivo* studies were conducted to investigate the biological properties of the prepared nanocomposites. The *in vitro* study revealed that the nanocomposite exhibits a potent antimicrobial activity and excellent biocompatibility toward fibroblasts. Results obtained from *in vivo* studies conducted on open excision type wounds in rat model demonstrated that nanocomposite accelerates wound repair and mediates a synergic effect including good antimicrobial ability, biocompatibility, wound appearance, and closure as well as improved swelling properties [7]. Gopal et al. [29] prepared copper/chitosan nanocomposite (CCNC) for wound healing. Copper nanoparticles were used in wound healing owing to their ability to modulate cells, cytokinase, and growth factors. Results obtained from *in vivo* study conducted on open excision wound in rats revealed that there was a significant decrease in wound size in the CCNC-treated rats compared to the control group. The acceleration in wound healing was ascribed to the ability of CCNC to promote angiogenesis, fibroblast proliferation, and collagen deposition via upregulation of vascular endothelial growth factor (VEGF) and transformation of growth factor-beta1 (TGF-β1) [29].

Aguzzi et al. [3] synthesized silver sulfadiazine loaded on 3D montmorillonite/chitosan nanocomposite for wound healing. Silver sulfadiazine is a topical

antimicrobial drug used for the treatment of burns. The silver sulfadiazine-loaded nanocomposite was prepared by intercalation solution technique and characterized by XRD, FTIR, and TEM. The characterization studies of nanocomposite confirmed that the nanocomposite has 3D structure and chitosan chains were successfully adsorbed into montmorillonite interlayer spaces. Moreover, characterization studies confirmed the silver sulfadiazine loading on the chitosan. *In vitro* studies demonstrated that the silver sulfadiazine loaded on 3D montmorillonite/chitosan nanocomposite showed an excellent biocompatibility, gap closure properties and antimicrobial activity, especially against *P. aeruginosa*, that commonly worsens skin lesions [3]. In another attempt to achieve wound dressing with superior antimicrobial and wound healing properties, Abdelgawad et al. [1] fabricated a novel antimicrobial silver (Ag) nanoparticles/PVA/chitosan nanocomposite in form of nanofibers. The Ag nanoparticles/chitosan nanocomposite was prepared first by reducing silver salt using glucose. Afterwards, the Ag nanoparticles/chitosan nanocomposite suspension was mixed with PVA solution and finally the Ag nanoparticles/PVA/chitosan nanofibers were obtained by electrospinning and cross-linked with glutaraldehyde. The antimicrobial activity of these nanofibers was investigated via viable cell counting. The viable cell counting revealed that silver (Ag) nanoparticles/PVA/chitosan nanofibers showed a potent antimicrobial activity against different bacterial species compared to PVA nanofibers/chitosan indicating the synergic antimicrobial activity is due to the combined effect of the antibacterial of chitosan and Ag nanoparticles [1].

3.3 Drug Delivery

The vast majorities of conventional drugs suffer from poor pharmacokinetic profiles such as short half-life and random biodistribution, resulting in lower drug bioavailability at the diseased site and suboptimal therapeutic effect. Since drug bioavailability is considered the key factor for achieving an optimum therapeutic effect as it controls therapy fates whether results in complete treatment or partial treatment with a high toxicity. Increasing the drug dose seems to be an appealing solution to increase the drug bioavailability and therapeutic effect, but it is restricted because the majority of drugs possess a dose-dependent systemic toxicity. Consequently, there is an urgent need to find a new therapeutic approach, which can deliver a drug with the optimal therapeutic concentration to the targeted site, while minimizing the adverse side effects [111].

A century ago, Paul Ehrlich proposed a hypothetical drug called “magic bullet” aimed at controlling drug release profile and selectively killing diseased cells. Over the last years, the idea of targeted drugs has been the focus of many scientists. Though little progress has been achieved in this field, the evolution of nanotechnology and molecular biology has paved the way for converting Ehrlich’s hypothetical drug into clinical reality. Targeted drug delivery system, a novel therapeutic approach has been developed as a result of the integration between nanotechnology

and molecular biology results. The targeted drug delivery system is composed of three components: a nanocarrier, a drug, and a targeting moiety. This targeting drug delivery system is based on using nanocarriers (i.e., lipsomes and nanoparticles) as drug vehicles, where the drug is either encapsulate inside their core or chemically conjugate to their surfaces. The targeting moiety, a molecule can recognize and bind to its complementary receptor overexpressed on targeted cells' surfaces, is typically conjugated to nanocarriers' surfaces to guarantee the delivery of drug-loaded nanocarriers to their targeted site. The targeted drug delivery system aims to prolong drug circulation half-life, selectively kill diseased cells, and enhance the drug pharmacokinetics profiles. The formidable therapeutic advantages of targeted drug delivery system open up a new hope for fighting different complicated diseases such as cancer [70, 114].

3.3.1 Cancer-Targeted Drug Delivery System

Cancer is one of the leading causes of death worldwide. Cancer is a unique disease characterized by abnormal cell proliferation, eventually leads to the formation of a mass of cells known as malignant tumor. Chemotherapy is commonly used for the treatment of different cancers such as breast cancer, lung cancer, prostate cancer, etc. Over the past decades, different classes of chemotherapy have been developed aiming at inhibiting the rapid proliferation of cancer cells. Although chemotherapy showed a potent anticancer activity, it suffers from many limitations which in some cases limit its clinical use. The main limitations of chemotherapy are (1) short half-life, (2) nonselective anticancer action, and (3) severe adverse side effects [34, 128].

To overcome these limitations, targeted drug delivery system has emerged as an alternative to conventional chemotherapy. The targeted drug delivery system has shown a great potency in targeting cancer cells, prolonging drug half-life, and controlling drug release. The targeted drug delivery system prolongs chemotherapy circulation half-life due to the small size of nanocarreirs along with their ability to shield the drug allowing it to escape the enzymatic degradation as well as renal filtration. Although drug-loaded nanocarriers can escape enzymatic degradation and renal filtration, it was found that drug-loaded nanocarriers are eliminated by the reticuloendothelial system (RES) uptake. Recently, PEGylated nanocarriers, PEG-coated nanocarriers have been developed and considered as a major breakthrough owing to their stealth effect, which allows drug-loaded nanocarriers to escape renal filtration, enzymatic degradation, and in turn circulates freely in the blood circulation resulting in elevating drug bioavailability at the targeted site and increasing its therapeutic efficiency [12, 34].

Besides the prolonged chemotherapy circulation half-life, targeted drug delivery system offers great possibilities to selectively kill cancer cells. The cancer-targeted drug delivery system is based on two targeting mechanisms namely, passive and active targeting mechanism (Fig. 10). On the one hand, the passive mechanism relies on the enhanced permeability and retention (EPR) effect, a characteristic property of tumor referring to their leaky blood vessels and poor lymphatic

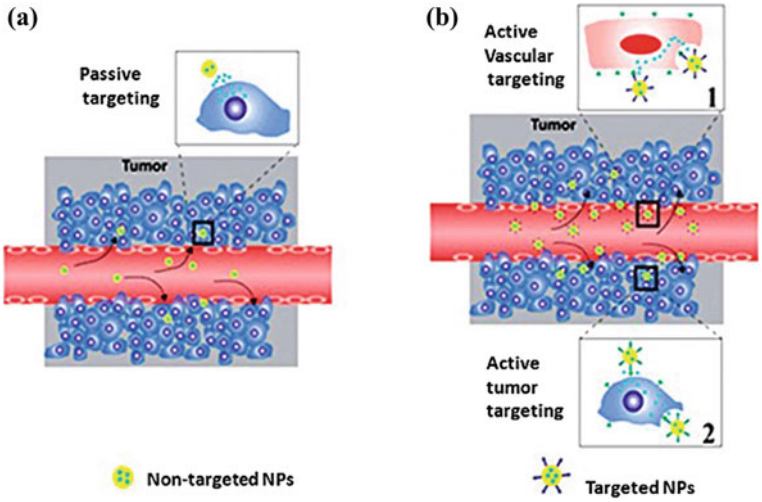

Fig. 10 **a** Passive targeting mechanism and **b** active targeting mechanism. Adapted from Ref. [130]

drainage. The leaky blood vessels of tumor are ascribed to its rapid and improper angiogenesis process in order for obtaining the needed supplement to compensate its rapid growth. As a result, the small and high molecular weight molecules such as nanocarriers can preferentially pass through these leaky blood vessels and accumulate into the extracellular matrix of tumor. On the other hand, active targeting is based on another unique property of cancer cells namely, the overexpression of specific surface receptors. Active targeting is achieved by coupling a targeting moiety such as antibodies or aptamers over the nanocarriers' surfaces. Once the targeting moiety binds to its complementary receptors/proteins overexpressed on cancer cells' surfaces, the nanocarriers penetrate cancer cells where drug release [21, 34, 128, 130].

The choice of nanocarriers is of a great importance because it greatly influences the pharmacokinetics and pharmacodynamic of the payload chemotherapeutic agents. Liposomes are the most extensive nanocarriers employed and investigated in drug delivery applications. However, liposomes showed some drawbacks such as poor reproducibility, stability, and low drug loading efficiency. Polymeric nanoparticles (NPs) have been alternatively used for drug delivery purposes such as parental, oral, and colon drug delivery [13, 112]. Polymeric NPs have been extensively used as drug vehicles owing to their small sizes, large surface area to volume ratio, and ease of surface modification. Moreover, polymeric nanoparticles have shown superior properties compared to liposomes such as better reproducibility, stability, and large drug loading capacity. Among different polymeric nanoparticles, chitosan NPs have been widely used in drug delivery applications owing to their unique physicochemical and biological properties such as mucoadhesivness, biodegradability, biocompatibility, nontoxicity, improved dissolution

rate of poor soluble chemotherapeutic agents, and improved absorption [49]. In an attempt to find better cancer therapy, several chitosan NPs-based chemotherapeutics formula have been widely developed and studied *in vitro* and *in vivo* on different cancers. To beneficial from the stealth effect of PEGylated chitosan derivatives, PEGylated chitosan NPs have been developed and loaded with chemotherapeutics. Bae et al. [8] designed chitosan-g-PEG/heparin nanocomplexes for studying the apoptotic death of cancer cells. The nanocomplexes demonstrated an excellent cellular internalization compared to free heparin alone. It was also observed that following cellular internalization, heparin releases inducing apoptotic death of cancer cells through caspase activation [8]. Que et al. [76] also prepared paclitaxel (PTX) loaded polyethylene glycol monomethylether (m-PEG)-*N*-octyl-O-sulfate chitosan micelles and were studied *in vitro* and *in vivo* on ovarian cancer cells. The *in vitro* and *in vivo* studies showed that PTX-m-PEG micelles exhibit high targeting efficiency to the uterus; moreover, they are able to escape the phagocytosis [76]. To further improve the circulation half-life of chemotherapy, hydrophobically modified glycochitosan (HCG) NPs, NPs composed of hydrophilic glycol–chitosan shell and hydrophobic multicores of bile acid analogs were developed [63]. Min et al. [62] synthesized camptothecin (CPT) lactone loaded on hydrophobically modified glycochitosan (HCG) NPs and were *in vitro* tested on breast cancer cell line. The *in vitro* study revealed that hydrophobically modified glycochitosan (HCG) NPs protect the drug from enzymatic degradation, prolong drug circulation half-life, and preferentially accumulate in the tumor site [62]. Liu et al. [53] also utilized quaternized chitosan derivatives, TMC, and developed trimethylchitosan (CPT-TMC) NPs encapsulating CPT drug through micro-precipitation and sonication. The *in vitro* and *in vivo* studies performed on melanoma (B16-F10) cell line and melanoma xenografts observed a potent inhibition of cell proliferation and apoptosis induction *in vitro*, while *in vivo*, tumor apoptosis and a significant decrease in cell proliferation and angiogenesis were reported [53]. Tan et al. [96] developed HER-2 antibody conjugated to small interfering (siRNA)-loaded chitosan/quantum dot NPs and *in vitro* tested on HER-2 overexpressing SKBR3 breast cancer cells. The *in vitro* test revealed that HER-2-conjugated chitosan/quantum dot NPs specifically target HER-2 receptors overexpressed over cancer cells mediating cellular internalization via endocytosis [51, 96].

3.3.2 Oral Drug Delivery System

Oral route of administration is the most convenient route of administration especially for the treatment of chronic diseases. Oral route of administration has many advantages including patient convenience and compliance, selective pharmacological action, painless and low toxicity profile. The major absorption site of oral administration is the small intestine which offers 100 m^2 surface epithelia allowing systemic drug delivery. Unfortunately, oral route of administration is not suitable for many drugs such as chemotherapeutics, proteins and peptides drugs due to their poor stability, short half-life, poor penetration of the intestine membrane,

immunogenicity, and high susceptibility to enzymatic degradation [111]. In order to overcome these limitations, several NPs-based oral drug delivery systems have been precisely formulated aiming at protecting the drug from gastrointestinal degradation, delivering it to its targeted site, translocating through the intestinal barrier via paracellular pathway and enhance its absorption. Among different polymers used in NPs formulation, chitosan seems to be advantageous in oral drug delivery compared to other polymers because of its ability to open the cellular tight junctions and hence improving the permeability of drug especially peptide/protein drugs [11, 68]. Several studies also demonstrated that chitosan NPs have proven to be promising candidates for oral drug delivery owing to their absorption enhancing, controlled drug release, and mucoadhesive property.

Indeed, with the increasing demand for developing oral insulin as an alternative route of administration to subcutaneous injections, chitosan NPs have been heavily explored for oral insulin delivery. Yin et al. [127] developed trimethyl chitosan–cysteine NPs for oral delivery of insulin. The prepared NPs possess a combined mucoadhesion and permeation enhancing the effect of both trimethyl chitosan and thiolated polymer. The insulin-loaded trimethyl chitosan–cysteine NPs demonstrated 2.1–4.7 fold increases in mucoadhesion compared to insulin-loaded trimethyl chitosan NPs. The *in vivo* studies also showed that trimethyl chitosan–cysteine NPs causes an elevation in insulin transport through rat intestine by 3.3–11.7 and 1.7–2.6 times as well as exhibits an increase in the cellular internalization by 7.5–12.7 times. The DSC measurements showed that the increase in mucoadhesion of trimethyl chitosan–cysteine NPs was ascribed to disulfide bond formation between trimethyl-cysteine and mucin. These findings indicate that the trimethyl chitosan–cysteine NPs are promising nanocarriers for oral insulin delivery [127]. Qian et al. [75] also designed novel functionalized graft copolymer NPs composed of chitosan methyl methacrylate (MMA), *N*-dimethylaminoethyl methacrylate hydrochloride (DMAEMC), and *N*-trimethylaminoethyl methacrylate chloride (TMAEMC) for oral insulin delivery. The copolymer NPs exhibit up to 100 % drug loading efficiency. These copolymer NPs also showed an initial burst release of insulin followed by slowly sustained release for more than 24 h. Moreover, results obtained from *in vivo* studies showed that the copolymer NPs enhanced the absorption and bioavailability of insulin in the GIT [75]. Garrait et al. [28] developed chitosan NPs encapsulated into alginate microparticles for oral drug delivery applications. Amaranth red was used as a drug model to investigate the encapsulation efficiency as well as the drug release kinetics of the prepared NPs under gastric and intestinal conditions. It was found that the encapsulation efficiency was 21.9 %, and the drug release was less 5 % at gastric pH, while at intestine pH, the drug was completely released. These results indicate that the prepared chitosan NPs encapsulated into alginate microparticles have pH-sensitive property, which allows the selective drug delivery and releasing at the intestine [28].

In addition to the oral delivery of peptides/protein drug, chitosan NPs showed a great potential to formulate efficient oral delivery systems for lipophilic drugs and chemotherapeutics. Jana et al. [36] prepared chitosan/egg albumin stabilized PEG NPs via interpolymeric complexation for oral delivery of lipophilic drugs such as

alprazolam. The *in vitro* drug release showed that the NPs demonstrated a sustained drug release over 24 h [36]. Huang et al. [35] also developed multifunctional polyelectrolyte complex NPs (CNPs) composed of hyaluronic acid (HA) grafted polycaprolactone (PCL) NPs (HA-***g***-PCL NPs) coated with chitosan. Studies showed that the chitosan layer remains intact under gastric pH, while degraded gradually at pH 7.4 followed by the release of core–shell HA-***g***-PCL NPs. The *in vitro* study showed that NPs penetrated the cells via receptor-mediated endocytosis followed by rapid drug release, which was triggered by hyaluronidase-1 enzyme abundant in the cancer cells guaranteeing a selective payloads release inside cancer cells [35]. Feng et al. [26] designed pH-sensitive chitosan and o-carboxymethyl chitosan (CMC) nanocomposite in the form of NPs for oral delivery of doxorubicin (DOX). The stability under stimulated GI tract conditions and cytotoxicity of the prepared DOX-loaded NPs were studied. It was observed that the release rate of DOX was higher in neutral pH than acidic pH. The *in vivo* studies also demonstrated that NPs enhanced the absorption and bioavailability of DOX in the small intestine and allowed DOX systemic delivery [26]. Hosseinzadeh et al. [33] formulated an oral drug delivery system for gemcitabine using pluronic/chitosan NPs. The prepared pluronic/chitosan NPs were spherical in shape with size range between 80 and 170 nm. The *in vitro* study conducted on (HT-29) colon cancer cell line showed that gemcitabine-loaded NPs possess much higher anticancer action than free gemcitabine [33].

3.4 Biosensors

Research and development in biosensors field have become a focus of many research groups due to their advantageous properties as diagnostic tools including miniaturization, portability, and low cost in comparison with other well-established laboratory techniques. Basically, sensor is a device which detects and responds to a certain signal/stimulus from the surrounding environment such as heat and light and then converts it into an analog or digital representative. Sensors specialized for biological systems are known as biosensors. In other words, biosensors are devices rely on detecting the biochemical reactions mediated by biological/targeting moiety, immobilized onto the signal transducer. The biological/targeting moiety is a biological element such as antibody, enzyme or DNA, which can recognize and bind to its complementary or targeted element such as receptors or substrates, signaling its presence, activity, concentration via producing a chemical change, which is detected by transducer and finally converted into a quantifiable signal. The advantages of biosensors include adaptability, portability, simplicity, high sensitivity and selectively [92, 98].

Recently, much focus has been on developing multipurpose, long-lived, implantable, and low-cost biosensors. In order to develop multipurpose biosensors fulfilling these criteria, researchers were directed toward using polymers, composites and nanocomposites-based biosensors. Chitosan has been extensively used

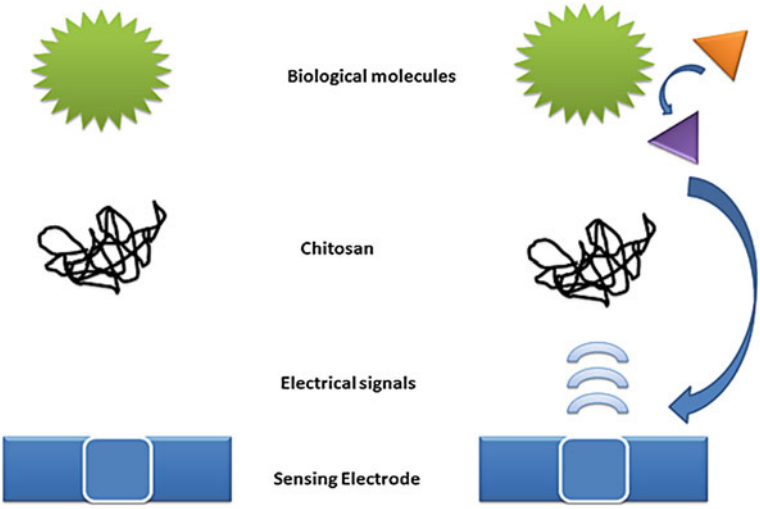

Fig. 11 Schematic illustration of chitosan-based biosensor. Adapted from Ref. [92]

for biosensor purposes (Fig. 11) due to its biocompatibility, biodegradability, inertness, ease of surface modification, hydrophilicity, gel-forming properties, binding affinity to proteins, and low cost. Chitosan-based nanocomposites have been used in the development of different biosensors such as amperometric-, potentiometric- and conductimetric sensors and were tested for diagnosis of different biological elements [92, 98, 133]. Wang et al. [118] synthesized a novel amperometric tryosinase biosensors based on iron oxide (Fe_3O_4) NPs/chitosan nanocomposite for catechol detection. The characterization studies showed that chitosan exhibited a porous structure and large surface area owing to the presence of iron oxide NPs which offer a large loading capacity for tryosinase enzyme [118]. Kaushik et al. [42] developed Fe_3O_4 NPs/chitosan nanocomposite film immobilizing glucose oxidase (GOx) deposited on indium–tin oxide (ITO) glass plate for glucose detection. It was found that the sensitivity of GOx-Fe_3O_4 NPs–chitosan nanocomposite electrode was 9.3 μA/(mg dL cm2) [42]. Kaushik et al. [43] also synthesized superparamagnetic iron oxide Fe_3O_4 NPs/chitosan-based nanocomposite film immobilizing urease and glutamate dehydrogenase modified onto indium-tin-oxide (ITO) coated glass plate for urea detection. This study revealed that Fe_3O_4 NPs provide larger surface area for immobilization of enzymes, enhanced electron transfer, and increased shelf life of electrode. It was also revealed that the biosensor sensitivity was in the range between 5 and 100 mg/dl urea concentration and detection limit was 0.5 mg/dl [43]. On the other hand, Bansi and Ajeet (2009) fabricated a new cholesterol biosensor; composed of cerium oxide NPs/chitosan nanocomposites immobilizing cholesterol oxidase (ChOx) depositing onto ITO-coated glass plate. This biosensor demonstrated high sensitivity toward detecting cholesterol in the range of 10–400 mg/dl with detection limit of 5 mg/dl and response time of 10 s [60]. In another study, nanocomposites composed of

Prussian blue NPs/multiwall carbon nanotubes/chitosan deposited on glassy carbon electrode was designed and used for detecting glucose. The Prussian blue NPs/multiwall carbon nanotubes/chitosan nanocomposite showed a great potential to amplify the reduction signal of hydrogen peroxide by about 35 folds [129].

To enhance the electrocatalytical activity and sensitivity of chitosan-based biosensors, noble metal NPs have been incorporated within chitosan nanocomposite. Shan et al. [53] synthesized gold (Au) NPs/graphene/chitosan nanocomposite deposited on gold electrode for glucose sensing. The studies revealed that the biosensor possesses an extraordinary electrocatalytical activity and sensitivity toward the hydrogen peroxides and oxygen. This extraordinary electrocatalytical activity was probably due to the synergic effect of both graphene and AuNPs. It was also found that the prepared biosensor has good amperometric response to glucose with linear response in the range between 2 and 10 mM at 0.5 V, high reproducibility and detection limit of 180 μM [89]. Safavi and Farjami [83] designed Au/platinum (Pt)/chitosan nanocomposites for cholesterol detection. It was revealed that this new biosensor has two wide linear responses to cholesterol in concentration ranges of 0.05–6.2 mM and 6.2–11.2 mM. Moreover, the sensitivity of this biosensor was 90.7 μA mM^{-1} cm^{-2} with detection limit of 10 μM and response time of 7 s [83]. Sun et al. [95] also developed a novel acetyl cholinesterase (AChE) biosensor for pesticides detection. The novel AChE biosensors is composed of Au NPs/O-carboxymethyl chitosan (CMCS) nanocomposites immobilizing acetyl cholinesterase (AChE) deposited onto the glassy carbon electrode (GCE). Such AChE biosensor detects pesticides depend on the inhibition of pesticides (e.g., chlorpyrifos) on AChE activity. Results demonstrated that the inhibition of chlorpyrifos is directly proportional to its concentration and limit of detection was 0.07 μg/L. The AChE biosensor seems to be a promising tool of pesticides detection as it exhibits fast response, accepted stability, good reproducibility, and low detection limit [95].

4 Conclusion and Future Perspective

Chitosan is a natural polymer derived from chitin and has been widely investigated in the field of biomedicine owing to its biological properties such as biocompatibility, biodegradability, nontoxicity, mucoadhesivness, and antimicrobial activity. However, chitosan has many drawbacks which limits its biomedical use such as low aqueous solubility; low thermal stability, poor mechanical properties, and higher swelling degree in aqueous solutions. Consequently, a great deal of research and effort has been performed to utilize the abundant functional groups of chitosan to produce different chitosan-based materials such as chitosan derivatives and composites with enhanced properties. Chitosan derivatives as well as composites were found to possess good solubility at neutral pH, in addition to high thermal and mechanical stability. Due to these enhanced properties of chitosan-based materials, several pharmaceutical companies invest millions of dollars to support research and development of chitosan-based materials in the biomedical fields.

Recently, the advent of nanotechnology paved the way for producing nanocomposites possessing superior properties compared to their bulk counterpart. Recently, several chitosan nanocomposites have been developed and shown a great potential in biomedical applications such as tissue engineering, wound healing, drug delivery and biosensors. In tissue engineering, the intrinsic biological properties of chitosan nanocomposites render them promising scaffolding biomaterials for different organs/tissues. Chitosan nanocomposites were also extensively studied in wound healing applications. Chitosan nanocomposites have demonstrated a considerable wound healing ability owing to their composition, which resembles the skin and positively charged surface which effectively supports and promotes cell growth and healing process. In addition, chitosan nanocomposites play an important role in the development of different targeted drug delivery systems. In particular, chitosan nanoparticles, which allow the selective delivery of payload therapeutics to the diseased cells and provide controlled payloads release. Furthermore, several chitosan nanocomposites were used in biosensor applications. Chitosan-based biosensors have shown a potential diagnostic ability toward different biological elements such as glucose, catechol, and thiocholine. Eventually, chitosan-based nanocomposites seem to be advantageous in the formulation of novel treatment and diagnosis strategies for complicated medical issues. However, several chitosan nanocomposite-based biomedical applications are still in infancy stage and are needed more effort and further research for being clinically implemented.

References

1. Abdelgawad AM, Hudson SM, Rojas OJ (2014) Antimicrobial wound dressing nanofiber mats from multicomponent (chitosan/silver-NPs/polyvinyl alcohol) systems. Carbohydr Polym 100:166–178
2. Abolhasani M, Arefazar A, Mozdianfard M (2010) Effect of dispersed phase composition on morphological and mechanical properties of PET/EVA/PP ternary blends. J Polym Sci, Part B: Polym Phys 48:251–259
3. Aguzzi C, Sandri G, Bonferoni C, Cerezo P, Rossi S, Ferrari F, Caramella C, Viseras C (2014) Solid state characterisation of silver sulfadiazine loaded on montmorillonite/chitosan nanocomposite for wound healing. Colloids Surf B 113:152–157
4. Aimin C, Chunlin H, Juliang B, Tinyin Z, Zhichao D (1999) Antibiotic loaded chitosan bar: an *in vitro*, *in vivo* study of a possible treatment for osteomyelitis. Clin Orthop Relat Res 366:239–247
5. Anitha A, Divya Rani V, Krishna R, Sreeja V, Selvamurugan N, Nair S, Tamura H, Jayakumar R (2009) Synthesis, characterization, cytotoxicity and antibacterial studies of chitosan, O-carboxymethyl and N,O-carboxymethyl chitosan nanoparticles. Carbohydr Polym 78:672–677
6. Anitha A, Rejinold NS, Bumgardner JD, Nair SV, Jayakumar R (2012) Approaches for functional modification or cross-linking of chitosan. Chitosan-Based Systems for Biopharmaceuticals: Delivery, Targeting and Polymer Therapeutics, pp 107–124
7. Archana D, Singh BK, Dutta J, Dutta P (2013) *In vivo* evaluation of chitosan–PVP–titanium dioxide nanocomposite as wound dressing material. Carbohydr Polym 95:530–539

8. Bae KH, Moon CW, Lee Y, Park TG (2009) Intracellular delivery of heparin complexed with chitosan-g-poly (ethylene glycol) for inducing apoptosis. Pharm Res 26:93–100
9. Berger J, Reist M, Mayer J, Felt O, Peppas N, Gurny R (2004) Structure and interactions in covalently and ionically crosslinked chitosan hydrogels for biomedical applications. Eur J Pharm Biopharm 57:19–34
10. Bhattarai N, Edmondson D, Veiseh O, Matsen FA, Zhang M (2005) Electrospun chitosan-based nanofibers and their cellular compatibility. Biomaterials 26:6176–6184
11. Bowman K, Leong KW (2006) Chitosan nanoparticles for oral drug and gene delivery. Int J Nanomed 1:117
12. Brannon-Peppas L, Blanchette JO (2012) Nanoparticle and targeted systems for cancer therapy. Adv Drug Deliv Rev 64:206–212
13. Cho K, Wang X, Nie S, Shin DM (2008) Therapeutic nanoparticles for drug delivery in cancer. Clin Cancer Res 14:1310–1316
14. Chouwatat P, Polsana P, Noknoi P, Siralertmukul K, Srikulkit K (2010) Preparation of hydrophobic chitosan using complexation method for PLA/chitosan blend. J Met, Mater Miner 20:41–44
15. Chow KS, Khor E (2000) Novel fabrication of open-pore chitin matrixes. Biomacromolecules 1:61–67
16. Chrissafis K, Paraskevopoulos KM, Papageorgiou GZ, Bikiaris DN (2008) Thermal and dynamic mechanical behavior of bionanocomposites: fumed silica nanoparticles dispersed in poly (vinyl pyrrolidone), chitosan, and poly (vinyl alcohol). J Appl Polym Sci 110: 1739–1749
17. Costa-Júnior ES, Barbosa-Stancioli EF, Mansur AA, Vasconcelos WL, Mansur HS (2009) Preparation and characterization of chitosan/poly (vinyl alcohol) chemically crosslinked blends for biomedical applications. Carbohydr Polym 76:472–481
18. Dai T, Tanaka M, Huang Y-Y, Hamblin MR (2011) Chitosan preparations for wounds and burns: antimicrobial and wound-healing effects
19. Darder M, Aranda P, Ruiz-Hitzky E (2007) Bionanocomposites: a new concept of ecological, bioinspired, and functional hybrid materials. Adv Mater 19:1309–1319
20. Dash M, Chiellini F, Ottenbrite R, Chiellini E (2011) Chitosan—a versatile semi-synthetic polymer in biomedical applications. Prog Polym Sci 36:981–1014
21. Davis ME (2008) Nanoparticle therapeutics: an emerging treatment modality for cancer. Nat Rev Drug Discovery 7:771–782
22. Denis TGS, Dai T, Huang Y-Y, Hamblin MR (2012) Wound-healing properties of chitosan and its use in wound dressing biopharmaceuticals. Chitosan-Based Systems for Biopharmaceuticals: Delivery, Targeting and Polymer Therapeutics pp 281–304
23. Depan D, Venkata Surya P, Girase B, Misra R (2011) Organic/inorganic hybrid network structure nanocomposite scaffolds based on grafted chitosan for tissue engineering. Acta Biomater 7:2163–2175
24. Dvir T, Timko BP, Kohane DS, Langer R (2011) Nanotechnological strategies for engineering complex tissues. Nat Nanotechnol 6:13–22
25. Elsabee MZ, Abdou ES (2013) Chitosan based edible films and coatings: a review. Mater Sci Eng, C 33:1819–1841
26. Feng C, Wang Z, Jiang C, Kong M, Zhou X, Li Y, Cheng X, Chen X (2013) Chitosan/o-carboxymethyl chitosan nanoparticles for efficient and safe oral anticancer drug delivery: *In vitro* and *in vivo* evaluation. Int J Pharm 457:158–167
27. Francesko A, Tzanov T (2011) Chitin, chitosan and derivatives for wound healing and tissue engineering, biofunctionalization of polymers and their applications. Springer, Berlin, pp 1–27
28. Garrait G, Beyssac E, Subirade M (2014) Development of a novel drug delivery system: chitosan nanoparticles entrapped in alginate microparticles. J Microencapsul 31:363–372
29. Gopal A, Kant V, Gopalakrishnan A, Tandan SK, Kumar D (2014) Chitosan-based copper nanocomposite accelerates healing in excision wound model in rats. Eur J Pharmacol 731:8–19

30. Gulrez SK, Al-Assaf S, Phillips GO (2011) Hydrogels: methods of preparation, characterisation and applications. Progress in Molecular and Environmental Bioengineering-From Analysis and Modeling to Technology pplications
31. Hein S, Wang K, Stevens W, Kjems J (2008) Chitosan composites for biomedical applications: status, challenges and perspectives. Mater Sci Technol 24:1053–1061
32. Hench LL (1991) Bioceramics: from concept to clinic. J Am Ceram Soc 74:1487–1510
33. Hosseinzadeh H, Atyabi F, Dinarvand R, Ostad SN (2012) Chitosan-Pluronic nanoparticles as oral delivery of anticancer gemcitabine: preparation and *in vitro* study. Int J Nanomed 7:1851
34. Hu C-MJ, Zhang L (2009) Therapeutic nanoparticles to combat cancer drug resistance. Curr Drug Metab 10:836–841
35. Huang P, Yang C, Liu J, Wang W, Guo S, Li J, Sun Y, Dong H, Deng L, Zhang J (2014) Improving the oral delivery efficiency of anticancer drugs by chitosan coated polycaprolactone-grafted hyaluronic acid nanoparticles. J Mater Chem B 2:4021–4033
36. Jana S, Maji N, Nayak AK, Sen KK, Basu SK (2013) Development of chitosan-based nanoparticles through inter-polymeric complexation for oral drug delivery. Carbohydr Polym 98:870–876
37. Jayakumar R, Menon D, Manzoor K, Nair S, Tamura H (2010) Biomedical applications of chitin and chitosan based nanomaterials—a short review. Carbohydr Polym 82:227–232
38. Jayakumar R, Prabaharan M, Nair S, Tokura S, Tamura H, Selvamurugan N (2010) Novel carboxymethyl derivatives of chitin and chitosan materials and their biomedical applications. Prog Mater Sci 55:675–709
39. Jayakumar R, Prabaharan M, Sudheesh Kumar P, Nair S, Tamura H (2011) Biomaterials based on chitin and chitosan in wound dressing applications. Biotechnol Adv 29:322–337
40. Jere D, Jiang H-L, Kim Y-K, Arote R, Choi Y-J, Yun C-H, Cho M-H, Cho C-S (2009) Chitosan-graft-polyethylenimine for Akt1 siRNA delivery to lung cancer cells. Int J Pharm 378:194–200
41. Jin J, Song M (2006) Chitosan and chitosan–PEO blend membranes crosslinked by genipin for drug release. J Appl Polym Sci 102:436–444
42. Kaushik A, Khan R, Solanki PR, Pandey P, Alam J, Ahmad S, Malhotra B (2008) Iron oxide nanoparticles–chitosan composite based glucose biosensor. Biosens Bioelectron 24:676–683
43. Kaushik A, Solanki PR, Ansari AA, Sumana G, Ahmad S, Malhotra BD (2009) Iron oxide-chitosan nanobiocomposite for urea sensor. Sens Actuators B: Chem 138:572–580
44. Kean T, Thanou M (2010) Biodegradation, biodistribution and toxicity of chitosan. Adv Drug Deliv Rev 62:3–11
45. Kim I-Y, Seo S-J, Moon H-S, Yoo M-K, Park I-Y, Kim B-C, Cho C-S (2008) Chitosan and its derivatives for tissue engineering applications. Biotechnol Adv 26:1–21
46. Kong M, Chen XG, Xing K, Park HJ (2010) Antimicrobial properties of chitosan and mode of action: a state of the art review. Int J Food Microbiol 144:51–63
47. Koo JH (2006) Polymer nanocomposites, McGraw-Hill Professional Pub
48. Kosaka T, Kaneko Y, Nakada Y, Matsuura M, Tanaka S (1996) Effect of chitosan implantation on activation of canine macrophages and polymorphonuclear cells after surgical stress. J Vet Med Sci: Jpn Soc Vet Sci 58:963–967
49. Kumar MR, Muzzarelli RA, Muzzarelli C, Sashiwa H, Domb A (2004) Chitosan chemistry and pharmaceutical perspectives. Chem Rev 104:6017–6084
50. Kumirska J, Weinhold MX, Thöming J, Stepnowski P (2011) Biomedical activity of chitin/chitosan based materials—influence of physicochemical properties apart from molecular weight and degree of N-acetylation. Polymers 3:1875–1901
51. Lakshmanan V-K, Snima K, Bumgardner JD, Nair SV, Jayakumar R (2011) Chitosan-based nanoparticles in cancer therapy, chitosan for biomaterials I. Springer, Berlin, pp 55–91
52. Liu DBDAT (2011) Tissue engineering. Asia-Pac J Chem Eng 6:813–815
53. Liu X-P, Zhou S-T, Li X-Y, Chen X-C, Zhao X, Qian Z-Y, Zhou L-N, Li Z, Wang Y-M, Zhong Q (2010) Research anti-tumor activity of N-trimethyl chitosan-encapsulated camptothecin in a mouse melanoma model

54. Liu Y, Kim H-I (2012) Characterization and antibacterial properties of genipin-crosslinked chitosan/poly (ethylene glycol)/ZnO/Ag nanocomposites. Carbohydr Polym 89:111–116
55. Lin M-F, Thakur VK, Tan EJ, Lee PS (2011) Dopant induced hollow $BaTiO_3$ nanostructures for application in high performance capacitors. J Mater Chem 21:16500–16504
56. Lin M-F, Thakur VK, Tan EJ, Lee PS (2011) Surface functionalization of $BaTiO_3$ nanoparticles and improved electrical properties of $BaTiO_3$/polyvinylidene fluoride composite. RSC Adv 1:576–578
57. Ma J, Liu C, Li R, Wang J (2012) Properties and structural characterization of chitosan/poly (vinyl alcohol)/graphene oxide nano composites. e-Polymers 12:386–398
58. Ma L, Gao C, Mao Z, Zhou J, Shen J, Hu X, Han C (2003) Collagen/chitosan porous scaffolds with improved biostability for skin tissue engineering. Biomaterials 24:4833–4841
59. Madihally SV, Matthew HW (1999) Porous chitosan scaffolds for tissue engineering. Biomaterials 20:1133–1142
60. Malhotra BD, Kaushik A (2009) Metal oxide–chitosan based nanocomposite for cholesterol biosensor. Thin Solid Films 518:614–620
61. Mi F-L, Tan Y-C, Liang H-F, Sung H-W (2002) *In vivo* biocompatibility and degradability of a novel injectable-chitosan-based implant. Biomaterials 23:181–191
62. Min KH, Park K, Kim Y-S, Bae SM, Lee S, Jo HG, Park R-W, Kim I-S, Jeong SY, Kim K (2008) Hydrophobically modified glycol chitosan nanoparticles-encapsulated camptothecin enhance the drug stability and tumor targeting in cancer therapy. J Control Release 127: 208–218
63. Nam HY, Kwon SM, Chung H, Lee S-Y, Kwon S-H, Jeon H, Kim Y, Park JH, Kim J, Her S (2009) Cellular uptake mechanism and intracellular fate of hydrophobically modified glycol chitosan nanoparticles. J Control Release 135:259–267
64. Nishikawa H, Ueno A, Nishikawa S, Kido J-I, Ohishi M, Inoue H, Nagata T (2000) Sulfated glycosaminoglycan synthesis and its regulation by transforming growth factor-β in rat clonal dental pulp cells. J Endod 26:169–171
65. Noh SM, Park MO, Shim G, Han SE, Lee HY, Huh JH, Kim MS, Choi JJ, Kim K, Kwon IC (2010) Pegylated poly-l-arginine derivatives of chitosan for effective delivery of siRNA. J Control Release 145:159–164
66. Okamoto Y, Watanabe M, Miyatake K, Morimoto M, Shigemasa Y, Minami S (2002) Effects of chitin/chitosan and their oligomers/monomers on migrations of fibroblasts and vascular endothelium. Biomaterials 23:1975–1979
67. Olteanu CE (2007) Applications of functionalized chitosan. Sci Study Res VIII:227–256
68. Pan Y, Li Y-J, Zhao H-Y, Zheng J-M, Xu H, Wei G, Hao J-S, Cui F-D (2002) Bioadhesive polysaccharide in protein delivery system: chitosan nanoparticles improve the intestinal absorption of insulin *in vivo*. Int J Pharm 249:139–147
69. Park BK, Kim M-M (2010) Applications of chitin and its derivatives in biological medicine. Int J Mol Sci 11:5152–5164
70. Patel MP, Patel RR, Patel JK (2010) Chitosan mediated targeted drug delivery system: a review. J Pharm Pharm Sci 13:536–557
71. Peter M, Binulal N, Soumya S, Nair S, Furuike T, Tamura H, Jayakumar R (2010) Nanocomposite scaffolds of bioactive glass ceramic nanoparticles disseminated chitosan matrix for tissue engineering applications. Carbohydr Polym 79:284–289
72. Pham GD, Nguyen XP, Vu DH, Nguyen NT, Tran VH, Mai TTT, Nguyen HB, Le QD, Nguyen TN, Ba TC (2011) Some biomedical applications of chitosan-based hybrid nanomaterials. Adv Nat Sci: Nanosci Nanotechnol 2:045004
73. Pillai C, Paul W, Sharma CP (2009) Chitin and chitosan polymers: chemistry, solubility and fiber formation. Prog Polym Sci 34:641–678
74. Qi B, Yu A, Zhu S, Chen B, Li Y (2010) The preparation and cytocompatibility of injectable thermosensitive chitosan/poly (vinyl alcohol) hydrogel. J Huazhong Univ Sci Technol [Med Sci] 30:89–93
75. Qian F, Cui F, Ding J, Tang C, Yin C (2006) Chitosan graft copolymer nanoparticles for oral protein drug delivery: preparation and characterization. Biomacromolecules 7:2722–2727

76. Qu G, Yao Z, Zhang C, Wu X, Ping Q (2009) PEG conjugated N-octyl-O-sulfate chitosan micelles for delivery of paclitaxel: *in vitro* characterization and *in vivo* evaluation. Eur J Pharm Sci 37:98–105
77. Rajam AM, Jithendra P, Rose C, Mandal AB (2012) *In vitro* evaluation of dual growth factor-incorporated chitosan nanoparticle impregnated collagen–chitosan scaffold for tissue engineering. J Bioact Compatible Polym 27:265–277
78. Ramanathan S, Ponnuswamy V, Mariappan R, Nazeer KP, Murugavel S (2012) Physical investigations on chitosan graft polyaniline. Elixir Org Chem 43:6952–6954
79. Risbud MV, Hardikar AA, Bhat SV, Bhonde RR (2000) pH-sensitive freeze-dried chitosan–polyvinyl pyrrolidone hydrogels as controlled release system for antibiotic delivery. J Control Release 68:23–30
80. Rosso F, Giordano A, Barbarisi M, Barbarisi A (2004) From cell–ECM interactions to tissue engineering. J Cell Physiol 199:174–180
81. Roy K, Ghosn B, Kasturi SP (2008) Enhancing polysaccharide-mediated delivery of nucleic acids through functionalization with secondary and tertiary amines. Curr Top Med Chem 8:331–340
82. Rúnarsson ÖV, Holappa J, Jónsdóttir S, Steinsson H, Másson M (2008) *N*-selective 'one pot'synthesis of highly *N*-substituted trimethyl chitosan (TMC). Carbohydr Polym 74: 740–744
83. Safavi A, Farjami F (2011) Electrodeposition of gold–platinum alloy nanoparticles on ionic liquid–chitosan composite film and its application in fabricating an amperometric cholesterol biosensor. Biosens Bioelectron 26:2547–2552
84. Samal SK, Dash M, Van Vlierberghe S, Kaplan DL, Chiellini E, Van Blitterswijk C, Moroni L, Dubruel P (2012) Cationic polymers and their therapeutic potential. Chem Soc Rev 41:7147–7194
85. Sanoj Rejinold N, Muthunarayanan M, Divyarani V, Sreerekha P, Chennazhi K, Nair S, Tamura H, Jayakumar R (2011) Curcumin-loaded biocompatible thermoresponsive polymeric nanoparticles for cancer drug delivery. J Colloid Interface Sci 360:39–51
86. Sarmento B, das Neves J (2012) Chitosan-based systems for biopharmaceuticals: delivery, targeting and polymer therapeutics, Wiley, New York
87. Sébastien F, Stéphane G, Copinet A, Coma V (2006) Novel biodegradable films made from chitosan and poly (lactic acid) with antifungal properties against mycotoxinogen strains. Carbohydr Polym 65:185–193
88. Shalumon K, Binulal N, Selvamurugan N, Nair S, Menon D, Furuike T, Tamura H, Jayakumar R (2009) Electrospinning of carboxymethyl chitin/poly (vinyl alcohol) nanofibrous scaffolds for tissue engineering applications. Carbohydr Polym 77:863–869
89. Shan C, Yang H, Han D, Zhang Q, Ivaska A, Niu L (2010) Graphene/AuNPs/chitosan nanocomposites film for glucose biosensing. Biosens Bioelectron 25:1070–1074
90. Shantha K, Bala U, Rao KP (1995) Tailor-made chitosans for drug delivery. Eur Polymer J 31:377–382
91. Shi C, Zhu Y, Ran X, Wang M, Su Y, Cheng T (2006) Therapeutic potential of chitosan and its derivatives in regenerative medicine. J Surg Res 133:185–192
92. Shukla SK, Mishra AK, Arotiba OA, Mamba BB (2013) Chitosan-based nanomaterials: a state-of-the-art review. Int J Biol Macromol 59:46–58
93. Sonia T, Sharma CP (2011) Chitosan and its derivatives for drug delivery perspective, chitosan for biomaterials I. Springer, Berlin, pp 23–53
94. Sultana N, Mokhtar M, Hassan MI, Jin RM, Roozbahani F, Khan TH (2014) Chitosan-based nanocomposite scaffolds for tissue engineering applications. Materials and Manufacturing Processes
95. Sun X, Zhai C, Wang X (2013) Amperometric acetylcholinesterase biosensor based on O-Carboxymethyl chitosan-gold nanoparticle nanocomposite by in-situ synthesis method. Sens J IEEE 13:172–179
96. Tan WB, Jiang S, Zhang Y (2007) Quantum-dot based nanoparticles for targeted silencing of HER2/neu gene via RNA interference. Biomaterials 28:1565–1571

97. Taranejoo S, Janmaleki M, Rafienia M, Kamali M, Mansouri M (2011) Chitosan microparticles loaded with *exotoxin A* subunit antigen for intranasal vaccination against *Pseudomonas aeruginosa*: an *in vitro* study. Carbohydr Polym 83:1854–1861
98. Teles F, Fonseca L (2008) Applications of polymers for biomolecule immobilization in electrochemical biosensors. Mater Sci Eng C 28:1530–1543
99. Thakur VK, Yan J, Lin M-F et al (2012) Novel polymer nanocomposites from bioinspired green aqueous functionalization of BNNTs. Polym Chem 3:962–969
100. Thakur VK, Lin M-F, Tan EJ, Lee PS (2012) Green aqueous modification of fluoropolymers for energy storage applications. J Mater Chem 22:5951–5959
101. Thakur VK, Ding G, Ma J et al (2012) Hybrid materials and polymer electrolytes for electrochromic device applications. Adv Mater 24:4071–4096
102. Thakur VK, Thakur MK (2014) Recent trends in hydrogels based on psyllium polysaccharide: a review. J Clean Prod 82:1–15
103. Thakur VK, Thakur MK (2014) Recent advances in graft copolymerization and applications of chitosan: a review. ACS Sustain Chem Eng 2:2637–2652
104. Thakur VK, Thakur MK (2014) Processing and characterization of natural cellulose fibers/thermoset polymer composites. Carbohydr Polym 109:102–117
105. Thakur VK, Thakur MK, Gupta RK (2014) Review: raw natural fiber-based polymer composites. Int J Polym Anal Charact 19:256–271
106. Thakur VK, Thakur MK, Raghavan P, Kessler MR (2014) Progress in green polymer composites from lignin for multifunctional applications: a review. ACS Sustain Chem Eng 2:1072–1092
107. Thakur VK, Vennerberg D, Madbouly SA, Kessler MR (2014) Bio-inspired green surface functionalization of PMMA for multifunctional capacitors. RSC Adv 4:6677–6684
108. Thakur VK, Thunga M, Madbouly SA, Kessler MR (2014) PMMA-g-SOY as a sustainable novel dielectric material. RSC Adv 4:18240–18249
109. Thakur VK, Grewell D, Thunga M, Kessler MR (2014) Novel composites from eco-friendly soy Flour/SBS triblock copolymer. Macromol Mater Eng 299:953–958
110. Thien DVH, Hsiao SW, Ho MH, Li CH, Shih JL (2013) Electrospun chitosan/hydroxyapatite nanofibers for bone tissue engineering. J Mater Sci 48:1640–1645
111. Tiyaboonchai W (2013) Chitosan nanoparticles: a promising system for drug delivery. Naresuan Univ J 11:51–66
112. van Vlerken LE, Amiji MM (2006) Multi-functional polymeric nanoparticles for tumour-targeted drug delivery. Expert opinion drug delivery 205–216
113. Varkouhi AK, Verheul RJ, Schiffelers RM, Lammers T, Storm G, Hennink WE (2010) Gene silencing activity of siRNA polyplexes based on thiolated N,N,N-trimethylated chitosan. Bioconjug Chem 21:2339–2346
114. Vasir JK, Reddy MK, Labhasetwar VD (2005) Nanosystems in drug targeting: opportunities and challenges. Curr Nanosci 1:47–64
115. Verheul RJ, van der Wal S, Hennink WE (2010) Tailorable thiolated trimethyl chitosans for covalently stabilized nanoparticles. Biomacromolecules 11:1965–1971
116. Wanchoo R, Thakur A, Sweta A (2008) Viscometric and rheological behaviour of chitosan-hydrophilic polymer blends. Chem Biochem Eng Q 22:15–24
117. Wang S-F, Shen L, Zhang W-D, Tong Y-J (2005) Preparation and mechanical properties of chitosan/carbon nanotubes composites. Biomacromolecules 6:3067–3072
118. Wang S, Tan Y, Zhao D, Liu G (2008) Amperometric tyrosinase biosensor based on Fe_3O_4 nanoparticles–chitosan nanocomposite. Biosens Bioelectron 23:1781–1787
119. Wang JJ, Zeng ZW, Xiao RZ, Xie T, Zhou GL, Zhan XR, Wang SL (2011) Recent advances of chitosan nanoparticles as drug carriers. Int J Nanomed 6:765–774
120. Xia W, Liu P, Zhang J, Chen J (2011) Biological activities of chitosan and chitooligosaccharides. Food Hydrocolloids 25:170–179
121. Xu XH, Ren GL, Cheng J, Liu Q, Li DG, Chen Q (2006) Self-assembly of polyaniline-grafted chitosan/glucose oxidase nanolayered films for electrochemical biosensor applications. J Mater Sci 41:4974–4977

122. Xu T, Xin M, Li M, Huang H, Zhou S (2010) Synthesis, characteristic and antibacterial activity of N,N,N-trimethyl chitosan and its carboxymethyl derivatives. Carbohydr Polym 81:931–936
123. Yadav VK, Gupta A, Kumar R, Yadav JS, Kumar B (2010) Mucoadhesive polymers: means of improving the mucoadhesive properties of drug delivery system. J Chem Pharm Res 2:418–432
124. Yang S, Leong K-F, Du Z, Chua C-K (2001) The design of scaffolds for use in tissue engineering. Part I. Traditional factors. Tissue Eng 7:679–689
125. Yang X, Tu Y, Li L, Shang S, Tao X-M (2010) Well-dispersed chitosan/graphene oxide nanocomposites. ACS Appl Mater Interfaces 2:1707–1713
126. Yannas JBI, Quinby W Jr, Bondoc C, Jung W (1981) Successful use of a physiologically acceptable artificial skin in the treatment of extensive burn injury. Ann Surg 194:413
127. Yin L, Ding J, He C, Cui L, Tang C, Yin C (2009) Drug permeability and mucoadhesion properties of thiolated trimethyl chitosan nanoparticles in oral insulin delivery. Biomaterials 30:5691–5700
128. Yu MK, Park J, Jon S (2012) Targeting strategies for multifunctional nanoparticles in cancer imaging and therapy. Theranostics 2:3
129. Zhai X, Wei W, Zeng J, Liu X, Gong S (2006) New nanocomposite based on prussian blue nanoparticles/carbon nanotubes/chitosan and its application for assembling of amperometric glucose biosensor. Anal Lett 39:913–926
130. Zhang L, Li Y, Jimmy CY (2014) Chemical modification of inorganic nanostructures for targeted and controlled drug delivery in cancer treatment. J Mater Chem B 2:452–470
131. Zhou HY, Zhang YP, Zhang WF, Chen XG (2011) Biocompatibility and characteristics of injectable chitosan-based thermosensitive hydrogel for drug delivery. Carbohydr Polym 83:1643–1651
132. Zohuriaan-Mehr MJ (2005) Advances in chitin and chitosan modification through graft copolymerization: a comprehensive review. Iran Polym J 14:235–265
133. Zou Y, Xiang C, Sun L-X, Xu F (2008) Glucose biosensor based on electrodeposition of platinum nanoparticles onto carbon nanotubes and immobilizing enzyme with chitosan-SiO_2 sol–gel. Biosens Bioelectron 23:1010–1016
134. Zuo P-P, Feng H-F, Xu Z-Z, Zhang L-F, Zhang Y-L, Xia W, Zhang W-Q (2013) Fabrication of biocompatible and mechanically reinforced graphene oxide-chitosan nanocomposite films. Chem Cent J 7:39

Graphene-Based Polymer Nanocomposites: Chemistry and Applications

Mehdi Mogharabi and Mohammad Ali Faramarzi

Abstract Graphene, a monolayer sp^2 hybridized carbon atom, received worldwide attention due to its extraordinary physical, chemical, thermal, and electrical properties. In recent years, the development of nanoscale dispersion techniques using graphene particles in a polymer matrix has been crowned a new and interesting horizon in material science. Graphene-based polymer nanocomposites reveal superior mechanical and thermal properties compared with the conventional graphite-based composites or neat polymers which are obtained through very low filler loadings in the polymer matrix. Graphene derivatives as unique nanofillers are used in the production of lightweight, low cost, and high-performance polymer nanocomposites with a wide range of applications, such as fuel cells, supercapacitors, solar cells, sensors, and lightweight gasoline tanks. This chapter reviews the preparation methods of graphene-based polymer nanocomposites, their characteristics, and their wide range of potential applications in technological fields.

Keywords Graphene · Polymer nanocomposites · Graphene modification · Preparation and functionalization · Applications · Biocompatibility

1 Introduction

The study of graphene, a monolayer of sp^2 hybridized carbon atoms arranged in a two-dimensional lattice, offers brilliant prospects for potential uses in many diverse products such as sensors, capacitors, solar cells, liquid crystal displays, and ceramic

M. Mogharabi · M.A. Faramarzi (✉)
Department of Pharmaceutical Biotechnology, Faculty of Pharmacy and Biotechnology Research Center, Tehran University of Medical Sciences, 14155–6451 1417614411 Tehran, Iran
e-mail: faramarz@tums.ac.ir

M. Mogharabi · M.A. Faramarzi
Pharmaceutical Sciences Research Center, Tehran University of Medical Sciences, 14155–6451, 1417614411 Tehran, Iran

V.K. Thakur and M.K. Thakur (eds.), *Eco-friendly Polymer Nanocomposites*, Advanced Structured Materials 74, DOI 10.1007/978-81-322-2473-0_7

composites [8, 10, 23, 53]. However, using graphene as nanoscale filler in polymer matrix composites is one of the most promising applications [89, 107]. Polymer nanocomposites not only demonstrate substantially improved chemical and mechanical properties at much lower loading of fillers, in contrast to the conventional micron-scale fillers of polymer composites, but also possess lower component weight and have simpler processing techniques [20, 76, 77, 138–142]. Different types of polymers, composites, and nanocomposites have been used in a number of applications [124–128, 143–145]. Moreover, the multifunctional enhanced properties of polymers and nanocomposites may result in new uses for polymers [49, 146–150]. Very recently in comparison to the traditional polymer composites, bio-based materials have been frequently used in a number of applications [122, 123]. In this direction, the use of natural cellulosic polymers as one of the components in new functional materials has been extensively explored. Indeed the composites containing natural fibers and biopolymers demonstrate unique advantages such as higher strength and better resistance to corrosion [135]. Cellulose, hemicellulose, and lignin are the main components of natural fibers. While cellulose forms the main structure of the cell, lignin provides the coupling on the hemicellulose–cellulose network as a protective barrier [143, 146–150]. Natural fibers are obtained from leaves, seeds, and stem of various plants (Fig. 1).

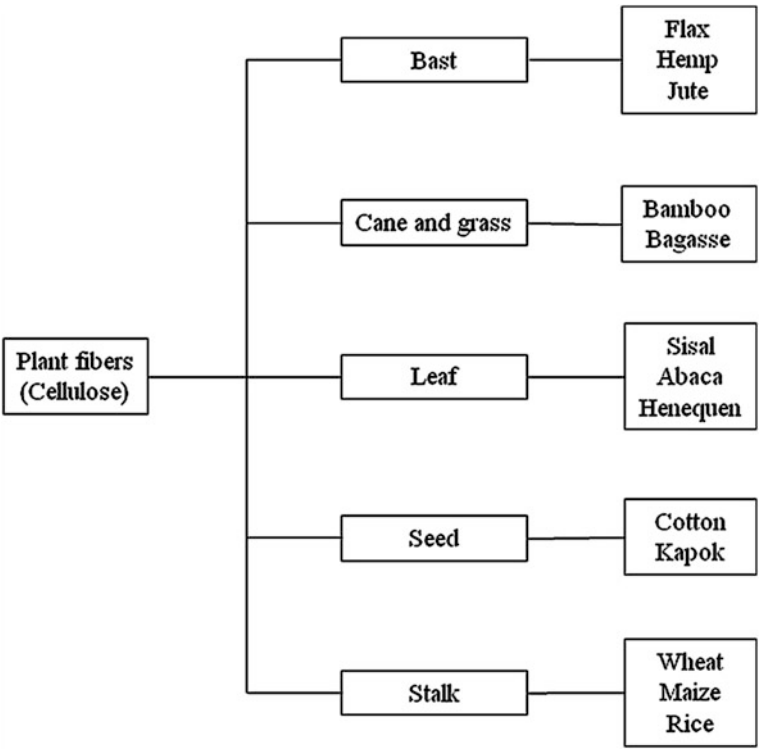

Fig. 1 The sources of cellulose

Cellulose nanoparticles are produced from two main factors including the biosynthesis of crystalline cellulose microfibrils and the extraction process of nanoparticles from the cellulose microfibrils. Surface modification of a cellulosic polymer is important to raise the physical and chemical properties of fibers to use as a green composite. The graft copolymerization of methyl methacrylate onto cellulosic biofibers is reported by using potassium persulfate in aqueous medium [135]. Cellulose-based biocomposites are widely applied in a broad range of applications such as paper, cosmetic, and electronic industries. The surface modifications of cellulose nanoparticles determine the properties of final composites and their surface functionalization generally are categorized as adsorption and covalent attachments [143, 146].

In addition to the use of bio-based materials such as cellulose, soy protein, etc. in polymer composites/nanocomposites, the use of graphene in the preparation of advanced materials has got greater attention all around the globe [146–150]. Recently, a lot of research work is being carried out in the field of cellulose and graphene-based materials for multifunctional applications.

Noncovalent physical attraction and covalent attachment approaches are employed to prepare graphene polymer nanocomposites [36, 60, 61, 172]. Combining pH-responsive polymers with functionalized graphene sheets is expected to be applied in graphene-based switching devices and sensors [9, 68, 71, 162, 163]. Interfacial interactions between graphene-based materials and polymers play an important role in the mechanical performance of the corresponding polymer nanocomposites. Graphene is produced using such techniques as the micromechanical cleavage of graphite and chemical vapor deposition [32]. Due to the relatively small yield of these two methods, the exfoliation of graphite or its derivatives, mainly graphite oxide, became an alternative approach to produce graphene and its chemically modified forms. The advantage of exfoliation is that it has a high yield production, is cost-effective, and is a scalable process, which makes it suitable for the production of polymer nanocomposites [37, 100, 131].

This chapter describes a brief history and recent advances in the synthetic strategies of functionalized graphenes and various characterization methods. It also discusses the importance of graphene and graphene derivatives as fillers in polymer nanocomposite matrices, along with their applications.

2 Graphene

Graphene is categorized into three types according to its number of stacked layers: single-layer, few-layer (2–10 layers), and multilayer (10–100 graphene layers; ~3–30 nm thick), which is also known as thin graphite [101]. While two-dimensional carbon sheets possess unique properties such as ballistic conductivity, high elasticity, very high mechanical strength, high surface area, and rapid heterogeneous electron transfer, multilayered graphene nanostructures are equally interesting and especially worthy of investigation (Fig. 2).

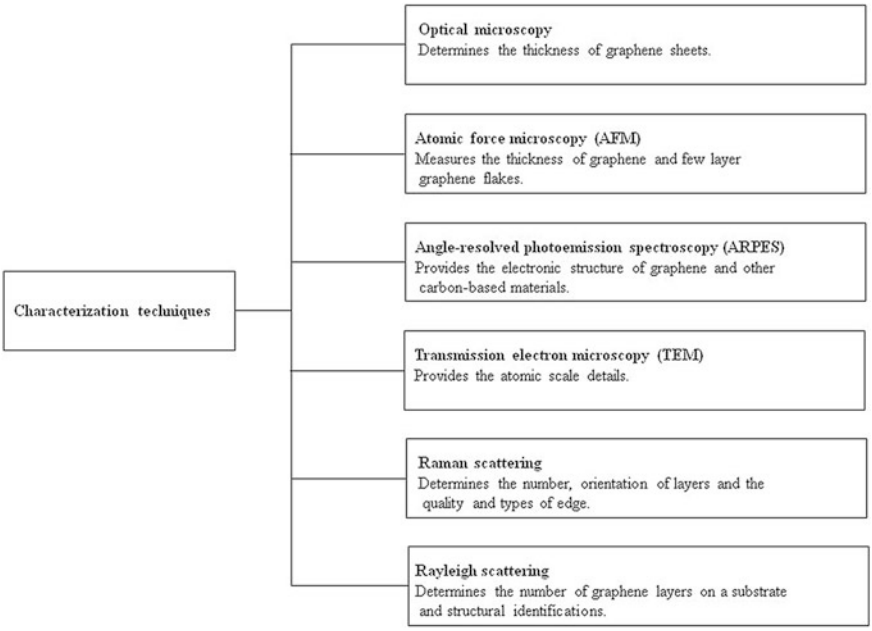

Fig. 2 Various characterization methods of graphene

2.1 Discovery, History, and Chemistry

A discussion of the history of graphene would be incomplete without briefly mentioning graphite oxide and graphite intercalation compounds. The insertion of a small molecule species, such as an acid or alkali metal, between carbon lamellae and the exfoliation of graphite with sulfuric and nitric acids was first reported by Schafhaeutl [114, 115]. The term "graphene" itself developed in the chemistry of graphite intercalation compounds, and was primarily employed by Boehm et al. [13]. In 1999, the tailoring of highly oriented pyrolytic graphite was applied to obtain graphene up to several microns in size [79, 81]. Novoselov et al. [95] characterized thin flakes of graphene only a few atoms thick, obtained when a highly oriented pyrolytic graphite surface was pressed against a silicon wafer surface. However, studies have since demonstrated that exfoliation of graphite in liquid media can produce few-layer or even monolayer graphene [19, 31].

Graphene nanoribbons may have zigzag or armchair configuration, which express different electrical properties (Fig. 3) [93]. It was shown that zigzagging ribbons possess localized edge states with energies close to the Fermi level, where the electrons are strongly localized near the zigzag edge [40]. While the detailed reactivity of graphene sheets—in terms of size, shape, and possibility for stoichiometric control—are currently not well understood, single-layer graphene sheets are found to be more reactive than two or more layers of graphene. Also, the reactivity

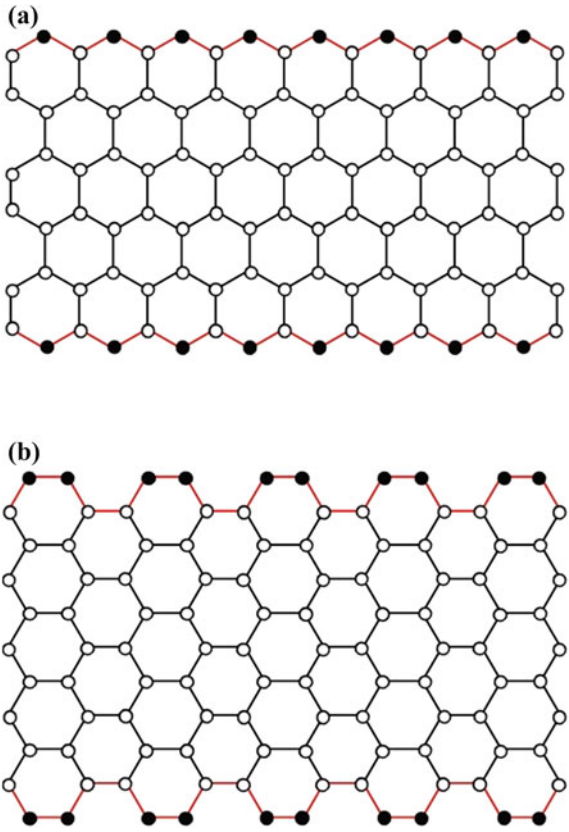

Fig. 3 The schematic illustration of the skeleton framework of an armchair ribbon (**a**) and a zigzag ribbon (**b**). Carbons of the edge sites are shown by *solid circles* on each side

of its edges is at least two times higher than the reactivity of the bulk single graphene sheet [78, 117]. The chemical functionalization of graphene is one way to control its electronic properties. The hydrogenation of graphene involves the change of electronic structure from sp^2 to sp^3 and results in a conversion from a metallic graphene to an insulator [33, 108].

The chemical modification of graphene oxide has become a promising route to achieve mass production of chemically modified graphene platelets. Graphene oxide contains a range of reactive oxygen functional groups, which nominate it for use in wide range applications through chemical functionalization [30, 41]. The precise chemical structure of graphene oxide, which depends on particular synthesis method and the degree of oxidation, is still subject to controversial debate. According to the widely accepted Lerf–Klinowski model, graphene oxide platelets have chemically reactive oxygen functionality groups, such as carboxylic acid, at their edges, and epoxy and hydroxyl groups on the basal planes [67]. Both polymers and small molecules can be covalently attached to the highly reactive oxygen functionalities, or noncovalently attached on the graphitic surfaces of chemically modified graphenes, for potential use in polymer composites.

2.2 Synthesis and Characterization Methods

During the last decade, numerous studies have investigated the most effective methods to produce high-quality single-layer graphene sheets, but large-scale procedures remain as a serious challenge. The synthesis of graphene can be classified into three main approaches: exfoliation, chemical vapor deposition, and chemicals-based techniques.

2.2.1 Exfoliation

Although the van der Waals attraction between the parallel layers in bulk graphite is weak enough to let them slide over each other in the direction perpendicular to the c-axis, the attraction is strong enough to make complete exfoliation into separate layers difficult. The production of graphene using the scotch tape technique inspired new efforts to produce two-dimensional materials via exfoliation [17]. The van der Waals attraction between adjacent layers decreases by expanding the distance between layers via chemical intercalation and oxidation. Inserted functional groups such as epoxide and hydroxyl to the graphitic layers raise the distance between graphite layers from 3.4 to 7.0 Å, facilitating the exfoliation process. Moreover, exfoliated graphene can also be obtained from graphite intercalation compounds such as alkali metal atoms or acid molecules.

Graphite oxide, derived from oxidation of graphite, is an excellent precursor to prepare single sheets. The most important mechanical approaches to exfoliating stacked materials involve stirring, shaking, and ultrasonication. Graphite oxide can be exfoliated in water by sonication due to the presence of polar functional groups and the increased distance between layers [19]. Furthermore, direct exfoliation of graphite oxide in certain organic solvents occurs without additional functionalization or intercalation with moderate sonication in dimethylformamide (DMF), n-methylpyrrolidone (NMP), tetrahydrofuran (THF), and ethylene glycol [97]. Although the mechanical exfoliation of graphite is similar to the exfoliation of graphite oxide, its lack of expanding groups such as epoxide and hydroxyl makes direct exfoliation of graphite significantly more difficult than from graphite oxide. Exfoliation of graphite in water is extremely challenging because of the hydrophobic nature of the sheets; one solution is to use surfactants to help exfoliate the sheets and keep them suspended [43].

Single-layer graphene can also be prepared by much faster thermal exfoliation techniques, which produce graphene in gaseous media, avoiding the use of liquids. Gases produced from the decomposition of functional groups attached to the graphitic layers during the heating process build the pressure between adjacent graphitic layers, which disrupt the van der Waals interlayer attractions [177]. Future work concentrating on controlling the number of layers and minimizing impurity levels must still develop an exfoliation process that can function at an industrial scale of production.

2.2.2 Chemical Vapor Deposition

Chemical vapor deposition (CVD) onto transition metal substrates such as copper, nickel, palladium, ruthenium, and iridium is known as the most promising, inexpensive, and readily accessible approach for the deposition of high quality graphene. Nickel was the first metal catalyst applied to produce graphene, but avoiding multilayer growth is very difficult [59, 116]. In general, during the CVD process, polycrystalline nickel films are exposed to the gas mixture containing hydrogen and methane at 900–1000 °C. Carbon atoms, derived from the thermal decomposition of methane, dissolve into the nickel film to form a solid solution. The material cools down in argon gas, which decreases its solubility; this leads to the diffusion of carbon atoms from the solid solution to precipitate on the nickel surface, forming graphene films [179, 181].

Copper has also been used to catalyze the growth of several carbon allotropes, including graphite, diamond, carbon nanotubes, and most recently graphene. The growth mechanism of graphene on copper is related to the surface because of the peculiar interactions between copper and carbon atoms. Due to the very low solubility of carbon in the copper bulk, the mobility of carbon is considered a purely surface-based process. Lia et al. [69] provide evidence demonstrating that the growth mechanism of graphene on copper is surface related using isotopic labeling of methane precursor gas. They introduced $^{12}CH_4$ and $^{13}CH_4$ to the growth in a specific sequence and measured the distribution of ^{12}C and ^{13}C graphene domains. Raman spectroscopy analysis showed a random mix of the carbon isotopes in the graphene film that was produced using nickel as a catalyst. In contrast, Raman analysis of graphene produced using a copper catalyst reflected the dosing sequence of two types of methane precursor. Production of graphene via chemical vapor deposition growth on copper foil using methane as a carbon source is strongly affected by hydrogen; the hydrogen acts as an activator of the surface-bound carbon that is necessary for monolayer growth and also controls the size and morphology of the graphene domains [155, 180].

Plasma-enhanced chemical vapor deposition (PECVD) can achieve deposition at low pressure and low temperature by using reactive species generated in the plasma [134]. PECVD technique has also shown favorable flexibility on any substrate, and is thus a promising method for the production of graphene. However, PECVD needs improvement to achieve better control over the thickness of the graphene layers and ensure its suitability for large-scale production.

2.2.3 Miscellaneous Methods

Carbon nanotubes are usually considered as rolled graphene sheets. One successful method of converting carbon nanotubes to graphene nanoribbons is the recently reported longitudinal unzipping using a mixture of concentrated sulfuric acid and potassium permanganate. The greatest challenge in producing graphene nanoribbons from carbon nanotubes is to develop ways of cleaving the ribbon

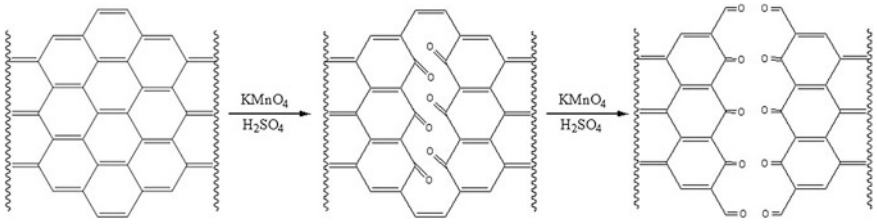

Fig. 4 The proposed chemical mechanism of nanotube unzipping

longitudinally without rapid etching along its circumference [160]. In addition, the over-oxidation of edges during this treatment may create defect sites, which hamper the electronic properties of graphene by diminishing electron mobility and conductivity [119]. The unzipping mechanism is based on the oxidation of alkenes by permanganate in acid and manganate ester formation, followed by further oxidation to form dione (Fig. 4) [64].

Epitaxial growth on electrically insulating surfaces such as silicon carbide is also applied to produce graphenes [98]. Thermal treatment of silicon carbide at about 1300 °C under vacuum condition results in the elimination of the silicon atoms while the carbon-enriched surface undergoes reorganization. However, control of the sublimation leads to the formation of very thin graphene coatings over the whole surface of the silicon carbide wafers [130]. This growth method encourages numerous hopes to incorporate graphene easily in the mainstream electronics industry.

2.3 Surface-Modified Graphenes

The surface modification of pristine graphene sheets with organic functional groups has been developed to raise the dispersibility of graphene in organic solvents that is usually achieved by attaching certain organic groups. The dispersion of graphene sheets in organic solvents is an effective move toward the production of nanocomposite materials containing graphene [42]. In addition, organic functional groups such as chromophores offer new properties that could have various applications such as photodetectors and electro-optics [62]. Covalent functionalization of pristine graphene typically is carried out via two general routes: (1) the formation of covalent bonds between dienophiles or free radicals and C=C bonds of pristine graphene, and (2) the formation of covalent bonds between organic functional groups and the oxygen groups of graphene oxide [66, 175].

Highly reactive free radicals produced from heating diazonium salt can attack the sp^2 carbon atoms of graphene and form covalent bonds [99]. The conductivity of a graphene sheet decreases during chemical functionalization with diazonium salts due to the aromatic system's disruption by the transformation of carbon atoms

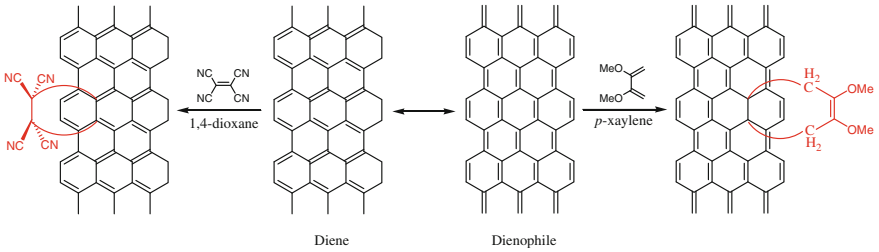

Fig. 5 Chemical structure of graphene as diene and dienophile

from sp^2 to sp^3 hybridization [129]. The ratio between carbon atoms with sp^2 and sp^3 hybridization, as an indication of the degree of oxidation or covalent functionalization reaction, is estimated using Raman spectroscopy as the I_D/I_G ratio, where I_D and I_G are the intensities of peaks corresponding to the number of sp^3 and sp^2 carbon atoms at 1350 and 1580 cm^{-1}, respectively [39].

Moreover, dienophiles also react with sp^2 carbons of graphene to afford a variety of organic derivatives with interesting applications in polymer composites. Graphene is known as a Diels–Alder substrate due to its ability to function as either diene or dienophile (Fig. 5) [113]. The covalent functionalization of graphene via Diels–Alder reactions is an efficient approach to reverse engineering the conductivity of graphene for electronic and optical applications [112]. As a result of the scope of Diels–Alder chemistry and the dual nature of graphene's reactivity, dienophiles and dienes with a wide range of chemicals can be employed to provide modified graphene [26]. The electron-rich nature of graphene results in the functionalization of graphene carbon networks based on electrophilic substitution reactions. The acylation of graphene via the Friedel–Crafts reaction has been successfully performed on a mild reaction condition with 4-aminobenzoic acid in the presence of PPA/P_2O_5 [24, 25].

2.4 Biofunctionalization of Graphene-Based Nanomaterials

The aromatic surface of graphene makes it a suitable substrate for adsorption of certain biomolecules such as single-stranded DNA, which can interact strongly with the surface of graphene. There is also a growing interest in employing graphene-based materials in biosensors, single-bacterium sensors, DNA transistors, and sensitive immunosensors for cancer biomarkers. Sequence-specific detection of very small amounts of DNA is used in a broad range of applications such as clinical diagnostics and forensics [2, 109]. Mohanty and Berry [91] demonstrated a graphene-based biodevice for DNA detection and bacterial (e.g., *Bacillus cereus*) assay. The water-soluble graphene oxide was also used as a platform for the selective and sensitive detection of various concentrations of human thrombin [80].

As well, the interactions of functionalized graphene oxide with bioactive proteins such as enzymes and its potential in enzyme engineering are interesting topics of research. Jin et al. [55] investigated the interactions between serine proteases and functionalized graphene oxide with various amine-terminated polyethylene glycols. Trypsin, chymotrypsin, and proteinase K, chemicals with important biomedical and industrial applications, were analyzed; results showed that functionalized graphene oxide selectively improves trypsin activity and thermal stability, while demonstrating insignificant effect on chymotrypsin and proteinase K.

2.5 Porous Graphene

Porous carbons are the most frequently applied porous materials due to their high surface areas, hydrophobic nature, and low cost to manufacture. Porous graphene is a graphene sheet that is missing carbon atoms from plane, resulting in some holes [181]. Fabrication of porous graphene by self-assembly of a hexaiodo-substituted molecular building block on a silver surface has been reported; the resulting porous graphene demonstrated a regular pore size with one missing hexagon per unit cell passivated by hydrogens (Fig. 6) [12]. Porous graphene displays remarkable features such as a low mass density, large specific surface area, preferred gas permeability, and higher specific capacitance. This type of graphene has been proposed for various applications such as energy storage units in lithium batteries, supercapacitors, and gas separation membranes. Porous graphene has also been reported as an efficient sorbent with the ability to remove oil and organic liquid pollution from water [11].

The high electron density of its aromatic rings repels any atoms or molecules that try to pass through the graphitic plane. Therefore, porous graphene has been extensively studied for use as a membrane for gas separation because the holes in the graphene plane results in the gas' permeability [47]. Porous graphene nanosheets synthesized via the etching of graphene sheets by MnO_2 are used as electrode

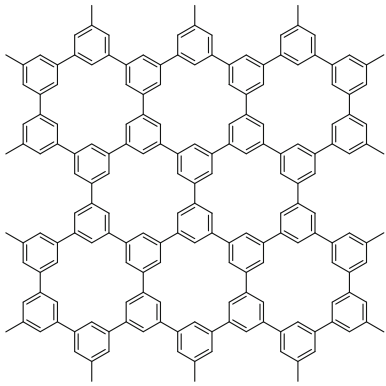

Fig. 6 Chemical structure of porous graphene

in supercapacitors. Research shows that porous graphene exhibits a higher specific capacitance at 500 mVs^{-1} than pure graphene nanosheets [34]. Moreover, porous graphene nanosheets demonstrate better capacitive performances at high rates because their mesopore structure facilitates the access of electrolytes to electrode material, leading to a shorter ion diffusion pathway through the pores than the active carbon electrodes [183].

3 Graphene–Polymer Nanocomposites

In past few decades, research related to polymer nanocomposites has been developed due to progress in creating advanced materials with a wide range of potential applications. A polymer nanocomposite is a combination of a polymer matrix with a large range of organic or inorganic filler materials which have at least one dimension of nanometer range [65]. Polymer nanocomposites based on fullerene, carbon black, carbon nanofiber, carbon nanotubes, and layered silicates have been exploited to improve the mechanical, thermal, electrical, and gas barrier properties of polymers [88]. The discovery of graphene with its unique extraordinary physical properties and capacity for dispersion in various polymer matrices created new horizons of polymer nanocomposites.

3.1 Preparation of Polymer Nanocomposites

Several methods such as in situ polymerization, melt processing, and solvent processing mixing were used to disperse graphene homogeneously and also to provide the strong interactions between the polymer matrix and its fillers. In situ polymerization begins with the dispersion of graphene or modified graphene into the monomer matrix, followed by a polymerization process in the presence of a suitable initiator [29, 164, 165]. In situ polymerization is an easy approach to prepare polyimide films containing functionalized graphene sheets, which demonstrated the improvements in both electrical conductivity and mechanical properties [85]. Graphene/carbon nanotube/polystyrene hybrid nanocomposites prepared by water-based in situ microemulsion polymerization were used as filler in a host polystyrene matrix to form composite films; the process improves the mechanical and thermal properties compared with the neat polymer [96].

Melt mixing is based on a molten state system in which graphene or modified graphene is mixed with the polymer matrix [1]. Several studies have reported the use of graphene as dispersed filler into a polymer matrix without applying any surfactants or solvents [6, 84]. Solution-based approaches generally involve mixing colloidal suspensions of graphene oxide platelets or other chemically modified graphene materials with the preferred polymer solution via simple stirring. The resulting suspension is then precipitated to obtain polymer chains that contain

graphene. Solution mixing has been broadly reported to incorporate fillers derived from graphene oxide into a wide range of polymers including polyacrylamide, polycarbonate, polyimides, and poly(methyl methacrylate) [7, 118]. The production of aqueous graphene oxide platelet suspensions via sonication is so simple that the solution mixing technique has become particularly appealing for the synthesis of nanocomposites containing water-soluble polymers such as poly(vinyl alcohol) and poly(allylamine) [182]. The dispersion of platelets in the polymer matrix via solution mixing depends significantly on the level of exfoliation of the platelets. However, this approach offers a potentially simple route to disperse single-layer chemically modified graphenes into a polymer matrix.

3.2 Polymer Matrices

While polymer nanocomposites based on a wide range of nanofillers, such as carbon nanotubes and nanofibers, have been investigated extensively, more research on graphene-based polymer nanocomposites is still needed. This section discusses the effectiveness of graphene as a nanofiller in various polymeric matrices such as epoxy, polyaniline, polystyrene, polyurethane, and polycarbonate (Table 1).

3.2.1 Epoxy

While epoxy resins are broadly used as adhesives, coatings, and composite matrices, their applications are limited by the fragile nature of polymer. Extensive studies have been conducted to improve epoxy resins using rubbers, thermoplastics, and inorganic particles [21]. Martin-Gallego et al. [86] reported the preparation of functionalized graphene sheets/epoxy coatings cured via cationic photopolymerization. Results clearly demonstrated a significant increase on the mechanical performance of the hybrid films, probably due to interaction between the graphene platelets and the polymeric chains, consequently increasing T_g values and toughness. Recently, Shokrieh et al. [120] investigated the effects of graphene nanoplatelets and graphene nanosheets on the fracture toughness and tensile properties of epoxy resin. It was found that the graphene nanoplatelets have greater impact on both fracture toughness and tensile strength of nanocomposites than graphene nanosheets. Optimal improvement was observed in critical stress intensity factor and Young's modulus for 0.5 wt% graphene nanoplatelet epoxy with an average increase compared with neat epoxy of about 39 and 15 %, respectively [120]. The glass transition temperature of neat epoxy increased from 94.7 to 108.6 °C with 2.5 wt% modified graphene, which had been produced through grafting 4,4′-methylene diphenyl diisocyanate into graphene platelets [176]. The filler percolation network of multiwalled carbon nanotubes grown by chemical vapor deposition

Table 1 Mechanical properties of graphene–polymer nanocomposites

Polymer matrix	Filler	Filler loading (vol. %)	Processing	Modulus increase	E_{matrix} (MPa)	Reference
Epoxy	Reduced graphene	0.05	In situ polymerization	31	2850	Rafiee et al. [104]
Polycaprolactone	Graphene oxide	2.4	Solvent	108	340	Kai et al. [56]
Polycaprolactone	Graphene oxide	0.46	Solvent	50	260	Cai and Song [16]
Polycarbonate	Reduced graphene	1.3	Melt	25	2080	Kim and Macosko [57, 58]
Poly (ethylenenaphthalate)	Reduced graphene	2.4	Melt	57	2350	Kim and Macosko [57]
Poly(methyl methacrylate)	Graphene oxide	1.7	In situ polymerization	54	520	Jang et al. [54]
Poly(methyl methacrylate)	Reduced graphene	0.5	Solvent	80	2100	Ramanathan et al. [105]
Poly(vinyl alcohol)	Graphene oxide	2.5	Solvent	128	2100	Xu et al. [167]
Poly(vinyl alcohol)	Graphene oxide	0.49	Solvent	62	2130	Liang et al. [72]
Poly(vinyl alcohol)	Functionalized graphene	0.4	Solvent	35	660	Das et al. [27]
Poly(vinylidene fluoride)	Reduced graphene	3.1	Solvent	92	1280	Ansari and Giannelis [5]
Polystyrene	Functionalized graphene	0.4	Solvent	57	1450	Fang et al. [35]
Polyurethane	Reduced graphene	1.5	Solvent	43	458	Nguyen et al. [94]
Polyurethane	Reduced graphene	1.6	Melt	250	ND	Kim et al. [60, 61]
Silicone foam	Reduced graphene	0.12	In situ polymerization	200	250	Verdejo et al. [153]

was compared with thermally reduced functionalized graphene sheets in an epoxy resin; it was found that functionalized graphene did not raise the system's viscosity as much as carbon nanotubes [87]. The tensile tests performed on the cured samples showed significant improvements in the elastic moduli and final strength of the polymer composites, particularly in the case of nanocomposites containing functionalized graphene sheets.

3.2.2 Polystyrene

Polystyrene is a widely used general polymer due to its unique properties such as low density, good chemical resistance, high performance–price ratio, and convenience of processing. However, its high flammability and severe dripping during combustion greatly restrict the application of polystyrene in buildings, transportation, and electrical instruments. Conventional flame retardant additives containing halogen elements are currently being replaced by phosphorus and nitrogen-based compounds. In addition, carbon nanoadditives such as expanded graphite, carbon nanotubes, graphite oxide, and graphene are extensively exploited into various polymer matrices to improve their flame retardant properties [46]. Polystyrene/modified graphene oxide nanocomposites were effectively prepared via an in situ miniemulsion polymerization process.

The obtained nanocomposites demonstrate superior anticorrosion properties compared to pure polystyrene. The results show that the efficiency of corrosion protection increases from 37.90 to 99.53 % with the incorporation of 2 wt% modified graphene oxide in the polystyrene polymer matrix. Its mechanical properties and thermal stability also impressively improved compared to pure polymer. The incorporation of 2 wt% modified graphene oxide in the polymer matrix increased the storage modulus from 1808.76 to 2802.36 MPa, and thermal decomposition temperature improved from approximately 73–372 °C [174]. An effective dispersion strategy was developed to prepare the well-defined magnetic Fe_3O_4@graphene oxide/polystyrene nanocomposite by one-pot in situ radical bulk polymerization of styrene in the presence of the Fe_3O_4 nanoparticles and surface-modified graphene oxide [75]. The immobilization of Fe_3O_4 nanoparticles on graphene oxide sheets not only avoids the magnetic aggregation of the magnetic nanoparticles in polymer matrices, but oleic acid molecules also adsorb onto the surfaces of the Fe_3O_4 nanoparticles on the graphene oxide nanosheets, efficiently improving the dispersibility of the nanosheets in styrene, which produces the well-dispersed tricomponent nanocomposite. He et al. [48] showed that the dielectric permittivity of polystyrene composite containing graphene nanosheets is 42 times higher than that of a pure polymer system. The AC electrical conductivity at 1000 Hz also increased from 3.6×10^{-10} S/m for pure polystyrene to 2.82×10^{-4} S/m for the composite containing graphene [48].

3.2.3 Polyaniline

Due to their unique morphology and structure, conductive polymers are suitable for various technological applications such as sensors, light-emitting diodes, and solar cells. Polyaniline, with its desirable electrical, electrochemical, and optical properties, is one of the most promising conducting polymers. The electrical properties of polyaniline can reversibly be controlled by changing the oxidation level of the main chain and protonation of the imine nitrogen atoms [28, 38]. Various nanofillers are added in a polyaniline matrix to synthesize nanocomposites with superior electrical, mechanical, and thermal properties. Because of their unique properties, graphene, graphene oxide, and chemically modified graphenes are now more widely applied than conventional nanofillers in the production of conductive polymer nanocomposites [158]. Stoller et al. [133] found that chemically modified graphene showed large capacitances for aqueous and organic electrolytes of 135 and 99 F g^{-1}, respectively. Recently, Imran et al. [52] developed a systematic approach to disperse graphene oxide during the emulsion polymerization of polyaniline to produce nanocomposites with improved electrical conductivities. The polymerization process was performed in the presence of dodecyl benzene sulfonic acid, which acts as both an emulsifier and protonating agent. The electrical conductivities of the nanocomposites containing graphene were considerably enhanced compared with those of the pure polyaniline samples. Polyaniline/graphene nanocomposites with porous structure and microspherical morphology are produced using porous graphene microspheres as the substrates for the growth of polyaniline nanowire arrays via an in situ polymerization process [18]. A specific capacitance of 338 F g^{-1} obtained at a scan rate of 20 mV s^{-1}, and a high capacity retention rate of 87.4 % after 10,000 cycles at a current density of 3 A g^{-1} suggest that the polyaniline/graphene composite can be used in high-performance supercapacitors [18]. The graphene/polymer composites are ideally proper for portable and wearable electronics due to their flexibility, and also because they can retain these properties even under harsh mechanical stress [102, 161].

3.2.4 Poly(Vinyl Alcohol)

Nanocomposites which are used as nanoscale fillers possess the potential to raise the performance of conventional composites. Maximal mechanical enhancement is achieved when the nanofiller is dispersed homogeneously in the matrix and strong interactions at the interface arise between the filler and the matrix [111]. Liang et al. [72] prepared the first poly(vinyl alcohol) nanocomposite using graphene oxide as a mechanical reinforcement material. Significant enhancement of the mechanical properties was obtained at fairly low concentrations of graphene oxide: the addition of only 0.7 wt% graphene oxide results in a 62 % improvement of Young's modulus and a 76 % increase in tensile strength. Layer-aligned poly(vinyl alcohol)/graphene nanocomposites in the form of films were formed by reducing the graphite

oxide in the polymer matrix via a simple solution mixing process [169]. The modulus and tensile stress of poly(vinyl alcohol)/graphene (3.5 wt%) nanocomposite were 16 and 32 % higher, respectively, than those of pure polymer. Wang et al. [156, 157] successfully synthesized high-performance poly(vinyl alcohol)/graphene nanocomposites by incorporating graphene oxide into a polymeric aqueous solution, which was subsequently reduced to form graphene sheets containing polymer nanocomposite. They showed that the addition of graphene nanofiller decreases the hydrophilicity of poly(vinyl alcohol) films and significantly improves the water resistance of the polymer matrix. Morimune et al. [92] reported the excellent barrier properties of poly(vinyl alcohol)/graphene oxide nanocomposites against water, which is comparable with the conventional high barrier polymer such as poly(vinylidene chloride).

3.3 Polyurethane

Thermoplastic polyurethanes are known as unique polymeric materials with a wide range of physical and chemical properties which are utilized in various applications due to their wide range of commercially available monomeric materials [70]. Functionalized graphene sheets can be finely dispersed on the nanoscale in a thermoplastic polyurethane matrix simply by solution mixing. The addition of 2 wt % modified graphene effectively improved the conductivity of the polymer nanocomposite compared with pristine thermoplastic polyurethane [94]. Dispersion of graphene oxide into thermoplastic polyurethane via melt compounding, solvent mixing, and in situ polymerization was compared, and results showed that solvent-based processes were more effective than melt processing and in situ polymerization in obtaining well-distributed graphene oxide throughout the matrix [60, 61].

Yousefi et al. [171] produced polyurethane-based composite films containing highly aligned graphene sheets through an environmentally benign process, resulting in excellent electrical conductivity with an extremely low percolation threshold of 0.078 vol%. Liao et al. [74] reported the first polymer nanocomposites with 3 wt% aqueous reduced graphene and thermoplastic polyurethane. It was reported that incorporating functionalized graphene nanoplatelets synthesized via a diazotization reaction and a coupling reaction between GNP and 4-aminophenethyl alcohol is an effective way to fabricate high-performance polyurethane nanocomposites [168]. The modulus of the polyurethane/functionalized graphene nanocomposites at 2 wt% graphene nanoplatelets loading was not only ten times greater than that of the pristine polymer sample, but the breaking stress and shape recovery also remarkably improved.

3.4 Poly(Vinylidene Fluoride)

Poly(vinylidene fluoride) is widely used to prepare conducting composites for self-regulated heaters, over current protectors, antistatic shielding, and conducting electrodes for lithium batteries. Its variation of electrical conductivity with temperature enables conductive nanocomposites to be employed as temperature sensors and capacitor [136, 137]. Adding exfoliated graphite, expanded graphite, graphene, and functionalized graphene sheets in poly(vinylidene fluoride) matrix to prepare conductive nanocomposites, which has potential applications for electronics industries, has been investigated extensively in recent years [5]. A nanocomposite of poly(vinylidene fluoride) was prepared with graphene sheets, and the results of differential scanning calorimetry and X-ray diffraction show that adding graphene to the polymer matrix promotes an α-phase to β-phase transformation of the polymer crystal. However, the nanocomposites show significant increases in thermal stability and dynamic mechanical properties compared with neat poly(vinylidene fluoride) [173].

In recent years, enormous effort has been concentrated on improving the energy harvesting ability of piezoelectric materials. Wu et al. [164, 165] added reduced graphene oxide to poly(vinylidene fluoride) to produce piezoelectric nanocomposite films. Their results showed significant enhancement in the piezoelectricity of the fabricated poly(vinylidene fluoride)/reduced graphene oxide nanocomposite at an optimally reduced graphene oxide content of 0.05 wt%. In addition, compared to pristine polymer, the open-circuit voltage, the density of harvested power of alternating current, and direct current of the poly(vinylidene fluoride)/reduced graphene oxide nanocomposite films increased by 105, 153, and 233 %, respectively, implying a potentially wide range of applications [164, 165]. Han et al. [45] demonstrated that with the presence of reduced graphene nanosheets in the poly (vinylidene fluoride) nanocomposite, the polymer structure not only tends to transform from α-phase to β-phase, but the resulting β-phase fractions are significantly influenced by the reduced graphene content.

4 Biocompatibility Graphene-Based Materials

There has in recent years been a surge of interest in research on graphene-based material with various potential biomedical applications such as biosensing, bioimaging, drug delivery, cancer therapy, and antibacterial materials [22, 83, 156, 157, 159]. However, concern has been raised regarding the biocompatibility of graphene-based nanomaterials and their effects on environment and human health [90]. One of the most important characteristics of graphene materials is their high surface area, which can act as a potent sorbent for a variety of small molecule solutes in physiological fluids. Adsorption on the surface of graphene derivatives is preferred for molecules with partial hydrophobicity, low solubility, and molecules with

conjugated π-bonds that allow π–π interactions [110]. Hu et al. [50] first explored the antibacterial properties of graphene oxide. They found that graphene oxide at a concentration of 85 μg mL^{-1} significantly suppresses the growth of *E. coli* after 2 h incubation at 37 °C, with an inhibition rate of over 90 %. In addition, graphene oxide may adsorb metal ions such as Mn^{+2} and Cu^{+2} via complexation or chelation on oxygen functional groups [106, 152].

Functionalized graphenes demonstrate several unique modes of interaction with DNA and RNA that include preferential adsorption of single-stranded over double-stranded forms, steric protection of adsorbed nucleotides from attack by nuclease enzymes and DNA intercalation by graphene-derived materials [82]. The toxicity of functionalized graphene or graphene oxide sheets to various cell lines was investigated in monolayer cultures of lung epithelial cells, fibroblasts, and neuronal cells. Zhang et al. [178] compared the toxicity of various types of carbon nanomaterials such as carbon nanotubes and graphene oxide to HeLa cells. Results showed that although graphene oxide possesses the lowest cell uptake ratio compared to carbon nanotubes, both of them exhibited a dose-dependent toxicity. The generation of reactive oxygen species to induce oxidative stress was considered a mechanism which leads to the toxicity of graphene-based materials [44, 121]. However, further investigations are essential to better understand their toxicity pathways, emphasizing especially the study of cellular interactions of materials containing graphene with cell membrane lipids on a molecular level.

5 Preparation and Characterization of Graphene Oxide

Single-layer transferable graphene nanosheets were first obtained by mechanical exfoliation of bulk graphite or chemical vapor deposition. The main obstacle to achieve individual or few-layer graphene is overcoming the enormous interlayer van der Waals forces. The most common approach to graphite exfoliation is the use of strong oxidizing agents to yield graphene oxide. Brodie [14] reported the synthesis of graphene oxide by adding a portion of potassium chlorate to slurry of graphite in fuming nitric acid. This protocol was later improved by Staudenmaier [132] by using the concentrated sulfuric acid as well as fuming nitric acid and then adding the chlorate which effectively led to formation of highly oxidized graphene oxide in a single reaction vessel. Hummers and Offeman [51] reported the most common method for oxidizing graphite by treating the starting material with $KMnO_4$ and $NaNO_3$ in the concentrated H_2SO_4. The following procedure describes the Hummer method for preparation of graphene oxide.

5 g graphite (purity degree 99.5 %, ~30 μm) was mixed with 115 mL concentrated H_2SO_4 and 2.5 g $NaNO_3$; and stirred in ice bath for half an hour. Then, 15 g $KMnO_4$ was slowly added into the mixture within 1 h while the temperature of the mixture not exceeding 5 °C. The mixture was heated to 35 °C and kept stirring for 2 h. The temperature was adjusted to a constant 98 °C for 60 min while 230 mL distilled water was drop-wise added to the mixture. Finally, the oxidation reaction

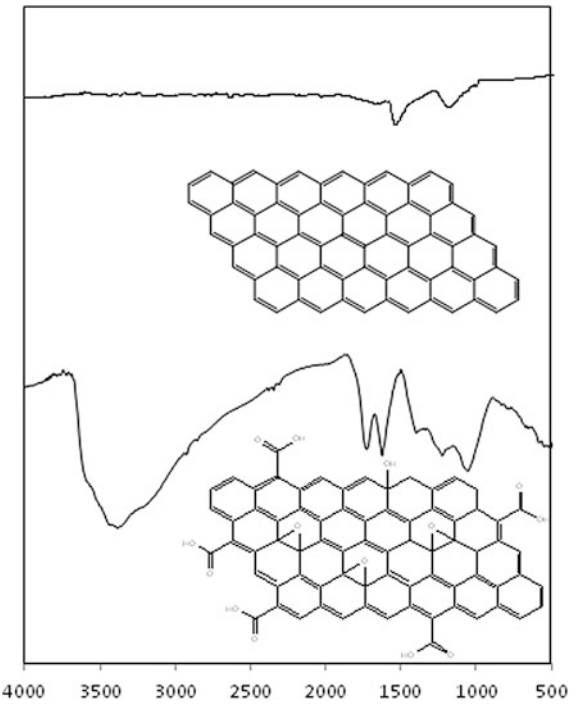

Fig. 7 IR spectra of reduced graphene oxide and graphene oxide

was terminated by adding 700 mL distilled water and 50 mL of 30 % H_2O_2 solution. The resultant solid product was repeatedly washed with 5 % HCl aqueous solution and then with distilled water and dried at 60 °C under vacuum for 12 h.

The Fourier transform infrared spectra of graphene oxide indicates the structure of graphene oxide showing apparent adsorption bands for the alkoxy (1000–1245 cm^{-1}), epoxy (1184–1297 cm^{-1}), aromatic C=C (1590–1620 cm^{-1}), carboxyl (1720–1740 cm^{-1}), and hydroxyl (3590–3650 cm^{-1}) groups (Fig. 7). Besides, scanning electronic microscopy (SEM) provides high-resolution images of graphene and atomic force microscopy (AFM) in tapping mode can directly determine the thickness of graphene layers. Raman spectroscopy indicates D peaks $\sim$1590 cm^{-1} and G peaks $\sim$1350 cm^{-1} which confirm the lattice distortions.

6 Potential Applications of Graphene-Based Polymer Nanocomposites

Graphene materials play a key role in the production of polymer nanocomposites with novel functionalities such as enhanced optical, electrical, thermal, or barrier properties which may be applied for prospective applications, including supercapacitors, transparent conducting electrodes, gas barrier membranes, and biosensors [10].

Efficient dispersion of graphene components through a polymer matrix without aggregation is crucial to improve the functional performance of the nanocomposite. Therefore, efforts to use reduced graphene oxide or surface functionalized graphene with various functional groups are required to improve dispersibility [15, 73].

Graphene nanosheets dispersed in Nafion solution were applied in combination with in situ plated bismuth film electrodes to produce an improved electrochemical sensing platform that can determine Pb^{2+} and Cd^{2+} via differential pulse anodic stripping voltammetry. The prepared Nafion–graphene composite film demonstrated enhanced sensitivity for detecting metal ions [69]. Al-Mashat et al. [4] reported the synthesis of a graphene/polyaniline nanocomposite and its application in the development of a sensitive hydrogen gas sensor. Moreover, several studies discuss the production of multicomponent polymer nanocomposites from silica and other oxide particles coated with graphene oxide for the detection of dopamine [177]. Enhanced electrochemical electrodes for peroxide and glucose detection [103], methanol-sensitive nanocomposites with improved characteristics from polyaniline–graphene oxides [63], amplified colorimetric sensors for target DNA detection [166] have also been reported.

Nanocomposites containing graphene are also exploited for gas barrier and gas separation applications. Yang et al. [170] deposited single layers of graphene oxide with branched polyethylenimine to investigate the oxygen barrier properties of obtained polymer nanocomposites. The addition of only 0.001 wt% of graphene oxide in a polyimide matrix resulted in a nanocomposite that exhibits not only the enhanced resistance to moisture but also retains enhanced mechanical strength, superior visible light transmission, and excellent dimensional stability [151]. Surface-functionalized graphene oxide with bis(triethoxysilylpropyl)tetrasulfide is used as a multifunctional nanofiller for natural rubber and the obtained composite showed improved mechanical and gas barrier properties at a significantly low concentration of filler [181]. Responsive graphene/polymer nanocomposites have also been described with various external stimuli such as light, electrical field, and temperature [154].

Polymer–inorganic nanofiller composite electrolytes show remarkably improved thermal, mechanical, and ionic conductivity properties compared to solid state polymer electrolytes. Highly effective and advanced graphene–polyethylene oxide composite electrolytes were applied as solid state electrolytes for the production of dye-synthetized solar cells [3].

7 Conclusions and Outlook

Although the production, properties, and potential applications of graphene polymer nanocomposites remain in an early stage of development, the growing interest and huge potential of this field have become obvious. The preparation and transfer of high quality graphene in a cost-effective manner is still a challenge, although new research strategies constitute promising steps forward. In recent years, a combined

experimental and theoretical effort has provided considerable progress in understanding and controlling the functionalization of graphene surfaces. Moreover, the full exploitation of graphene-filled nanocomposites will be determined by the level of graphene dispersion and the cost-effective manufacturing of the final material. The structural and functional performances of graphene/polymer nanocomposites are strongly affected by the level of dispersion. Several studies have already demonstrated the potential of developing strong interfacial bonding between chemically modified graphene and the polymer matrix, but further investigations are still crucial to understand the effects of the graphene/polymer interactions in matrix conformations.

References

1. Achaby ME, Arrakhiz F-E, Vaudreuil S, Qaiss AE, Bousmina M, Fassi-Fehri O (2012) Mechanical, thermal, and rheological properties of graphene-based polypropylene nanocomposites prepared by melt mixing. Polym Compos 33:733–744
2. Akhavan O, Ghaderi E, Rahighi R (2012) Toward single-DNA electrochemical biosensing by graphene nanowalls. ACS Nano 6:2904–2916
3. Akhtar MS, Kwon SJ, Stadlerc FJ, Yang OB (2013) High efficiency solid state dye sensitized solar cells with graphene-polyethylene oxide composite electrolytes. Nanoscale 5:5403–5411
4. Al-Mashat L, Shin K, Kalantar-zadeh K, Plessis JD, Han SH, Kojima RW, Kaner RB, Li D, Gou X, Ippolito SJ, Wlodarski W (2010) Graphene/polyaniline nanocomposite for hydrogen sensing. J Phys Chem C 114:16168–16173
5. Ansari S, Giannelis EP (2009) Functionalized graphene sheet-poly(vinylidene fluoride) conductive nanocomposites. J Polym Sci, Part B: Polym Phys 47:888–897
6. Appel A-K, Thomann R, Mülhaupt R (2012) Polyurethane nanocomposites prepared from solvent-free stable dispersions of functionalized graphene nanosheets in polyols. Polymer 53:4931–4939
7. Araby S, Meng Q, Zhang L, Kang H, Majewski P, Tang Y, Ma J (2014) Electrically and thermally conductive elastomer/graphene nanocomposites by solution mixing. Polymer 55:201–210
8. Artiles MS, Rout CS, Fisher TS (2011) Graphene-based hybrid materials and devices for biosensing. Adv Drug Deliv Rev 63:1352–1360
9. Bae S-H, Lee Y, Sharma BK, Lee H-J, Kim J-H, Ahn J-H (2013) Graphene-based transparent strain sensor. Carbon 51:236–242
10. Basu S, Bhattacharyya P (2012) Recent developments on graphene and graphene oxide based solid state gas sensors. Sens Actuators, B 173:1–21
11. Bi H, Xie X, Yin K, Zhou Y, Wan S, He L, Xu F, Banhart F, Sun L, Ruoff RS (2012) Spongy graphene as a highly efficient and recyclable sorbent for oils and organic solvents. Adv Funct Mater 22:4421–4425
12. Bieri M, Treier M, Cai J, Aït-Mansour k, Ruffieux P, Gröning O, Gröning, Kastler M, Rieger R, Feng X, Müllen K, Fasel R (2009) Porous graphenes: two-dimensional polymer synthesis with atomic precision. Chem Commun 6919–6921
13. Boehm HP, Setton R, Stumpp E (1986) Nomenclature and terminology of graphite intercalation compounds. Carbon 24:241–245
14. Brodie BC (1859) On the atomic weight of graphite. Philos Trans R Soc Lond 149:249–259
15. Butler SZ, Hollen SM, Cao L, Cui Y, Gupta JA, Gutiérrez HR, Heinz TF, Hong SS, Huang J, Ismach AF, Johnston-Halperin E, Kuno M, Plashnitsa VV, Robinson RD, Ruoff RS, Salahuddin S, Shan J, Shi L, Spencer MG, Terrones M, Windl W, Goldberger JE (2013)

Progress, challenges, and opportunities in two-dimensional materials beyond graphene. ACS Nano 7:2898–2926
16. Cai D, Song M (2009) A simple route to enhance the interface between graphite oxide nanoplatelets and a semi-crystalline polymer for stress transfer. Nanotechnology 20:315708/1–315708/
17. Cai M, Thorpe D, Adamson DH, Schniepp HC (2012) Methods of graphite exfoliation. J Mater Chem 22:24992–25002
18. Cao H, Zhou X, Zhang Y, Chen L, Liu Z (2013) Microspherical polyaniline/graphene nanocomposites for high performance supercapacitors. J Power Sources 243:715–720
19. Ciesielski A, Samorì P (2014) Graphene via sonication assisted liquid-phase exfoliation. Chem Soc Rev 43:381–398
20. Chang H, Wu H (2013) Graphene-based nanocomposites: preparation, functionalization, and energy and environmental applications. Energy Environ Sci 6:3483–3507
21. Chikhi N, Fellahi S, Bakar M (2003) Modification of epoxy resin using reactive liquid (ATBN) rubber. Eur Polym J 38:251–264
22. Choi W, Lahiri I, Seelaboyina R, Kang YS (2010) Synthesis of graphene and its applications: a review. Crit Rev Solid State Mater Sci 35:52–71
23. Choi HJ, Jung SM, Seo JM, Chang DW, Dai L, Baek JB (2012) Graphene for energy conversion and storage in fuel cells and supercapacitors. Nano Energy 1:534–551
24. Chua CK, Pumera M (2012) Friedel-Crafts acylation on graphene. Chem Asian J 7:1009–1012
25. Chua CK, Pumera M (2012) Covalent chemistry on graphene. Chem Soc Rev 42:3222–3233
26. Chua CK, Pumera M (2013) Covalent chemistry on graphene. Chem Soc Rev 42:3222−3233
27. Das B, Prasad KE, Ramamurty U, Rao CNR (2009) Nano-indentation studies on polymer matrix composites reinforced by few-layer graphene. Nanotechnology 20:125705/1–125705/5
28. Detsri E, Dubas ST (2013) Interfacial polymerization of polyaniline and its layer-by-layer assembly into polyelectrolytes multilayer thin-films. J Appl Polym Sci 128:558–565
29. Ding P, Su S, Song N, Tang S, Liu Y, Shi L (2014) Highly thermal conductive composites with polyamide-6 covalently-grafted graphene by an in situ polymerization and thermal reduction process. Carbon 66:576–584
30. Dreyer DR, Park S, Bielawski CW, Ruoff RS (2010) The chemistry of graphene oxide. Chem Soc Rev 39:228−240
31. Du W, Jiang X, Zhu L (2013) From graphite to graphene: direct liquid-phase exfoliation of graphite to produce single- and few-layered pristine graphene. J Mater Chem A 1:10592–10606
32. Edwards RS, Coleman KS (2013) Graphene synthesis: relationship to applications. Nanoscale 5:38–51
33. Elias DC, Nair RR, Mohiuddin TMG, Morozov SV, Blake P, Halsall MP, Ferrari AC, Boukhvalov DW, Katsnelson MI, Geim AK, Novoselov KS (2009) Control of graphene's properties by reversible hydrogenation: evidence for graphene. Science 323:610–613
34. Fan Z, Zhao Q, Li T, Yan J, Ren Y, Feng J, Wei T (2012) Easy synthesis of porous graphene nanosheets and their use in supercapacitors. Carbon 50:1699–1703
35. Fang M, Wang K, Lu H, Yang Y, Nutt S (2009) Covalent polymer functionalization of graphene nanosheets and mechanical properties of composites. J Mater Chem 19:7098–7105
36. Faramarzi MA, Forootanfar H (2011) Biosynthesis and characterization of gold nanoparticles produced by laccase from *Paraconiothyrium variabile*. Colloids Surf 87:23–27
37. Faramarzi MA, Sadighi A (2013) Insights into biogenic and chemical production of inorganic nanomaterials and nanostructures. Adv Colloid Interface Sci 189:1–20
38. Feliciano FJ, Monteiro OC (2014) New nanocomposite materials by incorporation of nanocrystalline TiO_2 particles into polyaniline conductive films. J Mater Sci Technol 30:449–454
39. Ferrari AC, Basko DM (2013) Raman spectroscopy as a versatile tool for studying the properties of graphene. Nat Nanotechnol 8:235–246

40. Fujii S, Enoki T (2012) Nanographene and graphene edges: electronic structure and nanofabrication. Acc Chem Res 46:2202–2210
41. Gao W, Alemany LB, Ci L, Ajayan PM (2009) New insights into the structure and reduction of graphite oxide. Nat Chem 1:403–408
42. Georgakilas V, Otyepka M, Bourlinos AB, Chandra V, Kim N, Kemp KC, Hobza P, Zboril R, Kim KS (2012) Functionalization of graphene: covalent and non-covalent approaches, derivatives and applications. Chem Rev 112:6156–6214
43. Guardia L, Fernández-Merino MJ, Paredes JI, Solís-Fernández P, Villar-Rodil S, Martínez-Alonso A, Tascón JMD (2011) High-throughput production of pristine graphene in an aqueous dispersion assisted by non-ionic surfactants. Carbon 49:1653–1662
44. Guo X, Mei N (2014) Assessment of the toxic potential of graphene family nanomaterials. J Food Drug Anal 22:105–115
45. Han P, Fan J, Jing M, Zhu L, Shen X, Pan T (2014) Effects of reduced graphene on crystallization behavior, thermal conductivity and tribological properties of poly(vinylidene fluoride). J Compos Mater 48:659–666
46. Han Y, Wu Y, Shen M, Huang X, Zhu J, Zhang X (2013) Preparation and properties of polystyrene nanocomposites with graphite oxide and graphene as flame retardants. J Mater Sci 48:4214–4222
47. Hauser AW, Schwerdtfeger P (2012) Nanoporous Graphene Membranes for Efficient $^{3}He/^{4}He$ Separation. J Phys Chem Lett 3:209–213
48. He F, Lam K, Ma D, Fan J, Chan LH, Zhang L (2013) Fabrication of graphene nanosheet (GNS)-Fe_3O_4 hybrids and GNS–Fe_3O_4/syndiotactic polystyrene composites with high dielectric permittivity. Carbon 58:175–184
49. Hu K, Kulkarni DD, Choi I, Tsukruk VV (2014) Graphene-polymer nanocomposites for structural and functional applications. Prog Polym Sci. doi:10.1016/j.progpolymsci.2014.03.001
50. Hu W, Peng C, Luo W, Lv W, Li X, Li D, Huang Q, Fan C (2010) Graphene-based antibacterial paper. ACS Nano 4:4317–4323
51. Hummers WS, Offeman RE (1958) Preparation of graphitic oxide. J Am Chem Soc 80:1339
52. Imran SM, Kim YN, Shao GN, Hussain M, Choa Y-H, Kim HT (2014) Enhancement of electroconductivity of polyaniline/graphene oxide nanocomposites through in situ emulsion polymerization. J Mater Sci 49:1328–1335
53. Janas D, Koziol KK (2014) A review of production methods of carbon nanotube and graphene thin films for electrothermal applications. Nanoscale 6:3037–3045
54. Jang JY, Kim MS, Jeong HM, Shin CM (2009) Graphite oxide/poly(methyl methacrylate) nanocomposites prepared by a novel method utilizing macroazoinitiator. Compos Sci Technol 69:186–191
55. Jin L, Yang K, Yao K, Zhang S, Tao H, Lee S-T, Liu Z, Peng R (2012) Functionalized Graphene Oxide in Enzyme Engineering: A selective modulator for enzyme activity and thermostability. ACS Nano 6:4864–4875
56. Kai W, Hirota Y, Hua L, Inoue Y (2008) Thermal and mechanical properties of a poly(ε-caprolactone)/graphite oxide composite. J Appl Polym Sci 107:1395–1400
57. Kim H, Macosko CW (2009) Morphology and properties of polyester/exfoliated graphite nanocomposites. Macromolecules 41:3317–3327
58. Kim H, Macosko CW (2009) Processing-property relationships of polycarbonate/graphene composites. Polymer 50:3797–3809
59. Kim KS, Zhao Y, Jang H, Lee SY, Kim JM, Kim KS, Ahn J-H, Kim P, Choi J-Y, Hong BH (2009) Large-scale pattern growth of graphene films for stretchable transparent electrodes. Nature 457:706–710
60. Kim H, Abdala AA, Macosko CW (2010) Graphene/polymer nanocomposites. Macromolecules 43:6515–6530
61. Kim H, Miura Y, Macosko CW (2010) Graphene/polyurethane nanocomposites for improved gas barrier and electrical conductivity. Chem Mater 22:3441–3450

62. Kim M, Safron NS, Huang C, Arnold MS, Gopalan P (2012) Light-driven reversible modulation of doping in graphene. Nano Lett 12:182–187
63. Konwer S, Guha AK, Dolui SK (2013) Graphene oxide-filled conducting polyaniline composites as methanol-sensing materials. J Mater Sci 48:1729–1739
64. Kosynkin DV, Higginbotham AL, Sinitskii A, Lomeda JR, Dimiev A, Price BK, Tour JM (2009) Longitudinal unzipping of carbon nanotubes to form graphene nanoribbons. Nature 458:872–877
65. Kuilla T, Bhadra S, Yao D, Kim NH, Bose S, Lee JH (2010) Recent advances in graphene based polymer composites. Prog Polym Sci 35:1350–1375
66. Kuila T, Bose B, Mishra AK, Khanra P, Kim NH, Lee JH (2012) Chemical functionalization of graphene and its applications. Prog Mater Sci 57:1061–1105
67. Lerf A, He H, Forster M, Klinowski J (1998) Structure of graphite oxide revisited. J Phys Chem B 102:4477–4482
68. Leszczynski P, Han Z, Nicolet AA, Piot BA, Kossacki P, Orlita M, Bouchiat V, Basko DM, Potemski M, Faugeras C (2014) Electrical switch to the resonant magneto-phonon effect in graphene. Nano Lett 14:1460–1466
69. Lia J, Guo S, Zhai Y, Wang E (2009) High-sensitivity determination of lead and cadmium based on the Nafion-graphene composite film. Anal Chim Acta 649:196–201
70. Li Y, Pan D, Chen S, Wang Q, Pan G, Wang T (2013) In situ polymerization and mechanical, thermal properties of polyurethane/graphene oxide/epoxy nanocomposites. Mater Des 47:850–856
71. Li P, Jing G, Zhang B, Sando S, Cui T (2014) Single-crystalline monolayer and multilayer graphene nano switches. Appl Phys Lett 104:113110
72. Liang J, Huang Y, Zhang L, Wang Y, Ma Y, Guo T, Chen Y (2009) Molecular-level dispersion of graphene into poly(vinyl alcohol) and effective reinforcement of their nanocomposites. Adv Funct Mater 19:2297–2302
73. Liang L-J, Wu T, Kang Y, Wang Q (2013) Dispersion of graphene sheets in aqueous solution by oligodeoxynucleotides. Chem Phys Chem 14:1626–1632
74. Liao K-H, Park YT, Abdala A, Macosko C (2013) Aqueous reduced graphene/thermoplastic polyurethane nanocomposites. Polymer 54:4555–4559
75. Liu P, Zhong W, Wu X, Qiu J (2013) Facile synergetic dispersion approach for magnetic Fe_3O_4@graphene oxide/polystyrene tri-component nanocomposite via radical bulk polymerization. Chem Eng J 219:10–18
76. Lin M-F, Thakur VK, Tan EJ, Lee PS (2011) Dopant induced hollow $BaTiO_3$ nanostructures for application in high performance capacitors. J Mater Chem 21:16500–16504
77. Lin M-F, Thakur VK, Tan EJ, Lee PS (2011) Surface functionalization of $BaTiO_3$ nanoparticles and improved electrical properties of $BaTiO_3$/polyvinylidene fluoride composite. RSC Adv 1:576–578
78. Loh KP, Bao Q, Ang PK, Yang J (2010) The chemistry of graphene. J Mater Chem 20:2277–2289
79. Lu X, Huang H, Nemchuk N, Ruoff RS (1999) Patterning of highly oriented pyrolytic graphite by oxygen plasma etching. Appl Phys Lett 75:193–195
80. Lu C-H, Yang H-H, Zhu C-L, Chen X, Chen G-N (2009) A graphene platform for sensing biomolecules. Angew Chem Int Ed 48:4785–4787
81. Lu X, Yu M, Huang H, Ruoff RS (1999) Tailoring graphite with the goal of achieving single sheets. Nanotechnology 10:269–272
82. Lu CH, Zhu CL, Li J, Liu JJ, Chen X, Yang HH (2010) Using graphene to protect DNA from cleavage during cellular delivery. Chem Commun Cambridge U. K. 46:3116–3118
83. Lü K, Zhao G, Wang X (2012) A brief review of graphene-based material synthesis and its application in environmental pollution management. Chin Sci Bull 57:1223–1234
84. Luechinger NA, Booth N, Heness G, Bandyopadhyay S, Grass RN, Stark WJ (2012) Surfactant-free, melt-processable metal-polymer hybrid materials: use of graphene as a dispersing agent. Adv Mater 20:3044–3049

85. Luong ND, Hippi U, Korhonen JT, Soininen AJ, Ruokolainen J, Johansson L-S, Nam J-D, Sinh LH, Seppälä J (2011) Enhanced mechanical and electrical properties of polyimide film by graphene sheets via in situ polymerization. Polymer 52:5237–5242
86. Martin-Gallego M, Verdejo R, Lopez-Manchado MA, Sangermano M (2011) Epoxy-graphene UV-cured nanocomposites. Polymer 52:4664–4669
87. Martin-Gallego M, Bernal MM, Hernandez M, Verdejo R, Lopez-Manchado MA (2013) Comparison of filler percolation and mechanical properties in graphene and carbon nanotubes filled epoxy nanocomposites. Eur Polym J 49:1347–1353
88. Mittal V (2014) Functional polymer nanocomposites with graphene: a review. Macromol Mater Eng. doi:10.1002/mame.201300394
89. Mittal G, Dhand V, Rhee KY, Park SJ, Lee WR (2014) A review on carbon nanotubes and graphene as fillers in reinforced polymer nanocomposites. J Ind Eng Chem. doi:10.1016/j.jiec.2014.03.022
90. Mogharabi M, Abdollahi M, Faramarzi MA (2014) Safety concerns to application of graphene compounds in pharmacy and medicine. Daru J Pharm Sci 22:23
91. Mohanty N, Berry V (2008) Graphene-based single-bacterium resolution biodevice and DNA transistor: interfacing graphene derivatives with nanoscale and microscale biocomponents. Nano Lett 8:4469–4476
92. Morimune S, Kotera M, Nishino T, Goto T (2014) Uniaxial drawing of poly(vinyl alcohol)/graphene oxide nanocomposites. Carbon 70:38–45
93. Nakada K, Fujita M, Dresselhaus G, Dresselhaus MS (1996) Edge state in graphene ribbons: nanometer size effect and edge shape dependence. Phys Rev B 54:17954–17961
94. Nguyen DA, Lee YR, Raghu AV, Jeong HM, Shin CM, Kim BK (2009) Morphological and physical properties of a thermoplastic polyurethane reinforced with functionalized graphene sheet. Polym Int 58:412–417
95. Novoselov KS, Geim AK, Morozov SV, Jiang D, Zhang Y, Dubonos SV, Grigorieva IV, Firsov AA (2004) Electric field effect in atomically thin carbon films. Science 306:666−669
96. Patole AS, Patole SP, Jung S-Y, Yoo J-B, An J-H, Kim T-H (2012) Self assembled graphene/carbon nanotube/polystyrene hybrid nanocomposite by in situ microemulsion polymerization. Eur Polym J 48:252–259
97. Paredes JI, Villar-Rodil S, Martínez-Alonso A, Tascón JMD (2008) Graphene oxide dispersions in organic solvents. Langmuir 24:10560–10564
98. Park S, Ruoff RS (2009) Chemical methods for the production of graphenes. Nat Nanotechnol 4:217–224
99. Peng C, Xiong Y, Liu Z, Zhang F, Ou E, Qian J, Xiong Y, Xu W (2013) Bulk functionalization of graphene using diazonium compounds and amide reaction. Appl Surf Sci 280:914–919
100. Potts JR, Dreyer DR, Bielawski CW, Ruoff RS (2011) Graphene-based polymer nanocomposites. Polymer 52:5–25
101. Pumera M (2010) Graphene-based nanomaterials and their electrochemistry. Chem Soc Rev 39:4146–4157
102. Pumera M (2011) Graphene-based nanomaterials for energy storage energy. Environ Sci 4:668–674
103. Qiu J-D, Shi L, Liang R-P, Wang G-C, Xia X-H (2012) Controllable deposition of a platinum nanoparticle ensemble on a polyaniline/graphene hybrid as a novel electrode material for electrochemical sensing. Chem Eur J 18:7950–7959
104. Rafiee MA, Rafiee J, Wang Z, Song H, Yu ZZ, Koratkar N (2009) Enhanced mechanical properties of nanocomposites at low graphene content. ACS Nano 3:3884–3890
105. Ramanathan T, Abdala AA, Stankovich S, Dikin DA, Herrera-Alonso M, Piner RD, Adamson DH, Schniepp HC, Chen X, Ruoff RS, Nguyen ST, Aksay IA, Prud'Homme RK, Brinson LC (2008) Nat Nanotechnol 3:327–331
106. Ren H, Wang C, Zhang J, Zhou X, Xu D, Zheng J, Guo S (2010) DNA cleavage system of nanosized graphene oxide sheets and copper ions. ACS Nano 4:7169–7174

107. Ren G, Zhang Z, Zhu X, Ge B, Guo F, Men X, Liu W (2013) Influence of functional graphene as filler on the tribological behaviors of Nomex fabric/phenolic composite. Compos A 49:157–164
108. Ryu S, Han MY, Maultzsch J, Heinz TF, Kim P, Steigerwald ML, Brus LE (2008) Reversible basal plane hydrogenation of graphene. Nano Lett 8:4597–4602
109. Sadighi A, Faramarzi MA (2013) Congo red decolorization by immobilized laccase through chitosan nanoparticles on the glass beads. J Taiwan Inst Chem Eng 44:156–162
110. Sanchez VC, Jachak A, Hurt RH, Kane AB (2012) Biological interactions of graphene-family nanomaterials: an interdisciplinary review. Chem Res Toxicol 25:15–34
111. Saravanan N, Rajasekar R, Mahalakshmi S, Sathishkumar TP, Sasikumar KSK, Sahoo S (2014) Graphene and modified graphene-based polymer nanocomposites–A review. J Reinf Plast Compos. doi:10.1177/0731684414524847
112. Sarkar S, Bekyarova E, Niyogi S, Haddon RC (2011) Diels-alder chemistry of graphite and graphene: graphene as diene and dienophile. J Am Chem Soc 133:3324–3327
113. Sarkar S, Bekyarova E, Haddon RC (2012) Chemistry at the dirac point: diels–alder reactivity of graphene. Acc Chem Res 45:673–682
114. Schafhaeutl C (1840) Ueber die verbindungen des kohlenstoffes mit silicium, eisen und anderen metallen, welche die verschiedenen gallungen von roheisen, stahl und schmiedeeisen bilden. J Prakt Chem 21:129–157
115. Schafhaeutl C (1840) LXXXVI. On the combinations of carbon with silicon and iron, and other metals, forming the different species of cast iron, steel, and malleable iron. Philos Mag 16:570–590
116. Seah C-M, Chai S-P, Mohamed AR (2014) Mechanisms of graphene growth by chemical vapour deposition on transition metals. Carbon 70:1–21
117. Sharma R, Baik JH, Perera CJ, Strano MS (2010) Anomalously large reactivity of single graphene layers and edges toward electron transfer chemistries. Nano Lett 10:398–405
118. Shen J, Yan B, Li T, Long Y, Li N, Ye M (2012) Study on graphene-oxide-based polyacrylamide composite hydrogels. Compos A 43:1476–1481
119. Shinde DB, Debgupta J, Kushwaha A, Aslam M, Pillai VK (2011) Electrochemical unzipping of multi-walled carbon nanotubes for facile synthesis of high-quality graphene nanoribbons. JACS 133:4168–4171
120. Shokrieh MM, Ghoreishi SM, Esmkhani M, Zhao Z (2014) Effects of graphene nanoplatelets and graphene nanosheets on fracture toughness of epoxy nanocomposites. Fatigue Fract Eng Mater Struct. doi:10.1111/ffe.12191
121. Shvedova AA, Pietroiustic A, Fadeeld B, Kagan VE (2012) Mechanisms of carbon nanotube-induced toxicity: focus on oxidative stress. Toxicol Appl Pharmacol 261:121–133
122. Singha AS, Thakur VK (2008) Saccaharum cilliare fiber reinforced polymer composites. E-J Chem 5:782–791
123. Singha AS, Thakur VK (2008) Synthesis and characterization of pine needles reinforced RF matrix based biocomposites. J Chem 5:1055–1062
124. Singha AS, Thakur VK (2009) Physical, chemical and mechanical properties of *Hibiscus sabdariffa* fiber/polymer composite. 58:217–228
125. Singha AS, Thakur VK (2009) Grewia optiva fiber reinforced novel, low cost polymer composites. J Chem 6:71–76
126. Singha AS, Thakur VK (2009) Synthesis, characterization and analysis of hibiscus sabdariffa fibre reinforced polymer matrix based composites. Polym Polym Compos 17:189–194
127. Singha AS, Thakur VK (2010) Mechanical, morphological, and thermal characterization of compression-molded polymer biocomposites. Int J Polym Anal Charact 15:87–97
128. Singha AS, Thakur VK (2010) Synthesis, characterization and study of pine needles reinforced polymer matrix based composites. J Reinf Plast Compos 29:700–709
129. Sinitskii A, Dimiev A, Corley DA, Fursina AA, Kosynkin DV, Tour JM (2010) Kinetics of diazonium functionalization of chemically converted graphene nanoribbons. ACS Nano 4:1949–1954

130. Soldano C, Mahmood A, Dujardin E (2010) Production, properties and potential of graphene. Carbon 48:2127–2150
131. Stankovich S, Dikin DA, Dommett GH, Kohlhaas KM, Zimney EJ, Stach EA, Piner RD, Nguyen ST, Ruoff RS (2006) Graphene-based composite materials. Nature 442:282–286
132. Staudenmaier L (1898) Verfahren zur darstellung der graphitsäure. Ber Dtsch Chem Ges 31:1481–1487
133. Stoller MD, Park S, Zhu Y, An J, Ruoff RS (2008) Graphene-based ultracapacitors. Nano Lett 8:3498–3502
134. Terasawa T, Saiki K (2012) Growth of graphene on Cu by plasma enhanced chemical vapor deposition. Carbon 50:869–874
135. Thakur VK, Singha AS, Misra BN (2011) Graft copolymerization of methyl methacrylate onto cellulosic biofibers. J Appl Polym Sci 122:532–544
136. Thakur VK, Tan EJ, Lin M-F, Lee PS (2011) Polystyrene grafted polyvinylidenefluoride copolymers with high capacitive performance. Polym Chem 2:2000–2009
137. Thakur VK, Tan EJ, Lin M-F, Lee PS (2011) Poly (vinylidene fluoride)-graft-poly (2-hydroxyethyl methacrylate): a novel material for high energy density capacitors. J Mater Chem 21:3751–3759
138. Thakur VK, Ding G, Ma J et al (2012) Hybrid materials and polymer electrolytes for electrochromic device applications. Adv Mater 24:4071–4096. D
139. Thakur VK, Singha AS, Thakur MK (2012) Biopolymers based green composites: mechanical, thermal and physico-chemical characterization. J Polym Environ 20:412–421
140. Thakur VK, Yan J, Lin M-F et al (2012) Novel polymer nanocomposites from bioinspired green aqueous functionalization of BNNTs. Polym Chem 3:962–969
141. Thakur VK, Lin M-F, Tan EJ, Lee PS (2012) Green aqueous modification of fluoropolymers for energy storage applications. J Mater Chem 22:5951–5959
142. Thakur VK, Singha AS, Misra BN (2012) Modification of natural biomass by graft copolymerization. Int J Polym Anal Charact 17:547–555
143. Thakur VK, Thakur MK (2014) Processing and characterization of natural cellulose fibers/thermoset polymer composites. Carbohydr Polym 109:102–117
144. Thakur VK, Thakur MK (2014) Recent trends in hydrogels based on psyllium polysaccharide: a review. J Cleaner Prod 82:1–15
145. Thakur VK, Thakur MK (2014) Recent advances in graft copolymerization and applications of chitosan: a review. ACS Sustain Chem Eng 2:2637–2652
146. Thakur VK, Thakur MK, Gupta RK (2014) Review: raw natural fiber-based polymer composites. Int J Polym Anal Charact 19:256–271
147. Thakur VK, Thunga M, Madbouly SA, Kessler MR (2014) PMMA-g-SOY as a sustainable novel dielectric material. RSC Adv 4:18240–18249
148. Thakur VK, Grewell D, Thunga M, Kessler MR (2014) Novel Composites from eco-friendly soy flour/SBS triblock copolymer. Macromol Mater Eng 299:953–958
149. Thakur VK, Vennerberg D, Madbouly SA, Kessler MR (2014) Bio-inspired green surface functionalization of PMMA for multifunctional capacitors. RSC Adv 4:6677–6684
150. Thakur VK, Thakur MK, Raghavan P, Kessler MR (2014) Progress in green polymer composites from lignin for multifunctional applications: a review. ACS Sustainable Chem Eng 2:1072–1092
151. Tseng I-H, Liao Y-F, Chiang J-C, Tsai M-H (2012) Transparent polyimide/graphene oxide nanocomposite with improved moisture barrier property. Mater Chem Phys 136:247–253
152. Tung VC, Allen MJ, Yang Y, Kaner RB (2009) High-throughput solution processing of large-scale graphene. Nat Nanotechnol 4:25–29
153. Verdejo R, Saiz-Arroyo C, Carretero-Gonzalez J, Barroso-Bujans F, Rodriguez-Perez MA, Lopez-Manchado MA. (2008) Physical properties of silicone foams filled with carbon nanotubes and functionalized graphene sheets. Eur Polym J 44:2790−2797
154. Verdejo R, Bernal MM, Romasanta LJ, Lopez-Manchado MA (2011) Graphene filled polymer nanocomposites. J Mater Chem 21:3301–3310

155. Vlassiouk I, Regmi M, Fulvio P, Dai S, Datskos P, Eres G, Smirnov S (2011) Role of hydrogen in chemical vapor deposition growth of large single-crystal graphene. ACS Nano 5:6069–6076
156. Wang Y, Li Z, Wang J, Li J, Lin Y (2011) Graphene and graphene oxide: biofunctionalization and applications in biotechnology. Trends Biotechnol 29:205–212
157. Wang J, Wang X, Xu C, Zhang M, Shang X (2011) Preparation of graphene/poly(vinyl alcohol) nanocomposites with enhanced mechanical properties and water resistance. Polym Int 60:816–822
158. Wang L, Yao Q, Bi H, Huang F, Wang Q, Chen L (2014) Large thermoelectric power factor in polyaniline/graphene nanocomposite films prepared by solution-assistant dispersing method. J Mater Chem. doi:10.1039/C4TA01541J
159. Wang X-M, Zhang W-H (2014) Application of graphene derivatives in cancer therapy: a review. Carbon 67:795–797
160. Wei D, Xie L, Lee KK, Hu Z, Tan S, Chen W, Sow CH, Chen K, Liu Y, Wee ATS (2013) Controllable unzipping for intramolecular junctions of graphene nanoribbons and single-walled carbon nanotubes. Nat Commun 4:1374
161. Wu Q, Xu Y, Yao Z, Liu A, Shi G (2010) Supercapacitors based on flexible graphene/polyaniline nanofiber composite films. ACS Nano 4:1963–1970
162. Wu S, He Q, Tan C, Wang Y, Zhang H (2013) Graphene-based electrochemical sensors. Small 9:1160–1172
163. Wu J, Huang G, Li H, Wu S, Liu Y, Zheng J (2013) Enhanced mechanical and gas barrier properties of rubber nanocomposites with surface functionalized graphene oxide at low content. Polymer 54:1930–1937
164. Wu L, Xue J, Itoi T, Hu N, Li Y, Yan C, Qiu J, Ning H, Yuan W, Gu B (2014) Improved energy harvesting capability of poly(vinylidene fluoride) films modified by reduced graphene oxide. J Intell Mater Syst Struct. doi:10.1177/1045389X14529609
165. Wu T, Xu X, Zhang L, Chen H, Gao J, Liu Y (2014) A polyaniline/graphene nanocomposite prepared by in situ polymerization of polyaniline onto polyanion grafted graphene and its electrochemical properties. RSC Adv 4:7673–7681
166. Xing XJ, Liu XG, He Y, Lin Y, Zhang CL, Tang HW, Pang DW (2012) Amplified fluorescent sensing of DNA using graphene oxide and a conjugated cationic polymer. Biomacromolecules 14:117–123
167. Xu Y, Hong W, Bai H, Li C, Shi G (2009) Strong and ductile poly(vinyl alcohol)/graphene oxide composite films with a layered structure. Carbon 47:3538–3543
168. Yadav SK, Cho JW (2013) Functionalized graphene nanoplatelets for enhanced mechanical and thermal properties of polyurethane nanocomposites. Appl Surf Sci 266:360–367
169. Yang X, Li L, Shang S, Tao X-M (2010) Synthesis and characterization of layer-aligned poly(vinyl alcohol)/graphene nanocomposites. Polymer 51:3431–3435
170. Yang Y-H, Bolling L, Priolo MA, Grunlan JC (2013) Super gas barrier and selectivity of graphene oxide-polymer multilayer thin films. Adv Mater 25:503–508
171. Yousefi N, Gudarzi MM, Zheng Q, Aboutalebi SH, Sharif F, Kim J-K (2012) Self-alignment and high electrical conductivity of ultralarge graphene oxide–polyurethane nanocomposites. J Mater Chem 22:12709–12717
172. Yousefi N, Sun X, Lin X, Shen X, Jia J, Zhang B, Tang B, Chan M, Kim J-K (2014) Highly aligned graphene/polymer nanocomposites with excellent dielectric properties for high performance electromagnetic interference shielding. Adv Mater. doi:10.1002/adma.201305293
173. Yu J, Jiang P, Wu C, Wang L, Wu X (2011) Graphene nanocomposites based on poly(vinylidene fluoride): structure and properties. Polym Compos 32:1483–1491
174. Yu Y-H, Lin Y-Y, Lin C-H, Chan C-C, Huang Y-C (2014) High-performance polystyrene/graphene-based nanocomposites with excellent anti-corrosion properties. Polym Chem 5:535–550

175. Yuan F-Y, Zhang H-B, Li X, Ma H-L, Li X-Z, Yu Z-Z (2014) In situ chemical reduction and functionalization of graphene oxide for electrically conductive phenol formaldehyde composites. Carbon 68:653–661
176. Zaman I, Phan TT, Kuan H-C, Meng Q, La LTB, Luong L, Youssf O, Ma J (2011) Epoxy/graphene platelets nanocomposites with two levels of interface strength. Polymer 52:1603–1611
177. Zeng Z, Zhou Y, Kong L, Zhou T, Shi G (2013) A novel composite of SiO_2-coated graphene oxide and molecularly imprinted polymers for electrochemical sensing dopamine. Biosens Bioelectron 45:25–33
178. Zhang X, Hu W, Li J, Tao L, Wei Y (2012) A comparative study of cellular uptake and cytotoxicity of multi-walled carbon nanotubes, graphene oxide, and nanodiamond. Toxicol Res 1:62–68
179. Zhang C, Lv W, Xie X, Tang D, Liu C, Yang Q-H (2013) Towards low temperature thermal exfoliation of graphite oxide for graphene production. Carbon 62:11–24
180. Zhang C, Lv W, Xie X, Tang D, Liu C, Yang Q-H (2013) Towards low temperature thermal exfoliation of graphite oxide for graphene production. Carbon 62:11–24
181. Zhang Y, Zhang L, Zhou C (2013) Review of chemical vapor deposition of graphene and related applications 46:2329–2339
182. Zhao X, Zhang Q, Chen D (2010) Enhanced mechanical properties of graphene-based poly (vinyl alcohol) composites. Macromolecules 43:2357–2363
183. Zheng C, Zhou X, Cao H, Wang G, Liu Z (2014) Synthesis of porous graphene/activated carbon composite with high packing density and large specific surface area for supercapacitor electrode material. J Power Sources 258:290–296

Natural Nano-based Polymers for Packaging Applications

Behjat Tajeddin

Abstract Natural nanoscale materials can be used in many applications like packaging industry. The main reason is to provide packaging which would protect the food from dust, gases, light, pathogens, and moisture. These materials are mainly safe, inert, cheap to produce, easy to dispose, and reuse. In addition, the characteristics of these nanocomposites such as mechanical, electrical, thermal, optical, and electrochemical properties will differ markedly from that of the component materials. One of the most practical uses of nanocomposites in the food packaging is adding the nanosized components to the traditional packaging materials such as metal, glass, paper, various synthetic plastics like PE, PP, PS, PVC. Also, the use of nanofiller materials in the biofilm preparation has been subjected in the many recent studies. Therefore, this chapter is an attempt to introduce various bionanocomposites to readers and provide a general overview of these natural nanopolymer applications in the food packaging industry as well as some practical examples. In effect, nanopackaging materials were developed by clay minerals, e.g., montmorriolonite, in 1986 and are still being grown using many different natural polymers. However, natural nanopolymer applications in the packaging industry can be organized around the main topics, to introduce nanocomposite organic/inorganic materials and to introduce some good examples to produce films, coatings, etc. Detailed discussions about each of these topics are also considered in this chapter.

Keywords Assessment tests · Food packaging · Nanobiopolymers · Nanocomposites · Natural polymers

B. Tajeddin (✉)
Packaging Engineering, Food Engineering and Post-Harvest Technology Research Department, Agricultural Engineering Research Institute, P. O. Box: 31585-845, Karaj, Iran
e-mail: behjattajeddin@gmail.com; behjat.tajeddin@yahoo.com

V.K. Thakur and M.K. Thakur (eds.), *Eco-friendly Polymer Nanocomposites*, Advanced Structured Materials 74, DOI 10.1007/978-81-322-2473-0_8

1 Introduction

It has been a long time since synthetic polymers such as polyethylene, polypropylene, polystyrene, polyethylene terephthalate, and polyvinyl chloride are being used as packaging materials. The reasons for this are the availability of abundant raw materials, low cost, good mechanical properties, and suitable barrier characteristics against oxygen, carbon dioxide, and aromatic compounds [106, 107]. The main problem of these synthetic packing materials is their long degradation time, which causes environmental pollution. In addition, the contamination of food by the migration of plastic packaging monomers is the other problem which reduces food safety and ends to the changes in its flavor [31]. Therefore, in order to meet environmental and economic issues in the plastics industry, it is important to reduce the environmental effluence of synthetic materials production by decreasing the environmental impact in every stage of their life cycle [108–112]. Thus, composites where the reinforcing or filler phase and/or the matrix are based on renewable resources (natural fibers/natural polymers) have currently been the subject of many researches for a number of applications [94–98]. For example, Poly vinyl chloride (PVC), as a hard thermoplastic, is widely used due to it being inexpensive, durable, and flexible in the applications such as in building materials pipe and plumbing. Mixing PVC with natural fibers is an interesting alternative. During the mixing with PVC, some natural fibers may act as reinforcing materials while other natural fibers only act as filler [129].

In general, the natural fiber-reinforced polymer composites are renewable, cheap, completely or partially recyclable, and biodegradable compared to their traditional synthetic counterparts [91–93]. These composites are having low density and cost as well as satisfactory mechanical properties make them attractive due to easy availability and renewability of raw materials. Natural fibers have been proven alternative to synthetic fiber in transportation such as automobiles, railway coaches, and aerospace [20, 113–117]. In fact, raw natural fiber-reinforced composites are the subject of numerous scientific and research projects, as well as many commercial programs. Other applications include military, building, packaging, consumer products, and construction industries for ceiling paneling, partition boards are subjected to use the natural fibers [20, 119]. Some properties of natural and synthetic fibers [127] are shown in Table 1.

Table 1 Selected properties of natural and synthetic fibers [127]

Fiber	Density (g/cm^3)	Tensile strength (Mpa)	Specific tensile strength (Mpa)	Elastic modulus (Gpa)	Specific elastic modulus (GPa)
Cotton	1.5–1.6	400	250–267	5.5–12.6	3.5–8.1
Kenaf	1.45	930	641	53	36.5
Sisal	1.5	511–635	341–423	9.4–22	6.3–14.7
E-glass	2.5	2,000–3,500	800–1,400	70	28
Carbon	1.4	4,000	2,857	230–240	164–171

Table 2 Chemical composition of some common natural vegetable fibers [49]

Type of fiber	Cellulose (%)	Lignin (%)
Cotton	85–90	0.7–1.6
Seed flax	43–47	21–23
Hemp	57–77	9–13
Abaca	56–63	7–9
Sisal	47–62	7–9
Bamboo	26–43	21–23
Kenaf	44–57	15–19
Jute	45–63	21–26
Papyrus	38–44	16–19
Sugarcane bagasse	32–37	18–26
Cereal straw	31–45	16–19
Corn straw	32–35	16–27
Wheat straw	33–39	16–23
Rice straw	28–36	12–16

The chemical content of natural fibers is very important in the composite formulation. Table 2 shows the chemical composition of some common natural vegetable fibers, as an example [49] which can be used in the biocomposites structure. The viability of the effective utilization of lignin (one of the three major components found in the cell walls of natural lignocellulosic materials) as an instance of potential sustainable green reinforcement in multifunctional polymer composites for advanced applications is discussed by Thakur et al. [120]. Natural cellulose fibers-based materials are the other example of natural fibers that are finding their applications in a number of fields ranging from automotive to biomedical. Natural cellulose fibers have been frequently used as the reinforcement component in polymers to add the specific properties in the final product. A variety of cellulose fibers-based polymer composite materials have been developed using various synthetic strategies [118]. Natural fibers can be used as packaging material especially to produce the packaging containers.

Different types of techniques have been frequently used to modify the multifunctional properties of natural cellulosic polymers [113–117]. On the other hand, natural polymers are widely used due to their properly characteristics to prepare biopolymers in some applications such as packaging industry. Mixing synthetic polymers with natural polymers is an interesting alternative as well as natural fibers. However, the hard works on the biocomposites and biopolymers have generated environment-friendly applications for many uses like packaging. Such ideas have led to the development of biodegradable packaging materials such as biocomposites, edible or inedible films, coatings, etc. In general, polysaccharides and protein-based materials or their blends are the worldwide interest examples of natural polymers or biopolymers [26, 41, 88, 123, 125, 132]. These polymers can be commonly used for preparation of film or coating forms in the food packaging area. Natural polymers and their some examples are mostly shown in Fig. 1 [3, 27, 104].

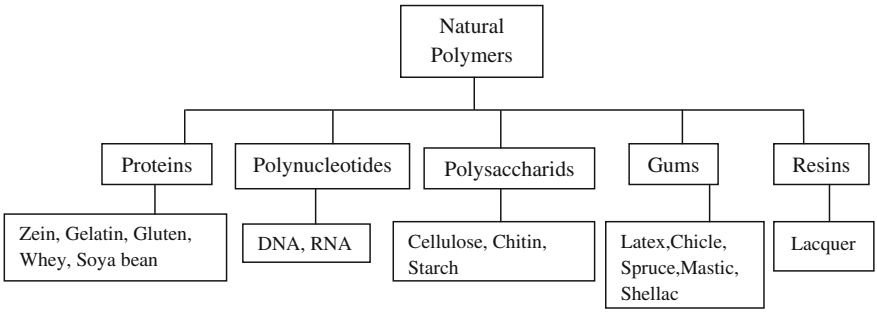

Fig. 1 A classification of natural polymers and some examples of them [3, 27, 104]

Several biopolymers have been exploited to develop materials for eco-friendly food packaging. However, the use of biopolymers has been limited because of their usually poor mechanical and barrier properties, which may be improved by adding reinforcing compounds (fillers), forming composites. Most reinforced materials present poor matrix–filler interactions, which tend to improve with decreasing filler dimensions. The use of fillers with at least one nanoscale dimension produces nanocomposites, a new class of composites [14]. Using natural fillers or natural reinforced materials with at least one nanoscale dimension creates nanobiocomposites. Therefore, nanobiocomposite application, as a novel issue and a new window in the packaging area is discussed mainly in this chapter.

To start, SCENIHR [83] defines nanocomposites, nanomaterials, nanocrystalline materials, and nanostructures as entities, the majority having one or more dimensions of the order of 100 nm or less. Based on their definition, nanocomposite is a multiphase material with the majority of the dispersed phase components in nanoscale; nanomaterial is any form of a material that is composed of discrete functional parts; nanocrystalline material is a material that is comprised of many crystals; and finally, nanostructure is any structure that is composed of discrete functional parts, either internally or at the surface.

Dispersing of the nano reinforcement into the matrix during processing leads to a lot of new properties [62, 63, 108]. The fillers in the food packaging applications may be in the different form of nanomaterials [48]. In general, depending on how many dimensions of the dispersed particles are in the nanometer range, nanocomposites can be classified as below [2, 48, 83, 90]:

1. Nanosheet, a discrete entity which has one dimension in the 100 nm level or less, and two long dimensions. Other things such as nanofilm, nanoplate, nanolayer, and very thin coatings comply with this definition, but may differ from each other by other characteristics (e.g., sheet is usually free and a layer is usually supported; there may be considerable differences in flexibility). The polymer-layered crystal nanocomposites is the other name for this family of composites. These materials are almost totally obtained by the intercalation of the polymer (or a monomer subsequently polymerized) inside the collection

of layered host crystals. There are many of both synthetic and natural crystalline fillers that are able to intercalate a polymer in the specific conditions.

2. Nanorod. This is a discrete entity which has two dimensions that are of the order of 100 nm or less, and one long dimension. Other entities such as nanofiber, nanowire, nanowhisker comply with this definition, but may differ from each other by other characteristics (e.g., rotational symmetry, flexibility). In general, a nanorod or nanofiber can be characterized by the aspect ratio, which is the ratio between length and diameter of the structure.
3. Nanotube. This is a discrete hollow entity which has two dimensions in the 100 nm level or less, and one long dimension. In fact, nanotubes are the nanometer-diameter cylinder forms. Nanotubes create an elongated structure. Carbon nanotubes and cellulose whiskers are examples of nanotubes which are considerably studied as reinforcing nanofiller materials. Although, nanotubes are said as an example of one-dimensional nanocomposites by Ajayan [1].
4. Nanoparticle or nanoparticulate matter. This is a discrete entity which has three dimensions with the 100 nm scale or less. Nanoparticles are typically defined as solids less than 100 nm in all three dimensions, such as spherical silica nanoparticles obtained by in situ sol–gel methods or by polymerization promoted directly from their surface. Azeredo [14] overviewed the main kinds of nanoparticles used in the food packaging systems and their effects and applications.

Haldorai et al. [47] reported that the nanoscale dimensions of particles such as metal oxides, carbon materials, semiconductor metallic nanocrystals, and clays can be incorporated to the polymers. Nanocomposites are currently being used in a number of fields and new applications are continuously being developed including thin-film capacitors, electrolytes for batteries, biomaterials, and a variety of devices in solar and fuel cells. The synthesis of polymeric composites usually involves solution chemistry, and because of this, a large amount of organic solvents may use.

In recent years, the use of nanomaterials has been considered in production of biodegradable packaging materials. Films of nanomaterials and biopolymers or the so-called nanocomposite biopolymers show better functional properties compared to other synthetic or biosynthetic films, particularly in their mechanical strength and the reduction of permeability to water vapor. The cause of the improved properties in nanocomposites is the interfacial interaction between the matrix and the nanomaterials; this interaction occurs more in nanocomposites than in conventional composites [28]. In general, nanobiocomposites are a class of biopolymer films that contain the following two main parts: biodegradable polymer, which acts as the matrix, and nanopolymers as the filler or reinforcement that must also be biodegradable [8]. Nanoparticles have proportionally larger surface area than their microscale counterparts, which favors the filler–matrix interactions and the performance of the resulting material. Besides nanoreinforcements, nanoparticles can have other functions when added to a polymer, such as antimicrobial activity, enzyme immobilization, biosensing, etc. [14].

2 Natural Nanocomposite Materials and Food Packaging

Rapid developments in nanotechnology have come to public attention as potentially one of the most significant technological advances for the food packaging industry contain a polymer plus a nano-additive in recent years. On the other hand, natural biopolymers have been paid more attention as alternatives to the petroleum-derived plastics for packaging films production. Mostly nanoclay particulates are used, although other composites containing nanoparticles, nanotubes, or nanofibers are also being developed. Biobased nanocomposites (PLA-clay, cellulose nanofibers) and metal (oxide)-polymer composites are also being developed. Therefore, different biopolymers with novel characteristics were proposed to the market and could be used in producing edible films. The thin films with thickness <50 μm [100] containing nanomaterials has created more novelty in the film properties. For example, the film containing nanoadditives like antimicrobial agents is a type of active packaging which is mainly designed to control microbial and chemical spoilage of food.

In general, the main role of nanopackaging is its small size that resulted in large surface area, and greater functionality per equivalent mass. Food packaging is the largest area of application of nanotechnology within the food sector, and clay particles at the nanoscale are the most common applications in food packaging. They are less expensive to produce than other nanomaterials because full-scale facilities already exist and basic materials are available from natural sources [90].

The nanoparticles are used in the food packaging in order to protect the food from dust, gases (O_2, CO_2), light, pathogens, and moisture. This packaging method is more safe, inert, inexpensive to produce, and easy to dispose. Traditional packaging materials such as metal, glass, paper, plastics (PP, PE, PS, PVC), or multilayers of polymers, are amended with nanosized components. The majority of nanopackaging contains nanoplatelets of clay minerals, where montmorriolonite can be mentioned as an example [54]. Among nanotechnical applications, nanocomposite food packaging, which combines the nanomaterials and conventional packaging, is at the front of applications in nanotechnologies, leading the whole industrial chain based on nanotechnologies with high-speed development [48]. Current usage of nanotechnology in the food packaging area includes nanoclays, cellulosic nanomaterials, nanoemulsions, electrospun nanofibers and nanocapsules, carbon based nanomaterials, nanoparticles of metal and metal oxides, and nanoparticle containing carriers. These nanomaterials are used as an efficient gas, UV light, and vapor barrier, to enhance mechanical and thermal properties, to reduce migration issues, and to provide controlled release, and active or bioactive functionalities to packaging. The high surface-to-volume ratio of many nanoscale structures which favors this improved performance of packaging materials, also becomes ideal for applications that involve chemical reactions, drug delivery, controlled and immediate release of substances in active functional food packaging technologies and energy storage in, for instance, intelligent food packaging [61].

Several applications of nanomaterials in food packaging and food safety including polymer/clay nanocomposites as high-barrier packaging materials, silver nanoparticles as potent antimicrobial agents, and nanosensors and nanomaterial-based assays for the detection of food relevant analytes (gases, small organic molecules, and food-borne pathogens) were reviewed by Duncan [32]. These applications were chosen because they do not involve direct addition of nanoparticles to consumed foods, and thus are more likely to be marketed to the public in the short term.

The main biodegradable polymers (natural and synthetic) are presented as a possible alternative to conventional plastics. These polymers may be adequate for food packaging applications, although there are some drawbacks such as their poor mechanical or barrier properties. One of the most promising ways to improve the functionality of biodegradable polymers is the incorporation of nanomaterials [55]. Rhim and Ng [78] reviewed the preparation of natural polymer-based films and their nanocomposites, and their potential use in packaging applications. The bio-based materials that are usually considered in the food packaging may be classified into four families that many of them can be used with nanoscale structure:

1. Polymers directly extracted from biomass, such as the polysaccharides like chitosan, starch, carrageenan, and cellulose; proteins such as gluten, soy, and zein; and various lipids.
2. Biomass-derived monomers which use classical chemical synthetic routes to obtain the final biodegradable and/or renewable polymers, including thermoplastics and thermosets. In regard to thermoplastics, this is the case of polylactic acid (PLA) and the nonbiodegradable sugarcane ethanol-derived biopolyethylene.
3. Polymers produced by natural or genetically modified microorganisms such as polyhydroxyalcanoates (PHA) and polypeptides.
4. Mixtures of biobased- and petroleum-based monomers, such as polycaprolactones (PCL), polyvinylalcohol (PVOH) and its copolymers with ethylene (EVOH), and some biopolyesters.

Sanchez-Garcia et al. [81] presented the properties of nanobiocomposites of solvent cast polyhydroxybutyrate-co-valerate (PHBV) and polycaprolactone (PCL) containing carbon nanofiber or carbon nanotubes as a function of filler content. They found that carbon nanotubes and nanofibers can be used to enhance the conductivity, thermal, mechanical, and gas barrier properties of thermoplastic biopolyesters.

Han et al. [48] reported that in the area of food packaging, the nanocomposite, which combines the traditional food packaging materials with the nanomaterials (NMs), has been subjected to high-speed development in the food packaging market with its excellent mechanical performance and good antibacterial and stronger resistant properties. The manufacturing methods and skills in combining NMs into packaging materials, such as polymers, paper and paperboard, glass and ceramic, and the surface of metals, are well developed. According to laboratory

research, market-oriented applications, and development trends, three main categories of nanotechnology are used in food packaging applications:

1. Nanoparticles (NPs)-reinforced packaging. The high surface area enables NPs to dramatically improve the mechanical performance, such as flexibility, reduced gaseous permeation, stability of temperature and humidity, and ultraviolet light and flame resistance, of packaging materials with a relatively low mass content (∼5 %, w/w). The matrix material properties are significantly affected in the vicinity of the reinforcement [84]. Apart from improving mechanical properties, the application of NPs can bring extra functions, such as an antibacterial property, to food packaging. Silver (Ag) NPs used in packaging or food contact materials can prolong foodstuff shelf life by restraining the growth of bacteria. For example, the NPs-polymer composites can form coatings on the surface of tableware and kitchenware to inhibit the growth of microorganisms.
   Engineered or manufactured NPs, nanosized particles occur naturally in many foodstuffs. For example, food proteins are globular structures between 10 and 100 nm (e.g., casein micelles in dairy products range from 300 to 400 nm) and most polysaccharides and lipids are linear polymers of 2 nm thickness. Fat globules can be considered as natural NPs as well, ranging in size from 100 nm to 20 μm, whereas fat globule membranes have a thickness of 4–25 nm. The homogenization of fat globules can be considered as a sort of "nanotechnology process" decreasing the average diameter and increasing the number and surface area of the fat globules [52]. The main challenge faced by nanocomposite materials is a good nanofiller–matrix interaction for reinforcing purposes. Nanocomposites usually contain 1–7 wt% nanofillers in the food biopackaging. It has been observed that the matrix–filler interactions significantly improve when reducing the size of the reinforcing agent [61].
2. Active and intelligent packaging. The active and intelligent food packaging category is a novel type of packaging compared with traditional methods. In active and intelligent food packaging, the "active" refers to the packaging which has the ability to remove undesirable tastes and flavor, and improve the color or smell of the packed food. "Intelligent" food packaging seems to have an extensive application than "active" packaging. In general, the "intelligent" aspect of food packaging refers to the concept of monitoring information about the quality of the packed food. Huyghebaert et al. [52] stated a number of applications that include smart packaging, nanosensors for pathogen detection or registration of storage conditions, nanoformulations of agrochemicals, nanoencapsulation/nanodelivery of food ingredients, etc.
3. Biodegradable nanocomposites food packaging. The biodegradable nanocomposite food packaging category involves new types of biodegradable materials, which in general can be made of polylactic acid (PLA) and montmorillonite (MMT). The naturally existing nanolayered structure limits the permeation of gases, and provides substantial improvements in gas barrier properties of the nanocomposite. Such improvements have led to the development of PLA-MMT nanocomposites for potential use in a variety of food packaging applications,

such as processed meats, cheese, confectionery, cereals, as well as boil-in-the-bag foods. Busolo et al. [22] studied the PLA biocomposites, obtained by solvent casting, containing a silver-based antimicrobial layered silicate additive for use in active food packaging applications. The silver-based nanoclay showed strong antimicrobial activity against gram-negative Salmonella spp. Despite the fact that no exfoliation of the silver-based nanoclay in PLA was observed, as suggested by TEM and wide angle X-ray scattering (WAXS) experiments, the additive dispersed nicely throughout the PLA matrix to a nanoscale, yielding nanobiocomposites. The films were highly transparent with enhanced water barrier and strong biocidal properties.

Avella et al. [10] prepared a biodegradable starch/clay nanocomposite films, to be used for food packaging, were obtained by homogeneously dispersing montmorillonite nanoparticles in different starch-based materials via polymer melt processing techniques. The results show, in the case of starch/clay material, a good intercalation of the polymeric phase into clay interlayer galleries, together with an increase of mechanical parameters, such as modulus and tensile strength.

Totally, the natural nanobiobased polymers applications in the packaging industry can be organized around the main topics, nanocomposite organic/inorganic materials. In fact, they can be entirely inorganic, entirely organic, or a mixture of inorganic and organic materials. Even where the final material may be entirely one class of material, multiple classes of materials may have been involved in the synthetic process, which may or may not remain in the final structure [21].

2.1 Inorganic Nanocomposite Materials

Inorganic layered materials exist in great variety. They possess well defined, ordered intralamellar space potentially accessible by foreign species. Inorganic materials play an important role in the creation of the nanostructured and nanocomposite materials so commonly found in nature. Materials scientists, chemists, and packaging specialists have made considerable efforts to create synthetic nanobiocomposites using inorganic materials. Considerable efforts have led to use many natural inorganic materials to create new packaging materials with different properties. The inorganic components can be three-dimensional framework systems (embedded networks) such as zeolites, two-dimensional layered materials (nanoscale coatings) like clays, metal oxides, metal phosphates, chalcogenides, one-dimensional and zero-dimensional materials (embedded clusters) such as molybdenum selenide $(Mo_3Se_{3-})_n$ chains and clusters [1].

Among all potential nanocomposite precursors, those based on clay and layered silicates are more widely investigated probably because the starting clay materials are easily available and because their intercalation chemistry has been studied for a long time. Owing to the nanometer-size particles obtained by dispersion, these nanocomposites exhibit markedly improved mechanical, thermal, optical, and

physicochemical properties when compared with the pure polymer or conventional (microscale) composites. Improvements can include, for example, increased strength and heat resistance, decreased gas permeability, and flammability [2].

Furthermore, inorganic materials are mostly utilized in the structure of magnetic nanoparticles. Magnetic nanoparticles are an important class of nanoparticle which can be manipulated using magnetic field. These are a class of functional materials, possessing unique magnetic properties due to their reduced size (below 100 nm) with potential for use in devices with reduced dimensions. Such particles commonly consist of magnetic elements such as iron, nickel, cobalt and their chemical compounds [128]. The synthesis of iron oxide magnetic nanoparticles via a reverse micelle system and modification of their surface through an organosilane agent was discussed by Osaka et al. [73]. Faraji and Fadavi [39] reported that magnetic iron oxide nanoparticles have been used in many fields, because of their unique properties such as large specific surface area and convenient separation in magnetic fields. These nanoparticles have high potential application in food science and technology such as enzyme immobilization, protein purification, and food analysis. However, there has been impulse for development of inorganic nanoparticles with structures that show novel physical, chemical, and biological properties [126]. For example, the potential benefits of nanosilver materials have been accepted in many applications due to the strong antimicrobial activity of silver against bacteria, viruses, and fungi [29, 79].

Braun [21] stated that bacteria in general are responsible for a vast amount of mineral deposition and in fact can contribute greatly to mineral deposits on the bottom of lakes and other aquatic environments. Mineral formation in the vicinity of bacteria is generally driven by a biologically induced change in the pH or ionic strength around individual bacteria. This change in the local environment reduces the solubility of certain mineral compounds, leading to precipitation of minerals.

2.1.1 Nanoclay

As cited in Alexandre and Dubois [2], Kojima and coworkers [59] studied the improvement of mechanical and the other properties of Nylon/clay nanocomposites first.

Lagaron [61] reported that the extensive research work has been performed in the study of nanocomposites for food packaging applications, since Toyota researchers in the late 1980s found that mechanical, thermal, and barrier properties of nylon–nanoclay composite material improved dramatically by reinforcing with less than 5 % of nanoclay. The nanoclay has a natural nanolayer structure that provides a barrier to permeation of gases (in 2–5 % conc.). It is commonly used in montmorillonite, derived from volcanic ash/rocks [90].

Montmorillonite, hectorite, and saponite types of clay are the most commonly used layered silicates [56]. Smectite clay is another type of clay [101].

Alexandre and Dubois [2] reported that there are four main strategies to prepare polymer-layered silicate nanocomposites. The whole range of polymer matrices is

covered, i.e., thermoplastics, thermosets, and elastomers. The four methods are stated below:

1. Exfoliation–adsorption: the layered silicate is exfoliated into single layers using a solvent in which the polymer (or a prepolymer in case of insoluble polymers such as polyimide) is soluble;
2. In situ intercalative polymerization: the layered silicate is swollen within the liquid monomer (or a monomer solution) so as the polymer formation can occur in between the intercalated sheets;
3. Melt intercalation: the layered silicate is mixed with the polymer matrix in the molten state;
4. Template synthesis: the silicates are formed in situ in an aqueous solution containing the polymer and the silicate building blocks have been widely used for the synthesis of double-layer hydroxide-based nanocomposites but is far less developed for layered silicates.

Dadashi et al. [28] examined the physical, mechanical, and structural properties of poly(lactic acid) (PLA)-based films containing nanoclay and microcrystalline cellulose (MCC, 3, 5 and 7 %) prepared by solvent (chloroform) casting method for packaging and other applications. Physical properties including thickness, transparency, and color did not change significantly with addition of nanoparticles to the polymer matrix. XRD patterns showed that pure PLA has a semicrystalline structure and addition of nanoclay into this polymer would produce more regular structure that results in improved crystallization. Because of the nature and particle size of the MCC, it did not interact sufficiently with the polymer. Tensile strength, elastic modulus, and elongation at break of neat PLA were 27.44 MPa, 1.84 GPa, and 24.53 % which with the addition of 7 % of nanoclay, was changed to 40.34, 2.62, and 10.36, respectively. As the results of XRD, MCC were indicated, there was no significant effect on the mechanical properties, AFM images were used to evaluate the surface morphology and roughness of PLA films. Neat PLA had smoother surfaces and a lower roughness parameter.

The effect of two types of polyethylene–clay nanocomposite films with thicknesses of 45 and 50 μm on the staling and the shelf life of sliced bread was studied by Keshavarzian et al. [57]. They packed the sliced bread in the polyethylene (control) and the nanocomposite films and stored them at 25 °C for 10 days. The results showed that water retention was higher for samples packed in nanocomposite film. The melting enthalpy of ice measured by DSC was lower, but the melting enthalpy of starch was higher for the control, indicating that nanocomposite packaging delayed the staling of the bread samples. The growth of mold was high in all samples. Although, the nanocomposite film retarded staling of sliced bread, it did not control mold growth because of the higher moisture content inside this type of packaging. The addition of antimicrobial agents to the nanocomposite film is required to take advantage of the increased preservation of freshness from this type of packaging.

2.1.2 Nanosilver

There is a special attention on the effects of silver nanoparticles and its antimicrobial impact, due to development of microbial resistance against chemical antimicrobial agents. The antimicrobial effect of silver additives is mostly used in a variety of injection-molded plastic products, textiles, coating-based applications such as food preparation areas, etc. [40, 42]. Silver-based antimicrobial additives consist of silver ions integrated into inert matrices consisting of ceramic, glass, or zeolite, in general. Other silver additives based on silver salts or metallic silver may be readily incorporated into thermoplastic polymers, such as polyethylene, polypropylene, polystyrene, or nylon [6]. Some important advantages of silver-based antimicrobials are their excellent thermal stability and their health and environmental safety [60]. However, application of the silver is sternly controlled by various national laws and control agencies, as well as the use of all biocide products.

Exposure of microorganisms to silver nanoparticles was shown to result in strong antimicrobial activity. In addition to the increased surface area and associated increased potential for the release of Ag^+, when dispersed in liquid suspensions, silver nanoparticles may accumulate in the bacterial cytoplasmic membrane, causing a significant increase in permeability and cell death [99]. Asadi Asadabadi et al. [11] studied the antibacterial effects of different concentrations of silver nanoparticles on *Staphylococcus aureus* and *Escherichia coli*. They produced the silver nanoparticles by chemical reduction. Manitol Salt Agar and Eosin Methylene Blue media were used as specific media for *S. aureus* and *E. coli*, respectively, and Mueller-Hinton medium was used to examine the antimicrobial properties of the cultures. Kind of bacterium, duration of microbial contact with nanosilver (1, 12, 24, 48 h), and the concentration of nanoparticles (5, 10, 25, 50 ppm) were the qualitative factors in their research. The results showed that all three factors have significant impacts on the microbial growth, but kind of bacterium and nanoparticle concentration showed more significant influence. In low concentration of nanosilver, *E. coli* showed more resistance to presence of nanoparticle in comparison with *S. aureus*. The minimum inhibitory concentration of silver nanoparticles for *S. aureus* and *E. coli* was 5 and 10 ppm. A concentration of 50 ppm of silver nanoparticles completely eliminated both bacteria.

Kumar and Münstedt [60] studied the effect of crystallinity on the silver ion release in the polyamide/silver composites by means of DSC. They reported that the bactericidal efficiency of polymer containing silver is based on the release of silver ions (Ag^+) in an aqueous medium. Egger et al. [34] used in vitro tests to display the antimicrobial activity of a silver–silica nanocomposite compared to the activities of conventional materials, such as silver nitrate ($AgNO_3$; 63.5 % Ag) and silver zeolite (38 % Ag bound to type A zeolite). A silver–silica-containing polystyrene material was produced using an industrial flame spray pyrolysis process. This process involves combustion of a flammable solvent containing homogeneously dissolved compounds as the source of components for the synthesis of the material. The scanning transmission electron micrograph results showed that the nanocomposite

consists of silver nanoparticles embedded in a matrix of amorphous silicon dioxide (SiO_2). The SiO_2 fine structure consists of aggregate matrix particles with an average diameter of approximately 1 μm. Silver metal particles are located on the surface of the silica and are also embedded within the matrix and each silica particle contains many small silver metal particles with a typical diameter between 1 and 10 nm. The specific surface area of the nanocomposite powder, as measured by nitrogen adsorption, is typically about 250 m^2/g, a value which is consistent with the open structure of the silica aggregate. To examine the antimicrobial properties of a typical application product, silver-containing polystyrene plates were manufactured from commercially available polystyrene polymer (clear, unfilled) using a thermoplastic injection-molding process. They concluded that the pure silver particles exhibits very good antimicrobial activity against a wide range of microorganisms due to releasing of silver ions, which represent the active antimicrobial principle.

Due to the quality changing of fruits and vegetables as living tissues after harvesting, Zandi et al. [131] studied the effect of nanocomposite-based packaging on the postharvest quality of strawberry fruit during storage. Two factors, including conventional polymer packaging (control) and nanocomposite in four types (nanosilver based on PE, nanosilver based on PP containing, nanosilicate based on PE, nanosilicate based on PP) and time of storage in four levels (0, 3, 7 and 10 days after storage) were investigated. The results showed that fruits stored in nanosilver and nanosilicate based on PE and PP containers generally emitted lower levels of weight loss compounds than those stored in conventional polymer.

Emamifar et al. [36] studied the potential of zinc oxide (ZnO-) and Ag-filled LDPE (low-density polyethylene) nanoparticle packaging to preserve the maximum nutritional value, freshness, and shelf life of orange juice. Nanocomposite LDPE films containing Ag and ZnO nanoparticles were prepared by melt mixing in a twin-screw extruder and were then filled with fresh orange juice and stored at 4 °C. The results of different tests showed that microbial growth significantly decreased due to using the nanocomposite packaging up to 28 days of storage ($p < 0.05$). Reduced degradation of ascorbic acid and development of brown pigments were also observed ($p < 0.05$) in the orange juice packaged in nanocomposite packages containing 0.25 % of nano-ZnO. Moreover, odor, taste, and overall sensory attributes ranked highest for the orange juice packed after 28 days of storage ($p < 0.05$). Packages containing nanosilver increased the shelf life of fresh orange juice to 28 days at 4 °C.

2.1.3 Other Examples

Researchers from the University of Leeds, UK, discovered the antimicrobial properties of nano-zinc oxide (ZnO) and magnesium oxide (MgO). Compared with Ag nanoparticles (NPs), the ZnO and MgO NPs are expected to provide not only more affordable and safe food packaging solutions in the future, but also a greater ability to inhibit the growth of microorganisms [48].

Ethylene plays an effective role in the loss of apple quality. Sardabi et al. [82] studied the effect of ethylene reduction on improving the quality of Golden and Red Delicious apples during cold storage by active packaging. They used 1-methylcyclopropene (1-MCP, 0 and 1 ppm) and 0 and 10 g of potassium permanganate-coated zeolite nanoparticles (ethylene absorber sachets) in their packaging design. Fruit quality important parameters were evaluated before storage and on a monthly basis during the storage period (0.5 °C and 90 % RH for up to 5 months). They concluded that the application of 1-MCP combined with ethylene absorber sachets had the best effect on the quality characteristics of both apple species. Red Delicious apples were firmer and fresher in appearance, indicating that this variety has better storability.

Many species of grass precipitate SiO_2 nanoparticles within their cellular structures. Due to some internal structure in their cells, the silica nanoparticles generated within the cells can be found in sheet-like, globular, or rod-like morphologies, with characteristic dimensions ranging from a few nanometers to tens of nanometers. The reason for the silica deposition may simply be a way for the plant to sequester silica, which it continuously takes in as dissolved silicic acid and other silica-containing soluble species. If the plant could not sequester silica, it would build up and potentially limit growth [21].

Nanotitanium nitride with the mechanical strength and as a processing aid is reported by Simoneau [90]. In addition, Nanoaluminium (as coating) is used in flexible packaging, improving the properties of foil surface, high barrier properties for gases (CO_2 and oxygen), UV screening effect, antiadhesive coating, color coatings, coatings reducing heat reflection. Antiadhesive coating or black coating of baking foil which does not reflect heat in an oven is an example of nanoaluminium application.

2.2 Organic Nanocomposite Materials

In general, lipid cellular membranes, ion channels, proteins, DNA, actin, spider silk, etc. are a few examples of nanoscale materials in biology. In all these structures, the characteristic dimension, at least in 1D, and often in 3D, is about a few nanometers. One completely organic nanocomposite with outstanding properties is spider silk; which makes up the spokes of a spider web. It is five times tougher than steel by weight and can stretch 30–40 % without breaking, while the elastic modulus of silk is significantly less than that of steel [21]. Although this particular nanocomposite is quite fascinating, it was just mentioned as an example of the organic nanocomposites and unfortunately does not yet have any applications in the food packaging industry. Compared with the synthetic polymers, natural polymers like proteins and polysaccharides are renewable, biocompatible, and biodegradable. Abundant polysaccharide polymers in nature such as cellulose, chitin, starch are increasingly being used for the preparation of nanocomposites.

Wang et al. [124] assessed the organic film-forming potential of six types of proteins (0–16 %), as well as six types of polysaccharides (0–4 %) at heating temperatures (60–80 °C). Sodium caseinate (SC), whey protein isolate (WPI), gelatine (G), carboxymethyl cellulose (CMC), sodium alginate (SA) and potato starch (PS) biopolymer films were evaluated. Optimal film-forming conditions were achieved using SC and G (4 and 8 %), WPI (8 and 12 %), PS, CMC (2 and 3 %), or SA (1 and 1.5 %) solutions heated to 80 °C in combination with 50 % (w/w) glycerol.

2.2.1 Polysaccharides

Polysaccharides such as cellulose, starch, chitin or chitosan, etc. are high molecular weight carbohydrates which can be derived from many sources. They can be used in the preparation of edible films and coatings. In recent years, the nanoscale of polysaccharide materials like cellulose and chitosan is used in the food packaging applications.

Nanocellulose

Cellulose is the most abundant biomass on the earth and its use in the preparation of biobased nanomaterials has gained a growing interest during the recent years. This interest can be illustrated by how the number of scientific publications on the cellulose nanomaterial research has grown very rapidly. The research topics have been published in the extraction of cellulose nanofibers and nanocrystals from different raw material sources, their chemical modification, characterization of their properties, their use as an additive or a reinforcement in different polymers, composite preparation, as well as their ability to self-assemble. Nanocelluloses, both fibers and crystals, have been shown to have promising and interesting properties, and the abundance of cellulosic waste residues has encouraged their utilization as a main raw material source. Cellulose nanofibrils have more advantages such as fine diameter, large aspect ratio, biocompatibility, high strength and modulus as well as other favorable physical properties associated with the highly crystalline extended chain conformation [19]. In addition, cellulose nanoparticles have high biodegradability rates and are less expensive than other nanofillers [30].

Dehnad et al. [30] prepared chitosan (powder form with a molecular weight of 600–800 kDa)-nanocellulose (20–50 nm in diameter) and absolute glycerol nanocomposites. The performance of the nanocomposite films on improving the shelf life of ground meat was studied. Results showed that increasing the nanocellulose level from 0 to 2 % (w/w chitosan) decreased the melting point and glass transition temperature of the nanocellulose. Chitosan–nanocellulose nanocomposites provided antimicrobial effects against gram-positive and gram-negative bacteria throughout the contact area. The application of chitosan–nanocellulose nanocomposites to ground meat decreased the lactic acid bacteria population of the product

up to three logarithmic cycles over the control sample. They recommended that the chitosan–nanocellulose nanocomposite with high thermal stability and antimicrobial properties is suitable as packaging material for products that undergo high spoilage rates and short shelf life, such as meat products.

Nanochitosan

Chitosan with $(C_6H_{11}NO_5)_n$ formula, is a natural polymer that is mainly found in the living organisms including exoskeleton and the inner structure of invertebrates residents as well as the crustaceans like shrimp and crab shell, insects, and some fungi [33, 77]. Chitosan is a natural antimicrobial compound against bacteria, yeast, and fungi [30].

Among different nanoparticles, chitosan nanoparticles are more significant [76]. Due to suitable mechanical, thermal, nontoxic, and antimicrobial characteristics, and natural compatibility with living organisms, chitosan nanoparticles have considerable potential as a nanobiopolymer packaging material [44, 65]. Chitosan has also reached a prominent position as carrier-forming material [15]. Grehna [44] reviewed a detailed description of methods used to produce chitosan nanocarriers.

Study results of Martínez-Camacho et al. [66] suggested that it is feasible to elaborate antifungal shrimp chitosan films, with good thermal stability and acceptable mechanical properties for food packaging. According to FTIR spectroscopic analysis of chitosan films, the fungistatic activity can be related to the hydrogen bonds' formation between the amino groups of chitosan with the hydroxyl groups from polymer or sorbitol.

Moradi et al. [70] studied the antimicrobial, antioxidant, and color properties of chitosan film incorporated with essential oil of Zataria multiflora Boiss (ZEO). In this experimental research, chitosan films containing 0, 0.5, 1, and 2 % ZEO, were obtained by casting method and subsequently, total phenol, antioxidant, color, and antimicrobial characteristics of films on *Listeria monocytogenes* were studied. The results indicated that an active film from chitosan could be achieved by incorporating ZEO. Addition of ZEO improves functional and antibacterial characteristics of chitosan film.

Yien Ing et al. [130] investigated the antifungal activity of chitosan nanoparticles and correlation with their physical properties. Antimicrobial effect of chitosan nanoparticles on *Streptococcus mutans* biofilms was studied by Paz et al. [75]. Since strawberries are highly sensitive to fungal agents and have a short shelf life, Eshghi et al. [37] used nanoemulsion chitosan instead of chemical fungicides to extend shelf life of strawberry fruit. Thus, they assessed the efficiency of an edible coating based on chitosan nanoemulsion in delaying perishability, quality preservation, and increasing the shelf life of strawberries. Strawberries were coated with 50–100 ± 10 nm particle sizes of nanoemulsion containing 0.5 % chitosan as an antimicrobial substance, and stored at a temperature of 4 °C ± 1 with 70 % RH. Qualitative tests were assessed at 4 day intervals. As compared to uncoated samples, the results showed that coating strawberries had the positive effects on their

quality parameters. The treated samples were firmer, and their weight loss, respiration rate, and percent damage were lower. Also, anthocyanins and ascorbic acid content were better preserved in the coated strawberries than in the uncoated sample. Changes in acidity and soluble solids were not considerable. They concluded that the coating strawberries with a nanoemulsion containing chitosan increased the shelf life of fruit from 8 to 20 days (2.5 times as long).

2.2.2 Proteins

Protein-based films (manufactured using casein, whey, collagen, egg white, gelatin, fish derived protein, etc.) have attracted enormous interest due to their biodegradability and good barrier properties. Soy protein isolated (SPI), corn, and wheat protein also are candidates for producing edible films. Furthermore, whey and zein protein are byproducts of the food industries and have good film-making properties [3, 43]. However, protein-based nanostructure formation is discussed very well by Angellier-Coussy et al. [3] and Braun [21].

Chang et al. [23] studied the effects of layered silicate structure on mechanical properties and structures of protein-based bionanocomposites. They filled a non-conventional protein source of pea protein isolate (PPI) with montmorillonite (MMT) and rectorite (REC) by solution intercalation, respectively. The reinforced PPI-based nanocomposites were then produced by hot press. The structure and interaction in the nanocomposites were investigated by FTIR, XRD, DSC, DMA, and pH and Zeta potential tests whereas the reinforcing effect was verified by tensile test. Furthermore, the origin of enhancing mechanical performances and the effects of layered silicate structure were explored. Although the MMT with lower negative charge surface and smaller apparent size of crude particles was easier to be exfoliated completely, the exfoliated REC nanoplatelets with more negative charge could form stronger electrostatic interaction with positive-charge-rich domains of PPI molecules, and hence produced the highest strength in two series of nanocomposites. In this case, the newly formed hydrogen bonds and electrostatic interaction on the surface of silicate lamellas guaranteed the transferring of the stress to rigid layered silicates. The cooperative effect of newly formed physical interaction between layered silicates and PPI molecules as well as the spatial occupancy of intercalated agglomerates of layered silicates destroyed the original microphase structure of PPI matrix and cleaved the entanglements among PPI molecules. The elongation and strength properties did not enhance.

Zein

Maize zeins are the main storage proteins of maize (Zea mays) seeds and account for 50 % or more of total endospermic proteins. The zein proteins are hydrophobic and insoluble in water even with low salt concentrations and thus ethanol at high concentrations (60–95 %) is required to maintain their molecular conformations.

Parris and Coffin [74] produced transparent unplasticized zein films, using two types of solvent, ethanol, and acetone. Their work results showed that tensile properties in films prepared with acetone (TS = 14.4 MPa) were stronger but less flexible than those prepared in ethanol (TS = 10.9 MPa). Incorporation of plasticizer (glycerol/poly(propylene glycol) ratio of 1/3) into zein films resulted in an almost doubling in water vapor permeability values.

Ghanbarzadeh and Oromiehi [43] studied the barrier, mechanical properties, and AFM analysis of biodegradable biocomposite single and laminated films based on whey protein and zein. Glycerol and olive oil were used as plasticizer. They reported that one of the important factors, which may cause the zein used in the preparation of films, is high tensile strength (TS) compared to other protein-based films. The laminated films exhibited higher ultimate tensile strength (UTS) than the single whey protein films (260 and 200 % in the whey–zein–glycerol and whey–zein–olive oil films, respectively). The UTS of the whey protein films increased two and three fold after lamination. The laminated films showed higher barrier properties than the single whey protein films (180 % in the whey protein–zein–glycerol films and 200 % in the whey protein–zein–olive oil films in comparison to single whey protein films) and lower than the single zein films.

Argüello-García et al. [7] investigated the effect of zein and film formulation on mechanical and structural properties of native (FNS), and oxidized with 2.5 % (FOSA) and 3.5 % (FOSB) banana starch. The oxidized starch showed differences from native starch due to the oxidation process, showing a decrease in lipids, proteins, and amylose. The increase of the sodium hypochlorite increased the content of carbonyl and carboxyl groups in the ranges 0.015–0.028 % and 0.022–0.031 %, respectively. The film obtained from FOSB displayed the highest TS (5.05 MPa) and satisfactory elongation value (27.1 %). The zein addition caused a decrease in these mechanical properties, as well as a significant decrease in water vapor permeability (WVP). However, films from FOSA and FOSB showed higher permeability than that of the native starch. The addition of glycerol and the level of oxidation increased the films moisture. Micrographs showed that, during the oxidation process, impurities were largely eliminated from the starch granule, noting more homogeneous structures both in granules and films.

AFM was used to investigate the nanostructure of zein from maize (Zea mays) by Guoa et al. [45]. In aqueous ethanol solution zein exists as small globules with diameters between 150 and 550 nm.

Gelatin

Gelatin is a protein that is commercially obtained from skins and bones of cattle and pigs following slaughter. There are some works on the gelatin as a biopolymer material. For example, Khoshnoudinia and Sedaghat [58] investigated the effect of gelatin coating, containing ascorbic acid (AA:1 % w/v) and propyl gallate (PG:100 ppm), on the instrumental and sensory properties of roasted pistachio (hardness and color). Pistachio nuts are packed and stored at 35 and 5 °C.

The results indicated that there are strong relationships between the instrumental and sensory hardness values, but sensory and instrumental color values had a weak correlation with each other. According to Wang et al. [124] in the screening of numerous food ingredients to establish the film-forming ability, gelatin was one of the biopolymer materials assessed which demonstrated desirable film-forming properties.

2.2.3 Lipids

Lipids are not polymers. However, they are natural macromolecules that mainly use as nanocarrier systems to stabilize the bioactive materials against a range of environmental and chemical changes in the encapsulation technologies or in the active packaging. Research and development on nanocarrier lipid systems, for example, using antimicrobials for the protection and preservation of foodstuffs in active packaging methods has remained relatively unexplored.

Various types of encapsulation methods are employed in the food industry through nanoparticles, nanospheres, nanoemulsions, nanocochleates, nanoliposomes, etc. Liposomes are found in the natural lipids. Nanoliposomes, or nanometric versions of liposomes, are lipid vesicles that are under intensive research and development by the different industries like food industries as nanocarrier systems for the protection and delivery of bioactive agents. Nanoliposomes are colloidal structures formed by the input of energy to a right combination of constituent molecules (mainly phospholipids) in an aqueous solution [71, 72, 87]. In fact, the encapsulation of nutraceutical compounds in lipid-based carrier systems, such as nanoliposomes, is an effective method in preserving their native properties throughout their shelf life. Liposomes are widely used in food industries because of their benefits, which include possible large-scale production using natural ingredients, nontoxic, entrapment and release of water-soluble, lipid-soluble, amphiphilic materials, and biodegradability [17, 69].

Mohammadi et al. [68] recommended the application of liposomes as a nanocarrier of ripening accelerated cheese enzyme in cheese production and ripening. Mohammadi et al. [69] studied vitamin D_3 nanoliposomes and characterized them using DCS and SEM. Nanoliposomes containing vitamin D_3 were prepared using different quantities of phosphatidylcholine (PC) and cholesterol (60–0, 50–10, 40–20, 30–30 mg) equivalents (8–0, 7–3, 5–5, 4–8 mM) using thin-film hydration and sonication. The physicochemical properties of the liposomes results showed that particle size was 78–89 nm and size distribution (span) was 0.77–0.84 nm. In all treatments, the encapsulation efficiency of vitamin D_3 was >90 %. The DSC thermogram of the vitamin-loaded liposome showed the disappearance of the melting endothermic peak of vitamin D_3 and a major endothermic peak at 227 °C, indicating that vitamin D_3 complex formed with the bilayers and was completely encapsulated by the lipid matrix of the nanoliposomes. The lower melting temperature of proliposome over bulk lecithin can be attributed to its small particle size. SEM analysis showed that the surface morphology of all freeze-dried liposome samples had a porous structure.

It is said that there is an inverse relationship between the consumption of omega-3 polyunsaturated fatty acids (PUFA) and risk of cardiovascular disease (CVD), thus Hadian et al. [46] suggested that liposomal nanocarriers can increase stability and improve bioavailability of omega-3 PUFAs.

2.3 Hybrid Inorganic/Organic Nanocomposite Materials

Nanocomposites including organic polymers and inorganic materials show a significant improvement in stiffness, toughness, impact resistance, and hardness when compared with the pure polymer.

Intralamellar space potential of inorganic layered materials enables them to act as matrices or hosts for polymers, yielding interesting hybrid nanocomposite materials. Lamellar nanocomposites can be divided into two distinct classes, intercalated and exfoliated. In the former, the polymer chains alternate with the inorganic layers in a fixed compositional ratio and have a well-defined number of polymer layers in the intralamellar space. In exfoliated nanocomposites the number of polymer chains between the layers is almost continuously variable.

However, organic/inorganic nanocomposites have become a well-known area of current research and development in the field of nanotechnology. Since the remarkable properties of conventional composites are mainly due to interface interactions, these hybrid materials may be provided a wide range of good properties. The general class of organic/inorganic nanocomposites may also be of relevance to issues of bioceramics and biomineralization in which in situ growth and polymerization of biopolymer and inorganic matrix are occurring. In addition, lamellar nanocomposites represent an extreme case of a composite in which interface interactions between the two phases are maximized. Haldorai et al. [47] overviewed on the synthesis of polymer–inorganic filler nanocomposites in supercritical carbon dioxide ($scCO_2$) as an alternative to the conventional processing.

Magnetic nanoparticles modified with organic molecules have been widely used for biotechnological and biomedical applications, because their properties can be magnetically controlled by applying an external magnetic field [73].

Although, clay is an inorganic material, Alexandre and Dubois [2] reported that the modified clay (or organoclay) is organophilic, its surface energy is lowered and is more compatible with organic polymers. Tiwari et al. [121] reported the synthesis and characterization of an organo-montmorillonite. They modified sodium Montmorillonite (NaMMT) via cation exchange reaction using three different organic cations. Basal spacings, interlamellar structure, and thermal stability of these organo-montmorillonite (OMMT) clays are characterized using wide angle X-ray diffraction (WAXRD) and thermogravimetric analysis (TGA) techniques. Increase in the basal spacing due to organic modification is in good agreement with

simple theoretical calculations based on van der Waals volume of the cationic ammonium ions. TGA characterization and analysis showed that the amount of organic modifier in the OMMTs is in good agreement with theoretically calculated stoichiometric content expected for almost complete exchange of Na + ions by organic cations. The OMMTs illustrated stepwise decomposition corresponding to initial weight loss from residual water desorption, followed by decomposition of the organic surfactant and the dehydroxylation of structural water of the montmorillonite layers.

There are two extremes of the mechanism for formation of inorganic/organic nanocomposites when the organic matrix forms first, followed by mineralization, and when the organic and inorganic materials coassemble into the nanostructured composite. There do not appear to be any examples in which the inorganic structure forms first, followed by organic structure formation [21]. Most biological composites appear to form through the first route, a process whereby an organic structure first forms, followed by the biologically directed nucleation and growth of a mineral phase. However, it is also clear that the organic matrix restructures and reorganizes continuously as the mineral deposits, which resembles the second mechanism. With both mechanisms, the organic material is generally composed of an amazing diversity of macromolecules, including proteins and other biopolymers. Considerable effort has been made to understand the mechanism of formation of these composite materials, a process that requires an understanding of both the structure and function of the organic matrix and the interactions between the organic matrix and the inorganic precursors and product [21].

The simplest examples of biological nanocomposites are those in which the mineral phase is simply deposited onto or within an organic structure. The next level of complexity is shown by examples in which the structure of the mineral phase is clearly determined by the organic matrix. The greatest complexity is where the mineral is intimately associated with the organic phase to create a structure with properties that are superior to those of either the mineral or organic phase. In the first and second examples, the organic phase forms first, but in the third, the organic and inorganic phases almost certainly coassemble into the final structure [21].

Sanchez et al. [80] believed that organic–inorganic hybrid materials do not represent only a creative alternative to design new materials and compounds for academic research, but their improved or unusual features allow the development of innovative industrial applications. Most of the hybrid materials processes are based on:

(a) the copolymerization of functional organosilanes, macromonomers, and metal alkoxides,
(b) the encapsulation of organic components within sol–gel derived silica or metallic oxides,
(c) the organic functionalization of nanofillers, nanoclays, or other compounds with lamellar structures, etc.

Chang et al. [24] studied the fabrication and characterization of Sb_2O_3[1]/carboxymethyl cellulose sodium and the properties of plasticized starch composite films. They prepared the Sb_2O_3 nanoparticles using CMC as the stabilizing agent. The nanocomposite was fabricated with Sb_2O_3/CMC nanoparticles as the filler in a glycerol plasticized starch (GPS) matrix. Characterization of Sb_2O_3/CMC nanoparticles revealed that Sb_2O_3 (about 84 wt%) was encapsulated by CMC (about 16 wt%) with the size of about 30–50 nm. Because there was good interaction between the Sb_2O_3/CMC filler and the GPS matrix, Sb_2O_3/CMC nanoparticles could be uniformly dispersed in the GPS matrix at a low filler loading level, resulting in obvious improvement in tensile strength and UV absorbance, and in the resistance of water vapor permeability. However, introduction of the nanoparticles into the matrix, decreased the elongation at break and the thermal stability of the nanocomposites.

Chitosan and nanoparticle silver are both materials with demonstrated antimicrobial properties, therefore, Huang et al. [51] investigated the synergistic combination of chitosan acetate with nanoparticle silver. They suggested that a dressing combining chitosan acetate with silver leads to improved antimicrobial efficacy against fatal burn infections.

Chang et al. [25] used polysaccharides as stabilizers for the synthesis of magnetic nanoparticles. They prepared individually the superparamagnetic Fe_3O_4 nanoparticles with soluble starch, carboxymethyl cellulose sodium (CMC), and agar as stabilizers. Since polysaccharides present the dynamic supramolecular associations facilitated by inter- and intramolecular hydrogen bonding, they can act as templates for the growth of nanosized Fe_3O_4. The resulting polysaccharide-Fe_3O_4 was characterized by FTIR spectroscopy, TGA, TEM, XRD, and magnetic properties. TEM revealed that Fe_3O_4 was encapsulated by polysaccharides. The particle size of starch-Fe_3O_4 (SF) was obviously smaller than those from CMC-Fe_3O_4 (CF) and agar-Fe_3O_4 (AF). TG analysis was used to calculate the Fe_3O_4 contents of SF, CF, and AF—62.7, 47.8, and 57.4 %, respectively. The saturation magnetization (20.43 emu/g) of AF was much lower than that of SF (36.16 emu/g) and CF (35.75 emu/g). The polysaccharide-Fe_3O_4 exhibited an extremely small hysteresis loop and low coercivity.

3 Quality Control or Assessments of Prepared Nanobiocomposites

In polymer/fiber composites in the food packaging system, all testing and assessment methods for nanobiomaterials should consider environmental degradation and accumulation, environmental toxicology, and food safety.

[1]Antimony trioxide (Sb_2O_3) is the inorganic compound with melting point of 656 °C, and boiling point of 1,425 °C. It is the most important commercial compound of antimony. It is found in nature as minerals, valentinite and senarmontite.

The study results of scientists and researchers on nanocomposites have revealed clearly the property advantages that nanomaterial additives can provide in comparison to both their conventional filler counterparts and base polymer. In food packaging, appropriately adding nanomaterials to a polymer matrix can enhance its performance, by simply capitalizing on the nature and properties of the nanoscale filler [38]. Understanding the effect of structure on the properties of nanobiocomposites is the key to obtain their design rules. To this end, it should be employed a vast number of structural and compositional characterization techniques. In fact, the large amount of reinforcement surface area of nanomaterials means that a relatively small amount of nanoscale reinforcement can have an observable effect on the macroscale properties of the nanocomposites. For example, adding some nanomaterials may improve the thermal conductivity, some of them may result in optical properties, heat resistance, or mechanical properties. However, it is necessary to assessment of prepared nanopackaging materials by various tests, depending on the nanopackaging production aims, production method, specific application, and the other factors. On the other hand, due to some disadvantages associated with nanoparticle incorporation like toughness and impact performance properties develop a better understanding of formulation/structure/property relationships leading to better results.

However, both natural fibers/natural polymers and biocomposites/nanocomposites should be characterized by some different tests. For example, fibers characterize by density, energy dispersive X-ray (EDX), X-ray diffraction (XRD), Fourier transform infrared spectroscopy (FTIR), and scanning electron microscopy (SEM), where as composites characterize by density, melt flow index (MFI), mechanical tests (tensile, flexural, and impact), thermogravimetric analysis (TGA), differential scanning calorimetry (DSC), field emission electron microscopy (FE-SEM), water uptake analysis, and so on [53]. Some of the important tests such as morphological characterization techniques and surface appearance; fundamental aspects; mechanical properties (e.g., strength, modulus, and dimensional stability); thermal stability and heat distortion temperature; permeability to gases, water, etc.; flammability (flame retardancy and reduced smoke emissions); optical transparency (optical clarity), chemical resistance; degradability of biodegradable nanocomposites, etc. are mentioned in the following paragraphs.

3.1 Film Thickness

If the final product is in the film form, the film thicknesses should be measured. It measures at several different points using a digital micrometer, and the average value of these determinations calculates as a film thickness, in normal. This average value may be used in other tests like to calculate the cross-sectional area of the samples (the area is equal to the thickness multiplied by the width of each sample) in mechanical tests.

3.2 Mechanical Properties

The mechanical properties include many tests such as the tensile strength (TS) and percent of elongation at break (%E), etc. Stress–strain mechanical properties of the films evaluate using a universal testing machine, equipped with a certain load cell, according to the conditions set by ASTM 882-09 method [12]. At least five specimens, with a size of 600 × 10 mm, were cut from films. Before characterization, all film samples were conditioned at 25 °C and 57 % RH (a saturated NaBr solution) relative saturation humidity (RH) for 72 h. The tensile strength calculates by dividing the applied force needed to break a sample, by the cross-sectional area. Percent elongation at break expresses as percentage of change of the original length of a specimen between grips at break. The %E in the films is also a very important characteristic, since it provides a flexibility index and shows the film capacity to absorb large amounts of energy before breaking.

In general, the mechanical performance of nanocomposites depends on many factors that are the keys of the interaction between nanofillers and matrix. Some of these factors are below [50]:

1. The adhesion and compatibility between the polymer matrix and nanofillers,
2. Degree of dispersion,
3. Nanofillers efficiency in the stress tolerance,
4. The filler volume (weight) fraction,
5. The filler geometry (aspect ratio); aspect ratio is defined as the ratio of the filler's longitudinal length to its transverse length,
6. Orientation of fillers,
7. Degree of the matrix crystalline.

In mechanical terms, nanocomposites differ from conventional composite materials due to the exceptionally high surface-to-volume ratio of the reinforcing phase and/or its exceptionally high aspect ratio [84].

3.3 Water Vapor Permeability (WVP)

The WVP evaluates using the modified ASTM E96-95 desiccant method, also known as "the test cell" [13].

3.4 Barrier Properties

The serious work on the barrier performance of nanobiocomposites is necessary. The requirement for a packaging system is to maintain the freshness and safety of food. The excellent gaseous barrier properties exhibited by nanocomposite polymer

systems will result in their substantial use as packaging materials. For example, incorporation of relatively small quantities of nanoclay materials improves the gaseous barrier property of nanocomposites.

3.5 Electron Microscopy

The morphology of film samples can be observed with scanning electron microscopy (SEM) instrument after coating by gold under vacuum conditions. There are different types of electron microscopy, for example, transmission electron microscopy (TEM) is used to characterize the nanocomposite morphology [2]. High resolution transmission electron microscopy (HRTEM) is also an imaging mode of the TEM that allows for direct imaging of the atomic structure of the sample. HRTEM is a powerful tool to study properties of materials on the atomic scale, such as nanoparticles. The contrast formation in HRTEM can only be explained by the wave nature of electrons. In HRTEM a virtually planar electron wave transmits a thin specimen (thickness <20 nm), in most cases a crystal [122]. In general, scanning and transmission electron microscopy are two of the few techniques that allow direct visualization of nanomaterials due to their high resolution. Conventional sample preparation techniques coupled to SEM and TEM imaging and (semi)automatic, threshold-based detection of NP in electron micrographs allow the detection of the primary subunits of nanomaterials and measure the physical characteristics of NP on a per particle basis. These include the size (distribution), shape, aggregation state, and the surface morphology of nanomaterials. Different methods for TEM imaging and image analysis in two and three dimensions were examined by Schneider et al. [85]. As an example, Fig. 2 shows SEM micrographs for an apricot (variety 58-Shahroud) coated with chitosan nanoemulsion with two particle sizes of 21.8 and 43.1 nm.

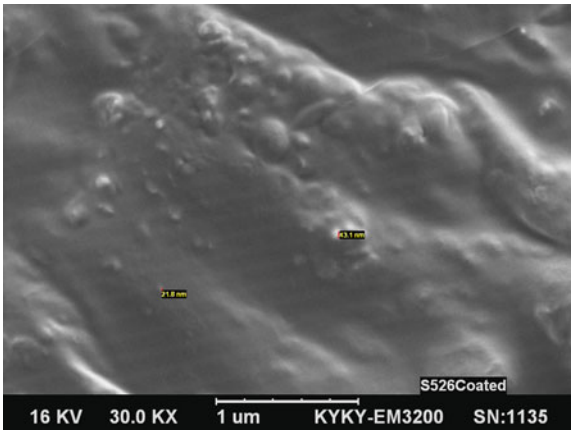

Fig. 2 SEM micrographs for an apricot (variety 58-Shahroud) coated with chitosan nanoemulsion. Two particle sizes, 21.8 and 43.1 nm can be seen here [103]

3.6 Nuclear Magnetic Resonance (NMR) Spectroscopy

NMR spectroscopy is a powerful and theoretically complex analytical technique used to determine a compound's unique structure. It identifies the carbon–hydrogen framework of an organic compound. Of all the spectroscopic methods, NMR is the only one for which a complete analysis and interpretation of the entire spectrum is normally expected. Although larger amounts of sample are needed than for mass spectroscopy, NMR is nondestructive, and with modern instruments good data may be obtained from samples weighing less than a milligram. Using NMR and other instrumental methods including infrared and mass spectrometry, scientists are able to determine the entire structure of a molecule. In this method, experiments are performing on the nuclei of atoms, not the electrons [64, 86].

3.7 Fourier Transform Infrared (FTIR) Spectroscopic Analysis

FTIR spectroscopy is one of the most important tools used to analyze food packaging films due to its sensitivity, relatively low cost, and speed [5]. Its applications are not limited to analyzing the properties of petrochemical-based plastics, but can also be used for biodegradable packaging films manufactured from polysaccharides or protein sources. Few researchers have investigated the use of FTIR as an analytical tool for determining biodegradable film properties [124].

Figure 3, as an example, shows the spectra of the two prepared films by Asgari et al. [9]. In their work, the nanocomposite LDPE with carbon nanotube films was prepared by solution casting in boiling xylene.

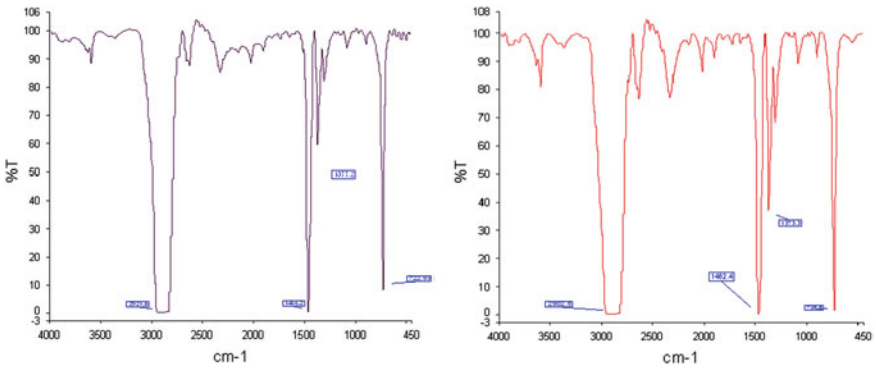

Fig. 3 FTIR spectra of nanocomposite LDPE with carbon nanotube films, the right; FTIR spectra of pure PE, the *left* [9]

3.8 Atomic Force Microscopy (AFM)

AFM can be used to nondestructively characterize the three-dimensional structure of food materials in the nanometer to 100 mm range, allowing the study of single molecules as well as complex composite structures. AFM may be conducted in ambient or fluid environments and requires minimal sample preparation. Studies in solution allow imaging of a specimen in its hydrated state under a controlled environment [45].

This technique allows measuring NPs in the Z-direction with a resolution in the order of one nanometre and hence optimally complements electron microscopy with the best resolution in the X- and Y-directions. The deflections of a cantilever with a sharp tip (mechanical probe) are measured when scanning a surface containing NPs. AFM can be operated in a number of modes, depending on the application. These can be divided into static (also called contact) modes and a variety of dynamic (or noncontact) modes where the cantilever is vibrated. As a result, the topography (Z-direction) of a sample is represented in function of its X- and Y-coordinates. In specific configurations, electric potentials can also be scanned using conducting cantilevers [85].

3.9 X-Ray Diffraction (XRD)

XRD is used to identify intercalated structures in nanocomposites [2]. In fact, due to the easiness and the availability of XRD, it is most commonly used to probe the nanocomposite structure, especially for general polymer/clay nanocomposites. However, the XRD can only detect the periodically stacked MMT layers; disordered (bunched together but not parallely stacked) or exfoliated layers are not detected. In general, in natural clay-filled polymers with favorable thermodynamics for nanocomposite formation, the structure is characterized by a coexistence of exfoliated, intercalated, and disordered layers. Figure 4 shows an example of XRD pattern for CMC/PVA/Nanoclay films.

3.10 Flame Retardancy

Montmorillonite-based fillers, for instance, promote the flame retardancy of polymers, across a wide range of different chemistries.

3.11 Optical Microscopy

Although this technique lacks the resolution to identify individual nanomaterials, it is widely applied to assess suspensions for the presence of large aggregates of

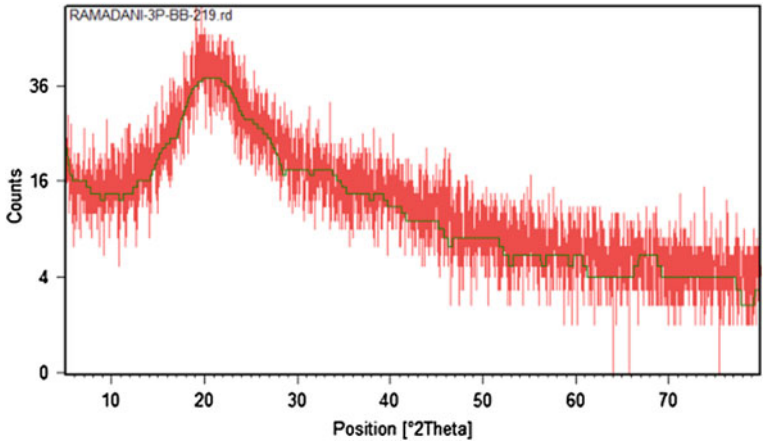

Fig. 4 XRD pattern of a CMC/PVA/nanoclay thin films [105]

nanoparticles. When the optical signal of an NP can be amplified (e.g., when the particles are autofluorescent or can be fluorescence labeled), optical microscopy can be a valuable tool to examine the distribution of NPs in cells and tissues [85].

3.12 Thermal Stability

A polymer may be completely amorphous in the solid state, semicrystalline, or perfectly crystalline. Amorphous polymers are characterized by a glass transition temperature, Tg and crystalline polymers are characterized by a melting transition temperature, T_m. When the polymer is cooled below the Tg temperature, it becomes hard and brittle, like glass. Some polymers are used above their glass transition temperatures, and some are used below [16, 18, 27]. However, there are some equipments and methods to determine the thermal properties of composites such as dynamic mechanical analysis (DMA), thermomechanical analysis (TMA), etc. Thermo gravimetric analysis (TGA) and differential scanning calorimetry (DSC) are the major techniques in thermal analysis. The objectives of calorimetric and gravimetric analysis of polymers are determination of two important thermal transitions observed in polymers, glass transition (T_g) and melting (T_m). Both Tg and Tm are important parameters, which serve to characterize a given polymer [102].

3.12.1 Thermo Gravimetric Analysis (TGA)

TGA is used to measure the mass or change in mass of a sample as a function of temperature or time or both. Changes of mass occur during sublimation, evaporation, decomposition, and chemical reaction, magnetic or electrical transformations [35].

TG curves show the component of samples (filler, matrix, plasticizer, etc.), due to their chemical characteristics and molecular structure. So, it is good to recognize the component in the composites. In TG, the change of a specimen mass is measured either absolutely in milligrams or relatively as a percentage of the starting mass, and plotted against temperature or time. Plastics may change mass in one or more steps. As shown in the Fig. 5, multistep TG curves often do not have a section of curve over which the mass remains constant. In such cases, m_i, the midpoint between m_{B1} and m_{A2}, is determined.

Figure 6 is an example of a two-step change of mass. Aside the TG curve, it contains derivative thermogravimetry (DTG) curve, which can be used to establish m_i, the smallest value on the curve between the two steps. The peak maximum T_P on the DTG curve represents the inflection point of the TG curve and thus the temperature of maximum rate of change of mass. This value is often used in practice for comparison purposes because evaluation is simple and reproducible [35].

3.12.2 Differential Scanning Calorimetric (DSC)

DSC is a well-established technique in which a sample is either heated or cooled while its temperature is monitored. Simultaneously, a reference sample located within the same chamber is also monitored. The temperature difference between the two samples is recorded and plotted. Any difference between the two specimens is a result of heat generation or absorption within the specimen because of

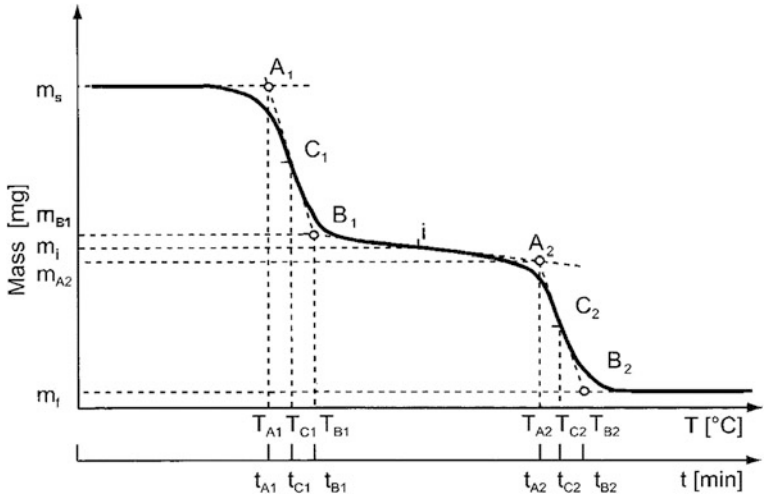

Fig. 5 TG curve example [35]; T_A onset temperature/time, T_B end temperature/time, T_C midpoint temperature/time, m_s starting mass, m_f final mass, m_i midpoint between m_{B1} and m_{A2}

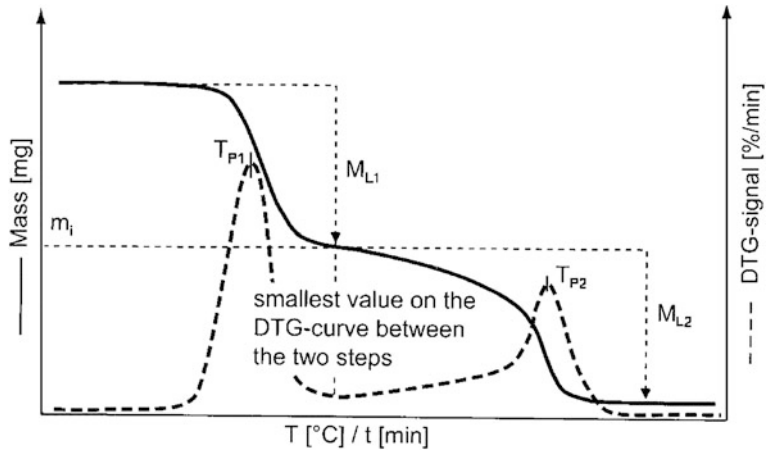

Fig. 6 An example of a two-step change of mass [35]; M_{L1}, M_{L2} loss of mass and T_{P1}, T_{P2}, Peak temperature on the DTG *curve*

polymerization or a phase change. Thus, this technique is used for monitoring the polymerization process, as well as determining the extent of crystallization of a sample [67]. On the other hand, calorimetry is a technique for determining the quantity of heat that is either absorbed or released by a substance undergoing a physical or a chemical change. Such a change alters the internal energy (enthalpy, ΔH) of the substance. Processes that increase ΔH such as melting, evaporation, or glass transition are said to be endothermic while those that lower ΔH such as crystallization, progressive curing, decomposition are called Exothermic [35]. Figure 7 shows a schematic diagram of a DSC curve.

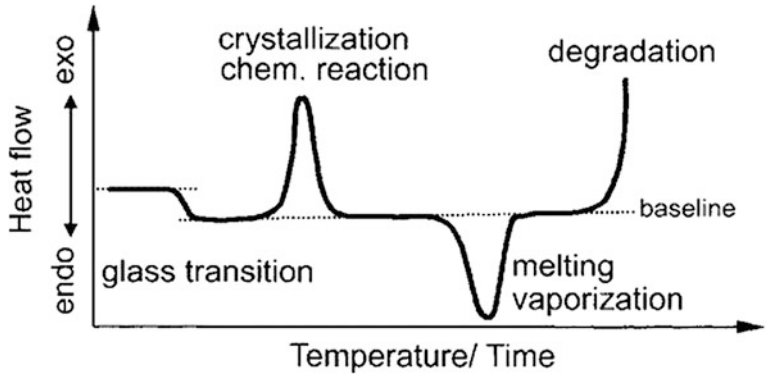

Fig. 7 Schematic diagram of a DSC *curve* [35]

3.13 Microbiology

The antimicrobial activity determines by using the different standard methods such as the Japanese industrial standard test (JIS Z 2801:2000), [4]. In this method, briefly, the test samples were placed in petri dishes and inoculated with 0.4 ml of a bacterial culture containing 10^5–10^6 CFU/ml. The inoculum was covered with a polyester film (X-131 transparent copier film; Folex Imaging), and the petri dishes were incubated at 37 °C for 24 h in a humid chamber to prevent desiccation. After the incubation period 20 ml of extraction solution (0.1 % [vol/vol] Tween 20, 145 mM sodium chloride, 20.5 mM sodium phosphate; pH 7.4) was added to the petri dishes and shaken for 2 min. Subsequently, serial dilutions of the extraction solution were spread on agar plates in triplicate and incubated at 37 °C overnight. Colonies were counted visually, and the numbers of CFU per sample were determined. The activity value was calculated from the mean value for the individual samples by subtraction of the log value determined for the test sample from the log value determined for the control.

3.14 Migration

Although nanotechnology or NPs have the potential to bring significant benefits to both the industry and consumers, they may also introduce potential risks for human health and the environment. Due to their small size, surface reactivity, and translocation possibility across biological membranes as well as potential interactions of NPs with the surrounding matrix and unexpected effects resulting from this specific data for risk assessment purposes are required [52]. The transfer of constituents of the food contact materials into the food is called migration. The main risk of consumer exposure to NPs from food packaging is likely to be through potential migration of NPs into food and drink. However, migration experimental data are not currently available, despite the fact that a number of food packaging types containing NPs are already available and in commercial use in some countries [48]. To ensure the protection of the health of the consumer and to avoid adulteration of the foodstuff, two types of migration limits have been established in the area of plastic materials [10]:

1. An overall migration limit (OML) of 60 mg (of substances)/kg (of foodstuff or food simulants) that applies to all substances that can migrate from the food contact material to the foodstuff,
2. A specific migration limit (SML) which applies to individual authorized substances and is fixed on the basis of the toxicological evaluation of the substance.

Simon et al. [89] presented a physicochemical perspective on the potential migration of engineered nanoparticles (ENPs) from packaging to food based on evaluation of the average distance traveled by ENPs in the polymer matrix.

The study has taken into account physicochemical properties of both ENPs and packaging polymers. From the properties, some general characteristics underpinning ENP migration can be predicted. The results indicate that any detectable migration of ENPs from packaging to food will take place in the case of very small ENPs with a radius in the order of 1 nm, from polymer matrices that have a relatively low dynamic viscosity, and that do not interact with the ENPs. These conditions are likely to be met in the case of nanocomposites of silver with polyolefins (LDPE, HDPE, PP). It can also be predicted that there will not be any appreciable migration in the case of bigger ENPs that are bound in polymer matrices with a relatively high dynamic viscosity such as polystyrene and polyethylene terephthalate. They concluded that only nanoparticles of 1 nm may diffuse from packaging material to food, bigger particles did not migrate. A study by Avella et al. [10] showed that there is no increase in mineral (Fe and Mg) content of the vegetables when the vegetables (lettuce and spinach) were in contact with starch/clay nanocomposite films.

Silver migration from the PLA containing a silver-based layered silicate films to a slightly acidified water medium, considered an aggressive food simulant, was measured by stripping voltammetry. Silver migration accelerated after 6 days of exposure. Nevertheless, the study suggests that migration levels of silver, within the specific migration levels referenced by the European Food Safety Agency (EFSA), exhibit antimicrobial activity, supporting the potential application of this biocidal additive in active food packaging applications to improve food quality and safety [22].

3.15 Statistical Analysis

In general, it is necessary using of a statistical method for analyzing the obtained data. For example, one-way, two-way, or *N*-way analysis of variance at a significance level of $\alpha = 0.05$ or $\alpha = 0.01$ usually apply to the data. In case of significance, the Tukey or the other multiple comparison methods can be concerned. Nowadays, there are many statistical softwares that can be also used.

4 Conclusions and Future Perspective

In the last decades there has been a significant increase in the amount of plastics being used in various sectors, particularly in food packaging applications. Plastics technology have enormous advantages, such as thermosealability, flexibility in thermal and mechanical properties, and they permit integrated processes, lightness, and a low price. Although technology has vast potential, it presents huge challenges too. The chief limitation of polymers being their inherent permissiveness to the transport of low molecular weight components, which leads to issues such as

food oxidation by penetration of oxygen, migration of toxic elements from the plastic, and scalping of food components on the packaging with the consequent losses in food quality and safety attributes. In addition, the substantial increase in the use of plastics has also raised a number of environmental concerns from a waste management point of view. As a result, there has been a strong research interest, pushed by authorities at national and international levels, and a concomitant industrial growing activity in the development and use of biodegradable and/or biobased materials. Inherent shortcomings of natural polymer-based packaging materials such as low mechanical properties and low water resistance can be recovered by applying a nanocomposite technology. Polymer nanocomposites exhibit markedly improved packaging properties due to their nanometer-size dispersion. These improvements include increased modulus and strength, decreased gas permeability, and increased water resistance. Additionally, biologically active ingredients can be added to impart the desired functional properties to the resulting packaging materials. Consequently, natural biopolymer-based nanocomposite packaging materials with biofunctional properties have an enormous potential for application in the active food packaging industry. However, in order to extend the degree of utilization of nanobiopolymers, future research has to focus on the production of nanomaterials based on proteins, polysaccharides, lipids, and/or their mixing with/without the other synthetic or natural polymers/natural fibers in the packaging industry specially in active packaging.

References

1. Ajayan PM (2003) Bulk metal and ceramics nanocomposites. In: Ajayan PM, Schadler LS, Braun PV (eds) Nanocomposite science and technology, pp 1–75. Wiley-VCH, New York
2. Alexandre M, Dubois P (2000) Polymer-layered silicate nanocomposites: preparation, properties and uses of a new class of materials. Mater Sci Eng 28:1–63
3. Angellier-Coussy H, Chalier P, Gastaldi E, Guillard V, Guillaume C, Gontard N, Peyron S (2013) Protein-based nanocomposites for food packaging. In: Dufresne A, Thomas S, Pothan LA (eds) Biopolymer nanocomposites: processing, properties, and applications, pp 613–654. Wiley, New York
4. Anonymous (2000) Antimicrobial products-test for antimicrobial activity and efficacy. Japanese industrial standard test (JIS Z 2801:2000) Japanese Standards Association Tokyo Japan
5. Anonymous (2001) Introduction to fourier transform infrared spectrometry. Thermo Nicolet Corporation 7 pp
6. Appendini P, Hotchkiss JH (2002) Review of antimicrobial food packaging. Innovative Food Sci Emerg Technol 3:113–126
7. Argüello-García E, Solorza-Feria J, Rendón-Villalobos JR, Rodríguez-González F, Jiménez-Pérez A, Flores-Huicochea E (2014) Properties of edible films based on oxidized starch and zein. Int J Polym Sci 2014 Article ID 292404 9 pp
8. Arora A, Padua GW (2010) Review: nanocomposites in food packaging. J Food Sci 75:43–49
9. Asgari P, Moradi O, Tajeddin B (2014) The effect of nanocomposite packaging carbon nanotube base on organoleptic and fungal growth of Mazafati brand dates. Int Nano Lett 4:98

10. Avella M, Vlieger JJ, Errico ME, Fischer S, Vacca P, Volpe MG (2005) Biodegradable starch/clay nanocomposite films for food packaging applications. Food Chem 93:467–474
11. Asadi Asadabadi M, Khosravi-Darani K, Mortazavi A, Hajseyed Javadi N, Azadnia E, Kiani Harchegani A, Ahmadi N (2014) Antimicrobial effect of silver nanoparticles produced by chemical reduction on *Staphylococcus aureus* and *Escheirchia coli*. Iran J Nutr Sci Food Technol 8(4):83–92 (Text in Persian)
12. ASTM 882-09 (2009) Standard test method for tensile properties of thin plastic sheeting. American Society for Testing and Materials West Conshohocken Pa USA
13. ASTM E96-95 (1995) Standard test methods for water vapour transmission of materials in sheet form. American Society for Testing and Materials West Conshohocken Pa USA
14. Azeredo HMC (2009) Nanocomposites for food packaging applications. Food Res Int 42:1240–1253
15. Balcerzak J, Kucharska M, Gruchała B (2013) Preparation of micro and nanostructures of chitosan by ultrasonic coalescence of w/o emulsions. Prog Chem Appl Chitin Deriv XVIII:13–20
16. Baker AMM, Mead J (2000) Thermoplastics. In: Harper CA (ed) Modern plastics handbook, 1.1–1.92. McGraw-Hill, New York
17. Barenholz Y (2001) Liposome application: problems and prospects. Curr Opin Colloid Interface Sci 7(1):66–77
18. Barry CMF, Orroth SA (2000) Processing of thermoplastics. In: Harper CA (ed) Modern plastics handbook, 5.1–5.125. McGraw-Hill, New York
19. Berglund L (2005) Cellulose-based nanocomposites. In: Mohanty AK, Misra M, Drzal LT (eds) Natural fibers, biopolymers, and biocomposites, pp 807–832. CRC Press
20. Bongarde US, Shinde VD (2014) Review on natural fiber reinforcement polymer composites. Int J Eng Sci Innovative Technol (IJESIT) 3(2):431
21. Braun PV (2003) Natural nanobiocomposites, biomimetic nanocomposites, and biologically inspired nanocomposites. In: Ajayan PM, Schadler LS, Braun PV (eds) Nanocomposite science and technology, pp 155–214
22. Busolo MA, Fernandez P, Ocio MJ, Lagaron JM (2010) Novel silver-based nanoclay as an antimicrobial in polylactic acid food packaging coatings. Food Addit Contam 27 (11):1617–1626
23. Chang PR, Yang Y, Huang J, Xia W, Feng L, Wu J (2009) Effects of layered silicate structure on mechanical properties and structures of protein-based bionanocomposites. J Appl Polym Sci 113(2):1247–1256
24. Chang PR, Yu J, Ma X (2009) Fabrication and characterization of Sb_2O_3/carboxymethyl cellulose sodium and the properties of plasticized starch composite films. Macromol Mater Eng 294(11):762–767
25. Chang PR, Yu J, Ma X, Anderson DP (2011) Polysaccharides as stabilizers for the synthesis of magnetic nanoparticles. Carbohydr Polym 83(2):640–644
26. Chen Z, Zhang L, Wang L (2011) Study on filming of oxidized starch/PVA. Frontiers Agric China 5(4):649–654
27. Cowie JMG (2008) Polymers: chemistry & physics of modern materials. Taylor & Francis, Boca Raton
28. Dadashi S, Mousavi SM, Emam D-Jomeh Z, Oromiehie A (2012) Films based on poly(lactic acid) biopolymer: effect of clay and cellulosic nanoparticles on their physical, mechanical and structural properties. Iran J Polym Sci Technol 25(2):127–136 (Text in Persian)
29. Damm C, Neumann M, Münstedt H (2006) Properties of nanosilver coatings on polymethyl methacrylate. Soft Mater 3:71–88
30. Dehnad D, Mirzaee H, Emam D-Jomeh Z, Jafari SM, Dadashi S (2014) Assessing thermal and antimicrobial properties of chitosan-nanocellulose nanocomposites to enhance the shelf life of ground meat. Iran J Nutr Sci Food Technol 8(4):163–173 (Text in Persian)
31. Del Nobile MA, Conte A, Buonocore GC, Incoronato AL, Massaro A, Panza O (2008) Active packaging by extrusion processing of recyclable and biodegradable polymers. J Food Eng 93:1–6

32. Duncan TV (2011) Applications of nanotechnology in food packaging and food safety: barrier materials, antimicrobials and sensors. J Colloid Interface Sci 363(1):1–24
33. Dutta PK, Tripathi S, Mehrotra GK, Dutta J (2008) Perspectives for chitosan based antimicrobial films in food applications. Food Chem 114:1173–1182
34. Egger S, Lehmann RP, Height MJ, Loessner MJ, Schuppler M (2009) Antimicrobial properties of a novel silver-silica nanocomposite material. Appl Environ Microbiol 75 (9):2973–2976
35. Ehrenstein GW, Riedel G, Trawiel P (2004) Thermal analysis of plastics, theory and practice. Carl Hanser Verlag, München
36. Emamifar A, Kadivar M, Shahedi M, Soleimanianzadeh S (2011) Effects of nanocomposite packaging containing silver and zinc oxide on the shelf-life of fresh orange juice. Iran J Nutr Sci Food Technol 6(1):57–67 (Text in Persian)
37. Eshghi S, Hashemi M, Mohammadi A, Badie F, Mohammad Hosseini Z, Ahmadi Sumehe K, Ghanati K (2013) Effect of nano-emulsion coating containing chitosan on storability and qualitative characteristics of strawberries after picking. Iran J Nutr Sci Food Technol 8(2):9–19 (Text in Persian)
38. Evangelos M (2007) Nanocomposites: stiffer by design. Nat Mater 6(1):9–11
39. Faraji M, Fadavi G (2013) Application of magnetic nanoparticles in food science and technology. Iran J Nutr Sci Food Technol 8(2):239–252 (Text in Persian)
40. Galeano B, Korff E, Nicholson WL (2003) Inactivation of vegetative cells, but not spores, of *Bacillus anthracis*, *B. cereus*, and *B. subtilis* on stainless steel surfaces coated with an antimicrobial silver- and zinc-containing zeolite formulation. Appl Environ Microbiol 69:4329–4331
41. Galus S, Lenart A, Voilley A, Debeaufort F (2013) Effect of oxidized potato starch on the physicochemical properties of soy protein isolate-based edible films. Food Technol Biotechnol 5(3):403–409
42. Gao Y, Cranston R (2008) Recent advances in antimicrobial treatment of textiles. Text Res J 78:60–72
43. Ghanbarzadeh B, Oromiehi AR (2008) Biodegradable biocomposite films based on whey protein and zein: barrier, mechanical properties and AFM analysis. Int J Biol Macromol 43:209–215
44. Grehna A (2012) Chitosan nanoparticles: a survey of preparation methods. J Drug Target 20 (4):291–300
45. Guoa Y, Liub Z, And H, Lia M, Hu J (2005) Nano-structure and properties of maize zein studied by atomic force microscopy. J Cereal Sci 41:277–281
46. Hadian Z, Sahari MA, Moghimi HR, Barzegar M, Abbasi S (2013) Preparation and characterization of nanoliposomes containing docosahexaenoic and eicosapentaenoic acids by extrusion and probe sonication. Iran J Nutr Sci Food Technol 8(1):219–230 (Text in Persian)
47. Haldorai Y, Shim JJ, Lim KT (2012) Synthesis of polymer–inorganic filler nanocomposites in supercritical CO_2. J Supercrit Fluids 71:45–63
48. Han W, Yu YJ, Li NT, Wang L (2011) Application and safety assessment for nano-composite materials in food packaging. Chin Sci Bull 56:1216–1225
49. Herrera F, Pedro J, Valadez-Gonzalez A (2005) Fiber- matrix adhesion in natural fiber composites. In: Mohanty AK, Misra M, Drzal LT (eds) Natural fibers, biopolymers, and biocomposites, pp 177–230, CRC Press
50. Hu H, Onyebueke L, Abatan A (2010) Characterizing and modeling mechanical properties of nanocomposites-review and evaluation. J Miner Mater Charact Eng 9(4):275–319
51. Huang L, Dai T, Xuan Y, Tegos GP, Hamblin MR (2011) Synergistic combination of chitosan acetate with nanoparticle silver as a topical antimicrobial: efficacy against bacterial burn infections. Antimicrob Agents Chemother 55(7):3432–3438
52. Huyghebaert A, Van Huffel X, Houins G (2010) Preface. In: International symposium on nanotechnology in the food Chain, Opportunities & Risks, pp 3–9

53. Islam MR, Beg MDH, Gupta A (2013) Characterization of Laccase-treated kenaf fibre reinforced recycled polypropylene composites. BioResources 8(3):3753–3770
54. Ivask A (2013) Potential and actual applications of nanoparticles as food ingredients and in food packaging. National Institute of Chemical Physics and Biophysics Laboratory of Environmental Toxicology Tallinn Estonia 16th April 2013 Warsaw
55. Jiménez A, Arab-Tehrany E, Sánchez-González L (2014) Progress in biodegradable packaging materials. Progress Nanomaterials Food Packag 50–56
56. Kato M, Usuki A (2006) Layerd silicates. In: Mai YW, Yu ZZ (eds) Polymer nanocomposites, pp 3–28. CRC Press
57. Keshavarzian F, Badii F, Seyedin Ardebili SM, Hashemi M, Ahmadi Z, Hosseini SE (2014) Effect of packaging in polyethylene-clay nanocomposite film on quality and storage life of sliced bread. Iran J Nutr Sci Food Technol 9(1):93–100 (Text in Persian)
58. Khoshnoudinia S, Sedaghat N (2013) Effect of gelatin edible coating containing antioxidant agents on hardness, and color of roasted pistachio nuts. Res Innovation Food Sci Technol 2 (4):295–310 (Text in Persian)
59. Kojima Y, Usuki A, Kawasumi M, Okada A, Fukushima Y, Karauchi T, Kamigaito O (1993) Mechanical properties of nylon-6-clay hybrid. J Mater Res 6:1185–1189
60. Kumar R, Münstedt H (2005) Polyamide/silver antimicrobials: effect of crystallinity on the silver ion release. Polym Int 54(8):1180–1186
61. Lagaron JM (2010) Nanotechnology trends to enhance biopackaged food, food quality and safety. In: Huyghebaert A, Van Huffel X, Houins G (eds) International symposium on nanotechnology in the Food Chain, Opportunities & Risks, pp 45–52
62. Lin M-F, Thakur VK, Tan EJ, Lee PS (2011) Dopant induced hollow $BaTiO_3$ nanostructures for application in high performance capacitors. J Mater Chem 21:16500–16504
63. Lin M-F, Thakur VK, Tan EJ, Lee PS (2011) Surface functionalization of $BaTiO_3$ nanoparticles and improved electrical properties of BaTiO3/polyvinylidene fluoride composite. Rsc Adv 1:576–578
64. Mamin HJ, Poggio M, Degen CL, Rugar D (2007) Nuclear magnetic resonance imaging with 90-nm resolution. Nat Nanotechnol 2:301–306
65. Martelli M, Barros T, Moura M, Mattoso L, Assis O (2012) Effect of chitosan nanoparticles and pectin content on mechanical properties and water vapor permeability of banana puree films. J Food Sci 78:98–104
66. Martínez-Camacho AP, Cortez-Rocha MO, Ezquerra-Brauer JM, Graciano-Verdugo AZ, Rodriguez-Félix F, Castillo-Ortega MM, Yépiz-Gómez MS, Plascencia-Jatomea M (2010) Chitosan composite films: thermal, structural, mechanical and antifungal properties. Carbohydr Polym 82(2):305–315
67. Miller E (1996) Introduction to plastics and composites, mechanical properties and engineering applications. Marcel Dekker Inc., New York
68. Mohammadi M, Jahadi M, Ehsani MR, Khosravi-Darani K (2013) Application of liposome nano carrier in cheese production and ripening. Iran J Nutr Sci Food Technol 7(4):25–34 (Text in Persian)
69. Mohammadi M, Ghanbarzadeh B, Hamishehkar H, Rezayi Mokarram R, Mohammadifar MA (2014) Physical properties of vitamin D3-loaded nanoliposomes prepared by thin layer hydration-sonication. Iran J Nutr Sci Food Technol 8(4):175–188 (Text in Persian)
70. Moradi M, Tajik H, Razavi Rohani SM, Oromiehie A, Malekinejad H, Saei-Dehkordi SS (2010) Antioxidant, color and antibacterial properties of edible chitosan film incorporated with Zataria multiflora Boiss essential oil against *Listeria monocytogenes*. Armaghane-Danesh 15(4):303–315 (Text in Persian)
71. Mozafari MR, Johnson C, Hatziantoniou S, Demetzos C (2008) J Liposome Res 18:309–327
72. Mozafari MR, Khosravi-Darani K, Borazan GG, Cui J, Pardakhty A, Yurdugul S (2008) Encapsulation of food ingredients using nanoliposome technology. Int J Food Prop 11:833–844
73. Osaka T, Matsunaga T, Nakanishi T, Arakaki A, Niwa D, Iida H (2006) Synthesis of magnetic nanoparticles and their application to bioassays. Anal Bioanal Chem 384:593–600

74. Parris N, Coffin DR (1997) Composition factors affecting the water permeability and tensile properties of hydrophilic zein films. J Agric Food Chem 45:1596–1599
75. Paz L, Reain A, Howard K, Sutherland D, Wejse L (2011) Antimicrobial effect of chitosan nanoparticles on *Streptococcus mutans* biofilms. Appl Environ Microbiol 77:3892–3895
76. Petersen K, Nielsen PV, Bertelsen G, Lawther M, Olsen MB, Nilsson NH, Mortense G (1999) Potential of biobased materials for food packaging. Trends Food Sci Technol 10 (2):52–68
77. Ravi Kumar MV (2001) A review of chitin and chitosan applications. React Funct Polym 46:1–27
78. Rhim JW, Ng PK (2007) Natural biopolymer-based nanocomposite films for packaging applications. Crit Rev Food Sci Nutr 47(4):411–433
79. Russell AD, Hugo WB (1994) Antimicrobial activity and action of silver. Prog Med Chem 31:351–370
80. Sanchez C, Julián B, Belleville P, Popall M (2005) Applications of hybrid organic–inorganic nanocomposites. J Mater Chem 15:3559–3592
81. Sanchez-Garcia MD, Lagaron JM, Hoa SV (2010) Effect of addition of carbon nanofibers and carbon nanotubes on properties of thermoplastic biopolymers. Compos Sci Technol 70 (7):1095–1105
82. Sardabi F, Mohtadinia J, Shavakhi F, Jafari AA (2013) Effect of 1-methylcyclopropene and potassium permanganate-coated zeolite nanoparticles on extending the shelf life and quality of Golden and Red Delicious apples. Iran J Nutr Sci Food Technol 8(2):135–144 (Text in Persian)
83. SCENIHR (Scientific Committee on Emerging and Newly Identified Health Risks) (2007) Opinion on the scientific aspects of the existing and proposed definitions relating to products of nanoscience and nanotechnologies. The 21st plenary on 29 Nov 2007, 22 pp
84. Schadler LS (2003) Polymer-based and polymer-filled nanocomposites. In: Ajayan PM, Schadler LS, Braun PV (eds) Nanocomposite science and technology, pp 77–154
85. Schneider YJ, Bazes A, Brasseur A, Geys J, Mast J, Pussemier L (2010) Toxicodynamic aspects of nanoparticles in food: interactions with the intestinal barrier. In: Huyghebaert A, Van Huffel X, Houins G (eds) International symposium on nanotechnology in the Food Chain, Opportunities & Risks, pp 59–65
86. Skewis LR, Demas V, Lowery TJ (2013) Nuclear magnetic resonance nanotechnology: applications in clinical diagnostics and monitoring. Encycl Anal Chem
87. Siegel DP, Tenchov BG (2008) Influence of the lamellar phase unbinding energy on the relative stability of lamellar and inverted cubic phases. Biophys J 94:3987–3995
88. Silva DA, Paula RCM, Feitosa JPA, Brito ACF, Maciel JS, Paula HCB (2004) Carboxymethylation of cashew tree exudate polysaccharide. Carbohydr Polym 58 (2):163–171
89. Simon P, Chaudhry Q, Bakos D (2008) Migration of engineered nanoparticles from polymer packaging to food-a physicochemical view. J Food Nutr Res 47(3):105–113
90. Simoneau C (2012) Nano in packaging. In: ILSI expert Workshop on nanotechnologies for food packaging. European Commission (JRC) 08–10 Feb 2012
91. Singha AS, Thakur VK (2008) Effect of fibre loading on urea-formaldehyde matrix based green composites. Iran Polym J 17:861–873
92. Singha AS, Thakur VK (2008) Saccaharum cilliare fiber reinforced polymer composites. E-J Chem 5:782–791
93. Singha AS, Thakur VK (2008) Synthesis and characterization of pine needles reinforced RF matrix based biocomposites. E-J Chem 5:1055–1062
94. Singha AS, Thakur VK (2009) Grewia optiva fiber reinforced novel, low cost polymer composites. J Chem 6:71–76
95. Singha AS, Thakur VK (2009) Synthesis, characterisation and analysis of hibiscus sabdariffa fibre reinforced polymer matrix based composites. Polym Polym Compos 17:189–194
96. Singha AS, Thakur VK (2009) Fabrication and characterization of *H. sabdariffa* fiber-reinforced green polymer composites. Polym-Plast Technol Eng 48:482–487

97. Singha AS, Thakur VK (2009) Fabrication and characterization of *S. cilliare* fibre reinforced polymer composites. Bull Mater Sci 32:49–58
98. Singha AS, Thakur VK (2009) Physical, chemical and mechanical properties of hibiscus sabdariffa fiber/polymer composite. Int J Polym Mater 58:217–228
99. Sondi I, Salopek-Sondi B (2004) Silver nanoparticles as antimicrobial agent: a case study of *E. coli* as a model for gram-negative bacteria. J Colloid Interface Sci 275:177–182
100. Sotirou GA, Blattmann CO, Pratsinis SE (2013) Flexible, multifunctional, magnetically actuated nanocomposite films. Adv Funct Mater 23(1):1616–3028
101. Strawhecker KE (2006) Nanocomposites based on water soluble polymers and unmodified smectite clays. In: Mai YW, Yu ZZ (eds) Polymer nanocomposites, pp 206–233. CRC Press
102. Tajeddin B (2009) Preparation and characterization of kenaf cellulose-polyethylene glycol-polyethylene biocomposites. Ph.D. thesis UPM Malaysia
103. Tajeddin B, Hashemi M, Khayam Nekouei SM (2013) The effect of a chitosan-based nano-emulsion on extending the shelf life of apricot. Final research report Iranian Agricultural Engineering Research Institute (IAERI) no 44007 (Text in Persian)
104. Tajeddin B, Ramedani N (2013) Shellac is a suitable natural production for using in food packaging. In: 6th congress on advances in agriculture research 15–16 May 2013 University of Kurdistan Sanandaj Iran (Text in Persian)
105. Tajeddin B, Ramedani N (2014) Investigation of nanostructure of CMC/PVA/Nanoclay films using XRD. In: 15th nanotechnology iranian student conference Tehran Tarbiat Modares University 24–25 April 2014 (Text in Persian)
106. Thakur VK, Tan EJ, Lin M-F, Lee PS (2011) Poly(vinylidene fluoride)-graft-poly (2-hydroxyethyl methacrylate): a novel material for high energy density capacitors. J Mater Chem 21:3751–3759
107. Thakur VK, Tan EJ, Lin M-F, Lee PS (2011) Polystyrene grafted polyvinylidenefluoride copolymers with high capacitive performance. Polym Chem 2:2000–2009
108. Thakur VK, Yan J, Lin M-F et al (2012) Novel polymer nanocomposites from bioinspired green aqueous functionalization of BNNTs. Polym Chem 3:962–969
109. Thakur VK, Ding G, Ma J et al (2012) Hybrid materials and polymer electrolytes for electrochromic device applications. Adv Mater 24:4071–4096
110. Thakur VK, Singha AS, Thakur MK (2012) Biopolymers based green composites: mechanical, thermal and physico-chemical characterization. J Polym Environ 20:412–421
111. Thakur VK, Singha AS, Thakur MK (2012) Graft copolymerization of methyl acrylate onto cellulosic biofibers: synthesis, characterization and applications. J Polym Environ 20:164–174
112. Thakur VK, Lin M-F, Tan EJ, Lee PS (2012) Green aqueous modification of fluoropolymers for energy storage applications. J Mater Chem 22:5951–5959
113. Thakur VK, Thakur MK, Gupta RK (2013) Development of functionalized cellulosic biopolymers by graft copolymerization. Int J Biol Macromol 62:44–51
114. Thakur VK, Thakur MK, Gupta RK (2013) Rapid synthesis of graft copolymers from natural cellulose fibers. Carbohydr Polym 98:820–828
115. Thakur VK, Thakur MK, Gupta RK (2013) Synthesis of lignocellulosic polymer with improved chemical resistance through free radical polymerization. Int J Biol Macromol 61:121–126
116. Thakur VK, Thakur MK, Gupta RK (2013) Graft copolymers from natural polymers using free radical polymerization. Int J Polym Anal Charact 18:495–503
117. Thakur VK, Thakur MK, Gupta RK (2013) Graft copolymers from cellulose: Synthesis, characterization and evaluation. Carbohydr Polym 97:18–25
118. Thakur VK, Thakur MK (2014) Processing and characterization of natural cellulose fibers/thermoset polymer composites. Carbohydr Polym 109:102–117
119. Thakur VK, Thakur MK, Gupta RK (2014) Review: raw natural fiber-based polymer composites. Int J Polym Anal Charact 19(3):256–271

120. Thakur VK, Thakur MK, Raghavan P, Kessler MR (2014) Progress in green polymer composites from lignin for multifunctional applications: a review. ACS Sustain Chem Eng 2 (5):1072–1092
121. Tiwari RR, Khilar KC, Natarajan U (2008) Synthesis and characterization of novel organo-montmorillonites. Appl Clay Sci 38(3–4):203–208
122. Tonejc A (1999) High resolution transmission electron microscopy (HRTEM): image processing analysis of defects and grain boundaries in nanocrystalline materials. Acta Chim Slov 46(3):435–461
123. Vroman I, Tighzert L (2009) Biodegradable polymer. Materials 2(2):307–344
124. Wang LZ, Liu L, Holmes J, Kerry JF, Kerry JP (2007) Assessment of film-forming potential and properties of protein and polysaccharide-based biopolymer films. Int J Food Sci Technol 42(9):1128–1138
125. Wang Y, Jiang L, Duan J, Shao S (2013) Effect of the carbonyl content on the properties of composite films based on oxidized starch and gelatin. J Appl Polym Sci 130(4):2753–2763
126. Weiss J, Takhistov P, McClements DJ (2006) Functional materials in food nanotechnology. J Food Sci 71(9):R107–R116
127. Westman MP, Laddha SG, Fifield LS, Kafentzis TA, Simmons KL (2010) Natural fiber composites: a review.Prepared for the U.S. Department of Energy, under Contract DE-AC05-76RL01830 (PNNL19220)
128. Willard MA, Kurihara LK, Carpenter EE, Calvin S, Harris VG (2004) Chemically prepared magnetic nanoparticles. Int Mater Rev 49(3–4):125–170
129. Wirawan R, Zainudin ES, Sapuan SM (2009) Mechanical properties of natural fibre reinforced PVC composites: a review. Sains Malaysiana 38(4):531–535
130. Yien Ing L, Zin N, Sarwar A, Katas H (2012) Antifungal activity of chitosan nanoparticles and correlation with their physical properties. Int J Biomater 632698:1–9
131. Zandi K, Weisany W, Ahmadi H, Bazargan I, Naseri L (2013) Effect of nanocomposite-based packaging on postharvest quality of strawberry during storage. Bull Environ Pharmacol Life Sci 2(5):28–36
132. Zavareze EDR, Pinto VZ, Klein B, Halal SLME, Elias MC, Prentice-Hernández C, Dias ARG (2012) Development of oxidised and heat-moisture treated potato starch film. Food Chem 132(1):344–350

Bionanocomposites for Magnetic Removal of Water Pollutants

F.L. Sousa, A.L. Daniel-da-Silva, N.J.O. Silva and T. Trindade

Abstract Magnetic separation in water remediation processes is of great interest in current environmental technologies. An important aspect in this field has been the development of efficient sorbents for water purification units, namely by exploiting other functionalities that might originate more sustainable technologies. This chapter describes the state-of-art on the chemical preparation of magnetic sorbents comprising inorganic particles and biopolymer matrices. Fundamental aspects related to nanoparticle synthesis of iron oxides and nanomagnetism will be first addressed. The use of these particles in biopolymers matrices such as polysaccharides will be then reviewed as an innovative strategy aiming at production of eco-friendly sorbents for magnetic separation.

Keywords Biopolymers · Magnetic nanoparticles · Bionanocomposites · Magnetic separation

1 Introduction

Water is the most essential resource for life. The population growth and fast development of industrialization and intensive agricultural activities has increased the demand for treated water. Contamination of surface and ground waters by effluent discharges has become a critical environmental issue and attracted global concern over the past years [3, 71, 96]. Heavy metal ions, dyes, phosphates and nitrates, radioactive species, and pharmaceuticals are examples of water contaminants [3]. These contaminants can compromise the integrity of ecological cycles and have an impact on human health through drinking water and by integration in the food

F.L. Sousa · A.L. Daniel-da-Silva · T. Trindade (✉)
Department of Chemistry and CICECO, University of Aveiro, 3810–193 Aveiro, Portugal
e-mail: tito@ua.pt

N.J.O. Silva
Department of Physics and CICECO, University of Aveiro, 3810–193 Aveiro, Portugal

V.K. Thakur and M.K. Thakur (eds.), *Eco-friendly Polymer Nanocomposites*,
Advanced Structured Materials 74, DOI 10.1007/978-81-322-2473-0_9

chain, causing serious health and environmental effects, which may include carcinogenicity, reproductive impairment, developmental and immune system changes, and endocrine disruption [3, 91].

Consequently, water treatment has been a subject of paramount importance that nowadays requires more sustainable technologies. In order to provide long-term high quality water or to enable water recycling, there has been research in alternative remediation processes, for example, involving chemically modified nanometer sized adsorbents, ion exchangers, or systems that can also be of interest for bioapplications [3, 71, 96]. Various materials have been used for these purposes such as activated carbon, clays, siliceous materials, zeolites, and biopolymers [1, 9, 32, 74, 92] among others. However, in some cases the applications have been limited by the associated costs, regeneration, and limited cycles of application, among other factors. Alternatively, the use of low-cost and eco-friendly sorbents composed of natural polymers has gained significant interest over the recent years owing to their unique intrinsic properties such as biodegradability, easy availability, flexibility, easy processing, and impressive physico-mechanical properties [92-88]. These biopolymers are renewable materials, environmentally friendly, generally nontoxic, biodegradable, and combine excellent functional properties [24]. The combination of magnetic nanoparticles (MNPs) and biopolymers can lead to bionanocomposites responsive to external magnetic stimuli [17]. Although magnetic properties have been extensively exploited in magnetically driven drug transport for target delivery, they can also be relevant for magnetic separation of water pollutants [96, 18, 67]. Other properties of magnetic bionanocomposites are equally important for their successful application as sorbents in water treatment. Among these, specific surface area, particle size, pore diameter, morphology, and chemical surface functionalization are particularly relevant [71]. High adsorption capacities are associated to sorbents with effective high specific surface areas and the required functional groups for interaction with target contaminants [3].

This chapter provides an overview of the literature disclosed in the past decade in the field of magnetic biocomposites for water treatment applications. Emphasis is given to the most common methodologies for preparation of magnetic composites of polysaccharides and to studies devoted to the above-mentioned applications. Some general concepts on the magnetic properties of magnetic nanoparticles (MNPs) are summarized, considering the specific properties required for magnetic separation.

2 Magnetic Polysaccharide Composites

A magnetic bionanocomposite is defined here as a material comprising magnetic nanoparticles dispersed in a biopolymer matrix. The performance of such materials in the context of sustainable nanotechnologies has attracted global interest in recent

Table 1 Polysaccharides commonly used in the preparation of bionanocomposites

Polymer	Source	Ionic character	Functional groups
Agarose	Marine red algae	Neutral	OH
Alginate	Brown algae	Anionic	OH, COO^-
Carrageenan	Red seaweeds	Anionic	OH, OSO_3^-
Chitosan	Shelfish and fungi cell wall	Cationic	OH, NH_3^+
Dextran	Produced by lactic acid bacteria	Neutral	OH
Gum arabic	Acacia tree	Anionic	OH, COO^-
Gum kondagogu	Cochlospermum gossypium tree	Anionic	OH, COO^-
Starch	Green plants	Neutral	OH

years, leading to extensive research into their synthesis and subsequent applications. In particular, polysaccharides have been commonly used for coating MNPs, including chitosan, dextran, alginate, agarose, carrageenan, gum Arabic, cellulose derivatives, and starch. Table 1 lists polysaccharides commonly used to prepare magnetic biocomposites in the context of environmental applications and the respective structural formulae are shown in Fig. 1. Nanoparticles coated with such biopolymers generally possess high adsorption capacities, rapid adsorption rates, even when present in low amounts and at short equilibrium times, and in certain conditions can be reusable [24].

2.1 Preparation Techniques of Magnetic Bionanocomposites

Herein we draw our attention to preparative routes for production of magnetic bionanocomposites composed of biopolymers and magnetic nanoparticles. This section starts to outline some chemical methods of iron oxide MNPs that are often used as fillers in composite materials envisaging water treatment procedures. The preparative routes for magnetic bionanocomposites are then reviewed, by distinguishing preparative methods that are based in blends of the components from those in which the MNPs are produced in situ.

2.1.1 Inorganic Nanoparticles

Among the most used MNPs, magnetite (Fe_3O_4) and maghemite (γ-Fe_2O_3) have sparked great interest in water treatment research [96, 39, 84]. These iron oxides show biocompatibility, low toxicity, size tuned magnetic behavior, and possibility to up-scale synthesis [71, 18, 36]. Several synthetic methods are available for preparation of iron oxide nanoparticles with appropriate size and distribution, these include: co-precipitation of Fe(II) and Fe(III) salts, hydrolysis and thermolysis of iron containing precursors, chemical reactions in microemulsions, hydrothermal

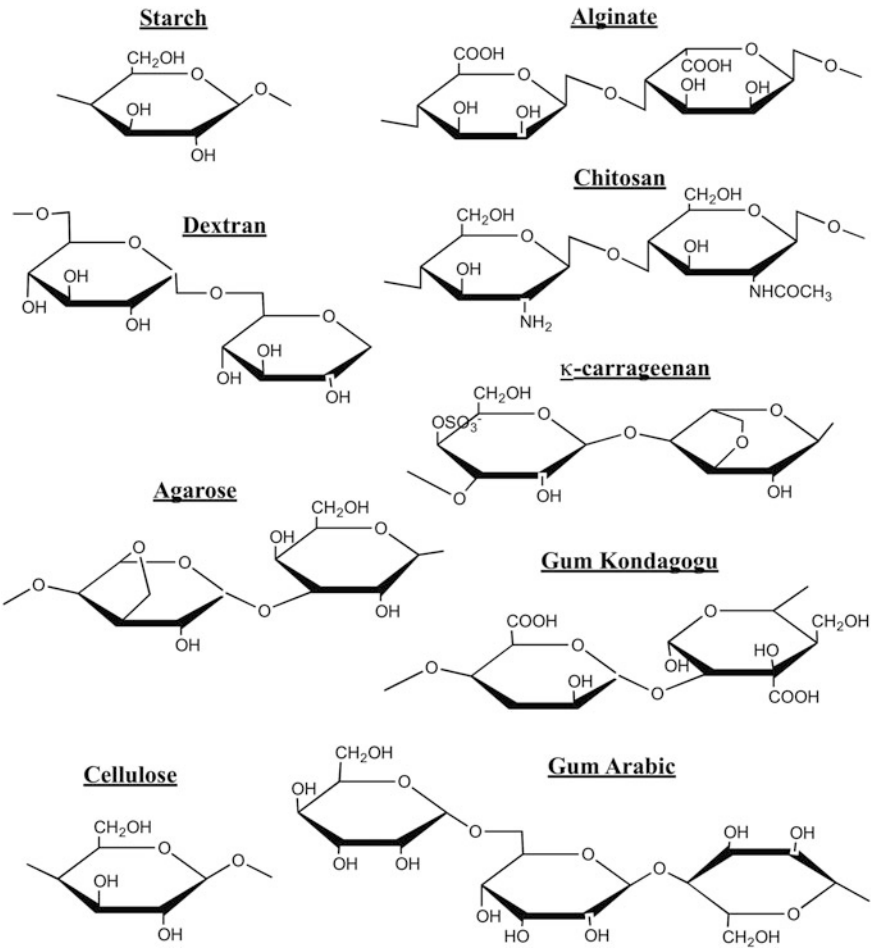

Fig. 1 Structural formulae of common polysaccharides

synthesis, sonochemical reactions [20, 43, 48]. By reaction of Fe_3O_4 with other cations such as Ni(II), Mn(II) and Co(II), ferrites with the general formula MFe_2O_4 can be obtained, which gives additional tools to tune the magnetic properties accordingly to the envisaged application [35, 42, 80]. A telegraphic description of the methods most used to prepare iron oxide nanoparticles is given below.

Co-precipitation

This is a widely used method to obtain iron oxide particles from mixtures of ferrous and ferric salts in aqueous basic medium [48]. The method involves the dissolution of a mixture of $FeCl_3 \cdot 6H_2O$ and $FeCl_2 \cdot 4H_2O$ in water under nitrogen atmosphere

with vigorous stirring at 70–85 °C and the subsequent addition of ammonia, leading to the formation of a dark precipitate [11, 55]. Although adaptations of this method have been employed, its simplicity and environmental friendly characteristics have made this process an elective method to prepare magnetite in aqueous medium.

Thermolysis of Precursors

The thermal decomposition of iron containing precursors in organic solvents of high boiling point temperature has been used to prepare crystalline iron oxide nanoparticles with narrow particle size distribution. Indeed, this method allows significant control of the mean size, size distribution, and provides organically protected surfaces. The reaction conditions, such as solvent, temperature, and time, are experimental parameters that can be used to adjust the final properties of the nanoparticles. Examples of precursors that have been used in this context include iron pentacarbonyl, $Fe(CO)_5$; iron(III) acetylacetonate, $Fe(C_5H_7O_2)_3$; iron(III) acetate, $Fe(CH_3CO_2)_3$, and iron(III) tri-(*N*-nitrosophenylhydroxyl-amine), i.e., $Fe(cupferron)_3$ [80, 11, 55].

Microemulsions

This method involves the use of surfactants to stabilize fine droplets of water dispersed in a nonpolar solvent. Iron salts are dissolved in water nanodroplets that are protected from the surrounding organic medium by the surfactant layer. Thus, these systems act as structured nanoreactors for synthesizing nanoparticles, proving a confined environment that limits particle nucleation and growth. A great advantage of this method is the diversity of NPs that can be obtained, both in terms of chemical composition and morphological features, by varying the chemical reactants, nature and amount of surfactant/cosurfactant, the oil phase, and the reacting conditions. For instance, $MnFe_2O_4$ nanoparticles with controllable sizes between 4 and 15 nm have been synthesized through the formation of water-in-toluene inverse micelles using sodium dodecylbenzenesulfonate (NaDBS) as surfactant [11, 55].

Hydrothermal Reactions

Hydrothermal syntheses have been used to prepare a broad range of MNPs. The reactions occur in aqueous media usually in autoclaves where the pressure can be higher than 2000 psi and the temperature can be above 200 °C. The two main routes for formation of magnetite via hydrothermal conditions involve forced hydrolysis of iron salts and thermolysis of mixed metal hydroxides. Hydrothermal reactions generally give high crystalline materials but surface capping is limited. Also, caution should be taken in the selection of the iron precursors that will be submitted to high pressure and high temperature reacting conditions. This method can be

extended to formation of other MNPs, thus $CoFe_2O_4$ nanoparticles with average size of 12 nm have been prepared by this route [11].

2.1.2 Magnetic Bionanocomposites

The preparation of magnetic bionanocomposites has involved two main approaches, the synthesis of MNPs in the presence of biopolymers (in situ) or blending of previously prepared MNPs with biopolymers (ex situ). Examples of both strategies are listed in Table 2. The synthesis in situ allows more intimate dispersion of the MNPs within the polymer matrix but control over their size and shape is limited, which in certain conditions can be crucial because nanoparticles have size and shape-dependent magnetic properties. In this situation, the biopolymer encapsulation of synthesized MNPs is an interesting alternative. Polysaccharide-based composites can be produced in the form of macroscopic networks ("bulk nanocomposites") or confined to smaller dimensions ranging the micron- to nano-metric range [18, 11]. In the latter, a variety of morphologies can be obtained depending on the preparation method employed but magnetic core–polymer shell and magnetic multi-cores homogeneously dispersed within the polymer matrix have been common structures (Fig. 2). Table 2 lists a number of magnetic sorbents used for water treatment procedures.

In situ preparation of magnetic bionanocomposites

In this strategy, magnetic bionanocomposites are prepared by promoting the synthesis of magnetic nanofillers in the biopolymer matrix. For example, polysaccharides possess functional moieties such as hydroxyl, carboxyl, and/or amine groups, which in aqueous solutions have the ability to interact with metal cations via electron rich donor atoms, which can act as nucleation sites. The cavities in the polymer network offer constrained environments that limit the growth of the in situ formed particles. The functional groups of the biopolymer present variable affinity for specific metallic ions and may determine the characteristics of the resulting inorganic phase [18, 19]. Although the one-step synthesis is relatively simpler and less time-consuming, magnetic bionanocomposites prepared by one-step procedures have been less reported. A few examples are outlined below that illustrate the usefulness of this preparative strategy.

Gum Kondagogu, an acetylated polysaccharide, was successfully used in co-precipitation of iron salts in aqueous solutions containing such biopolymer. The native gum contains various functional groups that facilitate the entrapment of MNPs within the biopolymer network by facilitating surface interactions. Transmission Electron Microscopy (TEM) images of these nanocomposites revealed spherical aggregates containing Fe_3O_4 nanoparticles with sizes ranging

Table 2 Magnetic bionanocomposites employed as sorbents in water treatment techniques

Biopolymer	MNP	Method	References
Alginate	γ-Fe_2O_3	ex situ	Rocher et al. [75]
			Ngomsik et al. [60]
			Rocher et al. [76]
			Idris et al. [40]
			Bee et al. [8]
	Fe_3O_4	ex situ	Tripathi et al. [89]
			Lee et al. [49]
	$Ni_xZn_{1-x}Fe_2O_4$	ex situ	Mahmoodi et al. [58]
	$CoFe_2O_4$	ex situ	Ai et al. [2]
Carrageenan	Fe_3O_4	ex situ	Salgueiro et al. [78]
		in situ	Mahdavinia et al. [57]
Cellulose	γ-Fe_2O_3	ex situ	Luo et al. [56]
	Fe_3O_4	ex situ	Shi et al. [81]
Carboxymethyl-β-cyclodextrin	Fe_3O_4	ex situ	Badruddoza et al. [5]
Chitosan	Fe_3O_4	ex situ	Liu et al. [52]
	γ -Fe_2O_3	in situ	Zhou et al. [105]
	γ-Fe_2O_3	ex situ	Zhou et al. [100]
		ex situ	Fan et al. [28]
			Fan et al. [27]
			Paulino et al. [63]
			Zhou et al. [102]
			Zhou et al. [103]
			Chen et al. [14]
			Zhou et al. [104]
			Liu et al. [53]
			Obeid et al. [61]
			Jiang et al. [44]
			Zhu et al. [106]
			Zhu et al. [107]
			Zhu et al. [108]
Guar gum	Fe_3O_4	ex situ	Yan et al. [97]
Gum arabic	Fe_3O_4	ex situ	Paulino et al. [64]
			Banerjee et al. [7]
Gum ghatti	Fe_3O_4	ex situ	Mittal et al. [59]
Gum kondagogu	Fe_3O_4	in situ	Saravanan et al. [79]
Sesbania gum	Fe_3O_4	ex situ	Lan et al. [46]
Humic acid	Fe_3O_4	ex situ	Peng et al. [65]
			Liu et al. [54]
			Yang et al. [98]

(continued)

Table 2 (continued)

Biopolymer	MNP	Method	References
Pectin	Fe_3O_4	ex situ	Gong et al. [33]
			Rakhshaeea et al. [70]
Poly(γ-glutamic acid)	Fe_3O_4	ex situ	Inbaraj et al. [41]
Polydopamine	Fe_3O_4	ex situ	Zhang et al. [99]
Starch	Fe_3O_4	ex situ	Pourjavadi et al. [68]

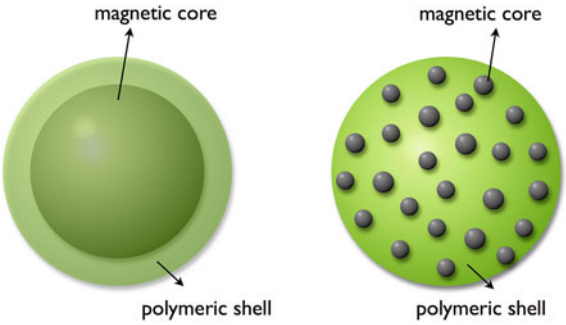

Fig. 2 Magnetic core–polymer shell (*left*) and magnetic multi-cores homogeneously dispersed in a polymer bead (*right*). Adapted from [71]

8–15 nm [79]. Magnetic iron-oxide nanoparticles have also been synthesized by in situ co-precipitation in the presence of other biopolymers such as carrageenan [57], chitosan [100, 14] and chitin/alginate [50]. Carrageenans, which are sulfated polysaccharides, were employed as stabilizers in the synthesis of magnetite nanoparticles via co-precipitation of ferric and ferrous ions and subsequent biopolymer cross-linking with K^+ ions [57], see Fig. 3. The composite beads have coarse and undulant surfaces with cubic-shaped sections, and contain Fe_3O_4 nanoparticles of sizes in the 3–7 nm range. The synthesis of magnetite nanoparticles in a chitosan matrix was prepared using W/O microemulsions containing chitosan and an Fe(II) salt [100]. The magnetic biocomposite was then treated with epichlorohydrine and grafted with ethylenediamine, in order to increase the extension of $-NH_2$ functionalization, hence increasing the adsorption capacity for anionic dyes via hydrogen bonding with protonated amine groups.

In another study, Chen et al. prepared Fe_3O_4-chitosan macroscopic beads with spherical shape of approximately 1 mm diameter by the in situ co-precipitation of Fe^{2+} and Fe^{3+} in the presence of chitosan [14]. Similarly, magnetic chitin/alginate beads were prepared in situ by promoting ionic cross-linking between the oppositely charged biopolymer chains, leading to iron oxide nanoparticles (30 nm average) uniformly dispersed and immobilized in the polymer matrix [50].

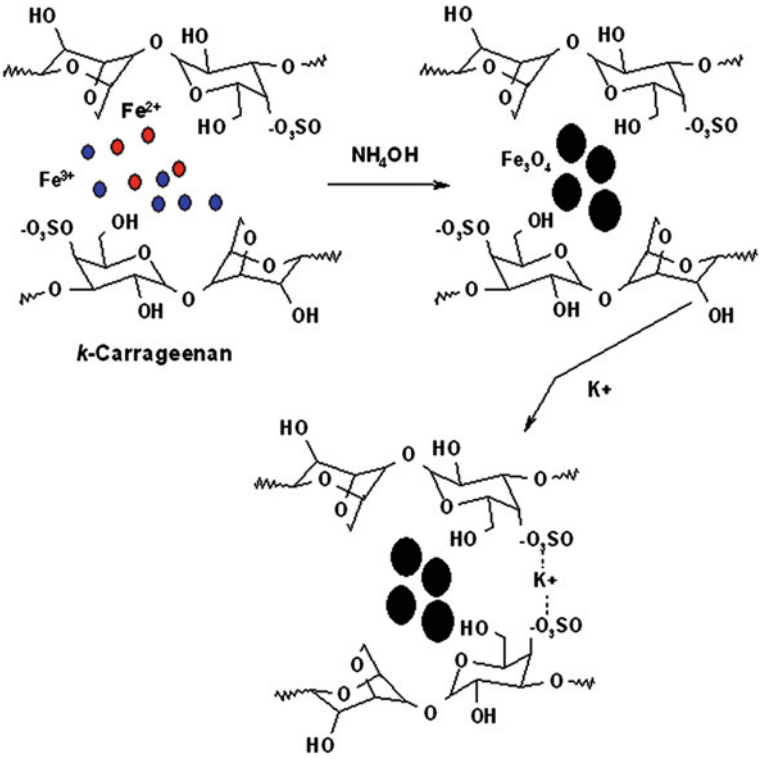

Fig. 3 Schematic representation of the preparation of magnetic κ-carrageenan beads. Reprinted with permission from [57]. Copyright 2014 Springer

Blending of magnetic nanoparticles with biopolymers

The ex situ method involves blending of MNPs with the biopolymer using a variety of methods which can be just the simple mixture of components or by inducing changes in the biopolymer, such as a cross-linking step. Typically, magnetite (Fe_3O_4) or maghemite (γ-Fe_2O_3), and more rarely a ferrite (MFe_2O_4), are obtained by synthesis methods such as those described in Sect. 2.1.1. In a second step, the MNPS are dispersed into the bulk biopolymer or its solutions, and the final composite is usually obtained by precipitation or cross-linking [71]. Surface modification of the MNPs and/or the biopolymer chains can be applied in order to ensure homogeneity of the final composite.

Alginate, a natural polysaccharide extracted from brown seaweed, was used as matrix to prepare magnetic bionanocomposites containing γ-Fe_2O_3 nanoparticles and activated carbon (AC), using Ca^{2+} ions as cross-linking agents. The resulting composite has shown spherical particles with an average diameter of 2.8 mm [76]. This route was also used to prepare macroscopic alginate beads containing cobalt ferrite and AC, which in the swollen state have an average diameter of about 2 mm. The

magnetic beads exhibited an egg-like morphology with a wrinkle and porous surface, which are characteristics that can improve the uptake of certain pollutants [2].

κ-Carrageenan coated Fe_3O_4 nanoparticles have been prepared by K^+ ions cross-linking of carrageenan chains in the presence of magnetite [78]. Acid treated and nontreated MNPs were used in order to vary the surface chemistry of the nanofillers. It was found that the bionanocomposites prepared with acid treated NPs appeared less aggregated and more homogeneously coated with the polysaccharides (Fig. 4). Acid treatment renders the surface charge of the MNP positive, thus promoting a more homogeneous dispersion in the anionic polymer. These composites were effective in the removal of methylene blue from aqueous solutions.

Chitosan-coated magnetic nanoparticles prepared by ex situ methods have been extensively reported in the literature (Table 2). Usually the preparation of magnetic chitosan composites is achieved by employing either cross-linking or precipitation methods. Zhu et al. [107] reported the preparation of crosslinked chitosan/γ-Fe_2O_3 using W/O microemulsions and glutaraldehyde as cross-linking agent. The final composite appeared as polydispersed microparticles whose average sizes range between 2 and 10 μm. Jiang et al. [44] prepared millimeter-sized γ-Fe_2O_3/chitosan

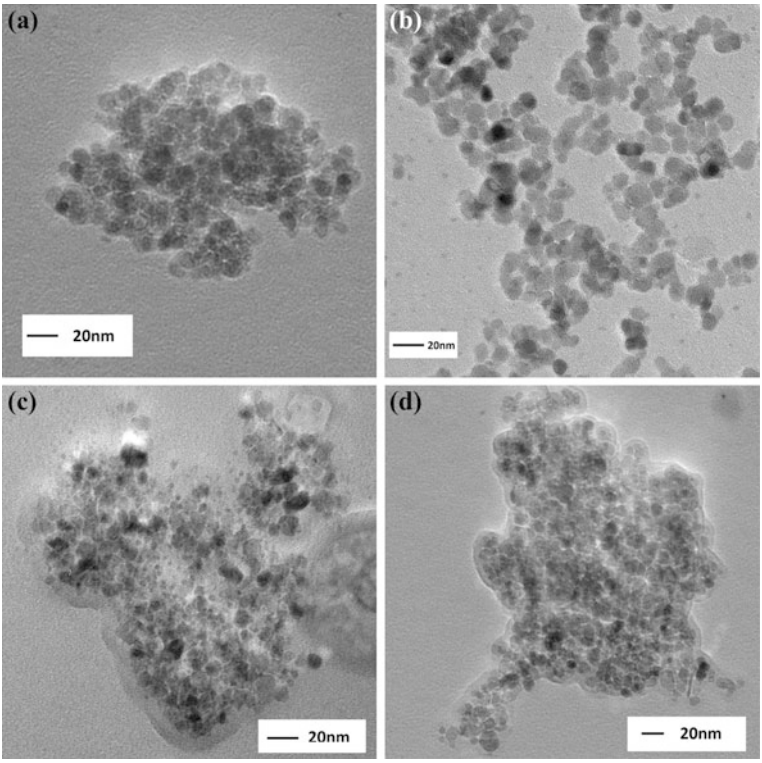

Fig. 4 TEM micrographs of **a** bare Fe_3O_4 NPs, **b** acid-treated Fe_3O_4 NPs, **c** coated Fe_3O_4 NPs and **d** coated acid-treated Fe_3O_4 NPs. Adapted with permission from [78]. Copyright 2013 Elsevier

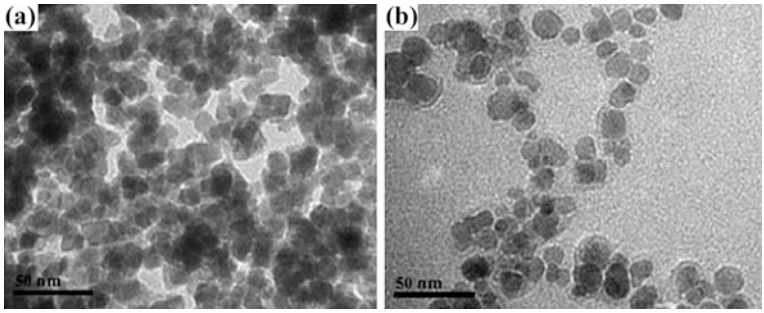

Fig. 5 TEM micrographs of **a** bare Fe_3O_4 NPs and **b** Fe_3O_4@HA NPs. Adapted with permission from [98]. Copyright 2012 American Chemical Society

beads with variable content in MNPs, which influenced the removal capacity of the composites toward Cr(VI). The composites exhibited superparamagnetic behavior and were collected from the solution by application of an external magnetic field. Magnetic chitosan biosorbents composites containing graphene oxide [27, 28] and multi-walled carbon nanotubes have been reported [108]. The incorporation of multi-walled carbon nanotubes enhanced the adsorption capacity of the composites and also improved their mechanical properties [108].

One-step coating of Fe_3O_4 nanoparticles with cellulose and chitosan was performed using ionic liquids as solvents [52]. Cellulose was used here as a blending agent for chitosan, leading to materials (average size 200 μm) with superior mechanical strength as well as to improve chemical stability in acidic medium. On the other hand, the chitosan coating prevented particle agglomeration and also provided free amine groups for coordination to aqueous heavy metal ions. Magnetite cellulose/graphene oxide composites were prepared using a co-precipitation method [81]. By loading cellulose with Fe_3O_4 NPs and GO, a rough texture at the surface of the matrix was achieved, which improved the sorption capacity of the composite in the magnetic removal of an azo dye.

Humic acid (HA) coated Fe_3O_4 nanoparticles were synthesized by co-precipitation method [98] leading to a core–shell type structure. The Fe_3O_4@HA particles appeared as spheroidal shaped with nearly uniform sizes. HA coating significantly enhanced the dispersion of Fe_3O_4@HA particles in solution compared to bare MNPs (Fig. 5).

3 Magnetism Aspects on Water Treatment Separation Technologies

3.1 General Principles of Magnetic Separation

Magnetic separation concerns overcoming a viscous flow and the associated drag force by application of a magnetic force. In the context of micro- and nano-objects,

forces associated to the mass (inertial forces) are in general negligible. In other words, such objects move within a low Reynolds number environment [69]. Thus, by removing the external (magnetic) force, MNPs will immediately stop or, in general, follow the original flow.

Magnetism can be mostly described as an interaction between dipoles, in the present case that of the magnetic particle and that of the external magnet producing a magnetic induction B. The distance between both is quite large compared to the atomic distance and therefore their interaction is solely Coulombic. This interaction has two effects: a torque that tends to align the dipoles and an attractive force that tends to bring together the dipoles.

$$\begin{aligned} \vec{F}_m &= (\vec{\mu} \cdot \nabla)\vec{B} \\ \vec{\tau} &= \vec{\mu} \times \vec{B} \end{aligned} \tag{1}$$

where μ is the moment of the dipole. It follows that magnetic separation occurs when this magnetic force is equal or larger than the drag force

$$\vec{F}_d = 6\pi\eta R\Delta\vec{v} \tag{2}$$

When the magnetic and drag forces are equal, the difference between the velocity of the nanoparticle and that of the fluid can be expressed as [62]

$$\Delta\vec{v} = \frac{R^2\Delta\chi}{9\mu_0\eta}\nabla\left(\vec{B}\cdot\vec{B}\right) \tag{3}$$

In Eq. 3, the relevant parameters are the radius (R) of the magnetic nanoparticle, the difference between the susceptibility of the nanoparticle and that of the (diamagnetic) fluid ($\Delta\chi$), and the fluid viscosity (η). Equation 3 has essentially a term associated to the magnetic properties of the system where separation occurs $(R^2\Delta\chi)/(9\mu_0\eta)$ and another term associated to the system producing the external magnetic force $\nabla\left(\vec{B}\cdot\vec{B}\right)$; both can be optimized to achieve an efficient magnetic separation. Concerning the properties of MNPs, in general, larger particles with higher magnetic susceptibility yield larger velocities. For the case of MNPs with polymer coating, Eq. 3 can be rewritten as

$$\Delta\vec{v} = \frac{R_m^3\Delta\chi}{9\mu_0\eta R_t}\nabla\left(\vec{B}\cdot\vec{B}\right) \tag{4}$$

where R_m is the radius of the magnetic nanoparticle and R_t is the total radius of the particle, such that a thicker polymer coating leads to smaller velocity difference.

Neodymium Iron Boron (NdFeB) magnets are currently the common choice to apply the external field. The $\vec{B}$ field produced by such a magnet bar is depicted in Fig. 6, showing an increase of $\vec{B}$ and its gradient when approaching the magnet pole; this increase is larger between points A and C (Fig. 6, right). More

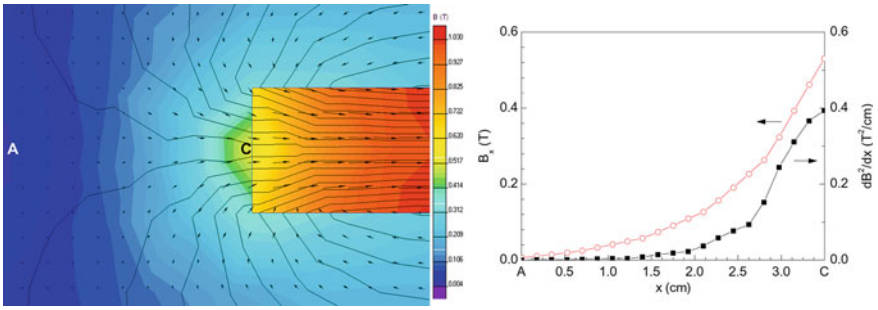

Fig. 6 *Left* color map of a typical magnetic induction created by a permanent magnet bar. *Arrows* show the direction and relative intensity of $\vec{B}$ while continuous lines represent the magnetic flux lines. Simulation performed using QuickField™ Student Edition 6.0.1.1521 by Tera Analysis Ltd using typical parameters of Neodymium Iron boron permanent magnets (1.5 × 5 cm bar, H_C = 1000 kA/m, m_r = 1.05). *Right* graph showing the dependence of the component of $\vec{B}$ along x between points A and C (B_x, open symbols, *left* scale) and the associated dependence of the term related to the magnetic force $\nabla(\vec{B}\cdot\vec{B}) = \partial B_x^2/\partial x$ (full symbols, *right* scale)

sophisticated systems using a combination of magnets yielding different field gradient profiles are also used. Another strategy is the use of micrometer sized ferromagnetic wires as a way of locally increasing the magnetic field gradient [73].

Equation 1 shows that the magnetic force is associated to the magnetic field gradient produced by a dipole.[1] As such, the MNPs will tend to move toward higher magnetic field values, usually placed at the top of the magnet (as shown in Fig. 6). In fact, the magnetic nature of a given material, diamagnetic, paramagnetic, or ferromagnetic is usually defined by the effect caused by an external magnetic field gradient, if it is repulsive, attractive, or strongly attractive, respectively. The media is usually diamagnetic and for superparamagnetic nanoparticles (to be defined below), the MNPs are attracted by the magnetic field gradient and the fluid is slightly repulsed. This is the reason why in Eq. 3 a relevant parameter is the difference between the susceptibility of the magnetic material and the media. Although magnetic forces occur only in the presence of magnetic field gradients, magnetic susceptibility χ is usually defined as the linear response of a magnetic material in the presence of a small external field H constant in space

$$M = \chi H \tag{5}$$

As stated above, in this situation torques will be developed and susceptibility quantifies the magnetization of the material that is aligned with the applied external field, i.e., it quantifies how large is the response of the stimuli to the field. A high and positive susceptibility means that a large dipolar moment appears in the direction of the field for a given field value, while a negative susceptibility means

[1] A constant magnetic field would just produce a torque.

that a dipolar moment appears in the opposite direction. Note also that we started by indistinguishably calling both the external field and the nanoparticle as 'dipoles'. In fact, they are similar in nature and magnetization of the material and intensity of the magnetic field are both a measure of the intensity of those dipoles and thus it is expectable that at magnetization and external field have equivalent units such that (volume) magnetic susceptibility is a dimensional.

3.2 Magnetic Nanoparticles for Separation Technologies

In certain situations, the atomic (ionic) magnetic moments of neighboring atoms (ions) tend to align. The origin of this alignment is in the quantum mechanical exchange integral, often introduced in the discussion of the hydrogen molecule [34], where it can be noticed that there is an energy difference between a symmetrical wave function and an antisymmetrical function, each one corresponding to a singlet spin and a triplet spin state, respectively. The singlet corresponds to an antiparallel (antiferromagnetic) coupling of spins, while the triplet corresponds to a parallel (ferromagnetic) coupling. In certain conditions, ferromagnetic and antiferromagnetic coupling leads to cooperative phenomena and properties including large magnetic moments, net magnetic moments in the absence of an external field, and hysteresis. Such phenomena occur in the case of ferromagnetic interactions and also in the case of antiferromagnetic ones, particularly when the magnitude of the coupling spins is different (as in the case of magnetite) or where the number of spins in one direction is larger than that of the opposite direction (as in the case of maghemite).

However, exchange is a short-range interaction and observation of cooperative phenomena depends on a number of factors. First, ordering can be destroyed by thermal fluctuations. Second, macroscopic ordering is favored by exchange interaction but is unfavoured by the magnetostatic energy associated with the creation of two macroscopic magnetic poles. In fact, if we take two magnetic bars into close proximity they will collapse coupling their opposite poles in order to reduce the magnetostatic energy associated to the two "isolated" magnetic poles. Third, the global energy balance has at least another important term: the anisotropy energy. This means that the energy of the system depends on the relative direction between the spins and specific directions of the material. Anisotropy energy can have different origins, being the most relevant magnetocrystalline and shape anisotropy. The magnetic state of a material will depend, in this simple description, on the balance between exchange, magnetostatic, and anisotropy energy. If anisotropy and exchange energy dominate, the system will behave as a permanent magnet. If magnetostatic energy dominates, the material will break into magnetic domains such that inside each domain the spins point in the same direction while different domains are oriented in different directions, usually forming close loops (Fig. 7a). In the case of materials forming multiple domains (such as bulk magnetite and maghemite, for instance), size changes this energy balance. Unlike magnetostatic

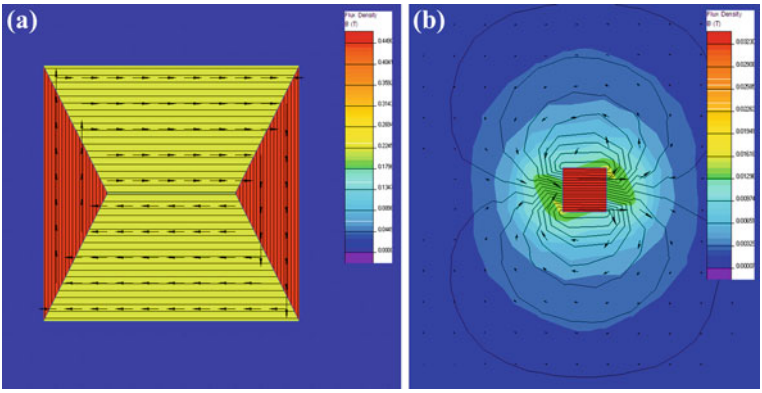

Fig. 7 **a** Color map of a typical magnetic induction created by a cubic magnetite bulk sample arbitrarily broken into four magnetic domains. Arrows show the direction and relative intensity of $\vec{B}$, while continuous lines represent the magnetic flux lines. Note that the induction outside the sample and the net magnetization of the sample are negligible. Yet, inside each domain the magnetic moments are aligned and the magnetization is not zero. **b** Similar map created by a magnetite single domain particle, where induction outside the sample is now visible and the net magnetization of the particle is not zero. Simulation performed using QuickField™ Student Edition 6.0.1.1521 by Tera Analysis Ltd using typical parameters of magnetite (H_C = 50 kA/m, m_r = 5)

energy, exchange is a short-range energy, dominating at small sizes. This means that below a given size, the system is always a single magnetic domain (Fig. 7b). This characteristic size is in the nanometric range for many materials and it is one of the key features of magnetic nanoparticles: they are intrinsically monodomains (nanodipoles). These nanoparticles are said to be superparamagnets since they are a sort of one giant classic paramagnet.

Although magnetic nanoparticles do not break into domains, the nanodipoles may have a direction fixed in space or fluctuate. The nanodipole, i.e., the magnetic moment of the nanoparticle has an intrinsic dynamic character (it fluctuates) and the fact that the direction is fixed in space or not depends on the relation between its relaxation time and the observation time window associated with a given experiment. Here, relaxation may occur between directions where anisotropy energy is minimum (the easy axis, where the dipole lies most of the time) which are separated by directions where anisotropy energy is maximum (hard directions). If the dipole is trapped in an easy axis and is not able to overcome hard axis and visit different easy directions within the observation window, the nanoparticle is said to be blocked and behaves as a nano permanent magnet. Therefore, a system composed of such nanoparticles has a nonzero net magnetization in the absence of an external field (nonzero remanence), which implies that an opposite field (the coercive field) is necessary to bring this net magnetization to zero. Otherwise, if the dipole is able to cross the anisotropy energy barrier and visit different easy axis, it is said to be unblocked, being remanence and coercivity zero. The nanoparticle is then no longer

a permanent magnet but other interesting magnetic properties arise. Many times in the literature, these are the nanoparticles termed superparamagnetic.

The fluctuation between easy axis over hard axis is usually a thermally activated process that follows an Arrhenius relation, termed Néel-Arrhenius law in this context

$$\tau_N = \tau_0 \exp\left(\frac{E_a}{k_B T}\right) \tag{6}$$

This equation gives the expected relaxation time of the nanoparticle (τ_N) for a given set of conditions: characteristic microscopic time τ_0, effective anisotropy barrier $E_a = K_{eff}V$ (proportional to the volume of the nanoparticles), and thermal energy $k_B T$. The magnetic moment of the nanoparticles is blocked (or unblocked) if τ_N is larger (or smaller) than the characteristic time of our experiment. τ_N depends exponentially on the volume and so, the design of the nanoparticles should be carefully performed concerning size, since the exponentially grows fast and we can easily pass from a situation where the nanoparticles fluctuate too fast form another where geological time scales are needed to see relaxation.

When nanoparticles which are unable to relax by the thermally activated Néel-Arrhenius mechanism are dispersed in a fluid, as usually occurs in the context of separation, another mechanism for relaxation comes into play, the Brownian relaxation. Here, the whole nanoparticle can rotate overcoming the energy associated with the viscosity of the fluid. The characteristic time for this relaxation is given as

$$\tau_B = \frac{3\eta V_H}{k_B T} \tag{7}$$

where V_H is the hydrodynamic volume of the whole nanoparticle (magnetic core plus coating). Beads composed of multi-magnetic cores wrapped by a polymer can also relax as a hole under this Brownian mechanism. Here, the dependence of the relaxation time with the volume is not so severe and a small variation in size leads to a small variation in τ_B. Particles behaving as blocked nanomagnets are usually difficult to stabilize and tend to aggregate due to the strong interparticle interactions. By contrast, unblocked nanoparticles are better dispersible yet maintaining one of their most appealing and distinctive characteristics in the context of separation: their high magnetic moment and thus high susceptibility. In unblocked superparamagnetic nanoparticles, susceptibility is given by a Curie law

$$\chi = \frac{\mu_0 N \mu^2}{3 k_B T} \tag{8}$$

where N is the number of nanoparticles per units of volume (or mass, in the case of mass susceptibility) and μ is the magnetic moment of each nanoparticle. χ is proportional to the square of μ meaning that, for instance, the susceptibility of two

nanoparticles with moment μ is less than the susceptibility of one nanoparticle made from the coalescence of these two, as long as it remains a superparamagnetic nanoparticle.

4 Application of Magnetic Bionanocomposites in Water Treatment

This section reviews the recent literature concerning application of magnetic bionanocomposites for removal of pollutants from water, thus illustrative examples will be presented for cations, dyes, and anions (Table 3). Due to the relevance of mathematical modeling of the adsorption processes involved, a brief overview of the most common models are given first. A detailed review of the several expressions for kinetics and isotherms sorption modeling can be found in the literature [66, 30].

Table 3 Magnetic bionanocomposites employed in removal of pollutants from aqueous solutions

Adsorbent	Pollutant	Optimum pH	Maximum adsorption capacity[a] (mg/g)	References
γ-Fe_2O_3—alginate—Cyanex 272	Ni(II)	5.3	0.52	Nogmsik et al. [60]
$Ni_xZn_{1-x}Fe_2O_4$-alginate	Basic Blue 9 and 41	8.0	106 and 25	Mahmoodi [58]
	Basic Red 18		56	
γ-Fe_2O_3—alginate beads containing activated carbon	Methylene Blue		5.9×10^{-2} mmol/g	Rocher et al. [76]
	Methyl Orange		2×10^{-3} mmol/g	
γ-Fe_2O_3—alginate	Pb(II)	7.0	50	Idris et al. [40]
Fe_3O_4—alginate-agarose	U(VI)	5.0	120.5	Tripathi et al. [89]
Fe_3O_4—alginate-chitosan beads	La(III)	2.8	97.1	Wu et al. [94]
Fe_3O_4—cellulose-graphene oxide	Methylene Blue		70.03	Shi et al. [81]
Fe_3O_4—Gum ghatti	Rhodamine B	7.0	654.87	Mittal and Mishra [59]
Iron oxide—Gum kondagogu (modified)	Cd(II), Cu(II), Pb (II), Ni(II), Zn (II), Hg(II)	5.0 ± 0.1	106.8, 85.9, 56.6, 49.0, 37.0, 35.0	Saravanan et al. [79]
Fe_3O_4—Humic acid	Eu(III)	8.5	6.95×10^{-5} mol/g	Yang et al. [98]
Fe_3O_4—κ-carrageenan	Methylene Blue	9	185.3	Salgueiro et al. [78]

(continued)

Table 3 (continued)

Adsorbent	Pollutant	Optimum pH	Maximum adsorption capacity[a] (mg/g)	References
Fe_3O_4—chitosan-graphene oxide composite	Methylene Blue	10.0	180.83	Fan et al. [27]
Iron oxide—chitosan composite	UO_2(II), Th(IV)		666.67, 312.50	Hritcu et al. [38]
Fe_3O_4—chitosan microspheres	Hg(II), Cu(II), Ni(II)	5.0	60.06, 42.93, 12.15	Zhou et al. [102]
γ-Fe_2O_3—chitosan	Cr(VI)	5.0	106.5	Jiang et al. [44]
γ-Fe_2O_3/SiO_2—chitosan	Methyl Orange	2.95	34.29	Zhu et al. [109]
Fe_3O_4—thiourea-chitosan imprinted Ag^+	Ag(I)	5.0	5.29	Fan et al. [26]

[a]Experimental or estimated values from applied models

4.1 Modeling the Adsorption Process

The adsorption of pollutants onto bionanocomposites is a complex process that can involve different mechanisms, including chemisorption, metal complexation, ion-exchange, precipitation, and physical adsorption [23]. The chemical nature of the pollutants and bionanocomposites, the removal conditions (e.g. pH, temperature, and ionic strength) and structural features (e.g. porosity) play an important role in determining the mechanisms involved that, in turn, will affect the adsorption rate. Moreover, the rate of the overall adsorption process might also be limited by the steps that anticipate the adsorption of the solute to the sorbent's surface, including the transport of solute from the bulk of the solution to the surroundings of the sorbent, the diffusion of the solute across the liquid film surrounding the sorbent (external diffusion), and the diffusion of the solute in the liquid within sorbent pores (intraparticle diffusion) [66]. The establishment of appropriate adsorption equilibrium correlation is indispensable for assessing the performance of a sorbent aiming at quantitative comparison of the adsorption capacity of different sorbents. Additionally, predicting the rate at which the pollutants removal takes place is crucial for effective design of adsorption systems. In this perspective, attempts have been made to describe the kinetics and the equilibrium sorption conditions using mathematical models. Table 4 lists the most representative isotherm and kinetic equations used for describing the adsorption of water pollutants.

The Langmuir equation [47] derives from an isotherm model commonly applied to describe the equilibrium of sorption on magnetic bionanocomposites [60, 40, 81, 102, 14, 104, 59, 98, 94, 26]. This empirical model assumes monolayer adsorption at a finite number of sites that are identical and equivalent, without any interaction between molecules adsorbed on adjacent sites. According to this model once a molecule occupies a site, no further adsorption can take place. The Freundlich isotherm [31] is an empirical model that describes the nonideal and reversible

Table 4 Isotherm and kinetic equations commonly used for describing the adsorption process of water pollutants

Isotherm models		Kinetic models	
Langmuir	$q_e = \frac{q_m K_L C_e}{1+K_L C_e}$	Pseudo-first order	$q_t = q_e(1 - e^{-k_1 t})$
Freundlich	$q_e = K_F C_e^{1/n_F}$	Pseudo-second order	$q_t = \frac{k_2 q_e^2 t}{1+k_2 q_e t}$
Sips	$q_e = q_m \frac{K_s C_e^{n_S}}{1+K_s C_e^{n_S}}$	Elovich	$q_t = \frac{1}{B}\ln(1 + ABt)$
Redlich-Peterson	$q_e = K_{RP} \frac{C_e}{1+\alpha_{RP} C_e^{\beta}}$	Intraparticle Diffusion	$q_t = C + k_P t^{1/2}$
Tempkin	$q_e = \frac{RT}{b_t}\ln(a_t C_e)$		

q_t is the adsorption capacity, i.e., the amount of solute adsorbed at time t; q_e is the adsorption capacity at equilibrium; q_m is the maximum adsorption capacity estimated by the model; C_e is the concentration of the solute at equilibrium; K_L is the Langmuir equilibrium constant; K_F and n_F are Freundlich constants and β is a parameter in the range 0–1; K_S and n_S are Sips constants; K_{RP} and α_{RP} are Redlich-Peterson constants; R is the gas constant; T is the absolute temperature; b_t is a constant related to the heat of adsorption and a_t is the Tempkin isotherm constant; k_1 is the pseudo-first order rate constant; k_2 is the pseudo-second order rate constant; A and B are Elovich constants; k_p is the intraparticle rate constant and C is the intercept

adsorption and accounts for the formation of multilayers with nonuniform distribution of adsorption heat and affinities over heterogeneous surfaces. Because the equation is exponential, usually it provides good fitting only in low to moderate concentration ranges of the sorbate. The Sips isotherm [82] combines the Langmuir and Freundlich expressions and it is usually applied for describing heterogeneous adsorption. At low adsorbate concentration it reduces to Freundlich isotherm while at high concentration it predicts the monolayer adsorption characteristic of the Langmuir isotherm. Similar to the Sips equation, the Redlich-Peterson isotherm [72] is an empirical model that also compromises the features of the Langmuir and Freundlich equations. It is a versatile equation than can be applied either in homogeneous or heterogeneous adsorption, over a wide sorbate concentration range. This isotherm equation described very well the adsorption of Pb(II), Cd(II) Cu(II) and Cr(VI) ions onto magnetic chitosan-based biocomposites [63, 21]. The Tempkin isotherm [85] assumes that adsorption heat of molecules in the layer decreases linearly with coverage. This is explained due to the sorbent–sorbate interactions and the distribution of binding energies in the adsorption is uniform. This isotherm fitted well the removal of the dye Basic Blue 9 using magnetic alginate composites [58].

The pseudo-first and the pseudo-second order equations are expressions commonly used for describing sorption kinetics, although they cannot be considered sorption kinetic models in their physical sense since they are used to describe the kinetics of other phenomena as well. The pseudo-first-order equation has been widely used to predict the adsorption of solutes from liquid solutions in systems near equilibrium and in systems with a time-independent solute concentration or linear behavior in equilibrium adsorption isotherms [83]. In contrast with the previous model, the pseudo-second-order kinetic equation predicts the behavior over the

whole range of adsorption [37]. The Elovich model [77] neglects the rate of simultaneously occurring desorption and therefore its applicability if often restricted to the initial times of the sorption process [66]. This model was suitable for describing the kinetic behavior of the adsorption of the reactive dye red 222 in chitosan-based materials [95]. In the same work the authors analyzed the kinetic data found in the literature for several biopolymer-based adsorption systems and found that the Elovich model fits well the adsorption kinetics of those systems with mildly rising tendency. The intraparticle diffusion model was proposed by Weber and Morris [93] who found that in many adsorption systems, the adsorption capacity varies almost proportionally with $t^{1/2}$ rather than with contact time t. This model assumes that the intraparticle–diffusion is the rate-limiting step of the solute uptake.

4.2 Removal of Metal Ions

Hazardous metal ions are commonly found in natural and wastewaters as dissolved contaminants. Some of these cations have been considered priority pollutants, such as Hg(II), thus requiring effective processes for their removal from water. A range of bionanocomposites has been investigated as effective sorbents for metal ions removal; here only those with ability for magnetic separation will be considered.

Alginate magnetic beads have shown great efficiency in the uptake of Pb(II) ions from aqueous solutions [40]. The adsorption equilibrium was achieved in less than 3 h in the pH range 6–10, with maximum adsorption observed at pH 7. The results fitted well to the Langmuir adsorption model with maximum adsorption capacity about 50 mg/g. Also, alginate-agarose magnetite composites have been applied in the removal of U(VI) from aqueous medium. The maximum uranium adsorption (97 ± 2 %) was observed in the pH range of 4.5–5.5. The thermodynamic parameters suggested passive endothermic adsorption behavior [89]. The performance of magnetic alginate-chitosan beads for the adsorption of lanthanum ions from aqueous solutions was evaluated. The materials showed selective high adsorption for lanthanum among other coexisting ions, such as Pb(II), Cd(II), Co (II), Ni(II) and Cu(II), with a maximum uptake of 97.1 mg/g. The adsorption data correlated well with the Langmuir isotherm model, while the kinetic data fit well the pseudo- second-order model [94]. Ngomsik et al. [60] evaluated the adsorption of Ni(II) from aqueous solutions using magnetic alginate microcapsules containing Cyanex 27 extractant. A two-stage kinetics behavior was observed with 70 % of maximum sorption capacity achieved within 8 h. An increase on Ni(II) removal was observed by increasing the pH, with a maximum uptake capacity of 0.42 mmol/g at pH 8. The adsorption isotherm (pH about 5.3) was obtained for a range of Ni(II) initial concentrations; the experimental data fitted the Langmuir model and the maximum adsorption capacity was reported as 0.52 mmol/g.

Humic acid (HA) coated Fe_3O_4 nanoparticles were investigated as sorbents for removal of various aqueous cations such as Hg(II), Pb(II), Cd(II), and Cu(II) [54].

The sorption of these ions reached equilibrium in less than 15 min, and agrees well with the Langmuir adsorption model with maximum adsorption capacities ranging from 45 to 100 mg/g. The composite was able to remove over 99 % of Hg(II) and Pb(II), and over 95 % of Cu(II) and Cd(II) in natural and tap water at optimized pH. More recently, Yang et al. [98] investigated the removal of Eu(III) ions from aqueous solutions by Fe_3O_4@HA composites. A fast sorption kinetics was observed, equilibrium reached in less than 30 min, with high sorption capacity attributed to abundant surface sites for coordination provided by the HA macromolecules. The composites were able to remove ~99 % of Eu(III) in aqueous solution at pH 8.5. The sorption isotherm agreed well with the Langmuir model, having a maximum sorption capacity of 6.95×10^{-5} mol/g.

The adsorption ability of Gum kondagogu modified Fe_3O_4 nanoparticles was investigated in the removal of a variety of metal ions [30]. The removal efficiencies of the different cations followed the order: Cd(II) > Cu(II) > Pb(II) > Ni(II) > Zn (II) > Hg(II), while for the overall desorption (%) of these ions the following series was established: Pb(II) > Cu(II) > Cd(II) > Hg(II) > Ni(II) > Zn(II), at pH = 5.0 ± 0.1 and temperature of 30.0 ± 1.0 °C. A maximum of 106.8 mg/g and a minimum of 35.07 mg/g adsorption capacities were observed, respectively, for Cd (II) and Hg(II), using the Langmuir isotherm model.

Sebasnia gum magnetic nanocomposites were used as adsorbents to remove Cd (II), Cu(II), and Pd(II). Consecutive sorption–desorption cycles were repeated thrice to establish the reusability of the adsorbent. The composite shows desorption efficiencies after the regeneration process above 91.19 % for Cu (II), 96.69 % for Cd (II), and 87.61 % for Pb (II) ions [46].

Chitosan and derivative composites have been widely used as sorbents to remove heavy metal ions from aqueous solutions. Figure 8 illustrates the overall process of adsorption, desorption and recycling in using magnetite cellulose–chitosan hydrogels for the removal of metal ions [52]. These studies have shown that the hydrogels had scarce affinity to Mn(II), Zn(II), and Ni(II), but exhibited high affinity to Cu(II), Fe(II), and Pb(II), with corresponding equilibrium adsorption capacities (mg/g) of, respectively, 44.7 ± 5, 94.1 ± 7 and 28.1 ± 3 of the adsorbent (dried weight).

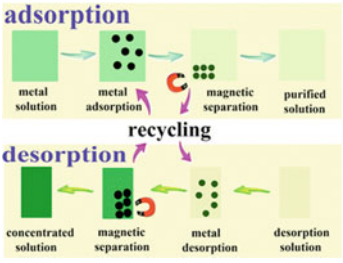

Fig. 8 Overall process of metal adsorption, desorption and recycling of magnetite cellulose-chitosan hydrogels. Reprinted with permission from [52]. Copyright 2012 Royal Society of Chemistry

Zhou et al. [104] prepared chitosan-coated maghemite nanoparticles modified with α-ketoglutaric acid and evaluated the ability to remove Cu(II) ions from the aqueous solution. Equilibrium studies have shown that Cu(II) adsorption data follow the Langmuir model, and the maximum adsorption capacity for Cu(II) ions was estimated as 96.15 mg/g. Also, magnetite chitosan hydrogels, graft-copolymerized with methylenebisacrylamide, and poly(acrylic acid) were employed in studies on the adsorption kinetics of Pb (II), Cd(II), and Cu(II) in aqueous solution [63]. The best experimental parameters for removal of metal ions have been observed at pH 4.5–5.5, initial metal concentration of 300 mg/dm^3 and 100 mg of dried hydrogel mass as sorbent. Isotherm models of Langmuir, Freundlich, and Redlich–Peterson were applied and revealed that the adsorption efficiency decreased with the presence of magnetite. The removal of Hg(II), Cu(II), and Ni(II) ions from aqueous solutions mediated by thiourea modified magnetite chitosan microspheres was investigated [104]. The adsorption kinetics followed the mechanism of pseudo-second-order equation for all systems studied, evidencing chemical sorption as the rate-limiting step of adsorption mechanism and not involving mass transfer in solution. The best interpretation for the equilibrium data was given by a Langmuir isotherm, and the maximum adsorption capacities were 625.2, 66.7 and 15.3 mg/g for Hg(II), Cu(II), and Ni(II) ions, respectively. Fan et al. [26] prepared magnetite thiourea-chitosan composites using Ag(I) as an imprinted ion and were able to show that this resin is strongly selective for the adsorption of Ag(I) over Cd(II), Zn(II), Pb(II), and Cu(II). The equilibrium adsorption was achieved within 50 min and the maximum adsorption capacity was 4.93 mmol/g observed at pH 5 and temperature 30 °C. The kinetic data, obtained at optimum pH 5, could be fitted with a pseudo-second order equation. Furthermore, the adsorption process was well described by Langmuir adsorption. In another study, monodisperse chitosan-coated Fe_3O_4 nanoparticles were used as adsorbents for recovery of Au(III) ions from aqueous solutions. Au(III) ions could be fast and efficiently adsorbed, and the adsorption capacity increased with decrease in pH due to protonation of the amino groups of chitosan. The adsorption data obeyed the Langmuir equation with a maximum adsorption capacity of 59.52 mg/g (1210 mg/g based on weight of chitosan) and a Langmuir adsorption equilibrium constant of 0.066 mg^{-1}. From the studies on the adsorption kinetics and thermodynamics of Au(III) ions, it was found that the adsorption process obeyed the pseudo-second-order kinetic model [12]. Magnetic chitosan composites were used as sorbents for removal of radioactive species from aqueous medium [14, 38, 101]. Magnetic chitosan composite particles exhibited high adsorption capacity for both UO_2(II) (666.67 mg/g) and Th(IV) (312.50 mg/g) and the authors conclude that the OH and –NH_2 groups were involved in this process [38]. In another study, Chen et al. [14] evaluated the capacity of Fe_3O_4-chitosan beads to remove Sr(II) ions from aqueous solutions. The adsorption equilibrium was reached at 6 h and the maximum adsorption capacity was calculated to be 11.58 mg/g using the Langmuir isotherm.

4.3 Removal of Dyes

In addition to metal ions, magnetic bionanocomposites have also been applied in the removal of dyes from aqueous solutions. These organic pollutants can be present in the effluents of industries of a number of products that include textiles, papers, plastics, among others. The discharge of dyes in water supplies is a matter of concern due to their harmful impact on the environment. Most of these compounds are potentially harmful to aquatic life and several dyes and their degradation products exhibit toxicity and potential mutagenic and carcinogenic effects [90].

Magnetic alginate composites have been investigated as sorbents for magnetic removal of dyes from aqueous solutions [76, 58, 2]. Ai et al. [2] reported the preparation of AC-$CoFe_2O_4$-alginate composites for effective removal of methylene blue (MB) from aqueous solutions. The kinetic studies revealed that the adsorption process followed the pseudo-first-order kinetic model. In addition, the adsorption equilibrium was well described by the Langmuir and Freundlich models. In another study, Mahmodi [58] investigated the ability of a nickel-zinc ferrite-alginate composite to remove dyes from both single and binary systems. Basic Blue 9 (BB9), Basic Blue 41 (BB41) and Basic Red 18 (BR18) were selected as model pollutants. The data obtained in single systems showed that the experimental data correlated reasonably well by the Tempkin (BB9) and Langmuir (BB41 and BR18) isotherm models. The data also indicated that the adsorption kinetics of dyes on the adsorbents followed the intraparticle diffusion model at different adsorbent dosages.

Rocher et al. [76] combined the adsorption properties of AC and the magnetic properties of γ-Fe_2O_3 NPs in an alginate matrix to produce a magnetic sorbent. The sorbent ability toward cationic MB and anionic methyl orange (MO) dyes was then evaluated. The adsorption kinetics reached equilibrium after 180 min, 50 % of the amount of MB was adsorbed in 10 min, while for MO this percentage of adsorption was achieved at 17 min contact time. Also, cellulose beads entrapping γ-Fe_2O_3 NPs and AC have been investigated for removal of such dyes from aqueous medium. Although the beads effectively adsorbed both dyes, these systems have shown higher adsorption capacity for MO than for MB. This reveals that the negatively charged MO was easier to bind with the beads through hydrogen bonding and electrostatic interaction. So the system could adsorb more strongly the negatively charge organic dyes (MO) than positively charged MB, indicating a selective adsorption behavior [56].

Mittal and Mishra [59] incorporated Fe_3O_4 NPs in a matrix of gum ghatti cross-linked with poly(acrylic acid-co-acrylamide) for removal of rhodamine B (RhB) from aqueous solutions. The adsorption at pH 7 of RhB onto the nanocomposite was endothermic and involved an increase in entropy. The process followed the Langmuir adsorption model and a maximum adsorption capacity of 654.87 mg/g was reported. The pseudo-second-order kinetic model described better the adsorption process than other kinetic models with high correlation coefficients.

Furthermore, the adsorbent showed good reproducibility and reusability for successive three cycles.

κ-Carrageenan coated Fe_3O_4 nanoparticles were tested as adsorbents for the magnetically assisted removal of MB from aqueous solutions [78]. The dye uptake was found to vary with solution pH and was higher in alkaline conditions. Both pseudo-first-order and pseudo-second-order equations predicted well the kinetics with the maximum adsorption achieved very fast, within 5 min. Interestingly, in this case MB adsorption has shown an unusual Z-type isotherm, which was interpreted by the generation of new adsorbing sites with increasing MB initial concentration. Under the experimental conditions used (23 °C, pH 9) the materials displayed MB adsorption capacity of 185.3 mg/g.

A chitosan-coated magnetite composite containing alizarin red (AR) as imprinted molecules was prepared and used to remove AR from aqueous solutions [26]. A maximum adsorption capacity of 40.12 mg/g was observed at pH 3 and temperature 30 °C. Equilibrium adsorption was achieved within 50 min. The kinetic data, obtained at the optimum pH 3, could be fitted with a pseudo-second-order equation. Furthermore, the adsorption process could be well described by Langmuir adsorption isotherms. The same group reported the preparation of similar magnetic chitosan composites but containing GO for the removal of MB [27]. The MB maximum adsorption capacity was 180.83 mg/g and the adsorption process was well fitted by the pseudo-second-order kinetic model. The incorporation of carbon nanostructures in magnetic chitosan-based sorbents was also explored by wrapping multiwalled carbon nanotubes and γ-Fe_2O_3 nanoparticles for the purpose of removal of MO [108].

Zhu et al. [109] prepared a γ-Fe_2O_3-SiO_2-chitosan composite and investigated the adsorption performance of this composite toward MO dissolved in water. The adsorption kinetics was found to follow the pseudo-second-order kinetic model, and intraparticle diffusion was related to adsorption, but not as a sole rate-controlling step. The equilibrium adsorption data were well described by the Freundlich isotherm model. The same group investigated the adsorptive potential of chitosan-kaolin-γ-Fe_2O_3 [106] and γ-Fe_2O_3-crosslinked chitosan [107] composites for removal of MO. Kalkan and co-workers [45] prepared magnetite nanoparticles coated with chitosan and applied it for removal of the reactive textile dye Reactive Yellow 145. The dye adsorption occurs according to the Langmuir model in the temperature range of 25–45 °C with a maximum adsorption capacity of 47.63 mg/g at 25 °C.

Magnetite NPs were synthesized onto guar gum-grafted carbon nanotubes to prepare a magnetic composite for adsorption of red (MR) and methylene blue (MB) from aqueous solutions [97]. The grafting of guar gum onto the carbon nanotubes (CNTs) enhances their hydrophilicity, thus improving their dispersion in aqueous solutions. The adsorption behavior of the composite for MB and NR could be described well by the pseudo second-order model. The adsorption isotherm experiments revealed that the adsorption data fitted Langmuir isotherm model, and the maximum adsorption of MB and NR reached 61.92 and 89.85 mg/g.

Multiwall carbon nanotubes-starch-Fe_3O_4 composite was used as an adsorbent for removing anionic dye methyl orange (MO) and cationic dye methylene blue (MB) from aqueous solutions [13]. The use of hydrophilic starch improved the dispersion of the composite in aqueous solutions and increased the number of surface sites available for dyes adsorption. The adsorption behavior was well described by the pseudo second-order model and the maximum adsorption capacities at equilibrium were 135.6 mg/g for MO and 93.7 mg/g for MB.

Debrassi et al. [22] prepared magnetic *N*-benzyl-O-carboxymethylchitosan nanoparticles and applied these nanosorbents on removal of three cationic dyes: MB, crystal violet (CV), and malachite green (MG). A pseudo-second-order equation was the best-fitted equation to characterize the adsorption process for the three dyes, among four kinetic models applied. The Langmuir–Freundlich equation was the best isotherm model, and maximum adsorption capacities of 223.58, 248.42 and 144.79 mg/g were reported for MB, CV, and MG, respectively.

4.4 Removal of Anions

The major sources of water contamination by large amounts of certain anions are domestic and agriculture activities. The intensive use of fertilizers in agriculture and forestry sectors has strong impact on contamination of natural waters by certain anions [3]. There have been attempts to use magnetic biocomposites for removal of such anions from contaminated water. For example, Lee and Kim [49] developed magnetic alginate-layered double hydroxide composites for phosphate removal. The results have shown that the magnetic composites were effective in the removal of phosphate and equilibrium was reached at 24 h. The maximum phosphate sorption capacity was determined to be 39.1 mgP/g. In addition, phosphate removal was not much sensitive to the initial solution pH (between 4.1 and 10.2).

Chitosan beads containing nanosized γ-Fe_2O_3 were prepared for Cr(VI) removal in the form of dissolved dichromate ($Cr_2O_7^{2-}$) and the effect of pH and coexisting ions on the magnetic removal was investigated [44]. The sorbent showed excellent performance in removal of $Cr_2O_7^{2-}$ from water with a maximum sorption capacity

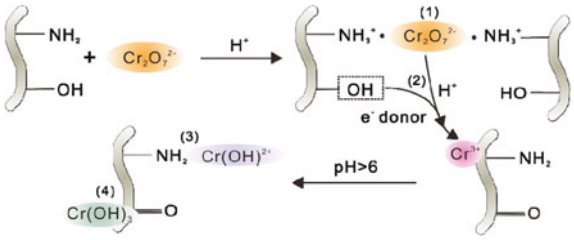

Fig. 9 Scheme for the mechanism proposed in the interaction of Cr(VI) with γ-Fe_2O_3—chitosan beads. Reprinted with permission from [44]. Copyright 2013 American Chemical Society

of 106.5 mg/g in the concentration range 0–200 ppm. The determination of the thermodynamic parameters indicates the spontaneous and exothermic nature of the sorption process. The γ-Fe_2O_3- chitosan bionanocomposite beads kept their performance after six cycles regeneration. The sorption of Cr(VI) on the beads has been described by a series of processes as illustrated in Fig. 9. Hence, dichromate species were first adsorbed on the beads surface via electrostatic attraction, occurring reduction to Cr(III) by the –OH groups of chitosan and coordination of the Cr(III) ions by the amine groups on the bead surfaces. In these processes there is consumption of hydrogen ions, which result in increase of the solution pH.

In some regions, arsenic can be present as a dangerous contaminant of water in the form of arsenate (AsO_4^{3-}) and/or arsenite (AsO_3^{3-}). The toxicity and mobility of arsenic are affected by its oxidation state, with arsenite as more toxic and mobile than arsenate in aqueous environments. Arsenate removal by calcium alginate-encapsulated magnetic sorbents has been investigated [51]. Fourier transform infrared spectroscopy (FTIR) and X-ray photoelectron spectroscopy (XPS) were used to assess the interaction between arsenic species and available sites of the sorbent. These studies indicate that surface oxygen of the magnetite and hydroxyl groups of the calcium alginate composite play an important role in the sorption of arsenate ions. Based on the XPS analysis it has been proposed that arsenate is reduced to arsenite after adsorption onto the sorbent.

Water-soluble molybdate anions represent a threat to the environment for concentrations exceeding 5 ppm. Therefore, the development of materials for treatment of water with high levels of such anions is an important issue. Elwakeel et al. [25] prepared two chemically modified chitosan resins incorporating magnetite NPs for removal of Mo oxoanions from aqueous solutions via anion exchange. Chitosan resins bearing both amine and quaternary ammonium chloride moieties (R2) displayed higher uptake capacity than the analog with only amine (R1) groups.

5 Conclusions and Future Perspectives

The application of magnetic bionanocomposites as sorbents for magnetic separation in water treatment has emerged as an interesting alternative to conventional sorbents. These materials offer clear advantages due to their potential bio- and eco-compatibility, tuned magnetic behavior, and affinity for a variety of pollutants, aiming at development of magnetic separation technologies of interest for water treatment units. Implementation of surface chemical modifications to adjust the affinity/specificity toward distinct pollutants has been demonstrated in various contexts, but more research is required, namely evaluation in real samples of diverse chemical composition and from different sources. These sorbents offer the clear advantage of magnetic separation by applying an external magnetic field in confined spaces. This aspect has important consequences in terms of waste storage, or recycling and reuse of sorbents, but on the other hand implies further developments on magnetic separation technology.

Acknowledgments F.L. Sousa acknowledges FCT (Fundação para a Ciência e a Tecnologia) for SFRH/BPD/71033/2010 grant. A.L. Daniel-da-Silva and N.J.O. Silva acknowledge FCT for funding from Ciência 2008 program and IF2013 contract, respectively. The authors thank funding by FEDER through COMPETE- Programa Operacional Factores de Competitividade and national funding from FCT in the frame of the project PTDC/CTM-NAN/120668/2010 and FCOMP-01-0124-FEDER-037271 (Ref. Pest-C/CTM/LA0011/2013).

References

1. Ahmaruzzaman M (2011) Industrial wastes as low-cost potential adsorbents for the treatment of wastewater laden with heavy metals. Adv Colloid Interface Sci 166:36–59
2. Ai L, Li M, Li L (2011) Adsorption of methylene blue from aqueous solution with activated carbon/cobalt ferrite/alginate composite beads: kinetics, osotherms, and thermodynamics. J Chem Eng Data 56:3475–3483
3. Ali I (2012) New generation adsorbents for water treatment. Chem Rev 112:5073–5091
4. Babel S, Kurniawan TA (2003) Low-cost adsorbents for heavy metals uptake from contaminated water: a review. J Hazard Mater 97:219–243
5. Badruddoza AZM, Tay ASH, Tan PY, Hidajat K, Uddin MS (2011) Carboxymethyl-β-cyclodextrin conjugated magnetic nanoparticles as nano-adsorbents for removal of copper ions: Synthesis and adsorption studies. J Hazard Mater 185:1177–1186
6. Bailey SE, Olin TJ, Bricka RM, Adrian DD (1999) A review of potentially low-cost sorbents for heavy metals. Water Res 33:2469–2479
7. Banerjee SS, Chen D-H (2007) Fast removal of copper ions by gum arabic modified magnetic nano-adsorbent. J Hazard Mater 147:792–799
8. Bee A, Talbot D, Abramson S, Dupuis V (2011) Magnetic alginate beads for Pb(II) ions removal from wastewater. J Colloid Interface Sci 362:486–593
9. Bhattacharyya KG, Gupta SS (2008) Adsorption of a few heavy metals on natural and modified kaolinite and montmorillonite: A review. Adv Colloid Interface Sci 140:114–131
10. Blackburn RS (2004) Natural polysaccharides and their interactions with dye molecules: applications in effluent treatment. Environ Sci Technol 38:4905–4909
11. Carlos L, Einschlag FSG, González MC, Mártire DO (2013) Waste water – treatment technologies and recent analytical developments. Intech – Open Access Publisher
12. Chang Y-C, Chen D-H (2006) Recovery of gold(III) ions by a chitosan coated magnetic nano-adsorbent. Gold Bulletin 39:98–102
13. Chang PR, Zheng P, Liu B, Anderson DP, Yu J, Ma X (2011) Characterization of magnetic soluble starch-functionalized carbon nanotubes and its application for the adsorption of the dyes. J Hazard Mater 186:2144–2150
14. Chen Y, Wang J (2012) Removal of radionuclide Sr^{2+} ions from aqueous solution using synthesized magnetic chitosan beads. Nucl Eng Des 242:445–451
15. Crini G (2005) Recent developments in polysaccharide-based materials used as adsorbents in wastewater treatment. Prog Polym Sci 30:38–70
16. Crini G (2006) Non-conventional low-cost adsorbents for dye removal: A review. Bioresour Technol 97:1061–1085
17. Daniel-da-Silva AL, Carvalho RS, Trindade T (2013) Magnetic hydrogel nanocomposites and composite nanoparticles – a review of recent patented works. Recent Pat Nanotechnol 7:153–166
18. Daniel-da-Silva AL, Silva NJO, Gil AM, Trindade T (2011) Nano-composite particles for bio-applications: Materials and bio-interfaces. Pan Stanford Publishing Pte. Ltd., Singapore
19. Daniel-da-Silva AL, Trindade T (2011) Advances in nanocomposite technology. Intech – Open Access Publisher

20. Dave SR, Gao X (2009) Monodisperse magnetic nanoparticles for biodetection, imaging, and drug delivery: a versatile and evolving technology. Wires Nanomed Nanobi 1:583–609
21. Debnath S, Maity A, Pillay K (2014) Magnetic chitosan–GO nanocomposite: Synthesis, characterization and batch adsorber design for Cr(VI) removal. J Environ Chem Eng 2:963–973
22. Debrassi A, Corrêa AF, Baccarin T, Nedelko N, Slawska-Waniewsk A, Sobczak K, Dłuzwskib P, Greneche J-M, Rodrigues CA (2012) Removal of cationic dyes from aqueous solutions using N-benzyl-O-carboxymethylchitosan magnetic nanoparticles. Chem Eng J 183:284–293
23. Demirbas A (2008) Heavy metal adsorption onto agro-based waste materials: A review. J Hazard Mater 157:220–229
24. Dias AMGC, Hussain A, Marcos AS, Roque ACA (2011) A biotechnological perspective on the application of iron oxide magnetic colloids modified with polysaccharides. Biotechnol Adv 29:142–155
25. Elwakeel KZ, Atia AA, Donia AM (2009) Removal of Mo(VI) as oxoanions fromaqueous solutions using chemically modified magnetic chitosan resins. Hydrometallurgy 97:21–28
26. Fan L, Luo C, Lv Z, Lu F, Qui H (2011) Removal of Ag^+ from water environment using a novel magnetic thiourea-chitosan imprinted Ag^+. J Hazard Mater 194:193–201
27. Fan L, Luo C, Sun M, Li X, Lu F, Qiu H (2012) Preparation of novel magnetic chitosan/graphene oxide composite as effective adsorbents toward methylene blue. Bioresour Technol 114:703–706
28. Fan L, Luo C, Sun M, Li X, Qiu H (2013) Highly selective adsorption of lead ions by water-dispersible magnetic chitosan/graphene oxide composites. Colloids Surf B 103:523–529
29. Fan L, Zhang Y, Li X, Luo C, Lu F, Qiu H (2012) Removal of alizarin red from water environment using magnetic chitosan with Alizarin Red as imprinted molecules. Colloids Surf B 91:250–257
30. Foo KY, Hameed BH (2010) Insights into the modeling of adsorption isotherm systems. Chem Eng J 156:2–10
31. Freundlich HMF (1906) Over the adsorption in solution. J Phys Chem 57:385–471
32. Girginova PI, Daniel-da-Silva AL, Lopes CB, Figueira P, Otero M, Amaral VS, Pereira E, Trindade T (2010) Silica coated magnetite particles for magnetic removal of Hg2+ from water. J Colloid Interface Sci 345:234–240
33. Gong J-L, Wang X-Y, Zeng G-M, Chen L, Deng J-H, Zhang X-R, Niu Q-Y (2012) Copper (II) removal by pectin–iron oxide magnetic nanocomposite adsorbent. Chem Eng J 185–186:100–107
34. Goodenough JB (1963) Magnetism and the chemical bond. John Wiley and Sons, New York
35. Guglielmo CD, López DR, Lapuente JD, Mallafre JML, Suàrez MB (2010) Embryotoxicity of cobalt ferrite and gold nanoparticles: a first in vitro approach. Reprod Toxicol 30:271–276
36. Gupta AK, Gupta M (2005) Synthesis and surface engineering of iron oxide nanoparticles for biomedical applications. Biomater 26:3995–4021
37. Ho YS, McKay G (1999) Pseudo-second order model for sorption processes. Process Biochem 34:451–465
38. Hritcu D, Humelnicu D, Dodi G, Popa MI (2012) Magnetic chitosan composite particles: Evaluation of thorium and uranyl ion adsorption from aqueous solutions. Carbohydr Polym 87:1185–1191
39. Hu J, Lo IMC, Chen G (2004) Removal of Cr(VI) by magnetite. Water Sci Technol 50:139–146
40. Idris A, Ismail NSM, Hassan N, Misran E, Ngomsik A-F (2012) Synthesis of magnetic alginate beads based on maghemite nanoparticles for Pb(II) removal in aqueous solution. J Ind Eng Chem 18:1582–1589
41. Inbaraj BS, Chen BH (2011) Dye adsorption characteristics of magnetite nanoparticles coated with a biopolymer poly(γ-glutamic acid). Bioresour Technol 102:8868–8876

42. Indira TK, Lakshmi PK (2010) Magnetic nanoparticles–a review. Int Pharm Sci Nanotech 3:1035–1042
43. Jeong U, Teng X, Wang Y, Yang H, Xia Y (2007) Superparamagnetic colloids: controlled synthesis and niche applications. Adv Mater 19:33–60
44. Jiang Y-J, Yu X-Y, Luo T, Jia Y, Liu J-H, Huang X-J (2013) γ-Fe_2O_3 Nanoparticles encapsulated millimeter-sized magnetic chitosan beads for removal of Cr(VI) from water: Thermodynamics, kinetics, regeneration, and uptake mechanisms. J Chem Eng Data 58:3142–3149
45. Kalkan NA, Aksoy S, Aksoy EA, Hasirci N (2012) Adsorption of reactive yellow 145 onto chitosan coated magnetite nanoparticles. J Appl Polym Sci 124:576–584
46. Lan S, Leng Z, Guo N, Wu X, Gan S (2014) Sesbania gum-based magnetic carbonaceous nanocomposites: Facile fabrication and adsorption behavior. Colloids Surf A 446:163–171
47. Langmuir I (1918) The adsorption of gases on plane surfaces of glass, mica and platinum. J Am Chem Soc 40:1361–1406
48. Laurent S, Forge D, Port M, Roch A, Robic C, Elst LV, Muller RN (2008) Magnetic iron oxide nanoparticles: synthesis, stabilization, vectorization, physicochemical characterizations, and biological applications. Chem Rev 108:2064–2110
49. Lee C-G, Kim S-B (2013) Magnetic alginate-layered double hydroxide composites for phosphate removal. Environ Technol 34:2749–2756
50. Li G, Du Y, Tao Y, Deng H, Luo X, Yang J (2010) Iron(II) cross-linked chitin-based gel beads: Preparation, magnetic property and adsorption of methyl orange. Carbohydr Polym 82:706–713
51. Lim S-F, Zheng Y-M, Zou S-W, Chen JP (2009) Uptake of arsenate by an alginate-encapsulated magnetic sorbent: Process performance and characterization of adsorption chemistry. J Colloid Interface Sci 333:33–39
52. Liu Z, Wang H, Liu C, Jiang Y, Yu G, Mu X, Wang X (2012) Magnetic cellulose–chitosan hydrogels prepared from ionic liquids as reusable adsorbent for removal of heavy metal ions. Chem Commun 48:7350–7352
53. Liu B, Wang D, Li H, Xu Y, Zhang L (2011) As(III) removal from aqueous solution using α-Fe_2O_3 impregnated chitosan beads with As(III) as imprinted ions. Desalination 272:286–1292
54. Liu J-F, Zhao Z-S, Jiang G-B (2008) Coating Fe_3O_4 magnetic nanoparticles with humic acid for high efficient removal of heavy metals in water. Environ Sci Technol 42:6949–6954
55. Lu A-H, Salabas EL, Schüth F (2007) Magnetic nanoparticles: synthesis, protection, functionalization, and application. Angew Chem Int Ed 46:1222–1244
56. Luo X, Zhang L (2009) High effective adsorption of organic dyes on magnetic cellulose beads entrapping activated carbon. J Hazard Mater 171:340–347
57. Mahdavinia GR, Iravani S, Zoroufi S, Hosseinzadeh H (2014) Magnetic and K+-cross-linked kappa-carrageenan nanocomposite beads and adsorption of crystal violet. Iran Polym J 23:335–344
58. Mahmoodi NM (2013) Magnetic ferrite nanoparticle–alginate composite: Synthesis, characterization and binary system dye removal. J Taiwan Inst Chem Eng 44:322–330
59. Mittal H, Mishra SB (2014) Gum ghatti and Fe_3O_4 magnetic nanoparticles based nanocomposites for the effective adsorption of rhodamine B. Carbohydr Polym 101:1255–1264
60. Ngomsik A-F, Bee A, Siaugue J-M, Cabuil V, Cote G (2006) Nickel adsorption by magnetic alginate microcapsules containing an extractant. Water Res 420:1848–1856
61. Obeid L, Bée A, Talbot D, Jaafar SB, Dupuis V, Abramson S, Cabuil V, Welschbillig M (2013) Chitosan/maghemite composite: A magsorbent for the adsorption of methyl orange. J Colloid Interface Sci 410:52–58
62. Pankhurst QA, Connolly J, Jones SK, Dobson J (2003) Applications of magnetic nanoparticles in biomedicine. J Phys D: Appl Phys 36:R167–R181
63. Paulino AT, Belfiore LA, Kubota LT, Muniz EC, Almeida VC, Tambourgi EB (2011) Effect of magnetite on the adsorption behavior of Pb(II), Cd(II), and Cu(II) in chitosan-based hydrogels. Desalination 275:187–196

64. Paulino AT, Guilherme MR, Mattoso LHC, Tambourgi EB (2010) Smart hydrogels based on modified gum arabic as a potential device for magnetic biomaterial. Macromol Chem Phys 211:1196–1205
65. Peng L, Qin P, Lei M, Zeng Q, Song H, Yang J, Shao J, Liao B, Gu J (2012) Modifying Fe_3O_4 nanoparticles with humic acid for removal of Rhodamine B in water. J Hazard Mater 209–210:193–198
66. Plazinski W, Rudzinski W, Plazinska A (2009) Theoretical models of sorption kinetics including a surface reaction mechanism: A review. Adv Colloid Interface Sci 152:2–13
67. Polyak B, Friedman G (2009) Magnetic targeting for site-specific drug delivery: applications and clinical potential. Expert Opin Drug Del 6:53–70
68. Pourjavadi A, Hosseini SH, Seidi F, Soleyman R (2013) Magnetic removal of crystal violet from aqueous solutions using polysaccharide-based magnetic nanocomposite hydrogels. Polym Int 62:1038–1044
69. Purcell EM (1977) Life at low reynolds number. Am J Phys 45:3–11
70. Rakhshaeea R, Panahandeh M (2011) Stabilization of a magnetic nano-adsorbent by extracted pectin to remove methylene blue from aqueous solution: A comparative studying between two kinds of cross-likened pectin. J Hazard Mater 189:158–166
71. Reddy DHK, Lee SM (2013) Application of magnetic chitosan composites for the removal of toxic metal and dyes from aqueous solutions. Adv Colloid Interface Sci 201–202:68–93
72. Redlich O, Peterson DL (1959) A useful adsorption isotherm. J Phys Chem 63:1024–1026
73. Ritter JA, Ebner AD, Daniel KD, Stewart KL (2004) Application of high gradient magnetic separation principles to magnetic drug targeting. J Magn Magn Mater 280:184–201
74. Rivera-Utrilla J, Sánchez-Polo M, Gómez-Serrano V, Alvarez PM, Alvim-Ferraz M CM, Dias JM (2011) Activated carbon modifications to enhance its water treatment applications. An overview. J Hazard Mater 187:1–23
75. Rocher V, Bee A, Siaugue J-M, Cabuil V (2010) Dye removal from aqueous solution by magnetic alginate beads crosslinked with epichlorohydrin. J Hazard Mater 178:434–439
76. Rocher V, Siaugue J-M, Cabuil V, Bee A (2008) Removal of organic dyes by magnetic alginate beads. Water Res 42:1290–1298
77. Roginsky S, Zeldovich Y (1934) Acta Physicochim USSR 1:554
78. Salgueiro AM, Daniel-da-Silva AL, Girão AV, Pinheiro PC, Trindade T (2013) Unusual dye adsorption behavior of κ-carrageenan coated superparamagnetic nanoparticles. Chem Eng J 229:276–284
79. Saravanan P, Vinod VTP, Sreedhar B, Sashidhar RB (2012) Gum kondagogu modified magnetic nano-adsorbent: An efficient protocol for removal of various toxic metal ions. Mater Sci Eng C 32:581–586
80. Sharifi I, Shokrollahi H, Amiri S (2012) Ferrite-based magnetic nanofluids used in hyperthermia applications. J Magn Magn Mater 324:903–915
81. Shi H, Li W, Zhong L, Xu C (2014) Methylene blue adsorption from aqueous solution by magnetic cellulose/graphene oxide composite: Equilibrium, kinetics, and thermodynamics. Ind Eng Chem Res 53:1108–1118
82. Sips R (1948) Combined form of Langmuir and Freundlich equations. J Chem Phys 16:490–495
83. Soto ML, Moure A, Dominguez H, Parajó JC (2001) Recovery, concentration and purification of phenolic compounds by adsorption: A review. J Food Eng 105:1–27
84. Tang SCN, Lo IMC (2013) Magnetic nanoparticles: Essential factors for sustainable environmental applications. Water Res 47:2613–2632
85. Tempkin MJ, Pyzhev V (1940) Recent modification to Langmiur isotherms. Acta Physiochim USSR 12:217–222
86. Thakur VK, Thakur MK (2014) Processing and characterization of natural cellulose fibers/thermoset polymer composites. Carbohydrate Polymers 109:102–117

87. Thakur VK, Thakur MK, Raghavan P, Kessler MR (2014) Progress in green polymer composites from lignin for multifunctional applications: A review. ACS Sustain Chem Eng 2:1072–1092
88. Tong J, Chen L (2013) Review: Preparation and application of magnetic chitosan derivatives in separation processes. Anal Lett 46:2635–2656
89. Tripathi A, Melo JS, D'Souza SF (2013) Uranium (VI) recovery from aqueous medium using novel floating macroporous alginate-agarose-magnetite cryobeads. J Hazard Mat 246–247:87–95
90. Umbuzeiro GA, Freeman HS, Warren SH, de Oliveira DP, Terao Y, Watanabe T, Claxton LD (2005) The contribution of azo dyes to the mutagenic activity of the Cristais River. Chemosphere 60:55–64
91. Vettorazzi G (1979) International regulatory aspects for pesticide chemicals. CRC Press Inc.: Boca Raton, Florida
92. Wang Ngah WS, Teong LC, Hanafiah MAKM (2011) Adsorption of dyes and heavy metal ions by chitosan composites: A review. Carbohydrate Polymers 83:1446–1456
93. Weber Jr WJ, Morris JC (1963) Kinetics of adsorption on carbon from solution. J Sanit Eng Div Am Soc Civ Engrs 89:31–59
94. Wu D, Zhang L, Wang L, Zhu B, Fan L (2011) Adsorption of lanthanum by magnetic alginate-chitosan gel beads. J Chem Technol Biotechnol 86:345–352
95. Wu F-C, Tseng R-L, Juang R-S (2009) Characteristics of Elovich equation used for the analysis of adsorption kinetics in dye-chitosan systems. Chem Eng J 150:366–373
96. Xu P, Zeng GM, Huang DL, Feng CL, Hu S, Zhao MH, Lai C, Wei Z, Huang C, Xie GX, Liu ZF (2012) Use of iron oxide nanomaterials in wastewater treatment: A review. Sci Total Environ 424:1–10
97. Yan L, Chang PR, Zheng P, Ma X (2012) Characterization of magnetic guar gum-grafted carbon nanotubes and the adsorption of the dyes. Carbohydr Polym 87:1919–1924
98. Yang S, Zong P, Ren X, Wang Q, Wang X (2012) Rapid and highly efficient preconcentration of Eu(III) by core–shell structured Fe_3O_4@humic acid magnetic nanoparticles. ACS Appl Mater Interfaces 4:6891–6900
99. Zhang S, Zhang Y, Bi G, Liu J, Wang Z, Xu Q, Xu H, Li X (2014) Mussel-inspired polydopamine biopolymer decorated with magnetic nanoparticles for multiple pollutants removal. J Hazard Mater 270:27–34
100. Zhou L, Jin J, Liu Z, Liang X, Shang C (2011) Adsorption of acid dyes from aqueous solutions by the ethylenediamine-modified magnetic chitosan nanoparticles. J Hazard Mater 185:1045–1052
101. Zhou L, Shang C, Liu Z, Huang G, Adesina AA (2012) Selective adsorption of uranium(VI) from aqueous solutions using the ion-imprinted magnetic chitosan resins. J Colloid Interface Sci 366:165–172
102. Zhou L, Wang Y, Liu Z, Huang Q (2009) Characteristics of equilibrium, kinetics studies for adsorption of Hg(II), Cu(II), and Ni(II) ions by thiourea-modified magnetic chitosan microspheres. J Hazard Mater 161:995–1002
103. Zhou Y, Fu S, Zhang L, Zhang H, Levit MV (2014b) Use of carboxylated cellulose nanofibrils-filled magnetic chitosan hydrogel beads as adsorbents for Pb(II). Carbohydr Polym 101:75–82
104. Zhou Y-T, Nie H-L, Branford-White C, He Z-Y, Zhu L-M (2009) Removal of Cu^{2+} from aqueous solution by chitosan-coated magnetic nanoparticles modified with α-ketoglutaric acid. J Colloid Interface Sci 330:29–37
105. Zhou Z, Lin S, Yue T, Lee T-C (2014a) Adsorption of food dyes from aqueous solution by glutaraldehyde cross-linked magnetic chitosan nanoparticles. J Food Eng 126:133–141
106. Zhu H-Y, Jiang R, Xiao L (2010) Adsorption of an anionic azo dye by chitosan/kaolin/γ-Fe_2O_3 composites. Appl Clay Sci 48:522–526
107. Zhu H-Y, Jiang R, Xiao L, Li W (2010) A novel magnetically separable γ-Fe_2O_3/crosslinked chitosan adsorbent: Preparation, characterization and adsorption application for removal of hazardous azo dye. J Hazard Mater 179:251–257

108. Zhu H-Y, Jiang R, Xiao L, Zeng GM (2010) Preparation, characterization, adsorption kinetics and thermodynamics of novel magnetic chitosan enwrapping nanosized γ-Fe_2O_3 and multi-walled carbon nanotubes with enhanced adsorption properties for methyl orange. Bioresour Technol 101:5063–5069
109. Zhu HY, Jiang R, Fu Y-Q, Jiang J-H, Xiao L, Zeng G-M (2011) Preparation, characterization and dye adsorption properties of γ-Fe_2O_3/SiO_2/chitosan composite. Appl Surf Sci 258:1337–1344

Magnetite Nanocomposites Thin Coatings Prepared by *MAPLE* to Prevent Microbial Colonization of Medical Surfaces

Alina Maria Holban, Alexandru Mihai Grumezescu and Crina Maria Saviuc

Abstract MAPLE (matrix-assisted pulsed laser evaporation) technique revealed a significant relevance in the deposition of bioactive nanostructures on different surfaces for the prevention and/or treatment of microbial infections associated with medical devices. Recent research progress highlights the development of two new directions for biomedical applications of magnetite nanoparticles: the antimicrobial therapy and microbial virulence and biofilm modulation. The aim of this chapter is to highlight the usefulness of functionalized magnetite nanoparticles as efficient anti-infective agents. In this respect, different type of nanocomposites based on hydrophilic/hydrophobic polymers and iron oxide nanostructures combined with natural and synthetic therapeutic agents are discussed. We offer a wide perspective regarding their synthesis, characterization, biocompatibility, and the ability to modulate the microbial attachment and biofilms development on different type of prosthetic devices or metal implants. All reported data demonstrate that magnetite-based bioactive coatings significantly inhibit the microbial colonization on the coated medical surfaces, features that together with their high in vivo viability recommend these type of thin coatings for the development of anti-infective surfaces for biomedical applications.

Keywords Matrix-assisted pulsed laser evaporation · MAPLE · Thin films · Coatings · Antimicrobial-coatings · Drug delivery · Magnetite nanoparticles · Magnetite nanocomposites · Medical surfaces

A.M. Holban · C.M. Saviuc
Faculty of Biology, Microbiology Department, University of Bucharest, Aleea Portocalelor no 1-3, 060101 Bucharest, Romania

A.M. Holban · A.M. Grumezescu (✉)
Faculty of Applied Chemistry and Materials Science, Department of Science and Engineering of Oxide Materials and Nanomaterials, University Politehnica of Bucharest, Polizu Street no 1-7, 011061 Bucharest, Romania
e-mail: grumezescu@yahoo.com
URL: http://grumezescu.com/

C.M. Saviuc
Biotehnos S.A, Otopeni, Romania

V.K. Thakur and M.K. Thakur (eds.), *Eco-friendly Polymer Nanocomposites*, Advanced Structured Materials 74, DOI 10.1007/978-81-322-2473-0_10

1 Introduction

Microorganisms may attach to and colonize most known surfaces and this ability represents one of the major risks for hospitalized patients, especially for critical care units. The infection sources are represented by different medical surfaces, which get in contact with patients and medical personnel, but also permanent implants and explorative devices [108]. Colonizing bacteria are usually resistant and multiresistant strains and most of them are able to produce biofilms on the colonized surface. These sessile, multicellular arrangements, called biofilms, represent the major complication of a medical device infection. Bacteria embedded in biofilms have a modified metabolism, being resistant and tolerant to most used antimicrobials, therefore the current anti-infectious therapy is usually ineffective [56, 57]. Surface modification of the medical devices could represent a very efficient strategy in order to inhibit microbial attachment, colonization and biofilm formation, thus fighting against device-associated resistant infections. Recent studies revealed that nanotechnology and laser techniques may be efficiently used in order to customize medical surfaces [36–40, 42, 43].

The most desired characteristics of a customized surface with medial purpose is to reduce bacterial adhesion and multiplication, but in the same time to support and promote eukaryotic cell adhesion. Biocompatibility and applicability of surface modification with current uses of metallic, polymeric, and ceramic biomaterials allow the modification of properties to enhance performance in a biological environment, while retaining bulk properties of the device [60, 61, 97–101]. Using biomaterials for developing improved medical surfaces, the resulting device will present increased biocompatibility and will usually reduce the environmental damage associated with many surface modification methods [81, 102, 103, 109].

Magnetic materials have been used for many years in medical applications and many modern technologies are currently emerging on the biomedical field. Magnetite can be used for cell separation, magnetic resonance imaging (MRI), diverse immunoassays, drug and gene delivery, minimally invasive surgery, radionuclide therapy, hyperthermia, artificial muscle applications, implants, and anti-infectious therapies [4, 42, 43, 53]. Not only the physicochemical properties, but also its great biocompatibility recommend magnetite as preferred option for developing diverse coatings for medical devices [36, 64].

There were described various characterization and surface modification methods based on nanocomposite biomaterials, containing magnetite, with useful applications in many biomedical areas. Advanced laser techniques flourished in recent years and due to their accuracy and malleability they are preferred coating methods for many applications, including the ones developed for the biomedical field [42, 43, 77]. Despite the advantages and wide usage of advanced laser techniques in the last 10 years, only few research papers regarding Matrix-Assisted Pulsed Laser Evaporation (MAPLE) surface modification using magnetite nano-formulations can be found [13, 23]. This relatively new procedure brings new insights in medical surfaces modification because it allows the deposition of uniform thin films

independent on the composition of deposited and target material and ensures the controlled release of the active drug contained within the bioactive nanosystem.

In this chapter we discuss the rates and main complications of biofilm-associated infections; but also the implications of magnetite-based nano-formulations on anti-infectious therapy, highlighting the possible impact of such nanosystems on the development of customized medical devices with improved anti-biofilm surfaces using advanced laser techniques. We also reveal the medical perspectives of MAPLE and related technologies on the technological progress aiming to obtain smart prosthetic devices able to control microbial colonization.

2 Microbial Colonization of Medical Surfaces

It has been estimated that about 20 million individuals have different implanted medical devices in United States only, the associated costs exceeding 300 billion dollars per year, and representing about 8 % of health care practiced throughout the world [82].

Applications covering areas range from the cardiovascular, orthopedic, ophthalmology domains to the dental and regenerative surgery (substitutes for tissues), or to the pharmaceutical industry (e.g., controlled delivery systems or matrix-embedded sensors for diagnosis). Therefore, materials industry recently flourished with several types of materials intended for medical use [94–96, 102, 103].

Developing a new biomaterial involves compatibility with biomedical application tests. Characterization should include mechanical, physicochemical and biological properties, but also stability/instability traits, the ultimate goal being to satisfy clinical and economical requirements.

Even though in the manufacture process, the properties of biomaterials and also the surgical procedure are strictly controlled and risk factors are efficiently predicted in implantology, the high rate of associated infections currently limit the use of most implants.

The adhesion in biology is a concept of a fundamental importance, attachment mechanisms being necessary precursors of most biological processes. The complex architectural organization and biological role of cell coatings that interfere in all biological processes, determined cell surface structures to become one of the privileged subjects of cellular and molecular biology, as well as immunology.

The adhesion of microorganisms to different surfaces have been widely investigated, in order to identify the adhesion-related properties, according to the incriminated species or type of microorganism, as well as the properties of the substrates and environmental conditions that significantly influence the process (e.g., temperature, pH, electrolyte concentration). Therefore, any study of the adhesion must be well-defined to meet a specific question. Controlling this phenomenon in the sense of attachment or detachment of microorganisms in conjunction with highly diverse mechanisms of microbial adhesion represents an important interdisciplinary research topic [3, 5, 57].

2.1 Structures, Biomolecules, and Filamentous Appendages Involved in Adhesion to the Inert Substratum

Bacterial cell wall is the support of all structures involved in adhesion (filamentous appendix and biomolecules), being a stiff shell structure which completely surrounds the bacterial cells. Common constituent of the cell wall of Gram-positive, Gram-negative, and acid–alcohol fast bacteria is the peptidoglycan. The differential elements between different groups of bacteria are the ratio, site, quantity, and structural arrangement of proteins, polysaccharides, and lipids. Teichoic acids are long and flexible molecules, polymers of 1,3-poly(glycerol phosphate) or 1,5-poly (ribitol phosphate), linked through phosphodiester bonds, often substituted with different glycosyl or amino acid residues and terminally linked to the muramic acid of peptidoglycan [11]. The literature mentioned the contribution of teichoic acids in biofilm formation. *Staphylococcus aureus* contains a widely studied polysaccharide with demonstrated role in bacterial adhesion and biofilm formation, PIA or PNAG (**p**olysaccharide **i**ntercellular **a**dhesin or **p**oly-**Na**cetyl**g**lucosamine). PIA associated with other parietal anchored structures, such as teichoic acids are achieved by multiple ionic bonds. Variable content of D-alanine in teichoic acids reduce the net negative charge. The absence of D-alanine in mutant strains causes deficiencies in the ability to form biofilms on the polystyrene or glass surfaces, probably due to the increase in the net negative charge resulting in electrostatic repulsions that inhibit the initial adhesion step in the biofilms formation.

Lipopolysaccharides (LPS) embedded in the outer membrane of Gram-negative bacteria can form hydrogen bonds with various inert substrates; strength of the bonds is approximately 2.5kT J (where k is Boltzmann's constant and T is absolute temperature). It was estimated that 1000 hydrogen bonds may bind irreversibly the bacterial cells to the substrate [44]. Identifying and quantifying the relationship between the physical properties of LPS and strength of the bonds in the adhesion to the inert substrate was reported as a convenient way to differentiate virulent phenotypes in vitro. Also, it was confirmed that the influence of the LPS three-dimensional structure and the number of repeating chemical moieties on the strength of the adhesion forces, using a bacterial related model, investigated by atomic force microscopy technique.

Exopolymeric substances (EPS = extracellular polymeric substances) of bacterial origin are extraparietal structures that develop on the surface of bacterial cells, such as capsules and glicocalix, different in terms of thickness, structure, chemical composition, and complexity. Polysaccharides are major constituents of this type of structures, being responsible for bacterial adhesion to the inert or cellular substratum and biofilms formation. The binding forces involved in such interactions are electrostatic forces or hydrogen bonds [44].

The S layer is a component of the cell cover, consisting of a three-dimensional crystalline network of protein subunits. S-layer now can be considered as one of the most commonly observed bacterial cell surface structures. Most S-layers are composed of a single protein or glycoprotein species endowed with the ability to

assemble into a monomolecular lattice by an entropy-driven process. S-layers can provide the organism with a selection advantage, by functioning as protective coats, molecules sieve, molecule and ion traps, and structures implicated in cell adhesion and surface recognition [92].

Bacterial fimbriae are the best studied adhesions. They are filamentous protein structures composed of fimbrillin subunits, of different lengths, usually present in large numbers on the surface of many bacteria. It has been suggested that the type-1 fimbriae, as well as outer membrane proteins participating in the adhesion of the bacteria at different material surfaces, in particular in the initial stage of adhesion, by stabilizing the contact of the cells with hydrophobic surfaces.

Pili are rigid hairlike, tubular, elongated structures, present in small numbers, often isolated on the bacterial cell surface, primarily composed of oligomeric pilin, a phosphoglycoprotein. Pili are defined by structural, biochemical, morphological, and antigenic features. It seems that the type IV pili, particularly found in Gram-negative bacteria, are involved in bacterial adhesion to the inert substratum, as well as in the specific adhesion [7, 44]. The ability of *Acinetobacter venetianus* to adhere to different substrates correlates with the presence of pili [35]. [106] described that MvaT, a global transcription factor in *Pseudomonas aeruginosa* inhibits the expression of *cup* genes, which are involved in the chaperone/usher pathway of fimbrial assembly. MvaT—defective mutants have a superior adhesion capacity, compared with type IV pili and flagellar-defective mutants, indicating that the initial adhesion and biofilm formation are mediated by these extraparietal structures [106].

2.2 The Kinetics of Microbial Adhesion and Biofilm Formation

Bacterial adhesion to a surface involves the following sequence of events: (1) transport near to the substrate, (2) initial adherence to the substrate, (3) molecular interactions with the substrate/conditioning film, which causes irreversible adhesion (in normal environmental conditions, including the presence of shear forces due to fluid flow in biological environments), followed by the (4) biofilm formation.

Simplifying the actual parameters of bacterial adherence, followed by the biofilms formation, this process could be treated as a process of heterocoagulation in mixed colloidal systems, which represents the interaction between the particles that differ in composition and/or size, and is dependent on the concentration of the electrolyte, specific adsorption of the hydrolyzed ionic species and steric stability. It has been demonstrated that the physical–chemical properties of the substrate influence the initial adsorption of microorganisms and subsequent development of biofilms [25]. These properties are: the available surface area, hydrophobicity, surface energy, adsorption of conditioning film, the presence of humic material (in natural environments) and fibronectin (in humans and animals), physical defects

(such as granular structure or surface topography), and the cracks. Other involved factors are: corrosion, surface catalytic activity, and the photochemical reactivity of the surface oxidized layer [57].

Physical–chemical interactions between bacterial cells and inert surfaces depend on the distance between the two surfaces and the electrolytes concentration, as well as the presence of additional binding sites. The first theory used to explain the interactions involved in bacterial adhesion was the DLVO theory (Derjaguin, Landau, Verwey, Overbeek), developed for macromolecules and particles. This theory considers that the total energy of adhesion is the result of the van der Waals attractive forces and the general repulsive interactions due to the interpenetration of the electrical double layers. The DLVO theory does not consider short-range interactions that are also important for adhesion, mainly Brownian movement forces and polar interactions (e.g., hydrophobic interactions). van Oss 1994, proposed an extension of the DLVO theory, generally known as XDLVO theory, this new approach considering the sum of the Lifshitz–van der Waals forces, polar interactions, electrical double layer interactions, and Brownian movement forces as terms of total free energy evaluation [6]. Due to the heterogeneity of macromolecules on the bacterial cell surface, there are some limitations in the application of DLVO theory to accurately estimate the quantitative bacterial adherence: (1) separation distance requires the existence of a clear separation between the surface and the environment. The reference point setting for it could not be fixed at the cell surface, consequently, the electrical charges involved in electrostatic interactions will be disperse distributed on the bacterial glicocalix. (2) flat plate geometry is generally assumed, because the dimensions of the surface are usually several orders of magnitude above those of an individual cell or bacterial surface macromolecules. (3) steric hindrance or specific covalent bonds between surface bacterial molecules with molecules of the film conditioning. (4) the zeta potential and Hamaker constant (van der Waals interactions characteristic) are parameters estimated by discrete values, which do not characterize accurately enough the entire cell surface. (5) the DLVO theory expresses a state of a thermodynamic equilibrium, that for the biological systems involved is reached in a time interval difficult to estimate, requiring complex molecular rearrangements to attain a minimum free energy. In this context, it is not surprising that the application of DLVO theory to study the dynamics of microbial biofilms developed on inert substrates yielded conflicting results reported in the literature, even if qualitative assessment tests were considered. Quantitative estimation approach of the microbial adhesion process becomes feasible only after the introduction of AFM technique (atomic force microscopy), which allowed the use of appropriate probes for determining the interaction forces and surface characteristics of the microbial cell [52]. A brief representation of biofilm formation stages can be found in the Fig. 1.

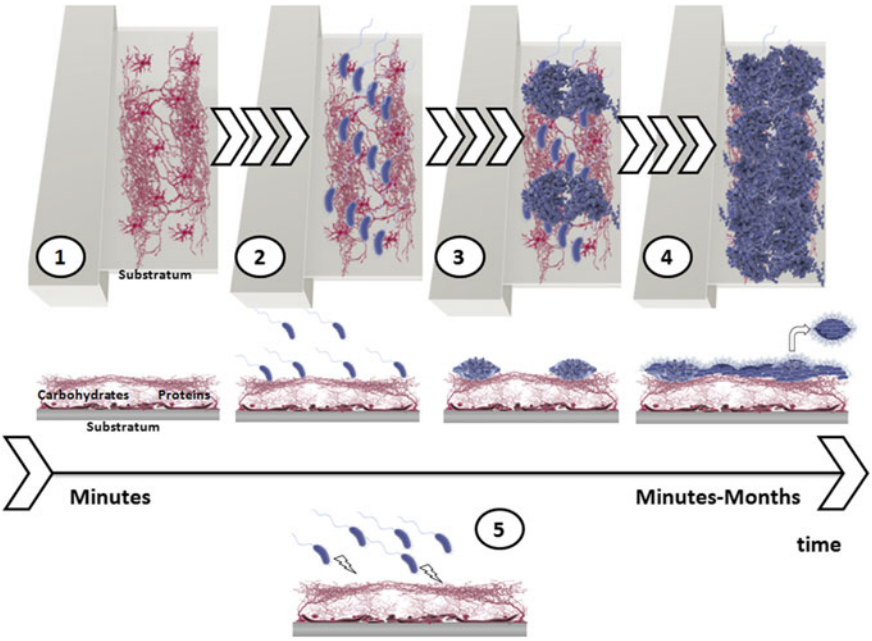

Fig. 1 Biofilm development on medical surfaces: Bacterial adhesion to a surface involves the following sequence of events: (*1*) transport near to the substrate, (*2*) initial adherence to the substrate, (*3*) molecular interactions with the substrate/conditioning film, which causes irreversible adhesion (in normal environmental conditions, including the presence of shear forces due to fluid flow in biological environments) followed by the (*4*) biofilm maturation and (*5*) dissemination of bacterial cell detached from the mature biofilm

2.3 *Mechanisms of Pathogenesis in Infections Associated with Medical Devices*

A plethora of Gram-positive and Gram-negative bacteria, as well as microfungi were identified as etiologic agents of infections in humans subsequent to a foreign body "introduction" (FBRI = foreign body related infections), *Staphylococcus epidermidis,* and other coagulase-negative staphylococci being the most often involved in FBRI after the implantation of temporary or permanent medical devices (MD). FBRI include all nosological entities with microbial etiology, localized infection, or bacteremia associated with implanted MD.

Mechanisms and presumptive pathogenesis conditions of infections caused by the biofilms included bacteria are: (1) cell detachment and aggregates release from the biofilms developed on the prosthetic devices, (2) resistance development to the host defense mechanisms, (3) toxigenesis, (4) establishment of a niche for generating resistant bacteria [11]. An extensively studied phenomenon that should be mentioned concerning biofilms-related infections is the QS (quorum sensing)

intercellular signaling mechanism. QS is an almost ubiquitous regulatory mechanism in the bacterial world involved both in physiological properties expression based on a certain cell density, and communication between bacteria. It was demonstrated that the QS works not only between individuals of the same species, but also between different species and is important for survival. Apart from their genetic apparatus for recognizing different types of prokaryotic or eukaryotic organisms bacteria exhibit a phenomenon known as crosstalk signaling system. This allows the regulation of gene expression for cooperation with other species in the same ecological niche. Synergistic behavior of several species causes a synchronization of various important functions, which allows the survival of the whole community, for example through the formation of mature multispecies biofilms [48].

However, the formation of microbial biofilms is an important reason for failure of the antimicrobial therapy. Resistance to the antimicrobial treatments, known as tolerance (recalcitrance) is a multifactorial process, a combination of physical and physiological factors, and research on biofilms requires complex experimental designs to understand this phenomenon. Biofilm resistance to antimicrobials remain incompletely elucidated, several mechanisms have been proposed to explain the phenomenon: (a) mechanisms related to the EPS matrix (antimicrobials diffusion limitation, accumulation of metabolites involved in the log phase inactivation, ion exchange capacity of the polymeric extracellular material), (b) up/down regulation of gene expression (40–60 % of the prokaryotic genome), (c) cell metabolism resting within the biofilm (due to the diffusion gradient of the nutrients in the biofilm matrix), (d) genetic plasticity within the biofilm—persister cells, (e) intercellular exchange of genetic material in multiclonal or multispecies communities [34, 58].

2.4 Foreign Body-Related Infections

Orthopedic implant infections may arise from peri- or postoperative contamination. Most infections occur within three months of implantation and are due to perioperative inoculation of the infectious agent, the microorganism being introduced directly into the tissue during, or immediately after the surgery. Staphylococci cause approximately 75 % of this FBRI and almost all of them are caused by aerobic Gram-positive cocci: coagulase-negative staphylococci are present in 30–43 % of cases, and *S. aureus* is present in 12–23 %. The incidence of *S. aureus* infections is an important issue, especially due to the emergence of multidrug-resistant strains such as MRSA. Other associated pathogens include *Enterococcus* sp. (3–7 %), *Streptococcus* sp. (9–10 %), *P. aeruginosa, Enterobacter* sp. (3–6 %), *Mycobacterium* sp., as well as anaerobic bacteria and fungal species (in particular *Candida* sp.) [89]. Also, when isolated from patients with prosthetic bone devices, *S. lugdunensis* should be considered pathogenic [33]. Relevant information about the etiology of these infections could be obtained by culturing peri-implant tissue biopsy samples or sonicated explanted devices samples [28, 104].

Ventilation-associated pneumonia (VAP) is the most common hospital-acquired infection in patients requiring respiratory assistance, being the main cause of mortality in intensive care units [2]. Approximately 8–28 % of mechanically ventilated patients are affected [55, 89]. The mortality rate of nosocomial pulmonary infection is 9–70 %. It is estimated that 50 % of antibiotics prescribed in the ICU are managed for nosocomial lower respiratory tract infections. Endotracheal intubation remains the most important risk factor for the development of nosocomial pneumonia. There is growing evidence that the epidemiology of VAP is closely related to the oral health [70, 80]. Recently, more than 700 species have been identified in the oral cavity by the use of molecular methods [112], populations of these species are selected as earlier colonizers of the endotracheal lumen, in a preconditioning step, among the microorganisms involved in VAP being developed mutual or synergistic relationships involving co-adherence and interspecies communication. Significant evidence exists for microorganisms as *P. aeruginosa* and *C. albicans*, *Streptococcus mutans*, and *C. albicans*, and *Porphyromonas gingivalis* and *Str. gordonii* [89]. The organisms responsible for VAP vary according to case mix, institution, prior antibiotic exposure, local resistance patterns, and length of mechanical ventilation. Organisms responsible for early-onset VAP are largely *Staphylococcus aureus*, *Streptococcus pneumoniae*, and *Haemophilus influenzae*, while late-onset VAP is often caused by resistant nosocomial pathogens such as *P. aeruginosa*, methicillin resistant *Staphylococcus aureus*, *Klebsiella* spp., and *Acinetobacter baumannii* [46].

Oral microbiota diversity, subject to a still open database, Human Oral Microbiome Database, has a role in the emergence and evolution of gingival pathology associated with dental implant rejection. As in the case of natural teeth, dental plaque is associated with inflammatory changes in the marginal soft tissue, peri-implant. Although the surface properties of the implant biomaterial are of importance for the initial microbial adhesion step, the long-term running it is no longer correlated to any possible pathogenesis or oral explant for therapeutic purposes [89].

CAUTI (catheter-associated urinary tract infections)—approximately one million cases are reported annually in the United States, representing approximately 40 % of all nosocomial infections. Primary risk factor in the pathogenesis is hospitalization/catheterization period, followed by colonization with nosocomial multidrug-resistant microbial species [49].

Chronic hemodialysis. Renal disorders with diverse etiology can be managed in three ways: hemodialysis, peritoneal dialysis, and renal transplantation. In all these cases may occur infectious complications with biofilm developing microorganisms, the pathogenesis of such species being influenced by specific factors. The principle of hemodialysis relies on the liquid–liquid extraction carried out by a semi-permeable filtering membrane, which is the boundary between extracorporeal blood flow and dialysate, a saline solution in purified water. Water purification systems (used for dialysate solution) have been identified as sources of microorganisms producing biofilms, although the current level of technology is impressive. The supplied water should be uncontaminated, but the quantity and quality issues

associated with the process could explain the associated risks. The amount of filtered water is by hundreds m^3 per day. For a single patient are required 200 L of water in 2 h of dialysis, which makes the number of filtered microorganisms to be very large and using the systems for the sterile water production impossible. Quality membrane filter usually prevents contamination, but the maintenance operations could be the moment of possible contamination. System contamination is a major problem, since the use of disinfectant solutions for filtered water is restricted. Contaminating microorganisms are selected oligotrophic species (due to the lack of nutrients in the system), able to attach to all available surfaces exposed, mainly as a survival strategy. The samples of water from contaminated dialysis systems usually contain Gram-negative bacteria species, fungi, and mycobacteria.

Factors which determine the pathogenesis are related to water purification system (physicochemical conditions: oligotrophic environment, various sites for adhesion, chemical composition of concentrated salt solution), and the absence of competitive relationships between populations of microorganisms associated, and especially the microorganism properties, pathogenicity, and virulence. Diffusion into the bloodstream of microbial components is also a major risk factor associated with hemodialysis. These substances are collectively referred to as pyrogenic factors or inducers of the synthesis of cytokines and diffuse through the membrane filter due to the small size of the molecules, triggering in the host organism the inflammatory cascade.

Intraperitoneal catheterization in chronic peritoneal dialysis subsequent to renal failure is also a risk factor for FBRI statistics, indicating an incidence of FBRI peritonitis of 0.82/patient. In these cases, often were isolated in culture strains of the *S. aureus* and *S. epidermidis* species, 27.8 and 19.3 % in peritonitis from positive blood cultures [89].

Infections of intravascular devices. Vascular path is used in modern medicine for administration of fluids and electrolytes, blood products, medications, parenteral nutrition, or hemodynamic monitoring. A major problem of using medical devices for venous catheterization is that it can be a reservoir for systemic infections with biofilms-related microorganisms. Central venous catheters are actually vascular surgical approaches most often associated with systemic infections.

Bacterial endocarditis. Infections are known for many decades to trigger heart diseases. The etiology of these infections is varied, as well as locating sites of infection (virtually all segments of the heart may be affected: pericardium, myocardium, endocardium, heart valves, and coronary arteries). A new problem in the infections of the heart, however, is about the rising incidence of various cardiac implants and post-implantation bacterial endocarditis. This is determined, in 80 % of cases, of species belonging to the *Staphylococcus*, *Streptococcus* and *Enterococcus* genus, and most severe complications are related with bacterial biofilm formation. Initial adhesion of microorganisms to the prosthetic devices is determined by conditioning film formation, composed of fibrinogen, fibrin, fibronectin, other plasma proteins and platelets, favoring microorganisms' adherence and colonization as well as determining a transient bacteremia. The adhesion of *S. aureus* to the heart valves and other prosthetic devices is mediated by surface adhesins, as FNbp

(**f**ibronectin **b**inding**p**rotein) A and B, clumping factor, and collagen adhesins. Coagulase-negative staphylococci adhere to the surface of intracardiac prosthetic devices by a different mechanism, caused by nonspecific factors, such as surface tension, hydrophobicity, and electrostatic forces, or by specific adhesins, autolysins, or capsular polysaccharides [89].

Contact lenses. The bacteria are able to adhere to all kinds of materials from which the lenses are made, the rate of attachment being influenced by various factors: the type of material, the water content of the material, the ionic character of the material, the pH, concentration of electrolytes, lachrymal layer of proteins (lactoferrin, immunoglobulin, mucin, lysozyme), etc. Microbial keratitis etiology associated with contact lens wear, includes microorganisms belonging to different genera and species, e.g. *P. aeruginosa*, *S. aureus*, *S. epidermidis*, *Serratia* spp, *Escherichia coli*, *Proteus* spp, *Candida* spp., microbial biofilms formed on contact lenses being multispecies communities. Contact lenses storing cases are typically the sources of contamination [89].

Currently used intrauterine devices (IUDs) are of two types: (a) nonabsorbable polymers, such as polyethylene impregnated with barium sulfate, and (b) controlled release devices, which release an active substance, such as copper or a progestational agent. A common complication of the use of these devices is pelvic inflammation with infectious etiology (*S. aureus*, *E. coli*, β-hemolytic streptococci, anaerobic microorganisms). IUD explanted from asymptomatic patients were contaminated with *Lactobacillus plantarum*, *S. epidermidis*, *Corynebacterium* sp., group B streptococci, *Micrococcus* sp., *C. albicans*, *S. aureus*, and *Enterococcus* sp. [27].

Neurological prostheses. Neurostimulation therapy involves the application of low voltage currents in different regions of the central or peripheral nervous system. Using this therapy it is aimed the management of neuropathic pain and therefore the motor disorders (e.g., Parkinson's disease). Literature data concerning infections related to these types of devices are relatively few, indicating *Staphylococcus* spp and *Ps. aeruginosa* as causative pathogens [89].

Cochlear implants. These are electronic devices that facilitate improved auditory function for the hearing impaired persons. Manufacture of cochlear implants is supervised by the FDA (Food and Drug Administration). The basic model consists of two parts, one for internal and one for external use. The rate of infectious complications of these devices ranges between 3.3 and 17 %. In most cases, the infection begins at the surgical incision site, tissue necrosis, or adjacent wound dehiscence in the first three months after the surgery. The etiologic agent most commonly found in such infections is *S. aureus*. FBRI related to the cochlear implant is a major complication requiring explantation of the device and could be associated with bacterial meningitis, especially in children. Causative agents of this complication are *Str. pneumoniae* and *Hemophilus influenzae* [89].

The breast reconstruction for esthetic purposes has become a common surgical practice. The rate of infection in such cases is 1.7–2.5 %. Etiology has been less studied than in other FBRI, but most commonly reported microorganisms involved are *S. aureus*, *Peptostreptococcus* spp, and *Clostridium perfringens* [89].

Prosthetic penile implants are designed to restore erectile function. The rate of infectious complications in these cases is 8–20 %. The organism most often involved in the etiology of these infections is *S. epidermidis* [68]. The introduction of new devices with modified surfaces, although it seems to have decreased the incidence of this type of infections, but caused a change in the etiology of these infections [110].

3 Matrix-Assisted Pulsed Laser Evaporation Customized Surfaces

MAPLE (Matrix-Assisted Pulsed Laser Evaporation) technique is an extension of PLD method (Pulsed Laser Deposition) that was successfully used to prepare thin films of organic (macro) molecules [72]. MAPLE allows the preparation of thin films with greater surface morphology than PLD, due to the laser beam energy used for target ablation that does not damage the molecules [15, 17–20, 22, 23]. The principle of this technique is very simple: organic (macro) molecules/nanostructures are solubilized/dispersed in a solvent, subsequently frozen and placed in a vacuum chamber. A laser is used to irradiate the solubilized/dispersed organic (macro) molecules/nanostructures, while the solvent is evaporated and the organic macro (molecules)/nanostructures are deposited on a substrate, which may be represented by glass, silicone, different medical devices and surfaces, etc. (Fig. 2) [15, 17–20, 22, 23].

There are two problems regarding MAPLE processing: (i) the laser beam can alter the functional groups of organic (macro) molecules/nanostructures; (ii) if the

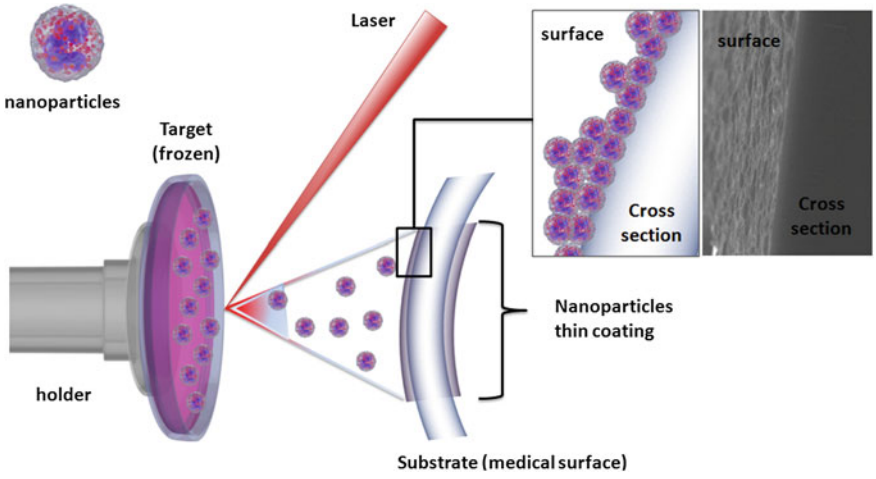

Fig. 2 Schematic representation of MAPLE technique

organic (macro) molecules/nanostructures are not well dispersed/solubilized, large aggregates may be transferred [10]. The solvent is required to absorb the laser light, protecting the functional groups of (macro) molecules/nanostructures. A series of published papers demonstrate that MAPLE can provide an improved approach to growing high-quality thin films of organic or inorganic materials [15, 17–20, 22, 23]. Table 1 presents the principal thin films and coatings prepared by MAPLE, selected fluence and their biomedical applications.

4 Magnetite Nanoparticles with Antimicrobial Loadings

Preparation of magnetite nanoparticles via coprecipitation is one of the most used methods in the last years, being safe for the preparation of high-purity magnetite nanocrystals, with a very good reproducibility and with the ability to control the size of prepared particles. Magnetite was firstly prepared by Massart method in 1981 [63]. The principle to prepare crystalline magnetite suppose the utilization of ferric and ferrous salts in molar ration 2:1, and the precipitation of these ions in basic aqueous solution [29]. In the coprecipitation are involved two mechanisms: (i) nucleation process and (ii) growth of nuclei. It has been proved that pH influence the mechanism of this reaction. The process is favored if the pH $\sim$ 11 for NH_4OH and pH $\sim$ 9–14 if NaOH is used [111]. It is required that coprecipitation of magnetite nanostructures to be realized in an atmosphere without oxygen to avoid the oxidation of magnetite to maghemite [62]. This inconvenient can be eliminated if the particles are functionalized with different organic molecules, starting from simple molecules (sulfanilic acid) to more complex molecules (amoxicillin and other antibiotics) in the coprecipitation step [39].

Coprecipitation method allow a higher amount of magnetite nanoparticles to be synthesized, but to obtain a restricted diameter of particles it is necessary to control the following parameters: molar ratio of Fe^{2+}/Fe^{3+}; pH value; concentration of ferric and ferrous ions; coprecipitation temperature and for a high restriction of dimension, surfactants are required [65, 88].

Medical applications of magnetite nanostructures are impressive, from medical imaging and diagnosis to antimicrobial therapy [37–39]. Applications of magnetite in antimicrobial therapy are related to: (i) the stimulation of the antimicrobial activity of currently used antimicrobial compounds and (ii) the modulation of microbial attachment and biofilm formation. Prepared by coprecipitation of ferric and ferrous salts, in aqueous basic solution, or by other methods (hydrothermal, solvothermal, microwaves, ultrasounds), magnetite nanoparticles can be functionalized with various organic molecules using few general routers: (i) incorporation of therapeutic agents in the coprecipitation step; (ii) preparation of magnetite nanoparticles, functionalization and chemical bonding with therapeutic agents; (iii) preparation of magnetite–polymers nanocomposites and the entrapment of therapeutic agents onto polymer network. Different molecules were used for the

Table 1 Thin films and coatings prepared by MAPLE used in medical field

Deposited compound	Fluence (mJ/cm^2)	Application
Lysozyme [79]	2000	Antimicrobial surface
SWCNTs [26]	100–200	Electromagnetic devices
Triacetate-pullulan [15]	500	Drug delivery
Cryoglobulin [16]	200	Diagnosis
Hydroxyapatite–silk fibroin [67]	400–500	Orthopedical applications
Alendronate–Hydroxyapatite [8]	750	Promote bone formation
Silicate glass–polymethylmetacrylate [31]	550	Implants and prostheses
Mg and Sr doped octacalcium phosphate [9]	750	Implants
Fibrinogen [93]	440	–
Polysiloxane [45]	30–130	Chemical sensor
Polyethylene glycol [83]	5400	–
Polyfluorene [105]	200	
Polycaprolactone [17]	500	Drug delivery
Poly(D,L-lactide) [18]	625	Drug delivery
Cinnamate-pullulan, tosylate-pullulan [50]	75–90	Drug delivery
Bovine serum albumin [51]	100–500	Protein films
Poly(1,3-bis-(p-carboxyphenoxy propane)-co-(sebacic anhydride)) [19]	1100	Drug delivery systems
Lactoferrin [14]	400–700	Vehicle delivery
Polyvinyl alcohol derivatives [20]	300	Delayed drug delivery
Mussel adhesive proteins [21]	600–1000	Antifouling affect
PEG:PLGA blends [73]	200	Drug release
Mn(III) metalloporphyrin [22]	300	Chemical/biological sensors
Peg:plga:indometacin [74]	300	Drug release
Fe_3O_4/C_{18}/cephalosporins [23]	200	Anti-biofilm surface
PLA/gentamicin [24]	500	Antimicrobial therapy
Porphyrin [47]	200–300	enzymatic biosensors
Poly(ethylene glycol)-block-poly (caprolactone) methyl ether [84]	500	Anti-biofouling
Poly(lactide-co-glycolide)/polyurethane [75]	800	Substrates for cell culture
Poly(lactic acid)–Poly (vinyl alcohol)-usnic acid [36]	300	Antimicrobial surface
poly(N-isopropylacrylamide) [85]	200–600	Cells attachment–detachment
Cellulose derivates [71]	450	Drug release
Magnetite@eugenol and (3-hidroxybutyricacid-co-3-hidroxyvaleric acid)–polyvinyl alcohol [37]	300	Anti-biofilm surface
Sulfonated phthalocyanines [30]	100–600	Gas sensors
Poly(lactic acid)-fibronectin [91]	550–700	Controlled release

(continued)

Table 1 (continued)

Deposited compound	Fluence (mJ/cm^2)	Application
Apatite [107]	750	Metallic implant coatings
Poly lactide/chitosan/dexamethasone [18]	600–1000	Drug delivery and tissue engineering
Urease [41]	400	Blood diagnostic applications
Dextran–iron oxide [78]	500	Coatings for medicine
Glass/poly(methyl methacrylate) [32]	550	Coatings for medicine
Fibronectin [90]	700	Coatings for medicine
Fe_3O_4/SiO_2/Antibiotics [66]	400	Anti-biofilm surfaces
PLGA-PVA-Fe_3O_4-UA [38]	300	Anti-biofilm surfaces

functionalization of magnetite nanoparticles: antibiotics (kanamycin, cefotaxime, penicillin, erytromycin, bacitracin), natural products (essential oils and high purity natural compounds), or macromolecules (chitosan, cellulose, alginates, polyvinyl-pyrrolidone, polyvinyl alcohol, poly lactic acid) [37, 54]. Functionalization of magnetite nanoparticles is required for improving the chemical stability in various medical environments and to prevent oxidation.

Uncoated magnetite nanoparticles present a series of disadvantages caused by: (i) aggregation in aqueous media; (ii) chemical instability (iii) low biodegradability; (iv)agglomeration in vivo; (v) nonspecific interactions with proteins; (vi) fast elimination by the immune system [69].

One of the first papers that report the ability of magnetite nanostructures to modulate microbial biofilm was reported by Saviuc et al. [86]. In this study, cover slips were coated with oleic acid functionalized magnetite nanoparticles. This type of nanostructures inhibited the colonization and biofilm formation of different fungi. Starting from this research paper, improved magnetite nanocomposites were prepared in order to modulate microbial biofilm development [86]. Deposition of magnetite nanoparticles by MAPLE on the surface of medical devices has been first reported by Cristescu et al. [23]. After that, a series of research papers has been reported highlighting the importance of magnetite nanocomposites as coating surfaces for different medical surfaces in order to improve their resistance to microbial colonization (Fig. 3).

5 Bioevaluation of Magnetite Nanoparticles and Magnetic MAPLE Deposited Surfaces

Trying to find the best formulations for antipathogenic modified surfaces, authors seek firstly for biocompatible materials with great effect against microbial development when used alone or functionalized with different antimicrobial agents. The excellent biocompatibility combined with magnetic properties make magnetic

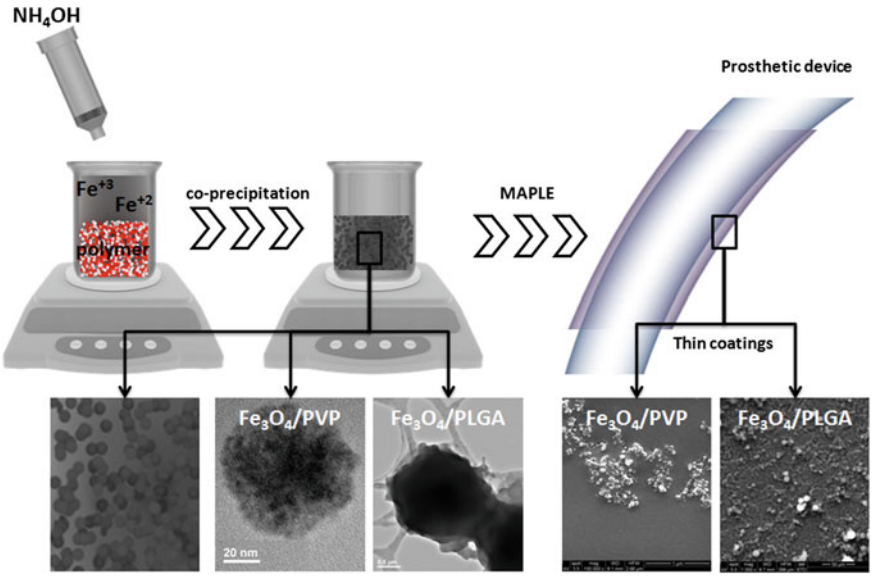

Fig. 3 Schematic representation of magnetite nanocomposite synthesis and thin coatings deposition using MAPLE technique

nanoparticles the focus of rapidly growing research efforts in controlled drug release, drug targeting, and microbial biofilm inhibition on coated surfaces. MAPLE proved to ensure a uniform deposition of magnetite thin films, the precise control of film thickness, roughness and homogeneity, slow release of active components, increased absorption into the systemic circulation, improved dispersion, and dry and sterile coating processing [66].

5.1 In Vitro Evaluation

In vitro studies revealed that thin films containing magnetite/salicylic acid/silica shell functionalized with antibiotics (Fe_3O_4/SA/SiO_2/ATB), deposited by MAPLE at a fluence of 400 mJ cm^{-2}, inhibited the attachment and biofilm formation of two main human pathogens, *P. aeruginosa* and *S. aureus* [66]. Previous studies of the same research group demonstrated that the incorporation of second, third, and fourth generation cephalosporins into magnetic microspheres improved the delivery of antibiotics in active forms [12] and this result should explain the antimicrobial effect of the Fe_3O_4/SA/SiO_2/ATB thin films. The fact that the inhibitory effect of the magnetite silica nanobiocoating is maintained during time, for at least 72 h [66], demonstrates that this MAPLE deposited thin film ensures not only the delivery but also the controlled release and stability of the therapeutic compounds. Furthermore,

this controlled release magnetic thin film proved also a good biocompatibility, the death rate of in vitro cultured human cells grown in the presence of this material being less than 5 % [66].

Cristescu et al. [23] reported a similar nanobiocoating composed of Fe_3O_4/oleic acid/ceftriaxone and Fe_3O_4/oleic acid/cefepime, deposited by MAPLE and drop-cast on polished Si and optic glass substrates. Authors demonstrated that both MAPLE and drop-cast prepared thin films exhibited great anti-attachment properties, inhibiting adherence and biofilm formation of a wide range of clinical microbial strains with diverse etiology, but biofilm inhibition was higher for thin films prepared by MAPLE. The intensity of microbial inhibition varied with the tested strain. The most obvious biofilm inhibitory effects were observed for the Gram-positive species *S. aureus* and *B. subtilis,* but also for the Gram-negative opportunistic pathogen *E. coli*, where both tested MAPLE deposited thin films were efficient. On the other hand, in the case of *P. aeruginosa* and *K. pneumonia*, only Fe3O4/oleic acid/ceftriaxone thin film proved antipathogenic properties, biofilm inhibition being in most cases significantly higher as compared with the plain antibiotic [23]. These results lead to the conclusion that either magnetite/oleic acid nanoparticles have an intrinsic antimicrobial effect or that these thin films improve the diffusion rate of the antibiotic in the liquid medium and thus the efficiency of the active drug.

In vitro biocompatibility studies performed by the same research group revealed that, despite the antibacterial attachment properties manifested against several bacteria species, Fe_3O_4/oleic acid/ATB thin films, have no impact on eukaryotic cells adherence. Studies performed on HeLa cultured cells demonstrate no morphological changes in cell morphology as revealed by microscopy analysis, demonstrating that the nanofilms have no cytotoxic effect on the eukaryotic cells [23].

Recently, Ciobanu et al. [13] reported the fabrication of dextran-coated iron oxide thin films with an estimated thickness ranging 280–360 nm using MAPLE technique. The obtained biocompatible magnetic film showed a granular surface morphology, which allowed and improved the adhesion and growth of living HepG2 cells. Authors stated also that cells developed on dextran surfaces coated with 1–5 % maghemite exhibit a normal actin cytoskeleton, suggesting that tested hepatocytes underwent normal cell cycle progression. The practical application proposed of the research group is that the thin film attached hepatocytes may be used as biosensors for different xenobiotics [13].

Due to the possibilities offered by Advanced Laser Techniques, currently there is a trend to use biopolimers in order to design micro- and nano platforms with multifunctional therapeutic properties [76]. Due to a mixture of properties such as biocompatibility, availability, relative low price and low toxicity, polylactic acid (PLA) and polyvinyl alcohol (PVA) have been extensively studied for biomedical applications [87, 114]. PLA–PVA microspheres were recently used for developing antimicrobial surfaces. These polymeric microspheres were loaded with natural agents with proved antimicrobial effect, such as Usnic Acid (UA), and deposited by MAPLE onto Ti substrates. The obtained coatings proved antimicrobial properties, reducing *S.aureus* biofilm development, as well as a good in vitro biocompatibility.

This microsphere-based thin coating proved to be efficient vehicle for UA delivery and controlled release, inhibiting microbial colonization and biofilm formation [36, 38]. These results are opening new perspectives for the prevention and therapy associated to biofilm-related infections developed on Ti prosthetic devices.

Magnetite polymeric microsphere were also developed for the delivery of natural plant derived compounds and extracts. Magnetite—polylactic-co-glycolic acid–polyvinyl alcohol (PLGA–PVA) microsphere thin films fabricated by MAPLE were used for the delivery and controlled release of UA. In vitro results showed that these magnetic nanocoatings deposited on 8 mm titanium discs, double-sided polished silicon and glass offer an increased resistance to staphylococcal colonization and also biofilm formation [36, 38].

One of our recent studies reports the fabrication and biological applications of a water dispersible nanostructure, based on magnetite and eugenol (E), prepared in a well-shaped spherical form by precipitation method, which were embedded into poly(3-hidroxybutyric acid-co-3-hidroxyvaleric acid)–polyvinyl alcohol (P (3HB-3HV)–PVA) microspheres by an oil-in-water emulsion technique [37]. The functionalized polymeric microspheres were deposited by MAPLE onto glass and both side polished silicon for investigating their effect on microbial colonization. The results revealed that the obtained thin coatings reduce the formation of *S. aureus* and *P. aeruginosa* biofims at least 3-folds after 24–48 h of incubation. After 72 h of development on the nanocoated surfaces, biofilms are less affected by the bioactive coating, although a biofilm inhibition is easily observable for both *S. aureus* and *P. aeruginosa* [37]. The reduction of the biofilm inhibitory effect may be explained by the high volatility of the active compound, eugenol, whose therapeutic effect may fade during time, as it is released from the magnetite nanostructures embedded in the polymeric microspheres.

Fe_3O_4 nanoparticles may be used also as bare nanosystems for the delivery and controlled release of plant extracts. Anghel et al. [4] reported the MAPLE deposition of *Cinnamomum verum*-functionalized Fe3O4 nanoparticles of 10 nm average diameter on the surface of gastrostomy tubes (G-tubes). Study revealed that these surface modified prosthetic devices are more resistant to *S. aureus* and *E. coli* colonization, which are the most frequent etiologies for severe and persistent infections associated with G-tube implantation. Attachment and biofilm formations of these bacterial strains on the surface of MAPLE modified G-tubes was inhibited to 3–5 folds in less than 72 h, as revealed by the in vitro experiments based on viable bacterial count assay [4]. This surface modification did not affect the biocompatibility of the G-tube, the obtained thin surfaces allowing the normal growth and development of human cultured endothelial cells for at least 5 days of contact incubation, as revealed by the microscopy analysis and mitochondrial activity of the cells [4].

Altogether, these studies demonstrate that functionalized magnetite-based bioactive coatings prepared by MAPLE may be successfully used for developing improved prosthetic devices and medical surfaces made by glass, silicone, titanium and plastic, with antimicrobial properties (Fig. 4).

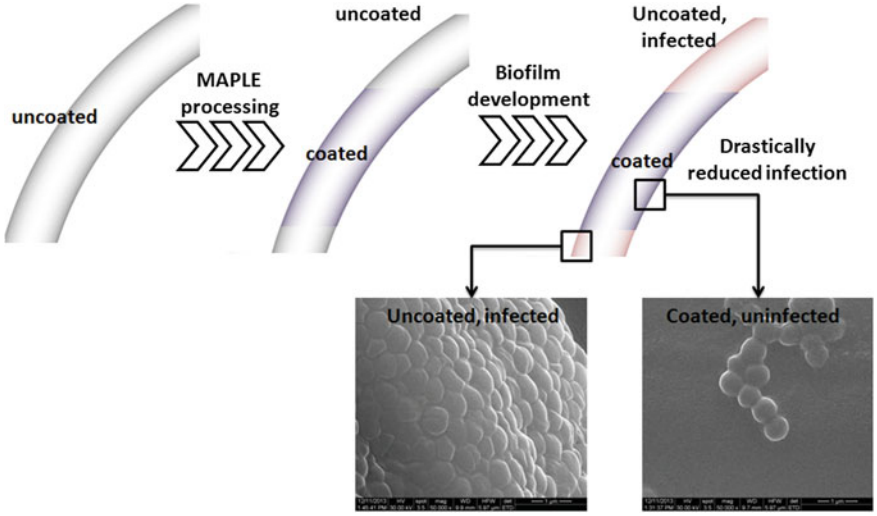

Fig. 4 Schematic representation of modified catheter surface using MAPLE and the ability of the modified surface to inhibit microbial biofilm development

5.2 In Vivo Evaluation and Biodistribution

Most in vivo assays performed to establish the potential cytotoxic effect of a coated medical surface include the insertion of a small fragment of the surface modified material in an animal model body, depending on the intended purpose of the material or final device. When using nanoparticles for thin coatings, because of their small dimensions, physicochemical properties, the potential bioactive loadings, and the fact that they can detach from the film, special attention should be paid to the potential cytotoxicity and biodistribution of the nanosystems included in the films.

Proton MRI follow-up of a rat model revealed that inhaled or instilled magnetic nanoparticles are vehiculized through the lungs and tend to accumulate in certain areas of the lungs, without being present in other vital organs as liver, spleen, and kidney [1]. Along with the administration procedure, one of the most important parameter for the biodistribution of nanoparticles is the surface coating. Yaseen and coworkers revealed that capsules' coatings influence the biodistribution of nanoparticles to a greater extent than their size, even though the circulation kinetics seems to remain the same [113]. Intravenously administrated coated nanoparticles (including magnetite) were found in the organs of the reticuloendothelial system, namely in the liver and spleen, as well as in the lungs [113].

Our recent unpublished studies performed on a Balb/c mouse model revealed that magnetite nanoparticles functionalized with antibiotics with proved antimicrobial and anti-biofilm effect are vehiculized through the blood flow and localize in certain organs. Intraperitoneally injected nanoparticles from a suspension obtained

in sterile phosphate buffered saline (PBS) were found clustered preferentially within the kidney, lungs, and spleen (Figs. 5, 6, 7, 8 and 9) at 72 h after the injection. Microscopy analysis of transversal sections obtained from mice organs revealed no clustered nanoparticles in the brain and liver (Figs. 5 and 6).

In the lungs nanoparticles were observed mainly in the perivascular macrophages found in the intra-alveolar septum. Nanoparticles were also found in the intravascular cells of the monocyte–macrophage system. It seems that the monocytes, which are the red bone marrow precursor cells of macrophages, have embedded in the nanostructures and this could explain the presence of nanoparticles in the vascular lumen. In the vascular lumen, isolated extracellular nanoparticles were found, which may be aggregated within the platelets (Fig. 7).

In the kidney, nanoparticles were observed in the blood vessels only. The rest of the renal parenchyma (glomeruli, tubules, renal stroma) did not reveal nanoparticles (Fig. 8).

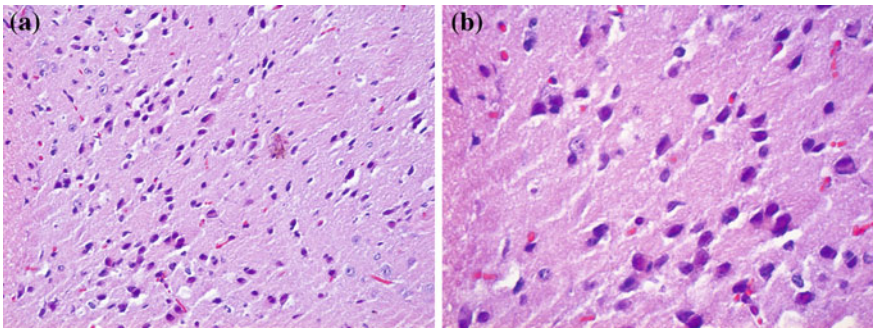

Fig. 5 Transversal section through the brain of a mouse treated with magnetite nanoparticles functionalized with cefotaxime. Hematoxilin–eosin staining: **a** ×100; **b** ×200

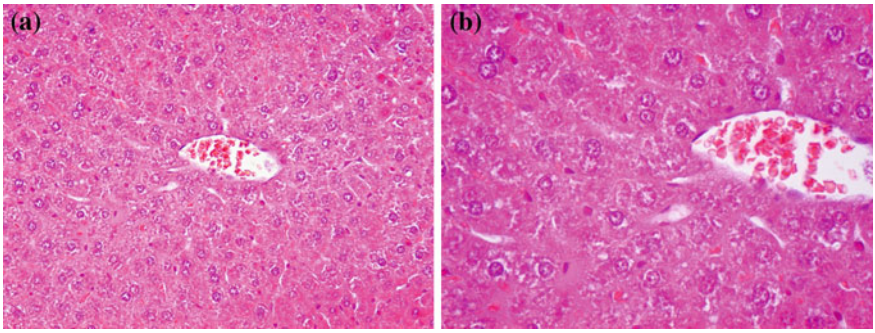

Fig. 6 Transversal section through the liver of a mouse treated with magnetite nanoparticles functionalized with cefotaxime. Hematoxilin–eosin staining: **a** ×100; **b** ×200

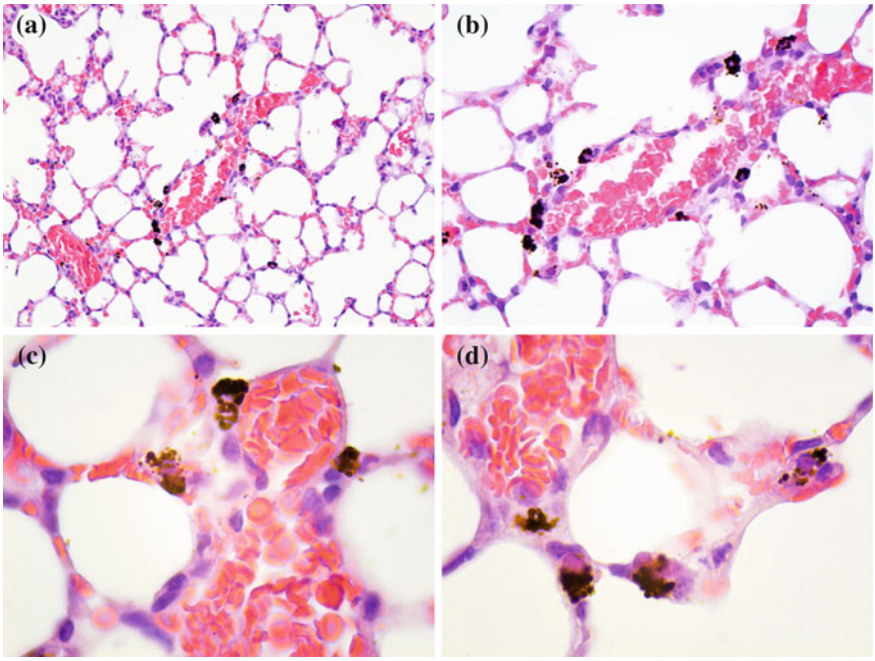

Fig. 7 Transversal section through the lung of a mouse treated with magnetite nanoparticles functionalized with cefotaxime. Hematoxilin–eosin staining: **a** ×100; **b** ×200; **c** ×400; **d** ×1000

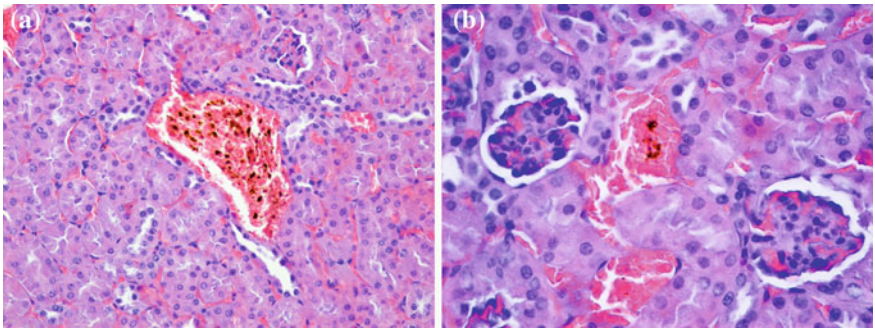

Fig. 8 Transversal section through the kidney of a mouse treated with magnetite nanoparticles functionalized with cefotaxime. Hematoxilin–eosin staining: **a** ×200; **b** ×400

Nanoparticles were present in the spleen sections, but only in the red pulp. In the white pulp, nanoparticles were absent. In the red pulp, nanoparticles have been identified in cells of the macrophages found both in Billroth cords and in the sinusoidal capillaries. Under the microscopy analysis of these sections, nanoparticles appear as granular structures, usually spherical, of various sizes, with diameters

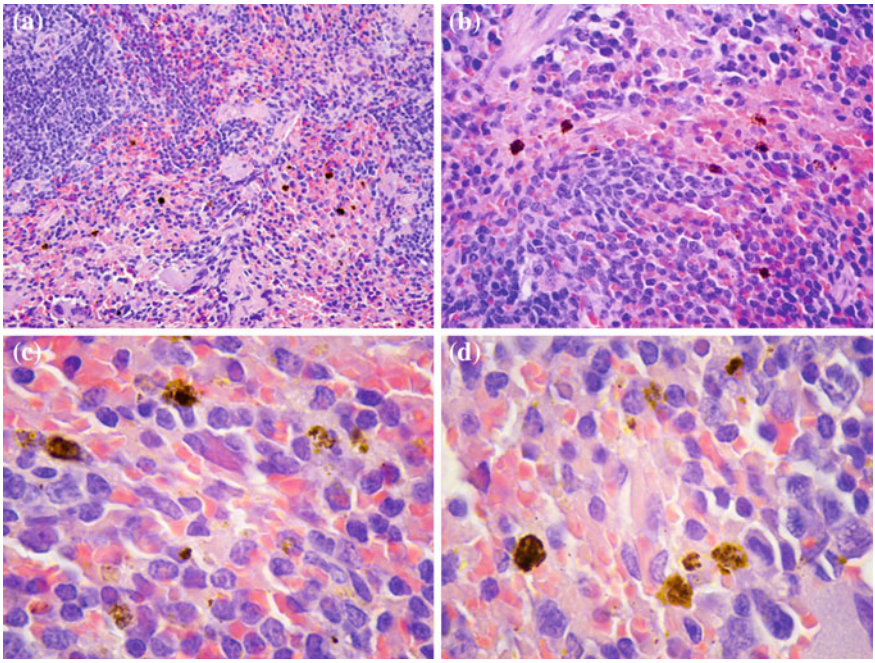

Fig. 9 Transversal section through the spleen of a mouse treated with magnetite nanoparticles functionalized with cefotaxime. Hematoxilin–eosin staining: **a** ×200; **b** ×400; **d**, **e** ×1000

up to 3 μ, black brown colored. The density of the nanoparticles varied from one cell to another: some cells revealing a higher concentration of intracellular nanoparticles (Fig. 9).

6 Conclusions and Perspectives

This chapter reports the current status of magnetite nanocomposites research with direct application on the biomedical field. Magnetite nanocomposites can be used successfully as thin coatings prepared by advanced laser techniques, to prevent contamination, colonization, and microbial biofilm development of different Gram-positive, Gram-negative, and fungal species. This new trend in antimicrobial therapy, involving nanotechnology is a promising approach for medical surfaces to prolong the life and utility of different prosthetic devices. MAPLE represents a recently developed technique ($\sim$10 years ago) with unique advantages regarding preparation of nanometric films and coatings on different surfaces. MAPLE processing allows the modulation of the releasing rate of the therapeutic agents due to the ability of varying the thickness of films/coatings and also offers the possibility to

use compounds, biomaterials, and biopolimers which cannot be processed through other deposition techniques.

The development of improved prosthetic devices coated with magnetite nanocomposites that function as controlled release systems for natural or synthetic therapeutic agents with antimicrobial activity and enhanced biocompatibility represent a new and effective strategy for reducing health risks by increasing durability and quality of prosthetic devices and also patients' comfort, reducing also the cost of their maintenance. In addition, this strategy once optimized can be applied in the future to most medical surfaces with the potential to revolutionize the market production of medical prosthetics.

Acknowledgments The work has been funded by the Sectoral Operational Programme Human 687 Resources Development 2007–2013 of the Ministry of European Funds through the Financial 688 Agreement P

References

1. Al Faraj A, Lacroix G, Alsaid H, Elgrabi D, Stupar V, Robidel F, Gaillard S, Canet-Soulas E, Crémillieux Y (2008) Longitudinal 3He and proton imaging of magnetite biodistribution in a rat model of instilled nanoparticles. Magn Reson Med 59:1298–1303
2. Alp E, Voss A (2006) Ventilator associated pneumonia and infection control. Ann Clin Microbiol Antimicrobials 5:7
3. An H, Friedman J (2000) Handbook of bacterial adhesion: principles, methods, and applications. Humana Press Inc, Totowa
4. Anghel AG, Grumezescu AM, Chirea M, Grumezescu V, Socol G, Iordache F, Oprea AE, Anghel I, Holban AM (2014) MAPLE fabricated Fe3O4@Cinnamomum verun antimicrobial surface for improved gastrostomy tubes. Molecules 19:8981–8994
5. Atlas RM, Bartha R (1999) Microbial ecology: fundamentals and applications. Benjamin/Cummings Publ. Comp., Inc, Calif
6. Azeredo J, Visser J, Oliveira R (1999) Exopolymers in bacterial adhesion: interpretation in terms of DLVO and XDLVO theories. Colloids Surf B 14:141–148
7. Beloin C, Roux A, Ghigo JM (2008) *Escherichia coli* biofilms. Curr Top Microbiol Immunol 322:249–289
8. Bigi A, Boanini E, Capuccini C, Fini M, Mihailescu IN, Ristoscu C, Sima F, Torricelli P (2009) Biofunctional alendronate–hydroxyapatite thin films deposited by matrix assisted pulsed laser evaporation. Biomaterials 30:6168–6177
9. Boanini E, Torricelli P, Fini M, Sima F, Serban N, Mihailescu IN, Bigi A (2012) Magnesium and strontium doped octacalcium phosphate thin films by matrix assisted pulsed laser evaporation. J Inorg Biochem 107:65–72
10. Canulescu S, Schou J, Fæster S, Hansen KV, Conseil H (2013) Deposition of matrix-free fullerene films with improved morphology by matrix-assisted pulsed laser evaporation (MAPLE). Chem Phys Lett 588:119–123
11. Chifiriuc MC, Pircalabioru G, Lazăr V, Gîlea B, Dascălu L, Enache G, Bleotu C (2011) Immunogenicity of different cellular fractions of *Vibrio parahaemolyticus* strains grown under sub-lethal heat and osmotic stress. Afr J Microbiol Res 5:65–72
12. Chifiriuc CM, Grumezescu AM, Saviuc C, Croitoru C, Mihaiescu DE, Lazar V (2012) Improved antibacterial activity of cephalosporins loaded in magnetic chitosan microspheres. Int J Pharm 436:201–205

13. Ciobanu CS, Iconaru SL, Gyorgy E, Radu M, Costache M, Dinischiotu A, Le Coustumer P, Lafdi K, Predoi D (2012) Biomedical properties and preparation of iron oxide-dextran nanostructures by MAPLE technique. Chem Cent J 6:17
14. Constantinescu C, Palla-Papavlu A, Rotaru A, Florian P, Chelu F, Icriverzi M, Nedelcea A, Dinca V, Roseanu A, Dinescu M (2009) Multifunctional thin films of lactoferrin for biochemical use deposited by MAPLE technique. Appl Surf Sci 255:5491–5495
15. Cristescu R, Dorcioman G, Ristoscu C, Axente E, Grigorescu S, Moldovan A, Mihailescu IN, Kocourek T, Jelinek M, Albulescu M, Buruiana T, Mihaiescu D, Stamatin I, Chrisey DB (2006) Matrix assisted pulsed laser evaporation processing of triacetate-pullulan polysaccharide thin films for drug delivery systems. Appl Surf Sci 252:4647–4651
16. Cristescu R, Kocourek T, Moldovan A, Stamatin L, Mihaiescu D, Jelinek M, Stamatin I, Mihailescu IN, Chrisey DB (2006) Laser deposition of cryoglobulin blood proteins thin films by matrix assisted pulsed laser evaporation. Appl Surf Sci 252:4652–4655
17. Cristescu R, Doraiswamy A, Socol G, Grigorescu S, Axente E, Mihaiescu D, Moldovan A, Narayan RJ, Stamatin I, Mihailescu IN, Chisholm BJ, Chrisey DB (2007) Polycaprolactone biopolymer thin films obtained by matrix assisted pulsed laser evaporation. Appl Surf Sci 253:6476–6479
18. Cristescu R, Doraiswamy A, Patz T, Socol G, Grigorescu S, Axente E, Sima F, Narayan RJ, Mihaiescu D, Moldovan A, Stamatin I, Mihailescu IN, Chisholm B, Chrisey DB (2007) Matrix assisted pulsed laser evaporation of poly(d, l-lactide) thin films for controlled-release drug systems. Appl Surf Sci 253:7702–7706
19. Cristescu R, Cojanu C, Popescu A, Grigorescu S, Nastase C, Nastase F, Doraiswamy A, Narayan RJ, Stamatin I, Mihailescu IN, Chrisey DB (2007) Processing of poly(1,3-bis-(p-carboxyphenoxy propane)-co-(sebacic anhydride)) 20:80 (P(CPP:SA)20:80) by matrix-assisted pulsed laser evaporation for drug delivery systems. Appl Surf Sci 254:1169–1173
20. Cristescu R, Popescu C, Popescu AC, Grigorescu S, Duta L, Mihailescu IN, Caraene G, Albulescu R, Albulescu L, Andronie A, Stamatin I, Ionescu A, Mihaiescu D, Buruiana T, Chrisey DB (2009) Functionalized polyvinyl alcohol derivatives thin films for controlled drug release and targeting systems: MAPLE deposition and morphological, chemical and in vitro characterization. Appl Surf Sci 255:5600–5604
21. Cristescu R, Mihailescu IN, Stamatin I, Doraiswamy A, Narayan RJ, Westwood G, Wilker JJ, Stafslien S, Chisholm B, Chrisey DB (2009) Thin films of polymer mimics of cross-linking mussel adhesive proteins deposited by matrix assisted pulsed laser evaporation. Appl Surf Sci 255:5496–5498
22. Cristescu R, Popescu C, Popescu AC, Grigorescu S, Mihailescu IN, Ciucu AA, Iordache S, Andronie A, Stamatin I, Fagadar-Cosma E, Chrisey DB (2011) MAPLE deposition of Mn(III) metalloporphyrin thin films: structural, topographical and electrochemical investigations. Appl Surf Sci 257:5293–5297
23. Cristescu R, Popescu C, Socol G, Iordache I, Mihailescu IN, Mihaiescu DE, Grumezescu AM, Balan A, Stamatin I, Chifiriuc C, Bleotu C, Saviuc C, Popa M, Chrisey DB (2012) Magnetic core/shell nanoparticle thin films deposited by MAPLE: investigation by chemical, morphological and in vitro biological assays. Appl Surf Sci 258:9250–9255
24. Cristescu R, Popescu C, Dorcioman G, Miroiu FM, Socol G, Mihailescu IN, Gittard SD, Miller PR, Narayan RJ, Enculescu M, Chrisey DB (2013) Antimicrobial activity of biopolymer–antibiotic thin films fabricated by advanced pulsed laser methods. Appl Surf Sci 278:211–213
25. de Avila ED, de Molon RS, Vergani CE, de Assis Mollo F, Salih V (2014) The relationship between biofilm and physical-chemical properties of implant abutment materials for successful dental implants. Materials 7:3651–3662
26. del Pino ÁP, György E, Cabana L, Ballesteros B, Tobias G (2012) Deposition of functionalized single wall carbon nanotubes through matrix assisted pulsed laser evaporation. Carbon 50:4450–4458
27. Donlan RM, Costerton JW (2002) Biofilms: survival mechanisms of clinically relevant microorganisms. Clin Microbiol Rev 15(2):167–193

28. Esteban J, Gomez-Barrena E, Cordero J, Martín-de-Hijas NZ, Kinnari TJ, Fernandez-Roblas R (2008) Evaluation of quantitative analysis of cultures from sonicated retrieved orthopedic implants in diagnosis of orthopedic infection. J Clin Microbiol 46:488–492
29. Fayas APA, Vinod EM, Joseph J, Ganesan R, Pandey RK (2010) Dependence of pH and surfactant effect in the synthesis of magneite (Fe_3O_4) nanoparticles and its properties. J Magn Magn Mater. doi:10.1016/j.jmmm.2009.09.064
30. Fitl P, Vrnata M, Kopecky D, Vlcek J, Skodova J, Bulir J, Novotny M, Pokorny P (2014) Laser deposition of sulfonated phthalocyanines for gas sensors. Appl Surf Sci 302:37–41
31. Floroian L, Sima F, Florescu M, Badea M, Popescu AC, Serban N, Mihailescu IN (2010) Double layered nanostructured composite coatings with bioactive silicate glass and polymethylmetacrylate for biomimetic implant applications. J Electroanal Chem 648:111–118
32. Floroian L, Florescu M, Sima F, Popescu-Pelin G, Ristoscu C, Mihailescu IN (2012) Synthesis of biomaterial thin films by pulsed laser technologies: Electrochemical evaluation of bioactive glass-based nanocomposite coatings for biomedical applications. Mater Sci Eng C 32:1152–1157
33. Frank KL, Del Pozo JL, Patel R (2008) From clinical microbiology to infection pathogenesis: how daring to be different works for Staphylococcus lugdunensis. Clin Microbiol Rev 21:111–133
34. Gilbert P, Maira-Litran T, McBain A, Rickard A, Whyte F (2002) The physiology and collective recalcitrance of microbial biofilm communities. Adv Microb Physiol 46:203–256
35. Gohl O, Friedrich A, Hoppert M, Averhoff B (2006) The thin pili of *Acinetobacter* sp. strain BD413 mediate adhesion to biotic and abiotic surfaces. Appl Environ Microbiol 72:1394–1401
36. Grumezescu V, Socol G, Grumezescu AM, Holban AM, Ficai A, Truşcă R, Bleotu C, Balaure PC, Cristescu R, Chifiriuc MC (2014) Functionalized antibiofilm thin coatings based on PLA–PVA microspheres loaded with usnic acid natural compounds fabricated by MAPLE. Appl Surf Sci 302:262–267
37. Grumezescu V, Holban AM, Iordache F, Socol G, Mogoşanu GD, Grumezescu AM, Ficai A, Vasile BŞ, Truşcă R, Chifiriuc MC, Maniu H (2014) MAPLE fabricated magnetite@eugenol and (3-hidroxybutyric acid-co-3-hidroxyvaleric acid)–polyvinyl alcohol microspheres coated surfaces with anti-microbial properties. Appl Surf Sci 306:16–22
38. Grumezescu V, Holban AM, Grumezescu AM, Socol G, Ficai A, Vasile BS, Trusca R, Bleotu C, Lazar V, Chifiriuc CM, Mogosanu GD (2014) Usnic acid loaded biocompatible magnetic PLGA-PVA microspheres thin films fabricated by MAPLE with increased resistance to staphylococcal colonization. Biofabrication 6:035002
39. Grumezescu AM, Gestal Cartelle M, Holban AM, Grumezescu V, Vasile BS, Mogoantă L, Iordache F, Bleotu C, Mogosanu GD (2014) Biocompatible Fe3O4 increases the efficacy of amoxicillin delivery against Gram-positive and Gram-negative bacteria. Molecules 19:5013–5027
40. Grumezescu V, Holban AM, Iordache F, Socol G, Mogosanu GD, Grumezescu AM, Ficai A, Vasile BS, Truşcă R, Chifiriuc MC, Maniu H (2014) MAPLE fabricated magnetite@eugenol and (3-hidroxybutyric acid-co-3-hidroxyvaleric acid)—polyvinyl alcohol microspheres coated surfaces with anti-microbial properties. Appl Surf Sci 306:16–22
41. György E, Sima F, Mihailescu IN, Smausz T, Hopp B, Predoi D, Sima LE, Petrescu SM (2010) Biomolecular urease thin films grown by laser techniques for blood diagnostic applications. Mater Sci Eng: C 30:537–541
42. Holban AM, Grumezescu V, Grumezescu AM, Vasile BS, Truscă R, Cristescu R, Socol G, Iordache F (2014) Anti-microbial nanospheres thin coatings prepared by advanced pulsed laser technique. Beilstein J Nanotechnol 5:872–880
43. Holban AM, Grumezescu V, Grumezescu AM, Vasile BS, Truşcă R, Cristescu R, Socol G, Iordache F (2014) Anti-microbial nanospheres thin coatings prepared by advanced pulsed laser technique. Beilstein J Nanotechnol 5:872–880
44. Hori K, Matsumoto S (2010) Bacterial adhesion: from mechanism to control. Biochem Eng J 48:424–434

45. Houser EJ, Chrisey DB, Bercu M, Scarisoreanu ND, Purice A, Colceag D, Constantinescu C, Moldovan A, Dinescu M (2006) Functionalized polysiloxane thin films deposited by matrix-assisted pulsed laser evaporation for advanced chemical sensor applications. Appl Surf Sci 252:4871–4876
46. Hunter JD (2006) Ventilator associated pneumonia. Postgrad Med J 82:172–178
47. Iordache S, Cristescu R, Popescu AC, Popescu CE, Dorcioman G, Mihailescu IN, Ciucu AA, Balan A, Stamatin I, Fagadar-Cosma E, Chrisey DB (2013) Functionalized porphyrin conjugate thin films deposited by matrix assisted pulsed laser evaporation. Appl Surf Sci 278:207–210
48. Israil AM, Balotescu-Chifiriuc MC (2009) Fenomenul de comunicare interbacteriana - noi concepte in terapia antiinfectioasa, Ed. Asclepius, Bucureşti
49. Jacobsen SM, Stickler DJ, Mobley HL, Shirtliff ME (2008) Complicated catheter-associated urinary tract infections due to *Escherichia coli* and *Proteus mirabilis*. Clin Microbiol Rev 21:26–59
50. Jelinek M, Cristescu R, Axente E, Kocourek T, Dybal J, Remsa J, Plestil J, Mihaiescu D, Albulescu M, Buruiana T, Stamatin I, Mihailescu IN, Chrisey DB (2007) Matrix assisted pulsed laser evaporation of cinnamate-pullulan and tosylate-pullulan polysaccharide derivative thin films for pharmaceutical applications. Appl Surf Sci 253:7755–7760
51. Jelinek M, Remsa J, Brynda E, Houska M, Kocourek T (2007) Thin layers of bovine serum albumin by matrix assisted pulsed laser evaporation. Appl Surf Sci 254:1240–1243
52. Katsikogianni M, Missirlis YF (2004) Concise review of mechanisms of bacterial adhesion to biomaterials and of techniques used in estimating bacteriamaterial interactions. Eur cells Mater 8:37–57
53. Kempe M, Kempe H, Snowball I, Wallén R, Arza CR, Götberg M, Olsson T (2010) The use of magnetite nanoparticles for implant-assisted magnetic drug targeting in thrombolytic therapy. Biomaterials 31:9499–9510
54. Kim JJ, Singh RK, Seo SJ, Kim TH, Kim JH, Leeab EJ, Kim HW (2014) Magnetic scaffolds of polycaprolactone with functionalized magnetite nanoparticles: physicochemical, mechanical, and biological properties effective for bone regeneration. RSC Adv 4:17325–17336
55. Koenig SM, Truwit JD (2006) Ventilator-associated pneumonia: diagnosis, treatment, and prevention. Clin Microbiol Rev 19:637–657
56. Lazar V (2011) Quorum sensing in biofilms–how to destroy the bacterial citadels or their cohesion/power? Anaerobe 17280–17285
57. Lazăr V (2003) Aderenţa microbiană, *Bucureşti,* Edit. Acad. Rom 88–146
58. Lazăr V (2011) Quorum sensing in biofilms-how to destroy the bacterial citadels or their cohesion/power? Anaerobe 17:280–285
59. Lazar V, Balotescu MC, Cernat R, Bulai D, Niţu G, Ilina L (2003) Phenotypic antibioticresistance of some enterobacterial strains adhered to an inert substratum. In vitro models for biofilm formation in liquid and solid media. Clin Microbiol Infect 9:227
60. Lin M-F, Thakur VK, Tan EJ, Lee PS (2011) Dopant induced hollow BaTiO3 nanostructures for application in high performance capacitors. J Mater Chem 21:16500–16504
61. Lin M-F, Thakur VK, Tan EJ, Lee PS (2011) Surface functionalization of BaTiO3 nanoparticles and improved electrical properties of BaTiO3/polyvinylidene fluoride composite. RSC Adv 1:576–578
62. Lodhia J, Mandarano G, Ferris NJ, Eu P, Cowell SF (2010) Development and use of iron oxide nanoparticles (Part 1): synthesis of iron oxide nanoparticles for MRI. Biomed Imaging Interv J 6(2):e12. http://www.biij.org/2010/2/e12/
63. Massart R (1981) Preparation of aqueous magnetic liquids in alkaline and acidic media. IEEE Trans Magn 17:1247–1248
64. Mbeh DA, França R, Merhi Y, Zhang XF, Veres T, Sacher E, Yahia L (2012) In vitro biocompatibility assessment of functionalized magnetite nanoparticles: biological and cytotoxicological effects. J Biomed Mater Res A. 100:1637–1646

65. Meng H, Zhang Z, Zhao F, Qiu T, Yang J (2013) Orthogonal optimization design for preparation of Fe_3O_4 nanoparticles via chemical coprecipitation. Appl Surf Sci 280:679–685
66. Mihaiescu DE, Cristescu R, Dorcioman G, Popescu C, Nita C, Socol G, Mihailescu I, Grumezescu AM, Tamas D, Enculescu M, Negrea RF, Ghica C, Chifiriuc C, Bleotu C, Chrisey DB (2013) Functionalized magnetite silica thin films fabricated by MAPLE with antibiofilm properties. Biofabrication 5:015007
67. Miroiu FM, Socol G, Visan A, Stefan N, Craciun D, Craciun V, Dorcioman G, Mihailescu IN, Sima LE, Petrescu SM, Andronie A, Stamatin I, Moga S, Ducu C (2010) Composite biocompatible hydroxyapatite–silk fibroin coatings for medical implants obtained by matrix assisted pulsed laser evaporation. Mater Sci Eng B 169:151–158
68. Mulcahy H, Charron-Mazenod L, Lewenza S (2008) Extracellular DNA chelates cations and induces antibiotic resistance in *Pseudomonasaeruginosa* biofilms. PLoS Pathog 4:11
69. Muthiah M, Park I-K, Cho C-S (2013) Surface modification of iron oxide nanoparticles by biocompatible polymers for tissue imaging and targeting. Biotechnol Adv 31:1224–1236
70. Paju S, Scannapieco FA (2007) Oral biofilms, periodontitis, and pulmonary infections. Oral Dis 13:508–512
71. Palla-Papavlu A, Rusen L, Dinca V, Filipescu M, Lippert T, Dinescu M (2014) Characterization of ethylcellulose and hydroxypropyl methylcellulose thin films deposited by matrix-assisted pulsed laser evaporation. Appl Surf Sci 302:87–91
72. Pate R, Stiff-Roberts AD (2009) The impact of laser-target absorption depth on the surface and internal morphology of matrix-assisted pulsed laser evaporated conjugated polymer thin films. Chem Phys Lett 477:406–410
73. Paun IA, Ion V, Moldovan A, Dinescu M (2011) Thin films of polymer blends deposited by matrix-assisted pulsed laser evaporation: effects of blending ratios. Appl Surf Sci 257:5259–5264
74. Paun IA, Moldovan A, Luculescu CR, Dinescu M (2011) Biocompatible polymeric implants for controlled drug delivery produced by MAPLE. Appl Surf Sci 257:10780–10788
75. Paun IA, Mihailescu M, Calenic B, Luculescu CR, Greabu M, Dinescu M (2013) MAPLE deposition of 3D micropatterned polymeric substrates for cell culture. Appl Surf Sci 278:166–172
76. Pérez-Artacho B, Gallardo V, Ruiz MA, Arias JL (2012) Maghemite/poly(d, l-lactide-co-glycolyde) composite nanoplatform for therapeutic applications. J Nanopart Res. doi:10.1007/s11051-012-0768-x
77. Pique A, Auyeung RCY, Stepnowski JL, Weir DW, Arnold CB, McGill RA, Chrisey DB (2003) Laser processing of polymer thin films for chemical sensor applications. Surf Coat Technol 163–164:293–299
78. Predoi D, Ciobanu CS, Radu M, Costache M, Dinischiotu A, Popescu C, Axente E, Mihailescu IN, Gyorgy E (2012) Hybrid dextran-iron oxide thin films deposited by laser techniques for biomedical applications. Mater Sci Eng: C 32:296–302
79. Purice A, Schou J, Kingshott P, Dinescu M (2007) Production of active lysozyme films by matrix assisted pulsed laser evaporation at 355 nm. Chem Phys Lett 435:350–353
80. Raghavendran K, Mylotte JM (2000) Scannapieco FA (2007) Nursing home-associated pneumonia, hospital-acquired pneumonia and ventilator-associated pneumonia: the contribution of dental biofilms and periodontal inflammation. Periodontol 44:164–177
81. Ratner BD (1993) New ideas in biomaterials science—a path to engineered biomaterials. J Biomed Mater Res 27:837–850
82. Ratner BD, Hoffman AS, Schoen FJ, Lemons JE (2004) Biomaterials science introduction to materials in medicine. Elsevier Academic Press, San Diego
83. Rodrigo K, Czuba P, Toftmann B, Schou J, Pedrys R (2006) Surface morphology of polyethylene glycol films produced by matrix-assisted pulsed laser evaporation (MAPLE): dependence on substrate temperature. Appl Surf Sci 252:4824–4828
84. Rusen L, Mustaciosu C, Mitu B, Filipescu M, Dinescu M, Dinca V (2013) Protein-resistant polymer coatings obtained by matrix assisted pulsed laser evaporation. Appl Surf Sci 278:198–202

85. Rusen L, Dinca V, Mitu B, Mustaciosu C, Dinescu M (2014) Temperature responsive functional polymeric thin films obtained by matrix assisted pulsed laser evaporation for cells attachment–detachment study. Appl Surf Sci 302:134–140
86. Saviuc C, Grumezescu AM, Chifiriuc MC, Bleotu C, Stanciu G, Hristu R, Mihaiescu DE, Lazar V (2011) In vitro methods for the study of microbial biofilms. Biointerface Res Appl Chem 1:31
87. Shen J, Burgess DJ (2012) Accelerated in vitro release testing of implantable PLGAmicrosphere/PVA hydrogel composite coatings. Int J Pharm 422:341–348
88. Shen L, Qiao Y, Guo Y, Meng S, Yang G, Wu M, Zhao J (2014) Facile co-precipitation synthesis of shape-controlled magnetite nanoparticles. Ceram Int Part B 40:1519–1524
89. Shirtliff M, Leid J (2009) The role of biofilms in device-related infections. Springer, Berlin
90. Sima F, Davidson P, Pauthe E, Sima LE, Gallet O, Mihailescu IN, Anselme K (2011) Fibronectin layers by matrix-assisted pulsed laser evaporation from saline buffer-based cryogenic targets. Acta Biomater 7:3780–3788
91. Sima F, Axente E, Iordache I, Luculescu C, Gallet O, Anselme K, Mihailescu IN (2014) Combinatorial matrix assisted pulsed laser evaporation of a biodegradable polymer and fibronectin for protein immobilization and controlled release. Appl Surf Sci 306:75–79
92. S-Layer Proteins, Sara M, Uwe BS (2000) Crystalline bacterial cell surface proteins. J Bacteriol 182:859–868
93. Stamatin L, Cristescu R, Socol G, Moldovan A, Mihaiescu D, Stamatin I, Mihailescu IN, Chrisey DB (2005) Laser deposition of fibrinogen blood proteins thin films by matrix assisted pulsed laser evaporation. Appl Surf Sci 248:422–427
94. Thakur VK, Thakur MK (2014) Recent trends in hydrogels based on psyllium polysaccharide: a review. J Clean Prod 82:1–15
95. Thakur VK, Thakur MK (2014) Recent advances in graft copolymerization and applications of chitosan: a review. ACS Sustainable Chem Eng 2:2637–2652
96. Thakur VK, Thakur MK (2014) Processing and characterization of natural cellulose fibers/thermoset polymer composites. Carbohydr Polym 109:102–117
97. Thakur VK, Thakur MK, Gupta RK (2013) Rapid synthesis of graft copolymers from natural cellulose fibers. Carbohydr Polym 98:820–828
98. Thakur VK, Thakur MK, Gupta RK (2013) Development of functionalized cellulosic biopolymers by graft copolymerization. Int J Biol Macromol 62:44–51
99. Thakur VK, Thakur MK, Gupta RK (2013) Synthesis of lignocellulosic polymer with improved chemical resistance through free radical polymerization. Int J Biol Macromol 61:121–126
100. Thakur VK, Thakur MK, Gupta RK (2013) Graft copolymers from natural polymers using free radical polymerization. Int J Polym Anal Charact 18:495–503
101. Thakur VK, Thakur MK, Gupta RK (2013) Graft copolymers from cellulose: synthesis, characterization and evaluation. Carbohydr Polym 97:18–25
102. Thakur VK, Thakur MK, Gupta RK (2014) Review: raw natural fiber-based polymer composites. Int J Polym Anal Charact 19:256–271
103. Thakur VK, Thakur MK, Raghavan P, Kessler MR (2014) Progress in green polymer composites from lignin for multifunctional applications: a review. ACS Sustainable Chem Eng 2:1072–1092
104. Trampuz A, Zimmerli W (2006) Antimicrobial agents in orthopaedic surgery: prophylaxis and treatment. Drugs 66:1089–1105
105. Tunno T, Caricato AP, Caruso ME, Luches A, Martino M, Romano F, Valerini D, Anni M (2007) Matrix-assisted pulsed laser evaporation of polyfluorene thin films. Appl Surf Sci 253:6461–6464
106. Vallet I, Diggle SP, Stacey RE, Cámara M, Ventre I, Lory S, Lazdunski A, Williams P, Filloux AJ (2004) Biofilm formation in *Pseudomonas aeruginosa*: fimbrial cup gene clusters are controlled by the transcriptional regulator MvaT. J Bacteriol 186:2880–2890

107. Visan A, Grossin D, Stefan N, Duta L, Miroiu FM, Stan GE, Sopronyi M, Luculescu C, Freche M, Marsan O, Charvilat C, Ciuca S, Mihailescu IN (2014) Biomimetic nanocrystalline apatite coatings synthesized by matrix assisted pulsed laser evaporation for medical applications. Mater Sci Eng, B 181:56–63
108. Wang L, Lansing B, Symons K, Flannery EL, Fisch J, Cherian K, McNamara SE, Mody L (2012) Infection rate and colonization with antibiotic-resistant organisms in skilled nursing facility residents with indwelling devices. Eur J Clin Microbiol Infect Dis 31:1797–1804
109. Wei QF, Gao WD, Hou DY, Wang XQ (2005) Surface modification of polymer nanofibers by plasma treatment. Appl Surf Sci 245:16–20
110. Wilson SK, Costerton JW (2012) Biofilm and penile prosthesis infections in the era of coated implants: a review. J Sex Med 9:44–53
111. Wu S, Sun A, Zhai F, Xu W, Yhang Q, Volinsky A (2011) Fe_3O_4 magnetic nanoparticles synthesis from tailings by ultrasonic chemical co-precipitation. Mater Lett. doi:10.1016/j.matlet.2011.03.065
112. Xie G, Chain PSG, Lo C, Liu KL, Gans J, Merritt J, Qi F (2010) Community and gene composition of a human dental plaque microbiota obtained by metagenomic sequencing. MolOral Microbiol 25:391–405
113. Yaseen MA, Yu J, Jung B, Wong MS, Anvari B (2009) Biodistribution of encapsulated indocyanine green in healthy mice. Mol Pharm 6:1321–1332
114. Zhao H, Cui Z, Wang X, Turng LS, Peng XF (2013) Processing and characterization of solid and microcellular poly(lactic acid)/polyhydroxybutyrate-valerate(PLA/PHBV) blends and PLA/PHBV/Clay nanocomposites. Compos Part B 5179–91

Eco-Friendly Chitosan-Based Nanocomposites: Chemistry and Applications

Catalina Natalia Cheaburu-Yilmaz, Onur Yilmaz and Cornelia Vasile

Abstract The deacetylated chitin derivative, chitosan (CS), as a linear polysaccharide having reactive side amino groups is among the favorite bio-based materials due to its nontoxicity, biodegradability, biocompatibility, antimicrobial properties mucoadhesivity among other advantages. Chitosan as a hydrophilic biopolymer exhibits a variety of physicochemical and biological properties resulting in numerous applications in fields such as pharmaceutical and biopharmaceutical, cosmetics, biomedical engineering, biotechnology, agriculture, textiles, food processing nutrition, etc. The mechanical properties and hardness of CS are frequently not enough to meet some of the biomedical applications requirements. The addition even of a very small amount of nanoparticles leads to obtain materials with improved mechanical, chemical, and antimicrobial properties targeted to particular application. The mechanical, thermal, and antibacterial properties of the nanocomposites as well as their biodegradability and applications are reviewed.

Keywords Eco-friendly · Bio-nanocomposites · Chitosan · Clay · Montmorillonite

1 Introduction

During the last few decades, synthetic polymers and polymer-based materials have become indispensable materials in people's lives [109–113]. Due to their ease of processing, low cost, and availability, they are used in a very wide range of

C.N. Cheaburu-Yilmaz · C. Vasile (✉)
Laboratory of Physical Chemistry of Polymers, Petru Poni Institute of Macromolecular Chemistry of the Romanian Academy, 41A Grigore Ghica Voda Alley, Iasi 700487, Romania
e-mail: cvasile@icmpp.ro

C.N. Cheaburu-Yilmaz
Faculty of Pharmacy, Department of Pharmaceutical Technology, Ege University, Izmir 35100, Turkey

O. Yilmaz
Faculty of Engineering, Leather Engineering Department, Ege University, Bornova, Izmir 35100, Turkey

V.K. Thakur and M.K. Thakur (eds.), *Eco-friendly Polymer Nanocomposites*, Advanced Structured Materials 74, DOI 10.1007/978-81-322-2473-0_11

applications from household to aerospace applications, from agriculture to medicine or pharmacy [119–125]. They have even replaced traditional metals, ceramic and glass-based materials for a number of applications [119, 120, 135]. However, due to the growing awareness on environmental care and human health as well as the scarcity and increase in price of the fossil resources, particular attention and efforts have been given to the environmentally friendly materials in the last years [126–130]. Therefore, eco-friendly products based on biopolymers such as biodegradable polyester [35, 89, 107, 138], proteins [21, 36, 90], polysaccharides [6, 30, 77, 142] have attracted a tremendous attention because of their possibility to reduce the dependence on fossil fuel and its derivatives.

Biodegradable polymers are defined as those that undergo microbially induced chain scission finally leading to the mineralization. Specific conditions in term of pH, humidity, oxygenation, and the presence of some metals are required to ensure the biodegradation of such polymers. Biodegradable polymers can be obtained from bio-sources like corn, wood, cellulose, chitin, etc., or can also be synthesized by bacteria, e.g., butyric acid or valeric acid that give polyhydroxybutyrate (PHB) and polyhydroxyvalerate (PHV) [67, 114].

Nowadays, available biopolymers are relatively expensive and rather in small quantities. This has been a limiting factor to extend their applications in various fields. However, recent signs show that increasing environmental awareness and more stringent legislations regarding recyclability and restrictions on waste disposal will give a rise for the use of biopolymers as well as decrease in their prices.

Polysaccharides are the most promising bio-based natural polymers to be used in the preparation of advanced functional composite materials. From the polysaccharide family, cellulose and lignin derivatives have been successfully used for the preparation of natural biopolymer reinforced polymer composites. The reviews on the preparation, characterization, and successful applications of these composites have been reported in detail by Thakur and coworkers [131, 134, 135]. A member of polysaccharide family, the deacetylated chitin derivative, chitosan, as a cationic polymer is another promising bio-based material used in bio-nanocomposite preparations. Chitosan and its derivatives are being considered to be materials of great futuristic potential with immense possibilities for structural modifications to impart desired properties and functions, research and development work on chitin and CS have reached a status of intense activities in many parts of the world [51, 83, 85, 94]. The positive attributes of excellent biocompatibility and admirable biodegradability with ecological safety and low toxicity with versatile biological activities such as antimicrobial activity and low immunogenicity have provided ample opportunities for further development [42, 47, 59, 72, 95, 166]. It has become of great interest not only as an under-utilized resource but also as a new functional biomaterial of high potential in various fields [41, 55, 58].

Despite its huge annual production and easy availability, chitin still remains an under-utilized resource primarily because of its intractable molecular structure [59, 175]. On the other hand, chitosan as deacetylated chitin derivative can be dissolved in acidic solutions, and its unique physicochemical and biological properties gives

opportunity to use it in various application fields e.g. cosmetics, biomedical engineering, pharmaceuticals, ophthalmology, biotechnology, agriculture, textiles, food processing nutrition, etc. However, the mechanical properties, hardness, and barrier properties of chitosan-based materials are frequently not enough to meet standards for a wide range of applications [114]. In the last decade, the nanotechnology field has opened up new ways in materials science exploiting the use and functionalities of biopolymers, particularly chitin and chitosan (CS) derivatives. Among these, polymer-nanocomposite technology especially took attention due to the substantial property enhancements with respect to the neat polymer matrix by the addition of nanoparticles into polymer matrix even in low amounts (up to 5 %). The interactions between the filler and polymer at nanometric scale explain the superior properties in comparison to the conventional polymer composites [82]. The developments in polymer nanocomposite technology have given the opportunity to improve the inherent properties of biodegradable polymers and to combine advantageously the unique characteristics of the biopolymers to the new composite materials.

The most common way to improve the mechanical, thermal, and barrier properties of chitosan is the use of nanolayered silicates [46, 73, 74]. The addition of layered silicates and in particular montmorillonite (MMT) in chitosan has also been extensively studied and many property enhancements have been reported for the chitosan-based nanocomposites which were found to be strongly affected by the preparation method of the nanocomposite and the interactions of the nanolayers with chitosan chains. The chitosan/clay bio-nanocomposite technology constitutes an important research field in material science and gives possibility to expand the use and value of this unique and natural biomaterial. Present chapter discusses the preparation techniques, characterization, and properties of the chitosan/clay bio-nanocomposites. A detailed review on various applications of these bio-nanocomposites also has been reported.

2 Chitosan as Biopolymer

Chitosan is a natural deacetylated chitin derivative and a cationic linear polysaccharide which is very similar to cellulose and consists of 1,4-linked d-glucosamine with a variable degree of N-acetylation, except that the acetylamino group replaces the hydroxyl group on the C2 position. Thus, chitosan is a copolymer consisting of N-acetyl-2-amino-2-deoxy-d-glucopyranose and 2-amino-2-deoxy-d-glucopyranose, where the two types of repeating units are linked by (1 → 4)-glycosidic bonds. Chitosan has a rigid crystalline structure through inter- and intramolecular hydrogen bonding.

The source of chitosan is a naturally occurring polymer, chitin, which is the second most abundant polysaccharide in nature after cellulose. Chitin is found in the exoskeleton of crustacea, insects, and some fungi types. The main commercial sources of chitin are the shell waste of shrimps, lobsters, krills, and crabs. In the

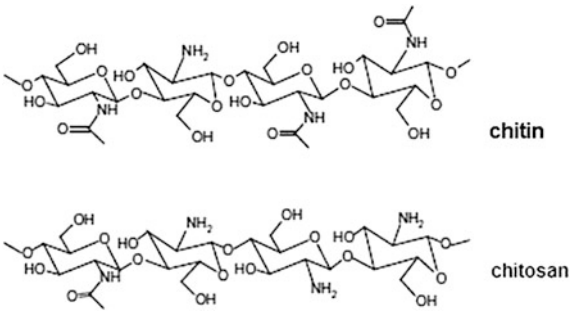

Fig. 1 Structure of chitin and chitosan

world, several millions tons of chitin are harvested annually and hence this biopolymer represents a cheap and readily available source. Chitosan is obtained by the thermochemical deacetylation of chitin in the presence of an alkali and naturally it may occur only in certain fungi types (Mucoraceae) [99]. Chitosan can be obtained via alkaline-based methods which usually involve the hydrolysis of the acetated position using sodium or potassium hydroxide solutions as well as a mixture of anhydrous hydrazine and hydrazine sulfate [25]. The treatment of chitin with an aqueous 40–45 % (w/v) NaOH solution at 90–120 °C for 4–5 h results in N-deacetylation of chitin. The structures of chitin and chitosan (CS) are given in Fig. 1. The conditions used for deacetylation determine the molecular weight of the biopolymer and the degree of deacetylation (DD). The active primary amino groups on the molecule provide reactive sites for a variety of side group attachment employing mild reaction conditions. The facile derivatization makes chitosan an ideal candidate for biofabrication. In addition, the characteristic features of chitosan such as being cationic, hemostatic, and insoluble at high pH, can be reversed by sulfating the amine which makes the molecule anionic and water soluble, with the introduction of anticoagulant properties. The attachment of different side groups on chitosan molecule can open up new ways to obtain versatile materials with specific functionality and altered biological and physical properties.

The main difference between chitin and CS is their solubility in various organic and inorganic solvents. The chemistry related with the solubility of chitosan and chitin was reviewed by Pillai et al. [83]. Due to the extended hydrogen bonds, chitin is insoluble in water or diluted acidic solutions and organic solvents. By comparison, chitosan is readily soluble in dilute acidic solutions below pH 6.0. This is because chitosan can be considered a strong base as it possesses primary amino groups with a pKa value of 6.3. The presence of the amino groups indicates that pH substantially alters the charged state and properties of chitosan [167]. At low pH, these amine groups get protonated and become positively charged and that makes CS a water soluble cationic polyelectrolyte. On the other hand, as the pH increases above 6, CS amine groups become deprotonated and the polymer loses its charge and becomes insoluble. The soluble–insoluble transition occurs at its pKa value around pH between 6 and 6.5. As the pKa value is highly dependent on the degree of N-acetylation, the solubility of CS is dependent on the deacetylation degree

(DD) and the method of deacetylation used [17]. The degree of ionization depends on the pH and the pKa of the acid with respect to studies based on the role of protonation of CS in the presence of acetic acid and hydrochloric acid [96, 97].

The polycationic nature of chitosan also gives antifungal or antimicrobial activities to the molecule. The antimicrobial action of chitosan is hypothesized to be mediated by the electrostatic forces between the protonated amino group (NH_2) in chitosan and the negative residues at cell surfaces [137]. The number of protonated amino groups (NH_2) present in chitosan increases with increased DD which influences the antimicrobial activity [70].

Chitosan is also an excellent film forming material [26]. Chitosan films have a selective permeability to gasses (CO_2 and O_2) and good mechanical properties. However, the fact that chitosan films are highly permeable to water vapor limits their use as being an important drawback since an effective control of moisture transfer is a desirable property for most foods, especially in moist environments.

The unique properties of chitosan such as biodegradability, biocompatibility, bioadhesivity, antimicrobial activity, having relatively good mechanical and barrier properties make it a perfect candidate for preparing bio-nanocomposites to be used in various applications.

3 Preparation and Characterization of Bio-nanocomposites Containing Layered Silicates

As the interest in industrial application of biodegradable polymers is growing, biodegradable polymer/silica nanocomposites have attracted much attention. Several biopolymers like chitosan, alginate, pectin, carragenan, were intercalated through ionic exchange mechanism into inorganic solid layers [11, 22, 153, 160]. Layered silicates (e.g., montmorillonite) are the most preferred nano additives for the preparation of bio-nanocomposites.

The commonly used layered silicates for the preparation of bio-nanocomposites belong to the same general family of 2:1 layered or phyllosilicates. Their crystal structure consists of layers made up of two silica tetrahedral layers fused to an edge-shared octahedral sheet of either aluminum or magnesium hydroxide (Fig. 2). These silicates are characterized by large active specific surface area (700–800 m^2/g) and a moderate negative surface charge. The particle size of the commercially available montmorillonite clay ranges between 6 and 13 μm. Each particle consists of 6000–10000 platelets of 1 nm thickness and 100–1000 nm width [80].

The surface of clay layers have a net negative electric charge which is balanced by a corresponding positive charge at some location. The charge in the naturally occurring clay is balanced, typically, by a sodium cation which lies between the layers in what is called the gallery space. The ability of the clay to improve the properties of the polymers is primarily determined by the extent of its dispersion in the polymer matrices, which, in turn, depends on the clay particle size. However,

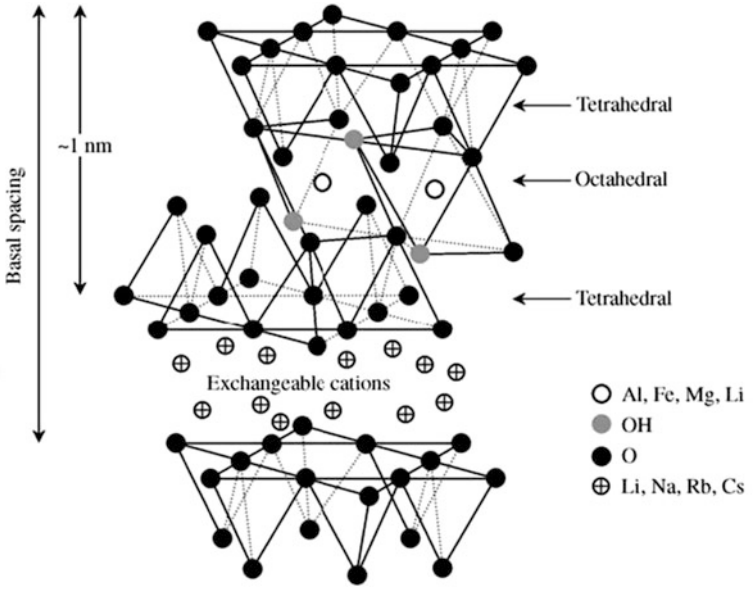

Fig. 2 Layered crystalline structure of montmorillonite (Reprinted from Ref. [87] Copyright (2003), with permission from Elsevier)

the hydrophilic nature of the clay surfaces impedes homogeneous dispersion in the organic polymer phase. To overcome this problem, it is usually necessary to render the surface organophilic prior to its use. The modification is usually made by substitution of the cations (Na^+, K^+, Li^+) on the surface of clay layers with cationic surfactants including primary, secondary, tertiary, and quaternary alkyl ammonium or alkyl phosphonium cations. These surfactants change the nature of the clay surface from hydrophilic to hydrophobic one as well as increasing the interlayer spacing of the clay and accordingly, they promote more affinity and space for the polymers [8, 54]. The role of the organic compounds in the organically modified montmorillonites (OMMT) is to reduce the surface energy of the montmorillonites, thereby improving the wetting characteristics on the interface with the polymer or monomer. Moreover, the choice of the organically modified clay type for each individual system is an important issue for the success of nanocomposite preparations. The hydrophilic–hydrophobic balance of the clay and matrix polymer should be well suited. Nowadays, different kinds of organically modified clays modified by various surfactants leading to varied interlayer spacings are commercially available in the market. They offer clay materials with different hydrophobicity to be suitable for various types of polymers.

As mentioned above, the successful formation of a hybrid is, to a large extent, determined by the miscibility of individual components of the system [174]. Along with the compatibility of clay material and polymer matrix, the procedure and

technique used for the preparation of nanocomposites are also crucial. Three main techniques are usually used in preparation of bio-nanocomposites; (i) in situ polymerization, (ii) solution casting, and (iii) melt processing. Recently, other preparation techniques, such as electrospinning and processing under supercritical conditions (e.g., supercritical carbon dioxide), have gained interest. Supercritical carbon dioxide has primarily been used because achieving its super critical conditions (Tc = 31.1 °C and Pc = 73.8 bar) is easy. Processing under supercritical carbon dioxide, either as a foaming agent or a medium where in situ polymerization or melt processing occurs is promising to be a particularly apt approach because this solvent is greener than other organic solvents. In clay-based nanocomposites, the use of super critical carbon dioxide has been a useful method to expand the interlayer distances and consequently aid in the dispersion of the same in polymer matrices. The selection of any of the techniques depends on the type of biopolymer involved and to a large extent, the nanoparticle in question. However, of the three primary techniques, melt processing is always a preferred method because it aligns well with the currently established industrial processing routes [79].

3.1 In Situ Polymerization

During in situ polymerization, the nanoparticles are premixed with the liquid monomer or monomer solution. Then, polymerization is initiated by either heat, radiation, or suitable initiators. However, its technique is not applicable for preparation of bio-nanocomposites since biopolymers are usually extraction products from natural sources.

3.2 Solvent Intercalation Process

This elaboration process is based on a solvent system in which the biopolymer is soluble and the silicate layers are swellable. Generally, the polymer is first dissolved in an appropriate solvent and mixed further with the swollen clay suspension that is prepared separately. The nanocomposite formation is based on the diffusion of polymer chains into the clay galleries by mixing. Therefore, mixing procedure is usually done within a prolonged period ($\sim$24–72 h) and preferably at elevated temperatures. Nevertheless, for non-water soluble polymers, this process involves the use of large amount of organic solvents, which is environmental unfriendly and cost prohibitive. This technique is widely used for the preparation of polysaccharide/clay hybrid materials in aqueous systems especially for chitosan-based nanocomposites.

3.3 Melt Intercalation Process

In the melt processing technique, the nanoparticles are mixed with the polymer in the molten state. The process involves mixing of the particles with the polymer and heating the mixture above the softening point of the polymer, statically or under shear [139, 141]. In the case of clay-containing bio-nanocomposites, this method has considerable advantages over the other preparation techniques. First, this method is environmentally benign due to the absence of organic solvents. Second, the melt processing is compatible with current industrial processes, such as extrusion and injection molding. The melt intercalation method allows the use of biopolymers that are not suitable for in situ polymerization.

The formation of bio-nanocomposites via polymer melt intercalation depends upon the thermodynamic interactions between the polymer and the nanoparticles. For clays, these interactions will also depend upon the transport/diffusion of polymer chains from the bulk melt into the silicate interlayers [140, 141]. The polymer needs to be sufficiently compatible with nanoparticle surface to ensure proper dispersion [79].

In the preparation of bio-nanocomposites, the key feature is to provide a good dispersion of clay in the polymer matrix which leads to enhancement of polymer properties. These well-dispersed systems are known as intercalated and exfoliated structures. Generally, the state of dispersion and the interlayer spacing of the clay platelets are typically investigated by using X-ray diffraction (XRD) analysis and transmission electron microscopy (TEM). Usually both techniques are essential for evaluating the nanocomposite structure since TEM is time intensive, and only gives qualitative information on the sample as a whole, while wide-angle peaks in XRD allow quantification of changes in layer spacing but not giving information on high layer spacing (>6–7 nm) and/or relatively disordered structures. Examples of the XRD patterns and TEM images obtained from a series of chitosan/montmorillonite nanocomposites with different MMT concentrations are shown in Figs. 3 and 4 [153]. The XRD pattern of the MMT (Fig. 3) shows a reflection peak at about $2\theta = 7.1°$ corresponding to a basal spacing of 1.25 nm. The XRD pattern of CS shows the characteristic crystalline peaks at around $2\theta = 10°$, 20°, and 25°. After incorporating MMT within CS, the basal plane of MMT at $2\theta = 7.1°$ disappears, substituted by a new weakened broad peak at around $2\theta = 3–5°$. The movement of the basal reflection of MMT to lower angle indicates the formation of an intercalated nanostructure, while the peak broadening and intensity decreases most likely indicate the disordered intercalated or exfoliated structure. However, it is difficult for XRD to give definitive conclusions about the defined structure. Thus TEM technique is necessary to characterize the morphology. The TEM images (Fig. 4a–b) show the good dispersion of MMT in the CS matrix. At lower MMT content (2.5 wt%, Fig. 3), the MMT shows the coexistence of both intercalated (stacks of multilayers of MMT) and exfoliated structures. With increasing the content of the MMT (5 wt%, Fig. 4b) the MMT clearly shows intercalated morphology with occasional flocculation. It is believed that the formation of flocculated structure in

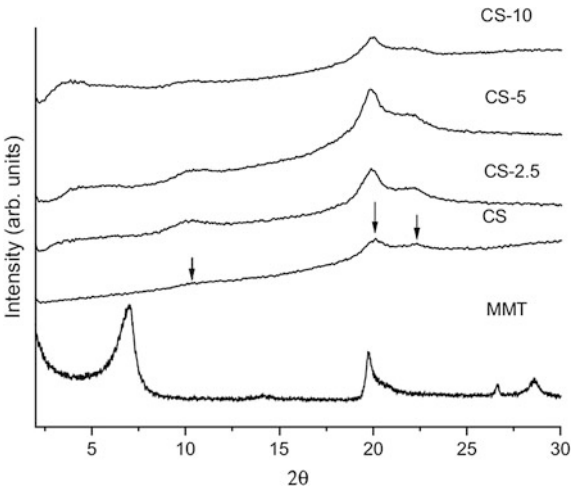

Fig. 3 XRD patterns of the montmorillonite (MMT), pure chitosan (CS), and its nanocomposites with MMT/CS ratios of 2.5 % (CS-2.5), 5 % (CS-5) and 10 % (CS-10) (Reprinted from Ref. [153], Copyright (2005), with permission from Elsevier)

CS/MMT nanocomposites is due to the hydroxylated edge-edge interaction of the silicate layers [88]. Since one chitosan unit possesses one amino and two hydroxyl functional groups, these functional groups can form hydrogen bonds with the silicate hydroxylated edge groups, which lead to the strong interactions between matrix and silicate layers.

Scanning electron microscopy (SEM) has also been used to investigate the surface morphology of bio-nanocomposites. However, in most cases, it was very difficult to image the degree of dispersion of nanoparticles in a polymer matrix because the inherent resolution of most SEM instruments is approximately 1 nm. However, SEM is a very valuable tool for studying the fracture-surface morphology

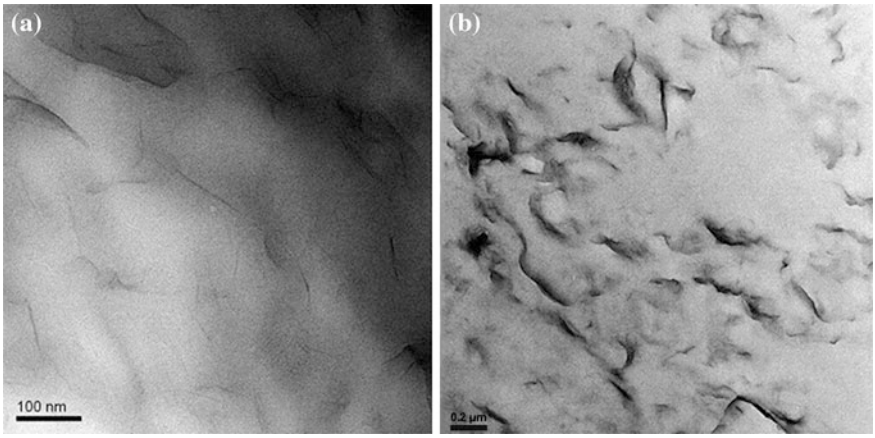

Fig. 4 Bright field TEM images of chitosan/MMT nanocomposite: **a** CS-2.5; **b** CS-5 (Reprinted from Ref. [153], Copyright (2005), with permission from Elsevier)

of bio-nanocomposites. Recently, SEM combined with energy dispersive X-ray spectroscopy has been frequently used to study the degree of dispersion of nanoparticles on the fractured surface of bio-nanocomposites [79].

Since no in situ polymerization techniques can be applied to naturally extracted biopolymers, the mixing procedures are very important and should be done efficiently for the preparation of bio-nanocomposites. Along with the well dispersion of the silicate layers within polymer matrix, the interactions of the components are also of importance to obtain improved polymer properties. Next section discusses the preparation techniques and properties of the particular chitosan/clay nanocomposites.

4 Chitosan/Clay Nanocomposites

The addition of layered silicates and in particular MMT in chitosan has been extensively studied [37, 43, 78, 91, 118, 152, 153, 163]. The polycationic nature of the chitosan in acidic media makes it an excellent candidate for intercalation in layered silicates by means of cationic exchange process. In general procedure, the chitosan solutions are prepared by dissolving in diluted acetic acid solutions and the pH is adjusted to milder acidic values ($\sim$4.0–5.0). Subsequently, the chitosan solution is slowly added to the clay suspension at selected temperatures and they are mixed for 24 h to few days. In the end, they are washed with purified water to remove the free acetate anions from the resulting mixtures [114]. The mixing ratios of chitosan/clay are usually varied to from 0.25/1 to 10/1, respectively, depending on the purpose and final desired properties. However, it has been shown that both the structure of chitosan/MMT nanocomposites and their thermal stability are strongly affected by the solvent-casting procedure used [37]. Wang et al. [153] investigated the effect of both acetic acid residue and the hydrogen bonds formed between chitosan and MMT on the nanocomposite properties. They demonstrated that the residual acetic acid accelerates the thermal decomposition of chitosan and decreases its crystallinity level. The effect of the solution's temperature and acidity (e.g., pH 5, 8, and 12) on the MMT dispersion has been also documented by Potarniche et al. [84]. It was found that for pH 5 and high solution temperatures a higher quantity of chitosan was intercalated between the silicate layers compared to the samples processed at room temperature or at other pHs. It can be assumed that at pH 5 the chitosan chains are oriented preferentially between the silicate layers.

The solution casting technique is the method of choice for the preparation of chitosan/clay nanocomposites due to the aforementioned polycationic nature of chitosan. For this reason, sodium montmorillonite is the most commonly used clay type in the preparation of chitosan/clay nanocomposites and generally intercalated/exfoliated structures are obtained. However, there are also some other techniques that can be used for nanocomposite preparations. The preparation of ultrafine polymeric nanoparticles with narrow size distribution could be achieved using reverse micellar medium. Reverse micelles are thermodynamically stable systems,

but they are also a liquid mixture of water, oil, and surfactant. Coacervation is another type of ionotropic gelation method. This process avoids the use of toxic organic materials as cross-linking agents; however, the prepared chitosan particles are poorly soluble in aqueous media. Covalently cross-linked chitosan nanoparticles can be prepared by several different methods: emulsion cross-linking, reverse micellar, solvent evaporation, spray-drying, or thermal cross-linking. The solvent evaporation method can be performed in a w/o emulsion, and the aqueous phase is removed by evaporation at high temperature. Spray-drying is a well-known technique to produce a cross-linked chitosan suspension. This method is based on drying of finely dispersed droplets of chitosan solution in a stream of hot air followed by the addition of a cross-linking agent. Thermal cross-linking is a very simple method for preparing chitosan particles; however, high temperature is necessary to establish cross-linking. Chitosan nano- and microsystems can be employed in a wide range of biomedical application, such as drug or gene-delivery systems.

Bodnar et al. [9] prepared nanoparticles based on chitosan via covalently cross-linking of the amino groups of chitosan chain with natural di- or tricarboxylic acids in aqueous media at room temperature. The solubility, structure, and size of these nanoparticles was found as pH dependent, by decreasing the pH, the transmittance of cross-linked particles increased, caused by the protonation of free amino groups of chitosan chains. Therefore, depending on the pH, cross-linked chitosan nanoparticles can become a macromolecular solution.

The examples of the studies on chitosan-based nanocomposites prepared via different methods comprising information regarding the method type, composition, obtained results and the application of the synthesized materials are summarized in Table 1. Some specific methods, e.g., in situ sol-gel intercalation, hot intercalation technique, electrospinning or microwave were also reported for the preparation of different types of chitosan-based nanocomposites. Anirudhan et al. [3] prepared montmorillonite/N-(carboxyacyl) chitosan-coated magnetic particles (MMT/CACS-MPs) for the controlled delivery of drugs (e.g., paracetamol) (MMT/CACS-MP) via hot intercalation technique to combine the advantages of biopolymer with clay. They obtained fibrous chitosan like white flakes located on the surface of MP indicating that chitosan was coated successfully on the surface of MP. After intercalation of CACS-MP in the interlayer space of MMT, the basal distance of MMT increased and its surface morphology changed also dramatically, becoming fluffy favoring the delivery process of the drug.

Another report was questioning the ability of pure chitosan for spinning which is limited due to its polycationic nature and high viscosity in solution, and the presence of specific intra- and intermolecular interactions [173]. In this respect, synthetic polymers such as polyethylene oxide (PEO) [27] and polyvinyl alcohol (PVA) [170] were mentioned as being mostly used in the ultrafine fiber production. Zhou et al. [173] produced carboxyethyl chitosan (CECS)/PVA nanofibers using electrospinning technique.

Similar method was used by Naseri et al. [75] to produce nanofibrous mats based on chitosan/PEO blend as matrix phase and chitin nanocrystals as reinforcing

Table 1 Preparation of chitosan-based nanocomposites via different methods and nanocomposite properties

System	Concentration	Preparation method	Properties	Applications	Literature
CS-OREC (organic rectorite)		Solution mixing	Increased thermal stability and stronger antimicrobial activity toward Gram-positive bacteria[a]	Coating, materials with antimicrobial activity	Wang et al. [152]
CS-Na^{+}MMT (sodium montmorillonite)	2w/v % and 1 wt%	Reflux-solution method	• For 2 w/v% solutions	Packaging material	Giannakas et al. [34]
			Decreased hydrated crystallinity		
			• Stiffness and strength (up to 100 %)		
			Decrease of elongation at break (up to 75 %)		
			Water vapor permeability (WVP) (up to 65 %)[b]		
Chitosan-grafted-poly Acrylonitrile silver nanocomposites (CS-g-PAN/Ag)	Solution of CS in 1 % acetic acid[c]	In situ chemical reduction of Ag ions in graft copolymerization of acrylonitrile onto chitosan	Antibacterial activity on *E. coli* and *S. aureus* presence of silver nanoparticles affects crystallography of chitosan	Antimicrobial material In medical field	Hebeish et al. [40]
			• Size of particles 15–20 nm • Thermal stability of nanocomposites		
Sulfonated graphene-chitosan (SPG-CS) and AuNPs	1 wt% CS with 1 % SPG[d]	AuNPs were used to modify SPG-CS deposited on an Indium tin-oxide (ITO) glass electrode via solution casting method	• Amperometric response of the GO x/SPG–AuNPs–CS/ITO bioelectrode • Fast response time (10 s), good stability (70 days), and high reproducibility	Glucose biosensor in human blood serum	Singha et al. [108]
Electrospun chitosan/polyethylene oxide-randomly	CS solution 3w% Matrix phase chitosan blended with PEO in a 1:1 mass	Electrospinning method	Fibers mats with: increased Young Modulus (∼10 times) tensile strenght (65 MPa) high	Wound dressing	Naseri et al. [75]

(continued)

Table 1 (continued)

System	Concentration	Preparation method	Properties	Applications	Literature
oriented fiber mats reinforced with chitin nanocrystals (CSNC)	ratio; reinforcing phase: Chitin nanocrystals		surface area mats (35 m^2 g^{-1}) water vapor water transmission rate: 1290–1548 gm^{-2} day^{-1}		
Titania–chitosan nanocomposites		In situ sol–gel	Particle size of 4.5–10.5 nm	Biomaterial for orthopedic and tissue engineering applications	Kavithaa et al. [49]
			Higher surface area (114–265 m^2/g)		
			Specific antibacterial		
			Action toward *Staphylococcus aureus*		
			Increased cell viability,		
			Controlled swelling		
			Degrading rate[e]		
Low density polyethylene (LDPE) with chitosan sodium montmorillonite clay nanocomposites (CSnano)	2.7 and 5.5 wt% chitosan or chitosan nanocomposites and 0.5 wt% Irganox or vitamin E[f]	Melt processing of neat LDPE and the corresponding composites with chitosan, chitosan nanocomposites or/and antioxidant agent CS/montmorillonite nanocomposites were prepared via solution mixing followed by solvent casting method.	Antimicrobial activity of films against Salmonella enteritidis, *E. coli* and Listeria monocytogenes	Materials for food packaging with antimicrobial and antioxidant activity	Vasile et al. [145]
			Higher mechanical properties[g]		
			Antioxidant activity—higher oxidation induction period (OIP)[h]		
Chitosan/hydroxy-aluminum pillared montmorillonite nanocomposites		Incorporation of hydroxy-aluminum pillared montmorillonite into chitosan solution prepared by dissolving the chitosan into diluted acetic acid		Absorbent of organic and metal ions from dying and finishing effluent	Tan et al. [117]

(continued)

Table 1 (continued)

System	Concentration	Preparation method	Properties	Applications	Literature
Mt/CACS-MP[j]	Chitosan solution 5 %	Hot intercalation technique; reverse-dispersion cross-linking technique was used for the preparation of CS-MP	• Delivery of paracetamol was pH dependent being more efficient in basic medium; maximum loading of the drug is at pH 6.0 (84 %) • Sips isotherm fit the best as model for drug binding	Targeted drug delivery	Anirudhan et al. [3]
Ag NP-loaded QCS/clay nanocomposites[k]	Mass ratio of QCS to MMT was fixed at 2:1	Ag NP-loaded QCS/clay nanocomposites were prepared at 800 W and 85u C for 70 min in the microwave irradiation	• Spherical Ag NPs occurred in the QCS matrix, 26 nm size uniformly, with polymer on the shell • Antimicrobial activity against *Pseudomonas aeruginosa* and *B. subtilis*	Antimicrobial materials for medicine and coating	Liu et al. [68]

[a]Proportional to the amount and the interlayer distance of the layered silicates

[b]Upon Na^+MMT addition; the addition of glycerol had a negative effect on the stiffness, strength, and WVP, and a positive effect on the elongation at break and the water absorption

[c]DA 90 %, M_W~ 350 kDa

[d]The optimized ratio of SPG, CS, and AuNPs was 1:2:1, and that 15 L was the optimum amount of SPG–AuNPs–CS solution, standardized for the dispersion, to deposit onto the ITO surface when preparing the SPG–AuNPs–CS/ITO film, in order to achieve the maximum amperometric current; optimum pH 7.0

[e]Favorably achieved at 2:1 nanocomposite ratio

[f]LDPE/3CS, LDPE/3CSnano/VE

[g]2.7 wt% CS in LDPE matrix led to a slightly increase of Young modulus in respect with that of the neat LDPE, 11 % higher when using the same percent of CS nanocomposites. Doubling the amount of CSnano in LDPE, an elastic modulus of 235.4 MPa was obtained, 12 % higher than the neat LDPE ones

[h]The antioxidant character of vitamin E is the most efficient in case of LDPE/6CSnano/VE, registering a delay in oxidation with about 59 % in comparison with material 7, LDPE/6Csnano

[i]Covalently immobilizing of anti-PSA and redox mediator (thionine) onto gold nanoparticles—incorporated polyamidoamine dendrimer (AuNPs–PAMAM) and multiwalled carbon nanotubes/ionic liquid/chitosan nanocomposite (MWCNTs/IL/CS) as the support platform

[j]Montmorillonite/N-(carboxyacyl) chitosan-coated magnetic particles

[k]Quaternized chitosan (QCS), montmorillonite (MMT), silver nanoparticles (Ag NPs)

phase. After the preparation of the fiber mats, they used genipin to cross-link them in order to enhance the mechanical properties and pH stability. This method allowed the preparation of fiber mats with a content of chitin nanocrystals of 50 wt % with high surface area (35 $m^2\ g^{-1}$) which is considered likely for wound healing materials. These electrospun fiber mats showed compatibility toward adipose derived stem cells.

A series of titania–chitosan nanocomposites were prepared by using in situ sol-gel method by Kavithaa et al. [49]. Compared with the conventional synthesis method (blending) of TiO_2—chitosan nanocomposite [49, 164], in situ sol-gel mediated synthesis produced homogenous dispersion of particles with strong interactions, thus enhancing the physicochemical properties and long-term functionalities. The method of in situ sol-gel proposed by Yang et al. [164] was based on the dissolution of titanium isopropoxide with isopropyl alcohol followed by the addition of acetyl acetone (to control hydrolysis) in the molar ratio of 1:4:0.7, respectively. Additionally, chitosan was dissolved in 2 % acetic acid solution and the prepared solutions were then added drop wise to dilute titanium isopropoxide separately under vigorous stirring. As an outcome of the method, the solutions turned into semisolid.

Liu et al. [68] reported a rapid and green method to synthesize silver nanoparticles (Ag NPs) and simultaneously achieve exfoliated chitosan/clay nanocomposite under microwave irradiation, in which quaternized chitosan (QCS), montmorillonite (MMT) and Gemini surfactant were used as reducing and stabilizing agents. They proposed the preparation of Ag NPs on the base of reducing action of quaternary ammonium groups in QCS. In addition, MMT and surfactant did not take part in the synthesis of Ag NPs, but they were conductive to the formation of Ag NPs. During the formation of Ag NPs, when QCS was reduced to form the Ag NP, the large driving force for intercalation was obtained to make the MMT layers peel.

Giannakas et al. [34] has prepared chitosan/Na-MMT nanocomposites the use of a reflux-solution method. They prepared chitosan acetate solution at 70 °C with two different concentrations which were added to clay suspension and refluxed for 1 h. They reported that the reflux treatment led to a significant decrease of the chitosan's hydrated crystallinity observed at XRD, a pronounced increase of the stiffness and strength, a considerable reduction of the elongation at break and water vapor permeability (WVP) of the nanocomposite films.

Xie et al. [161] prepared plasticized chitosan/clay nanocomposites by thermomechanical kneading. They used two different types of chitosan in their study. Lower molecular weight CS was used as an organic modifier for the sodium clay, whereas higher molecular weight CS used as matrix polymer. In the preparation of the nanocomposites glycerol (Gly) was first introduced into the chitosan powder and manually mixed, followed by the addition of CS-modified nanoclay (in the form of either paste or dried powder) with further manual mixing. Then, acetic acid aqueous solution (3 %, v/v) was added dropwise to the chitosan-glycerol-nanoclay mixture with continuous manual mixing to obtain a paste with a final chitosan concentration of 25 wt%. The mixtures were then thermomechanically kneaded in an internal batch mixer with twin roller rotors at 80 °C for 15 min, with a rotor

speed of 100 rpm. Finally, the resulting materials were compression molded at 110 °C temperature and 160 bar pressure. They stated that comparing to a typical solution casting method which has been used in many other studies of chitosan-based materials, this process demonstrated a high efficiency and great ability in well dispersing of the nanoclay into the chitosan matrix. Their XRD and TEM results showed that MMT could be largely exfoliated in the chitosan matrix during thermal kneading, no matter organo-modification of MMT with chitosan was carried out.

Chiu et al. [15] prepared chitosan/clay nanocomposites using different amounts of trimethoxysilylpropyl octadecyl dimethyl ammonium chloride treated clays and compared the results with nanocomposites containing unmodified clay. Their results revealed that exfoliated clay was attained at the higher intercalant dosages. The treated clay gave higher reinforcement than untreated clay in general. However, they also stated that with increasing modifier content, hydrophobic character of modified clay continued to increase, which in turn appeared to reduce available specific interactions between organic modifier and functional group on chitosan and to result in a slight drop of Young's modulus, even though they exhibited a high extent of dispersed clay. They also added that high dispersion of modified clay might not guarantee high mechanical properties of (nano) composites where dispersion status and interfacial interaction were both the major factors influencing the polymer properties.

Nanocomposites based on chitosan (CS) with nanoclay (montmorillonite, MMT) and/or nanoclays after surface modification were prepared by Lewandowska et al. [63]. In their study they used (1) unmodified clay, (2) nanoclay, surface modified—contains 25–30 wt% of octadecylamine, (3) nanoclay, surface modified—contains 0.5–5 wt% of aminopropyltriethoxysilane and 15–35 wt% of octadecylamine, (4) nanoclay, surface modified—contains 25–30 wt% of trimethyl stearyl ammonium. Their findings showed that in the case modified nanoclays better improvements were obtained for the nanocomposites. They explained the improvements based on the interactions that were associated with the presence of amino groups in the nanoclay and the hydroxyl or amino groups in chitosan.

Lertsutthiwong et al. [62] investigated the effects of the characteristics of chitosan (i.e., molecular weight and DD) and the chitosan/montmorillonite mass ratio on the properties of chitosan–montmorillonite. They used three different CS having molecular weights of 71.000, 220.000, 583.000 g/mol and chitosan with DD of 80 and 90 %. The nanocomposites were prepared by simple solution mixing method. In their results they indicated that the amount of chitosan intercalated into montmorillonite increased with the decrease of M_w of chitosan. Regardless of the M_w of chitosan, the d-spacing of chitosan–montmorillonite increased by about 18 % compared to that of sodium montmorillonite. Thus, the ability of chitosan to expand montmorillonite layers was independent of the M_w of chitosan. They also found that greater amount of chitosan with DD 80 % intercalated into the montmorillonite layers. When the ratio of CS to MMT was increased the d-spacing of sodium montmorillonite was more expanded. This was probably because higher amounts of chitosan in the ratio provided more cationic charges, and consequently a stronger electrostatic interaction with the anionic silicate layers of montmorillonite.

As a conclusion, it can be said that preparation methods and conditions highly affect either the intercalation efficiency or the properties of the resulting nanocomposites. The type of the preparation method, process temperature, ratio of CS to nanoclay, modification of the clay, molecular weight, and deacetylation degree of CS play a crucial role for the final properties of the nanocomposites which should be determined for each studied nanocomposite system.

4.1 Mechanical and Thermal Properties of Chitosan-Based Nanocomposites

Polymer/clay composites show often various attributes, including mechanical, thermal, and biodegradable properties that are superior to conventional composites. Tensile strength, Young's modulus, and elongation at break are generally used to quantify the mechanical properties of materials.

In recent years, more and more reports are related with the natural polymeric composites which contain organic and/or inorganic additives. Such composites can be used in medical and/or biomedical applications [1, 12, 16, 52, 64, 66, 100, 101, 103, 156, 163, 168].

The knowledge of physico-chemical properties of composites and their use in various applications is a key factor. The development of biodegradable biopolymer-based nanocomposites may open the way toward innovative applications of polymers in several fields. Characterization of films made of chitosan with addition of montmorillonite has been reported [1, 12, 13, 22, 37, 52, 61, 103, 153]. It has been shown that the tensile strength of chitosan/clay films increased significantly with increasing clay concentrations [1, 61, 163]. Moreover, the nanodispersed clay improves the thermal stability with the increase of clay loadings.

4.1.1 Mechanical Performance of the Chitosan-Based Nanocomposites

Generally, mechanical performance of a material can be evaluated by analyzing mechanical tests parameters (e.g., Young's Modulus, E; tensile strength, stress at break, thermomechanical parameters from dynamical mechanical thermal characterization (i.e., DMTA). Additionally, the transition temperature can be calculated from dynamical mechanical tests.

Different results were obtained by varying the amount of clay within the polymer matrix. So that, at higher amount of clay, especially over 5 wt%, the increase of the Young Modulus (E) occurs [13, 29, 34, 61]. This phenomenon could be explained by an increase of the matrix crystallinity due to the presence of clay particles. As expected, with the increase of the Young's modulus, the elongation at break decreases, making materials more brittle in the case of nanocomposites with

Table 2 Dependence of mechanical properties on the clay content and clay type

NC-based chitosan	Clay content %	Stress at break (MPa)	Young's modulus (MPa)	Tensile strength (MPa)	Elongation (%)	References
CS	0	97.44	3996	26.01[i]	5.3	Duncianu and Vasile [29]
CS-C30B1	1.0	79.10	3327.38		15.02	
CS-C30B3	3.0	78.67	3038.00		15.99	
CS-C30B5	5.0	88.93	5093.00		14.20	
CS-C30B7	7.0	113.08	5647.00		14.07	
CS-Na^+MMT1	1.0	106.73	7016.50		2.32	
CS-Na^+MMT3	3.0	53.80	4337.50	26.95[i]	2.12	
CS-Na^+MMT5	5.0	104.43	8625.90		1.85	
CS/GLY	0		1700[i]	8.20		Lavorgona et al. [61]
CS/3MMT/GLY	3			9.07		
CS/10MMT/GLY	10		3700[i]	17.97		
CS/10MMT	10		6300[i]	32.59		
CS	0		5700[i]	26.01		
CS-Na^+MMT3	3			26.95		
CS[ii]	0		3527	108.00	15	Giannakas et al. [34]
CS3MMT	3		4264	111	5.15	
CS5MMT	5		4748	126	9.58	
CS30G[iii]	0		1178	67	50,68	

[i]From DMTA curves (storage modulus, E′); GLY-glycerol
[ii]Chitosan solution 1 % in 1 % acetic acid
[iii]With 30 % glycerol

Na^+MMT, while for nanocomposites with organically modified montmorillonite (e.g. C30B) the elongation at break may show increase even at very small amount of clay loading as reported by Duncianu and Vasile [29]. In Table 2 mechanical properties of some chitosan-based nanocomposites are summarized.

Abdolmohammadi et al. [1] studied also the effect of addition of Na^+MMT and organically modified montmorillonite (OMMT) on the mechanical properties of polycaprolactone (PCL)/chitosan blends. They obtained improved tensile moduli mostly based on the reinforcement effect and the higher moduli of the rigid inorganic clay. Compared to Na^+MMT, OMMT was more compatible with PCL/chitosan, where the clay sheets were easily dispersed and intercalated into PCL/chitosan composite. Hence, the tensile modulus for the PCL/chitosan/OMMT was higher than that of PCL/chitosan/Na^+MMT. It increased proportionally by increasing OMMT concentration in the composites.

For the system PCL/chitosan/Na^+MMT microcomposites, it was shown that by increasing the Na^+MMT content the tensile strength decreased. This inverse relation between tensile strength and clay contents was due to the agglomeration and poor dispersion of Na^+MMT in the matrix. However, increasing the OMMT contents increased the tensile strength and peaks up to 3 wt% of OMMT loading due to good

dispersion of organoclay into the matrix, yielding higher reinforcement effect. By further loading of OMMT, the tensile strength gradually decreased, implying that for the OMMT loadings of higher than 3 wt%, the clay was not fully intercalated by the matrix. A reduction in elongation at break was found with the increase of OMMT and Na^+MMT contents. It indicates that the ductility of the matrix gradually decreases by increasing the clay content due to the aggregates of silicates at high clay content. The elongation at break of PCL/chitosan/OMMT was higher than that of PCL/chitosan/Na^+MMT, indicating that modification of clay improved the compatibility between clay and PCL/chitosan matrix.

Cheaburu et al. [13] studied the thermomechanical parameters of the systems based on chitosan and montmorillonite under film form. The dynamic mechanical analysis curves are given in Fig. 5 and the obtained transition/relaxation temperatures, (reading at the middle point of the inflection of the curve) are summarized in Table 3.

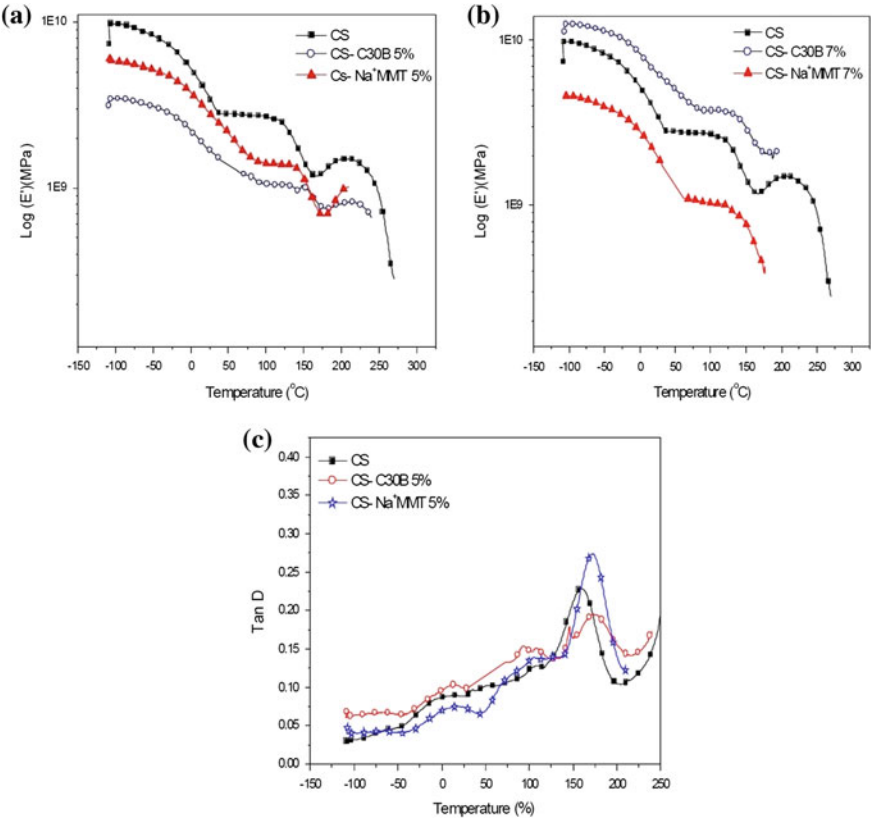

Fig. 5 DMTA spectra of nanocomposites based on chitosan: **a**, **b** nanocomposites with 5 wt% clay content, **c** nanocomposites with 7 wt% modified (C30B) and unmodified ones (Na^+MMT) clay content, respectively. (Adapted from Ref. [29])

Table 3 Transition/relaxation temperatures of chitosan and chitosan/clay nanocomposites (Adapted from [29])

Sample	From E′—Fig. 3 a_1, b_1		From tanδ—Fig. 3 a_2, b_2			
	T_1 (°C)	T_2 (°C)	T_3 (°C)	T_1 (°C)	T2 (°C)	T_4 (°C)
CS	6.0	142.0	−67.0	6.0	51.0	156.0
					105.0	
CS-C30B 5 %	17.5	165.0	−70.0	12.8	91.8	145.0
						175.0
CS-C30B 7 %	15.0	155.0	−79.0	8.0	84.0	168.0
CS-Na^+MMT 5 %	14.5	152.0	−73.0	15.0	100.0	170.0
CS-Na^+MMT 7 %	15.0	163.5	−75.0	12.8	75.0	167.0

A similar nonlinear viscoelastic behavior of the matrix with different content and type of clay was observed, but with a shift in transition temperatures in respect to that of pure chitosan. Two transitions/relaxation temperatures were found from the elastic modulus (E′ curves—Figs. 5a and 3b) while in the dependence of tanδ on temperatures (Fig. 5c) four transition/relaxation phenomena appeared. All transition/relaxation temperatures found took higher values in nanocomposites materials. From tanδ—T dependence, a transition at very low temperature, around –70 °C (T3) was detected. The low transition temperature of 6 °C (T_1) was shifted to higher temperature with approximately 9–10 °C in nanocomposites. The transition temperature (T_2) occurs at ∼80–100 °C was attributed to plasticized effect of the residual interchain water or to its removal. According to Britto and de Assis [10], the peak in the tan δ curve appeared at about 156 °C for chitosan and around 170 °C for the chitosan-based nanocomposites in the heating run might be due to some α—relaxation of molecular motions when the chitosan molecules were in the pseudo-stable state. Increase in transition/relaxation temperature values was in accordance with high stiffness found by tensile tests.

Quijada-Garrido et al. [86] plotted the storage (E′) and loss tangent (tanδ) as a function of temperature for neat chitosan and nanocomposites prepared with and without glycerol as plasticizer. The tanδ plot of neat chitosan without glycerol (Fig. 6b) showed a prominent relaxation process at around 160 °C. This peak was attributed to the glass transition temperature of chitosan arising from the relaxation of two glucopyranose rings via the glucosidic oxygen and assisted by a cooperative hydrogen bonds reordering. The shoulder at around 100 °C could be associated with the evaporation of residual water molecules. Some reactions involving functional groups of chitosan, such as the decomposition of chitosonium groups to chitin, can take place in the range of temperature between 80 and 100 °C ($–NH_3 + –OOCCH_3 \rightarrow –NH–OC–CH_3 + H_2O$) [136]. The presence of non-intercalated or poorly intercalated Na-MMT stacks, as revealed by WAXD analysis, did not significantly affect the thermomechanical behavior of materials in terms of both T_g and height of the tanδ peak. As for the materials obtained using glycerol as plasticizer, the storage modulus increased with the Na^+MMT contents in the glassy region.

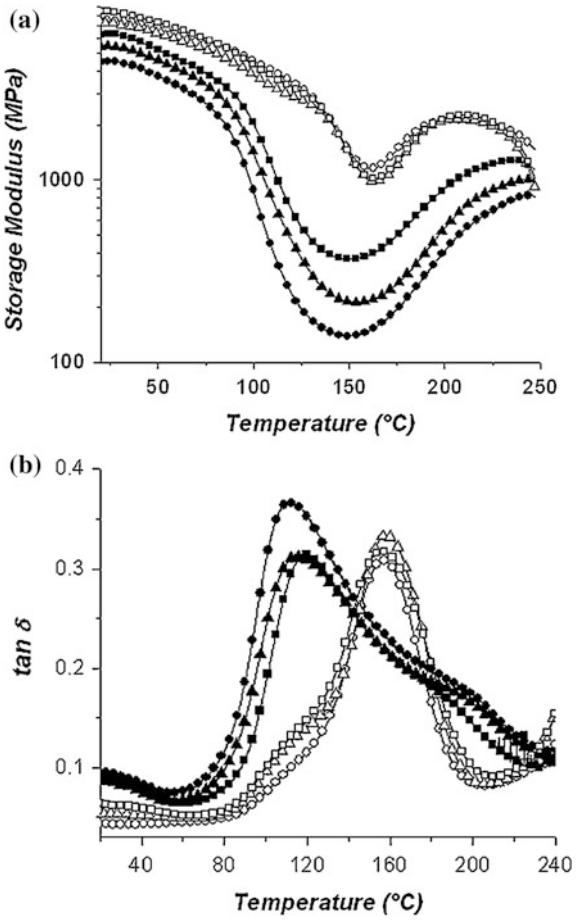

Fig. 6 DMA curves including storage modulus (**a**) and tan δ (**b**) as a function of temperature for chitosan and its nanocomposites. ○ CS, Δ CS/3MMT and □ CS/10MMT, ■ CS/GLY, ▲ CS/3MMT/GLY and (■) CS/10MMT/GLY (Reprinted from Ref. [61] with the permission from Springer)

This increase suggested that the interactions between chitosan matrix and Na^{+}MMT platelets were strong enough to allow an efficient load transfer between the matrix and the fillers.

The glass transitions of the nanocomposites is slightly higher than that of neat chitosan and the area under the tanδ curves is reduced, which is indication of a restriction to the relaxation movements of chitosan macromolecules probably due to the higher extent of the chitosan intercalation. The glass transition temperature decreases when glycerol is added, confirming its plasticizing effect on the chitosan polymeric network [86].

4.1.2 Thermal Properties of Chitosan/Clay Nanocomposites

Thermal stability and transition temperatures are analyzed generally by means of thermogravimetry and DSC measurements. For a system based on chitosan and montmorillonite with different clay types and amounts under film form were reported by Cheaburu et al. [13] Two processes have been detected in the studied temperature range (room temperature –200 °C) (Table 3) which the first in 110–125 °C and second in 168–173 °C region. The first one was not influenced by the nanocomposite content while the second one increased with both Na-MMT and Cloisite 30B content up to 6 °C in respect with that of chitosan film. The data were in accordance with those obtained by DMTA analysis, but the first temperature region was situated at high temperature in DSC curves due to the different heating rates used (2 °C/min in DMTA and 20 °C/min in DSC) (Fig. 7). The first peak was assigned to the water loss while the second to the decomposition of the components of the system being related to the thermal stability of nanocomposites. Thus the incorporation of Na^{+}MMT and Cloisite 30B led to improved thermal stability of chitosan.

The rise in the degradation temperature is due to restrain of the heat transfer by clay which also reduces the diffusion of volatile products released by substances.

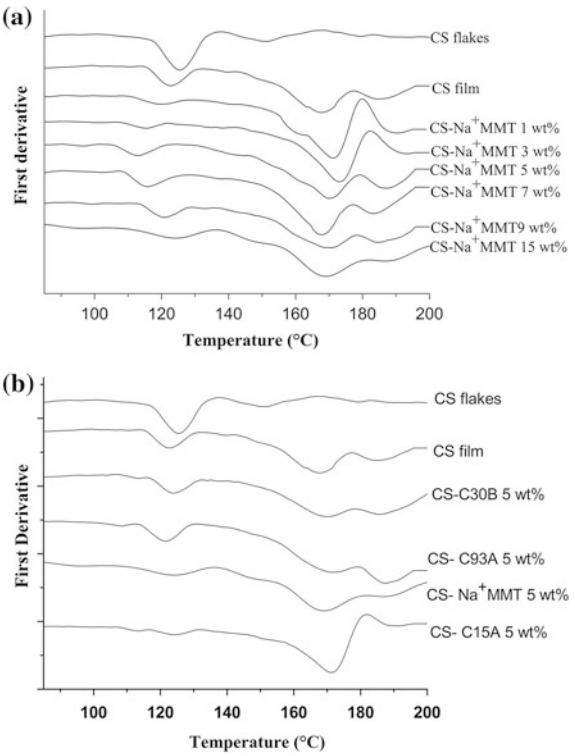

Fig. 7 DSC thermograms for the nanocomposites based on chitosan with various amounts of clay (**a**); and with a constant amount of clay (5 wt %) with different types (**b**) (Reprinted from Ref. [13], with the permission from Trans Tech. Pub.)

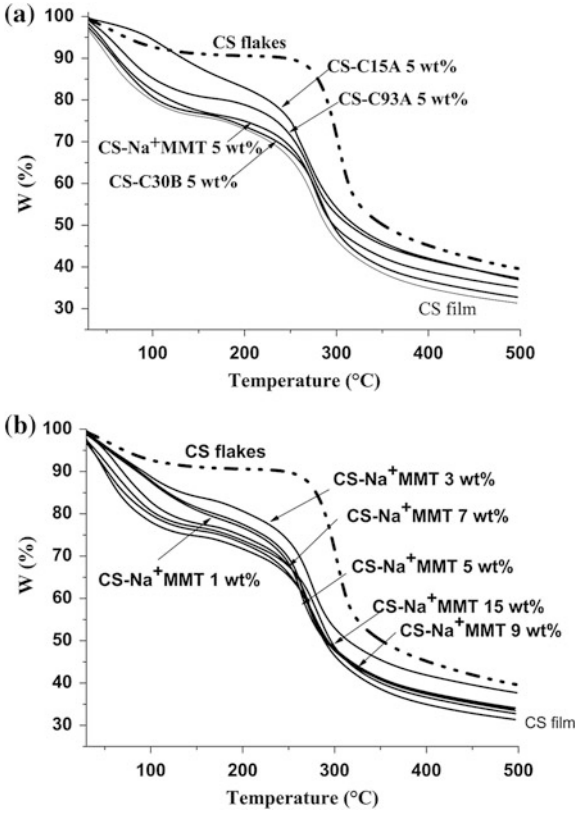

Fig. 8 Thermogravimetric curves for the Chitosan-based clay nanocomposites with; **a** different clay types, **b** different amounts of Na^+MMT (Adapted from Ref. [13], with the permission from Trans Tech. Pub.)

In Fig. 8 the weight loss curves of chitosan and chitosan/clay nanocomposite specimens containing different clay types and different ratios of sodium montmorillonite as function of temperature are given. The clay incorporation gives a rise in thermal stability of the CS films. However, the type of clay also had influence on the thermal degradation. Interestingly, the nanocomposites prepared with organically modified clays had higher thermal stability whereas the ones having clays with hydrophilic character had smaller improvements (Na^+MMT, Cloisite 30B). This shows that the organic modifier of the clay had better interactions with the chitosan molecule leading to a better intercalated system and improved properties. The effect of different ratios of Na^+MMT on thermal degradation of the nanocomposites was demonstrated by the data in Fig. 8b. With the incorporation of Na^+MMT layers, the thermal stability of the chitosan increased. However, the maximum enhancement was obtained at 3 wt% ratio of Na^+MMT, whereas further increase in clay amount did not lead to increase in thermal stability. This was probably due to the flocculation and tactoid formation of the clay layers at higher clay loading ratios. Therefore, usually an optimum clay loading ratio is reached for each particular system giving maximum property enhancements that should be investigated.

The addition of CS into the LDPE matrix, even in very small amount, strongly influenced the thermal behavior of chitosan–low density polyethylene (LPDE) composites as reported by Vasile et al. [145]. Chitosan was stable till higher temperatures (up to 150 °C). The LDPE/CS thermograms showed first degradation step within a temperature range of 290–420 °C, where an overlapping of thermal degradation of CS and of LDPE might occur. The second degradation stage is occured within the temperature range of 420–492 °C. The values of onset degradation temperature (T_i) had higher values than 260–290 °C while CS started to degrade at 249 °C lower than T_i of pure LDPE (323 °C). Also, the effect of additives, tocopherol, and Irganox 1076, which had a synergistic effect with the nanoclay in enhancing thermal stability, was found to be in accordance with the oxidation induction period (OIP) results. The degradation mechanism was significantly changed by CS incorporation whose decomposition interferes with that of LDPE giving a complex decomposition pathway characterized by two steps instead of one in LDPE, and also each additive influenced the decomposition processes.

4.2 Barrier Properties

Polymer/layered silicate nanocomposites are well known to have enhanced barrier properties. The high aspect ratio of the nanolayers exfoliated in the polymer matrix results in a tortuous pathway for permeating molecules that retards their diffusion through the matrix. The increase in barrier efficiency depends on the degree of tortuosity created by clay layers, which in turn, related to filler concentration, exfoliation degree, and lateral length of the clay sheets within the polymer matrix. The tortuous factor is defined as the ratio of the actual distance that the penetrant must travel to the shortest distance that it would travel in the absence of barriers. Since chitosan is a promising biomaterial to produce biodegradable materials (i.e., for food packaging) the barrier properties of the chitosan/clay nanocomposites are of importance and have been investigated by the researchers. Oguzlu and Tihminlioglu [78] prepared chitosan nanocomposite films using solvent-casting method by incorporation of an organically modified montmorillonite (Cloisite 10 A) and investigated the effect of filler concentration on the water vapour permeability (WVP) and oxygen permeability of the nanocomposite films. In their study, they obtained mostly intercalated structures. They reported that the WVP of the pure chitosan was very sensitive to relative humidity and showed a sharp increase above 50 % RH. The water vapor and oxygen permeability of the nanocomposite films were significantly reduced by the tortuosity created by the clay layers. Giannakasa et al. [34] investigated the effect of the use of reflux-solution method and addition of glycerol for 3,5,10 wt% Na^+MMT containing—chitosan nanocomposites. The lowest WVP values were found for films obtained from 2 w/v % chitosan solution and their nanocomposites. The nanocomposites prepared from more-diluted chitosan solution as well as the addition of glycerol in the system resulted in a two fold increase in the WVP values for tested chitosan-based films.

However, the nanocomposites prepared with the addition of Na^+MMT and refluxing resulted in a pronounced reduction of the WVP values (up to 60 %). In a similar study, Lavorgna et al. [61] studied the combined effect of clays and glycerol plasticizer on the barrier and water sorption properties of chitosan and its nanocomposites prepared with different Na^+MMT loadings by solution casting. They found out that the presence of glycerol enhanced the chitosan intercalation in the silicate galleries, hindered the flocculation process, and modified the hydrogen bonding network within the material that allowed better interaction between filler and matrix. As a result, the water sorption values were much lower in plasticized nanocomposites whereas they had lower reduction (30 %) in WVP. A higher reduction of permeability (50 %) was obtained in chitosan films not containing glycerol due to the alignment and flocculation of MMT stacks. Vartianien et al. [143] prepared chitosan/hydrophilic bentonite nanocomposites with higher clay loadings of 0, 17, 50, and 67 wt% by using sonication in solvent-casting method. They also applied the biohybrid coatings onto argon–plasma-activated LDPE coated paper. In their results, they showed that both the intercalated nanocomposite films and the coated paper indicated much improved barrier properties against oxygen, water vapor, grease, and UV light transmission. Oxygen transmission was significantly reduced under all humidity conditions. In dry conditions, over 99 % reduction and at 80 % relative humidity almost 75 % reduction in oxygen transmission rates was obtained. In another study by Casariego et al. [12], blends of chitosan (from Cuban lobster) and clay micro/nanoparticles were prepared by dispersion of clay particles in the film matrix. They used lactic acid solutions for the dispersion of chitosan and clay in the preparations. They reported that the WVP of the films was reduced by incorporation of such particles, while the water solubility was decreased as the clay concentration increased. Moreover, the addition of clay did not show significant effect on oxygen and CO_2 permeability whereas initial chitosan concentration had positive effect on oxygen permeability. It can be concluded that in all cases the addition of clay layers has positive effect on barrier properties especially for water vapor and oxygen permeability, however, the addition of glycerol as plasticizer leads to lower reduction in permeability whereas it helps to decrease water sorption of the nanocomposite films.

4.3 Antibacterial Properties of CS/Clay Nanocomposites

Unmodified nanoclays may adsorb bacteria from a solution enabling better interaction with antimicrobial polymers such as chitosan [24, 152]. Han et al. [38] observed that chitosan–MMT nanocomposites were significantly more effective against *Staphylococcus aureus* and *Escherichia coli* than both pure chitosan and Na^+MMT. Since the antimicrobial activity of chitosan has been ascribed to its cationic character, the increased antimicrobial activity of the nanocomposites seems contradictory, because the cations of chitosan are neutralized via electrostatic interactions with anionic silicate layers. The authors concluded that the

nanocomposites exhibited synergistic effects between the components, because the chitosan molecules were evenly distributed through the inorganic matrix.

Wang et al. [156] carried out a series of studies on antibacterial effect of chitosan/rectorite nanocomposites. In their study, unmodified Ca^{+2}-rectorite and organic rectorite modified by cetyltrimethyl ammonium bromide were used for chitosan nanocomposites via solution mixing technique. The antibacterial activity of the nanocomposites was measured by the minimum inhibition concentration (MIC) against Gram-positive (*S. aureus* and *Bacillus subtilis*) and Gram-negative (*E. coli* and *Pseudomonas aeruginosa*) bacteria. The results showed that the pristine rectorite could not inhibit the growth of bacteria, but chitosan/layered silicate nanocomposites had stronger antimicrobial activity than pure chitosan, particularly against Gram-positive bacteria. With the increase of the amount and the interlayer distance of the layered silicates in the nanocomposites, the nanocomposites showed a stronger antibacterial effect on Gram-positive bacteria, while the nanocomposites showed a weaker antibacterial effect on Gram-negative bacteria. In a study of Wang et al. [155], they prepared chitosan/organic rectorite (chitosan/OREC) nanocomposite films with different mass ratios of chitosan to organic rectorite and corresponding drug-loaded films by a casting/solvent evaporation method. In their results, they divided the antibacterial process of chitosan/OREC nanocomposites into two stages. The first stage was the adsorption of the bacteria from solution and immobilization on the surface of the clay and the second stage was related to the accumulation of chitosan on the surface of clay where they inhibit the bacterial growth. They found that the nanocomposite film with the highest amount of OREC and the film with the largest interlayer distance exhibited the strongest antibacterial behavior as a result of the increased surface areas for the absorption of the bacteria. In a recent study, Liu et al. [69] used microwave irradiation to intercalate quaternized carboxymethyl chitosan oligosaccharide (QCMCO) into the layer of rectorite (REC) to prepare QCMCO/REC (QCOR) nanocomposites which was faster than conventional heating method of 48 h. In their results they found out that in comparison with QCMCO, QCOR nanocomposites showed stronger antibacterial activity in the presence of REC. They also stated that the inhibition effect on Gram-positive bacteria was better than that of Gram-negative bacteria and fungus.

Chiu et al. [15] prepared chitosan/clay (nano) composites using a special quaternary ammonium intercalating agent coupled with a silanol group. In their study, they tested the antibacterial property of the nanocomposites against Gram-negative bacteria which chitosan is known to be less effective. They stated that pristine chitosan showed the antibacterial property at 79.2 ± 4.0 % against *E. Coli* while CS/OMMT nanocomposite displayed the highest antibacterial property among all the samples due to the quaternary ammonium group of the clay modifier that disrupted the bacterial cell membranes and caused cell lysis. Han et al. [38] prepared chitosan–montmorillonite nanocomposites by anion exchange reaction between water soluble oligomeric chitosan and Na^{+}-montmorillonite.

The antimicrobial activity of pure chitosan, Na^+-montmorillonite, and chitosan-based nanocomposites was tested quantitatively by the MIC measurement. They found out that generally all chitosan-based materials, including chitosan and chitosan nanocomposites exhibited antimicrobial activity, however, chitosan–montmorillonite nanocomposites show significantly higher antimicrobial activity against *S. aureus* and *E. coli* than pure chitosan and Na-montmorillonite. They also stated that the results were contradictory since the positive charge of chitosan molecules was neutralized via an electrostatic interaction with anionic silicate layers. Therefore, the nanocomposites had a synergic effect due to the uneven distribution of chitosan molecules are in the inorganic matrix that resulted in enhanced antimicrobial activity.

Hsu et al. [45] reported the preparation and antimicrobial properties of the nanocomposites based on chitosan and previously delaminated montmorillonite particles (DMP). During the nanocomposite preparations, one gram of CS was dissolved in 0.5 % (m/m) acetic acid (100 ml) and stirred for 24 h which was followed by the addition of DMP dispersion in different ratios to give the concentrations of DMP in the final composite of 10, 10^2, 10^3, or 10^4 ppm. The antimicrobial effect of DMP/CS nanocomposites was measured by the width of inhibition zone of *S. aureus*. The antimicrobial effect of DMP/CS 10 ppm and CS was similar; however, at increased concentrations of DMP much wider inhibition zones were obtained. They also measured the antimicrobial activity by the decrease of colony formation on the surface of DMP/CS nanocomposites (microbiostasis). The microbiostasis ratio of pure CS against *S. aureus* was about 40 %, but the ratio increased to 90 % as CS was mixed with DMP. The greatest microbiostasis ratio was 99 % when the DMP concentration was 10^4 ppm. Therefore, DMP/CS nanocomposites had much higher antimicrobial activity than the pure CS. Zhou et al. [172] studied the combined antibacterial effects of chitosan/silver/clay nanocomposites to improve the antibacterial function of biomedical catheter materials. They first prepared silver embedded chitosan materials by simple solution mixing of $AgNO_3$ with chitosan at pH = 7. Subsequently, they mixed CS–Ag with clay suspension to obtain CS–Ag–Clay composites that can be used as material for a drug-controlled release system in indwelling urinary catheters. Finally, they also synthesized polydimethyloxane (PDMS)/Clay–CS–Ag nanocomposite synthesized using an intercalation reaction. According to the outcome of the Inhibition Ring Test, PDMS/silver–chitosan/clay nanocomposites killed the mass of predominant urinary bacteria. Compared with chitosan and $AgNO_3$, the rate of killing bacteria was improved. In a similar study, Lavorgna et al. [60] prepared multifunctional bio-nanocomposites by loading chitosan matrix with silver–montmorillonite antimicrobial nanoparticles obtained by replacing Na^+ ions of natural montmorillonite with silver ions. They tested the effectiveness of silver nanoparticles immobilized in chitosan against *Pseudomonas spp.* as food-borne bacteria. A significant delay in microbial growth was obtained in presence of the active chitosan films. In particular, after 24 h a microbial load substantially lower than the control samples was

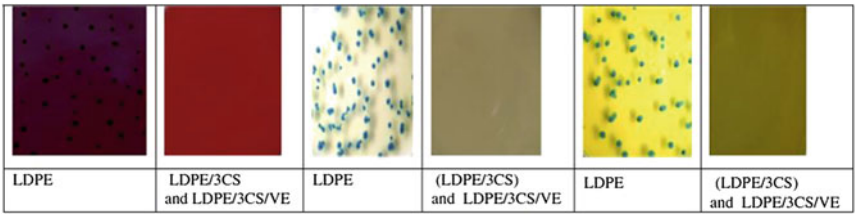

Fig. 9 Microscopical aspects of the colonies of *Salmonella enteritidis*, *Escherichia coli,* and *Listeria monocytogenes* grown over LDPE and LDPE/CS composites (Reprinted from Ref. [145], with permission from Elsevier)

found for the films containing Ag-MMT. However, after 48 h an increasing cell loads was also observed as a result of reversible stress of the cells.

Incorporation of vitamin E in the LDPE/CS systems [145] led to a total inhibition of bacteria growth, for the majority of LDPE composites. The most efficient antimicrobial action was obtained when testing the studied materials against *E. coli* and *L. monocytogenes* (Fig. 9).

It has been established that vitamin E beside antioxidant activity also shows an antimicrobial effect. It was associated with immune modulation by cumulating its activities with that of CS resulting in a synergistic effect. The obtained materials had a superior antimicrobial activity as it was demonstrated by testing as packaging material for mince poultry meat [146]. Thus, the use of CS in LDPE/clay composites exhibited 100 % inhibition after 24 h and even 48 h testing time.

4.4 Mucoadhesive Properties

Chitosan is also known to possess mucoadhesive properties due to the presence of many amino groups in the polymer chains that form hydrogen bonds with glycoproteins in the mucus [65] and also ionic interactions between positively charged amino groups and negatively charged sialic acid residues of mucin. Salcedo et al. [105] performed mucoadhesion measurements of chitosan nanocomposite matrices. Chitosan was characterized by the highest mucoadhesive potential (2.75 ± 0.10). Clay mineral was also able to interact with the mucin, although the normalized mucoadhesion parameter (0.71 ± 0.03) was significantly lower compared with CS (pb0.001, one-way ANOVA post hoc Scheffé test). Nanocomposite showed an intermediate behavior (0.85 ± 0.03) due to the mobility of the polymer chains which was reduced by the interactions of the clay mineral, reducing contact/interpenetration with the substrate.

4.5 Biodegradation of Chitosan-Based Nanocomposites

Biodegradation can be regarded as a process in which the degradation results from the action of microorganisms such as bacteria, fungi, or algae. Biodegradation can be generally divided into two steps. The first step is depolymerization or chain cleavage where the longer polymer chain undergoes backbone scission into smaller oligomeric fragments with the help of enzymes secreted by microorganisms. The second step is mineralization, which occurs inside the cell in which small oligomeric fragments are converted to biomass, minerals and salts, water, and gaseous substances such as carbon dioxide under aerobic environments and methane under anaerobic environments. Bio-based and biodegradable polymers (e.g., chitosan) and their composites may be broken down by the enzymes secreted by microorganisms. Once broken down to monomeric level, the polymer is used as the carbon source for the microorganism metabolism.

Chemical degradation usually refers to acid catalyzed degradation, i.e., in the stomach. Even though depolymerization through oxidation–reduction reaction and free radical degradation [44, 176] of chitosan have been reported these are unlikely to play a significant role in the in vivo degradation. Chitosan can be degraded by enzymes which hydrolyze glucosamine–glucosamine, glucosamine–N-acetyl-glucosamine, and N-acetyl-glucosamine–N-acetyl-glucosamine linkages [50].

Xie et al. [161] studied the biodegradation of plasticized chitosan-based nanocomposites according to the Australian Standard AS ISO 14855. During a degradation period of 160 days, the compost moisture content was maintained at 48–50 % and the pH at 7.8–8.5 to ensure favorable conditions for the compost microorganisms involved in the biodegradation process. Aerobic conditions were maintained by continuous supply of sufficient air flow to the bioreactors and the contents of each of the bioreactors were mixed once a week to ensure uniform distribution of air throughout the compost. The cumulative CO_2 and percentage biodegradation profiles for each test sample are shown in Fig. 10a, b, respectively. Steady rates of carbon dioxide evolution from each composting vessel indicate that test materials were actively metabolized by microbial population present in the compost. Similar results were observed by Xu et al. [162] during their biodegradation studies on acetylated chitosan films. It was shown that the biodegradation of the plasticized chitosan samples, with or without the addition of nanoclay (i.e., G10, G25, G25M2.5, G25M5.0, G25O2.5p, and G25O5.0p) was initiated immediately after incubation in compost, without any lag phase, whereas the unplasticized chitosan (G0) degraded relatively much slower. All plasticized samples achieved more than 50 % biodegradation within the first two weeks of composting. In comparison, G0 had an initial lag phase (3 days) and it reached approximately 18 % biodegradation at the end of second week. The increased susceptibility of the plasticized chitosan to biodegradation was favorized by the presence of glycerol (Gly).

The biodegradation rate of CS in the MMT/CS nanocomposite was much faster than that of the pure CS polymer. The biocompatibility of MMT/CS at 103 ppm was even better than that of pure chitosan and the proliferation of fibroblasts on

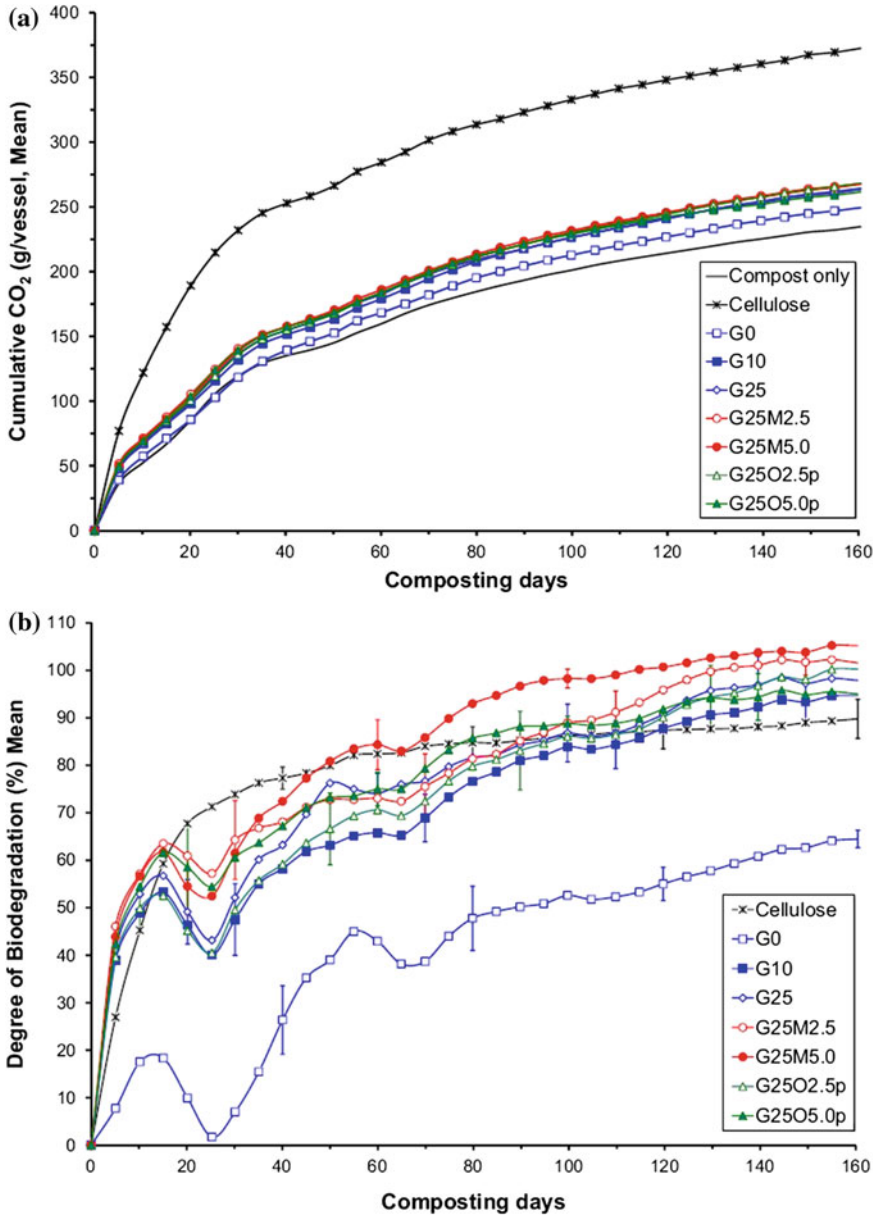

Fig. 10 The cumulative CO_2 data (**a**) and the degrees of biodegradation (**b**) as a function of composting time for cellulose and different chitosan samples (Sample codes; G0: Pure CS; G10: CS/Gly(10 %); G25: CS/Gly(25 %);G25M2.5: CS/Gly(25 %)/MMT(2.5 %); G25M5.0: CS/Gly (25 %)/MMT(5.0 %); G25O2.5p: CS/Gly(25 %)/OMMT-paste(2.5 %); G25O5.0p: CS/Gly(25 %)/ OMMT-paste(5.0 %). (Reprinted from Ref. [161], Copyright (2013), with permission from Elsevier)

MMT/CS at 103 ppm was found to be significantly greater than other materials. The inflammatory responses of MMT in vitro and in subcutaneous rats were not obvious until the concentration of MMT was >103 ppm.

Wu et al. [160] analyzed the biodegradable poly(lactic acid) (PLA)/chitosan modified MMT nanocomposites. In vitro degradation behaviors of PLA and PLA/m-MMT nanocomposites have been systematically investigated for up to 7 weeks in phosphate buffer saline (PBS) solution at 37.5 °C. The changes of number and weight average molecular weights (M_n and M_w) as a function of degradation time. Both M_n and M_w of PLA and PLA/m-MMT nanocomposites were decreased exponentially with degradation time throughout the degradation period. The degradation rates of PLA/chitosan—MMT nanocomposites were slower than that of PLA matrix. All results showed that introducing the m-MMT into PLA/chitosan system could enhance the physical properties of PLA/m-MMT nanocomposites due to the presence of inorganic layered silicates and better interaction between m-MMT and PLA in the fabricated nanocomposites.

Biodegradable nanocomposites of cellulose acetate phthalate (CAP) and chitosan reinforced with functionalized nanoclay (NC) were prepared by Gaurav et al. [33]. The blend showed an increase in the rate of biodegradation and water uptake with higher loading of nanoparticles. Chitosan was more biodegradable than CAP as the hydroxyl groups in the latter were replaced by ester groups. The blends showed a retarded degradation for the first 3 days but, thereafter, the biodegradation was higher than either CAP or chitosan as observed in the first 30 days. The addition of NC further lowered the biodegradation up to 4 % NC loading. This was explained to be due to the interaction between CAP and chitosan with the amine groups of modified NC, which restricted the segmental motion at the interface causing the effective path length and diffusion time to increase. A similar observation was made by Rindusit et al. [98] for methylcellulose–montmorillonite composites obtaining broader range of biodegradability and other essential properties of Methyl Cellulose (MC) through nanocomposite formation. However, beyond 4 % NC, the blend exhibited a higher degradation than for lower NC loadings. The higher ratios of modified nanoclay induced large amorphous regions and these regions were easily accessible during the degradation process. Gaurav et al. [33] found that there is a correlation between water uptake and degradability as higher water uptake accelerates the degradation process. Thus, increase in hydrophilicity leads to an increase in biodegradability. Thus, for water uptake, the blends loaded with lower content of NC show a lower uptake while blends loaded with >4 % NC show increased water absorption characteristics and hence higher biodegradability. However, in the case of high interactions between MMT and the macromolecular chains, the degradation process can also be decreased with increased MMT ratios, as observed by Zheng et al. [171]. This phenomenon was explained as MMT sheets consumed some hydrophilic groups and depressed the solvent uptake, which protected the macromolecules from hydrolyzing. Meanwhile, the presence of MMT also served as physical cross-linking sites, which enhanced the stability of the network. It seems that the biodegradation of the chitosan-MMT-based nanocomposites also depends on the interactions of the silicate sheets with the macromolecular chains of the polymer matrix.

5 Applications of Chitosan/Clay Nanocomposites

Due to the unique properties of chitosan/clay nanocomposites as mentioned in previous sections, they have many potential applications in various fields such as environment, food packaging, drug delivery, tissue engineering, and other biomedical applications which are here discussed.

5.1 CS/Clay Nanocomposites as Adsorbent for Removal of Dyes and Heavy Metals

Chitosan can be used as an adsorbent to remove heavy metals and dyes due to the presence of amino and hydroxyl groups, which can serve as the active sites [159]. Amino groups of chitosan can be cationized, after which they adsorb anionic dyes strongly by electrostatic attraction in the acidic media [56, 149].

Montmorillonite has a net negative surface charge and has little or no affinity to anionic or neutral contaminants such as acid dyes. For this reason, the clay surface charge should be modified to incorporate positively charged sites prior to any anion adsorption attempts. If the hydrated interlayer cations are replaced by certain organic cations, the resulting organoclay minerals have the capability to absorb anions as well as nonionic organic compounds. Chitosan, a natural biopolymeric cation, is an excellent candidate to modify montmorillonite for the adsorption of anions. Recent research works have shown that chitosan/montmorillonite composites represent an innovative and promising class of sorbent materials [117].

Wang and Wang [150] prepared a series of biopolymer chitosan/montmorillonite (CS/MMT) nanocomposites for the adsorption of Congo Red dye. They investigated the different molar ratios of CS and MMT, initial pH value of the dye solution and temperature on adsorption capacities of the samples. The results indicated that the adsorption capacity of CS/MMT nanocomposite was higher than the mean values of those of CS and MMT. The maximum adsorption capacities were obtained with molar ratio of CS to MMT as 5:1, at pH = 4 and higher temperatures (T = 50 °C).

Wan Ngah et al. [148] prepared cross-linked chitosan/bentonite composites to adsorb tartrazine, an azo group containing dye which is harmful to organisms. The chitosan composites, cross-linked with epichlorohydrin were able to improve the chitosan performance as an adsorbent. In another study, by Wan Ngah et al. [147] they investigated the removal of Malachite green from aqueous solutions by cross-linked chitosan-coated bentonite (CCB) beads. They stated that CCB was a promising adsorbent for the removal of the dye from aqueous solutions due to the rapid adsorption and the high value of maximum adsorption capacity. Similar studies were also conducted reporting the enhancement of the adsorption of different dyes with the addition of layered silicates in chitosan matrix [71, 76, 154].

The chitosan/clay nanocomposites were also studied for the adsorption of heavy metals from aqueous solutions. The Chitosan–PVA/Bentonite (CS-PVA/BT) nanocomposites were synthesized by Wanga et al. [157] with combination of BT and CS–PVA polymer matrix. The CS–PVA/BT nanocomposites possessed a mesoporous structure, good adsorption capacity, and selectivity for Hg(II) ions from aqueous solutions. Fan et al. [31] produced chitosan-coated montmorillonite for the removal of Cr(VI). They evaluated the effects of pH, initial concentration, and temperature on adsorption capacity. Their results indicated that the adsorption between the nanocomposite and Cr(VI) was significantly physical and the optimal removal was observed at high concentrations, lower temperatures, and at pH = 4. Zhang et al. [169] introduced an experiment on the removal of mercury vapor (Hg^0) by chitosan/bentonite composites. It was reported that chitosan/bentonite composites had a much lower surface area compared to bentonite. This could possibly be due to the blockage of micropores in bentonite after chemical modification. This resulted in a decrease in the amount of Hg^0 removed. In contrast, Yang and Chen [165] found that chitosan/bentonite composites were a good adsorbent for removing mercury ions from wastewater. There are also studies reporting the improved efficiency of chitosan/clay nanocomposites for the removal of other heavy metals like As^{3+} [4], Cu(II), Ni(II), and Pb(II) [32]. The researches have revealed that these bio-nanocomposites seem to be a way to establish inexpensive large-scale barrier filters or permeable reactive barriers in removing dyes and heavy metals from wastewater or contaminated groundwater plumes.

5.2 *CS/Clay Nanocomposites in Food Packaging Applications*

In the food packaging industry, the use of proper packaging materials and methods to minimize food losses and provide safe and wholesome food products has always been the main interests. Due to the improved performance in the properties of nanocomposite packaging materials such as (i) gas (oxygen, carbon dioxide) and water vapor barrier properties, (ii) high mechanical strength, (iii) thermal stability, (iv) chemical stability, (v) recyclability, (vi) biodegradability, (vii) dimensional stability, (viii) heat resistance, (ix) good optical clarity, as well as (x) developing active antimicrobial and antifungal surfaces, and (xi) sensing and signaling microbiological and biochemical changes, food packaging has been one of the most concentrated nanocomposite technology development. Nanocomposites have already led to several innovations with potential applications in the food packaging sector [93].

The present status and perspectives on application of nanocomposites in the food packaging sector are well documented in several review articles [2, 5, 23, 28, 39, 48, 81, 92, 115, 116, 144]. However, most applications are mainly focused on nanocomposites made from both thermoset and thermoplastic polymers. Examples of using bio-nanocomposites are very scarce though they are actively under development. The improved barrier properties for oxygen and water vapor,

enhanced mechanical properties, as well as antimicrobial and biodegradability properties of chitosan/clay nanocomposites mentioned in previous sections in detail make them promising materials to be used in food packaging applications. However, beyond the mention of its potential applications there are few reports using these nanocomposites in direct food packaging applications. Vartiainen et al. [143] prepared chitosan/bentonite nanocomposites by solution mixing under ultrasound assistance. Afterward, they applied the nanocomposite solutions onto plasma-activated LDPE coated paper with a total coating dry weight of 0.2–0.6 g/m to obtain coated multilayer structures. Nanocomposite films and multilayer coatings had improved barrier properties against oxygen, water vapor, grease, and UV light transmission. Oxygen transmission was significantly reduced under all humidity conditions. In dry conditions, over 99 % reduction and at 80 % relative humidity almost 75 % reduction in oxygen transmission rates was obtained. All coating raw materials were "generally recognized as safe" (GRAS) and the calculated total migration was ≤6 mg/dm^2 in all cases, thus the coatings met the requirements set by the packaging legislation. Processing of the developed biohybrid nanocomposite coated materials was safe as the amounts of released particles under rubbing conditions were comparable with the particle concentrations in a normal office environment. The developed nanocomposite films and coatings can be potentially exploited as safe and environmentally sound alternatives for synthetic barrier packaging materials. Vasile et al. [145] prepared low density polyethylene/chitosan nanocomposites for food packaging applications. They first prepared chitosan/sodium montmorillonite nanocomposites by solution mixing technique and obtained solid nanocomposites after freeze drying. Subsequently, they applied a melt processing of neat LDPE and chitosan nanocomposites and/or antioxidant agents to obtain final LDPE/CS/nanoclay composite materials. The composites were processed using 2.7 and 5.5 wt% chitosan or chitosan nanocomposites and 0.5 wt% Irganox or vitamin E antioxidants. Their results showed that the composites exhibited satisfactory mechanical and thermal properties. The commercial additive as Irganox 1076 (FDA approved) or tocopherol, played a synergistic role together with clay to obtain materials with good properties. Antimicrobial/antioxidant agent system, incorporated in LDPE by melt processing, did not affect the antimicrobial activity however led a slight decrease in mechanical properties. Addition of vitamin E within the matrix induced higher antioxidant character with longer oxidation induction period. The newly obtained materials showed good inhibition activity against Gram-positive (*L. monocytogenes*) or Gram-negative (*E. coli, S. enteritidis*) bacteria. The overall findings indicated that the LDPE/chitosan/clay nanocomposites were suitable candidates for food packaging applications.

5.3 Chitosan-Based Nanocomposites in Drug Delivery

Recently, there has been an increased interest in the use of natural polysaccharides in the development of hydrogels for applications in biomedical and water

purification along with many more fields [57]. The degree of swelling in selected hydrogels varies upon the type of material, composition, architecture, inherent properties of the aqueous solution (e.g., temperature, ionic strength) methods used in the synthesis as well as targeted applications [102, 158]. It is the most common parameter used to describe the swelling in hydrogels. The polymeric network in hydrogels is hydrophilic polymer chains that are linked to each other via covalent bondings that give rise to macro- or micro/nano dimensions. Along with the chemical bonds, other types of interactions are also possible in hydrogels that ranges from physical interactions (e.g., hydrogen bonding and electrostatic interactions) to hydrophobic interactions [102, 131–133].

The drug release behavior of any polymer network depends upon the nature of the polymer, solvent compatibility, and the degree of cross-linking. The nanoparticle drug delivery system was developed for the purpose of recruiting, internalizing, retaining, releasing, activating, localizing, and targeting the drugs to the correct location at the correct time and dose [53].

Rajan et al. [87] reported the high performance of the hyaluronidase enzyme core-5-fluorouracil-loaded chitosan-polyethylene glycol-gelatin polymer nanocomposites, which were prepared using an ionic gelation technique, as targeted and controlled drug delivery vehicles. These hyaluronidase-loaded nanoparticles have recently been proposed as targeted and controlled drug delivery vehicle systems to tissues due to their ability to lose the intercellular connective matrix of hyaluronic acid. The encapsulation efficiency and loading capacities of the nanoparticles demonstrated that these nanocomposites displayed sufficient binding ability, which depends on the pH and initial concentration of the drug. Increasing drug release times were observed after the addition of complexes containing PEG and gelatin as a consequence of the high polymeric chain, leading to slow water diffusion. The release of 5-fluorouracil (5-FU) was strongly dependent on the pH value. The drug was released slower at pH 1.2 than at pH 6.8 due to the very high degree of interaction between the polymers as it contains a large amount of free positive charges, possibly due to the pH-dependent interaction between 5-FU and the composites. As a result, the drug diffusion inside the composites was retarded and the release of 5-FU was suppressed.

Cojocariu et al. [18–20] reported the study of the system based on hydrogels from chitosan–montmorillonite nanocomposites with different clay types and also the delivery mechanism by using different drugs (i.e. paracetamol, theophylline, xanthine derivatives, and NO donor compounds). The swelling behavior of the cross-linked hydrogels containing nanoparticles was followed in acidic media at pH = 2.2. Incorporation of clay nanoparticles decreased the maximum swelling degree reaching a plateau value. The swelling mechanism changed with increasing Cloisite 15A content. Higher the content of clay within the matrix, the lower the amount of drug was released. The most efficient way for obtaining a slower release of the drugs was to increase the clay content.

Wang et al. [151] prepared quaternized chitosan/montmorillonite (HTCC/MMT) nanocomposites via intercalation technique. Wang et al. [151] proved that HTCC chains entered into the interlayers of MMT and the interactions between them had

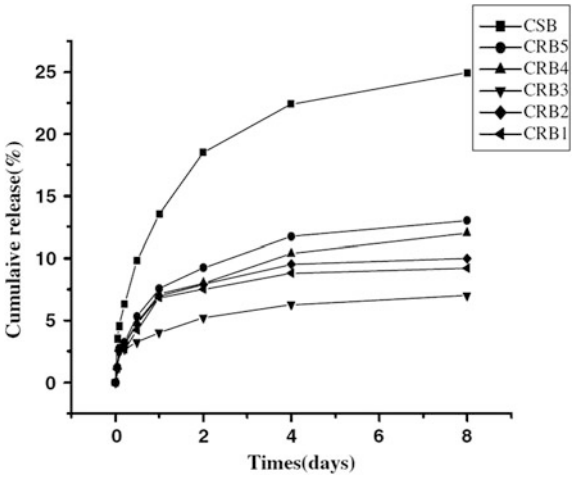

Fig. 11 In vitro release profiles of BSA from the chitosan/OREC nanocomposite films (BSA loaded films; CSB: Simple CS; CRB1-5: CS-OREC nanocomposites with mass ratios of 2:1, 6:1, 12:1, 20:1, 50:1, respectively). (Reprinted from Ref. [155], Copyright (2007), with permission from Elsevier)

taken place. Furthermore, HTCC/MMT nanocomposites were modified to prepare the nanoparticles and their drug-controlled release behaviors were evaluated. The results suggested that compared to pure HTCC nanoparticles, certain montmorillonite loadings on quaternized chitosan enhanced the drug encapsulation efficiency of the nanoparticles and slowed down the drug release from the nanocomposites. The effect of MMT in the drug release kinetics was found to be square root time dependent. The formulation with 1:1 mass ratio of HTCC/MMT was the most effective in encapsulating and releasing the drug and cytotoxicity.

Chitosan and chitosan/organic rectorite (OREC) nanocomposite films and corresponding drug-loaded films were prepared [155] by a casting/solvent evaporation technique in which chitosan and chitosan/OREC nanocomposite powder with different chitosan-OREC mass ratios (2:1, 6:1, 12:1, 20:1, 50:1). The bovine serum albumin (BSA) in vitro release behavior of chitosan and chitosan/OREC nanocomposite films containing BSA (Fig. 11) showed similar release profiles, and exhibited a small burst release in the first 12 h and then slow constant release but with different rates. Interestingly, all films showed equivalent drug release in the initial stages. But after several hours, all nanocomposite films showed slower release in comparison to pure chitosan film.

This initial burst effect could be attributed to the diffusion of the drug caused by rapid membrane swelling and also the faster release of the drug adsorbed toward the surface of the films matrix. So at the beginning, all films had similar swelling behavior and the equivalent rates of release of drug. This was particularly noticeable since a macromolecular model was used. Wang et al. [151] noted that the nanocomposite films, especially chitosan/OREC nanocomposite films with a ratio

(CRB3) with the largest interlayer distance, exhibited the subsequent slowest sustained release, and with the increase of the amount of OREC, the releases were slower. Higher hydrophobicity of the polymeric matrix and electrostatic attractive forces effectively improved the controlled drug release properties.

Chen et al. [14] reported chitosan/B-lactoglobulin core/shell nanoparticles, successfully prepared as nutraceutical carriers for nutrient delivery, increasing permeability of the molecules, increasing gastric residence time and providing the environmental stability. This encapsulated nutrient system was deemed safe for oral administration.

Salcedoa et al. [106] developed nanocomposite based on chitosan and montmorillonite as carrier to improve oral bioavailability of oxytetracycline. The nanocomposite was prepared by simple solid–liquid interaction and loaded with the drug. Caco-2 cell cultures were used to evaluate in vitro cytotoxicity and drug permeation. Their results showed that the nanocomposite was internalized into the cells and effectively enhanced drug permeation, being also biocompatible toward Caco-2 cells. The nanocomposite slightly decreased the permeation rate of the drug in the first phase of the permeation assay; nevertheless, the permeation was linear and proceeded all over the experiment time. The confocal laser scanning microscopy analysis showed that there was an interaction between the nanocomposites and the cell substrates thus causing the uptake of the nanocomposite into the cells. Even if a limited enhancement of drug permeation was determined by the nanocomposites the mechanism of internalization/uptake was found to be a chance for the drug to elude the P-glycoprotein.

5.4 Chitosan/Clay Nanocomposites in Tissue Engineering

Tissue engineering focuses on the regeneration of deficient or damaged tissues of the body and requires three basic elements: biomaterials, growth factors, and cell source. The scaffolds are expected to be degradable and absorbable with a proper rate to match the speed of new tissues' formation.

Azhar et al. [7] developed a novel composite based on chitosan–gelatin/nanohydroxyapatite-polyaniline (CS-Gel/nHA-PANI) by blending the synthesized nHA and PANI with chitosan and gelatin solution followed by lyophilization technique. The degradation behavior of biomaterials in physiological environments plays an important role in the engineering process of a new tissue. It was shown the in vitro biodegradation process of CS-Gel, CS-Gel/nHA, and CS-Gel/nHA-PANI composite scaffolds in PBS-containing lysozyme (≥30,000 U/mg) involved gelatin hydrolyzation and chitosan enzymatic degradation. Lysozyme is the primary enzyme responsible for in vivo degradation of chitosan through hydrolysis of acetylated residues [104]. Other proteolytic enzymes have shown to have lower level of degradation activity on the molecule.

It is known that the N-acetyl glucosamine groups of chitosan chains can be hydrolyzed by lysozyme. Its degradation leads to the release of amino sugars, which

can be incorporated into glycosaminoglycans and glycoprotein metabolic pathways or excreted. In the Azhar's study [7], it was presumed that the macromolecules of the scaffold surface underwent preferential hydrolytic scission into small molecules (oligomeric units), which could dissolve in PBS. Also the chains of gelatin, a hydrophilic polymer (presence of amide and carboxyl groups), hydrolyzed quickly in the presence of water [171]. In CS–Gel/nHA composite scaffold, the degradation was decreased by the addition of nHA compared to the CS–Gel matrix. Azhar et al. [7] found out that by the addition of PANI the degradation percentage was slowed down, demonstrating that the degradation rate might be controllable by adjusting the nHA and PANI contents in composite scaffolds.

Biocompatibility and cell attachment studies showed that the prepared scaffold based on chitosan is nontoxic to bovine leukemia virus fetal lamb kidney cell line and dental pulp stem cells being a good candidate for bone and tooth tissue regeneration.

6 Conclusion and Future Perspective

Present chapter reviewed chitosan bio-nanocomposites studies. Making a truly eco-friendly product keeps both environment and human safety in mind. At a minimum, the product is nontoxic. Other eco-friendly attributes include the use of sustainably ingredients, produced in ways that will not deplete the ecosystem.

A naturally occurring polysaccharide, chitosan, shows promise for safe use in healthcare products being a nontoxic, biocompatible material. However, care must be taken to ensure that it is pure, as protein, metal or other contaminants could potentially cause many effects both in derivative syntheses and in dosage forms. After derivatization (or cross-linking), unreacted reagents should be thoroughly removed to prevent confounding results as many reagents are cytotoxic uncoupled. It was shown that for special applications like biomedical, packaging, the mechanical and thermal properties of pure chitosan were not sufficient. Furthermore, many research studies focused on systems with chitosan preferred to synthesize chitosan derivatives at nanoscale level using various methods. The addition of a small amount of clay nanoparticles enhanced mechanical and thermal properties reducing the limitations of simple chitosan system to be applied in field which require a certain strength and thermal stability.

By combination of chitosan nanocomposites with other different polymeric systems, good results were obtained regarding the antimicrobial activity, solubility, drug release efficiency, enzyme immobilization, increased biocompatibility and cytotoxicity, barrier properties offering a wide range of applications (e.g., food packaging, biomedical and pharmaceutical, tissue engineering) which will be likely involved in our future lives.

Acknowledgments Chapter dedicated to the 65th anniversary of "Petru Poni" Institute of Macromolecular Chemistry of Romanian Academy, Iasi, Romania. Dr. C. Vasile acknowledge that

the research leading to these results has received partial funding from the Romanian—EEA Research Programme operated by the Ministry of National Education/Executive Agency for Higher Education, Research, Development and Innovation Funding (UEFISCDI) under the EEA Financial Mechanism 2009–2014 and Contract No 1SEE/30.06.2014 *ACTIBIOSAFE*

References

1. Abdolmohammadi S, Yunus WMZW, Rahman MZAB, Ibrahim NA (2011) Effect of organoclay on mechanical and thermal properties of polycaprolactone/chitosan/montmorillonite nanocomposites. J Reinf Plast Compos 30:1045–1054
2. Akbari Z, Ghomashchi T, Moghadam S (2007) Improvement in food packaging packaging industry with bio-based nanocomposites. Int J Food Eng 3(4):1–24
3. Anirudhan TS, Saranya Gopal S, Sandeep S (2014) Synthesis and characterization of montmorillonite/N-(carboxyacyl) chitosan coated magnetic particle (MP) nanocomposites for controlled delivery of paracetamol. Appl Clay Sci 88–89:151–158
4. Anjum A, Seth CK, Datta M (2013) Removal of As^{3+} using chitosan-montmorillonite composite: sorptive equilibrium and kinetics. Adsorpt Sci Technol 31:303–324
5. Arora A, Padua GW (2010) Review: nanocomposite in food packaging. J Food Sci 75(1): R43–R49
6. Averous L (2004) Biodegradable multiphase systems based on plasticized starch: a review. J Macromol Sci Part C Polym Rev 44:231–274
7. Azhar FF, Olad A, Salehi R (2014) Fabrication and characterization of chitosan–gelatin/nanohydroxyapatite–polyaniline composite with potential application in tissue engineering scaffolds. Des Monomers Polym 17:654–667
8. Blumstein A (1965) Polymerization of adsorbed monolayers: II. Thermal degradation of the inserted polymers. J Polym Sci A 3:65–73
9. Bodnar M, Hartmann JF, Borbely J (2005) Preparation and characterization of chitosan-based nanoparticles. Biomacromolecules 6:2521–2527
10. Britto D, de Assis OBG (2007) Synthesis and mechanical properties of quaternary salts of chitosan-based films for food application. Int J Biol Macromol 4:198–203
11. Calvo P, Remunan-Lopez C, Vila-Jato JL, Alonso MJ (1997) Novel hydrophilic chitosan-polyethylene oxide nanoparticles as protein carriers. J App Polym Sci 63:125–132
12. Casariego A, Souza BWS, Cerqueira MA, Teixeria JA, Cruz L, Díaz R, Vicente AA (2009) Chitosan/clay films' properties as affected by biopolymer and clay micro/nanoparticles' concentrations. Food Hydrocoll 23:1895–1902
13. Cheaburu CN, Vasile C, Duraccio D, Cimmino S (2009) Characterisation/Characterization of the Chitosan/layered silicate nanocomposites. Solid State Phenom 151:123–128
14. Chen L, Subirade M (2005) Chitosan/b-lactoglobulin core–shell nanoparticles as nutraceutical carriers. Biomaterials 26:6041–6053
15. Chiu FC, Lai SM, Hsieh IC, Don TM, Huang CY (2012) Preparation and properties of chitosan/clay (nano)composites: a silanol quaternary ammonium intercalated clay. J Polym Res 19:9781
16. Chivrac F, Pollet E, Avérous L (2009) Progress in nano-biocomposites based on polysaccharides and nanoclays. Mater Sci Eng R 67:1–17
17. Cho Y-W, Jang J, Park CR, Ko S-W (2000) Preparation and solubility in acid and water of partially deacetylated chitins. Biomacromolecules 1:609–614
18. Cojocariu A, Profire L, Aflori M, Vasile C (2012) In vitro drug release from chitosan/Cloisite 15A hydrogels. Appl Clay Sci 57:1–9
19. Cojocariu A, Profire L, Cheaburu C, Oprea A-M, Vasile C (2011) Evaluation of crosslinked chitosan hydrogels as carriers for prolonged delivery of some novel nitric oxide donor compounds based on theophylline and paracetamol. e Polym 11(1):334–351

20. Cojocariu A, Profire L, Cheaburu C, Vasile C (2012) Chitosan/montmorillonite composites as matrices for prolonged delivery of some novel nitric oxide donor compounds based on theophylline and paracetamol. Cellul Chem Technol 46:35–43
21. Cuq B, Gontard N, Guilbert S (1998) Proteins as agricultural polymers for packaging production. Cereal Chem 75:1–9
22. Darder M, Colilla M, Ruiz-Hitzky E (2003) Biopolymer—clay nanocomposites based on chitosan intercalated in montmorillonite. Chem Mater 15:3774–3780
23. de Azeredo HMC (2009) Nanocomposites for food packaging applications. Food Res Int 42:1240–1253
24. de Azeredo HMC (2013) Antimicrobial nanostructures in food packaging. Trends Food Sci Technol 30:56–69
25. Dmitriev BA, Knirel YA, Kochetkov NK (1975) Selective cleavage of glycosidic linkages: studies with the O-specific polysaccharide from Shigella dysenteriae type 3. Carbohydr Res 40:365–372
26. Domard A, Domard M (2001) Chitosan: structure–properties relationship and biomedical applications. Polymeric biomaterials. Marcel Decker Incorporated, New York
27. Duan B, Dong C, Yuan X, Yao K (2004) Electrospinning of chitosan solutions in acetic acid with poly (ethylene oxide). J Biomater Sci Polym Ed 15:797–811
28. Duncan TV (2011) Applications of nanotechnology in food packaging and food safety: barrier materials, antimicrobials and sensors. J Colloid Interface Sci 363:1–24
29. Duncianu CN, Vasile C (2008) In: Proceedings of the polymer processing society 24th Annual Meeting—PPS-24, Salerno (Italy), June 15–19 2008
30. Edgar KJ, Buchanan CM, Debenham JS, Rundquist PA, Seiler BD, Shelton MC, Tindall D (2001) Advances in cellulose ester performance and application. Prog Polym Sci 26: 1605–1688
31. Fan DH, Zhu XM, Xu MR, Yan JL (2006) Adsorption properties of chromium (VI) by chitosan coated montmorillonite. J Biol Sci 6:941–945
32. Futalan CM, Tsai WC, Lin SS, Hsien KJ, Dalida ML, Wan MW (2012) Copper, nickel and lead adsorption from aqueous solution using chitosan-immobilized on bentonite in a ternary system. Sustain Environ Res 22(6):345–355
33. Gaurav A, Ashamol A, Deepthi MV, Sailaja RRN (2012) Biodegradable nanocomposites of cellulose acetate phthalate and chitosan reinforced with functionalized nanoclay: mechanical, thermal, and biodegradability studies. J Appl Polym Sci 125(S1):e16–e26
34. Giannakas A, Grigoriadi K, Leontiou A, Barkoula NM, Ladavo A (2014) Preparation, characterization, mechanical and barrier properties investigation of chitosan–clay nanocomposites. Carbohydr Polym 108:103–111
35. Gross RA, Kalra B (2002) Biodegradable polymers for the environment. Science 297:803–807
36. Guilbert S, Gontard N, Gorris LGM (1996) Prolongation) Prolongation of the shelf-life of perishable food products using biodegradable films and coatings. LWT-Food Sci Technol 29:10–17
37. Günister E, Pestreli D, Ünlü CH, Atici O, Güngör N (2007) Synthesis and characterization of chitosan-MMT biocomposite systems. Carbohydr Polym 67:358–365
38. Han YS, Lee SH, Choi KH, Park I (2010) Preparation and characterization of chitosan–clay nanocomposites with antimicrobial activity. J Phys Chem Solids 71:464–467
39. Hatzigrigoriou NB, Papaspyrides CD (2011) Nanotechnology in plastic food-contact materials. J Appl Polym Sci 122:3720–3739
40. Hebeish AA, Ramadan MA, Montaser AS, Farag Ahmed M (2014) Preparation, characterization and antibacterial activity of chitosan-g-poly acrylonitrile/silver nanocomposite. Int J Biol Macromol 68:178–184
41. Hirano S (1996) Chitin biotechnology applications. Biotechnol Annu Rev 2:237–258
42. Hirano S (1999) Chitin and chitosan as novel biotechnological materials. Polym Int 48: 732–734

43. Hong SI, Lee JH, Bae HJ, Koo SY, Lee HS, Choi JH et al (2011) Effect of shear rate on structural, mechanical, and barrier properties of chitosan/montmorillonite nanocomposite film. J Appl Polym Sci 119:2742–2749
44. Hsu SC, Don TM, Chiu WY (2002) Free radical degradation of chitosan with potassium persulfate. Polym Degrad Stab 75:73–83
45. Hsu SH, Wang MC, Lin JJ (2012) Biocompatibility and antimicrobial evaluation of montmorillonite/chitosan nanocomposites. Appl Clay Sci 56:53–62
46. Jason B, Marroquin JB, Rhee KY, Park SJ (2013) Chitosan nanocomposite films: enhanced electrical conductivity, thermal stability, and mechanical properties. Carbohydr Polym 92 (2):1783–1791
47. Jayakumar R, Nwe N, Tokura S, Tamura H (2007) Sulfated chitin and chitosan as novel biomaterials. Int J Biol Macromol 40:175–181
48. Johansson C (2011) Bio-nanocomposites for food packaging applications. In: Mittal V (ed) Nanocomposites with biodegradable polymers. Oxford University Press, New York
49. Kavithaa K, Suthaa S, Prabhua M, Rajendrana V, Jayakumar T (2013) In situ synthesized novel biocompatible titania–chitosan nanocomposites with high surface area and antibacterial activity. Carbohydr Polym 93:731–739
50. Kean T, Thanou M (2010) Biodegradation, biodistribution and toxicity of chitosan. Adv Drug Delivery Rev 62:3–11
51. Khor E (2002) Chitin: a biomaterial inwaiting. Curr Opin Solid State Mater Sci 6:313–317
52. Kittinaovarat S, Kanosomwan P, Jiratumnukul N (2010) Chitosan/modified montmorillonite beads and adsorption reactive red 120. Appl Clay Sci 48:87–91
53. Korsmeyer RW, Peppas NA (1981) Effect of the morphology of hydrophilic polymeric matrices on the diffusion and release of water soluble drugs. J Membr Sci. 9:211–227
54. Krishnamoorti R, Vaia RA, Giannelis EP (1996) Structure and dynamics of polymer-layer silicate nanocomposites. Chem Mater 8:1728–1734
55. Kumar MNVR, Muzzarelli RAA, Muzzarelli C, Sashiwa H, Domb AJ (2004) Chitosan chemistry and pharmaceutical perspectives. Chem Rev 104:6017–6084
56. Kumar MNVR (2000) A review of chitin and chitosan applications. React Funct Polym 46:1–27
57. Kumari M, Chauhan GS (2011) Adsorption capacity, kinetics and mechanism of copper (II) uptake on gelatin-based hydrogels. J Appl Polym Sci 119:363–370
58. Kurita K (1995) Chemistry and application of chitin and chitosan. Polym Degrad Stab 59:117–120
59. Kurita K (2006) Chitin and chitosan: functional biopolymers from marine crustaceans. Mar Biotechnol 8:203–226
60. Lavorgna M, Attianese I, Buonocore GG, Conte A, Del Nobile MA, Tescione F, Amendola E (2014) MMT-supported Ag nanoparticles for chitosan nanocomposites: structural properties and antibacterial activity. Carbohydr Polym 102:385–392
61. Lavorgona M, Piscitelli F, Mangiacapra P, Buonocore GG (2010) Study of the combined effect of both clay and glycerol plasticizer on the properties of chitosan films. Carbohydr Polym 82:291–298
62. Lertsutthiwong P, Noomun K, Khunthon S, Limpanart S (2012) Influence of chitosan characteristics on the properties of biopolymeric chitosan–montmorillonite. Prog Nat Sci Mat Int 22(5):502–508
63. Lewandowska K, Sionkowska A, Kaczmarek B, Furtos G (2014) Characterization of chitosan composites with various clays. Int J Biol Macromol 65:534–541
64. Li B, Huang L, Wang X, Ma J, Xie F (2011) Biodegradation and compressive strength of phosphorylated chitosan/chitosan/hydroxyapatite bio-composites. Mater Des 32:4543–4547
65. Lim ST, Martin GP, Berry DJ, Brown MB (2000) Preparation and evaluation of the in vitro drug release properties and mucoadhesion of novel microspheres of hyaluronic acid and chitosan. J Control Release 66:281–292
66. Lin KF, Hsu CY, Huang TS, Chiu WY, Lee YH, Young TH (2005) A novel method to prepare chitosan/montmorillonite nanocomposites. J Appl Polym Sci 98:2042–2047

67. Lindblad MS, Liu Y, Albertsson AC, Ranucci E, Karlsson S (2002) Polymer from renewable resources. Adv Polym Sci 157:139–161
68. Liu B, Shen S, Luo J, Wang X, Sun R (2013) One-pot green synthesis and antimicrobial activity of exfoliated Ag NP-loaded quaternized chitosan/clay nanocomposites. RSC Adv 3:9714–9722
69. Liu B, Wang X, Pang C, Luo J, LuoY Sun R (2013) Preparation and antimicrobial property of chitosan oligosaccharide derivative/rectorite nanocomposite. Carbohydr Polym 92:1078–1085
70. Liu H, Du Y, Wang X, Sun L (2004) Chitosan kills bacteria through cell membrane damage. Int J Food Microbiol 95:147–155
71. Monvisade P, Siriphannon P (2009) Chitosan intercalated montmorillonite: preparation, characterization and cationic dye adsorption. Appl Clay Sci 42:427–431
72. Mourya VK, Inamdar NN (2008) Chitosan-modifications and applications: opportunities galore. React Funct Polym 68:1013–1051
73. Muzzarelli RAA (2011) Chitosan composites with inorganics, morphogenetic proteins and stem cells, for bone regeneration. Carbohydr Polym 83:1433–1445
74. Muzzarelli RAA, Muzzarelli C (2002) Natural and artificial chitosan-inorganic composites. J Inorg Biochem 92:89–94
75. Naseri N, Algan C, Jacobs V, John M, Oksman K, Mathew AP (2014) Electrospun chitosan-based nanocomposite mats reinforced with chitin nanocrystals for wound dressing. Carbohydr Polym 109:7–15
76. Nesic AR, Velickovic SJ, Antonovic DG (2012) Characterization of chitosan/montmorillonite membranes as adsorbents for Bezactiv Orange V-3R dye. J Hazard Mater 209–210:256–263
77. Neus Angles M, Dufresne A (2000) Plasticized Starch/tunicin whiskers nanocomposites. 1. structural analysis. Macromolecules 33:8344–8353
78. Oguzlu H, Tihminlioglu F (2010) Preparation and barrier properties of chitosan-layered silicate nanocomposite films. Macromol Symp 298:91–98
79. Ojijo V, Sinha Ray S (2013) Processing strategies in bionanocomposites. Prog Polym Sci 38:1543–1589
80. Okamoto M (2003) Polymer/Layered silicate nanocomposites. Rapra Review Reports 14:3–5
81. Părpăriţă E, Cheaburu CN, Paţachia SF, Vasile C, (2014) Polyvinyl alcohol/chitosan/montmorillonite nanocomposites preparation by freeze/thaw cycles and characterization, Acta Chemica Iasi: 22:75–96.
82. Pavlidou S, Papaspyrides CD (2008) A review on polymer-layered silicate nanocomposites. Prog Polym Sci 33:1119–1198
83. Pillai CKS, Paul W, Sharma CP (2009) Chitin and chitosan polymers: chemistrychemistry, solubility and fiber formation. Prog Polym Sci 34:641–678
84. Potarniche CG, Vuluga Z, Donescu D, Christiansen J de C, Eugeniu V, Radovici C, Serban S, Ghiurea M, Somoghi R, Beckmann S (2012) Morphology study of layered silicate/chitosan nanohybrids. Surf Interface Anal 44(2):200–207
85. Prashanth KVH, Tharanathan RN (2007) Chitin/chitosan: modifications and their unlimited application potential—an overview. Trends Food Sci Technol 18:117–131
86. Quijada-Garrido I, Iglesias-Gonzalez V, Mazon-Arechederra JM, Barrales-Rienda JM (2007) The role played by the interactions of small molecules with chitosan and their transition temperatures. Glass-forming liquids:1,2,3-Propantriol (glycerol). Carbohydr Polym 68:173–186
87. Rajan M, Raj V, Al-Arfaj AA, Murugan AM (2013) Hyaluronidase enzyme core-5-fluorouracil-loaded chitosan-PEG-gelatin polymer nanocomposites as targeted and controlled drug delivery vehicles. Int J Pharm 453:514–522
88. Ray SS, Okamoto M (2003) Polymer/layered silicate nanocomposites: a review from preparation to processing. Prog Polym Sci 28:3–1641
89. Reddy CSK, Ghai R, Rashmi Kalia VC (2003) Polyhydroxyalkanoates: an overview. Bioresour Technol 87:137–146

90. Redl A, Morel MH, Bonicel J, Vergnes B, Guilbert S (1999) Extrusion of wheat gluten plasticized with glycerol: influence of process conditions on flow behavior, rheological properties, and molecular size distribution. Cereal Chem 76:361–370
91. Rhim JW, Hong SI, Park HM, Ng PKW (2006) Preparation and characterization of chitosan-based nanocomposite films with antimicrobial activity. J Agric Food Chem 54:5814–5822
92. Rhim JW, Ng PK (2007) Natural biopolymer-based nanocomposite films for packaging applications. Crit Rev Food Sci Nutr 47:411–433
93. Rhim JW, Park HM, Ha CS (2013) Bio-nanocomposites for food packaging applications. Prog Polym Sci 38:1629–1652
94. Rinaudo M (2006) Chitin and chitosan: properties and applications. Prog Polym Sci 31:603–632
95. Rinaudo M (2008) Main properties and current applications of some polysaccharides as biomaterials. Polym Int 57:397–430
96. Rinaudo M, Pavlov G, Desbrieres J (1999) Influence of acetic acid concentration on the solubilization of chitosan. Polymer 40:7029–7032
97. Rinaudo M, Pavlov G, Desbrieres J (1999) Solubilization of chitosan in strong acid medium. Int J Polym Anal Charact 5:267–276
98. Rindusit S, Jingjid S, Damrongsappul S, Tiptikaporn S, Tapeichi T (2008) Biodegradability and property characterizations of methyl methyl cellulosecellulose: effect of nanocompositing and chemical crosslinking. Carbohydr Polym 72:444–455
99. Roberts GAF (1992) Chitin chemistry. Macmillan, London
100. Rodríguez FJ, Galotto MJ, Guarda A, Bruna JE (2012) Modification of cellulose acetate films using nanofillers based on organoclays. J Food Eng 110:262–268
101. Romero RB, Leite CA, Gonçalves MC (2009) The effect of the solvent on the morphology of cellulose acetate/montmorillonite nanocomposites. Polymer 50:161–170
102. Sahiner N (2013) Soft and flexible hydrogel templates of different sizes and various functionalities for metal nanoparticle preparation and their use in catalysis. Prog Polym Sci 38:1329–1356
103. Sahoo D, Nayak PL (2012) Synthesis and characterization of chitosan/cloisite 30B film for controlled release of ofloxacin. J Appl Polym Sci 123:2588–2594
104. Sahoo D, Sahoo S, Mohanty P, Sasmal S, Nayak PL (2009) Chitosan: a new versatile bio-polymer for various applications. Des Monomers Polym 12:377–404
105. Salcedo I, Aguzzi C, Sandri G, Bonferoni MC, Mori M, Cerezo P, Sánchez R, Viseras C, Caramella C (2012) In vitro biocompatibility and mucoadhesion of montmorillonite chitosan nanocomposite: a new drug delivery. Appl Clay Sci 55:131–137
106. Salcedo I, Sandri G, Aguzzia C, Bonferoni C, Cerezoa P, Sánchez-Espejoc R, Viseras C (2014) Intestinal permeability of oxytetracycline from chitosan-montmorillonite nanocomposites. Colloids Surf B 117:441–448
107. Sinclair RG (1996) The case for polylactic acid as a commodity packaging plastic. J Macromol Sci Part A Pure Appl Chem 33:585–597
108. Singha J, Khanra P, Kuila T, Srivastava M, Das AK, Kim NH, Jung BJ, Kim DY, Lee SH, Lee DW, Kim D-G, Lee JH (2013) Preparation of sulfonated poly(ether–ether–ketone) functionalized ternary graphene/AuNPs/chitosan nanocomposite for efficient glucose biosensor. Process Biochem 48:1724–1735
109. Singha AS, Thakur VK (2009) Synthesis, characterisation and analysis of hibiscus sabdariffa fibre reinforced polymer matrix based composites. Polym Polym Compos 17:189–194
110. Singha AS, Thakur VK (2009) Grewia optiva fiber reinforced novel, low cost polymer composites. J Chem 6:71–76
111. Singha AS, Thakur VK (2009) Fabrication and characterization of S. cilliare fibre reinforced polymer composites. Bull Mater Sci 32:49–58
112. Singha AS, Thakur VK (2009) Fabrication and characterization of H. sabdariffa fiber-reinforced green polymer composites. Polym Plast Technol Eng 48:482–487
113. Singha AS, Thakur VK (2009) Physical, chemical and mechanical properties of hibiscus sabdariffa fiber/polymer composite. Int J Polym Mater 58:217–228

114. Sinha Ray S, Bousmina M (2005) Biodegradable polymers and their layered silicate nanocomposites: in greening the 21st century materials world. Prog Mater Sci 50:962–1079
115. Smolander M, Chaudhry Q (2010) Nanotechnologies in food packaging. In: Chaudhry Q, Castle L, Watkins R (eds) Nanotechnologies in Food. RSC Publishing, Cambridge
116. Sorrentino A, Gorrasi G, Vittoria V (2007) Potential perspectives of bionanocomposites for food packaging applications. Trends Food Sci Technol 18:84–95
117. Tan W, Zhang Y, Szeto Y-S, Liao L (2008) A novel method to prepare chitosan/montmorillonite nanocomposites in the presence of hydroxy-aluminum. Compos Sci Technol 68:2917–2921
118. Tang C, Chen N, Zhang Q, Wang K, Fu Q, Zhang X (2009) Preparation and properties of chitosan nanocomposites with nanofillers of different dimensions. Polym Degrad Stab 94:124–131
119. Thakur VK, Tan EJ, Lin M-F, Lee PS (2011) Polystyrene grafted polyvinylidenefluoride copolymers with high capacitive performance. Polym Chem 2:2000–2009
120. Thakur VK, Tan EJ, Lin M-F, Lee PS (2011) Poly(vinylidene fluoride)-graft-poly(2-hydroxyethyl methacrylate): a novel material for high energy density capacitors. J Mater Chem 21:3751–3759
121. Thakur VK, Lin M-F, Tan EJ, Lee PS (2012) Green aqueous modification of fluoropolymers for energy storage applications. J Mater Chem 22:5951–5959
122. Thakur VK, Ding G, Ma J et al (2012) Hybrid materials and polymer electrolytes for electrochromic device applications. Adv Mater 24:4071–4096
123. Thakur VK, Singha AS, Thakur MK (2012) In-air graft copolymerization of ethyl acrylate onto natural cellulosic polymers. Int J Polym Anal Charact 17:48–60
124. Thakur VK, Singha AS, Thakur MK (2012) Surface modification of natural polymers to impart low water absorbency. Int J Polym Anal Charact 17:133–143
125. Thakur VK, Yan J, Lin M-F et al (2012) Novel polymer nanocomposites from bioinspired green aqueous functionalization of BNNTs. Polym Chem 3:962–969
126. Thakur VK, Thakur MK, Gupta RK (2013) Development of functionalized cellulosic biopolymers by graft copolymerization. Int J Biol Macromol 62:44–51
127. Thakur VK, Thakur MK, Gupta RK (2013) Synthesis of lignocellulosic polymer with improved chemical resistance through free radical polymerization. Int J Biol Macromol 61:121–126
128. Thakur VK, Thakur MK, Gupta RK (2013) Rapid synthesis of graft copolymers from natural cellulose fibers. Carbohydr Polym 98:820–828
129. Thakur VK, Thakur MK, Gupta RK (2013) Graft copolymers from natural polymers using free radical polymerization. Int J Polym Anal Charact 18:495–503
130. Thakur VK, Thakur MK, Gupta RK (2013) Graft copolymers from cellulose: synthesis, characterization and evaluation. Carbohydr Polym 97:18–25
131. Thakur VK, Thakur MK (2014) Processing and characterization of natural cellulose fibers/thermoset polymer composites. Carbohydr Polym 109:102–117
132. Thakur VK, Thakur MK (2014) Recent trends in hydrogels based on psyllium polysaccharide: a review. J Cleaner Prod 82:1–15
133. Thakur VK, Thakur MK (2014) Recent advances in graft copolymerization and applications of chitosan: a review. ACS Sustain Chem Eng 2:2637–2652
134. Thakur VK, Thakur MK, Gupta RK (2014) Review: raw natural fiber–based polymer composites. Int J Polym Anal Charact 19(3):256–271
135. Thakur VK, Thakur MK, Raghavan P, Kessler MR (2014) Progress in green polymer composites from lignin for multifunctional applications: A review. ACS Sustain Chem Eng 2 (5):1072–1092
136. Toffey A, Samaranayake G, Frazier CE, Glasser WG (1996) Chitin derivatives. I. kinetics of the heat-induced conversion of chitosan to chitin. J Appl Polym Sci 60:75–85
137. Tsai GJ, Su WH, Chen HC, Pan CL (2002) Antimicrobial activity of shrimp chitin and chitosan from different treatments and applications of fish preservation. Fish Sci 68(1): 170–177

138. Tsuji H, Ikada Y (1998) Blends of aliphatic polyesters. II. Hydrolysis of solution-cast blends from poly(L-lactide) and poly (ε-caprolactone) in phosphate-buffered solution. J Appl Polym Sci 67:405–415
139. Vaia RA, Giannelis EP (1997) Lattice model of polymer melt intercalation in organically-modified layered silicates. Macromolecules 30:7990–7999
140. Vaia RA, Giannelis EP (1997) Polymer melt intercalation in organically modified layered silicates: model predictions and experiment. Macromolecules 30:8000–8009
141. Vaia RA, Jandt KD, Kramer EJ, Giannelis EP (1996) Microstructural evolution of melt intercalated polymer organically modified layered silicates nanocomposites. Chem Mater 8:2628–2635
142. Van Soest JJG, Benes K, De Wit D, Vliegenthart JFG (1996) The influence of starch molecular mass on the properties of extruded thermoplastic starch. Polymer 37:3543–3552
143. Vartiainen J, Tuominen M, Nattinen K (2010) Bio-hybrid nanocomposite coatings from sonicated chitosan and nanoclay. J Appl Polym Sci 116:3638–3647
144. Vasile C, Cheaburu CN (eds) (2010) Noi ambalaje polimerice pentru alimente. Editura PIM, Iaşi
145. Vasile C, Darie RN, Cheaburu-Yilmaz CN, Pricope GM, Bracic M, Pamfil D, Hitruc GE, Duraccio D (2013) Low density polyethylene—Chitosan chitosan composites. Compos Part B 55:314–323
146. Vasile C, Darie RN, Sdrobis A, Paslaru E, Pricope G, Baklavaridis A, Munteanu SB, Zuburtikudis I (2014) Effectiveness of chitosan as antimicrobial agent in LDPE/CS composite films as minced poultry meat packaging materials. Cellul Chem Technol 48: 325–336
147. Wan Ngah WS, Ariff NFM, Hanafiah MAKM (2010) Preparation, characterization, and environmental application of crosslinked chitosan-coated bentonite for tartrazine adsorption from aqeous solutions. Water Air Soil Pollut 206:225–236
148. Wan Ngah WS, Ariff NFM, Hashim A, Hanafiah MAKM (2010) Malachite green adsorption onto chitosan coated bentonite beads: isotherms, kinetics and mechanism. Clean Soil Air Water 38:394–400
149. Wan Ngah WS, Teong LC, Hanafiah MAKM (2011) Adsorption of dyes and heavy metal ions by chitosan composites: a review. Carbohydr Polym 83:1446–1456
150. Wang L, Wang A (2007) Adsorption characteristics of congo red onto the chitosan/ montmorillonite nanocomposite. J Hazard Mater 147:979–985
151. Wang L, Zhang J, Wang A (2008) Removal of methylene blue from aqueous solution using chitosan-g-poly(acrylic acid) / montmorillonite superadsorbent nanocomposite. Colloids Surf A 322:47–53
152. Wang S, Chen L, Tong Y (2006) Structure–property relationship in chitosan-based biopolymer/montmorillonite nanocomposites. J Polym Sci A Polym Chem 44:686–696
153. Wang SF, Shen S, Tong YJ, Chen L, Phang IY, Lim PQ, Liu TX (2005) Biopolymer chitosan/ montmorillonite nanocomposites: preparation and characterization. Polym Degrad Stab 90:123–131
154. Wang X, Du Y, Luo J (2008) Biopolymer/montmorillonite nanocomposite: preparation, drug-controlled release property and cytotoxicity. Nanotechnology 19:065707
155. Wang X, Du Y, Luo J, Lin B, Kennedy JF (2007) Chitosan/organic rectorite nanocomposite films: structure, characteristic and drug delivery behavior. Carbohydr Polym 69:41–49
156. Wang X, Du Y, Yang J, Wang X, Shi X, Hu Y (2006) Preparation, characterization and antimicrobial activity of chitosan/layered silicate nanocomposites. Polymer 47:6738–6744
157. Wang X, Yang L, Zhang J, Wang C, Li Q (2014) Preparation and characterization of chitosan–poly(vinyl alcohol)/bentonite nanocomposites for adsorption of Hg(II) ions. Chem Eng J 251:404–412
158. White EM, Yatvin J, Grubbs JB, Bilbrey JA, Locklin J (2013) Advances in smart materials: stimuli-responsive hydrogel thin films. J Polym Sci Part B Polym Phys 51:1084–1099
159. Wu FC, Tseng RL, Juang TS (2001) Enhanced abilities of highly swollen chitosan beads for color removal and tyrosinase immobilization. J Hazard Mater 81:167–177

160. Wu TM, Wu CY (2006) Biodegradable poly(lactic acid)/chitosan-modified montmorillonite nanocomposites: pand characterization. Polym Degrad Stab 91:2198–2204
161. Xie DF, Martino VP, Sangwan P, Way C, Cash GA, Pollet E, Dean KM, Halley PJ, Averous L (2013) Elaboration and properties of plasticised chitosan-based exfoliated nano-biocomposites. Polymer 54:3654–3662
162. Xu J, McCarthy SP, Gross RA, Kaplan DL (1996) Chitosan film acylation and effects on biodegradability. Macromolecules 29(10):3436–3440
163. Xu Y, Ren X, Hanna MA (2006) Chitosan/clay nanocomposite film preparation and characterization. J Appl Polym Sci 99:1684–1691
164. Yang D, Li J, Jiang Z, Lu L, Chen X (2009) Chitosan/TiO_2 nanocomposite pervaporation membranes for ethanol dehydration. Chem Eng Sci 64:3130–3137
165. Yang YQ, Chen HJ (2007) Study on the intercalation organic bentonite and its adsorption. J Xinyang Norm Univ 20:338–340
166. Yi H, Wu L-Q, Bentley WE, Ghodssi R, Rubloff GW, Culver JN (2005) Biofabrication with chitosan. Biomacromolecules 6:2881–2894
167. Yi H, Wu LQ, Bentley WE, Ghodssi R, Rubloff GW, Culver JN et al (2005) Biofabrication with chitosan. Biomacromolecules 6:2881–2894
168. Yoksan R, Chirachanchi S (2010) Silver nanoparticle-loaded chitosan–starch based films: fabrication and evaluation of tensile, barrier and antimicrobial properties. Mater Sci Eng C 30:891–897
169. Zhang AC, Sun LS, Xiang J, Hu S, Fu P, Su S et al (2009) Removal of elemental mercury from coal combustion flue gas by bentonite–chitosan and their modifier. J Fuel Chem Technol 37:489–495
170. Zhang Y, Huang X, Duan B, Wu L, Li S, Yuan X (2007) Preparation of elec-trospun chitosan/poly (vinyl alcohol) membranes. Colloid Polym Sci 285:855–863
171. Zheng JP, Wang CZ, Wang XX, Wang HY, Zhuang H, Yao KD (2007) Preparation of biomimetic three-dimensional gelatin/montmorillonite–chitosan scaffold for tissue engineering. React Funct Polym 67:780–788
172. Zhou N-L, Liu Y, Li L, Meng N, Huang Y-X, Zhang J, Wei S-H, Shen J (2007) A new nanocomposite biomedical material of polymer/Clay–Cts–Ag nanocomposites. Curr Appl Phys 7(S1):e58–e62
173. Zhou Y, Yang D, Chen X, Xu Q, Lu F, Nie J (2008) Electrospun water-soluble carboxyethyl chitosan/poly(vinyl alcohol) nanofibrous membrane as potential wound dressing for skin regeneration. Biomacromolecules 9:349–354
174. Zhu J, Wilkie CA (2007) Intercalation compounds and clay nanocomposites, hybrid materials: synthesis, characterization and applications. Wiley-VCH Verlag GmbH & Co, Weinheim
175. Zohuriaan-Mehr MJ (2005) Advances in chitin and chitosan modification through graft copolymerization: a comprehensive review. Iran Polym J 14:235–265
176. Zoldners J, Kiseleva T, Kaiminsh I (2005) Influence of ascorbic acid on the stability of chitosan solutions. Carbohydr Polym 60:215–218

Environmental Applications of Polypyrrole—and Polyaniline–Bacterial Extracellular Polysaccharide Nanocomposites

V. Janaki and S. Kamala-Kannan

Abstract Nanotechnology is the engineering and art of developing new materials on a nanoscale. Due to its unique properties, the application of nanoparticles in various scientific fields, including environmental sciences, has increased greatly—numerous nanomaterials have been used for the treatment of wastewaters too. However, easy escaping and ecological risk associated with the nanomaterials limited the application in industrial scale. Recently, there has been considerable interest in the synthesis of nanocomposites from different chemical and biological materials—an important area of nanocomposite research because of its wide application in environmental sciences. Polypyrrole–bacterial extracellular polysaccharides (PPy–EPS) and polyaniline–bacterial extracellular polysaccharides (Pn–EPS) are nanocomposites with chemical and biological polymers and are good adsorbents for the removal of reactive dyes and detoxification of Cr(VI) from wastewaters. This chapter compiles the application of PPy–EPS and Pn–EPS nanocomposites in wastewater treatment.

Keywords Chromium · Extracellular polysaccharide · Nanocomposite · Polyaniline · Polymers · Polypyrrole · Reactive dyes

V. Janaki (✉)
Department of Chemistry, Paavai Engineering College, 637 018 Namakkal, Tamil Nadu, India
e-mail: janu.venki@gmail.com

S. Kamala-Kannan
Division of Biotechnology, Advanced Institute of Environment and Bioscience, College of Environmental and Bioresource Sciences, Chonbuk National University, 570752 Iksan, South Korea
e-mail: kannan@jbnu.ac.kr

V.K. Thakur and M.K. Thakur (eds.), *Eco-friendly Polymer Nanocomposites*, Advanced Structured Materials 74, DOI 10.1007/978-81-322-2473-0_12

1 Introduction

Nanotechnology is a branch of applied science that focuses on the development and application of nanomaterials in different scientific fields, including environmental sciences [21, 22]. Nanoparticles were shown to have highly desirable physical, chemical, and biological properties largely due to their size (1–100 nm) and quantum effects [51, 53]. High surface area and ability to interact specifically with pollutants have potentially increased the application of nanoparticles in wastewater treatment. However, easy escaping of nanomaterials from fixed bed or any other flow-through columns, difficulties in separation and reuse of nanoparticles for several cycles, ecological risk associated with the escaped nanoparticles, and massive aggregation of certain group of nanoparticles have reduced their application on a large/industrial scale [53]. These drawbacks are overcome by preparing nanocomposites, multiphasic materials with one of the phases having one, two, or three dimensions less than 100 nm. Nanocomposites are touted to be the materials of the twenty-first century because of their uniqueness and vital characteristics.

Polymers are macromolecules composed of many small molecules called monomers. These monomers are polymerized using different polymerization techniques [38–40]. Today, different kinds of biological and chemical polymers are available for wide applications [1, 27, 41, 42, 45]. These polymers are modified using different techniques to obtain materials with desired properties for a number of applications [30–37]. Biological polymers have been widely investigated for the wastewater treatment because of eco-friendly nature, biodegradability, low cost, acceptable specific strength, and low density [5, 42]. The commonly used biological polymers include cellulose, chitosan, chitin, starch, and bacterial extracellular polysaccharides (EPS) [4, 16, 45, 50].

EPS is a biopolymer secreted by microorganisms during growth. It consists of large amounts of proteins, lipids, and carbohydrates and smaller quantities of humic substances, nucleic acids, and uronic acids [18, 28]. It plays a vital role in the adhesion of microorganisms onto substrates, aggregation of microbial cells on biofilms, stabilization of biofilms and flocs, retention of water, sorption of organic compounds, protecting microorganisms from harmful effects, quorum sensing, and aggregation of microbial cells in flocs [47]. It has been reported that EPS contain different functional groups such as carboxyl, amine, hydroxyl, and phosphoric, which lead to enhanced interaction with different group of pollutants [9, 50, 52]. Wang et al. [46] reported the adsorption of Cu^{2+} and Zn^{2+} onto EPS. EPS reduce the highly toxic Cr(VI) into less toxic Cr(III) [10]. Similarly, the presence of EPS significantly enhances the microbial reduction of Cr(VI) [6].

Polyaniline (Pn) and polypyrrole (PPy), π-conjugated semiconducting polymers, have been widely investigated for the removal of heavy metals and dyes from aqueous solution [2, 3]. In the last decades, there has been considerable interest in the synthesis of nanocomposite that comprises Pn or PPy and biological polymers. Lignosulfonate–PPy nanocomposite was used for adsorption of Ag(I) and Pb(II) ions from aqueous solutions. Maximum adsorption capacities of Ag(I) and Pb(II)

were up to 759.3 mg g^{-1} and 207.5 mg g^{-1}, respectively [20]. Pn/rice husk ash nanocomposite was used for the removal of Zn from aqueous solution. The adsorption capacity (q_{max}) for Zn ion in terms of monolayer adsorption was 24.3 mg g^{-1} [8]. Esfandian et al. [7] reported that Pn-sawdust nanocomposite removed 97 % of Cr(VI) from aqueous solution at pH 2. Similarly, Pn–cellulose nanocomposite decolorized 82 % of simulated reactive dye bath effluent [14]. α-cellulose-PPy composite successfully removed Reactive Red from aqueous solution [24]. Pn–chitosan composite removed 95.4 % of Congo Red, 98.2 % of Coomassie Brilliant Blue, and 99.8 % of Remazol Brilliant Blue R from aqueous solution [11]. Pn-starch nanocomposite decolourized 87 % of simulated reactive dye bath effluent [12].

Reactive dyes gained popularity in the twentieth century, and they represent the largest classes of dyes used in textile processing industries. Around 30 % of the total dye market took up reactive dyes due to their bright color, excellent color fastness, and ease of application [48]. The reactive systems of these dyes react with ionized hydroxyl groups on the cellulose fiber. However, hydroxyl ions present in the dye bath can compete with the cellulose substrate, resulting in a percentage of hydrolyzed dyes that can no longer react with the cellulose fiber. Thus, 10–50 % of the initial dye load will be present in the dye bath, giving rise to a highly colored effluent [12, 44]. Thus, disposal of dye effluent into the ecosystem leads to undesirable problems including aesthetic displeasing, decrease in soil quality, alter microbial activity in soil and water, reduce in photosynthetic rate of aquatic systems, and, in some cases, toxicity to aquatic organisms [25, 26]. Therefore, there is a considerable need to treat reactive dye effluents before discharging into receiving water bodies.

Heavy metal pollution has been considered as a major environmental problem worldwide. Mining and metallurgical and industrial activities are the major sources of heavy metal pollution in ecosystem. Chromium is the most common heavy metal pollutant in the environment because of its wide application in leather processing, tanning, pulp and paper, dyeing, pigmenting, and wood preserving industries [29]. It exists in the ecosystem in different states such as hexavalent (Cr(VI)) and trivalent (Cr(III)). Cr(VI) is highly soluble and mobile in aquatic systems when compared with Cr(III). Moreover, Cr(VI) is highly toxic and the International Agency for Research and Cancer declared Cr(VI) as class I carcinogen. Thus, the removal of Cr(VI) from contaminated water before it is discharged into the environment is important.

Recently, EPS was loaded onto Pn and PPy and used for the removal and detoxification of reactive dyes and Cr(VI) from aqueous solution [11–13, 15]. The basic principle behind the pollutant removal is based on the chelating properties ascribed from the amine and secondary amino groups on the polyaniline/bacterial extracellular polysaccharide (Pn/EPS) and polypyrrole/bacterial extracellular polysaccharide (PPy/EPS) nanocomposites (Fig. 1). This chapter provides insight into the synthesis and unique properties of Pn–EPS and PPy–EPS nanocomposites, and their application in the removal of reactive dyes and chromium.

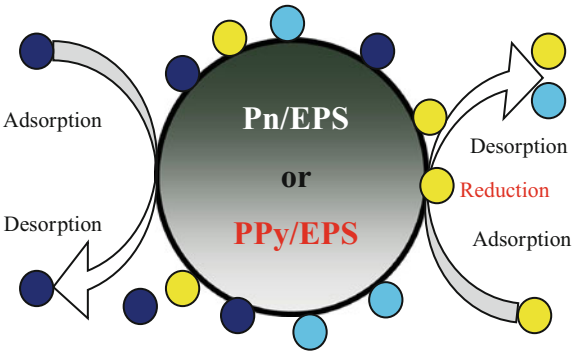

Fig. 1 Schematic representation for removal and detoxification of reactive dyes and Cr(VI) by Pn/EPS and PPy/EPS nanocomposites

2 Synthesis and Properties of Pn–EPS and PPy–EPS Nanocomposites

2.1 Extraction of EPS

EPS extracted from the *Bacillus* sp. were used for the preparation of Pn–EPS and PPy–EPS nanocomposites. In brief, the bacteria were cultivated in Luria Bertani (LB) broth at 30 °C for 24 h. After incubation, the bacteria were separated by centrifugation (10,000 rpm for 10 min), and the EPS present in the culture filtrate were precipitated with six volumes of ethanol. The precipitated EPS were separated by centrifugation (12,000 rpm for 20 min), freeze-dried (−80 °C), and used for the preparation of the composites.

2.2 Pn–EPS Nanocomposite

Pn–EPS nanocomposite was synthesized by in vitro oxidative polymerization of aniline and it is reported by Janaki et al. [13]. Briefly, EPS was dissolved in sterile water and mixed with 0.01 M aniline monomer to form a homogenous solution. The polymerization of aniline was induced by adding the oxidant, ammonium peroxydisulfate. The molar ratio of oxidant to monomer was 1:2. After polymerization, the greenish black product was separated by centrifugation and washed several times with methanol and water until the solution became colorless. The precipitates were freeze-dried (−80 °C) and used for the treatment of simulated reactive effluent and detoxification of Cr (VI). The proposed polymerization of aniline with EPS is schematically represented in Fig. 2. Janaki et al. [15] reported the morphological characters of Pn–EPS nanocomposite. The size of the nanocomposite varied from 40 to 80 nm. The Pn–EPS nanocomposite was irregular in shape and mostly presented in aggregates. The surface of the nanocomposite was granular, providing a

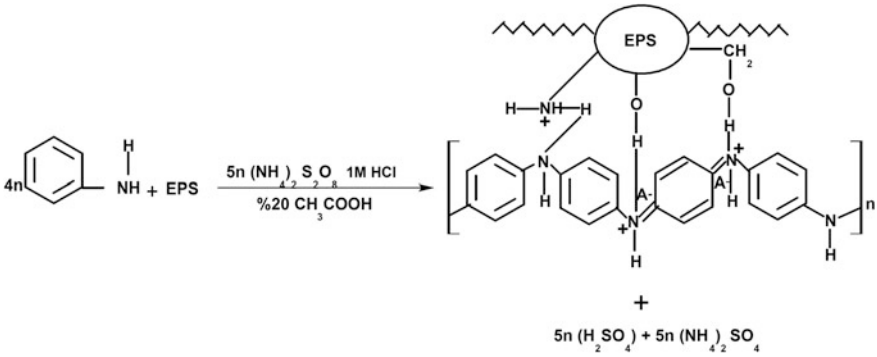

Fig. 2 Proposed polymerization of aniline with EPS (source [11–13])

good possibility for adsorbing different group of pollutants present in the aqueous solution.

Fourier transform infrared (FTIR) spectra and X-ray diffractogram of Pn–EPS nanocomposite are well reported by Janaki et al. [13, 15]. The FTIR spectrum indicates the presence of various functional groups in the nanocomposite. The O-H stretching vibration was reported between 3200–3231 cm^{-1}, and N-H stretching was reported at 2933, 2571, and 1560 cm^{-1}, respectively. The characteristic C-C aromatic stretching of benzenoid unit, exclusively expected for Pn, was reported at 1487 cm^{-1} [17]. In addition, alkane (743, 686, 593, and 504 cm^{-1}), aromatic (878 and 796 cm^{-1}), and carboxyl (1297, 1242, and 1138 cm^{-1}) groups were reported in the Pn–EPS nanocomposite. Some of these functional groups are preferentially reported for EPS extracted from other microorganisms [49]. Similarly, the X-ray diffractogram of the nanocomposite carries the peaks for both Pn and EPS. The polyaniline peaks were reported at $2\theta = 20.1$ and 26.2°, and EPS peaks are reported at 2θ = 6.0, 17.8, 30.4 and 40.8°. Also, based on the X-ray diffractograms, the nature of Pn–EPS nanocomposite was reported as partly amorphous and partly crystalline.

2.3 PPy–EPS Nanocomposite

PPy–EPS nanocomposite was also prepared by chemical oxidative polymerization of pyrrole. Briefly, oxidation in the reaction mixture (pyrrole (0.01 M) and EPS) was initiated by the addition of ammonium peroxydisulfate. The molar ratio of oxidant to monomer was 1:2. After polymerization, the blackish precipitate was separated by centrifugation and washed several times with methanol and water until the solution became colorless. The precipitates were freeze-dried (−80 °C) and used for the treatment of simulated reactive effluent and detoxification of Cr(VI). The proposed polymerization of pyrrole with EPS is schematically represented in Fig. 3.

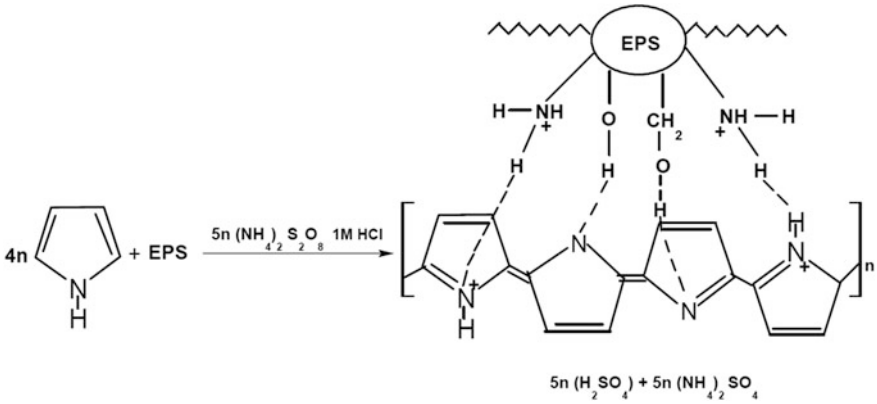

Fig. 3 Proposed polymerization of pyrrole with EPS

The size of the nanocomposite varied from 40 to 70 nm, irregular in shape, and mostly presented in aggregates. The surface of the PPy–EPS nanocomposite was rough, providing a possibility for trapping different groups of dyes and metals present in the aqueous solution.

Functional groups present in the PPy–EPS nanocomposite were reported based on the FTIR studies. The O-H stretching vibration of polymeric compounds was observed between 3400–3100 cm^{-1}, and C-N and C-C asymmetric and symmetric ring-stretching of PPy were observed at 1548 and 1463 cm^{-1} [19, 23]. The C-H stretching vibration of fatty acids and sugars was observed at 2934 cm^{-1}, and characteristic peaks of polymerized pyrrole were observed at 1302, 1048, 910, and 792 cm^{-1}. In addition, peaks for carboxyl and alkane groups, arising from the sugars and amino acids of EPS, were observed at 1165, 1045, 901, and 506 cm^{-1} [13]. X-ray diffractogram peak at $2\theta = 26°$ indicates the amorphous nature of the nanocomposite [43]. Moreover, a minor shift in XRD peak at $2\theta = 21.3°$ and a new peak at $2\theta = 28.3°$ in PPy–EPS indicates the successful integration of EPS during pyrrole polymerization.

3 Application of Pn–EPS and PPy–EPS Nanocomposites for the Treatment of Simulated Remazol Dye Effluent

Janaki et al. [13] reported the potential application of Pn–EPS composite for the removal of reactive dyes from simulated textile effluents; the composite removed 97 % of reactive dyes from simulated effluents at pH 3. Also, the study reported the influence of experimental variables (pH, contact time, and initial adsorbent dosage) on dye removal and possible mechanism of dye adsorption based on the isotherm and kinetic analysis. Pn–EPS nanocomposite at a dosage of 0.3 g L^{-1} effectively

removed the reactive dyes from the simulated effluent. A rapid removal of dyes was reported during the first 10 min, which gradually decreased with lapse of time, and reached equilibrium at 50 min. Similar to other variables, pH also highly influenced the dye removal rate. The study reported the maximum removal at pH 3 and minimum removal at pH 8. Higher decolorization at pH 3 was due to the protonation of functional groups in the Pn–EPS nanocomposite, which directly increases the electrostatic attraction between the Pn–EPS nanocomposite and the reactive dye molecules. The authors modeled the decolorization results with modified Freundlich model and reported high correlation coefficient (R^2 = 0.988), indicating the heterogeneous adsorption of reactive dyes onto the Pn–EPS nanocomposite. The kinetics of the simulated effluent followed pseudo first-order model (Q_e, k_1, and R^2 are as 0.3577 L/g, 0.0522 min^{-1}, and 0.9794, respectively); chemisorption being the rate controlling step.

PPy–EPS nanocomposite was also observed as an effective adsorbent for the removal of reactive dyes from simulated textile effluent. The PPy–EPS nanocomposite removed >90 % of reactive dyes from simulated effluent. Like Pn–EPS, the reactive dye removal rate in simulated effluent was highly influenced by initial adsorbent dosage, contact time, and pH. Maximum dye removal was observed at pH 3, and minimum removal at pH 8. The results of the biosorption isotherms of dye effluent were modeled using the modified Freundlich model. Very high correlation coefficient, R^2 = 0.9040, was obtained, indicating that the isotherm followed the Freundlich model. The K_F and n_F values were 2.6303 L g^{-1} and 0.0403, respectively. The kinetics of Remazol dye effluent followed pseudo first-order model. Values of Q_e, k_1, and R^2 were calculated as 2.1543 L g^{-1}, 0.0428 min^{-1}, and 0.9861, respectively. The correlation coefficient (R^2) was closer to unity, indicating the better fit of pseudo first-order kinetic model.

4 Application of Pn–EPS and PPy–EPS Nanocomposites for the Removal of Cr(VI) from Aqueous Solution

Janaki et al. [15] reported the Cr(VI) adsorption and detoxification potential of Pn–EPS nanocomposite. The study reported that the solution pH highly influence the adsorption rate of Cr(VI) onto Pn–EPS nanocomposite. Maximum Cr(VI) removal (65.1 %) was reported at pH 3, and minimum removal at pH 9. The protonation of amino group, at pH 3, enhances the electrostatic interaction between the constituent Pn–EPS nanocomposite and $HCrO_4^-$, a predominant form of Cr(VI) in acidic pH. The study also reported a rapid adsorption of Cr(VI) onto Pn–EPS nanocomposite during the first 10 min, which gradually decreased with lapse of time until it reached equilibrium (50 min). The rapid adsorption was due to the availability of more reactive sites. The authors modeled the removal rate with Langmuir, Freundlich, and Tempkin isotherm models and reported that Freundlich

model well described the adsorption equilibrium data with high correlation coeffecients ($R^2 > 0.9915$) than Langmuir and Freundlich models. The kinetics of Cr (VI) adsorption onto Pn–EPS nanocomposite followed pseudo first-order model, indicating that ionic interaction being the rate controlling step. The correlation coefficients were closer to 1, and the equilibrium adsorption capacity (Q_e) correlates well with the experimental (Q_e) values. Moreover, the study also reported that the adsorbed Cr(VI) was reduced into Cr(III). The Cr(VI) reduction was confirmed by XRD studies. Maximum detoxification was reported within 10 min, and gradually decreased with lapse of time. Similarly, PPy–EPS nanocomposite also detoxified Cr (VI) into less toxic Cr(III). The PPy–EPS nanocomposite reduced >80 % of Cr(VI) within 30 min. A rapid reduction of Cr(VI) was reported during the first 5 min, and gradually decreased with lapse of time. The rapid reduction during the initial time was due to availability of more reactive sites on the PPy–EPS nanocomposite.

5 Conclusion

Both Pn–EPS and PPy–EPS effectively removed reactive dyes and Cr(VI) from the aqueous solution, and both the composites reduced the highly toxic form of Cr(VI) into the less toxic Cr(III), suggesting that the composites could be effectively used as an adsorbent for the treatment of dyes and Cr-bearing industrial wastewaters. Research into the removal of dyes and heavy metals using Pn–EPS and PPy–EPS nanocomposites has provided greater understanding of the environmental applications of these nanocomposites. The reported results are completely based on in vitro studies and, thus, more remain to be learned from pilot scale studies. Moreover, some of the experimental variables altering the adsorption rate of pollutants need to be explained, such as salts in wastewater, presence of more than one type of pollutants in some industrial wastewaters, variation in the concentration of the pollutants, optimum physical conditions, and influence of temperature on pollutant removal. Answering these will help advance the application of these novel nanocomposites in wastewater treatment.

References

1. Ahmad R, Kumar R (2010) Conducting polyaniline/iron oxide composite: a novel adsorbent for the removal of amido black 10B. J Chem Eng Data 55:3489–3493
2. Ai L, Jiang J, Zhang R (2010) Uniform polyaniline microspheres: a novel adsorbent for dye removal from aqueous solution. Synthetic Met 160:762–767
3. Ayad MM, El-Nasr AA (2010) Adsorption of cationic dye (Methylene Blue) from water using polyaniline nanotubes base. J Phys Chem C 114:14377–14383
4. Cheng R, Xiang B, Li Y, Zhang M (2011) Application of dithiocarbamate modified starch for dyes removal from aqueous solutions. J Hazard Mater 188:254–260

5. Dobos AM, Stoica I, Olaru N, Olaru L, Ioanid EG, Ioan S (2012) Surface properties and biocompatibility of cellulose acetates. J Appl Polym Sci 125:2521–2528
6. Dogan NM, Kantar C, Gulcan S, Dodge CJ, Yilmaz BC, Mazmanci MA (2011) Chromium (VI) bioremoval by *Pseudomonas* bacteria: role of microbial exudates for natural attenuation and biotreatment of Cr(VI) contamination. Environ Sci Technol 45:2278–2285
7. Esfandian H, Jafari M, Alizadeh M, Rahmati HT, Katal R (2012) Synthesis of polyaniline nanocomposite and its application for chromium removal from aqueous solution. J Vinyl Addit Techn 18:250–260
8. Ghorbani M, Eisazadeh H, Ghoreyshi AA (2012) Removal of zinc ions from aqueous solution using polyaniline nanocomposite coated on rice husk. Iranica J Energy Environ 3:66–71
9. Gutnick DL, Bach H (2000) Engineering bacterial biopolymers for the biosorption of heavy metals; new products and novel formulations. Appl Microbiol Biotechnol 54:451–460
10. Harish R, Samuel J, Mishra R, Chandrasekaran N, Mukherjee A (2012) Bio-reduction of Cr (VI) by exopolysaccharides (EPS) from indigenous bacterial species of Sukinda chromite mine, India. Biodegradation 23:487–496
11. Janaki V, Oh BT, Shanthi K, Lee KJ, Ramasamy AK, Kamala-Kannan S (2012) Polyaniline/chitosan composite: an eco-friendly polymer for enhanced removal of dyes from aqueous solution. Synthetic Met 162:974–980
12. Janaki V, Vijayaraghavan K, Oh BT, Lee KJ, Muthuchelian K, Ramasamy AK, Kamala-Kannan S (2012) Starch/polyaniline nanocomposite for enhanced removal of reactive dyes from synthetic effluent. Carbohyd Polym 90:1437–1444
13. Janaki V, Oh BT, Vijayaraghavan K, Kim JW, Kim SA, Ramasamy AK, Kamala-Kannan S (2012) Application of bacterial extracellular polysaccharides/polyaniline composite for the treatment of remazol effluent. Carbohydr Polym 88:1002–1008
14. Janaki V, Vijayaraghavan K, Oh BT, Ramasamy AK, Kamala-Kannan S (2013) Synthesis, characterization and application of cellulose/polyaniline nanocomposite for the treatment of simulated textile effluent. Cellulose 20:1153–1166
15. Janaki V, Shin MN, Kim SH, Lee KJ, Cho M, Ramasamy AK, Oh BT, Kamala-Kannan S (2014) Application of polyaniline/bacterial extracellular polysaccharide nanocomposite for removal and detoxification of Cr(VI). Cellulose 24:463–472
16. Juang RS, Shao HJ (2002) A simple equilibrium model for sorption of heavy metal ions from aqueous solution on chitosan. Water Res 36:2999–3008
17. Karthikeyan M, Kumar KKS, Elango KP (2011) Batch sorption studies on the removal of fluoride ions from water using eco-friendly conducting polymer/biopolymer composites. Desalination 267:49–56
18. Liu H, Fang HP (2002) Characterization of electrostatic binding sites of extracellular polymers by linear programming analysis of titration data. Biotechnol Bioeng 80:806–811
19. Liu Y, Zhang Y, Ma G, Wang Z, Liu K, Liu H (2013) Ethylene glycol reduced graphene oxide/polypyrrole composite for supercapacitor. Electrochim Acta 88:519–525
20. Luo JJ, Lu QF (2014) Controllable preparation and heavy metal ion adsorption of lignosulfonate-polypyrrole composite nanosorbent. Polym Compos. doi:10.1002/pc.23062
21. Lin M-F, Thakur VK, Tan EJ, Lee PS (2011) Dopant induced hollow $BaTiO_3$ nanostructures for application in high performance capacitors. J Mater Chem 21:16500–16504
22. Lin M-F, Thakur VK, Tan EJ, Lee PS (2011) Surface functionalization of $BaTiO_3$ nanoparticles and improved electrical properties of $BaTiO_3$/polyvinylidene fluoride composite. RSC Adv 1:576–578
23. Naumann D, Helm D, Labischinski H (1991) Microbiological characterizations by FT-IR spectroscopy. Nature 351:81–82
24. Ovando-Medina VM, Vizcainoo-Mercado J, Gonzalez-Ortega O, Rodrıguez de la Garza JA, Martınez-Gutierrez H (2014) Synthesis of α-cellulose/polypyrrole composite for the removal of reactive red dye from aqueous solution: kinetics and equilibrium modeling. Polym Composite. doi:10.1002/pc.22945

25. Papic S, Koprivanac N, Bozic AL, Metes A (2004) Removal of some reactive dyes from synthetic wastewater by combined Al(III) coagulation/carbon adsorption process. Dyes Pigments 62:291–298
26. Robinson T, Chandran B, Nigam P (2002) Removal of dyes from a synthetic textile dye effluent by biosorption on apple pomace and wheat straw. Water Res 36:2824–2830
27. Salem MA (2010) The role of polyaniline salts in the removal of direct blue 78 from aqueous solution: a kinetic study. React Funct Polym 70:707–714
28. Sponza DT (2002) Extracellular polymer substances and physicochemical properties of flocs in steady and unsteady-state activated sludge systems. Process Biochem 37:983–998
29. Sukumar C, Janaki V, Kamala-Kannan S, Shanthi K (2014) Biosorption of chromium(VI) using *Bacillus subtilis* SS-1 isolated from soil samples of electroplating industry. Clean Technol Envir 16:405–413
30. Thakur VK, Tan EJ, Lin M-F, Lee PS (2011) Poly (vinylidene fluoride)-graft-poly (2-hydroxyethyl methacrylate): a novel material for high energy density capacitors. J Mater Chem 21:3751–3759
31. Thakur VK, Tan EJ, Lin M-F, Lee PS (2011) Polystyrene grafted polyvinylidenefluoride copolymers with high capacitive performance. Polym Chem 2:2000–2009
32. Thakur VK, Singha AS, Thakur MK (2012) Biopolymers based green composites: mechanical, thermal and physico-chemical characterization. J Polym Environ 20:412–421
33. Thakur VK, Singha AS, Thakur MK (2012) Graft copolymerization of methyl acrylate onto cellulosic biofibers: synthesis, characterization and applications. J Polym Environ 20:164–174
34. Thakur VK, Singha AS, Thakur MK (2012) Modification of natural biomass by graft copolymerization. Int J Polym Anal Charact 17:547–555
35. Thakur VK, Singha AS, Thakur MK (2012) Green composites from natural fibers: mechanical and chemical aging properties. Int J Polym Anal Charact 17:401–407
36. Thakur VK, Singha AS, Thakur MK (2012) In-Air graft copolymerization of ethyl acrylate onto natural cellulosic polymers. Int J Polym Anal Charact 17:48–60
37. Thakur VK, Singha AS, Thakur MK (2012) Surface modification of natural polymers to impart low water absorbency. Int J Polym Anal Charact 17:133–143
38. Thakur VK, Thakur MK (2014) Recent trends in hydrogels based on psyllium polysaccharide: a review. J Clean Prod 82:1–15
39. Thakur VK, Thakur MK (2014) Recent advances in graft copolymerization and applications of chitosan: a review. ACS Sustainable Chem Eng 2:2637–2652
40. Thakur VK, Thakur MK (2014) Processing and characterization of natural cellulose fibers/thermoset polymer composites. Carbohydr Polym 109:102–117
41. Thakur VK, Thakur MK, Raghavan P, Kessler MR (2014) Progress in green polymer composite from lignin for multifunctional applications: a review. ACS Sustainable Chem Eng 2:1072–1092
42. Thakur VK, Thakur MK, Gupta RK (2014) Review: Raw natural fiber-based polymer composites. Int J Polym Anal Charact 19:256–271
43. Vishnuvardhan T, Kulkarni V, Basavaraja C, Raghavendra S (2006) Synthesis, characterization and a.c. conductivity of polypyrrole/Y_2O_3 composites. Bull Mater Sci 29:77–83
44. Vijayaraghavan K, Won SW, Yun YS (2009) Treatment of complex Remazol dye effluent using sawdust- and coal-based activated carbons. J Hazard Mater 167:790–796
45. Wang L, Li J (2013) Adsorption of C.I. Reactive Red 228 dye from aqueous solution by modified cellulose from flax shive: kinetics, equilibrium, and thermodynamics. Ind Crop Prod 42:153–158
46. Wang J, Li Q, Li MM, Chen TH, Zhou YF, Yue ZB (2014) Competitive adsorption of heavy metal by extracellular polymeric substances (EPS) extracted from sulfate reducing bacteria. Bioresource Technol 163:374–376
47. Wingender J, Neu TR, Flemming HC (1999) Microbial extracellular polymeric substances: characterisation, structure and function. Springer, Berlin, p 123

48. Xing G, Liu S, Xu Q, Liu Q (2012) Preparation and adsorption behavior for Brilliant Blue X-BR of the cost-effective cationic starch intercalated clay composite matrix. Carbohydr Polym 87:1447–1452
49. Xu C, Zhang S, Chuang C, Miller EJ, Schwehr KA, Santschi PH (2011) Chemical composition and relative hydrophobicity of microbial exopolymeric substances (EPS) isolated by anion exchange chromatography and their actinide binding affinities. Mar Chem 126:27–36
50. Yin Y, Hu Y, Xiong F (2011) Sorption of Cu(II) and Cd(II) by extracellular polymeric substances (EPS) from *Aspergillus fumigatus*. Int Biodeterior Biodegrad 65:1012–1018
51. Zhang W (2003) Nanoscale iron particles for environmental remediation: an overview. J Nanopart Res 5:323–332
52. Zhang Z, Xia S, Wang X, Yang A, Xu B, Chen L, Zhu Z, Zhao J, Jaffrezic-Renault N, Leonard D (2009) A novel biosorbent for dye removal: Extracellular polymeric substance (EPS) of *Proteus mirabilis* TJ-1. J Hazard Mater 163:279–284
53. Zhao X, Lv L, Pan B, Zhang W, Zhang S, Zhang Q (2011) Polymer-supported nanocomposites for environmental application: a review. Chem Eng J 170:381–394

Synthesis, Chemistry, and Medical Application of Bacterial Cellulose Nanocomposites

Mazhar Ul-Islam, Shaukat Khan, Waleed Ahmad Khattak, Muhammad Wajid Ullah and Joong Kon Park

Abstract Bacterial cellulose (BC), an environmental friendly polymeric material, has recently received immense attention in the human society. Herein, we have focused on the biosynthesis, chemical structure, and physiological behavior of BC along with synthetic routes and medical applications of its nanocomposites. The structure of BC consists of nanofibrils made up of (1 → 4) β-glycosidic linked glucose units interconnected through intra- and intermolecular hydrogen bonds. The interconnected 3D network structure of BC nanofibers with a high degree of nanoporosity makes BC an ideal candidate for the incorporation of nanomaterials to form reinforced composites. BC nanocomposites have been synthesized through a number of routes that have not only improved the existing properties of BC, but also enhanced it with novel features. Among nanomaterials, metal, metal oxides, and organic nanomaterials have been effectively used to engender antimicrobial, biocompatible, conductive, and magnetic properties in BC. BC nanocomposites have been successfully employed in the medical field and have shown a high clinical value for wound healing and skin tissue repair. Recent interest has been focused on designing ideal biomedical devices like artificial skin and artificial blood vessels from BC. This study will provide an extensive background about the primary features of BC and discuss the synthetic routes and chemical feasibility of BC nanocomposites along with their current and future application in the medical field.

Keywords Bacterial cellulose · Biosynthesis · Composites · Synthetic approaches · Medical applications

M. Ul-Islam · S. Khan · W.A. Khattak · M.W. Ullah · J.K. Park (✉)
Department of Chemical Engineering, Kyungpook National University, Daegu 702–701, Korea
e-mail: parkjk@knu.ac.kr

M. Ul-Islam
Department of Chemical Engineering, College of Engineering, Dhofar University, Salalah 211, Oman

V.K. Thakur and M.K. Thakur (eds.), *Eco-friendly Polymer Nanocomposites*, Advanced Structured Materials 74, DOI 10.1007/978-81-322-2473-0_13

1 Introduction

Polymers and polymer-based materials have received immense interest in numerous field of life and have replaced synthetic materials [1]. These emerging materials are simplifying the human life and affecting all aspects of current development ranging from medical to defense fields [2–9]. Polymers-based materials are generally modified to meet the end-user applications [1, 10–14]. Polymers have been used in development of various materials including, plastic, elastomers, medical instruments, cosmetic products, paper making, etc. [8]. Among polymers, the biopolymers represent further advance and purified group that are renewable and environmental friendly materials [8]. The renewable biopolymers such as natural cellulose fibers, chitosan, and starch offer numerous advantages over the traditional synthetic materials regarding their biodegradability, eco-friendliness, cost effectiveness, purity, easy availability, low density, etc [15, 16]. For more advance and successful applications, these biopolymers have been combined with a number of metallic, nonmetallic, and synthetic materials in the form of composites [10]. To date, the most impressive applications of these biopolymers have been found in medical fields.

Bacterial cellulose (BC) is a biopolymer produced by different types of bacterial species of *Acetobacter genus* [17]. Since its discovery, it has received tremendous fame owing to its impressive physicomechanical properties [18]. Unlike plant cellulose, BC does not contain any impurities like lignin or hemicelluloses. This pure nature and better structural features like crystallinity, mechanical strength, etc. make BC much superior material than plan cellulose. Ultra-fine structural analysis studies reveal that BC consists of three-dimensional reticulated web-shaped networks of cellulose fibrils. These fibrils arrangement provide BC with porous geometry that is ultimately responsible for its wide-spread applications and composite developments. Its mechanical strength, thermal degradation temperature, crystallinity, and liquid-absorbing capabilities are very high, making it a valuable material for applications in the medical field and other disciplines [19, 20].

Regardless of all of these impressive features, pure BC comes through certain limitations that restrict its applications to some extent in several fields. BC is non-bactericidal in nature and hence cannot provide protection against the microbial invasion during its application as wound healing material. Further, its lower biocompatibility also affects the wound healing and tissue regeneration processes. Besides biological features, pure BC does not own conductive or magnetic properties that ultimately limit its applications in designing conductive and optoelectronic devices [21]. It is therefore important to investigate and develop some strategies that successfully incorporate these required important features in BC and extend its applications in medical, industrials, and other related fields.

Biopolymer composites synthesis technologies are currently in huge practice to improve the existing feature of polymers and bless them with new ones. Efforts are being made to prepare the biopolymers-based composites using more facile synthesis and techniques [22–24]. The physiological, chemical, and mechanical features of

various polymers have been improved in their composites [25]. Similarly, efforts have been made to overcome the limitations of BC by preparing its composites with bioactive materials, nanoparticles, and polymers [21, 26]. The production process (microbial fermentation during BC synthesis) and structural features (porous web-shaped structure) provide an ideal scenario for the synthesis of BC composites. A number of schemes have been introduced to synthesize BC composites with different materials. Among these schemes, the initial addition of materials to BC culture media (in situ addition), the treatment of BC with solutions and suspensions (ex situ addition), and the dissolution of BC in solvents with consequent blending are the most commonly used techniques [21]. It has been observed that BC composites have high levels of antibacterial, antifungal, antiviral, biocompatible, wound healing, conductive, magnetic, and optical properties [19, 27–29].

To date, BC composites have been synthesized with a variety of polymers and nanomaterials for specific applications. BC composites with chitosan (BC–Ch) were synthesized via in situ and ex situ addition strategies to enhance the physicochemical and biological features of BC [27, 30, 31]. These composites showed better impact in medical applications compared to pure BC. The conductive properties of BC were enhanced by synthesizing composites with graphene oxide (GO) and polyanaline (PAni) [29, 32]. Among nanomaterials, silver (Ag), gold (Au), zinc oxide (ZnO), palladium (Pd), carbon nanotubes (CNTs), iron oxide (FeO), platinum (Pt), and titanium oxide (TiO_2) have been utilized to enhance the antimicrobial, conductive, and magnetic properties of BC [21].

BC and BC composites have gained numerous applications in different fields. Among all, the most exciting applications are concerned with the medical field. Owing to its high mechanical properties and water-absorbing capabilities, BC has been used as dressing material in wound healing and tissue regeneration [19, 21]. The composites of BC enhanced its biological (bactericidal and biocompatible) properties and hence promoted its applicability in the medical field. Recent research work has been focused on developing artificial blood vessels and organs from BC composites [33, 34, 35]. Similarly, the inclusion of conductive materials in BC composites has led to the development of optoelectronic devices, displays, biosensors, and many advanced materials [18, 21, 26].

Herein, we discuss the synthetic pathways of BC, the chemical nature of BC, the efforts made to enable inexpensive and enhanced BC production, the need for developmental strategies to synthesize BC composites, the pros and cons of available composite synthesis strategies, and the applications of BC composites in the medical field and other related disciplines.

2 History of BC and BC Composites

Cellulose production from bacteria, specifically *Acetobacter xylinum,* was first reported by A.J. Brown in 1986 in the form of an extracellular gelatinous mat [36]. The material got fame by the name of “vinegar plant”. However, it did not receive

any serious attention until the twentieth century. Several decades after the discovery of microbial cellulose, C.A. Browne studied its production through the fermentation of Louisiana sugarcane juice, which attained a thickness of 25 mm under favorable conditions and thus affirmed the report of Browne [37]. Moreover, on removing the substance from the culture media, the cellulose took on a tough structure that was observed through its cross-section analysis. Its microscopic analysis showed that it contained living bacteria embedded in a structure less film [37]. Later studies have reported the production of BC by several other organisms, such as *Acetobacter pasteurianum*, *Acetobacter rancens*, *Sarcina ventriculi*, and *Bacterium xylinoides*. The first report on the production of bacterial cellulose was published by Tarr and Hibbert in 1931, who conducted a series of experiments to grow *A. xylinum* in culture media [38]. In the middle of the nineteenth century, Hestrin et al. [39] reported that glucose and oxygen were the principal requirements for BC synthesis. Colvin found that cellulose could also be produced by a cell-free extract obtained from *A. xylinum* once it was provided with glucose and ATP, an energy source [40]. This observation confirmed that BC synthesis was under the control of an enzymatic pathway.

Recent studies of bacterial cellulose have revealed several useful applications. Studies have also been focused on the controlled synthesis and characterization of BC, showing that the BC pellicle comprises a random assembly of microfibrils (2–4 nm in diameter) that result in a film or sheet upon drying [41]. Moreover, its crystallographic form is similar to that of plant cellulose, commonly known as "cellulose I," and its molecular orientation is similar to the direction of the cellulose chain axis [42].

BC encounters several problems if it is evaluated in its native form, such as the lack of antimicrobial activity and the absence of any protection against reactive oxygen species (ROS) during wound healing. In addition, pristine BC lacks optical transparency, electrical conductivity, magnetism, and hydrophobicity, and thus limiting its application in electrical devices, batteries, sensors, electromagnetic shielding, and electrochromic devices [29, 43]. These limitations necessitated the development of BC composite materials. To date, several composites of BC have been developed with various types of materials and evaluated for different useful applications. Several processing routes for the production of BC composites have been reported. Some have tried to disintegrate the cellulose network structure in order to blend it as a standard nanofibril. Others have reported routes that introduced a second phase during the development of BC networks. Touzel et al. developed a double-network gel of BC–pectin by adding pectin to the culture media [44]. Mormino et al. incorporated solid-reinforcing particles in the formation of a BC gel through a rotating disc bioreactor [45]. Recently, the introduction of starch in the BC network by modifying the BC culture media has been reported [46]. Various nano- and biomaterials have been incorporated in BC matrix through different methods for broad range of applications. Research is currently in progress to innovate new methods of synthesizing BC composites for the development of novel applications in different fields.

3 Synthesis of Bacterial Cellulose

BC is produced by specified classes of bacteria by utilizing various substrate sources that mainly contain glucose or fructose as a carbon source. The synthetic routes are comprised of a complex enzyme system that utilizes carbon and nitrogen sources through a series of metabolic reaction to produce BC. The details of BC synthetic mechanism have been described in coming topic. Along with utilizing synthetic culture media, BC has been produced from a diverse range of cheap waste media [47]. Among these, the most familiar are coconut media, pineapple media, beer wastes, agriculture wastes, and a number of fruit juices. The physiological appearance of the produced BC depends on the production methods. Currently, a number of methods have been introduced to enhance the production, productivity, and properties of BC. Some of the BC production approaches are described herein.

4 Development of Various Approaches for BC Production

A number of methods have been reported for the production of BC, including static culture [48, 49], agitating culture [50, 51], and the numerous designed bioreactors [52]. The BC production approaches were not merely based on cheap BC production but also on desired applications like medical and industrial, etc. To satisfy the commercial demand for BC, large-scale, semicontinuous, and continuous fermenters have been designed. The aim is to achieve maximum production of BC with suitable form and properties for the required application. Figure 1 outlines various strategies applied or the production of BC.

4.1 Static Cultures

Static cultivation is a simple method that is widely used for the production of cellulose pellicles. Shallow trays are filled with broth medium, inoculated, and incubated for 5–10 days until a thick cellulose sheet is produced on the surface of the medium. A gelatinous BC pellicle produced by *Gluconacetobacter xylinus* has a denser surface at the air interface. The BC production is directly related to the surface area of the air/liquid interface, provided that the depth is less than 4.5 cm [53]. The BC pellicle floats on the liquid surface due to the entrapped CO_2 generated from bacterial metabolism [54]. The BC pellicles produced through this strategy could be successfully applied in medical fields as dressing and healing material, etc. Furthermore, the thickness of the developed pellicles was easily controllable through variation of cultivation time. The low productivity and long cultivation time not only threatens the economic feasibility but also hinders the industrial application of the traditional static culture. Shezad et al. [49] proposed a

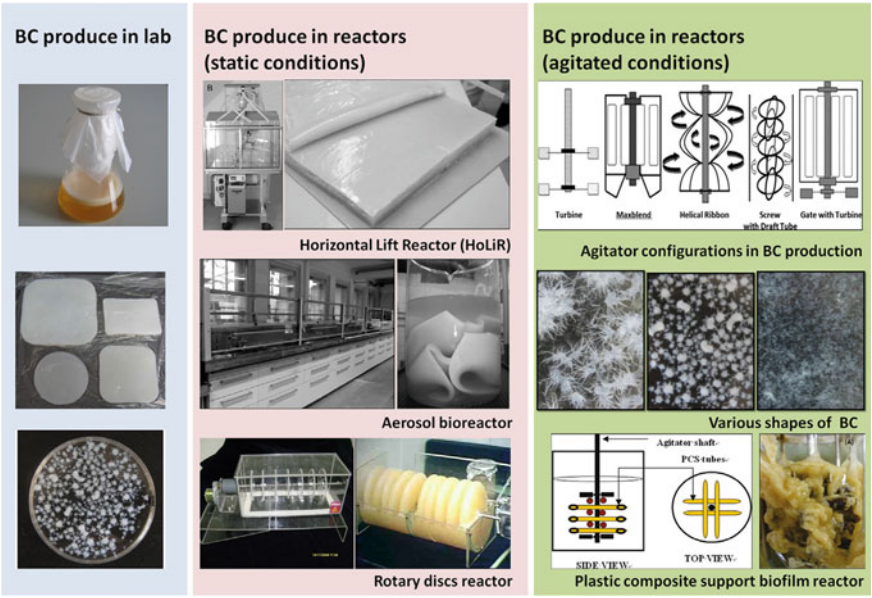

Fig. 1 BC production under static and agitated conditions. Various bioreactors for production under agitated conditions. Figure has been reproduced from [141] with permission from Elsevier

new simple fed-batch strategy for the static culture system to increase BC productivity, using waste from beer fermentation broth (WBFB) as a nutrient source. WBFB was found to be a better medium than the chemically defined medium (CDM) for BC production in a fed-batch process, and a two- to threefold increase in BC production was obtained compared with batch cultivation. The scanning electron micrographs revealed much denser and thinner BC fibrils cultivated with WBFB than those produced using CDM [55]. A novel bioreactor, named Horizontal Lift Reactor (HoLiR), having fleeces and foils of selectable length and adjustable height, was developed for the semicontinuous production of bacteria-produced nanocellulose (BNC) pellicles [48]. This method not only combined the advantages of static cultivation and continuous harvesting, but also significantly reduced cost compared to static cultivation.

4.2 Submerged (Agitated) Fermentation

Submerged fermentation is a convenient method for scale-up production of BC. Therein, BC is produced in environment where the constant rotation of culture media and cells make provide a homogenous contact resulting in better yield. The agitation method results in the production of BC pellets instead of pellicles (Fig. 1). *G. xylinus* JCM 9730 formed sphere-like BC particles under agitation cultures with

a rotational speed above 100 rpm [56]. When the structural properties were investigated with respect to agitation speed, it was found that spheres with diameters of 0.1–1 and 10 mm were produced at a rotational speed of 200 and 150 rpm, when cultured in a 250 and 150 mL Erlenmeyer flask, respectively, with 100 mL of medium. Field emission scanning electron microscopy (FE-SEM) analysis showed that cellulose spheres 200 rpm were hollow, while spheres produced at 150 rpm were solid.

The major problems associated in this technique are the insufficient oxygen supply, irregular shape of the produced BC, and the simultaneous accumulation of non-BC-producing mutants in agitation cultures [54, 57]. The overall yield of BC produced through agitation culture is much higher than the static cultures as observed in various studies. *G. xylinus* BPR2001 (ATCC® 700178) showed a 1.8-fold increase in BC productivity compared with the commonly used strain, *G. xylinus* (ATCC® 23769), cultivated under agitation [58]. Other strains, including *G. xylinus* BPR 3001A, *Gluconacetobacter hansenii* KCTC 10505BP, and *G. xylinus* NUST4.1, have also been successfully applied in the agitated fermentation method [55, 57, 59].

5 Various Bioreactors Designed for BC Production

Static and agitated culture methods have been applied for the production of BC. The static culture method suffers from low productivity due to long culture time and intensive man power. On the other hand, in the agitated cultures, the cellulose-producing strains are converted into cellulose-negative strains, which in turn take over the wild-type strain because of their rapid growth. This conversion reduces the production of BC [60]. In stirred tanks or airlift bioreactors, the produced BC adheres to the walls and upper parts of the reactors, creating problems and reducing BC production [61]. Therefore, it is necessary to design a bioreactor for BC production that will reduce culture time while improving production. Scientists have designed different bioreactors to optimize BC production.

5.1 Bioreactor with Spin Filters

A bioreactor with a spin filter was designed and tested for BC production [62]. The BC production was carried out in a bioreactor equipped with a six flat-blade turbine impeller and a spin filter surrounded by a stainless steel mesh whose bottom was attached to the agitator shaft. BC production of 4.57 g/L was achieved after 140 h of cultivation using *G. hansenii* PJK, which was 2.9 times higher than that obtained in a conventional jar fermenter [62].

5.2 Bioreactor with Silicone Membranes

Yoshino et al. designed a bioreactor in 1996 in which cellulose pellicles were formed on an oxygen-permeable synthetic membrane and on a liquid surface. The rate of BC production was doubled when the bottom end of the cylindrical vessel was covered with a silicone sheet of 100 mm in thickness. The rate of cellulose production depended strongly on the degree of roughness of the silicone membrane surface. The rate of BC production on a smooth silicone membrane was five times higher than that on a rough one [63].

5.3 Airlift Bioreactor

Airlift bioreactor is another important technique for improved BC production, which requires a lower power supply compared with the agitated bioreactor. The first airlift bioreactor for BC production was implemented in 1997 [64]. Air or oxygen-enriched air was supplied from the bottom of the reactor, which in turn drove the circulation of the culture media. Later, different modifications in the airlift bioreactor have been applied to enhance BC production. BC production of 3.8 g/L was obtained after 67 h of fermentation when a 50 L internal-loop airlift reactor was employed [65]. A modified airlift reactor, equipped with three wire-mesh draft tubes, yielded 7.7 g/L BC after 72 h of fermentation [66]. The highest BC production obtained to date through airlift bioreactor is 10.4 g/L with a production rate of 0.22 g/L/h [67].

5.4 Rotating Disk Bioreactor

Homogeneity is difficult to achieve in the agitation and airlift bioreactors because of the adhesion of produced BC to the different parts of the reactors. The produced BC pellets also face the limitation of having low mechanical strength compared to pellicles, restricting their practical applications. The first rotating disk bioreactor reported for BC production was comprised of an inlet for inoculation and several circular disks accumulated on a rotating central shaft [68]. During BC production, half of the area of the rotating disk was inside the medium while the other half was exposed to air. During rotation, the disk surface alternatively shifts between the medium and the atmosphere. Thus, the BC produced in this way is not only aerated but also gains its mechanical strength from being attached to the disk. BC composites were prepared by adding solid particles into the medium. It was found that the incorporation of solid particles into the BC was related to their concentration and the disk rotation speed [68]. BC composites have been produced using rotating disk bioreactors with plastic matrices for enhanced cell adhesion and paper fiber for improved mechanical properties [45, 69].

5.5 Cell Immobilization and Biofilm Reactors

Novel techniques such as immobilized-cell reactors, cell recycle reactors, and hollow fiber reactors are applied for improved BC production. A biofilm reactor is a type of immobilized-cell reactor that is efficient in cost reduction due to its consumption of high biomass density and production yield. BC production has been reported using a plastic composite support (PCS) biofilm reactor yielding 7.05 g/L BC, a 2.5-fold increase from the control [70]. An important aspect of this technique was the much improved mechanical properties of produced BC that can effectively lead toward enhanced applications in medical and other related fields.

6 BC Synthetic Pathway

Biosynthesis of BC is a precise, enzyme-regulated process involving a large number of specific enzymes and regulatory proteins. Though the mechanism of glucose polymerization into cellulose chains is still not completely known, the mechanism of uridine diphosphoglucose (UDPGlc) synthesis has been relatively well explained. Cellulose biosynthesis involves the production of UDPGlc, a precursor in cellulose synthesis, followed by polymerization of glucose units forming a β-1 → 4 glucan chain. The individual cellulose chains extrude outside the cell, resulting in a ribbon-like structure composed of hundreds and thousands of individual chains. In turn, the self-assembly of these ribbons leads to the formation of fibrils [71]. Cellulose biosynthesis in bacteria is associated with catabolic processes and does not interfere with other anabolic processes, including protein synthesis. *A. xylinum* follows either the pentose phosphate cycle or the Krebs cycle coupled with gluconeogenesis for cellulose synthesis [72, 73].

A. xylinum can convert hexoses, glycerol, dihydroxyacetone, pyruvate, and dicarboxylic acids into cellulose with almost 50 % efficiency. Pyruvate and dicarboxylic acids enter the Krebs cycle and undergo a conversion to hexoses via gluconeogenesis, similar to glycerol, dihydroxyacetone, and intermediates of the pentose phosphate cycle (Fig. 2). The direct cellulose precursor is UDPGlc, involving the glucokinase-catalyzed phosphorylation of glucose to glucose-6-phosphate (Glc-6-P). Isomerization of Glc-6-P leads to Glc-α-1-P, catalyzed by phosphoglucomutase, and conversion of Glc-a-1-P to UDPGlc is mediated by UDPGlc pyrophosphorylase. This enzyme is crucial for cellulose synthesis as the cellulose-negative species (Cel^{-}) are deficient in this enzyme [74]. The pyrophosphorylase activity varies among different strains of *A. xylinum* and the highest activity has been reported in the most effective cellulose producer, *A. xylinum* ssp. *sucrofermentans* BPR2001 [71].

Cellulose biosynthesis in bacteria is catalyzed by UDPGlc-forming cellulose synthase. It is a typical membrane-anchored protein tightly bound to the cytoplasmic membrane with a molecular mass of 400–500 kDa. The cellulose synthase

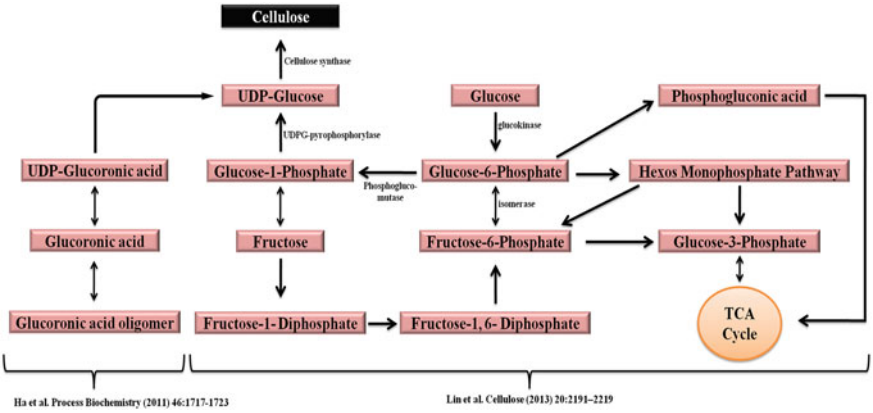

Fig. 2 BC synthetic pathway. The figure was modified from Lin et al. [100] and Shah et al. [21]

contains certain amino acids and other glycosyltranferases in the globular region, which is predicted to be cytoplasmic based on the analysis of the transmembrane segments and the presence of UDPGlc in the cytosol [75]. Cellulose biosynthesis by the UDPGlc-forming cellulose synthase is essentially a processing of 4-b-glucosyl transferase, as it transforms glucopyranose residues from UDPGlc into the newly founded polysaccharide chain. Oligomeric cellulose synthase complexes, often called terminal complexes, are responsible for β-1 → 4 glucan chain synthesis.

7 Self-Assembly and Crystallization of Cellulose Chains

The unique structural, physical, and mechanical properties of cellulose result from the extrusion and self-assembly of chains outside the cells. The cellulose export compounds or nozzles are responsible for the extrusion of the synthesized cellulose molecules out of the cells, forming protofibrils of approximately 2–4 nm in diameter. The protofibrils are in turn bundled into ribbon-shaped microfibrils of approximately 80 × 4 nm in size [76]. The formation of protofibrils and their assembly into ribbons and cellulose network structures are shown in Fig. 3.

Electron micrographs of the cell envelope have shown 50–80 pore-like sites arranged along the long axis of the cell and in combination with the extracellular cellulosic ribbon [77, 78]. These discrete pores are assumed to be the sites for the extrusion of pre-cellulosic polymer chains. Therefore, the initial assembly of cellulose comprises aggregates of β-1 → 4 glucan chains [79]. The existence of such aggregates suggests that the simultaneous synthesis of many β-1 → 4 glucan chains is a common feature of the assembly of cellulose microfibrils in both higher and

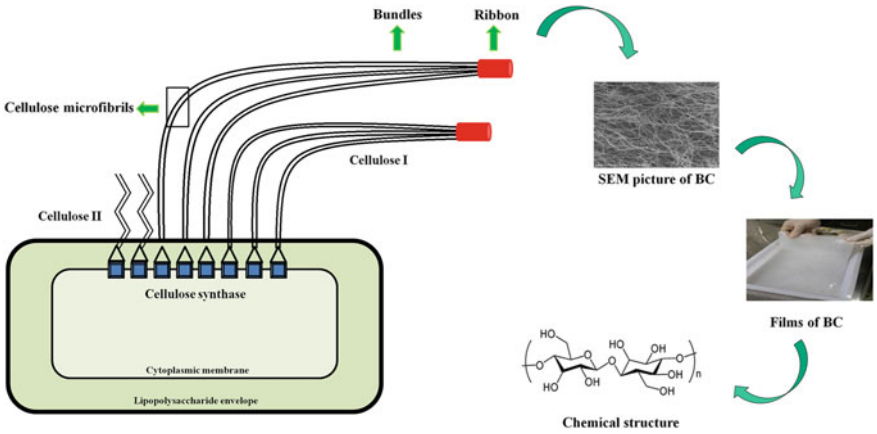

Fig. 3 Synthetic route, SEM image, films morphology, and chemical structure of bacterial cellulose

lower organisms [80]. As the mutual orientation and association of glucan chains, aggregates, microfibrils, bundles, and ribbons are governed by the original pattern of extrusion sites, the process of assembly and crystallization of cellulose is described as cell-directed [72].

A. xylinum produces cellulose in two distinctive physical forms: (i) the ribbon-like cellulose I, and (ii) a thermodynamically more stable amorphous form, cellulose II [81]. The β-1 → 4 glucan chains of cellulose I are aligned in parallel and arranged uniaxially whereas those of cellulose II are arranged in a random manner. Microfibrillar arrangements of BC and its pure nature compared with plant cellulose are responsible for most of its distinguishing properties, such as high tensile strength, high crystallinity, high water-holding capacity, etc.

8 Chemical Structure of BC

Cellulose is a homopolymer consisting of glucose molecules bonded through β-1 → 4 glycosidic linkages. The polymer unit consists of two glucose molecules bonded to each other in such a way that one molecule is rotated 180° with respect to the other (Fig. 3).

The chemical structure of BC is not different from plant cellulose. However, the degree of polymerization of plant cellulose is 13,000–14,000 while that of BC is 2000–6000 [82]. The repeated glucose units in BC produce a long unbranched polymer chain while the polymer chains form strong intermolecular hydrogen bonds. Cellulose from *A. xylinum* consists of microfibril ribbons, which are 3–4 nm thick and 70–80 nm wide. Hydrophobic interactions seem to be involved in

maintaining the shape of the BC sheet. The BC sheet is formed through the inter- and intrachain hydrogen bonds, whereas the crystalline structure of BC results from the hydrogen bonds between cellulose sheets [71].

Fourier transform infrared spectroscopy (FTIR) and nuclear magnetic resonance (NMR) have been utilized to study the structural differences between BC produced by stationary and agitated cultures [83, 84]. X-ray diffraction analysis has shown two distinct crystalline forms of cellulose as cellulose I and cellulose II [85]. Scanning electron microscopy (SEM) observation revealed a significant difference in the morphology of the BC surface and cross section. The surface showed irregular arrangements of fibers while the cross section showed layers of clustered fibers [86]. CP/MAS 13C NMR spectroscopy, wide-angle X-ray diffractometry, and transmission electron microscopy (TEM) were used to study the solid-phase nitration and acetylation of BC. The relative reactivity of OH groups in BC was found to be in the order of 6′OH > 2′OH > 3′OH. At lower concentrations of nitric acid in the reaction medium, the 6′OH groups were subjected to nitration, both in the crystalline and amorphous phases. However, at high concentrations, all OH groups were subjected to nitration. No regioselective reactivity was observed among the OH groups during solid-phase acetylation. This result shows that the reaction proceeds in a very thin layer between the acetylated and nonacetylated regions in the microfibrils [87].

9 BC Composites

The exciting structural and physiological features of BC have inspired its applications in a number of fields including food, textiles, paper, and electronics [17, 18, 43, 88]. Currently, the most important applications of BC are presented in the medical field, where BC has been incorporated in wound healing materials, artificial skin, scaffolds for tissue engineering, and artificial blood vessels [35, 89–92]. BC has been proposed as a potential material for preparing environmentally compatible ion-exchange membranes for fuel cells, biocompatible sensors, and actuators [17, 21, 93].

Despite its valuable features, pure BC has certain limitations that have restricted its application to some extent. For example, BC has no antimicrobial properties to prevent wound infection during its application as a dressing material [94]. Moreover, it lacks antioxidant properties and cannot provide protection against reactive oxygen species during wound healing. All these limitations reduce the wide-spread applicability of BC in medical fields. Pure BC does not possess properties like optical transparency, electrical conductivity, magnetism, and hydrophobicity, and hence cannot be utilized directly in electrical devices, batteries, sensors, electromagnetic shielding, and electrochromic devices [21, 29, 43].

10 Necessity of BC Composites

The above-mentioned deficiencies limit the application of BC. This situation demands the combination of BC with certain materials that can withstand the shortcomings of pure BC and extend the applicability of BC. The structural features, specifically the fibril arrangement, provide an excellent scenario for the use of BC in the synthesis of various composites. In fact, BC can be used as both a matrix and a reinforcement material for composite design [21, 27, 95, 96]. A number of BC composites have already been produced to overcome the inadequacies and enhance the physiological, biological, chemical, and mechanical features of BC [19, 20, 27–29, 43, 96–98]. Some of the BC composites, representing various combinations of materials, and their applications are described in Table 1.

It is observed that BC composites have been synthesized through a number of synthetic strategies. All composites bestowed BC with additional properties when compared with pristine BC. It is evident that the combination of nanomaterials (Ag, Au, ZnO, etc.) and polymers (chitosan, PAni, PEG, etc.) has helped in the synthesis of bactericidal and conductive BC [21]. The table is merely a presentation of the huge number of BC composites that have been synthesized to date. Recent advancements show the synthesis of BC composites for fabricating display devices, fuel cells, artificial organs, and more [21]. Comprehensive efforts are still required in order to develop new routes of composite synthesis and to explore new applications of BC in miscellaneous fields.

11 Synthetic Approaches for BC Composites

Polymer composites are usually synthesized through a number of synthetic strategies. The use of a particular strategy is mainly specified by the nature of the matrix and the reinforcement materials as well as the intended application [21]. The production route and structural features of BC provide the possibility to develop a variety of synthetic methods for preparing BC composite. Generally, polymeric composites are synthesized through three basic approaches: (a) adding the reinforcement materials to the polymer during its biosynthesis, (b) injecting the reinforcement materials inside the synthesized polymer matrix, and (c) blending the polymer solution with the reinforcement materials [21]. Being a typical biopolymer, BC composites are synthesized through all three aforementioned approaches. Herein, these approaches are described with specific examples. Figure 4a–c represents various approaches developed for the BC composites, while the mechanism of composite structure has been shown in Fig. 4d.

Table 1 Various BC composite materials showing the synthetic strategy, composites type, improved properties, and concerned applications (Reproduced from [141], with permission from Elsevier)

Reinforcement material	Synthetic approach	Composite type	Improved properties	Applications	Reference
Chitosan	Ex situ solution penetration	Polymer-polymer	Physical, mechanical antifungal	Biomedical, industrial	[27]
Gelatin			Physical, mechanical	Biomedical	[108]
Poly aniline			Conducting, medicinal	Electronic devices, biomedical	[29]
Polyethylene glycol			Thermal stability, biocompatibility	Biomedical	[154]
Graphine oxide (GO)			Thermal, mechanical, conducting properties	Electronic devices, industrial	[32]
Collagen	Insitu addition		Tissue engineering scaffold	Biomedical	[155]
Aloe vera gel			Mechanical, physical	Biomedical, Industrial	[28]
Montmorrilonite	Exsitu particle penetration	Polymer-particle	Physical, mechanical, antibacterial, thermal	Biomedical, industrial	[19, 20]
Silver nanoparticle			Antibacterial activities	Biomedical	[105]
Palladium			Conducting	Sensors, electronic	[43]
Gold nanoparticle			Optical, photocatalysis, biosensing	Biosensors, optical devices	[156, 157]
Hydroxy apatite			Biocompatible	Biomedical	[107]
Carbon nanotubes	Exsitu particle penetration/ Insitu addition		Mechanical, conducting	Electronic devices	[50], [111]
Silica			Mechanical properties	Industrial	[103]
Inorganic particles	Insitu addition		Mechanical properties	Industrial	[68]

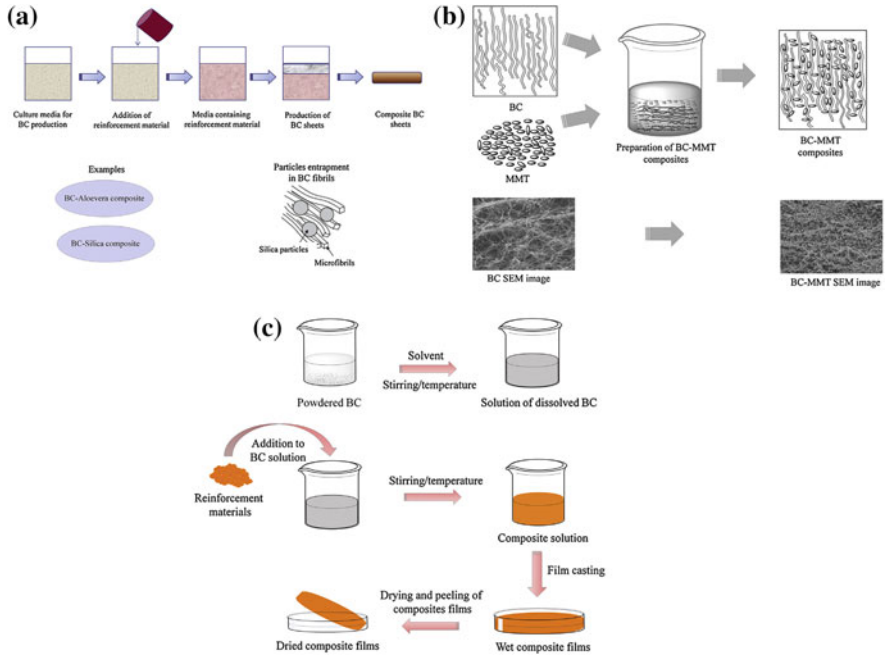

Fig. 4 **a** Schematic representation of BC composites synthesized through an in situ synthetic strategy. **b** Schematic representation of BC composites synthesized through an ex situ synthetic strategy. **c** Schematic representation of BC composites synthesized from dissolved BC solutions through casting approach. The figure is reproduced from [21] with permission from Elsevier. **d** Mechanism of BC composite structure synthesized with nanoparticles and polymers

11.1 In Situ BC Composite Synthesis

The in situ materials addition technique is the most common approach used for the synthesis of BC composites. The technique is principally based on the initial addition of the reinforcement materials to the BC culture media. As explained in the BC synthetic mechanism, the fibrils of BC aggregate to produce a dense fibril structure that ultimately produce a web shape. The reinforcement materials contained in the BC culture media can easily penetrate and accommodate in the fibril network. These added materials either bind through chemical bonding or establish physical interaction with BC fibrils, and consequently result in the synthesis of BC composites [96–99]. It is important to mention that these added materials influence both the production and properties of BC. These materials remain partly or completely attached to BC after cultivation and processing. The overall mechanism for the synthesis of such types of BC composites is illustrated in Fig. 4a.

The strategy of adding materials in situ has been widely utilized in synthesizing BC and other biopolymeric composites. These reinforcement materials range from nanoparticles to polymers. Depending upon their chemical nature and physical appearance, these materials bind differently to the BC network. Yan et al. [50] prepared BC composites with multiwalled carbon nanotubes (CNTs) through the in situ strategy. CNTs were well dispersed in the BC culture media. The growing fibrils trapped the CNTs that were detected through structural analysis, and the produced BC–CNT composites enhanced the physicomechanical and electrical properties of BC. In another study, Saibuatong and Phisalaphong prepared BC–aloe vera composite films via the in situ addition of different quantities of aloe vera to the synthetic media of BC. The aloe vera components were well entrapped in the BC fibrils and complemented BC with superior physicomechanical properties [28]. Similarly, chitosan (Ch) was added as a reinforcement to the BC culture media for in situ synthesis of BC–Ch composites. Consequently, the structural and physiological features of the BC–Ch composites improved significantly as compared with BC [100]. BC–Ch composite showed significant growth inhibitions against *E. coli* and *S. aureus*. Recently, BC composites were synthesized with a water-insoluble poly-3-hydroxybutyrate (PBH) via the in situ synthesis strategy [101]. The addition of PBH to the culture media not only affected BC production, but also changed the morphology and crystallinity of BC [101]. Literature studies revealed several other examples of BC composites synthesized through the in situ approach [102, 103].

The strategy of in situ composite synthesis proved effective in several cases and resulted in successful synthesis of various BC composites. However, the synthetic approach comes across through several limitations that reduced its broad applicability. The major problem lies in the nature of the culture media and the reinforcement materials. In the case where particles are used as reinforcement materials, they remain suspended for only a short period of time before they settle down in the media. BC is produced at the surface of the culture media, and uniform dispersion of the particles in the BC media is required for composite synthesis [70, 104]. However, once the particles have precipitated or moved to the bottom of the media, they can no longer be entrapped by the BC fibers that are produced on the surface. This inadequacy could be overcome using agitated cultures for BC production [50, 70, 104] or by designing special vessels containing rotating disks [68]. The constant movement in the agitated culture keeps the particles suspended throughout the culturing period and provides better chances for composite synthesis. Polymers, on the other hands, have a better chance of forming composites even in static cultivation cultures. Another important limitation concerning this strategy is the toxic nature of reinforcement materials. Being a biosynthetic process, it is very important to verify that the added reinforcement materials are not toxic to the BC-producing cells. Due to this important fact, various bioactive materials (Ag, ZnO, TiO_2, etc.) cannot be used to synthesize BC composites through this strategy [21].

12 Ex Situ BC Composites Synthesis

The ex situ strategy deals with the impregnation of reinforcement materials inside the BC matrix. The strategy was developed to resolve the problems encountered by the in situ composite developmental approach. Being a web-shaped porous structure, BC offers an excellent environment for polymeric solutions and nanomaterials to penetrate into the structural matrix of BC. Figure 4b illustrates the schematic of BC composite synthesis through the strategy of ex situ materials impregnation. Like in situ strategy, the interaction between the two combining partners could be physical or chemical. The porous structure of BC entraps the nanoparticles while the presence of OH moieties in cellulose chains provides sites for hydrogen bonding. The detailed binding mechanism can be viewed in Fig. 4d. Compared with the in situ method, the ex situ strategy is much simpler, broader ranged, and more effective. This strategy employs the BC sheets prepared through static culture that have important applications in the medical field [17, 96, 98, 105]. The basic structure of BC is not disturbed during the composite synthesis. Furthermore, this strategy is not affected by the toxic nature of the reinforcement materials. Particle suspension is not an issue, unlike the case of in situ composite development.

The strategy of ex situ synthesis has been applied to a number of BC composites, including those with polymers, inorganic materials, metals, and metallic oxides [29, 103]. Ul-Islam et al. developed BC–Ch composites through the ex situ impregnation strategy. It was evident that the penetrating Ch produced definite layers inside the BC matrix. The composites showed hydrogen bonding between the OH and NH groups on BC and Ch [31]. The composites exhibited higher physical, thermal, and mechanical properties than pure BC did. Other polymers, including gelatin, hydroxyapatite (HA), polyethylene glycol (PEG), etc., were combined with BC through the same strategy with the aim of enhancing the biological features and promoting the biomedical applications of BC [106–108].

Besides BC-polymer composites synthesized through the ex situ strategy, a number of BC composites with inorganic materials have been synthesized via the same approach. These composites were mainly developed to promote BC for particular applications. Novel nanostructured composite materials based on bacterial cellulose membranes (BC) and acrylate polymers were prepared by atom transfer radical polymerization (ATRP) [109]. Therein the BC fibrils were initially functionalized and then it was followed by the atom transfer radical polymerization reaction. The composites showed better thermal properties and flexibility compared to pure BC [109]. Yang et al. synthesized BC–Ag nanocomposites using this strategy, showing that the incorporated Ag nanoparticles enhanced the bactericidal properties of BC [110]. Ul-Islam et al. prepared BC composites with montmorillonite (MMT) clay with the same approach, mixing well-dispersed MMT particles into the BC fibril network. In a further extension of this work, modified MMTs were incorporated into the BC network, producing good bactericidal effects against *E. coli* and *Staphylococcus aureus* [98]. Numerous other types of BC composites

have been synthesized through the same ex situ production strategy, such as BC–Pd and BC–CNT [43, 111].

Like in situ approach, the ex situ strategy also faces certain limitations. The biggest problem is associated with the size of the combining materials. Although the strategy is highly successful for nanoparticles and water-soluble polymers, it is less effective for large-sized particles and water-insoluble or hydrophobic polymers. Large-sized particles cannot penetrate through the BC fibers, and hydrophobic materials are incapable of forming any bonds with BC. Furthermore, the ex situ strategy could be successful when the BC fibers take on a uniform arrangement. As it has been shown that the fiber arrangement is not always uniform, reproducible results are not guaranteed.

12.1 BC Composites Through Solution Blending

The limitations of in situ and ex situ techniques demand alternatives to cope with the requirements of BC composites. Solution blending is an important technique commonly used in polymeric composite synthesis. The technique utilizes a broad range of materials that can be combined with BC in composite form. Importantly, the composition of the matrix and the reinforcement materials can be easily controlled in this method. A generalized scheme of BC composite development using this approach is shown in Fig. 4c. Hard melting and the limited solubility of BC are the major concerns currently associated with the applicability of this technique. It has been observed that BC is insoluble in water and common organic solvents [112]. The lower solubility is mainly caused by strong inter- and intramolecular hydrogen bonding and the high crystallinity of BC [112]. This unusual behavior has generated high attention to explore various suitable solvents for dissolving BC.

Recently, a few classes of compounds have been reported to completely dissolve BC [112]. Among these solvents, N-methylmorpholine N-oxide (NMMO) [97], ionic liquids [102], $ZnCl_2$ ($3H_2O$) [113], NaOH [114], and LiOH/urea/thiourea [115] have been used for BC dissolution and composite synthesis. Based on these findings, BC composites have been prepared with nanomaterials through the solution casting method. Dissolved BC can be used to synthesize BC films, nanofibers, nanocrystals, and composite materials. After dissolution, various materials, specifically nanomaterials, are added in desired quantities and homogeneously dispersed through sonication [21, 97].

Literature studies revealed several examples of BC composites synthesized via the solution casting technique, imparting new properties in BC. Gao et al. dissolved BC in NMMO and prepared regenerated BC (RBC) films from dissolved BC [116]. It was found that fibril structure and arrangement in RBC is much uniform than BC and they possess higher thermal and mechanical properties. A recent study by Ul-Islam et al. [97] reported the synthesis of RBC–ZnO nanocomposites via the same approach. They added various quantities of ZnO nanoparticles to a BC solution dissolved in NMMO. After sufficient dispersion, the composite solution

was casted on glass plates and composite films were developed. The composites possessed high antibacterial properties and were nontoxic to animal cells. Furthermore, the dissolution of BC in various ionic solvents and their use in BC composite synthesis has also been reported.

The solution blending/casting technique is still new and has not been extensively applied to BC composites. However, the approach has been comprehensively employed for the synthesis of various polymeric composites with inorganic materials including clay, metals, and nanoparticles [117]. This approach provides certain advantages and can overcome the limitations faced by the methods discussed earlier. BC composites synthesized through this method have stronger interactions with the combining material. The use of multiple materials in a composite is possible and there is no issue of material size, shape, or toxic effects. It is expected that this approach will be very useful in future strategies of BC composite development.

13 Applications of BC Composites

Bacterial cellulose is a versatile polymer that has been used in numerous applications in various fields. The major applications take advantage of its structural and physiological characteristics. The most impressive applications of BC and BC composites are found in the medical field. In addition, they have been used as a food source and have also found use in food additives, cosmetics, pharmaceuticals, display devices, medical devices, biosensors, filter membranes, and optoelectronic devices [21]. Figure 5 illustrates a generalized scheme of various applications of BC composites. Herein, we describe some of the main applications of BC and its composites.

14 Medical Applications of BC and BC Composites

The unique structural and mechanical features of BC make it a better choice than plant cellulose for various applications. Precisely, BC fibers have a high aspect ratio with a diameter of 20–100 nm and very high surface area, conferring a very high liquid-loading capacity to BC. Moreover, several other salient features, such as biocompatibility, hydrophilicity, transparency, and nontoxicity make it a suitable candidate for a wide range of applications in various fields including biomedicine and biotechnology [118]. Generally, the choice of a biomaterial for medical applications is principally dependent on its biocompatibility (i.e., ability to remain in contact with living tissues without causing any toxic or allergic side effects). Likewise, a proposed medical application should advocate the choice of a particular cellulose structure. For instance, implantable cellulose should display high porosity with interconnected pores of 50–150 μm in diameter for artificial skin substitutes to facilitate skin cell integration into a cellulose scaffold, such as one made of plant

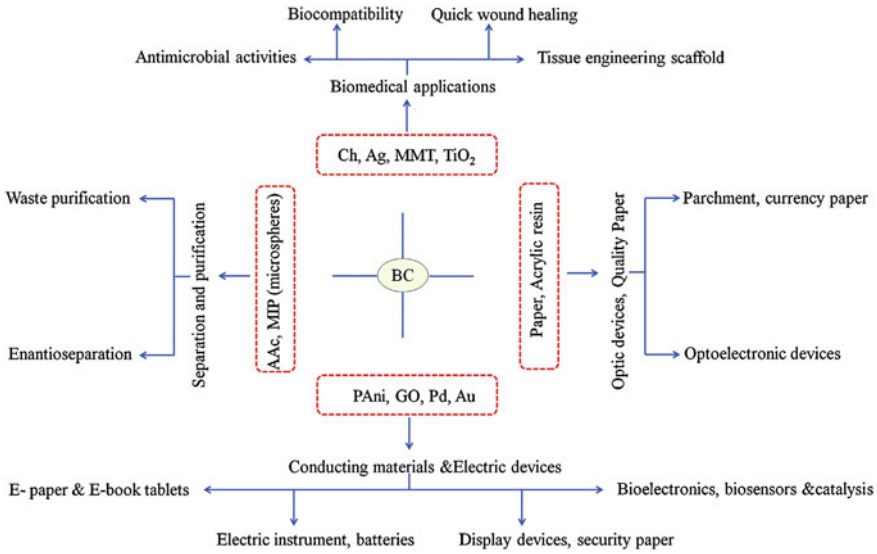

Fig. 5 Applications of BC composites in different fields. Figure is reproduced from [21] with permission from Elsevier

cellulose, reported to support bone tissues and hepatocytes [119]. Similarly, for temporary wound dressing purposes, cellulose should exhibit a nanoporous structure and keep the wound moist during the healing process. Several in vivo studies have reported the use of microbial cellulose (MC) on animal models, such as rabbit and mouse [120, 121]. To date, various biomedical applications of BC have been reported, including artificial organs (skin, blood vessels, cornea, urethra, bone, cartilage, and porcine knee meniscus), heart valve prosthesis, and deliveries of drugs, hormones, and proteins. Table 2 represents various composites of BC applied for specific medical applications.

14.1 Skin/Tissue Regeneration

Skin regeneration, or more precisely skin grafting, is usually carried out in situations of extensive wounding or trauma, severe burns, substantial skin loss due to infection, or specific surgeries that may require skin grafts for healing to occur. The materials used for dressing during skin regeneration should stop the exudates and should be easily removable from the wound surface after recovery. In addition, they should exhibit absorbent and permeable properties. Recently, interest in BC as a

Table 2 Illustration of various biomedical applications of BC-composites materials

BC-composite	Application	Improved features	References
BC-chitosan and silver NPs	Skin tissue regeneration	Antibacterial activity; improved transparency, flexibility, and mechanical properties	[123]
BC-collagen type I	Skin tissue regeneration	Reduced concentration of adsorbed proteases and interleukins; improved antioxidant activity	[125]
BC-hydroxyapatite	Cartilage and bone tissue engineering	Improved biological activity and mechanical strength	[158], [107]
BC-laponite	Drug delivery	Improved electrical properties and thermal stability	[159]
All BC composites	Small grafts, ligament or tendon substitute, drug delivery	Improved mechanical properties	[160], [161] [162]
BC-montmorillonite (BC-MMT)	Wound healing	Improved mechanical properties, thermal stability; antimicrobial activity	[19, 20]
BC-lysostaphin	Wound healing	Antimicrobial activity	[163]
BC films	Replacement of diseased arteries	Minimized blood clotting, increased biocompatibility, high mechanical strength, substantial permeability to water, high water retention, and low surface roughness	[164]
BC-chitosan	Wound healing and skin burns	Highly nonporous, enhanced wound healing, high mechanical properties	[89]
BC tubes (BASYC®)	Artificial blood vessels in microsurgery	High mechanical strength, highly moldable, high tensile strength, Improved Young modulus, inner smooth surface	[92]
BC membrane	Scaffold for mammalian cell	High permeability	[134]

wound dressing material has increased dramatically because of its potential applications in medicine and cosmetics [122]. BC serves as an attractive candidate material for skin tissue repair since it provides a moist environment for the injury site. However, BC by itself lacks antimicrobial activity to prevent wound infection, and it exhibits no significant influence on the biochemical state of chronic wounds. Various BC composites have been prepared, therefore, with materials that confer the antimicrobial activity against invading microorganisms, hence proving its applicability as a skin tissue repair material. Considering the properties of BC and its clinical performance, the commercialization of BC for wound care is very promising [89]. Figure 6 illustrates some of the medical applications of BC composites including regeneration of soft and hard tissues.

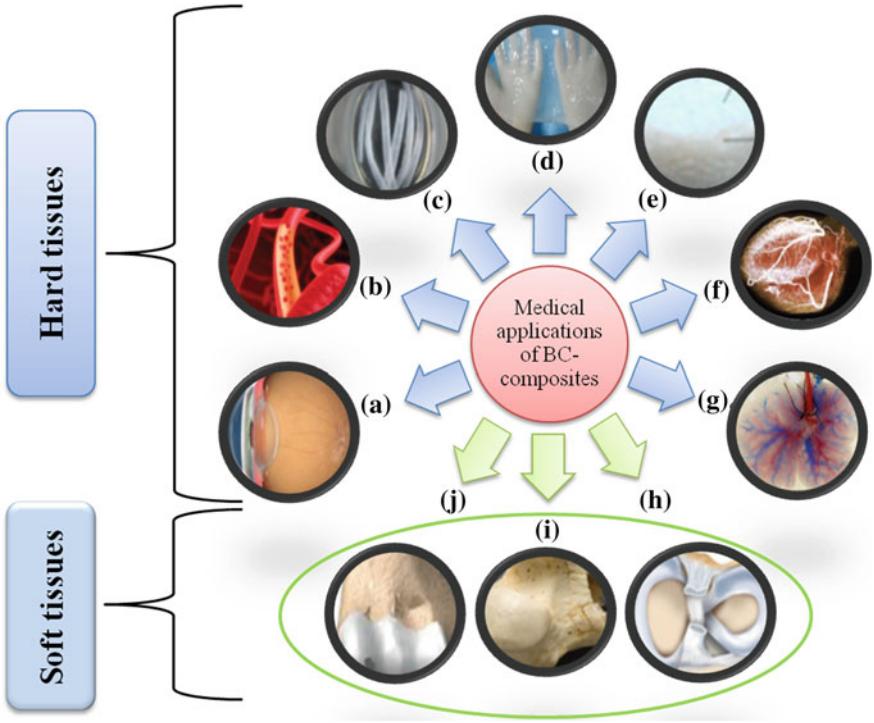

Fig. 6 Prospects of various biomedical applications of BC-based materials: hard tissues; **a** cornea **b** blood vessels, **c** urethra **d** skin, **e** scaffold, **f** heart valves, **g** liver, and soft tissues; **h** menisci, **i** bone, **j** cartilage

Several composites of BC synthesized with different materials have been reported to serve as substitutes for conventional biomaterials used in skin regeneration. The enhanced mechanical properties, high water-holding capacity, and slow water release rate make these composites attractive candidates for wound dressing and other medical applications [31]. BC–chitosan nanocomposites reinforced with silver nanoparticles to exhibit antibacterial activities have been prepared and thus serve as an appropriate biomaterial for skin regeneration. The nanocomposite films were highly transparent, flexible, and displayed better mechanical properties when compared with pure BC [123]. Similarly, BC–collagen type I composites showed that the collagen molecules were not only coated on the surface of the BC fibrils, but also penetrated inside the BC and thus formed hydrogen bonding between BC and collagen [124]. The composite was able to significantly reduce the adsorbed amounts of certain proteases and interleukins, showing a distinct antioxidant capacity [125]. A similar behavior was shown by BC–PEG (polyethylene glycol) composites. BC–gelatin double-network (DN) hydrogels showed high mechanical strength, improved fracture strength, and high elastic modulus under compressive stress. BC–gelatin membranes mediated the

proliferation of NIH/13 cells and served as a biodegradable skin tissue regeneration template. Composites of BC with several other polysaccharides, such as sodium alginate, gellan gum, and i-carrageenan, have also been reported [108]. BC-poly(3-hydroxubutyrate-co-4-hydroxubutyrate) (P(3HB-co-4HB)) composite scaffolds showed better proliferation of Chinese Hamster Lung (CHL) fibroblast cells than pure P(3HB-co-4HB) scaffold did [126]. The BC–alginate composite sponge has served as a promising material to be used as a nonadherent hydrogel dressing because of the many advantages it offers, such as skin tissue compatibility, excellent water uptake ability, high mechanical strength, and stability in both water and PBS.

14.2 Wound Healing

Wound healing is a dynamic process involving complex interactions between various cell types, extracellular matrix (ECM) molecules, and soluble compounds [127]. It requires the coordination of a series of events including homeostasis, inflammation, granulation tissue formation, and remodeling [127]. Problems in ulcer wound healing are mostly caused by the failure of one or more of these events to occur properly. Recent research in wound healing has been focused on improving the process by optimizing elements that accelerate healing and reduce scarring, developing novel tissue or organ substitutes, and identifying signals that gear up the healing process by regeneration and not repairing. For example, the healing of skin wounds requires the regeneration of different tissue types, cell types, and matrix components [128].

To date, various natural and synthetic wound dressing materials have been evaluated to treat surgical and nonsurgical lesions. Though these materials are successful in closing the wounds, efforts are being made to find appropriate materials that must be similar to autograft tissues, both structurally and functionally, in order to mediate complete wound healing. The healing of ulcers has been attempted using hydrogels, hydrocolloids, synthetic, and biological membranes, and alginate as dressing materials [129]. BC has been extensively explored as a wound dressing material due to its unique features, such as small-sized fibrils, wet nature, highly nanoporous structure, and ease of molding. These features confer several advantages, such as providing a moist environment for the wounds, facilitating the transfer of antibiotics and other medicines, and serving as a physical barrier against infections. The first commercial application of BC as a wound dressing material was reported by Johnson & Johnson Company in the 1980s. Czaja et al. [90, 91] found that BC serves as a better dressing than conventional wound dressings do in several aspects, such as conforming to the wound surface, maintaining a moist environment within the wound, significantly reducing pain, accelerating re-epithelialization, forming granulation tissues, and reducing scar formation. In another set of studies conducted by Fontana et al. [130] and Mayall et al. [131], who developed a BC product called Biofill, the product proved to be a

very successful wound dressing material for skin problems, such as burns and chronic ulcers. Biofill was shown to be more effective than other wound dressing materials in several ways, such as providing pain relief, protecting the wound against infection, accelerating the healing process, and reducing the cost of treatment. Moreover, it was also proven to be more effective than other skin treatments. Xylos Corporation developed another BC product called XCell, used in a study conducted by Alvarez et al. [132]. XCell was developed from never-dried BC and was used to treat chronic venous ulcers. This material proved to be more effective than conventional wound dressing materials in various aspects, such as promoting autolytic debridement, reducing pain, and accelerating granulation. XCell could simultaneously donate and absorb moisture from the wound, a feature that is particularly important for wounds with a large volume of exudates [133].

14.3 Artificial Blood Vessels

Artificial blood vessels are tubes made from synthetic materials to restore blood circulation. In case of coronary vessel blockage around the heart due to the hardening of arteries, a bypass operation is required, bearing a fatal risk due to the sophisticated and complex procedures that are involved. BC could be used for the synthesis of artificial blood vessels as it carries a lower risk of blood clots compared with chemically synthetic materials, such as vinyon, Teflon, and synthetic fiber Dacron. BC exhibits several mechanical properties useful for the synthesis of artificial blood vessels, including shape retention and tear resistance, which are superior to many synthetic materials. Compared to organic sheets like polypropylene, polyethylene terephthalate, or cellophane, BC processed into a film or sheet showed remarkable mechanical strength. Tubular-shaped BC served as an attractive candidate as a blood vessel replacement [92]. Moreover, cellulose works very well in contact with blood and thus may serve as a substitute for artificial blood vessels. BC fibers support the growth and proliferation of smooth muscle, endothelial, and fibroblast cells to eventually create a viable blood vessel. Its mechanical properties, shown in its tensile strength and flexibility, may also prove to be appropriate in order to withstand the forces generated by the circulatory system, hence proving to be effective for the generation of blood vessels. The artificially synthesized blood vessels (BASYC tubes) usually have an inner diameter of 1.0 mm, a length of 5 mm, and a wall thickness of 0.7 mm, allowing the cells to grow on their surfaces and thus ensure the prevention of blood clotting. High mechanical strength, resistance to mechanical strain, and blood pressure are the other important features of these artificial blood vessels.

The practical development of cardiovascular grafts has been limited by a compliance mismatch between the synthetic graft and the surrounding tissues. This limitation could be overcome by the development of biomaterials exhibiting properties close to the tissues being replaced. An anisotropic BC–PVA (polyvinyl alcohol) nanocomposite has been prepared that displayed the desired medical

properties showing high biocompatibility. The mechanical properties of nanocomposites, like anisotropy, were varied in broad range by controlling material and processing parameters. Furthermore, its properties were closely matched in both the circumferential and axial directions within the physiological range, with improved resistance to further stretch beyond the physiological strain. These observations led to the conclusion that the degree of anisotropy of BC–PVA nanocomposites could be controlled to closely match the mechanical properties of the soft tissues to be replaced, ranging from cardiovascular to other connective tissues. However, prior to the development of artificial blood vessels, the material to be evaluated, including BC, needs to be compared with conventional graft materials in terms of the potential to support endothelial cell proliferation and thrombogenic properties.

14.4 Scaffolding

The key element that determines the success of tissue regeneration in tissue engineering approaches is the development of a three-dimensional biomaterial scaffold that provides structural support for cell attachment, spreading, migration, proliferation, and differentiation, aside from the shape of the new growing tissues. Moreover, the scaffold should possess an interconnected network of pores allowing cell movement and transport of nutrients to the growing cells. The cells for the formation of a desired type of tissue are seeded onto the scaffold, which coaxes them to develop into the proper three-dimensional structure. This tissue construct, developed in vitro, is then implanted into the affected area of the body, which could be a burn, a nonhealing wound, or an ulcer, as either a replacement tissue or organ.

Earlier studies have suggested that scaffolding materials should be biodegradable so that the seeded cells would secrete their own extracellular molecules as they proliferate, eventually replacing the implanted material. Yet, this approach encountered several limitations as scaffolds often degrade faster than the rate at which cells replace it. This problem can be overcome through the development of a permanent scaffolding material that must be biocompatible, porous, and contains the mechanical properties required for normal tissue function. Various materials have been evaluated for the design of scaffolds including natural polymers like collagen, alginate, hyaluronic acid, fibrin glue, and chitosan, and synthetic polymers like polyglycolic acid (PGA), poly(lactic acid) (PLA), polyvinyl alcohol (PVA), polyhydroxy ethyl methacrylate (pHEMA), and poly(N-isopropylacrylamide) (pNIPAA) [17]. Preliminary studies indicated that BC could serve as an excellent material for scaffold development in tissue engineering since it is not harmful whether used as implant material or as a substrate. It has been extensively used as a scaffolding material both in its native and modified form. However, some studies have shown that native BC was an ineffective substrate for cell culture or tissue engineering because cells do not adhere to it and hence do not proliferate. Upon soaking native BC in serum and electrolytic solutions such as sodium hydroxide, cells began to adhere and proliferate, proving the ability of BC to be

used as a cell culture substrate for scaffold development [134]. *G. xylinus* has been evaluated as a novel material for scaffolding owing to its unique properties of biocompatibility, mechanical strength, and degradability. Native and chemically modified BC materials (phosphorylated and sulfonated BC) have also been evaluated using bovine chondrocytes. The results demonstrated that unmodified BC supported chondrocyte proliferation at levels of approximately 50 % of that of the collagen type II substrate and provided significant advantages in terms of mechanical properties. Compared with tissue culture plastic and calcium alginate, native BC promoted significantly higher levels of chondrocyte growth. Chemical sulfonation and phosphorylation of BC did not show improved chondrocyte growth, but the porosity of the material did affect chondrocyte viability.

14.5 Bone and Cartilage Regeneration

Natural bone is composed of a collagen matrix reinforced with hydroxyapatite (HAp). Bone tissues severely damaged by disease are often difficult to regenerate by the healing process. Every year, over two million bone-grafting surgeries are performed worldwide, costing more than $15 billion. Similarly, cartilage is an avascular tissue consisting of only one type of cells, chondrocytes, which are embedded in a matrix composed of collagen and proteoglycans. Adult cartilage tissues have a limited self-repair capacity due to the sparse distribution of highly differentiated and nondividing chondrocytes. In addition, the self-repair process is inhibited by a slow matrix turnover, a low supply of progenitor cells, and a lack of vascular supply. Bone transplantation is carried out either through autografting, allografting, or orxenografting, the latter two of which often face the problem of immune rejection. Despite the maximum chance of success, autografting is often avoided due to limited availability, size, and shape of the donor tissues as, well as surgical pain during the removal of autogenous bones. Thus, it may not be appropriate for the repair of large bone damages [135]. Besides, synthetics grafts made from metals, bioactive glass, alumina ceramics, calcium sulfate, poly(glycolic acid), poly(lactic acid), polycaprolactone, calcium phosphate, collagen, and natural corals or ceramics [136] do not provide optimal mechanical properties, exhibit poor overall osseointegration, and eventually fail due to infection or fatigue loading. These limitations necessitate a major clinical need for novel bone-grafting materials that can be readily processed into larger, more complex structures and guide the natural repair mechanism through tissue engineering.

Several synthetic polymers are currently in practice in biomedical engineering and some of their important properties, such as degradation time, can be improved during polymer processing. The scaffold in tissue engineering supports cell proliferation and maintains the cells' differentiated functions in addition to defining the shape of the new growing tissues. BC has served as a scaffold in tissue engineering practices for the regeneration of bone and cartilage tissues because of its biocompatibility, high tensile strength in dry and wet states, fine fibril networks, high

crystallinity, and moldability [136]. Studies have shown that BC supports the growth of several cells type, such as endothelial cells, smooth muscle cells, and chondrocytes, important components of bone and cartilage. BC has also shown nontoxic effect to these cells. However, a major limitations associated with BC is that nanofibrils from a dense mesh can limit the cell infiltration [137]. The problem was overcome by introducing porosity into the BC through incorporation of porogens during the fermentation of *A. xylinum* [138] that produced a network of interconnected pores. Studies with smooth muscle cells demonstrated better incorporation into the microporous BC material.

14.6 Other Medical Applications

Several other reports have shown various useful applications of BC and its composites including hemodialysis membranes, diffusion-controlling membranes, and membrane carriers for enzyme immobilization in biosensors, coating materials for drugs and drug-releasing scaffolds, and in vitro hollow fibers perfusion systems. BC has also been extensively used for cell culturing and implantation, either in its pure form or in the form of composites, which gave rise to important organ formation such as artificial liver, bones, and cartilage [139].

15 Applications of BC in Other Fields

It is noteworthy that BC has become very well-known biomaterial in the medical field as a result of its multiple applications. Besides medical as the primary applicable field, BC has gained applications in various other fields. For example, it has been used in the food industry as well as the paper and pulp industries. Additionally, BC has been applied as a membrane for separation and purification as well as in the development of conductive and electrical devices. Herein, we briefly discuss these miscellaneous applications of BC and BC composites.

15.1 Applications in the Food Industry

Dietary fibers are important constituents of daily food and offer several advantages, specifically in reducing the risks of chronic diseases [140]. BC is a type of dietary fiber that is "generally recognized as safe (GRAS)" in its classification [141]. BC offers several advantages over other dietary fibers including its highly pure nature that avoids harsh treatments processes, the easy inclusions of color and taste pigments, possible production in desired shapes, and the three-dimensional web-shaped structure [141]. BC gels have been used as a famous food named Nata in the

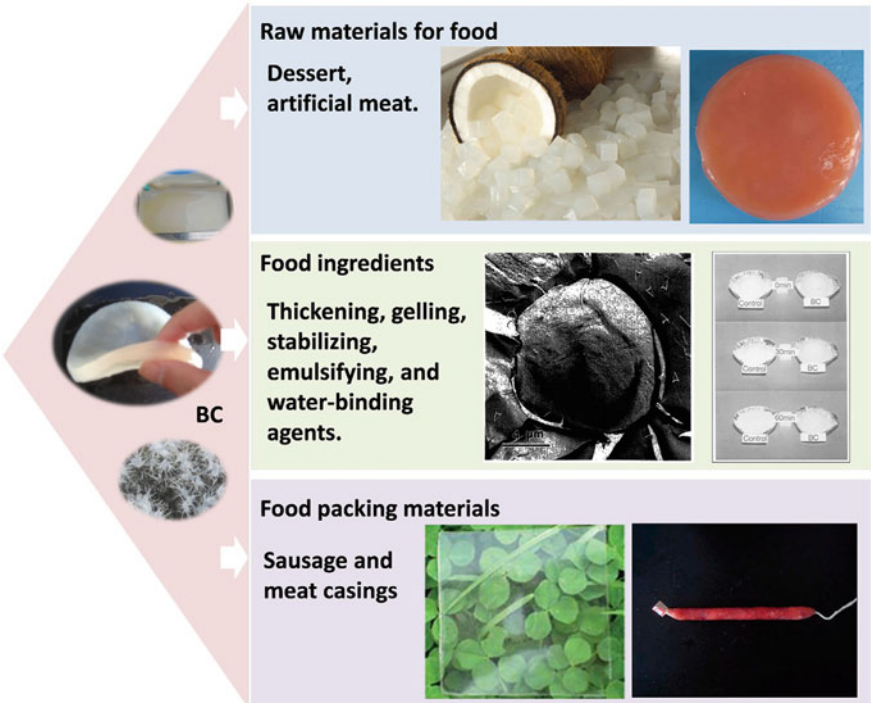

Fig. 7 Utilization of BC in food. Figure has been reproduced from [141] with permission from Elsevier

Philippines [142]. Various flavors have been incorporated in Nata based on the sources of medium, like coconut and pineapple. Figure 7 illustrates the application of BC in food industry. Owing to its simple manufacturing process and good taste, the market of BC as a type of food is quickly increasing, and it is becoming a popular food in South Asia, specifically Japan.

Besides pure food, BC fiber has been utilized successfully as a food additive to produce food items with low calories. Its use as an additive has been considered to replace fats in emulsified meat products [143]. It is noteworthy that BC fibers have been found to reduce cholesterol levels by producing low cholesterol products. Compared to fiber-free foods, an appreciable reduction in serum triglyceride, serum cholesterol, and liver cholesterol was observed in in vivo experiments involving BC fibers. The applicability of BC in the food industry is also boosted by its higher water-absorbing capabilities. BC complexes fused with monascus (natural red pigment) has a meat-like taste and can be used to replace meat. BC composites with poly(lactic acid) have been effectively used in the food packaging industry due to its high mechanical properties, transparent nature, and biocompatibility [144].

15.2 Separation and Waste Purifications

BC composites have shown tremendous potential as a purification or separation membrane. The porous membrane of BC offers an ideal scenario when combined with other polymeric materials (having effective separating capabilities). BC composites were prepared with acrylic acid (AAc), which possessed ion-exchange capabilities, for applications as separating membranes. Compared with commercial membranes, the BC–AAc composite membranes possessed improved electrochemical properties and showed excellent absorption capabilities for heavy metals through binding with metal ions and separating trace metals. The preparation of BC composites with biodegradable materials is an effective strategy because it not only shows good separation capabilities, but also avoids environmental problems as no disposal issues are associated with the preparation. With the capabilities of ion exchange and heavy metal absorption, these composites can effectively be utilized for wastewater treatment and purification [145].

With the development of BC membranes for separation purposes, an important application arose in affinity chromatography. BC composites with molecularly imprinted polymers can be used for the separation of desired isomers from racemic mixtures. MIP nanoparticles can be impregnated into BC through either of the composite synthesis techniques. These BC–MIP composites contain a huge number of binding sites that can pick up the desired enantiomer from a racemic mixture and carry out the separation. Jantarat et al. successfully dispersed MIP microspheres (S-propranolol selective) in a porous BC matrix with controlled allocation and availability of molecular recognition sites [146]. Similarly, in another study, BC–MIP composite membranes were developed for the separation of the S-propranolol enantiomer. The composites were successfully utilized for enantioselective separation [147].

15.3 Conductive Materials and Electrical Devices

BC has received a great deal of interest as substrates in the development of flexible optoelectronic and photonic devices [148]. Although structural features favor the development of BC for such devices, the main problem associated with its use is its nonconductive nature. Therefore, in the first step, BC is converted into electrically conductive sheets by the incorporation of conductive materials. The BC composites with conductive properties are then immobilized with electrochromic dyes and attached to electrodes. The application of a potential to the electrodes results in a reversible color change [149]. Display devices based on BC composites are highly flexible and biodegradable, having high contrast and high reflectivity [150]. A study performed by Okahisa et al. [148] reported the successful fabrication of OLED displays on cellulose and acrylic resin nanocomposites. These devices have several potential applications, including e-newspapers, e-book tablets, rewritable maps, and learning tools [149].

A number of conductive materials ranging from polymers to nanomaterials have been applied in the synthesis of BC composites with conductive properties. In this regard, BC–PAni composites, synthesized through the ex situ approach, produced a high degree of conductivity. BC–PAni composites were therefore recommended for implementation in biosensors, flexible electrodes, flexible displays, substrates to evaluate the effects of electrical signals on cell activity, and devices to direct desired cell function for applications in tissue engineering [29, 151]. Among nanoparticles, carbon nanotubes (CNTs) were incorporated both through in situ and ex situ strategies to develop BC with conductive properties. Besides a high conductivity of 1.4×10^{-1} S/cm, BC–CNT presented much better thermal and mechanical properties than pure BC did [50, 111]. Other BC composites fabricated for similar applications include BC–graphene oxide, BC–Pd, BC–Au, and BC–Pt.

15.4 Industrial Applications

Polymers with high mechanical properties have been implemented in numerous applications in various industries. Consequently, different materials are added to produce BC composites with improved mechanical properties. Materials were initially added to the BC growth media and incorporated in the growing fibrils, subsequently improving the mechanical properties of BC. Mormino and Bungay used scrap paper as reinforcement materials to enhance the mechanical properties of BC. The scrap paper was added in controllable quantities to the BC media and was found embedded inside the BC fibers. The resulting paper composites were stronger than pure BC and can be used as parchment or for currency [45]. In other related work, glucose phosphate was added to the BC culture media to produce a modified form of BC. The phosphate group was incorporated inside the resulting BC gels, and these BC gels containing phosphates were used in synthesizing BC composites with wood pulp for preparing paper sheets. Modified BC–pulp composites significantly enhanced the strength and fire-resistance properties of the paper sheets. Thus, these composites will likely play an important role in the synthesis of high-quality paper [152].

A number of optically transparent polymers seek applications in the development of optoelectronic devices. The major barrier associated with these polymers is their weak mechanical properties. It has been observed that composites of BC synthesized with such polymers can overcome this limitation, while possessing excellent mechanical properties. In developing such types of composites, BC is used as the reinforcement material where it does not inflict negative effects on the transparency of the polymeric materials [153]. Nogi et al. prepared BC nanocomposites with acrylic resins through the ex situ composite synthesis strategy, keeping BC sheets in an acrylic resin solution. The composites were transparent and had great potential in the development of optoelectronic devices. Moreover, the composites were much stronger than the polymeric materials alone and showed stable transmittance upon temperature variation [153].

16 Conclusion and Future Prospects

Pure BC produced by microorganisms offers several advantages and applications owing to its unique structural features. Further advancement in its applications has been achieved by synthesizing composites with nanomaterials and polymeric materials. The demand for advancement in the preparation and applications of BC has led to the innovation of several strategies for the synthesis of BC composites. BC composites have been implemented in impressive applications in the medical field, specifically in wound healing, tissue regeneration, and the development of artificial organs. Antimicrobial, conductive, separating, purifying, biocompatible, biosensing, and many other characteristics have also been enhanced in the BC composites. Additionally, current research on BC composites is leading toward the development of electronic papers, displays, LEDs, and various optoelectronic devices.

Currently, several challenges are hindering the versatile applications of BC and BC composites. Among these, one is to find an economically feasible method of producing BC. The synthetic media currently used in BC production are very expensive. It is of utmost importance to find cheap, economically, and environmentally feasible sources of BC production. Second, it is important to develop techniques that enhance the production and productivity of BC without disturbing its basic structural features. In this regard, the use of genetically stable bacterial strains could be one possible strategy. Among the different types of reactors, the rotating disk biofilm reactor should be enhanced so as to accumulate the BC-producing cells on the disks while continuously producing BC without further inoculation.

The third major issue is related to the strategies of composite synthesis, as all of the aforementioned studies are currently facing one or more problems. There is a strong need to develop new methods of composite synthesis that can cope with all the limitations of previous strategies and seek new applications.

Acknowledgment The research is supported by the BK21 plus (2014-2019) Korea, (21A.2013-1800001).

References

1. Thakur VK, Thakur MK, Raghavan P, Kessler MR (2014) Progress in green polymer composites from lignin for multifunctional applications: a review. ACS Sustain Chem Eng 2:1072–1092
2. Thakur VK, Yan J, Lin M-F et al (2012) Novel polymer nanocomposites from bioinspired green aqueous functionalization of BNNTs. Polym Chem 3:962–969
3. Thakur VK, Lin M-F, Tan EJ, Lee PS (2012) Green aqueous modification of fluoropolymers for energy storage applications. J Mater Chem 22:5951–5959
4. Thakur VK, Ding G, Ma J et al (2012) Hybrid materials and polymer electrolytes for electrochromic device applications. Adv Mater 24:4071–4096

5. Thakur VK, Singha AS, Thakur MK (2012) Biopolymers based green composites: mechanical, thermal and physico-chemical characterization. J Polym Environ 20:412–421
6. Thakur VK, Singha AS, Thakur MK (2012) Modification of natural biomass by graft copolymerization. Int J Polym Anal Charact 17:547–555
7. Thakur VK, Thakur MK (2014) Processing and characterization of natural cellulose fibers/thermoset polymer composites. Carbohydr Polym 109:102–117
8. Thakur VK, Thakur MK (2014) Recent trends in hydrogels based on psyllium polysaccharide: a review. J Clean Prod 82:1–15
9. Thakur VK, Thakur MK (2014) Recent advances in graft copolymerization and applications of chitosan: a review. ACS Sustain Chem Eng 2:2637–2652
10. Thakur VK, Thakur MK, Gupta RK (2014) Review: raw natural fiber-based polymer composites. Inter J Polym Anal Charact 19:256–271
11. Thakur VK, Vennerberg D, Kessler MR (2014) Green aqueous surface modification of polypropylene for novel polymer nanocomposites. ACS Appl Mater Interfaces 6:9349–9356
12. Thakur VK, Vennerberg D, Madbouly SA, Kessler MR (2014) Bio-inspired green surface functionalization of PMMA for multifunctional capacitors. RSC Adv 4:6677–6684
13. Thakur VK, Thunga M, Madbouly SA, Kessler MR (2014) PMMA-g-SOY as a sustainable novel dielectric material. RSC Adv 4:18240–18249
14. Thakur VK, Grewell D, Thunga M, Kessler MR (2014) Novel composites from eco-friendly soy flour/SBS triblock copolymer. Macromol Mater Eng 299:953–958
15. Singha AS, Thakur VK, Mehta IK et al (2009) Surface-modified hibiscus sabdariffa fibers: physicochemical, thermal, and morphological properties evaluation. Int J Polym Anal Charact 14:695–711
16. Singha AS, Thakur VK, Mishra BN (2009) Study of grewia optiva fiber reinforced urea-formaldehyde composites. J Polym Mater 26:81–90
17. Keshk SMAS (2014) Bacterial cellulose production and its industrial applications. J Bioproces Biotechniques 4:1–10
18. Mohite BV, Patil SV (2014) A novel biomaterial: bacterial cellulose and its new era applications. Biotechnol Appl Bioc 61:101–110
19. Ul-Islam M, Khan T, Park JK (2012) Water holding and release properties of bacterial cellulose obtained by in situ and ex situ modification. Carbohydr Polym 88:596–603
20. Ul-Islam M, Khan T, Park JK (2012) Nanoreinforced bacterialcellulose–montmorillonite composites for biomedical applications. Carbohydr Polym 89:1189–1197
21. Shah N, Ul-Islam M, Khattak WA, Park JK (2013) Overview of bacterial cellulose composites: a multipurpose advanced material. Carbohydr Polym 98:1585–1598
22. Singha AS, Thakur VK (2008) Effect of fibre loading on urea-formaldehyde matrix based green composites. Iran Polym J 17:861–873
23. Singha AS, Thakur VK (2008) Saccaharum cilliare fiber reinforced polymer composites. E J Chem 5:782–791
24. Singha AS, Thakur VK (2008) Synthesis and characterization of pine needles reinforced RF matrix based biocomposites. E J Chem 5:1055–1062
25. Fiayyaz M, Zia KM, Zuber M, Jamil T, Khosa MK, Jama MA (2014) Synthesis and characterization of polyurethane/bentonite nanoclay based nanocomposites using toluene diisocyanate. Korean J Chem Eng 31:644–649
26. Zhou T, Chen D, Jiu J, Nge TT, Sugahara T, Nagao S, Koga H, Nogi M, Suganuma K, Wang X, Liu X, Cheng P, Wang T, Xiong D (2013) Electrically conductive bacterial cellulose composite membranes produced by the incorporation of graphite nanoplatelets in pristine bacterial cellulose membranes. Express Polym Lett 7:756–766
27. Kim J, Cai Z, Lee HS, Choi GS, Lee DH, Jo C (2011) Preparation and characterization of a bacterial cellulose/chitosan composite for potential biomedical application. J Polym Res 18:739–744
28. Saibuatong O, Philsalaphong M (2010) Novo aloe vera–bacterial cellulose composite film from biosynthesis. Carbohydr Polym 79:455–460

29. Shi Z, Zang S, Jiang F, Huang L, Lu D, Ma Y, Yang G (2012) In situ nano-assembly of bacterial cellulose–polyaniline composites. RSC Adv 2:1040–1046
30. Ciechanska D (2004) Multifunctional bacterial cellulose/chitosan composite mate-rials for medical applications. Fibres Text East Eur 12:69–72
31. Ul-Islam M, Shah N, Ha JH, Park JK (2011) Effect of chitosan penetrationon physico-chemical and mechanical properties of bacterial cellulose. Korean J Chem Eng 28:1736–1743
32. Feng Y, Zhang X, Shen Y, Yoshino K, Feng W (2012) A mechanically strong, flexible and conductive film based on bacterial cellulose/graphene nanocom-posite. Carbohydr Polym 87:644–649
33. Bae E, Park HJ, Yoon J, Kim Y, Choi K, Yi J (2011) Bacterial uptake of silver nanoparticles in the presence of humic acid and $AgNO_3$, Korean. J Chem Eng 28:267–271
34. Rouabhia M, Asselin JM, Tazi N, Messaddeq Y, Levinson D, Zhang Z (2014) Production of biocompatible and antimicrobial bacterial cellulose polymers functionalized by RGDC grafting groups and gentamicin. ACS Appl Mater Interfaces 6:1439–1446
35. Wang J, Zhu Y, Du J (2011) Bacterial cellulose: a natural nanomaterial for biomedical applications. J Mech Med Biol 11:285
36. Brown AJ (1886) J Chem Soc 49, 51:172, 432, 643
37. Browne CA (1906) J Chem Soc 28:453
38. Tarr HLA, Hibbery H (1931) Can J Res 4:372
39. Hestrin S, Aschner M, Mager J (1947) Synthesis of cellulose by resting cells of *Acetobacter xylinum*. Nature Lond 159:64
40. Steinbuhel A (2001) Bacterial cellulose. Biopolymers. Wiley, Weinheim
41. Amano Y, Ito F, Kanda T (2005) Novel cellulose producing system by microorganisms such as *Acetobacter* sp. J Biol Macromol 5:3–10
42. Brown RM Jr, Montezinos D (1976) Cellulose microfibrils: visualization of biosynthetic and orienting complexes in association with plasma membrane. Proc Natl Acad Sci 73:143–147
43. Evans BR, O'Neill HM, Malyvanh VP, Lee I, Woodward J (2003) Palladium-bacterial cellulose membranes for fuel cells. Biosens Bioelectron 18:917–923
44. Touzel JP, Chabbert B, Monties B, Debeire P, Cathala B (2003) Synthesis and characterization of dehydrogenation polymers in *gluconacetobacter xylinus* cellulose and Cellulose/Pectin composite. J Agric Food Chem 51:981–986
45. Mormino R, Bungay H (2003) Composites of bacterial cellulose and paper made with a rotating disk bioreactor. Appl Microbiol Biotechnol 62:503–506
46. Grande CJ, Torres FG, Gomez CM, Troncoso OP, Canet-Ferrer J, Martínez-Pastor J (2009) Development of self-assembled bacterial cellulose-starch nanocomposites. Mater Sci Eng C 29:1098–1104
47. Ha JH, Park JK (2012) Improvement of bacterial cellulose production in *Acetobacter xylinum* using byproduct produced by *Gluconacetobacter hansenii*, Korean. J Chem Eng 29:563–566
48. Kralisch D, Hessler N, Klemm D, Erdmann R, Schmidt W (2010) White biotechnology for cellulose manufacturing—the HoLiR concept. Biotechnol Bioeng 105(4):740–747
49. Shezad O, Khan S, Khan T, Park JK (2010) Physicochemical and mechanical characterization of bacterial cellulose produced with an excellent productivity in static conditions using a simple fed-batch cultivation strategy. Carbohydr Polym 82(1):173–180
50. Yan Z, Chen S, Wang H, Wang B, Jiang J (2008) Biosynthesis of bacterial cellulose/multi-walled carbon nanotubes in agitated culture. Carbohydr Polym 74(3):659–665
51. Tse ML, Chung KM, Dong L, Thomas BK, Fu LB, Cheng KC, Lu C, Tam HY (2010) Observation of symmetrical reflection sidebands in a silica suspended-core fiber Bragg grating. Opt Express 18(16):17373–17381
52. Song H-J, Li H, Seo J-H, Kim M-J, Kim S-J (2009) Pilot-scale production of bacterial cellulose by a spherical type bubble column bioreactor using saccharified food wastes. Korean J Chem Eng 26(1):141–146

53. Okiyama A, Shirae H, Kano H, Yamanaka S (1992) Bacterial cellulose I. Two-stage fermentation process for cellulose production by *Acetobacter aceti*. Food Hydrocolloids 6 (5):471–477
54. Schramm M, Hestrin S (1954) Factors affecting production of cellulose at the air/liquid interface of a culture of *Acetobacter xylinum*. J Gen Microbiol 11:123–129
55. Zhou LL, Sun DP, Hu LY, Li YW, Yang JZ (2007) Effect of addition of sodium alginate on bacterial cellulose production by *Acetobacter xylinum*. J Ind Microbiol Biotechnol 34 (7):483–489
56. Hu Y, Catchmark JM (2010) Formation and characterization of spherelike bacterial cellulose particles produced by *Acetobacter xylinum* JCM 9730 strain. Biomacromolecules 11 (7):1727–1734
57. Park JK, Jung JY, Park YH (2003) Cellulose production by *Gluconacetobacter hansenii* in a medium containing ethanol. Biotechnol Lett 25(24):2055–2059
58. Toyosaki H, Naritomi T, Seto A, Matsuoka M, Tsuchida T, Yoshinaga F (1995) Screening of bacterial cellulose-producing acetobacter strains suitable for agitated culture. Biosci Biotech Bioch 59(8):1498–1502
59. Naritomi T, Kouda T, Yano H, Yoshinaga F, Shigematsu T, Moriumura S, Kida K (2002) Influence of broth exchange ratio on bacterial cellulose production by repeated-batch culture. Process Biochem 38(1):41–47
60. Kim JY, Kim JN, Wee YJ, Park DH, Ryu HW (2007) Bacterial cellulose production by *Gluconacetobacter* sp. RKY5 in a rotary biofilm contactor. Appl Biochem Biotechnol 137:529–537
61. Krystynowicz A, Czaja W, Wiktorowska-Jezierska A, Gonçalves-Mioekiewicz M, Turkiewicz M, Bielecki S (2002) Factors affecting the yield and properties of bacterial cellulose. J Ind Microbiol Biotechnol 29:189–195
62. Jung JY, Khan T, Park JK, Chang HN (2007) Production of bacterial cellulose by *Gluconacetobacter hansenii* using a novel bioreactor equipped with a spin filter. Korean J Chem Eng 24:265–271
63. Yoshino T, Asakura T, Toda K (1996) Cellulose production by *Acetobacter pasteurianus* on silicone membrane. J Ferment Bioeng 81:32–36
64. Chao YP, Sugano Y, Kouda T, Yoshinaga F, Shoda M (1997) Production of bacterial cellulose by *Acetobacter xylinum* with an air-lift reactor. Biotechnol Tech 11(11):829–832
65. Chao YP, Ishida T, Sugano Y, Shoda M (2000) Bacterial cellulose production by *Acetobacter xylinum* in a 50-L internal-loop airlift reactor. Biotechnol Bioeng 68(3):345–352
66. Cheng HP, Wang PM, Chen JW, Wu WT (2002) Cultivation of *Acetobacter xylinum* for bacterial cellulose production in a modified airlift reactor. Biotechnol Appl Biochem 35(Pt 2):125–132
67. Chao Y, Sugano Y, Shoda M (2001) Bacterial cellulose production under oxygen-enriched air at different fructose concentrations in a 50-L, internal-loop airlift reactor. Appl Microbiol Biotechnol 55(6):673–679
68. Serafica G, Mormino R, Bungay H (2002) Inclusion of solid particles in bacterial cellulose. Appl Microbiol Biotechnol 58(6):756–760
69. Lin SP, Cheng KC (2012) Bacterial cellulose production by *Gluconacetobacter xylinum* in the rotating PCS semicontinuous bioreactor and its materials property analysis. In: Paper presented at the 2012 mini symposium frontiers in biotechnology, National Taiwan University, Taipei
70. Cheng KC, Catchmark JM, Demirci A (2009) Enhanced production of bacterial cellulose by using a biofilm reactor and its material property analysis. J Biol Eng 3:12
71. Bielecki S, Krystynowicz A, Turkiewicz M, Kalinowska H (2005) Bacterial cellulose. In: Steinbüchel A, Rhee SK (eds) Polysaccharides and polyamides in the food industry. Wiley, Hoboken
72. Ross P, Mayer R, Benziman M (1991) Cellulose biosynthesis and function in bacteria. Microbiol Rev 55:35–58

73. Tonouchi N, Tsuchida T, Yoshinaga F, Beppu T, Horinouchi S (1996) Characterization of the biosynthetic pathway of cellulose from glucose and fructose in *Acetobacter xylinum*. Biosci Biotechnol Biochem 60:1377–1379
74. Valla S, Coucheron DH, Fjaervik E, Kjosbakken J, Weinhouse H, Ross P, Amikam D, Benziman M (1989) Cloning of a gene involved in cellulose biosynthesis in *Acetobacter xylinum*: Complementation of cellulose-negative mutant by the UDPG pyrophosphorylase structural gene. Mol Gen Genet 217:26–30
75. Brown RM, Saxena IM (2000) Cellulose biosynthesis: a model for understanding the assembly of biopolymers. Plant Physiol Biochem 38:57–67
76. Iguchi M, Yamanaka S, Budhiono A (2000) Bacterial cellulose—a masterpiece of nature's arts. J Mater Sci 35:261–270
77. Brown RM, Willison JHM, Richardson CL (1976) Cellulose biosynthesis in *Acetobacter xylinum*: visualization of the site of synthesis and direct measurement of the *in vivo* process. Proc Natl Acad Sci USA 73:4565–4569
78. Zaar K (1979) Visualization of pores (export sites) correlated with cellulose production in the envelope of the gram-negative bacterium *Acetobacter xylinum*. J Cell Biol 80:773–777
79. Benziman M, Haigler CH, Brown RM, White AR, Cooper KM (1980) Cellulose biogenesis: Polymerization and crystallization are coupled processes in *Acetobacter xylinum*. Proc Natl Acad Sci USA 77:6678–6682
80. Delmer DP (1987) Cellulose biosynthesis. Ann Rev Plant Physiol 38:259–290
81. Yu X, Atalla RH (1996) Production of cellulose II by *Acetobacter xylinum* in the presence of 2,6-dichlorobenzonitrile. Int J Biol Macromol 19:145–146
82. Jonas R, Farah LF (1998) Production and application of microbial cellulose. Polym Degrad Stabil 59:101–106
83. Tokoh C, Takabe K, Fujita M, Saiki H (1998) Cellulose synthesized by *Acetobacter xylinum* in the presence of acetyl glucomannan. Cellulose 5:249–261
84. Watanabe K, Tabuchi M, Morinaga Y, Yoshinaga F (1998) Structural features and properties of bacterial cellulose produced in agitated culture. Cellulose 5:187–200
85. Kuga S, Takagi S, Brown RM (1993) Native folded chain cellulose II. Polymer 34:3293–3297
86. Thompson NS, Carlson JA, Kaustinen HM, Uhlin KI (1988) Tunnel structures in *Acetobacter xylinum*. Int J Biol Macromol 10:126–127
87. Yamamoto H, Horii F, Hirai A (2006) Structural studies of bacterial cellulose through the solid-phase nitration and acetylation by CP/MAS 13C NMR spectroscopy. Cellulose 13:327–342
88. Cannon RE, Anderson SM (1991) Biogenesis of bacterial cellulose. Crit Rev Microbiol 17:435–447
89. Czaja W, Krystynowicz A, Bielecki S, Brown RJ (2006) Microbial cellulose-the natural power to heal wounds. Biomaterials 27:145–151
90. Czaja W, Krystynowicz A, Kawecki M, Wysota K, Sakiel S, Wroblewski P, Glik J, Nowak P, Bielecki S (2007) In Cellulose: Molecular and Structural Biology; Brown RM, Saxena IM, Eds, Springer Dordrecht: The Netherlands
91. Czaja W, Young DJ, Kawechi M, Brown RM (2007) The future prospects of microbial cellulose in biomedical applications. Biomacromolecules 8:1–12
92. Klemm D, Schumann D, Udhardt U, Marsch S (2001) Bacterial synthesized cellulose artificial blood vessels for microsurgery. Prog Polym Sci 26:1561–1603
93. Jeon JH, Oh IK, Kee CD, Kim SJ (2010) Bacterial cellulose actuator with electrically driven bending deformation in hydrated condition. Sensor Actuat B Chem 146:307–313
94. Maria LCS, Santos ALC, Oliveira PC, Valle ASS (2010) Preparation and antibacterial activity of silver nanoparticles impregnated in bacterial cellulose. Polímeros Ciência e Tecnologia 20:72–77
95. Stroescu M, Stoica-Guzun A, Jinga SI, Dobre T, Mihaela JI, Dobre LM (2012) Influence of sodium dodecyl sulfate and cetyl trimethylammonium bromide upon calcium carbonate precipitation on bacterial cellulose Korean. J Chem Eng 29:1216–1223

96. Ul-Islam M, Ha Jung Hwan, Khan Taous, Park JK (2013) Effects of glucuronic acid oligomers on the production, structure and properties of bacterial cellulose. Carbohydr Polym 92:360–366
97. Ul-Islam M, Khattak WA, Ullah MW, Khan S, Park JK (2014) Synthesis of regenerated bacterial cellulose-zinc oxide nanocomposite films for biomedical applications. Cellulose 21:433–447
98. Ul-Islam M, Khan T, Khattak WA, Park JK (2013) Bacterial cellulose-MMTs nanoreinforced composite films: novel wound dressing material with antibacterial properties. Cellulose 20:589–596
99. Tang W, Jia S, Jia Y, Yang H (2010) The influence of fermentation conditions and post-treatment methods on porosity of bacterial cellulose membrane. World J Microb Biotechnol 26:125–131
100. Lin WC, Lien CC, Yeh HJ, Yub CM, Hsu S (2013) Bacterial cellulose and bacterial cellulose–chitosan membranes for wound dressing applications. Carbohydr Polym 94:603–611
101. Ruka DR, Simon GP, Dean KM (2013) In situ modifications to bacterial cellulose with the water insoluble polymer poly-3-hydroxybutyrate. Carbohydr Polym 92:1717–1723
102. Chen HH, Chen LC, Huang HC, Lin SB (2011) In situ modification of bacterial cellulose nanostructure by adding CMC during the growth of *Gluconacetobacterxylinus*. Cellulose 18 (1573L):1583
103. Yano S, Maeda H, Nakajima M, Hagiwara T, Sawaguchi T (2008) Preparation and mechanical properties of bacterial cellulose nanocomposites loaded with silica nanoparticles. Cellulose 15:111–120
104. Cheng KC, Catchmark JM, Demirci A (2009) Enhanced production of bacterial cellulose by using a biofilm reactor and its material property analysis. J BIOL Eng 3:12
105. Maneerung T, Tokura S, Rujiravanit R (2007) Impregnation of silver nanoparticles into bacterial cellulose for antimicrobial wound dressing. Carbohydr Polym 72:43–51
106. Hong F, Guo X, Zhang S, Han SF, Yang G, Jönsson LJ (2012) Bacterial cellulose production from cotton-based waste textiles: Enzymatic saccharification enhanced by ionic liquid pretreatment. Bioresource Technol 104:503–508
107. Hong L, Wang YL, Jia SR, Huang Y, Gao C, Wan YZ (2006) Hydroxyapatite/bacterial cellulose composites synthesized via a biomimetic route. Mater Lett 60:1710–1713
108. Nakayama A, Kakugo A, Gong JP, Osada Y, Takai M, Erata T, Kawano S (2004) High mechanical strength double network hydrogel with bacterial cellulose. Adv Funct Mater 14:1124–1128
109. Lacerda PSS, Barros-Timmons AMMV, Freire CSR, Silvestre AJD, Neto CP (2013) Nanostructured composites obtained by ATRP sleeving of bacterialcellulose nanofibers with acrylate polymer. Biomacromols 14:2063–2073
110. Yang G, Xie J, Deng Y, Bian Y, Hong F (2012) Hydrothermal synthesis of bacterial cellulose/AgNPs composite: a green route for antibacterial application. Carbohyd Polym 87:2482–2487
111. Yoon SH, Jin HJ, Kook MC, Pyun YR (2006) Electrically conductive bacterial cellulose by incorporation of carbon nanotubes. Biomacromolecules 7:1280–1284
112. Lindman B, Karlström G, Stigsson L (2010) On the mechanism of dissolution of cellulose. J Mol Liq 156:76–81
113. Lu X, Shen X (2011) Solubility of bacteria cellulose in zinc chloride aqueous solutions. Carbohydr Polym 86:239–244
114. Łaszkiewicz B (1998) Solubility of bacterial cellulose and its structural properties. J Appl Polym Sci 67:1871–1876
115. Zhang S, Luo J (2011) Preparation and properties of bacterial cellulose/alginate, blend bio-fibers. J Eng Fiber Fabr 6:69–72
116. Gao Q, Shen X, Lu X (2011) Regenerated bacterial cellulose fibers prepared by the NMMO·H2O process. Carbohydr Polym 83:1253–1256
117. Gao F (2004) Clay/polymer composites: the story. Mater Today 7:50–55

118. Dahman Y (2009) Nanostructured biomaterials and biocomposites from bacterial cellulose nanofibers. J Nanosci Nanotechno 9:5105–5122
119. Kino Y, Sawa M, Kasai S, Mito M (1998) Multiporous cellulose microcarrier for the development of a hybrid artificial liver using isolated hepatocytes. J Surg Res 79:71–76
120. Kołodziejczyk M, Pomorski L (1999) Final report on the realization of the grant no. 7 S20400407 from the Polish State Committee for Scientific Research (in Polish)
121. Oster GA, Lantz K, Koehler K, Hoon R, Serafica G, Mormino R (2003) Solvent dehydrated microbially derived cellulose for in vivo implantation. U.S. Patent 6:599–518
122. Hornung M, Biener R, Schmauder HP (2009) Dynamic modelling of bacterial cellulose formation. Eng Life Sci 9:342–347
123. Fernandes SCM, Oliveira L, Freire CSR, Silvestre AJD, Neto CP, Gandini A, Desbriéres J (2009) Novel transparent nanocomposite films based on chitosan and bacterial cellulose. Green Chem 11:2023–2029
124. Cai ZJ, Yang G (2011) Bacterial cellulose/collagen composite: characterization and first evaluation of cytocompatibility. J Appl Polym Sci 1205:2938–2944
125. Wiegand C, Elsner P, Hipler UC, Klemm D (2006) Protease and ROS activities influenced by a composite of bacterial cellulose and collagen type I in vitro. Cellulose 13:689–696
126. Cai ZJ, Hou CW, Yang G (2011) Poly (3-hydroxubutyrate-co-4-hydroxubutyrate)/bacterial cellulose composite porous scaffold: preparation, characterization and biocompatibility evaluation. Carbohydr Polym 872:1073–1080
127. Eming SA, Smola H, Krieg T (2002) The treatment of chronic wounds: current concepts and future aspects. Cells Tissues Organs 172:105–117
128. Balasubramani M, Kumar TR, Babu M (2001) Skin substitutes: a review. Burns 27:534–544
129. Slêzak A, Kucharzewski M, Franek A, Twardokês W (2004) Evaluation of the efficiency of venous ulcer treatment with a membrane dressing. Med Eng Phys 26:53–60
130. Fontana JD, de Sousa AM, Fontana CK, Torriani IL, Moreschi JC, Gallotti BJ, de Sousa SJ, Narcisco GP, Bichara JA, Farah LF (1990) Acetobacter cellulose pellicle as a temporary skin substitute. Appl Biochem Biotechnol 24(25):253–264
131. Mayall RC, Mayall AC, Mayall LC, Rocha HC, Marques LC (1990) Tratamento das ulceras troficas dos membros com um novo substitute da pele. Rev Bras Cir 80:4
132. Alvarez O, Patel M, Booker J, Markowitz L (2004) Effectiveness of a biocellulose wound dressing for the treatment of chronic venous leg ulcers: results of a single center randomized study involving 24 patients. Wounds 16:224–233
133. Frankel VH, Serafica GC, Damien CJ (2004) Development and testing of a novel biosynthesized XCell for treating chronic wounds. Surg Technol Int 12:27–33
134. Watanabe K, Eto Y, Takano S, Nakamori S, Shibai H, Yamanaka S (1993) A new bacterial cellulose substrate for mammalian cell culture: a new bacterial cellulose substrate Cytotechnology 13:107–114
135. Deng HW, Liu YZ (2005) Current topics in bone biology. World Scientific, Hackensack, pp 125–128
136. Zimmermann KA, LeBlanc JM, Sheets KT, Robert W, Gatenholm FP (2011) Biomimetic design of a bacterial cellulose/hydroxyapatite nanocomposite for bone healing applications. Mater Sci Eng C 31:43–49
137. Bäckdahl H, Helenius G, Bodin A, Nannmark U, Johansson BR, Risberg B, Gatenholm P (2006) Mechanical properties of bacterial cellulose and interactions with smooth muscle cells. Biomaterials 27:2141–2149
138. Bäckdahl H, Esguerra M, Delbro D, Risberg B, Gatenholm P (2008) Engineering microporosity in bacterial cellulose scaffolds. J Tissue Eng Regenerative Med 2:320–330
139. Entcheva E, Bien H, Yin L, Chun CY, Farrell M, Kostov Y (2004) Functional cardiac cell constructs on cellulose-based scaffolding. Biomaterials 25:5753–5762
140. Cho S, Almeida N (2012) Dietary fiber and health. CRC Press, Boca Raton
141. Shi Z, Zhang Y, Phillips GO, Yang G (2014) Utilization of bacterial cellulose in food. Food Hydrocolloids 35:539–545

142. Phisalaphong M, Chiaoprakobkij N (2012) Applications and products-dNata de coco. Bacterial nanocellulose: a sophisticated multifunctional material. CRC Press, Boca Raton 9:143
143. Lin KW, Lin HY (2004) Quality characteristics of Chinese-style meatball containing bacterial cellulose (Nata). J Food Sci 69:107–111
144. Xiao L, Mai Y, He F, Yu L, Zhang L, Tang H, Yang G (2012) Bio-based green composites with high performance from poly (lactic acid) and surface modified microcrystalline cellulose. J Mater Chem 22:15732–15739
145. Choi YJ, Ahn Y, Kang MS, Jun HK, Kim IS, Moon SH (2004) Preparation and characterization of acrylic acid-treated bacterial cellulose cation-exchange membrane. J Chem Technol Biot 79:79–84
146. Jantarat C, Tangthong N, Songkro S, Martin GP, Suedee R (2008) S-Propranolol imprinted polymer nanoparticle-on-microsphere compositeporous cellulose membrane for the enantioselectively controlled delivery of racemic propranolol. Int J Pharm 349:212–225
147. Bodhibukkana C, Srichana T, Kaewnopparat S, Tangthong N, Bouking P, Martin GP, Suedee R (2006) Composite membrane of bacterially-derived cellulose and molecularly imprinted polymer for use as a transdermal enantio selective controlled-release system of racemic propranolol. J Control Release 113:43–56
148. Okahisa Y, Yoshida A, Miyagushi S, Yano H (2009) Optically transparent wood cellulose nanocomposite as a base substrate for flexible organic light emitting displays. Compos Sci Technol 69:1958–1961
149. Shah J, Brown RM Jr (2005) Towards electronic displays made from microbial cellulose. Appl Microbiol Biotechnol 66:352–355
150. Legnini C, Vilani C, Calil VL, Barud HS, Quirino WG, Achete CA, Ribeiro SJL, Cremona M (2008) Bacterial cellulose membrane as flexible substrate for organic light emitting devices. Thin Solid Films 517:1016–1020
151. Hu W, Chen S, Yang Z, Liu L, Wang H (2011) Flexible electrically conductive nanocomposite membrane based on bacterial cellulose and polyaniline. J Phys Chem B 115:8453–8845
152. Basta AH, El-Saied H (2009) Performance of improved bacterial cellulose application in the production of functional paper. J Appl Microbiol 107:2098–2107
153. Nogi M, Handa K, Nakagaito AN, Yano H (2005) Optically transparent bionanofiber composites with low sensitivity to refractive index of the polymermatrix. Appl Phy Lett 87:243110. doi:10.1063/1.2146056
154. Cai Z, Kim J (2010) Bacterial cellulose/poly (ethylene glycol) composite: characterization and first evaluation of biocompatibility. Cellulose 17:83–91
155. Luo H, Xiong G, Huang Y, He F, Wang Y, Wan Y (2008) Preparation and characterization of a novel COL/BC composite for potential tissue engineering scaffolds. Mater Chem Phys 110:193–196
156. Pinto RJB, Marques PA, Martins MA, Neto CP, Trindade T (2007) Electrostatic assembly and growth of gold nanoparticles in cellulosic fibres. J Colloid Interface Sci 312:506–512
157. Zhang T, Wang W, Zhang D, Zhang X, Ma Y, Zhou Y et al (2010) Biotemplatedsynthesis of gold nanoparticle–bacteria cellulose nanofiber nanocomposites and their application in biosensing. Adv Funct Mater 20:1152–1160
158. Wan YZ, Huang Y, Yuan CD, Raman S, Zhu Y, Jiang HJ, He F, Gao C (2007) Biomimetic synthesis of hydroxyapatite/bacterial cellulose nanocomposites for biomedical applications. Mater Sci Eng, C 27(4):855–864
159. Perotti GF, Barud HS, Messaddeq Y, Ribeiro SJL, Constantino VRL (2011) Bacterial cellulose-laponite clay nanocomposites. Polymer 52(1):157–163
160. Mathew AP, Oksman K, Pierron D, Harmand M-F (2012) Fibrous cellulose nanocomposite scaffolds prepared by partial dissolution for potential use as ligament or tendon substitutes. Carbohydr Polym 87(3):2291–2298

161. Pooyan P, Tannenbaum R, Garmestani H (2012) Mechanical behavior of a cellulose-reinforced scaffold in vascular tissue engineering. J Mech Behav Biomed Mater 7:50–59
162. Wang Y Chen L (2011) Impacts of nanowhisker on formation kinetics and properties of all-cellulose composite gels. Carbohydr Polym 83:1937–1946
163. Son WK, Youk JH, Park WH (2006) Antimicrobial cellulose acetate nanofibers containing silver nanoparticles. Carbohydr Polym 65:430–434
164. Charpentier PA, Maguire A, Wan WK (2006) Surface modification of polyester to produce a bacterial cellulose-based vascular prosthetic device. Appl Surf Sci 252(18):6360–6367

Chitin-Based Nanocomposites: Biomedical Applications

Carlos Filipe Cidre João, Jorge Carvalho Silva and João Paulo Borges

Abstract Chitin, the second most abundant polymer in nature, is a renewable, nontoxic, biodegradable, and antibacterial polysaccharide. This semicrystalline biopolymer exhibits hierarchical structure from nano to micro-scale and is responsible for interesting living tissue properties. Recently, the scientific interest in chitin nanofibrils for applications in biomedical and tissue engineering fields has increased due to their particular capabilities such as matrix reinforcements, bioactivity and morphology similar to natural tissues. This chapter is focused on composite materials reinforced with chitin nanofibrils and their biomedical applications.

Keywords Chitin · Nanofibrils · Nanowhisker · Biomaterials · Tissue engineering

1 Introduction

The Tissue Engineering and Regenerative Medicine fields have aimed, since their inception, at developing new therapeutic solutions based on materials that might present advantages in promoting tissue repair and regeneration. Among the available options, polymers emerged as valuable materials due to their ease of fabrication, structural control, low cost and availability [45, 48, 49].

Concomitantly, the importance of renewable, biodegradable and eco-friendly materials has been emphasized due to shortage of natural resources, increasing energy demand and exhaustion of nonrenewable fuels [36, 44], which has triggered researchers to explore the use of polysaccharides (cellulose, chitin/chitosan, starch, alginate) and animal protein-based biopolymers (gelatin, wool, silk, collagen) as materials for new bioapplications [48].

C.F.C. João · J.C. Silva · J.P. Borges (✉)
CENIMAT/I3N, Departamento de Ciência Dos Materiais, Faculdade de Ciências e Tecnologia - FCT, Universidade Nova de Lisboa, 2829-516 Caparica, Portugal
e-mail: jpb@fct.unl.pt

V.K. Thakur and M.K. Thakur (eds.), *Eco-friendly Polymer Nanocomposites*, Advanced Structured Materials 74, DOI 10.1007/978-81-322-2473-0_14

Cellulose and chitin (Fig. 1) are the first and second most abundant natural origin biomaterials and therefore have been extensively considered whenever bio-based polymers from renewable sources were sought. Cellulose is found primarily in plants and is a linear chain of ringed glucose molecules (poly-β-(1 → 4)-D-glucosamine units) with a flat ribbon-like conformation [30]. During biosynthesis, the hydrogen bond between hydroxyl groups and oxygen of adjacent molecules induces the formation of a parallel stacking of multiple cellulose chains. The continuous packing of the long chains gives rise to the formation of hierarchic structures starting from elementary fibrils and going to macro-fibers. Cellulosic fibers have been extracted from different sources (wood, plant, tunicate, algae, bacterial) and considered with different purposes. Its main use as reinforcement is due to easy renewability, biodegradability, availability, high toughness, low specific gravity, acceptable specific strength and enhanced energy recovery [4, 9, 46].

Chitin is a polysaccharide structurally similar to cellulose with huge biological and chemical attributes. Composed of poly-β-(1 → 4)-*N*-acetyl-D-glucosamine

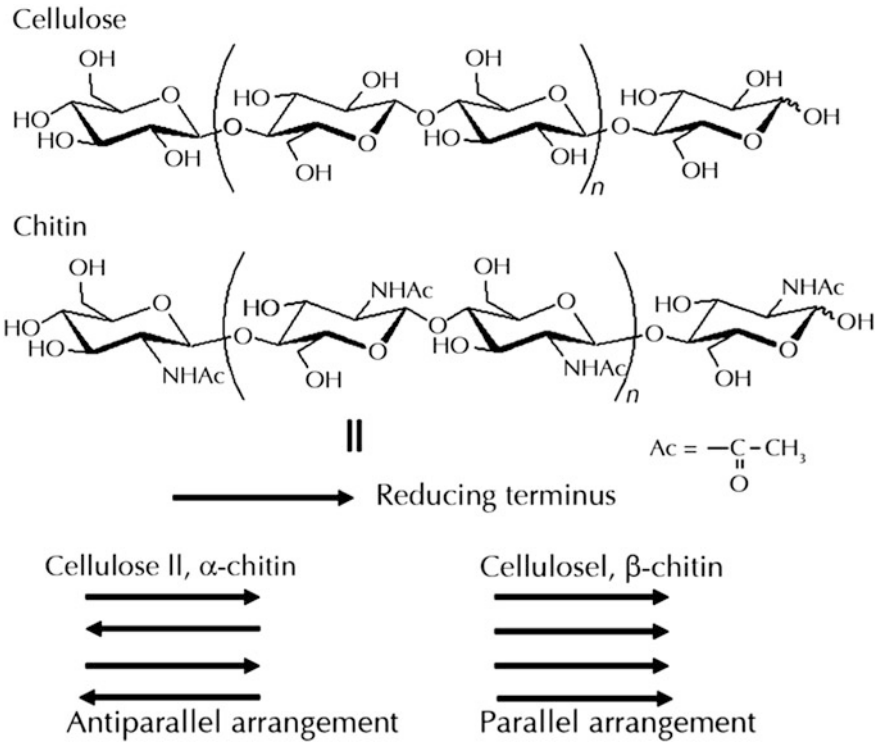

Fig. 1 Cellulose and chitin chemical and crystalline structure. From [5]

units (Fig. 1), it is found mainly in the exoskeleton of crustaceans and insects but also in mollusks and fungi [33]. Because of its linear structure with two hydroxyl groups and an acetamide group, chitin is predominantly crystalline with strong hydrogen bonding.

Notwithstanding their substantial applicability, native cellulose and chitin are somehow limited regarding properties, functionality, durability and uniformity required for the fulfillment of society's demand for high performance materials. For this reason, researchers have dedicated attention to the highly crystalline regions that compose these natural fibers—nanofibrils—to prepare nanoscaled polymeric assemblies [30]. Cellulose and chitin nanofibrils are anisotropic particles with high degree of biodegradability that exhibit extremely high modulus and strength along their axes, allowing also facile chemical modifications of their surfaces.

A large number of works have been developed involving nanocrystalline cellulose, also known as cellulose nanowhiskers or cellulose nanofibrils, which exhibit properties such as lightweight, stiffness, nontoxicity, transparency, low thermal expansion, gas impermeability, and outstanding mechanical properties. Electronic/optoelectronic, food, paper, packaging, medical, and pharmaceutical markets have all benefited from the advantages of applying cellulose nanofibrils in products like displays, sensors, intelligent windows, flavor carriers, suspension stabilizers, improvement of paper's mechanical properties, barriers in greaseproof-type papers, antimicrobial films, water absorbent pads, excipients, and biocoatings [10].

Also, an interesting feature has been explored regarding the self-assembly of anisotropic nanofibrils when in suspension. Liquid crystalline behavior of the rod-like cellulose nanowhiskers led to interesting studies based on cholesteric lyotropic mesophases [8, 11, 24]. The possibility of using nanofibrils' self-assembly to recreate the natural arrangement of fibrous proteins in living tissues opens a new and promising avenue regarding the production of biomimetic materials for tissue regeneration [6, 7, 40].

Cellulose and chitin show significant resemblance, the reason that the scientific community has been exploring chitin nanofibrils' capabilities supported by the knowledge of cellulose nanocrystalline production and application. In this chapter we invite the reader to become acquainted with and understand chitin nanofibril's potential in the production of biomedical and tissue engineering products.

2 Chitin: Structure and Properties

As a biomaterial, chitin is nontoxic, antimicrobial, biocompatible, bioabsorbable, and shows low antigenicity with the ability to induce healing effects, which make it a good candidate for applications in the biomedical and tissue engineering fields [54]. The largest chitin source for biomedical applications is the food industry waste, including shells of crabs and shrimps chemically treated and purified.

In living tissues, chitin generally appears as ordered semicrystalline fibrils that can create complex hierarchical architectures within multiple length scales (nano to micro) from simple molecules to composites.

First, chitosomes promote chitin synthesis through polymerization of glucosamine units. Depending on the species and molecular chain orientation, this biopolymer can be polymorphic originated as either α, β or γ - *chitin* [15]:

- α-chitin, present in shrimps and crabs, is the most stable and common form. The polymer units are disposed antiparallel (similar to cellulose type II) allowing maximum connection between the macromolecules through hydrogen bonds. This induces formation of strong and highly stable fibrils with crystallinity higher than 80 %.
- *β-chitin,* founded in squids, has its molecular units aligned parallel (similar to cellulose type I). Fibrils can reach 70 % crystallinity. A bigger distance between molecules makes it more reactive and more susceptible to dissolution in solvents. It can also reach a higher hydration degree which allows the formation of more flexible tissues.
- *γ-chitin* consists of a combination of α and β with the assembling of two parallel chains alternately, with one antiparallel chain.

The aggregation of 18–25 native chitin chains promotes the formation of fibrils, exhibiting a rod-like or spindle-like morphology of length approximately 300 nm and diameter 2–5 nm (Fig. 2). High crystalline chitin (which can be obtained by amorphous region dissolution after acid hydrolyses) is often called ***chitin whiskers***, ***chitin nanocrystals,*** or ***chitin nanofibrils*** (**CTN**). In the following sections, synthesis methods, characterization and applications of chitin nanofibrils are presented.

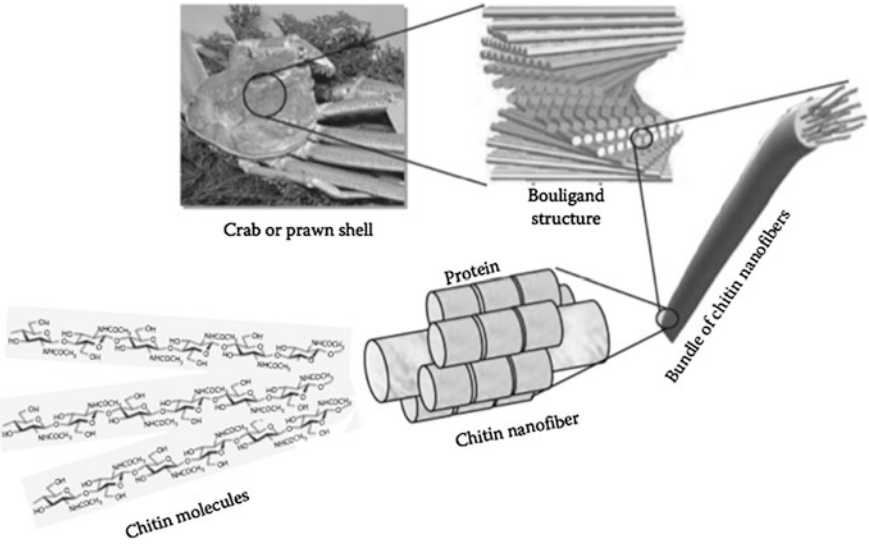

Fig. 2 Schematic of chitin hierarchical architecture in crabs. From [23]

Nanofibrils tend to group in clusters of polymer and proteins, which lead to the formation of long bundles of nanofibrils of diameter length 50–350 nm. These filaments distribute themselves parallel and equidistant to each other in long range of piled layers whose stacking levels rotate in periodic and small constant angles. When observed under polarized light microscopy the resulting structures reveal textures analogous of cholesteric liquid crystals, as a consequence of the molecular self-assembly, which suggests that tissue formation involves liquid crystalline states of matter.

Finally, the organic tissue loses its fluidity with the increase of rigidity through molecular cross-linking and calcification [12]. The tissue thus formed by this hierarchical organized setup achieves a unique combination of properties like stiffness and strength with low weight and crack deflection.

3 Chitin Nanofibrils

3.1 Synthesis and Characterization of Chitin Nanofibrils

A large number of natural nanofibrils like collagen, fibroin, keratin, and cellulose are already known to the scientific community, which has developed several methods for fibril extraction from bulk material. Due to the similarity with cellulose, many authors have applied analogous protocols for chitin nanofibril synthesis. The main approach consists in chitin hydrolysis either by acidic and/or enzymatic activity.

Although chitin treatment process can differ depending on its origin (crab shell, prawn shell, mushrooms, etc.), there are common steps to achieve the nanofibrils state, including extraction of chitin from the natural source, purification trough mineral and protein removal and isolation of the nanocrystals (Fig. 3).

Fig. 3 Schematic of chitin nanofibrils production

Food wastes remain the main source to obtain this polymer. Alongside to chitin (20–30 %), shrimps and crab wastes also contain proteins (30–40 %), calcium carbonate (30–50 %), lipids, and astaxanthin (<1 %) [59].

To extract chitin, the wastes are ground and treated with acid (hydrochloride or acetic) in order to remove all mineral and inorganic content. Then the resultant suspension is stirred, filtered, and washed with water several times before adding KOH to promote deproteinization. Alternative methods like enzymatic treatment (proteases) can also be applied in protein removal and chitin extraction [57]. The dissolution of pigments is achieved by adding an $NaClO_2$ aqueous solution [56]. Following this the samples are washed and centrifuged with ethanol and water and finally dried (heat, vacuum or freeze-drying) originating chitin flakes.

In order to achieve the nanowhisker state, the chitin flakes are subjected to a hydrolysis process involving an acid bath for a specific and well-defined combination of temperature and time. This process allows the dissolution of chitin amorphous content, when compared to the crystalline fibril content, due to the faster swelling and hydrolysis. In Table 1 the main procedures for chitin fibrils production are referenced, sorted by chitin source, fibrillation process, temperature, and time of hydrolysis and results of the procedures. Depending on source and hydrolysis condition parameters, fibrils with different diameters and lengths can be obtained, ranging from tens to hundreds of nanometers. The most used fibrillation process is performed with 3 N hydrochloric acid (HCL) at temperatures near HCL boiling point (104 °C) during periods of time close to 90 min.

After the acidic treatment, the chitin solution is centrifuged and the supernatant CTN suspension is dialyzed against distilled water to adjust pH. Depending on further use, chitin can be freeze-dried and recovered as cotton-like samples (as a result of the aggregation of millions of nanofibrils) or even kept as liquid suspensions (that can result in liquid crystalline solutions due to the self-assembly of the anisotropic chitin nanofibrils). In Figs. 4 and 5, typical scanning electron microscopy (SEM) and transmission electron microscopy (TEM) images of chitin nanofibrils are shown.

3.2 Chitin Nanofibrils for Biomedical Applications

Chitin nanowhiskers have been attracting growing interest for different applications like drug delivery [23], cosmetic [31], adsorbents in industry, and water purification or even protein biosensors [29]. A great number of nanofibers, nanoparticles, and nanocomposites have been developed using chitosan/chitin [18, 34]. In this section special attention will be given to the high crystalline region of chitin—chitin nanofibril—used in the development of scaffolds, hydrogels, drug release systems for wound healing, and in biomedical and tissue engineering applications.

Thanks to their size, mechanical strength, and relevant biological properties, CTN have been majorly applied as nanofillers in the reinforcement of both natural and synthetic composites [59].

Table 1 Chitin nanofibrils: source, fibrillation method, hydrolysis conditions, and fibrils characterization

Chitin Nanofibrils							
ID	Source	Fibrillation	Hydrolysis temperature/time	Length (nm)	Diameter (nm)	Aspect ratio	Reference
1	Crab	HCL	40 °C/60 min	–	–	–	[28]
2		HCL	90 °C/90 min	240	15	16	[14]
3		HCL	104 °C/90 min	500 ± 50	50 ± 10	10	[27]
4		Acetic Acid + Grinder	–	10–20	–	–	[17]
5		HCL	104 °C/90 min	200–500	5–20	15– 20	[56]
6		HCL	120 °C/360 min	255 ± 56	31 ± 6	8	[16]
7		HCL	95 °C/90 min	240	18	13	[50]
8		HCL	104 °C/90 min	200	15	13	[60]
9		Acetic Acid + Grinder	–	–	25–40	–	[42]
10	Shrimp	HCL	104 °C/90 min	417	33	17	[43]
11		HCL	104 °C/360 min	427	43	10	[55]
12		HCL	90 °C/90 min	200–500	10–15	20–33	[13]
13		HCL	105 °C/180 min	200–560	18–40	18	[39]
14		HCL	104 °C/360 min	343	46	8	[52]
15		HCL	-/360 min	300	20	15	[19]
16		HCL	120 °C/360 min	549	31	18	[21]
17	Squid	HCL	-/90 min	150	10	15	[38]
18	Riftia	HCL	104 °C/90 min	2200	18	120	[32]

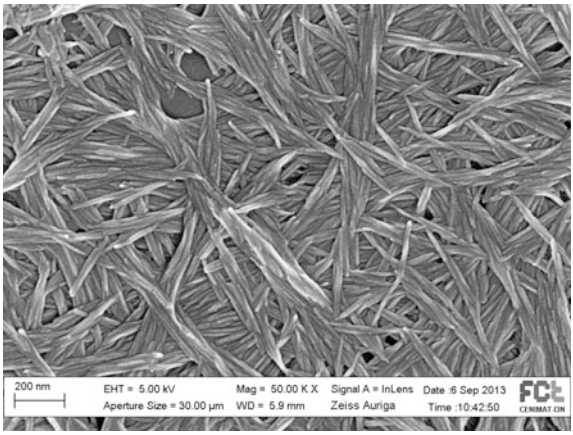

Fig. 4 SEM image of chitin nanobrils (shrimp). Scale bar 200 nm

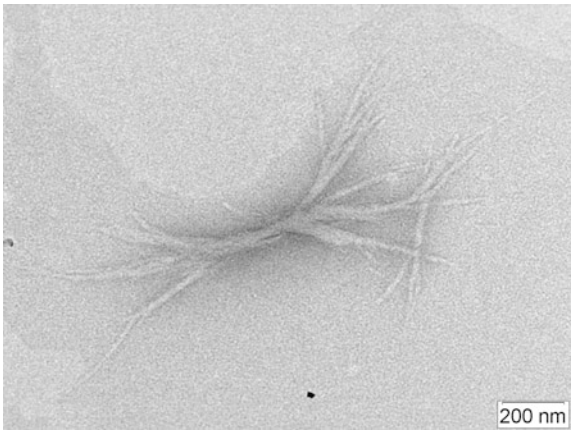

Fig. 5 TEM image of chitin nanofibrils (shrimp). Scale bar 200 nm

Morin and Dusfrene [29] developed solid films of policaprolactone (PCL) and chitin whiskers that highlighted the use of chitin nanofibril as fillers in different nanocomposites. Gopalan et al. [14] reinforced natural rubber with chemically modified CTN; Lu et al. [27] developed soy protein insulating thermoplastics with chitin nanofibers; Sriupayo et al. [43], produced chitosan films reinforced with chitin whiskers. Araki et al. [2] constructed chitosan hydrogels with rod-like chitin, Junkasem et al. [21, 22] produced electrospun nanofibers of composite CTN and polyvinylalcohol, Yudin et al. [58] fabricated composite chitosan and CTN fibers by wet spinning.

It was generally concluded that, at critical concentrations, nanofibrils form a percolation network where the fibril aspect ratio and high crystalline morphology play an important role as they influence the mechanical properties, allowing a higher performance of the resulting composite. At the same time, the CTN were responsible for swelling capacity decrease, enabling a more stable behavior in

aqueous environments, and also for increasing the glass transition temperature compared to the matrix.

Wongpanit et al. [55] studied the nanofiller influence of chitin whisker on the dimensional stability of silk fibroin sponges and tested its feasibility for tissue engineering applications with fibroblast-like cells. Aqueous suspensions of 4, 63 wt % chitin nanofibrils (Table 1—ID 10) were added to silk solutions in a proportion of 0, 1/8, 2/8 and 4/8 CTN/silk ratio. To produce the sponges, ultrasonication and mechanical stirring were applied to ensure complete solution homogenization, before freezing the samples at −40 °C overnight followed by freeze-drying at 10 Pa for 24 h. The sponges generated by this method were morphologically characterized by SEM revealing an interconnected pore network as a result of ice crystals removal, with 150 μm average pore size. Mechanical behavior was evaluated with compressive tests that have shown that mechanical properties were substantially enhanced by hydrogen bonding between the matrix and the chitin nanofibrils. The biological tests performed after seeding L929 cells on the sponges demonstrated that after 24 h, cell spreading was enhanced in the composite sponges (64 %) compared to initial silk fibroin sponge (31 %).

Phongying et al. [39] undertook the task of building a chitosan scaffold by direct transformation of chitin whiskers into its co-polymer. CTN were obtained after acid hydrolysis of chitin flakes (Table 1—ID 13) and then lyophilized to obtain solid CTN. Posterior to this the nanofibrils were treated with 40 % wt/v NaOH aqueous solution to promote deacetylation and transformation into chitosan. Different reaction temperatures (100–180 °C) and time (7–28 h) were applied to measure the influence on the deacetylation degree and molecular weight. FTIR analysis confirmed higher crystallinity of CTN compared with chitin flakes, although the opposite occurred for the CTN treated with NaOH, explained by the existence of amorphous regions typical of chitosan. SEM observation has shown that lyophilization induced the formation of a fibrous network of deacetylated CTN (chitosan) of pore diameter approximately 200 nm.

Watthanaphanit et al. [52] fabricated a nanocomposite wound-dressing material with CTN and alginate through wet spinning. With this combination researchers were seeking mechanical properties improvement and a faster wound healing process caused by the release of CTN present in the composite after enzymatic degradation by lysozyme. Chitin nanofibrils, prepared by acid hydrolysis (Table 1—ID 14), were added to a 6 % wt/v sodium alginate aqueous solutions in proportions of 0, 05–2, 00 wt% CTN. The final mixtures were extruded through a 30 holes spinneret in a first coagulation bath of 5 % wt/v $CaCl_2$ in 50 % v/v methanol aqueous solution and a second coagulation bath of 100 % methanol.

SEM images revealed an increase of roughness in the fibers surface with increase of CTN content due to nanofibrils aggregation. The evaluation of fiber's mechanical and thermal properties led to the conclusion of an existence of plateau region. The composite fibers present an increase of mechanical and thermal properties due to hydrogen bonding and electrostatic interactions between alginate molecules and CTN until a maximum CTN content is reached. After that, natural aggregation of CTN occurs decreasing the ability of the matrix to transfer the stress to fibrils and

also increasing the ionic radius between the alginate molecules and the CTN aggregates, thus reducing the restriction in the motion of alginate molecules. Biodegradability tests were conducted for 5 days in two different media of Tris-HCL buffer solution and buffer solution containing lysozyme. The presence of CTN accelerated the biodegradability of the composite fibers in buffer solution containing lysozyme mainly because of the partial degradation of CTN, although toughness values increased in the Tris-HCL buffer solution due to Ca^{2+} diffusion into the fibers, responsible for further cross-linking.

Later, and based on this work, Watthanaphanit et al. [53] also produced alginate/chitosan whiskers composite fibers by wet spinning, acetylating the CTN (average dimensions: length = 309 nm, width = 64 nm, aspect ratio = 4.8) to obtain its co-polymer. This alternative fiber also achieved great results as effectual wound dressing since the incorporated CS whisker could be released to the medium thanks to surface erosion, conferring antibacterial activity against microbial pathogens Gram-positive S. *aureus* and Gram-negative E. *coli*.

Muzzarelli et al. [35] developed wound healing applications based on chitin nanofibrils/chitosan and glycolate composites. They formulated three types of products: spray (97, 5 % CTN suspension; 0, 56 % glycolic acid; 0, 97 % chitosan and 0, 40 % chlorhexidine); gel (91, 1 % CTN suspension, 3, 13 % glycolic acid; 4, 81 % chitosan, 0, 40 % chlorhexidine and sodium hydroxymehtylglycinate) and gauze (0,8 g dibutyril chitin nonwoven, 1.0 % chitosan glycolate solution containing CTN (2 g/l) and 0,4 % chlorhexidine.

After implantation in the murine model for 7 days and gathering the morphological and immunohistochemical data, researchers concluded that spray could be applied as first aid tool for abrasions with little bleed; the gel was capable of enhancing physiological repair in particular areas with thin epidermal layer; and the gauze had excellent results in effective skin repair with scarless epidermis. Moreover, the gauze was clinically tested in hospitalized patients with diverse traumatic wounds and the results of treatment were considered as satisfactory.

Hariraksapitak and Supaphol [16] developed bone scaffolds through freeze-drying, from a combination of hyaluronan (HA) and gelatin (GEL) with the incorporation of α-chitin whiskers (Table 1–ID 6). Solutions of 2 wt% polymer in deionized water containing 50/50 % HA and GEL were used to prepare mixtures incorporating CTN at 0, 2, 5, 10, 20, and 30 % (w/w). The final solutions were introduced in specific molds and lyophilized at −50 °C for 24 h in order to produce cylindrical (10 mm diameter and 2 mm height) and disk shaped (1 mm thickness) structures. The scaffolds were characterized regarding their microstructure, mechanical properties, water-retention capacity, in vitro degradation, thermal analysis, and biological evaluation. Observation of SEM images has shown that all scaffolds preserved a well-defined porous structure with pores averaging 139 μm at transverse section and 166 μm at longitudinal section. Researchers also verified that scaffolds' mechanical properties were enhanced by increase of chitin nanofibrils content, although a maximum value of elasticity modulus was reached at 2 % CTN. The increase of CTN also gave higher thermal stability and lower biodegradation. Human osteosarcoma cells (SaOS-2) were seeded on the structures. Cytotoxicity

and in vitro response was evaluated revealing good cell adhesion and proliferation with best results in scaffolds containing 10 % CTN.

Yamamoto et al. [54] developed an inorganic/organic hydrogel inspired on the biomineralization of liquid crystalline chitin nanofibrils. Suspensions of CTN (Table 1—ID 5) and aqueous solution of poly (acrylic acid) with calcium chloride ($CaCl_2$) were placed together in a chamber containing a vial of ammonium carbonate, for 30 days.

Under cross-polarized optical microscopy the suspensions exhibit isotropic and liquid-crystalline mesophases around 5.3 wt% CTN, reaching a complete liquid crystalline state around 11.3 wt%. After introducing the suspensions in the ammonium chamber, an automatic conversion to gel (Fig. 6) was verified with the maintenance of the liquid-crystalline character. Fingerprint textures, typical of cholesteric liquid crystals were observed with spaces between fringes of 20–30 μm.

The chitin gels were immersed in the aqueous solution of $CaCl_2$ and after 3 days spherical $CaCO_3$ crystals appeared on the surface of the gels. Laser Raman spectra confirmed no existence of amorphous $CaCO_3$. After 30 days of experiment the gel matrix was completely filled with the calcium carbonate crystals, completing the production of hybrid $CaCO_3$/CTN hydrogels (Fig. 7).

Zhang et al. [60] developed cyclodextrin (CD) hydrogels with three kinds of polysaccharide nanofillers—cellulose, chitin, and platelet-like starch—with the objective of increasing mechanical properties and to regulate the drug release behavior of these structures. Chitin nanofibrils (Table 1—ID 8) were added to α-CD aqueous solutions in concentrations of 0.1, 0.5, 1.0, and 2.5 wt%. Biological assays performed with mouse muscle cell line L929 showed that the chitin composite hydrogels did not add cytotoxicity to the structure compared to CD hydrogel. The presence of polysaccharide fillers enhanced the mechanical properties and contributed to creation of a permanent network within the hydrogel, increasing strength

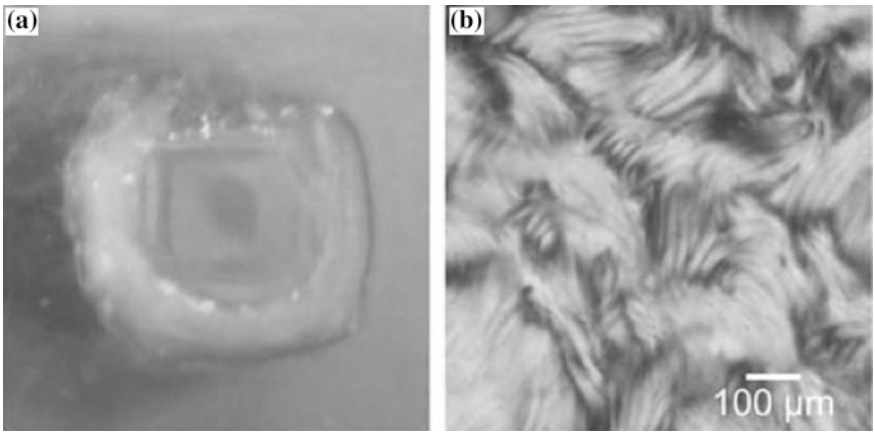

Fig. 6 Images of cholesteric chitin gel. **a** Photograph, **b** Polarized optical micrograph image. From [54]

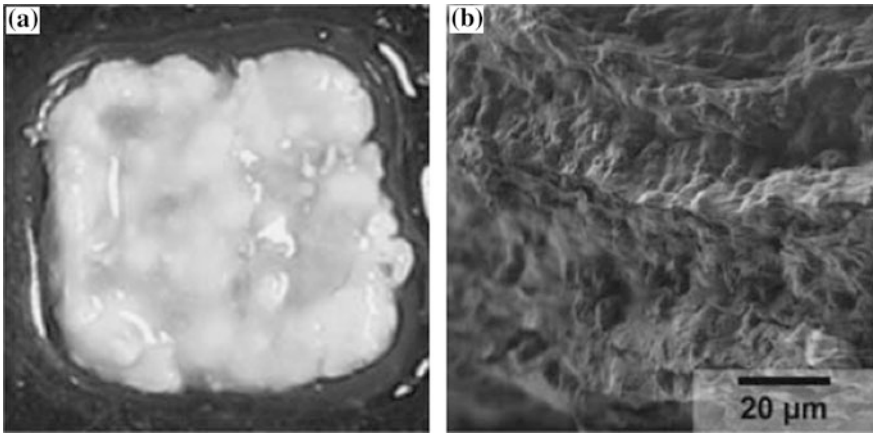

Fig. 7 Images of mineralized chitin gel. **a** Photograph **b** SEM image. From [54]

and rigidity. Shear-thinning and thermo-sensitive properties were also improved. The gelation process was faster and the retention of bovine serum albumin was more efficient compared to native CD hydrogel, indicating the potential use as injectable smart delivery biomaterial.

Lin et al. [26] investigated a new drug release product also using the three polysaccharide nanofillers integrated with alginate-based microspheres. Chitin nanofibrils (dimensions: length = 200–300 nm, width = 10–20 nm, aspect ratio = 20) suspensions were prepared in deionized water in which the same amount of sodium alginate (SA) was added to produce stock solutions of 2 wt% SA. In order to obtain the microspheres, the stock solution was injected in a 10 wt% $CaCl_2$ aqueous solution (promoting crosslinking) and the resulting product was washed with distilled water to remove non-reacting free Ca^{2+}.

Nanocomposite microspheres thus obtained were of diameter 3500 ± 50 µm in wet condition but 900 ± 20 µm after drying. With addition of CTN, the alginate microspheres exhibit higher values of storage modulus (G') and loss modulus (G'') confirming fibril reinforcing function. Morphologically, composite microspheres exhibit smoother surface and nonexistence of cracks compared to the wrinkled surface and cracked aspect of single alginate microspheres, suggesting that nanofibrils were responsible for adhesion and structural integrity.

Drug encapsulation efficiency was tested with theophylline (TP). Results demonstrated that nanofibrils had the capacity to induce more than 55 % encapsulation due to creation of a dense 3D network that behaved as a barrier, retaining more quantity of TP. The nanofibrils were also responsible for changing the in vitro drug release profile, evidencing a 3-step regime with lower, faster, and equilibrium releases. Despite having lower release at the beginning, composite microspheres were able to achieve higher accumulative release at the end of equilibrium stage by restricting the motion of SA molecules and consequently improving the drug load and controlled release action.

Shervani et al. [42] conducted a series of experiments where the combination of chitin nanofibrils (Table 1—ID 9) and gold nanoparticles was explored with possible applications in different fields like cosmetics and pharmaceutics. Researchers prepared suspensions of CTN (16 wt%) in which they added Au nanoparticles. After stirring and sonication, sheets of films, flakes, and powder were produced. To prove CTN—Au nanoparticles adhesion, characterization techniques like TEM, SEM, X-ray diffraction, and UV-spectra were used. Results indicated that 56 % polymer and 100 % nanoparticles phase transferred from polymer water solution to CTN suspension and that phase transfer phenomena was responsible for CTN–Au composite formation.

Ji et al. [19, 20] questioned the limitation of dispersing chitin nanofibrils only in aqueous solvents and produced composites of CTN and policaprolactone in non-aqueous medium. CTN (Table 1—ID 15) powders were first dispersed in deionized water and then the water was exchanged by acetone. The resulting CTN was finally dispersed in trifluoroethanol (TFE), the same solvent used for PCL dissolution. Cross-polarized optical microphotographs of CTN (0, 1 % w/v) dispersed in water and TFE revealed the existence of birefringent domains in both cases. In more concentrated suspensions (5 % w/v) fingerprint and band texture appeared, characteristic of cholesteric liquid crystal, proving that CTN could self-assemble in both solvents.

The two polymers were mixed at different mass ratios of 5:95, 10:90, 15:85, 20:80, 25:75, and 30:70 CTN/PCL. The final composite solution was used for production of films and electrospun fibers that were characterized regarding its wettability (static-water-contact-angle analysis), morphology (SEM), thermal (differential scanning calorimetry with thermogravimetric analysis—DSC/TG), mechanical (DMA), and biological properties.

Through micrographs and dynamic mechanical analysis (DMA) it was possible to conclude that CTN organize themselves differently in films and fibers. In films the nanofibrils form a rigid network caused by mutual interactions, while in fibers the CTN dispose themselves within the fiber and along the fiber's long axis. Significant fiber diameter decrease occurred compared to PCL fibers. Like previous works reported in this chapter, CTN was responsible for higher crystallinity degree conducting to mechanical properties improvement. Despite the fact that PCL is hydrophobic the electrospun composite fibers have shown hydrophilic behavior for CTN content greater than 25 wt%.

To perform biological evaluation, human dermal fibroblasts (hDF) were seeded on different disks (10 mm diameter) of fiber mat. Considering micrographs of scaffolds cross-section after 14 days of culture, the cells spread along the surface and migrated through the scaffold interior. Nevertheless, the fiber scaffold had smaller pores than cell size; the hDF penetrated more easily the composite scaffold probably because of lower hydrophobicity and higher wettability, facilitating adhesion and infiltration.

Azuma et al. [3] tested the anti-inflammatory and anti-fibrosis properties of chitin nanofibrils in inflammatory bowel disease mice model. For the experiments, C57BL/6 mice were used as model for dextran sulfate sodium (DSS)-induced acute

ulcerative colitis. Gels of 1 % α-chitin nanofibrils in 0, 3 % acetic acid aqueous solutions were administered at the site of injury.

Characterization was performed through quantitative digital morphometric analysis of extracellular matrix and immunohistochemical detection of nuclear factor-*K*B (NF-*K*B) in the colon. Results have shown that CTN gels suppressed clinical symptoms and tissue injury of the colon by decreasing serum MCP-1 (monocyte chemotactic protein 1) expression and NF-*K*B (nuclear factor-kB) activation. Likewise, CTN suppressed the fibrosis process with a decrease in collagen formation.

Rodriguez et al. [41] reported a preliminary study of an innovative bone scaffold based on gelatin sponges filled with hydroxyapatite (HAp), chitin nanofibrils and platelet-rich plasma (PRP). The introduction of the HAp and CTN fillers was designed to increase structural strength while PRP had the purpose of enhancing scaffold bioactivity.

To produce the scaffolds, solutions of 30 mg/ml gelatin in deionized water were used as base in which mixtures of 10 mg/ml of HAp, CTN, and PRP were added. After a cycle of slow freezing at −15 °C overnight, −20 °C for 4 h and −70 °C for another 4 h, the composites were lyophilized for 24 h, giving origin to gelatin/PRP/HA/CTN sponges.

In vitro tests were performed with MG-63 osteoblast-like cell line seeding on the proposed scaffolds. Further analysis demonstrated that sponges' absorption capacity was capable of eliciting cell infiltration into the scaffolds and controlled proteins release. Moreover, the composite was able to induce osteogenesis with cell-created mineral matrix.

Ang-atikarnkul et al. [1] fabricated bionanocomposite sponges of cellulose nanofibers (CN)/chitin whisker (CTN)/silk sericin (SS) and studied the potential for wound care application. Suspensions of CN, CTN, CN/CTN, and CN/CTN/SS were prepared with different composite mass ratios, poured into cell culture plates, and subjected to freeze-drying followed by cross-linking with gluraldehyde.

TEM images of the suspensions showed needle-like CN averaging width 7.3 nm and length 400 nm, with aspect ratio of 55. CTN with rod-like aspect averaged width 27, 1 nm, length 307.7 nm, and aspect ratio of 11. SEM images of the scaffolds have shown porous structures in all scaffolds, although some of them had closed pores at the surface, which prevents access to the interior of the structure (Fig. 8).

The complex CN/CTN/SS is the one that has a better architecture, with open porosity that grants oxygen transportation in a possible wound healing application. Due to higher aspect ratio, CN works as a support material, CN as wound healing accelerator and SS as binder for the different nanofibrils, preventing whiskers fluctuation and promoting a porous structure.

The structural effect of releasing SS from the sponges when in physiologic pH medium with and without lysozyme was investigated leading to the conclusion that SS follows a diffusion profile with a release rate that decreases with time. Complete SS release was not achieved due to previous cross-linking process. It is expected that the remaining SS trapped in the sponges can help to provide

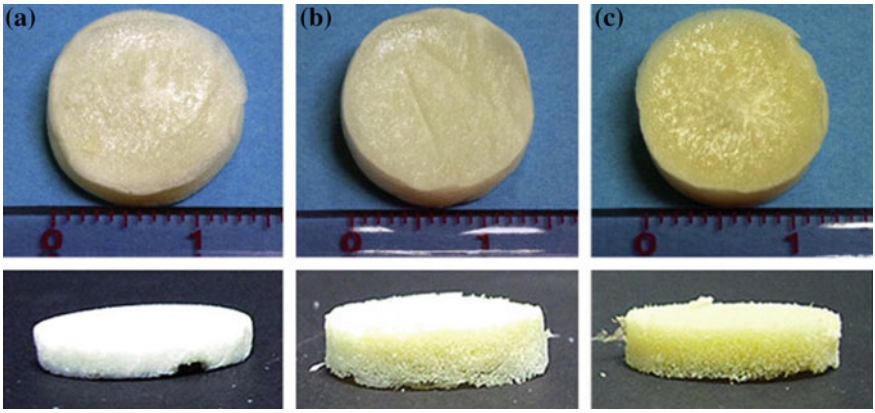

Fig. 8 Images of sponges. **a** CN, **b** CTN, **c** CN/CTN/SS. From [1]

moisturizing effect to the wound at the same time that chitin regulates collagen synthesis and facilitates granulation and damaged skin tissue repair.

Wang and Esker [51] developed nanocrystalline chitin films for enzyme immobilization. CTN suspensions were prepared by HCL hydrolyses of α-chitin (shrimp) that lead to the formation of nanofibrils ranging in length 200–600 nm and width 30–70 nm. The suspensions were spincoated onto a gold modified surface creating an ultrathin smooth and homogeneous layer of CTN film. The use of data from a quartz crystal microbalance with dissipation monitoring (QCM-D) allowed the acknowledgment of slower chitinase-catalyzed hydrolyses of CTN film compared to amorphous regenerated chitin films. To investigate film protein immobilization capacity BSA was used as model. Despite the adsorption dependency on the thickness BSA was highly adsorbed by the CTN films. The films lost very little quantity of BSA after washing with water, showing great loading capacity and indicating potential as bio-supports for sensors and catalysts.

Li et al. [25] applied salt leaching and thermally induced phase separation (TIPS) technique to produce poly(3-hydroxybutyrate-co-3-hydroxyvalerate) (PHBV) and chitin nanofibrils scaffolds for tissue engineering. The produced scaffolds, incorporating CTN with 200–500 nm length and 20–40 nm width, exhibit macro pores of 100–300 μm and micro pores of 10 μm.

When performing compressive tests the composite scaffolds showed enhanced mechanical properties with compressive modulus of (7.12 ± 0.24) MPa, while the PHBV scaffolds only achieved (5.21 ± 0.14) MPa. Bioactivity performance was also higher in the composite scaffolds. After 7 days of incubation of human adipose-derived stem cells (hADSCs), confocal microscopy images showed the adhesion of cells at the surface of PHBV scaffold while evidence of penetration and migration of hADSCs through the PHBV/CTN scaffold was observed.

Another product for wound dressing was proposed by Naseri et al. [37]. Chitosan-based nanocomposite fiber mats reinforced with chitin nanocrystals were

produced by electrospinning. For spinning solutions, chitosan and PEO were blended in 1:1 ratio and used as matrix, while CTN was used as reinforcement in order to produce final solutions of 3 wt% polymer in 50 % aqueous acetic acid solvent. With the purpose of verifying nanocrystals dispersion, flow birefringence was studied by placing the electrospinning solutions under stirring, between two cross-polarized filters, and visually compared with dilute water CTN suspensions birefringence.

After the electrospinning process, fiber (diameter = 223–966 nm) mats were cross-linked with genipin to enhance the mechanical properties and pH stability. This was confirmed by uniaxial tensile tests performed in mat samples with the best fibers (50 % CTN) exhibiting tensile strength of 64.9 MPa and elastic modulus of 10.2 GPa. Adipose stem cells were seeded on the fiber mats and after 7 days of culture, non-cytotoxicity was verified with conservation of cells morphology.

4 Conclusions

Chitin is after cellulose the most abundant polymer in nature. However, due to chain rigidity it is difficult to dissolve in most solvents, which has limited its applications in the biomedical field. Most of the applications found in the literature deal with the production of nanofibrils and its use as reinforcements in composite materials. These nanofibrils are highly crystalline and rigid (high Young Modulus) allowing the improvement of mechanical performance of composites. Recently, the attention of the scientific community has been attracted to assembling these nanofibrils when in suspension, giving rise to cholesteric lyotropic mesophases. These mesophases are able to mimic the supramolecular organization of collagen in living tissues and the possibility of developing new biomimetic products from it can be foreseen in the future.

Acknowledgments This work is funded by FEDER funds through the COMPETE 2020 Programme and National Funds throught FCT—Portuguese Foundation for Science and Technology under the project UID/CTM/50025/2013. C.F.C. João also acknowledges Portuguese Science Foundation—FCT for his PhD scholarship, ref: SFRH/BD/ 80860/2011.

References

1. Ang-atikarnkul P, Watthanaphanit A, Rujiravanit R (2014) Fabrication of cellulose nanofiber/chitin whisker/silk sericin bionanocomposite sponges and characterizations of their physical and biological properties. Compos Sci Technol 96:88–96. doi:10.1016/j.compscitech.2014.03.006
2. Araki J, Yamanaka Y, Ohkawa K (2012) Chitin-chitosan nanocomposite gels: reinforcement of chitosan hydrogels with rod-like chitin nanowhiskers. Polym J 44(7):713–717. doi:10.1038/pj.2012.11

3. Azuma K, Osaki T, Ifuku S, Saimoto H, Tsuka T, Imagawa T et al (2012) α-Chitin nanofibrils improve inflammatory and fibrosis responses in inflammatory bowel disease mice model. Carbohydr Polym 90(1):197–200. doi:10.1016/j.carbpol.2012.05.023
4. Bledzki AK, Gassan J (1999) Composites reinforced with cellulose based fibres. Prog Polym Sci 24(2):221–274
5. Chan CH, Chia CH, Thomas S (2014). Physical chemistry of macromolecules. Apple Academic Press, p 1–636
6. Dugan JM (2012) Cellulose nanowhiskers for tissue engineering skeletal muscle
7. Dugan JM, Gough JE, Eichhorn SJ (2013) Bacterial cellulose scaffolds and cellulose nanowhiskers for tissue engineering. Nanomedicine 8(2):287–298. doi:10.2217/nnm.12.211
8. Eichhorn SJ (2011) Cellulose nanowhiskers: promising materials for advanced applications. Soft Matter 7(2):303. doi:10.1039/c0sm00142b
9. Faruk O, Bledzki AK, Fink H-P, Sain M (2012) Biocomposites reinforced with natural fibers: 2000–2010. Prog Polym Sci 37(11):1552–1596. doi:10.1016/j.progpolymsci.2012.04.003
10. Gaspar D, Fernandes SN, de Oliveira AG, Fernandes JG, Grey P, Pontes RV et al (2014) Nanocrystalline cellulose applied simultaneously as the gate dielectric and the substrate in flexible field effect transistors. Nanotechnology 25(9):094008. doi:10.1088/0957-4484/25/9/094008
11. Geng Y, Almeida PL, Fernandes SN, Cheng C, Palffy-Muhoray P, Godinho MH (2013) A cellulose liquid crystal motor: a steam engine of the second kind. Sci Rep 3. doi:10.1038/srep01028
12. Giraud-Guille M-M, Belamie E, Mosser G (2004) Organic and mineral networks in carapaces, bones and biomimetic materials. CR Palevol 3(6–7):503–513. doi:10.1016/j.crpv.2004.07.004
13. Goodrich JD, Winter WT (2007) α-Chitin nanocrystals prepared from shrimp shells and their specific surface area measurement. Biomacromolecules 8:252–257
14. Gopalan Nair K, Dufresne A (2003) Crab shell chitin whisker reinforced natural rubber nanocomposites. 1. processing and swelling behavior. Biomacromolecules 4(3):657–665
15. Gupta NS (2010) Chitin. Springer
16. Hariraksapitak P, Supaphol P (2010) Preparation and properties of α-chitin-whisker-reinforced hyaluronan–gelatin nanocomposite scaffolds. J Appl Polym Sci 117(6):3406–3418. doi:10.1002/app.32095
17. Ifuku S, Morooka S, Morimoto M, Saimoto H (2010) Acetylation of chitin nanofibers and their transparent nanocomposite films. Biomacromolecules 11:1326–1330
18. Jayakumar R, Menon D, Manzoor K, Nair SV, Tamura H (2010) Biomedical applications of chitin and chitosan based nanomaterials-A short review. Carbohydr Polym 82(2):6. doi:10.1016/j.carbpol.2010.04.074
19. Ji Y-L, Wolfe PS, Rodriguez IA, Bowlin GL (2012) Preparation of chitin nanofibril/polycaprolactone nanocomposite from a nonaqueous medium suspension. Carbohydr Polym 87(3):7–7
20. Ji Y, Liang K, Shen X, Bowlin GL (2014) Electrospinning and characterization of chitin nanofibril/polycaprolactone nanocomposite fiber mats. Carbohydr Polym 101:68–74. doi:10.1016/j.carbpol.2013.09.012
21. Junkasem J, Rujiravanit R, Supaphol P (2006) Fabrication of α-chitin whisker-reinforced poly (vinyl alcohol) nanocomposite nanofibres by electrospinning. Nanotechnology 17(17):4519–4528. doi:10.1088/0957-4484/17/17/039
22. Junkasem J, Rujiravanit R, Grady BP, Supaphol P (2010) X-ray diffraction and dynamic mechanical analyses of Î ± -chitin whisker-reinforced poly (vinyl alcohol) nanocomposite nanofibers. Polym Int 59(1):85–91. doi:10.1002/pi.2693
23. Kim SK (2013) Chitin and Chitosan Derivatives. CRC Press
24. Lagerwall JPF, Schütz C, Salajkova M, Noh J, Park JH, Scalia G, Bergstrom L (2013) Cellulose nanocrystal-based materials: from liquid crystal self-assembly and glass formation to multifunctional thin films 6(1):e80–12

25. Li HY, Li H, Wang BJ, Gu Q, Jiang ZQ, Wu XD (2014) Synthesis and properties of poly (3-hydroxybutyrate-co-3- hydroxyvalerate)/chitin nanocrystals composite scaffolds for tissue engineering. Chin Chem Lett 1–4. doi:10.1016/j.cclet.2014.06.019
26. Lin N, Huang J, Chang PR, Feng L, Yu J (2011) Effect of polysaccharide nanocrystals on structure, properties, and drug release kinetics of alginate-based microspheres. Colloids Surf B:Biointerfaces 85(2):270–279. doi:10.1016/j.colsurfb.2011.02.039
27. Lu Y, Weng L, Zhang L (2004) Morphology and properties of soy protein isolate thermoplastics reinforced with chitin whiskers. Biomacromolecules 5(3):1046–1051. doi:10.1021/bm034516x
28. Marchessault RH, Morehead FF, Walter NM (1959) Liquid crystal systems from fibrillar polysaccharides. Nature 184:632–633
29. Mincea M, Negrulescu A, Ostafe V (2012) Preparation, modification, and applications of chitin nanowhiskers: a review. Rev Adv Mater Sci 30:225–242
30. Moon RJ, Martini A, Nairn J, Simonsen J, Youngblood J (2011) Cellulose nanomaterials review: structure, properties and nanocomposites. Chem Soc Rev 40(7):3941. doi:10.1039/c0cs00108b
31. Morganti P, Morganti G (2008) Chitin nanofibrils for advanced cosmeceuticals. Clin Dermatol 26(4):334–340. doi:10.1016/j.clindermatol.2008.01.003
32. Morin A, Dufresne A (2002) Nanocomposites of chitin whiskers from riftiatubes and poly (caprolactone). Macromolecules 35(6):2190–2199. doi:10.1021/ma011493a
33. Muzzarelli RAA (1977) Chitin, 1st edn. Pergamon, Great Britain
34. Muzzarelli RAA (2011) Biomedical exploitation of chitin and chitosan via mechano-chemical disassembly, electrospinning, dissolution in imidazolium ionic liquids, and supercritical drying. Mar Drugs 9(12):1510–1533. doi:10.3390/md9091510
35. Muzzarelli RAA, Morganti P, Morganti G, Palombo P, Palombo M, Biagini G et al (2007) Chitin nanofibrils/chitosan glycolate composites as wound medicaments. Carbohydr Polym 70 (3):274–284. doi:10.1016/j.carbpol.2007.04.008
36. Mülhaupt R (2012) Green polymer chemistry and bio-based plastics: dreams and reality. Macromol Chem Phys 214(2):159–174. doi:10.1002/macp.201200439
37. Naseri N, Algan C, Jacobs V, John M, Oksman K, Mathew AP (2014) Electrospun chitosan-based nanocomposite mats reinforced with chitin nanocrystals for wound dressing. Carbohydr Polym 109:7–15. doi:10.1016/j.carbpol.2014.03.031
38. Paillet M, Dufresne A (2001) Chitin wisker reinforced thermoplastic nanocomposites. Macromolecules 34:6527–6530
39. Phongying S, Aiba S-I, Chirachanchai S (2007) Direct chitosan nanoscaffold formation via chitin whiskers. Polymer 48(1):393–400. doi:10.1016/j.polymer.2006.10.049
40. Pooyan P, Tannenbaum R, Garmestani H (2012) Mechanical behavior of a cellulose-reinforced scaffold in vascular tissue engineering. J Mech Behav Biomed Mater 7:50–59. doi:10.1016/j.jmbbm.2011.09.009
41. Rodriguez IA, Sell SA, McCool JM, Saxena G, Spence AJ, Bowlin GL (2013) A preliminary evaluation of lyophilized gelatin sponges, enhanced with platelet-rich plasma, hydroxyapatite and chitin whiskers for bone regeneration. Cells 2(2):244–265. doi:10.3390/cells2020244
42. Shervani Z (2012) Preparation of gold nanoparticles loaded chitin nanofiber composite. Adv Nanopart 1(3):71–78. doi:10.4236/anp.2012.13010
43. Sriupayo J, Supaphol P, Blackwell J, Rujiravanit R (2005) Preparation and characterization of a-chitin whisker-reinforced poly(vinyl alcohol) nanocomposite films with or without heat treatment. Polymer 46(15):8. doi:10.1016/j.polymer.2005.04.069
44. Thakur VK, Singha AS, Mehta IK (2010) Renewable resource-based green polymer composites: analysis and characterization. Int J Polym Anal Charact 15(3):137–146. doi:10.1080/10236660903582233
45. Thakur VK, Singha AS, Kaur I et al (2011) Studies on analysis and characterization of phenolic composites fabricated from lignocellulosic fibres. Polym Polym Compos 19:505–511

46. Thakur VK, Singha AS, Thakur MK (2013) Ecofriendly biocomposites from natural fibers: mechanical and weathering study. Int J Polym Anal Charact 18(1):64–72. doi:10.1080/1023666X.2013.747246
47. Thakur VK, Thakur MK, Gupta RK (2014) Review: raw natural fiber-based polymer composites. Int J Polym Anal Charact 19(3):256–271. doi:10.1080/1023666X.2014.880016
48. Thakur VK, Thakur MK, Raghavan P, Kessler MR (2014) Progress in green polymer composites from lignin for multifunctional applications: a review. ACS Sustain Chem Eng 2(5):1072–1092. doi:10.1021/sc500087z
49. Thomas S, Visakh PM, Mathew AP (2012) Advances in Natural Polymers. Springer
50. Tzoumaki MV, Moschakis T, Biliaderis CG (2010) Metastability of nematic gels made of aqueous chitin nanocrystal dispersions. Biomacromolecules 11:175–181
51. Wang C, Esker AR (2014) Nanocrystalline chitin thin films. Carbohydr Polym 102:151–158. doi:10.1016/j.carbpol.2013.10.103
52. Watthanaphanit A, Supaphol P, Tamura H, Tokura S, Rujiravanit R (2008) Fabrication, structure, and properties of chitin whisker-reinforced alginate nanocomposite fibers. J Appl Polym Sci 110(2):890–899. doi:10.1002/app.28634
53. Watthanaphanit A, Supaphol P, Tamura H, Tokura S, Rujiravanit R (2010) Wet-spun alginate/chitosan whiskers nanocomposite fibers: preparation, characterization and release characteristic of the whiskers. Carbohydr Polym 79(3):9. doi:10.1016/j.carbpol.2009.09.031
54. Wise DL (2000) Biomaterials and bioengineering handbook, vol 63. Marcel Dekker New York
55. Wongpanit P, Sanchavanakit N, Pavasant P, Bunaprasert T, Tabata Y, Rujiravanit R (2007) Preparation and characterization of chitin whisker-reinforced silk fibroin nanocomposite sponges. Eur Polymer J 43(10):4123–4135. doi:10.1016/j.eurpolymj.2007.07.004
56. Yamamoto Y, Nishimura T, Saito T, Kato T (2010) CaCO3/chitin-whisker hybrids: formation of CaCO3 crystals in chitin-based liquid-crystalline suspension. Polym J 42(7):583–586. doi:10.1038/pj.2010.32
57. Younes I, Hajji S, Frachet V, Rinaudo M, Jellouli K, Nasri M (2014) Chitin extraction from shrimp shell using enzymatic treatment. antitumor, antioxidant and antimicrobial activities of chitosan. Int J Biol Macromol 69:489–498. doi:10.1016/j.ijbiomac.2014.06.013
58. Yudin VE, Dobrovolskaya IP, Neelov IM, Dresvyanina EN, Popryadukhin PV, Ivan'kova EM et al (2014) Wet spinning of fibers made of chitosan and chitin nanofibrils. Carbohydr Polym 108:176–182. doi:10.1016/j.carbpol.2014.02.090
59. Zeng J-B, He Y-S, Li S-L, Wang Y-Z (2012) Chitin whiskers: an overview. Biomacromolecules 13(1):1–11. doi:10.1021/bm201564a
60. Zhang X, Huang J, Chang PR, Li J, Chen Y, Wang D et al (2010) Structure and properties of polysaccharide nanocrystal-doped supramolecular hydrogels based on cyclodextrin inclusion. Polymer 51(19):4398–4407. doi:10.1016/j.polymer.2010.07.025

Eco-Friendly Cellulose–Polymer Nanocomposites: Synthesis, Properties and Applications

S. Karuppusamy, P. Vengatesh and M. Anbu Kulandainathan

Abstract Grafting or deposition is a powerful tool to modify the cellulose/textile surfaces permanently with precisely controlled structure in nanometer to micrometre scale, which leads to multifunctional applications. The properties that can be imparted through functionalization include superhydrophobicity, superoleopholicity, shape memory effect, high conductivity, drug storage/delivery, flame retardant, heat storage/release, and UV protection. Through this functionalization new applications for textile can be achieved such as waterproof textiles, textile actuators, fire resistive textiles, UV-protective materials, Band-Aids, transdermal batches, medical textiles, supercapacitor electrodes, separator of oil–water mixture, wearable textile electronics, conductive textiles, self-protection cloths. This chapter summarises recent publications about modifying the cellulose surfaces with biopolymers along with nanoparticles and their composites used for superhydrophobicity, oil–water separation, conducting fabrics and drug delivery devices leading to smart bandages. The main objective is to clarify the true significance of functionalization for each application. Thus, another important purpose of this chapter is to establish general guidelines for functionalization and propose future direction for cheaper devices that can elevate the textile industries.

Keywords Cellulose · Superhydrophobicity · Energy storage applications · Oil–water separation · Grafting

Abbreviations

LBL	Layer-by-Layer
PGMA-b-PTFEMA	Poly(2,2,2-trifuoroethyl methacrylate)-block-poly-(glycidyl methacrylate)
PVDF-HFP)/FAS	Poly(vinylidene fluoride-hexafluoropropylene)/ fluoroalkylsilane

S. Karuppusamy · P. Vengatesh · M.A. Kulandainathan (✉)
Electrochemical Process Engineering, CSIR-Central Electrochemical Research Institute, Karaikudi 630006, India
e-mail: manbu123@gmail.com

V.K. Thakur and M.K. Thakur (eds.), *Eco-friendly Polymer Nanocomposites*, Advanced Structured Materials 74, DOI 10.1007/978-81-322-2473-0_15

PEDOT/FD-POSS/FAS	Poly (ethylenedioxythiophene)/fluorinated decyl polyhedral oligomericsilsesquioxane/flouroalkylsilane
p(V4D4-L-PFDA)	Poly[(1,3,5,7-tetravinyl-1,3,5,7-tetramethylcyclotetrasiloxane), 1H,1H,2H,2H perfluorodecylacrylate]
PANI-PTES	Polyaniline-1H, 1H, 2H, 2H-perfluorooctyltriethoxysilane
CeO_2-DFTMS	Cerium oxide-Dodecafluoroheptyl-propyl-trimethoxylsilane
PAH-N_3/silica-N_3/FAS	Poly(allylamine hydrochloride)-azide terminated/silica azide terminated/fluoroalkylsilane
WCA	Water Contact Angle
PFDT	Perfluorodecanethiol
SiO_2/DFPA	Nanosilica/dodecafluoroheptyl-containing polyacrylate
PDMDAAC/SiO_2/HDFTDT	Poly-dimethyldiallylammonium chloride/nanosilica/heptadeca fluoro-1,1,2,2-tetradecyl) trimethoxysilane
MCTS	Methyltrichlorosilane
PMSQ	Polymethylsilsesquioxane
ATS/GPTMS	Alkyltrialkoxysilanes/(3-glycidyloxypropyl) trimethoxysilane
P(POSS-MMA-VBFC)	Poly(POSS-co-methyl methacrylate-co-4-vinylbenzyl fluoropolyether carboxylate)
P(FOEA-co-IPSMA)	Poly-[(perfluorooctylethyl acrylate)-co-(tri(isopropyloxy)silyl-propylmethacrylate)]
HDMS/TiO_2-SiO_2@PDMS	1,1,1,3,3,3-Hexamethyl disilazane/titania sol-silica sol @polydimethylsiloxane hybrid
PHEA	Poly(2-hydroxyethyl acrylate)
PNIPAAm	Poly(*N*-isopropylacrylamide)
PMETAC	Poly[2-(methacryloyloxy)ethyltrimethylammonium chloride]
SI-ATRP	Surface-initiated atom transfer radical polymerization
PFHEA-b-PIPSMA	Poly[2-(perfluorohexyl)ethyl acrylate]-block-poly[(triisopropyloxysilyl)propyl methacrylate]
PFHEA-b-PGM A	Poly[2-(perfluorohexyl)ethyl acrylate]-block-poly(glycidyl methacrylate)
AD-HFPS	3-Aryl-3-(trifluormethyl)diazirine functionalized highly fluorinated phosphonium salts
PLMA	Poly-laurylmethacrylate
PHMA	Poly-hexylmethacrylate
Ag NPs	Silver nanoparticles
ZnO NPs/PS	Zinc oxide nanoparticles/polystyrene
HDMSO	Hexamethyldisiloxane
rf-PECVD	Radio frequency-plasma enhanced chemical vapour deposition

1 Introduction

1.1 Biopolymers

Biopolymers are structurally classified into three major types by its linkage between the monomer units: polynucleotides (nucleotide monomers) such as DNA and RNA, polypeptides (amino acids) such as ribosome and protein, and polysaccharides (carbohydrate units) such as cellulose, starch, chitosan and lignin (Fig. 1) [89–91]. Biopolymers are acquired from the extraction from biomass, such as

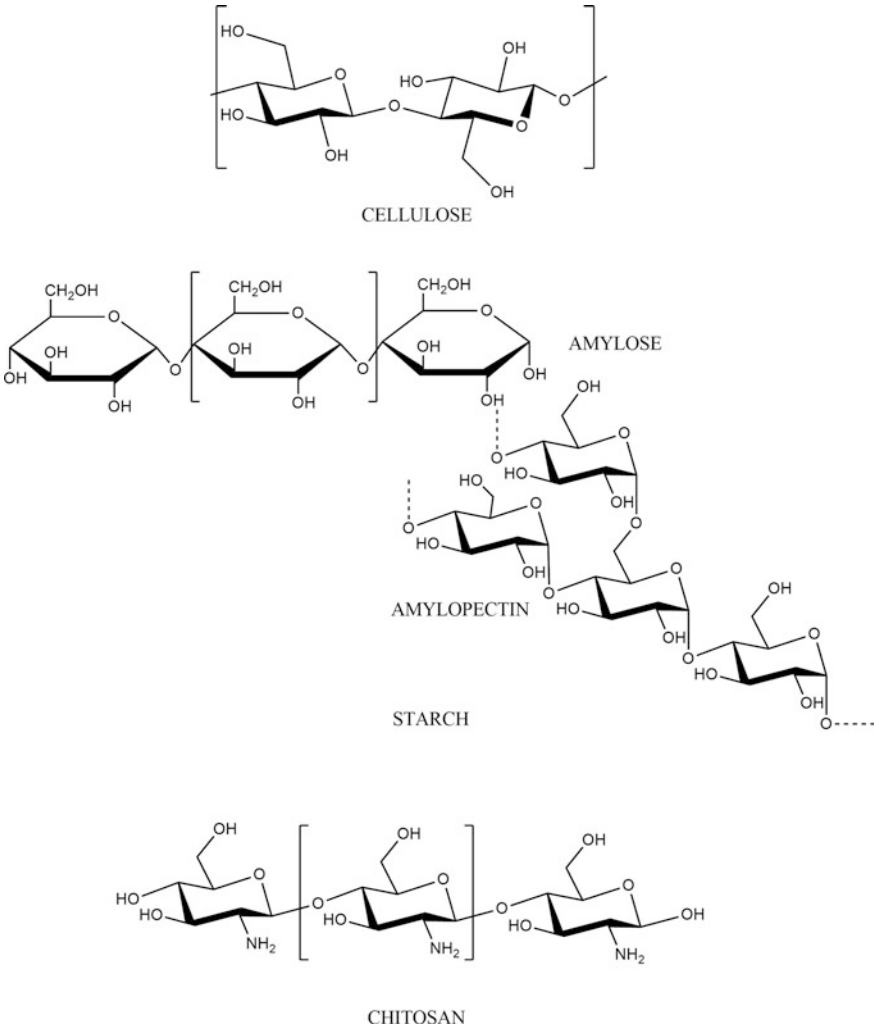

Fig. 1 Structures of some of the important biopolymers

Saccaharum cilliare [65, 66, 75], *Grewia optiva, Hibiscus sabdariffa* (Singha and Thakur [75, 76]), pine needles [76] and synthesised from bio-derived monomers/organisms such as bacterial cellulose, ethyl cellulose acetate [81–84, 92]. Different types of cellulose-based graft copolymers materials have been obtained using free radical polymerization techniques [81, 84–88].

The contemporary world have been utilising natural and synthetic polymer-based composite materials for important applications since the discovery of Bakelite resin [77–80]. Based on the renewable biopolymer application, this kind of materials has possible substituent for metal supported materials, petrochemical-based materials and natural fibres reinforced composite materials [59, 67, 68]. The contemporary world postulates applied materials as non-toxic, abundant, recyclable and biodegradable. Natural fibres are fulfilling the modern world's requirements that are 40–45 % cellulose, 26–34 % lignin and 7–14 % pentosan [18, 90].

Cellulose $(C_6H_{10}O_5)_n$, the polysaccharide is the most common organic biopolymer that can be classified based on their source, viz., bacterial, animal and plant (Fig. 1). The cellulose has hydroxyl groups (OH), on C2, C3 and C6, and further OH groups on C1 and C4 are utilised for the linkage of β(1 → 4) glycosidic bonds between the D-glucose units that brings up the linearity of structure [69, 74]. The extension of the linearity enables the molecules to get closer, and form a compact structure by virtue of intra- and intermolecular hydrogen bonding and thus increasing the cohesive energy. Moreover, the hydroxyl groups can be converted into some useful functional groups that in turn provide multifarious properties to such kind of compact OH structural materials [100].

Lignin is the second most abundant biopolymer next to the cellulose in nature and generated from the chemical industries about 50 million tons every year as both major and by-product. Lignin is a hydrophobic in nature, structurally linking with C–C and C–O bonds between the monomers, biodegradable and non-toxic. Like cellulose, lignin also has vital advantages of having the reactive functional groups, high carbon content, and good stability and can be able to make this as reinforcing materials in polymers, nanocomposite materials, cross-linking polymers, etc. Due to the problems associated with the disposal, variable and complex nature of lignin limits its applications [93].

Starch is another important biopolymer, which is a combination of two glucosidic macromolecules (amylose 18–28 % and amylopectin 72–82 %), amylose is linear macromolecules that are linked by α-(1 → 4) glycosidic bonds, whereas amylopectin linked by α-D-(1 → 6)-glycosidic bonds (Fig. 1). It is highly abundant (reserves in plants, tubers, seeds) and generated more than 50 million tons in 2012. Due to its own advantages of biodegradability, low cost, renewable, is useful in biomedical field, such as drug delivery systems and tissue engineering scaffolds, paper industries, adhesives and food industries [28]. The main disadvantages of the starch are weak absorbing functional groups, poor processability, stability and mechanical properties of its end products [28, 70].

Chitosan is a long chain copolymer of D-glucosamine and *N*-acetyl-D-glucosamine, linked by β-1, 4-D-glucosamine, and can be obtained from the

Table 1 Impact of biopolymers coating on fabrics for multifarious applications

S.No	Biopolymer	Application	References
1	Chitosan	Drug delivery, antimicrobial	Petkova et al. [51]
2	Polyvinyl alcohol	Wound healing	Gupta et al. [24]
3	Cyclodextrin	Drug carrier	Hebeish et al. [25]
4	Sericin	UV-resistant, drug delivery	Doakhan et al. [16]
5	Alginate	Moisture absorber, drug delivery	Yang et al. [102]
6	Polydopamine	Oil–water separation, hydrophobicity, conductivity, drug carrier	Liu et al. [38]
7	CASEIN	Flame retardant	Carosio et al. [11]
8	DNA	Flame retardant	Mateos et al. [43]
9	Polyphenol oxidase	UV protection	Zhuo and Sun [117]

deacetylation of chitin (Fig. 1). It is highly abundant in nature, biocompatible, non-toxic and biodegradable [103]. Due to these properties, it can be used in biomedical applications, such as antitumor, antifungal, antimicrobial, antioxidant activities, immune enhancing agent, water treatment, drug delivery, tissue engineering and food packaging [21]. The drawbacks of chitosan polymer nanocomposites are discoloration, surface cracking, lack in the mechanical properties and stiffening.

Some of the important applications of biopolymers have been listed in Table 1. However, due to large potential applications and plenty of resources of cellulose, its functionalization for the multifunctional applications is very important and needs literature reviewing. Hence, this chapter highlights the importance of functionalization of cellulose surfaces to introduce multifunctional properties and to develop the research focuses towards effective grafting/coating for innovative products to the modernised scientific community.

1.2 Cellulose

Cellulose is an easily available, renewable, soft and flexible fibre, hydrophilic in nature (water contact angle, WCA is 17–47°) and has very high breathability, and hence it is used in wearable materials, composites, smart textiles, adhesives, paper products, medical bandages and adsorbent materials [35, 60–64]. By changing, the nature of the cellulose through certain modifications, one can introduce the multifunctional properties to the cellulose fabrics. Depending on the type of modifications, either through physical or chemical processes, the cellulose fibres are used for several applications (Fig. 2). The chemical reactivity mainly depends on the hydroxyl groups on C2, C3 and C6 positions of cellulose and the relative reactivity is influenced by the steric effect between reacting group and the cellulose.

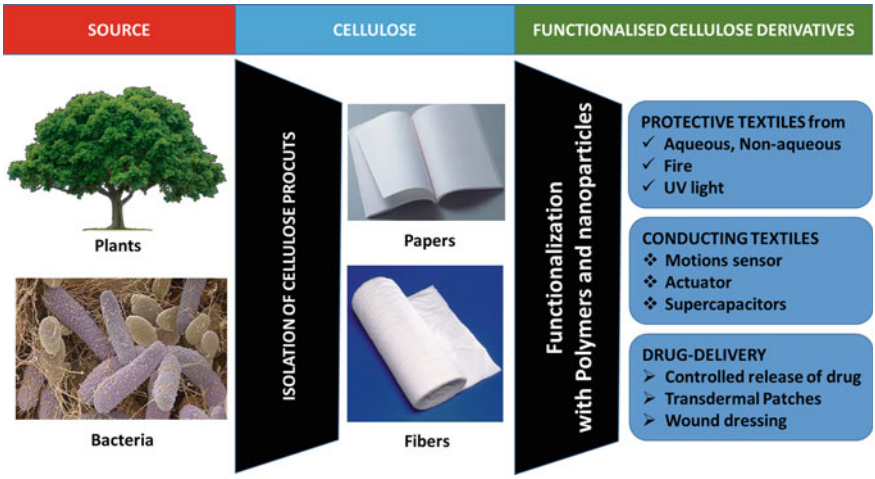

Fig. 2 Flow chart of cellulose materials towards future smart textiles

Nowadays, the cellulose or textile market mainly depends on introducing multifunctional properties to the cellulose. As the cellulose is weightless and flexible substrate; they find their application in energy storage devices (separator, supercapacitor), superhydrophobicity, membrane (oil–water separation), conducting materials and drug delivery.

Most of the functional garments that are used for high-performance applications such as protective wears from flame, UV rays, liquids and microbes lack comfort. Coating is the process that is mainly employed for obtaining such performance, which often closes the pores of the fabrics substrate providing very low air permeability, which reduces air and water vapour transmission, a reason for reduced comfort. Hence, protective wear with high performance and comfort level is to be focused and developed.

Thus, an idea of developing a functional garment with cellulose grafting using biopolymers along with nanocomposites that are comfortable, without compromising its functionalities and performance is proposed. The garment having hydrophilic group on one side, which wicks away the sweat from the skin, permeable to wear vapour, is expected to provide better microclimate comfort. Absorption of sweat leads to dampness, which is a media for microbial growth and malodours, hence, antimicrobial polymers, can also be blended with hydrophilic polymers to nullify such issues. Hydrophobic polymers that repel water and other fluids can be coated over the substrate in order to obtain superhydrophobic functionality, required for many applications including surgical theatre garments. Front side of the fabric can also be coated with UV-repellent finishes as well as flame-retardant finishes that find their application as protective wears for UV and firefighters respectively.

1.3 Functionalization of Cellulose

Effective functionalizations of cellulose have been achieved through various methods such as, some of which are mentioned as below.

1.3.1 Coating

The coating methods are simple, low cost and an efficient process to fabricate/introduce multifunctional properties onto cotton and in general onto the materials. To succeed in this method, it requires three to five individual processes that include preparation of coating mixture in suitable phase to apply, drying and curing. Using the above technique nanomaterials, dopants, fluoroalkylsilanes, polymers, and some inorganic compounds can be deposited over the substrate. The number of steps involved in this method will vary depending on the types of technique used including spin coating, spray coating and dip-coating. The coating thickness is more than 100 nm depending on the type of coating and thus enhance/produce the micro- to nanoroughness on the surface. The method is moderate-to-rapid process because of few steps of fabrication (sophisticated techniques producing even in a single step using spray coating) [47]. Moreover, the method has certain disadvantages like less durability, low laundering capacity and lack of strong attraction between the substrate and the coating mixture. These disadvantages can be outsmarted by using highly reactive coating mixture with the base substrate. This method brings up nanoroughness surface and synthesis the molecules bind with cellulose covalently and hence opening up a wide spectrum of possibilities for various levels of functionalization.

1.3.2 Plasma Etching

Plasma etching is one of the processes to get nanoscale roughness, low energy surface and porous on the cellulose surface. Plasma is the fourth state of matter in the universe, ionised gas or free electrons, bombarded on the surface with high energy under the electric field/super magnetic field so that it cuts the link between carbon, hydrogen and oxygen and making the surface into nanoroughed surface [45, 74]. This method is highly targetive, selective and a controlled process and further selective deposition can be achieved through chemical vapour deposition method. Disadvantages of this method are usage of costly instrument, batch processing, moderate durability and time-consuming (Example, oxygen plasma).

1.3.3 Surface Modification by Nanoparticle Growth

Roughness/hierarchical structure can be generated through dispersing organic/inorganic nanoparticles onto the cellulose surface. This kind of nanoparticle growth was formulated by dip-coating, spray coating and in situ generation of nanoparticles. In situ nanoparticles generation will be effective owing to its increased durability and laundering capacity. Superhydrophobic surface decorated by the nanoparticle deposition have nanoscale roughness and the hierarchical surface that can hold the air pockets in it which will not allow liquid phase to pass through it. Moreover, the conducting fibre can be prepared by several methods, and this kind of nanoparticle deposition will enhance the conductivity by effective transfer of electrons through it. Nanoparticle deposition on cellulose plays a vital role in introducing antimicrobial properties since the drug material of our interest can be imprinted on such fabrics, which would be used as smart bandages.

1.3.4 Grafting

Grafting is a process of making strong chemical bonding between the substrates. As discussed earlier cellulose has a number of reactive hydroxyl groups that can be functionalised through linking and deriving the required functional property [81–84]. The hydroxyl group can be reacted with the polymers, low surface energy molecules and utilised for nanoparticles formation and depositions by successful grafting with required functional group materials in a single material. The cellulose was fully/partially cross-linked with the substrate containing cyanate, epoxy, azide and polycarboxylic acid groups and such links existing as covalent bonding/hydrogen bonding (Fig. 3). The H-bonding is also existing between OH group and the heteroatom of applied substrate, for example direct adhesion of amide containing polymers forming hydrogen bonding between the cellulosic OH and heteroatom amide group. The way of polymer introduction on cellulose by covalent bonding is huge, but it belongs generally to direct reaction of polymer group with cellulose (polycarboxylic acids with cellulose) and in situ polymerisation. In situ polymerisation has three steps, preparation of monomer adhesive cellulose groups, introduction of monomers, polymerisation, after which the fibre washed with many times to remove the unreacted monomers. The main advantages of grafting process are strength arising from chemical bonding of the substrate with molecules, which is responsible for application so that it is highly robust, tuneable, withstand for several washes, the thickness of materials thus formed never exceeds 200 nm and long-lived surface. Sustained release of drug materials is the main problem in classic medical industries but layer-by-layer grafting and other grafting processes have effectively aided the modernised life-curing institutes in achieving sustained release of drug molecules. Some of the disadvantages of grafting process are time-consuming and sometimes exceeds more than five steps, hence making it expensive.

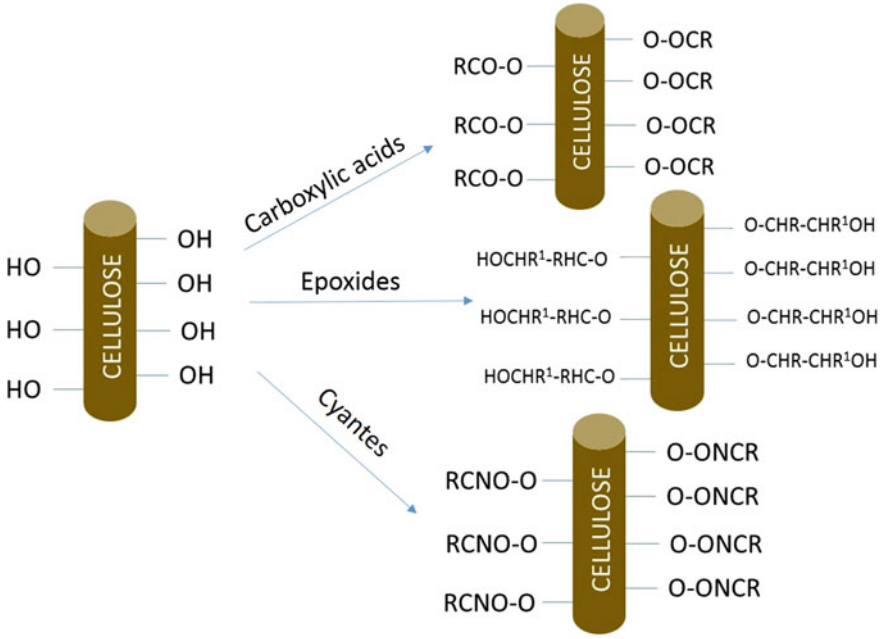

Fig. 3 The important functionalization of cellulose fabrics

1.3.5 Chemical Vapour Deposition

Chemical vapour deposition (CVD) is one type of chemical reaction, which can be carried out using gaseous precursor to achieve nanolevel solid deposition. This is the main tool to create nanoroughness as well as chemical functionalization. Chemical vapour deposition can be easily carried out on the surface along with plasma etching. These two processes are collectively called plasma etching–chemical vapour deposition (PECVD). PECVD technique is also useful in creating superhydrophobic surface on the cotton surface because this process is highly selective, useful for making thin film deposition and nanotexture surface. CVD process is carried out in high temperature chamber, the vapour of starting material is allowed to deposit over the cellulose surface, followed by the covalent formation between the hydroxyl group and the multifunctional precursors. During the reaction, the vapour generated as by-product might damage the cellulose fibre strength because cellulose can be easily damaged by acid/DMF. Some of the disadvantages of this technique are the fibre tensile strength is reduced and its durability becomes moderate. Yet, this is the simplest, short process, thin film (≤100 nm) with nanotextured on the surface.

2 Superhydrophobicity

Surface with superhydrophobicity possesses excellent water repellence behaviour because of their low surface energy and nanoscale surface roughness. The term "Superhydrophobicity", scaled by very high water contact angle (WCA > 150°), very low sliding angle (SA < 5°) and very low contact angle hysteresis (CAH < 5°) have aroused because of its potential applications in vast areas. This property has variety of applications from waterproof material to smart microfluidic devices, whereas wettable surfaces also used for printing, coating and adhesive applications. The hazardous liquids, highly corrosive materials and foreign materials affect the wettable surfaces so that the materials require protection from it to retain its properties. Moreover, the additional properties achieved by introducing superhydrophobicity depend on the materials used and types of preparation method [9, 10]. Such kinds of preparations need to be effective, highly durable, easy to prepare, environmental friendly and use of biodegradable materials. Hence, the method of preparation to attain the superhydrophobic behaviour is grandness to make multifarious cellulose-based textiles such as filter for oil–water separation, as separator in the battery applications, wearable cloths, raincoats, self-cleaning application, corrosion resistance, household applications and other industrial applications. In this part, the details about the method of preparation and improvements achieved in the superhydrophobic cellulose surface are being discussed further.

2.1 Methods of Preparation

Two different approaches were developed in the recent literature to get water repellence behaviour on the solid surfaces. That are, (a) making low energy or ultra low energy surfaces and (b) creating micro- and nanoscale roughness on the surface. The nanoscale roughness was observed by using the nanoparticles encapsulation on the cellulose fabrics or by layer-by-layer grafting. The grafting of molecules that contain muckle of hydrophobic functional groups, fluorine, silicone-containing polymers and layer-by-layer grafting process created low energy surface.

2.2 Functionalization with Low Surface Energy

Zhu et al. [118] reported coating methods for hydrophobic cotton and polyester (cellulose derivatives) by using various carbon atom having alkyltrialkoxysilane and/or else (3-glycidyloxypropyl)trimethoxysilane with alkyltrialkyloxysilane. According to Zhu et al., reported a generalised method with two ways, (1) first series involving hydrolysis of alkyltrialkoxysilane using NH_4OH in ethanol solution (Sol A) and (2) second series (Sol B) has additionally one step of adding

(3-glycidyloxypropyl)trimethoxysilane and alkyltrialkyloxysilane to the sol A. Generally, it is applied on the fabrics by pad-dry-cure method as explained below. The cotton/polyester fabric has to be immersed in a modified silica sol (either or both, Sol A and Sol B) for 30 s, drying at 80 °C and curing at 120 °C for an hour.

The authors [118] highlighted the

(1) Catalyst effect on the size: the optimised amount of NH_4OH for hydrolysis and depending on the amount the NH_4OH, the average size of the silica particle size increases,
(2) Substrate effect on the size: the number of carbon atom increases in the chain, the average particle size also increases.
(3) Substrate effect on CA: the number of carbon atom increases in the chain, the contact angle also increases. Based on these factors, optimization process for the preparation are easier to make the required contact angle to go with the textiles to fabricate drug delivery-orientated devices (Fig. 4).

Wang et al. [94] used cotton functionalization with low surface energy molecules (siloxanes) to get superhydrophobic surfaces. The author has hydrolysed the methoxy group containing silane molecules and further undergoes co-hydrolysis

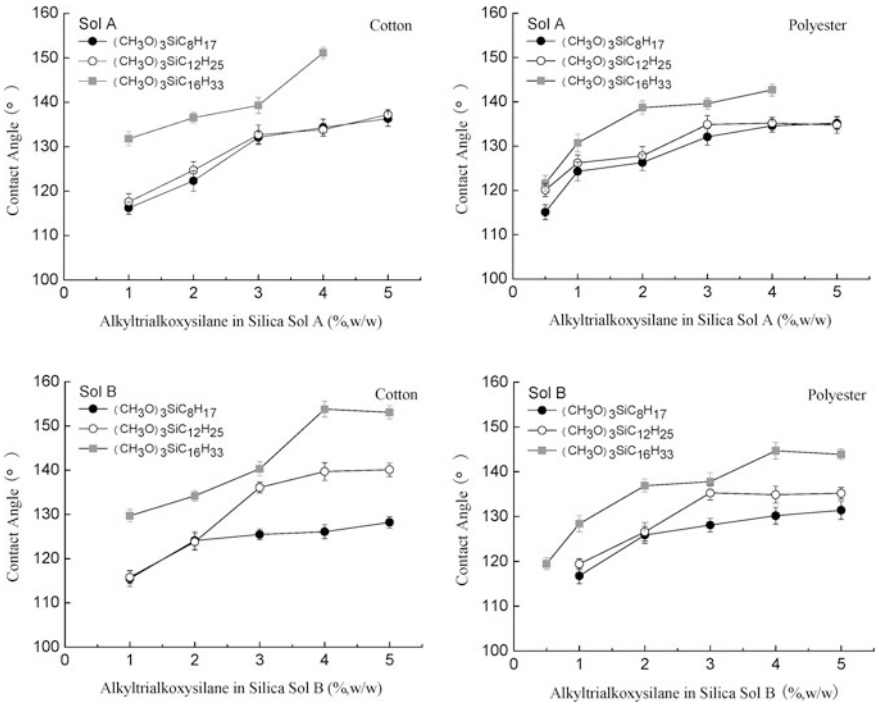

Fig. 4 Water contact angle of the cotton and polyester fabrics treated with different modified silica sol. Reprinted with permission from [118], copyright 2011, American Chemical Society

with other silane precursors to fabricate superhydrophobic coatings on fabrics. The fabrics were then dipped in the solution, padded, and dried at room temperature and further it was cured at 110 °C for 1 h. The cellulose having OH group has the tendency to bond with the epoxide group present in the 3-glycidoxypropyltrimethoxysilane (GPTMS) that can be achieved by adding cotton fabrics into the solution, the binding between these two was made of covalent bond to impart high laundering durability. WCA and SA on the cotton fabric coated with the GPTMS containing sol were approximately 170° and <10° respectively. It can have superhyphobicity behaviour with WCA of 160° even after 50 washing cycles.

Zhou et al. [114] reported superhydrophobic fabrics with highly durable behaviour by simple dip-coating method. The combination of long chain fluoro groups and siloxane bonds can enhance the superhydrophobic properties which were achieved by using tridecafluorooctyltriethoxysilane and polydimethylsiloxane (PDMS) precursor. To apply on the fabrics the molecules had to be dissolved in THF solution, then the fabrics were dip-coated and cured at 135 °C for 30 min to afford an excellent mechanical and chemical durability. The WCA of a pristine coated cotton and after 500 washes were 170° and 165° respectively, and the SA was changed from 3° to 6° correspondingly. The authors demonstrated that the fabrics retain its superhydrophobic properties while treating with boiling water and acid or base solutions.

2.3 Creation of Nanoroughness

Duan et al. [17] treated cotton fabrics with cerium dioxide (CeO_2) sol and dodecafluoroheptyl-propyl-trimethoxylsilane (DFTMS) using a dip-pad-cure process. The cotton fabrics were dipped into the solution of CeO_2, padded and cured at 170 °C for 3 min. The whole dip-pad-cure process was repeated until to get a dense film of CeO_2 xerogel of coating on cotton. After this process, the fabric was immersed in ethanol solution of hydrolysed DFTMS for a day and then it was further dried and cured at 120 °C for 1 h. The cotton fabrics showed superhydrophobic properties due to the irregular surface topography of aggregated CeO_2 nanoparticles with a size of 15 nm properties. The WCA of irregular topography with silicone bridged fabric and after completing 30 washing cycle were 158° and 150° respectively. Additionally, the fabrics show bifunctional behaviour of UV-shielding property and superhydrophobicity behaviour, which will be useful for functional materials.

2.4 Polymerization

Zhou et al. [115] fabricated a highly durable superamphiphobic coating with self-healing property on polyester, wool and cotton fabrics using two-step dip-coating method in which the cotton fabrics were immersed in a suspension of

fluoroalkylsilane + TEOS modified silica particles in ethanol for 1 min as a first step and the fabric was dried at room temperature for 10 min without rinsing and in the next step, it was immersed in a poly(vinylidene fluoride-hexafluoropropylene)/FAS containing DMF solution for 1 min and dried at 130 °C for 1 h. The coated fabrics showed great contact angles with low SAs 170°, 163°, 160° and 2°, 5° and 8° for water, soybean oil and hexadecane, respectively, and retains its superhydrophobicity behaviour after washing and acid/base etching. The coating was robust and self-healing, resistance to strong acid/base, boiling and ozone treatments, and showed high laundering capacity say 600 cycles.

Kivotidi et al. [33] fabricated superhydrophobic materials on cotton fabrics/cellulose papers by treating the samples with aqueous solutions and supercritical CO_2. High amount of $Ca(OH)_2$ was impregnated on the cellulose by immersion of cellulose substrates in the $CaCl_2$ solution and followed by immersion in the equimolar amount of NaOH and each process takes 40 min. After this, the fabric was exposed to supercritical CO_2 atmosphere for 40 min at 80-bar pressure to get corresponding carbonates. Further, this sample was immersed into the white spirit solution of silane–siloxane monomer solution for 20 min and dried in an air atmosphere. This sample showed superhydrophobic behaviour with contact angle between 145 and 154° and additionally it offered flame-retardant property as well.

Zhao et al. [113] and Basu et al. [8] demonstrated that LbL assembly of azido-functionalized silica nanoparticles and azido-grafted poly(allylamine hydrochloride) coated on the cotton fabrics to show the superhydrophobic properties. The poly(acrylic acid) treated cotton fabrics dipped in the 2.0 wt% FAS in hexane for 1 h and then dried at 100 °C for 30 min. The detail of the scheme is presented as Fig. 5. After coating, the fabrics were coated with 70 nm particles of diameter, hence showing the water contact angle on this multilayer-coated cotton fabric was measured to be 158°, and the superhydrophobicity coating showed good chemical resistance against various organic solvents and aqueous solutions of wide range of pH and washing durability.

Wu et al. [97] prepared highly durable superhydrophobic cotton fabric (SCF) obtained by the graft polymerization of lauryl methacrylate (LMA) and *n*-hexyl methacrylate (HMA). The cotton fabric were soaked in monomer solution in methanol and irradiated by γ-ray followed by polymerization, the fabric subjected to hot solvent extraction for 72 h. The fabrics were exhibiting the contact angle of 154° and after around 8000 and 9000 abrasion cycles for PHMA and PLMA-grafted fabrics lost their superhydrophobicity, respectively. However, if the cotton fabric is ironed at 200 °C, the fabric regains the superhydrophobicity behaviour within certain cycles. Interestingly, the fabric grafted with PHMA and PLMA after ironing at 200 °C does not lose its superhydrophobicity even after 24,000 abrasion cycles (Fig. 6). Further, without ironing only PLMA-grafted fabrics retains the superhydrophobicity up to 24,000 cycles.

Changes in water repellency with respect to various processes and usage of various compounds are listed in the Table 2.

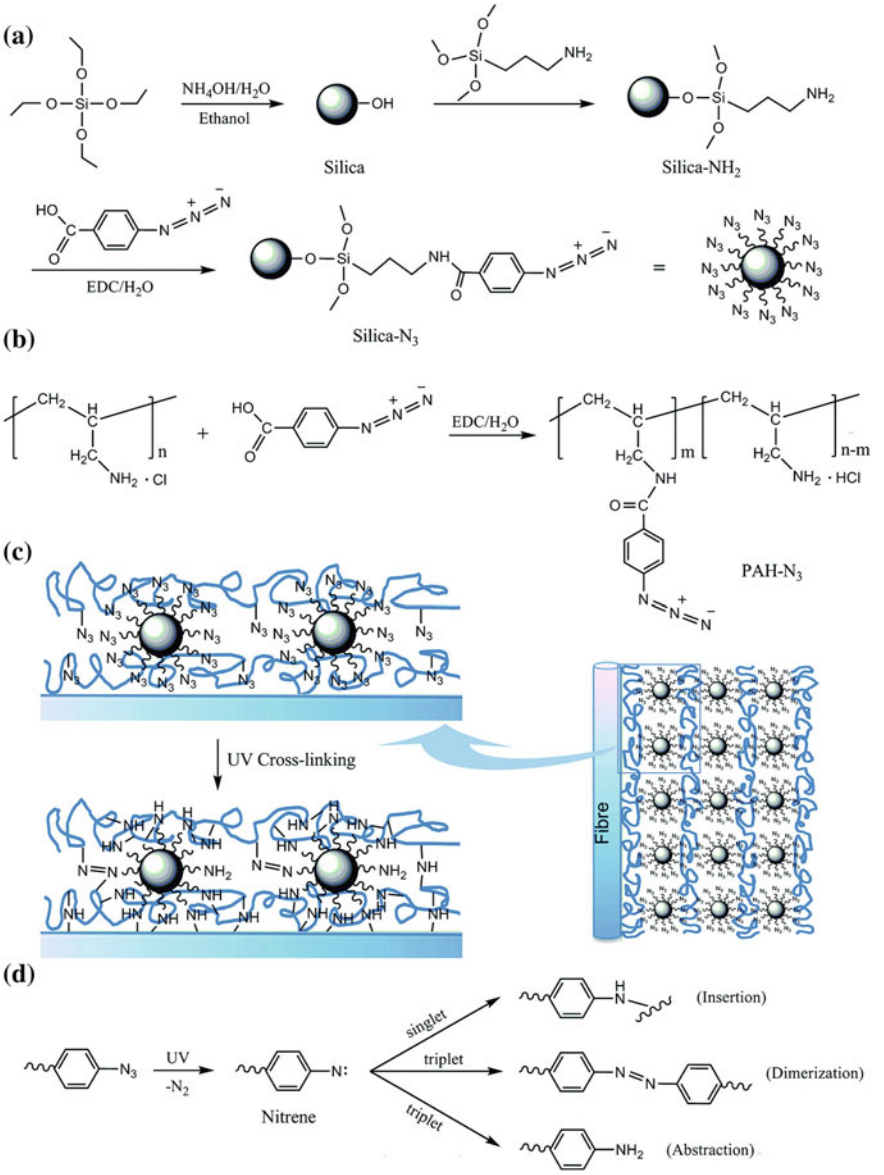

Fig. 5 Schematics for the synthesis of **a** silica-N_3 nanoparticles and **b** PAH-N_3, **c** the UV cross-linking of the PAH-N_3/silica-N_3 multilayers and **d** the possible photochemical reactions of phenyl azido groups. Reprinted with permission [113], copyright 2012, American Chemical Society

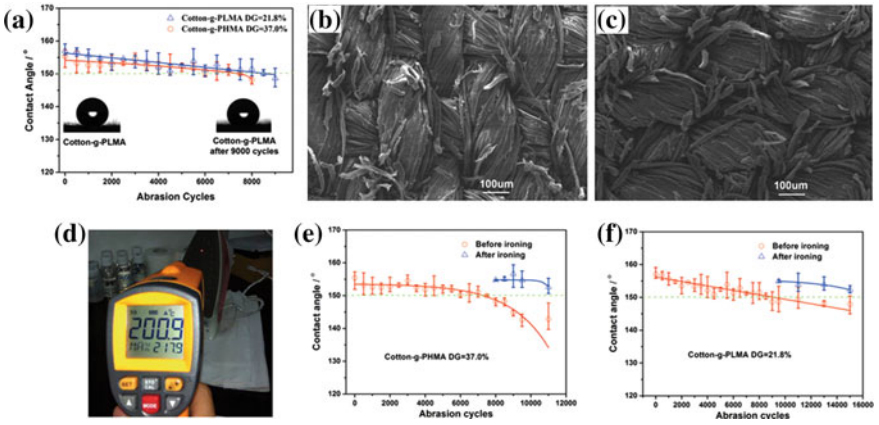

Fig. 6 **a** CA value versus the abrasion cycles of the Cotton-g-PHMA (DG 5 37.0 %) and the Cotton-g-PLMA (DG 5 21.8 %); inserted images: the image of a water droplet on the Cotton-g-PLMA (DG 5 21.8 %) before (*left*) and after (*right*) an abrasion test of 9,000 cycles; **b** SEM image of the Cotton-g-PHMA (DG 5 37.0 %) after an abrasion test of 8,000 cycles; **c** SEM image of the Cotton-g-PLMA (DG 5 21.8 %) after an abrasion test of 9,000 cycles; **d** The temperature measuring of the iron. **e** CA value before and after the steam ironing versus the abrasion cycles of the Cotton-g-PHMA(DG 5 37.0 %); **f** CA value before and after the steam ironing versus the abrasion cycles of the Cotton-g-PLMA (DG 5 21.8 %) [97]. Copyright © 2013 by Nature Publishing Group. Reproduced with permission of Nature Publishing Group in the format trade book via copyright clearance centre

3 Oil–Water Separation

The increasing interest of conserving water and oil/fuel/solvent and reflects in recyclability, reusability, protection from the foreign material mixing, saving for the future resources. The industrial oily wastewater, marine accidents and spillage influence environments and future energy so that the development of saving these things from each other also getting importance. The research efforts on flexible solid surfaces with well-controlled superhydrophobic and superoleophilic properties are useful to separate the oil–water after industrial and oil transport accidents, which leads to oil/fuel spills over aquatic environment. The modified cellulose surface should retain the inherent property of cellulose and porous structure in the network fibrils. This allows the flow of adsorbed liquid through capillary action. The immiscible oil–water mixture was then poured onto the functionalized fabrics, which permits the organic phase due to the superoleophilicity and Van der Waals force of attraction between the organic/composite interfaces. The permeability of the organic layer also depends on the micro texture, porous nature and additional gravitational force acting on the wetting organic liquid. Due to the superhydrophobic nature of the surface, the aqueous layer remains on the top of the membrane [110]. The separation capability of the composite membrane was checked with different amount of oil–water mixtures and successfully separated the oil such as

Table 2 Superhydrophobicity variations with respect to various compounds and type of process

Classification of materials	Materials	Method of preparation	Contact angle (°)	Remarks	References
Siloxane	MCTS	Solution-immersion process	160	Formation of a dense PMSQ nanofilament texture layer on the surface of fibres	Shirgholami et al. [57]
	ATS/GPTMS	Pad-dry-cure	154	Treated fabrics possessed negligible reduction in tensile strength, whiteness, and air permeability	Zhu et al. [118]
	HDMSO	rf-PECVD	163	Maintains its superhydrophobicity after water vapour condensation and after oil-wetting	Shin et al. [56]
Nanomaterials	HDMS/TiO_2-SiO_2@PDMS	Solution-immersion process	158	Thermally stable and photocatalytic superhydrophobic films	Deng et al. [15]
	Janus particles	Dip-coating	140	200 nm large Janus particles are very efficient for the design of water-repellent textiles	Synytska et al. [72]
	Nano-Al	Sol–gel technique	146	Excellent hydrophobic properties and UV protection efficiency with UPF value (164.06)	Pan et al. [48]
	Ag NPs	Solution-immersion process	153	Excellent antistatic, UV protection with ultraviolet protection factor (UPF) of 396.5	Guo et al. [23]
	Ag NPs	Dip-coating	151	High antibacterial activity against the gram-negative bacteria, *Escherichia coli*	Xue et al. [98]
	ZnO NPs/PS	Drop-coating	155	Excellent property in water–oil separation	Zhang et al. [111]
Polymers	PGMA-b-PTFEMA	Dip-coating	~163	Mechanical abrasion, strong laundering conditions	Zou et al. [120]
	p(V4D4-L-PFDA)	Chemical vapour deposition	153	Maintained its water repellence even after 20,000 cycles of the abrasion test and after 75 cycles of the laundry test	Yoo et al. [104]

(continued)

Table 2 (continued)

Classification of materials	Materials	Method of preparation	Contact angle (°)	Remarks	References
	P(POSS-MMA-VBFC)	Dip-coating	160	Excellent water and oil repellency	Gao et al. [19]
	PHEA	Cograft polymerization	~90	Enabled with a photocatalyzed self-cleaning effect under UV light radiation	Yu et al. [107]
	PNIPAAm	Grafting	152	Thermo responsive switchable wetting fabrics	Jiang et al. [29]
	PMETAC	Grafting (SI-ATRP)	154	Tunable wettability by counterion exchange	Jiang et al. [30]
	PFHEA-b-PIPSMA PFHEA-b-PGMA	Dip-coating	>150	Modestly water-repellent cotton fabrics with relatively poor stability Exhibited robust water repellency that withstood harsh test conditions	Shi et al. [58]
	PLMA, PHMA	Graft polymerization	152	Self-healing fabrics which could able to withstand at least 24,000 cycles of abrasion with periodic steam ironing	Wu et al. [97]
Combination of above	(PVDF-HFP)/FAS/ modified silica nanoparticles	Dip-coating	156	Self-healing ability to auto-repair against chemical damages	Zhou et al. [115]
	CeO_2-DFTMS	Dip-pad-cure	158	Rendered excellent protection against UV radiation	Zhou et al. [17]
	PEDOT/FD-POSS/FAS	Vapour-Phase polymerisation	169	Could able to withstand 500 cycles of standard laundry and 10,000 cycles of abrasion	Wang et al. [95]
	PANI-PTES	Vapour-phase deposition	156	Separation of water and oil mixture with separation efficiency as high as 97.8 %	Zhou et al. [116]
	PAH-N_3/ silica-N_3/ FAS	LBL	158	Stability of the silica nanoparticle/ polycation multilayer film was greatly improved after UV irradiation	Zhao et al. [113]

(continued)

Table 2 (continued)

Classification of materials	Materials	Method of preparation	Contact angle (°)	Remarks	References
	PFDT	Dip-coating	158	mechanical stability and easy repairability by a simple method	Zhu et al. [119]
	SiO2/DFPA	Dip-coating	153.6	Superhydrophobicity using microphase separation	An at al. [2]
	Poly-DMDAAC/ SiO_2/ HDFTDT	LBL/Dip-coating	155	Excellent chemical stability and outstanding non-wettability	Zhang et al. [112]
	P(FOEA-co-IPSMA)	Spray coating	160	Robust and resistant to both solvent extraction and NaOH etching	Zhang et al. [109]
	AD-HFPS	Solution-immersion process	139	High durability towards wash cycles and sonication in organic solvents	Ghiassian et al. [20]

petroleum ether, ethyl acetate, dichloromethane or chloroform from water. Apart from the separation efficiency the durability, preparation method, processing and high cost are also disadvantages to cut off for the good separator.

3.1 Siloxane Functionalization

Zhou et al. [116] fabricated the cotton textiles to introduce superhydrophobic properties in it for the separation of oil–water mixture. The preparation process involved vapour phase deposition of aniline at 70 °C for 30 min to previously coated cotton fabric with perfluorooctyltriethoxysilane, PTES and ferric chloride. The fabric was thoroughly rinsed with anhydrous ethanol, distilled water to remove all the residuals and dried at 100 °C for 30 min. The prepared PANI-PTES fabrics showed superhydrophobic behaviour with a WCA of 156°. Due to superhydrophobic and superoleophilic behaviour, cotton fabrics were useful in oil/water separation, with high separation efficiency up to 97.8 % and showing excellent durability (Fig. 7).

3.2 Metal Nanoparticles

Basu et al. [8] developed superhydrophobic behaviour on the glass substrate and cotton by depositing CuO film on the surface. Copper acetate and pyrrole were

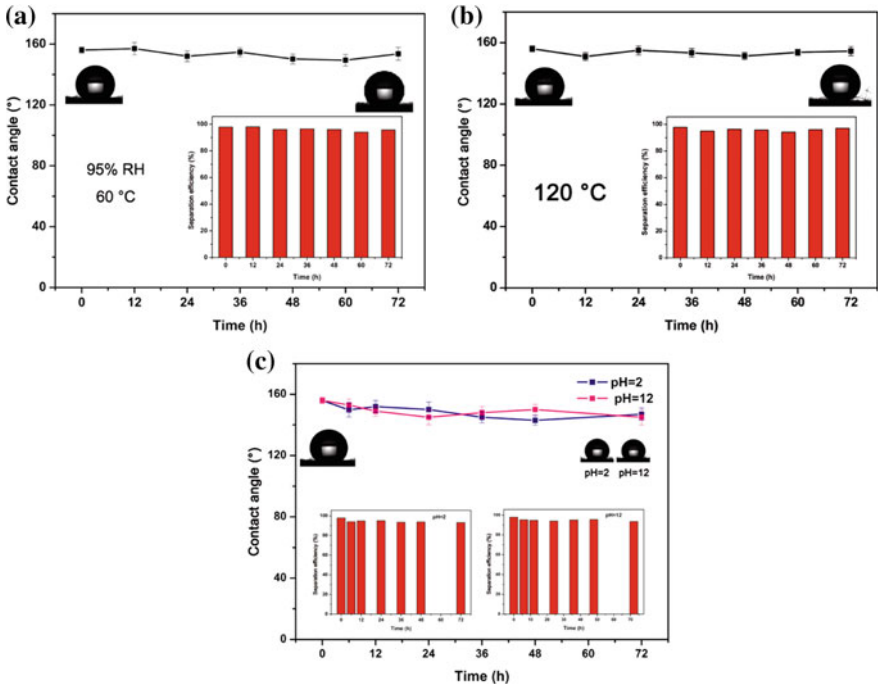

Fig. 7 Variation of water contact angles on the coated fabric **a** under 95 % RH at 60 °C, **b** at 120 °C, **c** exposed to acidic and alkaline solutions. Insets are the corresponding separation efficiencies for the oil–water mixture. Reprinted with permission [116], copyright 2013, American Chemical Society

poured in a vessel and heated for 1 h at 80 °C, after the appearance of blue colour, the cotton wool was immersed for an hour to become black, which indicates the deposition of CuO. The fabric was washed thoroughly, dried and reserved for the deposition of CuO by immersing and shaken well for an hour with the various thiol solution in ethanol. The prepared fabric having both superhydrophobicity with contact angle of 152° and superoleophilicity. Hence, the fabric was used for the separation of water immiscible solvents and the schematic representation of separation is shown in Fig. 8 and using that setup the solvents can be separated like hexane, petroleum ether, petrol, etc. from water in successful manner.

3.3 Nanocellulose

Cervin et al. [13] utilised the superhydrophobic ultra-porous nanocellulose aerogels as separation medium for oil/water mixtures. The aerogels had porosity greater than 99 % and their absorption capacity of hexadecane was up to 45 times of the aerogel

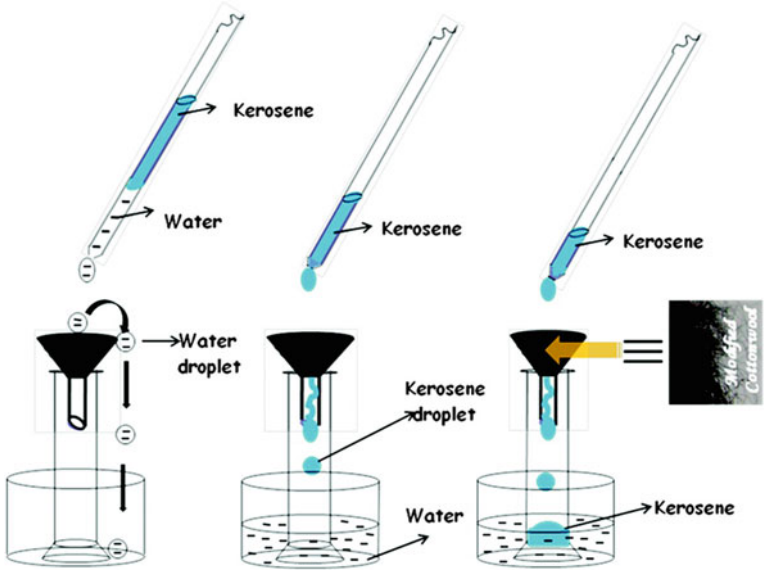

Fig. 8 Schematic representation of separation of kerosene–water mixture using modified cotton wool. Reprinted with permission [8], copyright 2011, American Chemical Society

weight. The aerogels could be reused several times as they did not show significant changes in volume upon sorption/desorption cycles.

4 Conductivity

The flexible conducting materials can be synthesised using metal wires (10^7 S/m) Ag(6.3) > Cu(5.85) > Au(4.25) > Al(3.45) > Al–Mn(2.95) > Na(2.1), conjugating polymers containing S, N and πC-πC backbone, charge-transfer complexes, anionic polymers and carbon materials such as CNT, graphene and its derivatives. After fabricating with these materials, the conductivity can be tuned using various dopants and doping methods. Conductive fibre are used in conducting wires, sensors, actuators, wearable displays, embedded health monitoring devices, electromagnetic interference shielding, textile-based circuits and energy harvesting devices, and collectively multifunctional fabrics in wearable textiles [42]. The method of preparation involves direct dip-coating, spray coating and sol–gel methods. These methods have several disadvantages like the problems associated with the conducting polymers solubility, viscosity, wettability with the substrate and non-uniform coating, which leads to lack in the homogeneity in the thickness decreasing the conductivity on the surface. The in situ polymerisation onto the substrate is the way to bringing up effective conductivity throughout the surface by several

methods such as electro-polymerization, chemical polymerization, plasma polymerization, etc. Layer-by-Layer method is a simple technique for using wide range of polymers, forming thin films onto the surface, which in turn helps in tuning the properties of the materials.

4.1 Conducting Polymers

Conductivity can be triggered on the nonconducting surfaces using conducting polymers with extensive π conjugation, metal implantation by electron transfer/flow and usage of graphene and its derivatives. Further, this was improved by various doping and applying procedures. Conducting polymers are conducting electricity by the flow of electrons in aromatic compounds (polypyrrole, polyaniline, polythiophenes, polyazulenes, etc.), aliphatic compounds (polyacetylenes) via effective delocalisation of electrons. These kind of organic conducting polymers have the conductivity in the range of 10^{-4}–10^{4} S/m.

4.1.1 Polypyrrole

Polypyrrole has been extensively studied in the past decades and pyrrole was polymerized by CVD, chemical, electrochemical, plasma polymerization techniques and the problems associated with the conductivity is the cross-polymerization of 2-3', 2-4', 2-5' by the rotation of pyrrole unit. The defects in the polymerization decrease the orientation of linearity in chains, conjugation between the rings, and thereby affecting the conductivity of PPy. The action of atmospheric oxygen attack on polypyrrole leads to formation of β-unsaturated carbonyl groups, which acts as an electron trap, thus decreasing the conductivity of the fabric day-by-day. This reduces the life span but there is no need of special design for disposal (biodegradable).

Effect of Dopants

Patil and Deogaonkar [49] used the in situ chemical polymerization of pyrrole on textile using oxidant at various temperatures with various dopants to study about the conductivity behaviour. From this study, for effective polymerization two electrons are required to polymerise the each pyrrole unit and the 1/3 electrons required to oxidise the dopants in a chain. The pyrrole units are interacting with H-bond with the cellulose fabrics, further treating with oxidant ($FeCl_3$) pyrrole gets polymerized product which observed by the colour change over the textile from white to black. After the polymerization, it was washed, dried to remove the unreacted monomers and water. The temperature affects the rate of polymerization that reflects in orientation of the pyrrole units and conductivity behaviour. The low temperature of

the reaction lowers the rate of the reaction, which eventually results pyrrole–pyrrole unit in 180° rotation, thus making it more conductive.

The polymer with sulfonic acid dopants can increase its atmospheric stability and conductivity of the fabrics with the extent of ½ to 1/3, due to peculiar positioning of dopants in the PPy chain facilitates interchain charge hopping more readily than small dopants like Cl^- ions. Based on this, the conductivity order changes with respect to the dopants as given below. AQSA > NSA > N@D2SA > DBSA, Cl.

Effect of Oxidant

Muller et al. [46] utilised hydrated bacterial cellulose to prepare electrically conductive nanocomposite using in situ polymerisation method. The polymerisation of pyrrole was carried out on the bacterial cellulose surface using $FeCl_3$/APS as an oxidant. After 4 h, grafted fabrics were washed with distilled water and dried at room temperature. Depending on the amount of polypyrrole and the type of oxidant used, the conductivity of the fabrics varies, i.e. 80 % of PPy content (0.05 mol of pyrrole, $FeCl_3$ as oxidant) grafted fabrics exhibited conductivity up to 270 S/m, whereas 32.5 % (0.05 mol pyrrole, APS as oxidant) exhibited 1.2 S/m. The 2nd order magnitude variation of conductivity observed in the fabrics was achieved by using same monomer concentration with different oxidants. Even though, the pyrrole having same doping degree, the counterion mobility and number of defects in the polymer chains contributing the 2nd order magnitude changes in the electrical conductivity.

Effect of Metal Nanoparticles

Babu et al. [4] prepared PPy-Ag embedded antimicrobial textiles by adding silver nitrate solution onto the 30 min impregnated cotton fabrics, stirred for 24 h, washed with methanol and water followed by drying. The silver nanoparticle greatly influenced the conductivity of the cotton fabric up to 4-fold (4.82×10^{-1} S/m) with respect to the polypyrrole-coated fabric (1.03×10^{-1} S/m) and additionally conductivity increased with the NPs concentration (Fig. 9) and Xu et al. fabricated the cotton with PPy/Ni [101]. They developed a textile-based electrode for the application of high-performance supercapacitors and DSSC applications.

4.1.2 Polyaniline

Li et al. [36] utilised the in situ polymerization grafting techniques to develop conducting textiles by the APS oxidative polymerization of aniline onto the previously grafted acrylamide using PPS. The polymerisation and dopants were carried out in two bath, viz., APS bath to oxidise the monomer and HCl bath to introduce

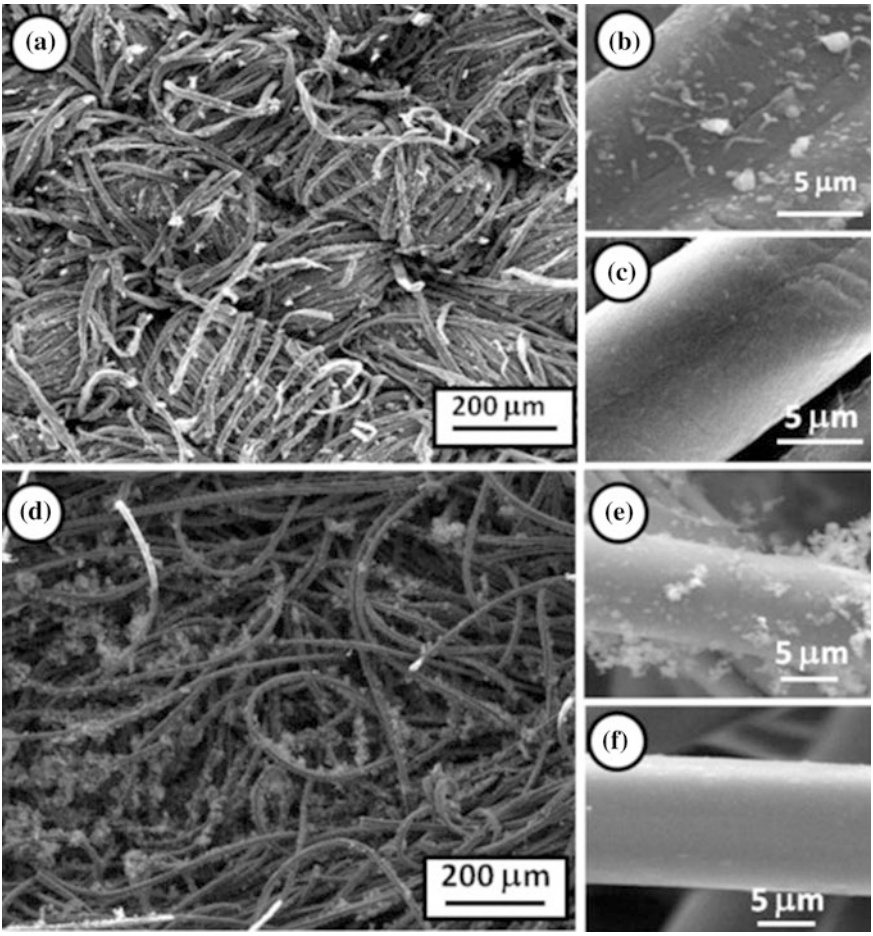

Fig. 9 Scanning electron microscopic images of textiles **a** PPy-Cotton at lower magnification, **b** PPy-Cotton and **c** bare cotton at higher magnification, **d** PPy-Viscose atlower magnification, **e** PPy-Viscose and **f** bare viscose at higher magnification. Adopted from [6] with permission, copyright 2013, Elsevier

the dopants on it. The authors extensively studied the problems associated with the grafting process such as concentration of oxidant affecting the conjugation due to over oxidation, and dopants making the salt formations at higher concentration. So the concentration of oxidant, monomer, dopant and processing time of chemical grafting process are import to impart reasonable conducting properties to the cellulose fabrics. While dipping the cotton fabric (previously soaked in 0.9 mol/L of APS and 0.6 mol/L aniline solutions) in 1 mol/L HCl for 30 min, the conductivity increases by one order magnitude with the value of 2.45×10^{-2} S/m.

Polyaniline with Nanoparticles

Savitha et al. [53] developed highly durable polyaniline–TiO_2 coated cotton fabrics with conductivity up to 10,000 S/m. The 1.3 ml of solution (2 ml of $TiCl_4$in 10 ml of alcohol) and 0.6 ml of aniline were added into the flask containing 40 ml of 1 M acetic acid at r.t. and the reaction mixture stirred at 80 °C for 4 h. The cotton fabric was completely immersed in the colloidal solution by continuous stirring for 1 h at room temperature. The fabric with aniline–$TiO_2$was polymerised using 1.0 molar ratio of APS and 0.5 molar ratio of CSA with respect to aniline. Then the fabric was washed with distilled water, dried and conductivity measured as 1.5×10^{-1} S/m. The conductivity of the fabrics is increased with TiO_2 concentration but it is reverted due to the higher TiO_2 concentration due to orientation defect and conjugation blocking of conjugation and hinder the carrier transport between different molecular chains of polyaniline.

4.1.3 PEDOT:PSS

Tarabella et al. [73] converted cotton yarns into semi-conductive yarns using the simple and economic by coating and baking method. Cotton yarns were soaked in the aq. PEDOT:PSS at 6 °C for 48 h followed by baking on the hot plate at 145 °C for an hour. Then the fabric was soaked in ethylene glycol for 3 min at room temperature to improve the conductivity and stickiness on the yarn. Fabrics showed low electrical resistivity of 25 x 10^3 Ω/cm, whereas modified aqueous solution of PEDOT:PSS with 5 % dodecyl benzenesulfonicacid (dopant, surfactant) and 20 % of ethylene glycol showed 430 Ω/cm due to the dopants and effective coating by reducing solubility of PEDOT:PSS in aqueous media. This process is simple, low cost and used as a channel of an organic electrochemical transistor for wearable health care electronics.

Mattana et al. [44] developed a technique in which metal nanoparticle (Au) imprinting onto the conducting polymer PEDOT-coated fibres. The cotton fabrics were soaked in the solution of metal nanoparticles for 24 h and then the fabric rinsed with water to remove the loosely bounded gold nanoparticles, after which it was dried in air oven. Previously, the cotton fabric was converted into cationic cellulose fabrics by immersing in aqueous solution of (2,3-epoxypropyl) triethylammonium chloride. The prepared gold nanoparticles decorated on cotton fabrics having the resistance up to 1.2 x 10^8 Ω/cm. The chemical vapour deposition techniques were employed to deposit thin film of PEDOT:tos on the cotton yarns. PEDOT:tos coated cotton yarn was soaked in a solution of 125:25:1 wt% of isopropanol:Fe(III)-tosylate:pyridine for 10 min and dried at 80 °C for 3 min followed by 50 °C for half an hour. The fabrics were finished with rinsing with ethanol and drying in oven for 12 h at room temperature. From the experimental results, PEDOT:tos coated over the Au NPs coated cotton fabrics exhibited improved conductance behaviour up to 4 orders of magnitude. This kind of nanoscale modification on natural cotton fibres with metal nanoparticles imprinting onto the

conjugative conducting polymers enhances the conductivity by 7.5 % comparing polymers and similarly 10^4 times with natural cotton yarn. Obviously the increasing order of conductivity will be cotton + Au NPs + PEDOT:tos > cotton + PEDOT: tos > cotton + Au NPs > Cotton. The fabric coated with Au NPs and PEDOT:tos have the good electrical and mechanical properties that can be useful for making conductors, electrochemical transistors.

4.2 Nanoparticles Coating

Cotton textiles conductivity was improved by electrochemical nanoparticle deposition method using three electrodes system [7]. The activated cotton textiles, ACT was made of dipping, drying and annealing processes which were carried out by dipping the textile in 1 M NaF solution for 1 h and drying at 120 °C, followed by annealed in tubular furnace at 800–1200 °C in argon atmosphere for an hour. Counter electrode, Pt foil and working electrode, ACT was immersed into the electrolyte solution of equimolar 0.1 M solution of Mn $(CH_3COO)_2$ and Na_2SO_4. A constant current 1 mA/cm^{2}was applied for 30–240 min to coat the MnO_2, and then fabrics were washed with deionised water to remove the electrolyte and then dried in oven at 100 °C for 3 h. Such fabrics have resistivity of 10–20 Ω/sq which is enough to get the supercapacitor behaviour on the textiles.

Wei et al. [96] developed a novel textile-based six-layer structured sensor including conductive layer, which was achieved by applying silver/polymer paste over cotton/polyester fabric and cured at 150 °C for 30 min. This kind of printing method for conductive applications gave satisfactory resistivity about 0.015 Ω/sq. They have developed cantilevers using the above conductive material as motion sensors to detect human arm movements that can sense both slow and fast motions.

Superhydrophobic antimicrobial cotton conductive fabrics with silver nanoparticles without using any conducting polymers were developed by Xue et al. [99]. 10 wt% NaOH treated cotton fabrics were dipped into the $[Ag(NH_3)_2]^+$ solution for 1 h and then fabric transferred into 0.1 M glucose solution and the reaction mixture were stirred with the dipped fabric for 15 min and then fabrics were washed, dried in air. The conductivity of the dried superhydrophobic fabrics was measured to be 37 Ω/cm.

In_2O_3/SnO_2nanoparticles:

Hu et al. [27] reported cotton fabric was dipped into the previously prepared ITO precursor solution (indium chloride and tin chloride) for 2 h under vacuum, dried at 60 °C for 0.5 h and the same process was repeated three times. After calcination at 350–550 °C for 4 h, the size of NTO particles over fabrics is changed to 20–30 nm resulting in conductive network. The conductivity of the regular nanoparticle network on cotton template was improved up to 5 S/m.

ZnO Nanoparticles:

Jur et al. [31] used atomic layer deposition method (ALD) technique to deposit nanoparticles conformal layer on the fabric with retainable inherent properties. One of the drawbacks of this method is mechanical cracking with increasing number of cycles (i.e. after 500 cycles). 20–200 nm thickness ZnO oxide films were deposited on the cotton fibre using diethylzinc and water in an ALD cyclic process (180–600). The conductivity of the fabrics increases with number of cycle and at the end of 240th cycle, the conductivity hits its highest notch at 2400 S/m.

4.3 Carbon Derivatives

Carbon derivatives such as graphene and carbon nanotubes have greater number of sp^2 carbon atom which allows extensive delocalization of electrons which increases the conductivity of the materials. Based on the effective coating the conductivity of the materials will vary due to lack of connectivity between the coated conductivity batches.

Yun et al. [108] fabricated highly conducting fibre by chemical reduction method of graphene oxide using HI. Bovine serum albumin (BSV), universal adhesive, was used to coating on cotton, nylon-6, polyester to improve the holding capacity of graphene oxide. BSV-coated fabric was further dipped in aqueous solution of graphene oxide after that reduced with HI and finally reduced graphene oxide coated on cotton. Thus, conductivity was achieved up to 10^3 S/m along with properties with highly durable and 400 bending cycles.

Guinorart et al. [22] built electrochemical sensors for wearable textile devices using commercial cotton yarns into electrical conductors through a simple dying process using a CNT ink. CNT ink was prepared by 3 mg/ml of SWCNT in an aqueous solution of sodium dodecyl sulphate. After drying, the resistivity of the textile fabric was decreased to 500 Ω/cm due to CNTs wrap around the cellulose fibres through strong supra molecular interaction. The improved conductivity by the supramolecular interaction is enough to make sensor and to sense the electrochemical reactions.

Mateos et al. [43] developed conducting recipe by dip-coating of polycation and polyanion in the industrial scale. The textile was coated with 1.0 wt% of branched polyethylenimine, (BPEI) as an adhesive to bind the polycation and polyanion effectively. The textile were rolled for 12 h in 0.25 wt% of positively charged aqueous solution of poly(diallyl dimethyl ammonium chloride), followed by sonication at 20 W for 1 h in a solution of 0.05 wt% of MWCNT and 1.0 % sodium deoxy cholate (DOC, stabilizer). After that, the solution pH was adjusted to 4 to bring out the effective deposition. A nip-roll techniques were used to remove excess solution after each deposition. The coated textile fabric was dried in an oven at 70 °C to remove moisture. The industrially scaled textile fabrics with MWCNT coating is bringing resistivity up to 8.1 x 10^4 Ω.

4.4 Applications

Conducting textiles used for several applications such as sensor [22, 31], supercapacitors, wearable electronics, DSSC [32, 37], drug delivery applications [4]. Due to its advantages, it can be useful as electrode material for supercapacitor applications [6, 105]. Phase memory polymers can respond to external stimuli due to the enthalpy changes during the phase change. Babu et al. [5] developed a thermally responsive textile pads with the polypyrrole-modified textiles. Polypyrrole-modified cellulose derivatives are one such type of materials that can respond to external thermal stimuli due to the molecular level/local dimensional changes and interfacial interaction between NWVR (nonwoven viscose rayon) and polypyrrole. Polypyrrole–NWVR strips are illustrating the upward movements and angle variation with respect to the actuation of thermal stimuli (Fig. 10). These kinds of highly responsive materials are useful for the electric fields and robotic engineering technological products.

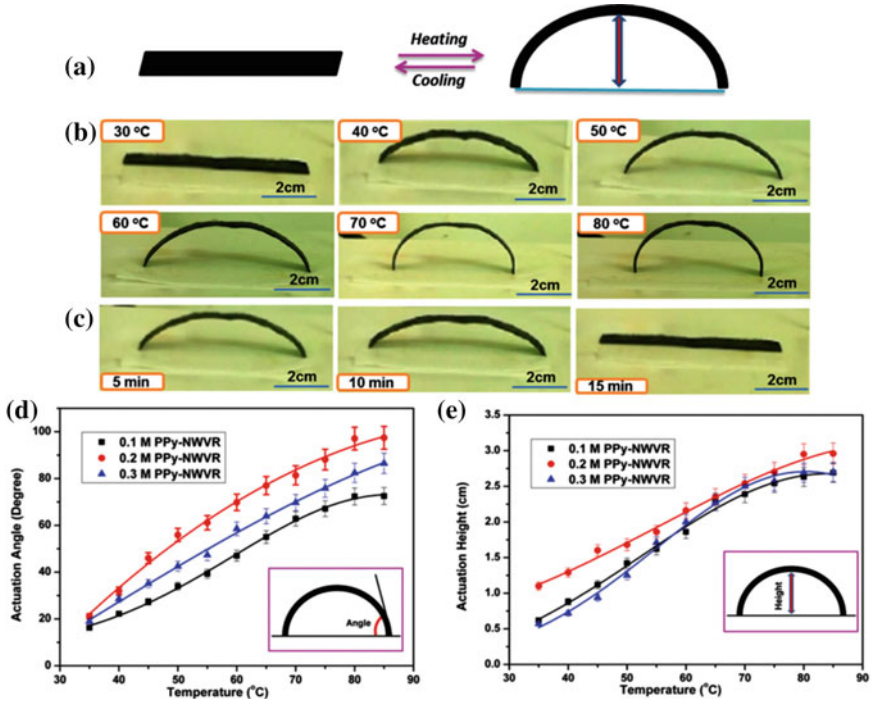

Fig. 10 **a** Schematic illustration of the bending movement/unbending of the PPy-NWVR strip towards temperature changes, **b** Digital photographic image of the bending movement at different temperatures, **c** time profile of unbending movement after removal from the hot plate and temperature-dependant actuation **d** angle and **e** height of the PPy-NWVR strip ($1 \times 7 \times 0.3$ cm^3). Reproduced with permission [5], copyright © 2014 WILEY-VCH Verlag Gm bH & Co. KGaA, Weinheim

5 Drug Delivery

Clothing materials, pressure garments, artificial body parts, wound dressing materials, transdermal patches and bandages are also made of cellulose materials that are having the high breathability, flexibility, fibrous in nature. Due to the wide usages, the production of such materials with high durability and recyclability against the increased problems of microbial contamination and fibre damages due to environmental factors. Hence, the highly durable antimicrobial textiles were prepared by coating/grafting with various metal nanoparticles, metal oxide nanoparticles, quaternary ammonium compounds, *N*-halamine derivatives and other class of antibiotics. Further, these materials can be useful for the water purification methods to kill the microbes present in the aquatic environment. Microbial survival percentage on the cellulose derivatives was calculated using the following formula:

$$\text{Reduction viability}, (\%) = \left(\frac{A - B}{A}\right) \times 100$$

Where, A and B are the average number of bacteria with the respect to time and zeroth time on the contact with the microbial.

5.1 Nanoparticles

Metal/metal oxide nanoparticles are effective antimicrobial agents used in drug delivery and other biomedical devices. Even though, certain metal/metal oxides are hazardous for the body, after optimization of the concentration level (non-hazardous) the drug can be delivered into the body for safety. The controlled release of such hazardous materials is usually done by encapsulating the drug molecules into the polymer matrix which also increases the stability and efficacy of the core drug molecules.

Perelshtein et al. [50] and Petkova et al. [51] developed an innovative approach of sonochemical method to develop antimicrobial dressings on cotton fabrics. ZnO NPs were coated sonochemically on the cotton fabrics using an ultrasonic transducer for 30 min in a solution containing aqueous ZnO NPs and chitosan. After coating, the samples were washed thoroughly with water and dried to obtain 12–40 nm of ZnO coating thickness. Antibacterial activity of the coated fabrics showed good antimicrobial activity which shows that more than 98 % of both *S. aureus* and *E. coli* survival was controlled within 60 min (Fig. 11). The antimicrobial coatings were highly resistant to multiple washings and temperature (up to 75 °C) for uses in a hospital environment.

Moreover, the cellulose-based fabrics were used for coating with combination of metal nanoparticles and metal nanoparticles/polymers giving efficient drug delivery.

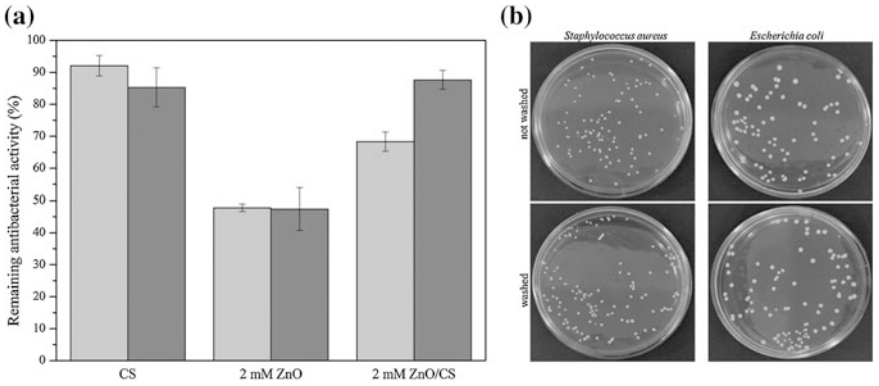

Fig. 11 **a** Percentage of remaining antibacterial activity of the coatings after 10 washing cycles at 75 °C against *S. aureus* (*light grey bars*) and *E. coli* (*dark grey bars*), after 15 min of contact. **b** Antibacterial activities of the Zn^{2+}/CS fabrics before and after washing. Reprinted with permission from [51], copyright 2014, American Chemical Society

Arain et al. [3] used a simple pad-dry-cure method to study about the antibacterial activity of AgCl–TiO_2/chitosan colloid coated fabric. The antimicrobial cotton fabrics were fabricated by dipping into solution containing chitosan and AgCl–TiO_2 colloid, nipped, dried for 3 min at 120 °C, curing for 3 min at 150 °C. Authors highlighted that the synergistic effect of the colloid (Chitoshan and AgCl) resulted in effective antimicrobial activity against the microbes. Several reports are also available on Ag NPs within PPy matrix [4], Ag with chitosan [1], Ag NPs with sericin [106], TiO_2 with sericin [16], MgO NPs [71], Zn NPs with CuO [41], Cu_2O [54] coating with the cellulose substrate.

5.2 Drug Molecules

Luo et al. [39] synthesised cellulose–EDTA conjugates by esterification of cotton fabrics with EDTAD (Ethylenediaminetetraaceticdianhydride) to show the initial protection of mammalian cells from microbial cells. 15 g of pre-treated cotton fabrics was added to the solution of 30 g of EDTAD in 500 ml of anhydrous DMF and the reaction was carried out under constant stirring at 75 °C. After completion of the reaction, the treated fabrics were washed, dried and stored for 72 h. The authors highlighted the antimicrobial efficacy of these materials with respect to different grafting yields, in which the fabrics having 15.7 % grafting yield is enough to kill the bacteria in 2 h minimum contact time.

Zhuo et al. [117] reported the development of anthraquinone-based light-induced antimicrobial cotton fabrics and evaluated against the microbes. 1–9 % of 2-Ethylantraquinone, 2EtAQ/0.5 % of Vat Yellow GCN was dispersed in water under alkaline conditions and then allowed to react with sodium dithionite for 10 min at

50 °C. To this 20 times diluted salt solution, the cotton fabrics were immersed and then dyeing for 50 min with agitation at room temperature. Upon dye exhaustion, the treated fabrics were dried, oxidised at r.t. in air, and then washed with boiling detergent water for 30 min, rinsed and dried at r.t for overnight. The light-induced antimicrobial function of the cotton fabrics were evaluated by *in vitro* studies which exhibited that the 99.99 % reduction rate of bacterial count was noticed in 30–60 min depends on the weight percentage of the drugs.

Hong and Sun [26] produced photoactive antimicrobial cotton fabrics by esterification of benzeophenonetetracarboxylicdianhydride (BPTCD) with cellulose. The cotton fabrics were immersed in a solution of BPTCD and sodium hypophosphite hydrate and then the reaction mixture shaken for 30 min. Further, the fabrics were padded to have a 130 % wet pickup rate, dried at 85 °C for 30 min and cured at 150 °C for 4 min followed by washing and air drying at 25 °C for 24 h. The antimicrobial activity was found to be increasing with increase for BPTCD, so that reduction rate of 99.99 % was achieved in 2 h for 0.2 M of BPTCD. The mechanical properties of the fabrics retain after the process.

Chen et al. [14] grafted an environmental friendly antibacterial cotton fabrics with siloxanesulfopropylbetaine (SSPB). The cotton textiles were functionalised covalently with Si of SSPB by dip-coating. In detail, the cotton textiles were ultrasonic washed with dimethylacetamide and water for 10 min and then the dried fabrics dipped in 2.0 wt% SSPB/alcohol to get the 0.03 mg/cm^2 of SSPB on textiles. The authors highlight that the drug materials is nontoxic, non-leachable from the fabrics, and does not induce skin stimulation. These hydrophilic antibacterial fabrics have a good killing efficiency of 89 % within first 1 h.

Shimanovich et al. [55] developed a sonochemical method to coat tetracyclin, TTCL-loaded proteinaceous microspheres were made of BSA and casein proteins. The authors made TTCL-encapsulated microspheres with proteinaceous proteins and optimised the optimal concentration to coat on the cotton/polyester is 5.4×10^{-3} M. Dodecane and aq. BSA/casein solution and cotton fabrics were taken in a reaction cell and to the solution 5 % of TTCL was added to it. The whole mixture was sonicated for 3 min and then ultrasonic horn was positioned bottom of the reaction cell to coat at constant temperature of 22 °C. After the reaction, the bandages were washed to remove the unbounded microspheres on 1328 nm cotton fabrics and 680 nm polyester fabrics. Such prepared fabrics show good antimicrobial activities and comparable with the 30 μg of TTCL tablet with a zone inhibition of 27 mm for 12 μg of TTCL.

Cerkez et al. [12] have used simple and layer-by-layer assembly technique for multiple time coatings onto cotton surface. 0.2 wt% of poly(2,2,6,6-tetramethyl-4-piperidyl methacrylate-co-trimethyl-2-methacryloxyethylammonium chloride), PMPQ and Poly(2,2,6,6-tetramethyl-4-piperidyl methacrylate-co-acrylic acid potassium salt), PMPA in water was made in two separate bath. Bleached cotton swatches were dipped alternatively into these solutions for 5 min followed by 2 min ethanol rinsing and drying at 100 °C for each dipping process. Between these two

dipping process, the fabrics is washed with deionized water for 30 s to remove the unbounded polyelectrolytes. The fabric is treated at 120 °C for 12 h, and then washed with detergent and subsequently with water. Finally, it undergoes chlorination to activate the drug. Chlorinated halamine drugs show effective bacterial activity against microbes within 15 min of contact time.

Ma et al. [40] reports the synthesis of *N*-halamine epoxide and grafting with cotton fabrics to apply for antimicrobial dressings. *N*-halamines-based antimicrobial activities depend on the stabilities of the halamine bond and structure (descending order imide > amide > amine). *N*-halamine based drugs are traditionally coated using pad-dry-cure process. 1-Glycidyl-s-triazine-2,4,6-trione, (GTT) was previously synthesised and dissolved in water with 3–10 %, to this solution, cotton swatches were soaked for 15 min. After two dips and two nips process, the swatches were dried at 95 °C for 5 min, cured for 10–20 min at 160–170 °C and then soaked with 0.5 % detergent solution for 15 min, washed and dried at ambient temperature. The cotton swatches were activated with 10 % sodium hypochlorite, NaOCl at pH 7 for 1 h at r.t. This fabric was further washed with distilled water and dried at 45 °C to remove the free chlorine and to get highly durable antimicrobial textiles. The authors demonstrated that the more than 99.98 % reduction against bacteria within 1 min contact time. The fabrics showed good stability of imide halamine after repeated washing 50 cycles with a loss of 30 %.

Kocer et al. [34] prepared *N*-halamine-based copolymers showing the antimicrobial activities on cotton swatches. The copolymer of 3-chloro-2-hydroxypropylmethacrylate and glycidyl methacrylate (called GM) and 3-glycidyl-5,5-dimethylhydantoin (M) were dissolved in acetone to obtain a homogeneous solution. The cotton swatches were soaked in the above solution for 15 min, and then padded, cured at 165 °C for an hour. After this process, the swatches were washed with detergent solution and water for several times. The coated fabrics were immersed in 5,5-dimethylhydantoin potassium salt solution in ethanol for 5 min under reflux conditions to afford stiffer and slightly yellow fabrics, after washing the fabrics with water, the fabrics became soft and white. The drug molecules were activated by the chlorination using household bleach solution. Thus prepared fabrics inactivates the bacteria within 5 min of contact time.

Ringot et al. [52] reported a simple synthesis of photosensitizer-bearing antimicrobial cellulose substrates for effective killing of gram-positive bacteria. Aminoporphyrin, (TPP-NH2)/anionic sulfonedaminoporphyrin, (TPPS-NH2)/cationictrans-pyridiniumaminoporphyrin, (trans-MePyþ-NH2), was dissolved in THF and then 1.2 eq of cyanuric chloride and 1.2 eq of DIPEA/$NaHCO_3$/DIPEA were added at 0 °C. The reaction mixture stirred for 15 min at 25 °C. The cotton fabric pre-treated with NaOH, the grafting was achieved with the above reaction mixture in 24 h at 70/80/70 °C. Finally, the fabrics were washed with THF, $CHCl_3$, and hot DMF for 24 h at 100 °C and then finishing with drying at 100 °C for an hour (as shown in Scheme 1). The prepared fabric will be called as neutral/anionic/cationic photosensitive cotton fabrics. The fabric showing good antimicrobial activity against *S.aureus* and following this order of better activity in the increasing order of anionic, neutral and cationic.

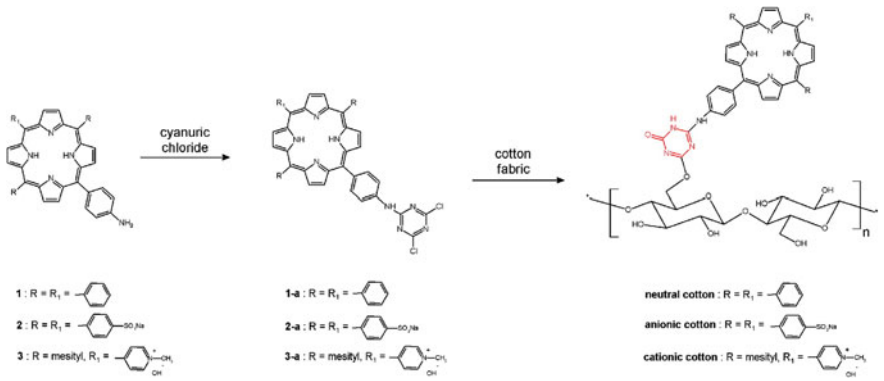

Scheme 1 Synthetic route to photo-antimicrobial cotton. Reprinted with permission from [52], copyright 2011, American Chemical Society

6 Conclusion and Future Perspective

The main part of cellulose research focused on various approaches from one-step to multi-step process for effective durability and properties. The polymerization and coating methods are extensively used to obtain superhydrophobic, conductive and biological properties on the biofibrous materials. The limitations that are yet to overcome are durability of the coating, problems associated with the conversion of lab scale to plant process, multi-step processing, coating thickness, economically viability processes and low grafting efficiency. The chemistry of biofibres with polymers and nanoparticles will satisfy modern world requirement with eco-friendly composites for multifunctional applications. The biofibre composite materials durability can be enhanced up to 20,000 usage cycles with retaining the properties through grafting polymerization methods. The research area opens to find such grafting methods with the cellulose for achieving highly durable, highly conductive (>1000 S/m), amphiophobic and eco-friendly biocomposites.

As can be seen from the above discussions, grafting of polymers along with nanocomposites with cellulose fabric is an exciting topic of research. Future developments in this polymer nanocomposites biofibres filled will surely revolutionise the textile industries. The promising future developments include,

(a) The novel functions to be introduced on textile surfaces include, detoxification (filtering of toxic chemicals), membrane for oil–water separation, sensor, actuators and flexible electrodes for energy storage devices.
(b) Health care materials, where sustained release of drug is required for wound healing especially in case of diabetic/cancer purposes.

Acknowledgments This research was financially supported by the Department of Science and Technology (DST), New Delhi (GAP 08/13) and Council of Scientific and Industrial Research (CSIR), New Delhi, India (12 FYP-CSC-0134, M2D).

References

1. Abou-Okeil A (2012) Ag nanoparticles growing onto cotton fabric using chitosan as a template. J Nat Fibers 9:61–72
2. An Q, Xu W, Hao L et al (2013) Fabrication of superhydrophobic fabric coating using microphase-separated dodecafluoroheptyl-containing polyacrylate and nanosilica. J Appl Polym Sci 128:3050–3056
3. Arain RA, Khatri Z, Memon MH, Kim I-S (2013) Antibacterial property and characterization of cotton fabric treated with chitosan/AgCl–TiO2 colloid. Carbohydr Polym 96:326–331
4. Babu KF, Dhandapani P, Maruthamuthu S, Kulandainathan MA (2012) One pot synthesis of polypyrrole silver nanocomposite on cotton fabrics for multifunctional property. Carbohydr Polym 90:1557–1563
5. Babu KF, Narayanan TN, Kulandainathan MA (2014) Molecular motions aided thermally responsive biocompatible textile pads. Adv. Mater. Interfaces 1:1300139
6. Babu KF, Subramanian SPS, Kulandainathan MA (2013) Functionalisation of fabrics with conducting polymer for tuning capacitance and fabrication of supercapacitor. Carbohydr Polym 94:487–495
7. Bao L, Li X (2012) Towards textile energy storage from cotton t-shirts. Adv Mater 24:3246–3252
8. Basu M, Sinha AK, Pradhan M et al (2011) Fabrication and functionalization of CuO for tuning superhydrophobic thin film and cotton wool. J Phys Chem C 115:20953–20963
9. Bittoun E, Marmur A (2012) The role of multiscale roughness in the lotus effect: is it essential for super-hydrophobicity? Langmuir 28:13933–13942
10. Bormashenko E, Musin A, Whyman G, Zinigrad M (2012) Wetting transitions and depinning of the triple line. Langmuir 28:3460–3464
11. Carosio F, Blasio AD, Cuttica F et al (2014) Flame retardancy of polyester and polyester-cotton blends treated with caseins. Ind Eng Chem Res 53:3917–3923
12. Cerkez I, Kocer HB, Worley SD et al (2011) N-Halamine biocidal coatings via a layer-by-layer assembly technique. Langmuir 27:4091–4097
13. Cervin N, Aulin C, Larsson P, Wågberg L (2012) Ultra porous nanocellulose aerogels as separation medium for mixtures of oil/water liquids. Cellulose 19:401–410
14. Chen S, Chen S, Jiang S et al (2011) Environmentally friendly antibacterial cotton textiles finished with siloxane sulfopropylbetaine. ACS Appl Mater Interfaces 3:1154–1162
15. Deng Z-Y, Wang W, Mao L-H et al (2014) Versatile superhydrophobic and photocatalytic films generated from TiO 2–SiO 2@ PDMS and their applications on fabrics. J Mater Chem 2:4178–4184
16. Doakhan S, Montazer M, Rashidi A et al (2013) Influence of sericin/TiO2 nanocomposite on cotton fabric: part 1. Enhanced antibacterial effect. Carbohydr Polym 94:737–748
17. Duan W, Xie A, Shen Y et al (2011) Fabrication of superhydrophobic cotton fabrics with UV protection based on CeO_2 particles. Ind Eng Chem Res 50:4441–4445
18. Dufresne A (2013) 8—Cellulose-Based Composites and Nanocomposites. Handb. Biopolym. Biodegrad. Plast. William Andrew Publishing, Boston, 153–169
19. Gao Y, He C, Qing F-L (2011) Polyhedral oligomeric silsesquioxane-based fluoroether-containing terpolymers: synthesis, characterization and their water and oil repellency evaluation for cotton fabric. J Polym Sci, Part A: Polym Chem 49:5152–5161
20. Ghiassian S, Ismaili H, Lubbock BDW et al (2012) Photoinduced carbene generation from diazirine modified task specific phosphonium salts to prepare robust hydrophobic coatings. Langmuir 28:12326–12333
21. Gong J, Zhou Z, Hu X et al (2009) Self-assembled chitosan nanotemplates for biomineralization of controlled calcite nano architectures. ACS Appl Mater Interfaces 1: 26–29
22. Guinovart T, Parrilla M, Crespo GA et al (2013) Potentiometric sensors using cotton yarns, carbon nanotubes and polymeric membranes. Analyst 138:5208–5215

23. Guo R, Li Y, Lan J et al (2013) Microwave-assisted synthesis of silver nanoparticles on cotton fabric modified with 3-aminopropyltrimethoxysilane. J Appl Polym Sci 130:3862–3868
24. Gupta B, Agarwal R, Alam MS (2013) Preparation and characterization of polyvinyl alcohol-polyethylene oxide-carboxymethyl cellulose blend membranes. J Appl Polym Sci 127:1301–1308
25. Hebeish A, Abdel-Mohdy FA, Fouda MM et al (2011) Green synthesis of easy care and antimicrobial cotton fabrics. Carbohydr Polym 86:1684–1691
26. Hong KH, Sun G (2011) Photoactive antibacterial cotton fabrics treated by 3,3′,4,4′-benzophenonetetracarboxylic dianhydride. Carbohydr Polym 84:1027–1032
27. Hu P, Wang H, Zhang Q, Li Y (2012) An indium tin oxide conductive network for flexible electronics produced using a cotton template. J Phys Chem C 116:10708–10713
28. Janaki V, Vijayaraghavan K, Oh B-T et al (2012) Starch/polyaniline nanocomposite for enhanced removal of reactive dyes from synthetic effluent. Carbohydr Polym 90:1437–1444
29. Jiang C, Wang Q, Wang T (2012) Thermoresponsive PNIPAAm-modified cotton fabric surfaces that switch between superhydrophilicity and superhydrophobicity. Appl Surf Sci 258:4888–4892
30. Jiang C, Wang Q, Wang T (2012) Tunable wettability via counterion exchange of polyelectrolyte brushes grafted on cotton fabric. New J Chem 36:1641–1645
31. Jur J, Sweet WJ, Oldham CJ, Parsons GN (2011) Atomic layer deposition of conductive coatings on cotton, paper, and synthetic fibers: conductivity analysis and functional chemical sensing using "all-fiber" capacitors. Adv Funct Mater 21:1993–2002
32. Kang TJ, Choi A, Kim D-H et al (2011) Electromechanical properties of CNT-coated cotton yarn for electronic textile applications. Smart Mater Struct 20:15004
33. Kivotidi S, Tsioptsias C, Pavlidou E, Panayiotou C (2013) Flame-retarded hydrophobic cellulose through impregnation with aqueous solutions and supercritical CO2. J Therm Anal Calorim 111:475–482
34. Kocer HB, Cerkez I, Worley SD et al (2011) Polymeric antimicrobial *n*-halamine epoxides. ACS Appl Mater Interfaces 3:2845–2850
35. Kontturi E, Suchy M, Penttilä P et al (2011) Amorphous characteristics of an ultrathin cellulose film. Biomacromolecules 12:770–777
36. Li R, Liu G, Gu F et al (2011) In situ polymerization of aniline on acrylamide grafted cotton. J Appl Polym Sci 120:1126–1132
37. Liu W, Yan X, Lang J et al (2012) Flexible and conductive nanocomposite electrode based on graphene sheets and cotton cloth for supercapacitor. J Mater Chem 22:17245–17253
38. Liu Y, Ai K, Lu L (2014) Polydopamine and Its Derivative Materials: Synthesis and Promising Applications in Energy, Environmental, and Biomedical Fields. Chem Rev 114:5057–5115
39. Luo J, Lv W, Deng Y, Sun Y (2013) Cellulose-ethylenediaminetetraacetic acid conjugates protect mammalian cells from bacterial cells. Biomacromolecules 14:1054–1062
40. Ma K, Liu Y, Xie Z et al (2013) Synthesis of novel *n*-halamine epoxide based on cyanuric acid and its application for antimicrobial finishing. Ind Eng Chem Res 52:7413–7418
41. Malka E, Perelshtein I, Lipovsky A et al (2013) Eradication of multi-drug resistant bacteria by a novel Zn-doped CuO nanocomposite. Small 9:4069–4076
42. Mason EC, Weber AP (2011) Polypyrrole: Properties, Performance and Applications. Nova Science Publishers, Incorporated, New York
43. Mateos AJ, Cain AA, Grunlan JC (2014) Large-scale continuous immersion system for layer-by-layer deposition of flame retardant and conductive nanocoatings on fabric. Ind Eng Chem Res 53:6409–6416
44. Mattana G, Cosseddu P, Fraboni B et al (2011) Organic electronics on natural cotton fibres. Org Electron 12:2033–2039
45. Mihailović D, Šaponjić Z, Molina R et al (2011) Multifunctional properties of polyester fabrics modified by corona discharge/air RF plasma and colloidal TiO2 nanoparticles. Polym Compos 32:390–397

46. Muller D, Rambo CR, Porto LM et al (2013) Structure and properties of polypyrrole/bacterial cellulose nanocomposites. Carbohydr Polym 94:655–662
47. Ogihara H, Xie J, Okagaki J, Saji T (2012) Simple method for preparing superhydrophobic paper: spray-deposited hydrophobic silica nanoparticle coatings exhibit high water-repellency and transparency. Langmuir : ACS J Surf colloids 28:4605–4608
48. Pan C, Shen L, Shang S, Xing Y (2012) Preparation of superhydrophobic and UV blocking cotton fabric via sol–gel method and self-assembly. Appl Surf Sci 259:110–117
49. Patil AJ, Deogaonkar SC (2012) Conductivity and atmospheric aging studies of polypyrrole-coated cotton fabrics. J Appl Polym Sci 125:844–851
50. Perelshtein I, Applerot G, Perkas N et al (2010) Ultrasound radiation as a "throwing stones" technique for the production of antibacterial nanocomposite textiles. ACS Appl Mater Interfaces 2:1999–2004
51. Petkova P, Francesko A, Fernandes MM et al (2014) Sonochemical coating of textiles with hybrid ZnO/Chitosan antimicrobial nanoparticles. ACS Appl Mater Interfaces 6:1164–1172
52. Ringot C, Sol V, Barrière M et al (2011) Triazinyl porphyrin-based photoactive cotton fabrics: preparation, characterization, and antibacterial activity. Biomacromolecules 12: 1716–1723
53. Savitha KU, Prabu HG (2013) Polyaniline-TiO_2hybrid-coated cotton fabric for durable electrical conductivity. J Appl Polym Sci 127:3147–3151
54. Sedighi A, Montazer M, Samadi N (2014) Synthesis of nano Cu_2O on cotton: morphological, physical, biological and optical sensing characterizations. Carbohydr Polym 110:489–498
55. Shimanovich U, Cavaco-Paulo A, Nitzan Y, Gedanken A (2012) Sonochemical coating of cotton and polyester fabrics with "antibacterial" BSA and casein spheres. Chem Eur J 18:365–369
56. Shin B, Lee K-R, Moon M-W, Kim H-Y (2012) Extreme water repellency of nanostructured low-surface-energy non-woven fabrics. Soft Matter 8:1817–1823
57. Shirgholami MA, Khalil-Abad MS, Khajavi R, Yazdanshenas ME (2011) Fabrication of superhydrophobic polymethylsilsesquioxane nanostructures on cotton textiles by a solution–immersion process. J Colloid Interface Sci 359:530–535
58. Shi Z, Wyman I, Liu G et al (2013) Preparation of water-repellent cotton fabrics from fluorinated diblock copolymers and evaluation of their durability. Polymer 54:6406–6414
59. Singha AS, Thakur VK (2008) Saccaharum cilliare fiber reinforced polymer composites. E-J Chem 5:782–791
60. Singha AS, Thakur VK (2009) Synthesis, characterisation and analysis of hibiscus sabdariffa fibre reinforced polymer matrix based composites. Polym Polym Compos 17:189–194
61. Singha AS, Thakur VK (2009) Fabrication and characterization of S. cilliare fibre reinforced polymer composites. Bull Mater Sci 32:49–58
62. Singha AS, Thakur VK (2009) Fabrication and characterization of H. sabdariffa fiber-reinforced green polymer composites. Polym-Plast Technol Eng 48:482–487
63. Singha AS, Thakur VK (2009) Grewia optiva fiber reinforced novel, low cost polymer composites. J Chem 6:71–76
64. Singha AS, Thakur VK (2009) Physical, chemical and mechanical properties of hibiscus sabdariffa fiber/polymer composite. Int J Polym Mater 58:217–228
65. Singha AS, Thakur VK (2010) Mechanical, morphological, and thermal characterization of compression-molded polymer biocomposites. Int J Polym Anal Charact 15:87–97
66. Singha AS, Thakur VK (2010) Synthesis, characterization and study of pine needles reinforced polymer matrix based composites. J Reinf Plast Compos 29:700–709
67. Singha AS, Thakur VK, Mehta IK et al (2009) Surface-modified hibiscus sabdariffa fibers: physicochemical, thermal, and morphological properties evaluation. Int J Polym Anal Charact 14:695–711
68. Singha AS, Thakur VK (2008) Saccaharum cilliare fiber reinforced polymer composites. E-J Chem 5:782–791
69. Song J, Rojas OJ (2013) Approaching super-hydrophobicity from cellulosic materials: a Review. Nord Pulp Pap Res J 28:216–238

70. Subramanian SB, Francis AP, Devasena T (2014) Chitosan–starch nanocomposite particles as a drug carrier for the delivery of bis-desmethoxy curcumin analog. Carbohydr Polym 114:170–178
71. Suresh J, Rajiv Gandhi R, Gowri S et al (2012) Surface modification and antibacterial behaviour of bio-synthesised mgo nanoparticles coated cotton fabric. J Biobased Mater Bioenergy 6:165–171
72. Synytska A, Khanum R, Ionov L et al (2011) Water-repellent textile via decorating fibers with amphiphilic janus particles. ACS Appl Mater Interfaces 3:1216–1220
73. Tarabella G, Villani M, Calestani D et al (2012) A single cotton fiber organic electrochemical transistor for liquid electrolyte saline sensing. J Mater Chem 22:23830–23834
74. Teisala H, Tuominen M, Kuusipalo J (2014) Superhydrophobic coatings on cellulose-based materials: fabrication, properties, and applications. Adv. Mater. Interfaces 1:1300026
75. Thakur VK, Singha AS, Kaur I et al (2010) Silane functionalization of saccaharum cilliare fibers: thermal, morphological, and physicochemical study. Int J Polym Anal Charact 15:397–414
76. Thakur VK, Singha AS, Mehta IK (2010) Renewable resource-based green polymer composites: analysis and characterization. Int J Polym Anal Charact 15:137–146
77. Thakur VK, Singha AS, Kaur I et al (2011) Studies on analysis and characterization of phenolic composites fabricated from lignocellulosic fibres. Polym Polym Compos 19:505–511
78. Thakur VK, Tan EJ, Lin M-F, Lee PS (2011) Polystyrene grafted polyvinylidenefluoride copolymers with high capacitive performance. Polym Chem 2:2000–2009
79. Thakur VK, Singha AS, Misra BN (2011) Graft copolymerization of methyl methacrylate onto cellulosic biofibers. J Appl Polym Sci 122:532–544
80. Thakur VK, Tan EJ, Lin M-F, Lee PS (2011) Poly (vinylidene fluoride)-graft-poly (2-hydroxyethyl methacrylate): a novel material for high energy density capacitors. J Mater Chem 21:3751–3759
81. Thakur VK, Singha AS, Thakur MK (2012) In-air graft copolymerization of ethyl acrylate onto natural cellulosic polymers. Int J Polym Anal Charact 17:48–60
82. Thakur VK, Singha AS, Thakur MK (2012) Surface modification of natural polymers to impart low water absorbency. Int J Polym Anal Charact 17:133–143
83. Thakur VK, Singha AS, Thakur MK (2012) Graft copolymerization of methyl acrylate onto cellulosic biofibers: synthesis, characterization and applications. J Polym Environ 20:164–174
84. Thakur VK, Singha AS, Thakur MK (2012) Modification of natural biomass by graft copolymerization. Int J Polym Anal Charact 17:547–555
85. Thakur VK, Thakur MK, Gupta RK (2013) Synthesis of lignocellulosic polymer with improved chemical resistance through free radical polymerization. Int J Biol Macromol 61:121–126
86. Thakur VK, Thakur MK, Gupta RK (2013) Graft copolymers from natural polymers using free radical polymerization. Int J Polym Anal Charact 18:495–503
87. Thakur VK, Thakur MK, Gupta RK (2013) Rapid synthesis of graft copolymers from natural cellulose fibers. Carbohydr Polym 98:820–828
88. Thakur VK, Thakur MK, Gupta RK (2013) Development of functionalized cellulosic biopolymers by graft copolymerization. Int J Biol Macromol 62:44–51
89. Thakur VK, Thakur MK (2014) Recent trends in hydrogels based on psyllium polysaccharide: a review. J Clean Prod 82:1–15
90. Thakur VK, Thakur MK (2014) Recent advances in graft copolymerization and applications of chitosan: a review. ACS Sustainable Chem Eng 2:2637–2652
91. Thakur VK, Thakur MK (2014) Processing and characterization of natural cellulose fibers/thermoset polymer composites. Carbohydr Polym 109:102–117
92. Thakur VK, Thakur MK, Gupta RK (2014) Review: raw natural fiber-based polymer composites. Int J Polym Anal Charact 19:256–271

93. Thakur VK, Thakur MK, Raghavan P, Kessler MR (2014) Progress in green polymer composites from lignin for multifunctional applications: a review. ACS Sustain Chem Eng 2:1072–1092
94. Wang H, Ding J, Xue Y et al (2010) Superhydrophobic fabrics from hybrid silica sol-gel coatings: structural effect of precursors on wettability and washing durability. J Mater Res 25:1336–1343
95. Wang H, Zhou H, Gestos A et al (2012) Robust, electro-conductive, self-healing superamphiphobic fabric prepared by one-step vapour-phase polymerisation of poly(3,4-ethylenedioxythiophene) in the presence of fluorinated decyl polyhedral oligomeric silsesquioxane and fluorinated alkyl silane. Soft Matter 9:277–282
96. Wei Y, Torah R, Yang K et al (2013) A screen printable sacrificial fabrication process to realise a cantilever on fabric using a piezoelectric layer to detect motion for wearable applications. Sensors Actuators A: Phys 203:241–248
97. Wu J, Li J, Deng B et al (2013) Self-healing of the superhydrophobicity by ironing for the abrasion durable superhydrophobic cotton fabrics. Sci. reports 3:2951
98. Xue C-H, Chen J, Yin W et al (2012) Superhydrophobic conductive textiles with antibacterial property by coating fibers with silver nanoparticles. Appl Surf Sci 258:2468–2472
99. Xue C-H, Ji P-T, Zhang P et al (2013) Fabrication of superhydrophobic and superoleophilic textiles for oil–water separation. Appl Surf Sci 284:464–471
100. Xue C-H, Ma J-Z (2013) Long-lived superhydrophobic surfaces. J Mater Chem 1:4146–4161
101. Xu J, Li M, Wu L et al (2014) A flexible polypyrrole-coated fabric counter electrode for dye-sensitized solar cells. J Power Sources 257:230–236
102. Yang JS, Zhou QQ, He W (2013) Amphipathicity and self-assembly behavior of amphiphilic alginate esters. Carbohydr Polym 92:223–227
103. Yang X, Tu Y, Li L et al (2010) Well-dispersed chitosan/graphene oxide nanocomposites. ACS Appl Mater Interfaces 2:1707–1713
104. Yoo Y, You JB, Choi W, Im SG (2013) A stacked polymer film for robust superhydrophobic fabrics. Polym Chem 4:1664–1671
105. Yuan C, Hou L, Li D et al (2011) Synthesis of flexible and porous cobalt hydroxide/conductive cotton textile sheet and its application in electrochemical capacitors. Electrochim Acta 56:6683–6687
106. Yue X, Lin H, Yan T et al (2014) Synthesis of silver nanoparticles with sericin and functional finishing to cotton fabrics. Fibers Polym 15:716–722
107. Yu M, Wang Z, Liu H et al (2013) Laundering durability of photocatalyzed self-cleaning cotton fabric with TiO_2nanoparticles covalently immobilized. ACS Appl Mater Interfaces 5:3697–3703
108. Yun YJ, Hong WG, Kim W-J et al (2013) A novel method for applying reduced graphene oxide directly to electronic textiles from yarns to fabrics. Adv Mater 25:5701–5705
109. Zhang G, Lin S, Wyman I et al (2013) Robust superamphiphobic coatings based on silica particles bearing bifunctional random copolymers. ACS Appl Mater Interfaces 5:13466–13477
110. Zhang L, Zhang Z, Wang P (2012) Smart surfaces with switchable superoleophilicity and superoleophobicity in aqueous media: toward controllable oil/water separation. NPG Asia Mater. 4:1–8
111. Zhang M, Wang C, Wang S, Li J (2013) Fabrication of superhydrophobic cotton textiles for water–oil separation based on drop-coating route. Carbohydr Polym 97:59–64
112. Zhang M, Wang S, Wang C, Li J (2012) A facile method to fabricate superhydrophobic cotton fabrics. Appl Surf Sci 261:561–566
113. Zhao Y, Xu Z, Wang X, Lin T (2012) Photoreactive azido-containing silica nanoparticle/polycation multilayers: durable superhydrophobic coating on cotton fabrics. Langmuir 28:6328–6335

114. Zhou H, Wang H, Niu H et al (2012) Fluoroalkyl silane modified silicone rubber/nanoparticle composite: a super durable, robust superhydrophobic fabric coating. Adv Mater 24:2409–2412
115. Zhou H, Wang H, Niu H et al (2013) Robust, self-healing superamphiphobic fabrics prepared by two-step coating of fluoro-containing polymer, fluoroalkyl silane, and modified silica nanoparticles. Adv Funct Mater 23:1664–1670
116. Zhou X, Zhang Z, Xu X et al (2013) Robust and durable superhydrophobic cotton fabrics for oil/water separation. ACS Appl Mater Interfaces 5:7208–7214
117. Zhuo J, Sun G (2013) Antimicrobial functions on cellulose materials introduced by anthraquinone vat dyes. ACS Appl Mater Interfaces 5:10830–10835
118. Zhu Q, Gao Q, Guo Y et al (2011) Modified silica sol coatings for highly hydrophobic cotton and polyester fabrics using a one-step procedure. Ind Eng Chem Res 50:5881–5888
119. Zhu X, Zhang Z, Yang J et al (2012) Facile fabrication of a superhydrophobic fabric with mechanical stability and easy-repairability. J Colloid Interface Sci 380:182–186
120. Zou H, Lin S, Tu Y et al (2013) Simple approach towards fabrication of highly durable and robust superhydrophobic cotton fabric from functional diblock copolymer. J Mater Chem A 1:11246–11260

Recent Development of Chitosan Nanocomposites with Multiple Potential Uses

Francisco Claudio de Freitas Barros, Vicente de Oliveira Sousa Neto, Tecia Vieira Carvalho, Rodrigo Silveira Vieira, Glória Maria Marinho Silva and Ronaldo Ferreira do Nascimento

Abstract This chapter reviews an actual relevant literature about the most important methods used in the processing of chitosan nanocomposites, which are based on most extensively used biodegradable polymer matrices. A particular attention has been focused on the biodegradable polymer chitosan because of their widespread use in the bionanocomposite films field. Thus, the processing procedures and the results obtained of various applications from chitosan nanocomposite films have been compiled. The current research trends in chitosan-based material films for applications, including biodegradable composites and the use of chitosan are presented. This chapter will increase the interest of researchers in chitosan-based chitosan nanocomposites and the development of new ideas in this field.

Keywords Chitosan film · Sustainable materials · Nanocomposites · Biodegradable polymer

V. de Oliveira Sousa Neto
Department of Chemistry, State University of Ceara (UECE-CECITEC), Ceara, Brazil

F.C. de Freitas Barros · R.F. do Nascimento (✉)
Department of Analytical Chemistry and Physical—Chemistry, Federal University of Ceara, Ceara, Brazil
e-mail: ronaldo@ufc.br

T.V. Carvalho
PADETEC (Parque de Desenvolvimento Tecnológico), Federal University of Ceara, Ceara, Brazil

R.S. Vieira
Department of Chemical Engineering, Federal University of Ceara, Ceara, Brazil

G.M.M. Silva
Department of Chemistry and Environment, Federal Institute of Ceara, Ceará, Brazil

V.K. Thakur and M.K. Thakur (eds.), *Eco-friendly Polymer Nanocomposites*,
Advanced Structured Materials 74, DOI 10.1007/978-81-322-2473-0_16

1 Introduction

Recently, there has been a continuing increase in the research of polymer-based materials starting from synthetic polymers to biorenewable and biodegradable polymer [1, 2]. Among the different polymeric materials, biopolymers are considered most environmental friendly, for various purposes, in particular for multifunctional applications, since many of these polymers, in addition to being biodegradable, also possess antimicrobial and antioxidant properties [3–6]. Among the biodegradable matrices of natural origin have, in particular, polysaccharides (starch, cellulose, pectin, or chitin/chitosan); proteins (casein or gluten); and lipids (fatty acids, resins, and waxes), that has ability to form nanocomposite films and nontoxic, and biocompatible, which have the advantage of being able to be in contact with food products.

1.1 Biopolymers: Bio-Based Matrix Material

Natural polymers belong to the special class of polymers found in nature such as natural fibers, starch, proteins, etc., [7, 8] and possess a well-defined structure [9–11]. The use of natural polymers-based materials by human beings is not new as these polymer materials have been used in the earlier civilization by many centuries ago. Polymers obtained from different biorenewable resources are generally refereed as bio-based polymers [12, 13]. It is well known that renewable resources such as plants (e.g., cellulose or chitin, vegetable oils, etc.), bacteria, as well as nonrenewable petroleum (e.g., aliphatic/aliphatic–aromatic co-polyester) are sources of a variety of polymeric materials. Accordingly, biodegradable polymeric materials have been classified as natural or synthetic depending on their origin. Also, biodegradable polymers themselves can be classified depending on their origin such as agro polymers (starch or cellulose), microbial poly (hydroxyalkanoate), chemically synthesized from agro-based resource monomers poly (lactic acid), and chemically synthesized from conventionally synthesized monomers.

Most natural polymers are water sensitive, in that they absorb water, and may even be water soluble, causing their properties to deteriorate (Figs. 1 and 2). This is normally overcome by blending them with polymers or plasticizers to enhance their performance (and value). These can lead to "new polymers" with attractive properties. To take advantage of this and their cost as well as the properties of "old polymers," several low-cost monomers are used. Thus, a change in the paradigm in polymers has been occurring during the last few decades to obtain functional polymer including structural polymers. The details of some biopolymers are given in Figs. 1 and 2.

1.2 Starch-Based Polymers and Composites

Starch is the main storage supply in botanical sources such as cereals (wheat, maize, rice), tubers (potato), and legumes (pea). In the past, studies carried on starch esters

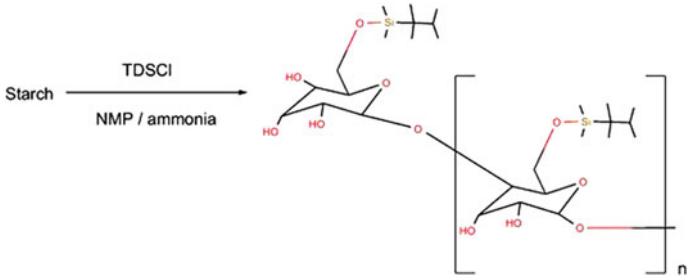

Fig. 1 Silylation of Starch with bulky thexyldimethylchlorosilane (TDSCl) in *N*-methylpyrrolidone (NMP)/ammonia. Reprinted with permission [14]. Copyright 2001, American Chemical Society

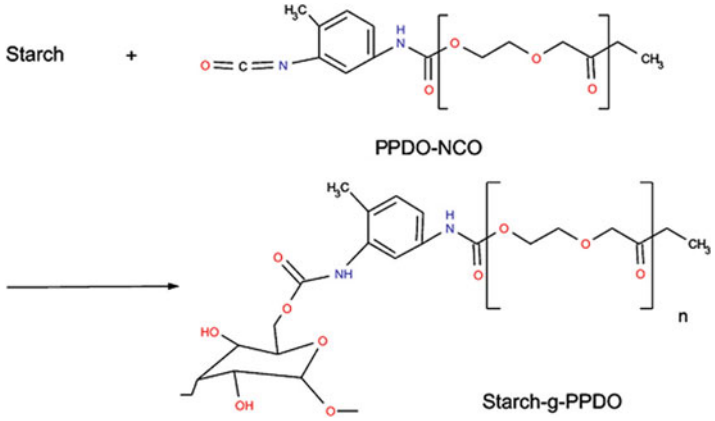

Fig. 2 Preparation of a starch-graft-poly(1,4-dioxan-2-one). The diisocyanate (NCO) group links the poly 1,4-dioxan-2-one (PPDO) to the starch chains. Reprinted with permission [15]. Copyright 2006. Elsevier

were abandoned due to their inadequate properties in comparison with cellulose derivates. Only in the recent years, a renewed interesting starch-based polymers has been aroused.

Starch consists of two major components, amylose and amylopectine. Amylose (Fig. 3a) is a linear or sparsely branched carbohydrate based on α(1-4) bonds with a molecular weight of 105–106. The chains show spiral-shaped single or double helixes. Amylopectine (Fig. 3b) is a highly multiple branched polymer with a high molecular weight of 107–109 based on α(1-4) bonds and α(1-6) links constituted branching points occurring every 22–70 glucose units [16, 17]. In nature starch is found as crystalline beads and in three crystalline modifications according to the botanical source.

The crystallinity of the starch granules is attributed mainly to the amylopectin and not to amylase, which is although linear, presents a confirmation that hinders its regular association with other chains. Starches exhibit poor melt processability and

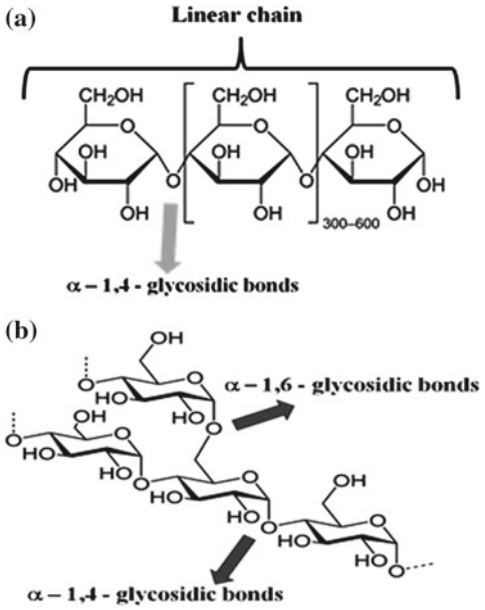

Fig. 3 Structures of **a** amylose and **b** amylopectine (depicted by Prof. Dr. Vicente de Oliveira Sousa Neto)

are highly water soluble, difficult to process, and brittle due to anarchical growth of one their constituents, and hence need a plasticizer [18, 19] to make them suitable for engineering applications.

Plasticizers such as water or glycols make starches flow and suitable for thermoplastic processing [18]. In this process, the glass transition temperature Tg and melting point of starch decrease due to the mechanical and heat energy. Also, by using the blends of some of these polymers, it is possible to tailor the mechanical properties of such thermoplastics to suit structural applications, depending on the source and processing conditions, or by using fillers, including cellulose micro/nanofibrils, and natural "macro" fibers [18, 20–23].

Modifications of starches, including blending them with other polymers, have been the subject matter of many studies. For example, blends of wheat starch with PLA (Fig. 4) or low density polyethylene (LDPE) have been prepared economically using twin-screw extruders, without affecting their biodegradability, by incorporating dry starch granules into the poly(lactic acid) (PLA) or LDPE, where the starch granules act as a filler resulting in an increased modulus, but also in further loss of ductility with increasing starch content.

1.3 Poly(lactide) (PLA)

Poly(lactide) (PLA) has been the frontrunner in these (bio)polymers due to its attractive mechanical properties, renewability, biodegradability, and relatively low

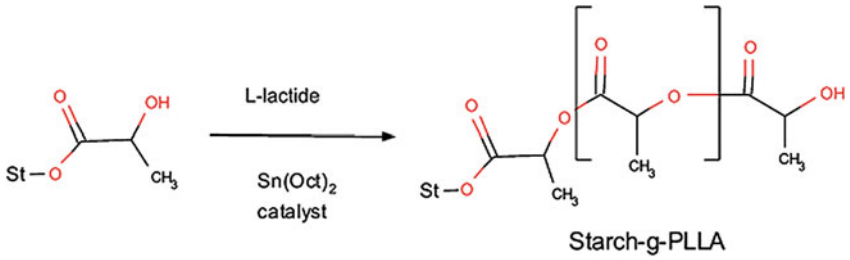

Fig. 4 The OH groups of the starch (St) are reacted with lactic acid and then the polymerization is started by adding $Sn(Oct)_2$ as catalyst. Reprinted with permission [24]. Copyright 2006. Elsevier

cost [25]. In the first method to prepare PLA, l-lactic acid was condensed and water was removed continuously, leading to low molecular weight PLA [26]. However, due to its reversibility, this polycondensation method suffers from several drawbacks such as the need of high temperature, the continuous removal of by-products (most often water) and long reaction times. In this respect, ring-opening polymerization (ROP) of lactide (LA) (cyclic dimer of lactic acid) promoted by protic compounds (water, alcohol, and amine) as initiators and tin(II) octoate (Sn(Oct)2) as catalyst is industrially preferred to obtain high molecular weight PLA in bulk (absence of solvent) (Fig. 5) [27].

Grafting of PLA chains on the surface of nanocelluloses has also been explored to enhance the compatibility between the nanocellulose and PLA through "grafting onto" or "grafting from" strategies. Li et al. [29] succeeded to graft epoxy-terminated copolymer of polylactide and glycidyl methacrylate onto the surface of BC nanofibers. The resulting polymer-grafted nanofibers showed a good ability to disperse in PLA matrix, but any of the thermomechanical properties was reported in this study. Through "grafting from" approach, polycaprolactone (PCL) chains were grown from the surface of CNs by microwave-assisted ring opening polymerization, and redisperse into PLA [30]. Although PCL and PLA are immiscible, the authors reported that the resulting PCL-g-CNs showed good dispersion in PLA, and consequently improved the mechanical properties of PLA at certain extent. "Grafting from" method was also exploited by Goffin et al. [31] to graft PLA chains from the surface of CNs (Fig. 6), which were then redispersed into PLA using

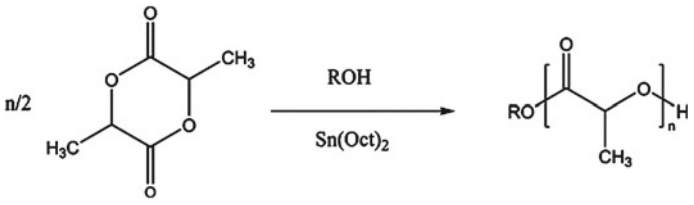

Fig. 5 ROP of LA promoted with ROH/$Sn(Oct)_2$. Reprinted with permission [28]. Copyright 2013. Elsevier

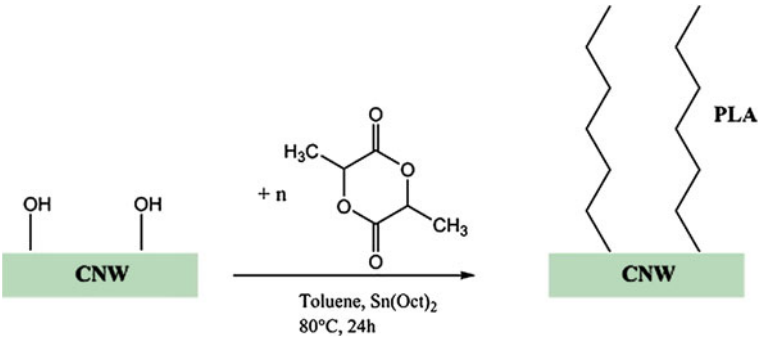

Fig. 6 Grafting from method based on ROP of LA carried out via hydroxyl functionalities present at the CNs surface. Reprinted with permission [28]. Copyright 2013. Elsevier

extrusion technology [31, 32]. The grafted PLA chains not only enhanced the compatibility with the matrix but also co-crystallized with PLA matrix, creating therefore a co-continuous network made of the filler within the PLA matrix. This played a key role in the good adhesion acquired and hence in the improvement of the mechanical properties for the final PLA-based nanocomposites.

1.4 Polycaprolactone (PCL)

Polycaprolactone (PCL) and its copolymers are a type of hydrophobic aliphatic polyester based on hydroxyalkanoic acids. They possess exceptional qualities: biocompatibility; FDA approval for clinical use; biodegradability by enzyme and hydrolysis under physiological conditions and low immunogenicity. These critical properties have facilitated their value as sutures, drug delivery vehicles, and tissue engineering scaffolds in pharmaceutical and biomedical applications. However, the hydrophobicity of PCL and its copolymers remains a concern for further biological and biomedical applications. One promising approach is to design and synthesize well-controlled PCL-based amphiphilic block copolymers.

PCL-based amphiphilic block copolymers are prepared by combing a hydrophilic segment with PCL blocks in various architectures which can then self-assemble into intriguing aggregates of various shapes and sizes in selected solvents such as micelles, vesicles, and hydrogels [33–36]. Hydrophilic components such as poly(ethylene glycol) (PEG), poly(acrylic acid), (PAA), poly(2-ethyl-2-oxazoline) (PEtOz), poly(*N*-isopropylacrylamide) (PNIPAAm), and poly(*N,N*-dimethylamino-2-ethyl methacrylate) (PDMAEMA) have been utilized to construct amphiphilic block copolymers with PCL as the hydrophobic segment.

PEG-PCL diblock copolymers were previously synthesized by ring opening polymerization (ROP) of ε-caprolactone using monomethyoxy poly(ethylene

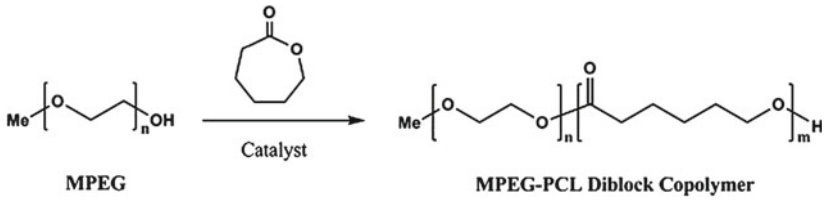

Fig. 7 MPEG-PCL diblock copolymers prepared by ring opening polymerization. Reprinted with permission [38]. Copyright 2013. Elsevier

glycol) MPEG as the macroinitiator (Fig. 7). Calcium ammoniate [37], HCl/Et_2O, rare earth catalyst yttrium tris(2,6-ditertbutyl-4-methylphenolate) [$Y(DBMP)_3$] [38], Lewis acid [37], and Tin compounds [38] are effective catalysts for the ROP of ε-caprolactone when using the terminal alcohol of PEG as initiators [38].

Triblock copolymers comprising of three different segments can be built into A-B-C triblock architecture. For example, a series of well-defined amphiphilic triblock copolymer MPEG-PCL-PDMAEMA were prepared by a three-step reactions in the combination of ROP, transesterification, and ATRP (Fig. 8). These PLA-based amphiphilic block copolymers have found a variety of bio-related applications; typical examples include: self-assembled nanoparticles for drug delivery and hydrogels for tissue engineering.

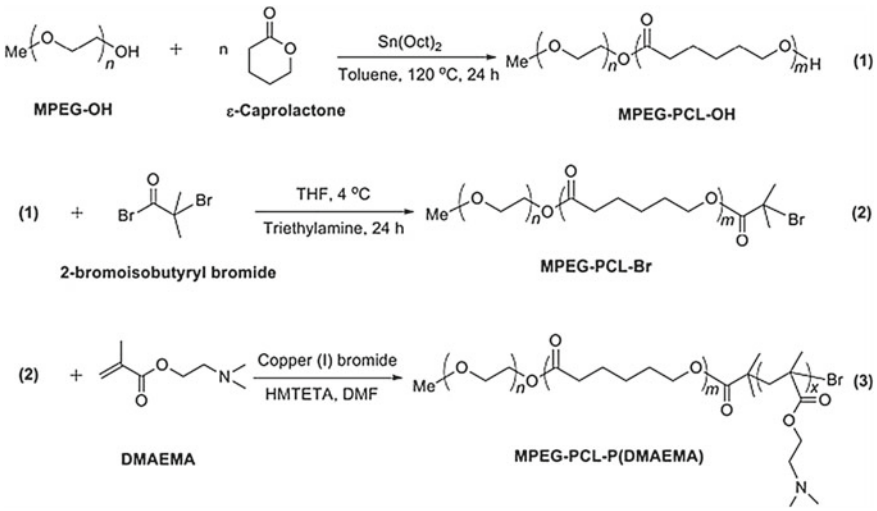

Fig. 8 Synthetic scheme of MPEG-PCL-PDMAEMA A-B-C triblock copolymer. Reprinted with permission [38]. Copyright 2013. Elsevier

1.5 Lignin

Lignin is the second most available polymer next to cellulose and comprises 25–30 % of the nonfossil organic molecules on earth [39, 40]. Lignin is hydrophobic in nature, thus making the cell wall impermeable to water and ensuring an efficient water and nutrition transport in the cells [41, 42]. It is known as a cross-linked macromolecular material based on a phenylpropanoid monomer structure. The Fig. 9 shows monomer structure has been reported to consist of the same phenyl propenoid skeleton [9, 11, 43].

Nair et al. [45] showed that on chitosan–lignin composites for adsorption of dyes and metal ions from wastewater all the interactions between chitosan and alkali lignin are likely due to the formation of weak hydrogen bonds. The hydroxyl group present in the phenolic ring of alkali lignin can interact with (a) β-1,4-glycosidic oxygen (shown as dashed line 1 in Fig. 10) and (b) hydroxyl group of chitosan (dashed line 3). A weak bond is also formed between hydroxyl group of chitosan and methoxy group of alkali lignin (dashed line 2). A weak interaction between aromatic ring of alkali lignin and secondary amino group of chitosan was also observed and then worked (dashed line 4).

Fernandes et al. [46] have obtained from high-density polyethylene (HDPE) and cork powder cork-polymer composites (CPC) with improved properties (Fig. 11). This work focuses on the development of cork–polymer composites (CPC) using suberin and lignin as bio-based coupling agents through a reactive extrusion (REX) process, in order to overcome with environmental benefits the insufficient adhesion between cork and a high-density polyethylene (HDPE) matrix. REX has the capability of functionalize, prepare the composite, and produce pellets in a single step. No environmental or health hazardous solvents are used, low investment costs, and high production yields are obtained [47]. Benzoyl peroxide (BPO) was used as initiator agent, and suberin or lignin isolated from cork-enhanced filler-matrix bonding and promoted mechanical reinforcement with

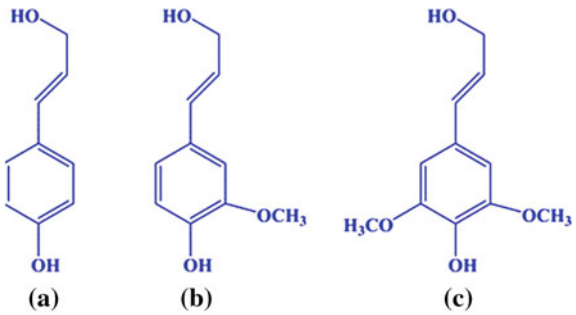

Fig. 9 Monolignol monomer species: **a** p-coumaryl alcohol (4-hydroxyl phenyl, H), **b** coniferyl alcohol (guaiacyl, G), **c** sinapyl alcohol (syringyl, S). Adopted with permission. Reprinted with permission [44]. Copyright 2011. Elsevier

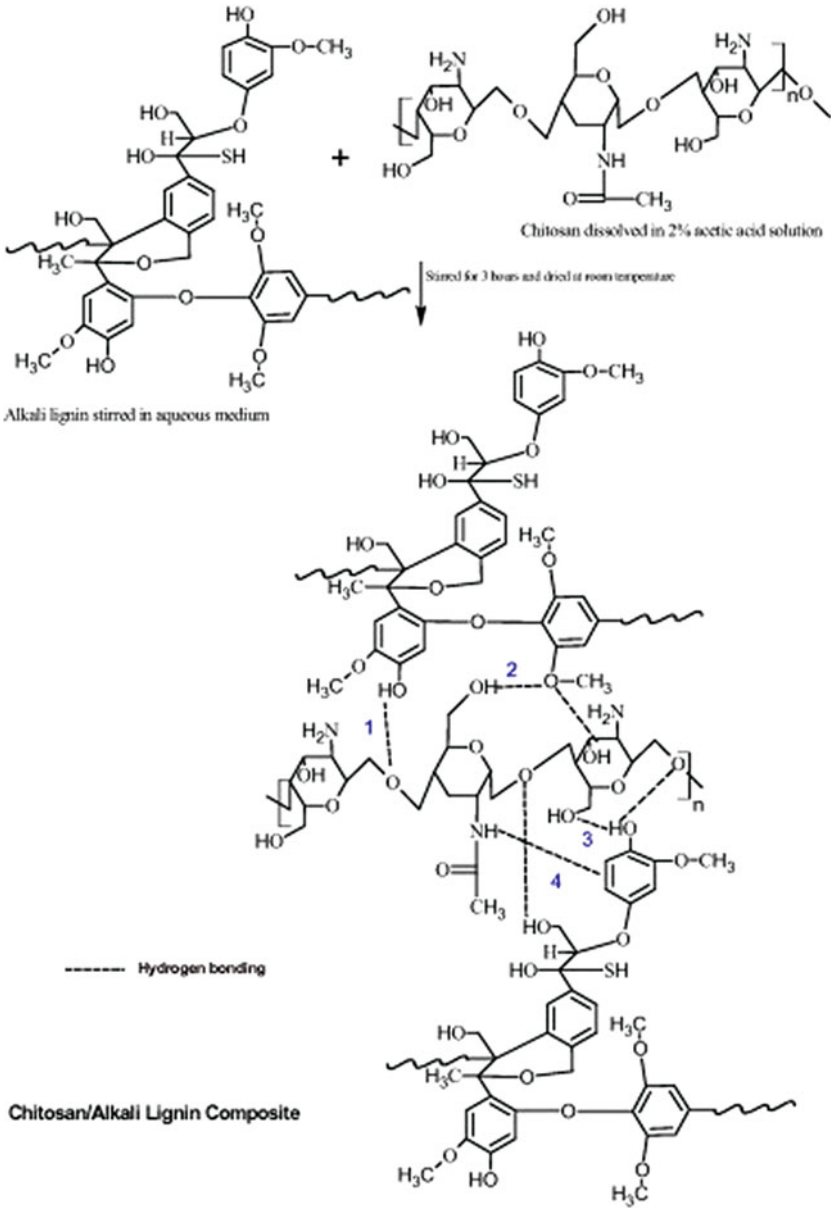

Fig. 10 Preparation of chitosan–alkali lignin composite. The *dashed lines* show the possible weak bonding between chitosan and alkali lignin. Reprinted with permission [45]. Copyright 2014. Elsevier

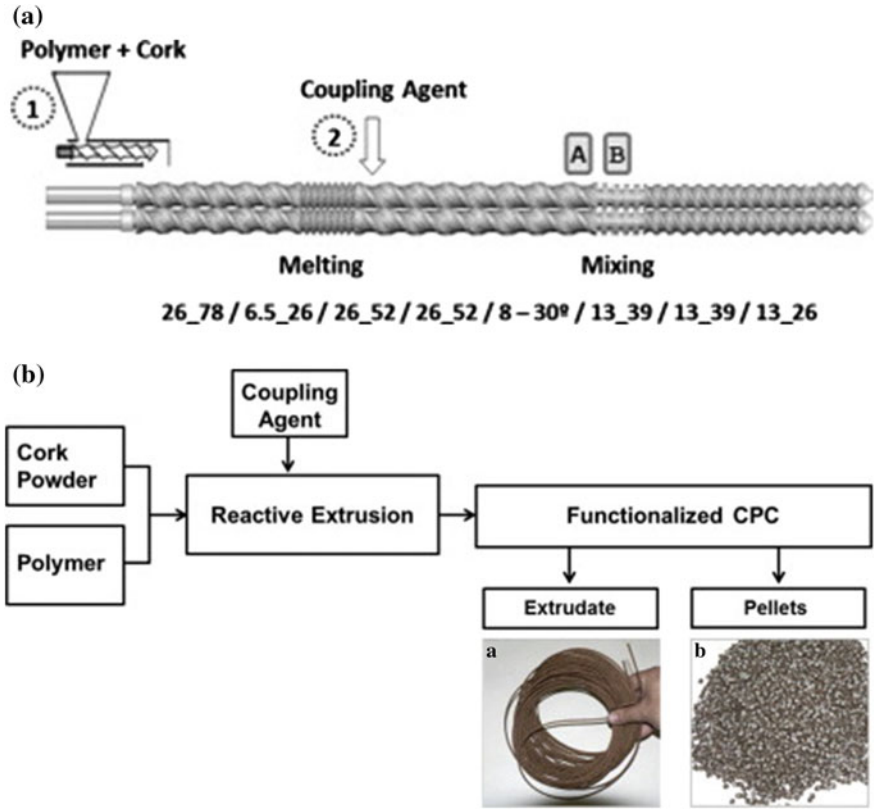

Fig. 11 **a** Twin-screw extruder setup. Screw profile is defined in terms of (pitch_length) of the various elements. **a** and **b** denote locations of material sampling; **b** Scheme for the production of extruded functionalized cork-polymer composites (CPC) from *a* CPC 3 composition with 2 wt% of suberin and *b* CPC 5 with 4 wt% of lignin as coupling agent in the pellet form. Reprinted with permission [46]. Copyright 2014. Elsevier

environmental benefits. According to the authors, the novel composites were characterized in terms of dimensional stability, evolution of morphology, thermal and mechanical properties, and their performance was compared with that of composites containing polyethylene-grafted maleic anhydride (PE-g-MA) as coupling agent. As expected, composites with coupling agent present higher mechanical properties, lower water uptake, and thickness swelling variation. Suberin acts as plasticizer with antioxidant benefits, while lignin works as a coupling agent, improving tensile modulus and maximum strength. Increasing lignin content does not improve the mechanical properties but improves thermal stability.

1.6 Cellulose

Cellulose is the world's most abundant natural, renewable, biodegradable polymer, and a classical extracellular high-performance skeletal biocomposite consisting of a matrix reinforced by fibrous biopolymer [48, 49].

1.7 Cellulose Chemical Composition

It is a linear homopolysaccharide consists of glucose (D-glucopyranose) units linked together by β-(1-4) glycosidic bonds (β-D-glucan), Fig. 12. This polysaccharide is widespread in nature, occurring in both primitive and highly evolved plants. The size of the cellulose molecule is normally given in terms of its degree of polymerization (DP), i.e., the number of anhydroglucose units present in a single chain. However, the conformational analysis of cellulose indicated that cellobiose (4-O-β-D-glucopyranosyl-β-D-glucopyranose) rather than glucose is its basic structural unit [50].

1.8 Cellulosic Chemical Features Versus Their Incorporation into Composites

Cellulose's chemical characteristics provide it a rich variety of options for chemistry and engineering for many material applications [52]. Cellulose's structure is based on a 180° turn-screw ß-1,4-glucopyranoside cellulose polymeric chain that gives rise to various crystalline domain formations that are considered allomorphs [53]. These domains possess very high strength, approximately on the order or greater than a comparable structural steel sample. This intrinsic strength is available in the fundamental domains, the nanocrystals, which can be obtained upon a variety of acid hydrolyses to yield rod-like crystals [54]. These nanocrystals are able to provide reinforcement in a variety of composites [55–59]; yet, a problem is that failures in a composite with these materials are really due to weak boundary layer

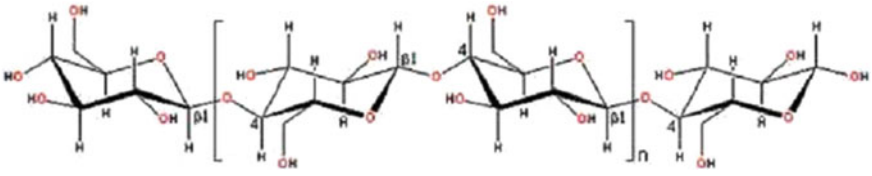

Fig. 12 Bassic chemical structure of cellulose [51]. http://www.lsbu.ac.uk/water/hycel.html, (September, 2010)

interactions, especially between polar (cellulose) and nonpolar components. Thus, chemical modification schemes are necessary, which can generally be done to the cellulosic portion followed up by cross-linking [60]. Cellulose can easily accommodate hydrophobic appending chains to overcome adverse interactions with nonpolar composite matrices. Moreover, the high melting temperature of the cellulose nanocrystals can positively affect the thermal transition properties of these appending chains, a very attractive feature for designing materials that need to perform at high temperatures. Likewise, the high hydrophilicity of cellulose is sometimes a disadvantage in certain applications; thus, a variety of surface modification strategies are available such as coating them with surfactants [61] or grafting hydrophobes onto them [59].

By utilizing ROP of monomers such as ε-caprolactone or l-lactide from cellulose, composite materials with new and/or improved properties can be obtained. Grafting of solid cellulose substrates, such as cotton, microfibrillated cellulose (MFC) or cellulose nanocrystals, renders cellulose that can easily be dispersed into polymer matrices and may be used as reinforcing elements to improve mechanical and/or barrier properties of biocomposites. A surface-grafted polymer can also tailor the interfacial properties between a matrix and the fibrillar structure of cellulose. When derivatives of cellulose are grafted with polymers in homogenous media, amphiphilic materials with interesting properties can be achieved anticipated to be utilized for applications such as encapsulation and release.

Yang et al. [62] grafted filter paper with hyperbranched poly(3-methyl-3-oxetanemethanol) (HBPO) by SI-ROP of 3-methyl-3-oxetanemethanol from the hydroxyl groups of cellulose (Fig. 13). The grafting of this hyperbranched polymer yielded an increased amount of hydroxyl groups on the surface of the fibers, as determined by XPS. The HBPO content of different samples varied between 44 and 99 %; however, the results calculated from XPS may overestimate the HBPO content, due to an underestimation of the O/C ratio in cellulose.

Lönnberg et al. [63] were the first to report ring-opening polymerisation from microfibrillated cellulose (MFC). The grafting was performed by SI-ROP of ε-CL

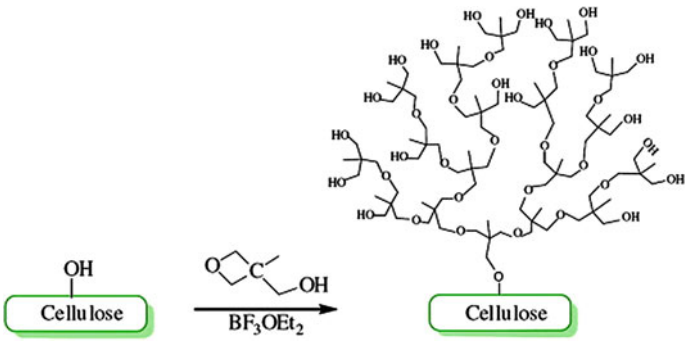

Fig. 13 Grafting of hyperbranched polyether from a cellulose fiber surface. Reprinted with permission [62]. Copyright 2011. Elsevier

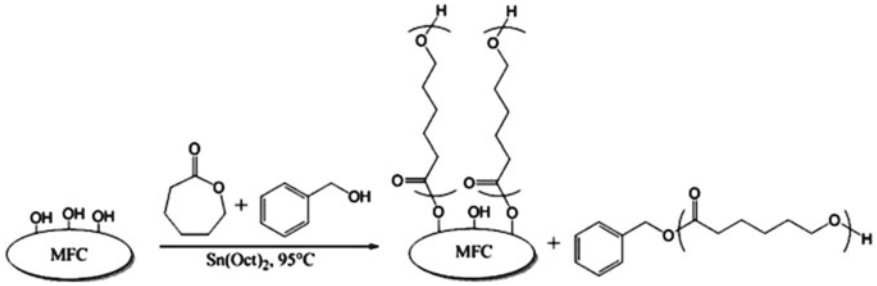

Fig. 14 ROP of ε-caprolactone from microfibrillated cellulose. Reprinted with permission [63]. Copyright 2014. Elsevier

in the presence of benzyl alcohol as a free initiator, Fig. 14, which created grafts on the MFC as well as an unbound, free polymer.

The grafted fibers commonly self-assemble into micelles in aqueous solutions which may lead to future applications as solubilizing agents for hydrophobic drugs. As grafted cellulose derivatives often have good mechanical properties in addition to good biocompatibility, they are utilized as material for surgical repair, an area that potentially could expand further.

1.9 Cellulose–Chitosan Composites

Tran et al. [64] developed a simple and one-step method to prepare biocompatible composites from cellulose (CEL) and chitosan (CS). [$BMIm^+Cl^-$], an ionic liquid (IL), was used as a green solvent to dissolve and prepare the [CEL + CS] composites. Since majority (>88 %) of IL used was recovered for reuse by distilling the aqueous washings of [CEL + CS], the method is recyclable (Fig. 15). According to the authors, the composite was found to have combined advantages of their components: superior mechanical strength (from CEL) and excellent adsorption capability for microcystin-LR, a deadly toxin produced by cyanobacteria (from CS).

Of these biopolymers, the chitosan is capable of forming nanocomposite materials that may be used as coating or packaging for food preservation [4]. Chitosan (Fig. 16a) 1is known as the most abundant natural biopolymer after cellulose, a copolymer primarily composed of poly(1-4)-β-D-glucosamine, is obtained by the enzymatic or alkaline (under heat-treatment) deacetylation of chitin (Fig. 16b), a homopolymer of (1-4)-linked *N*-acetyl-β-D-glucosamine residues [65, 66], is a biodegradable, hydrophilic, nontoxic, and biocompatible polysaccharide that presents a remarkable economic interest due to its functional versatility, with potential applications. It is also an abundantly available low-cost biopolymer for pollutant removal that can be obtained from natural resources [66–70]. When compared with other commercial adsorbents, it has received a lot of focus due to its specific

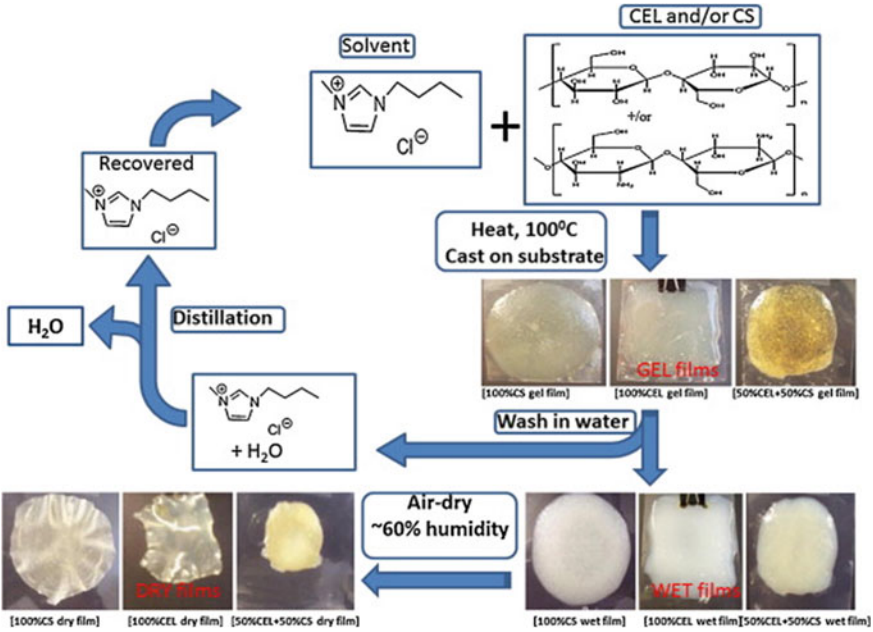

Fig. 15 Summary of the procedure used to dissolve and to regenerate films of CEL and/or CS with [BMIm + Cl−] as solvent. Reprinted with permission [64]. Copyright 2013. Elsevier

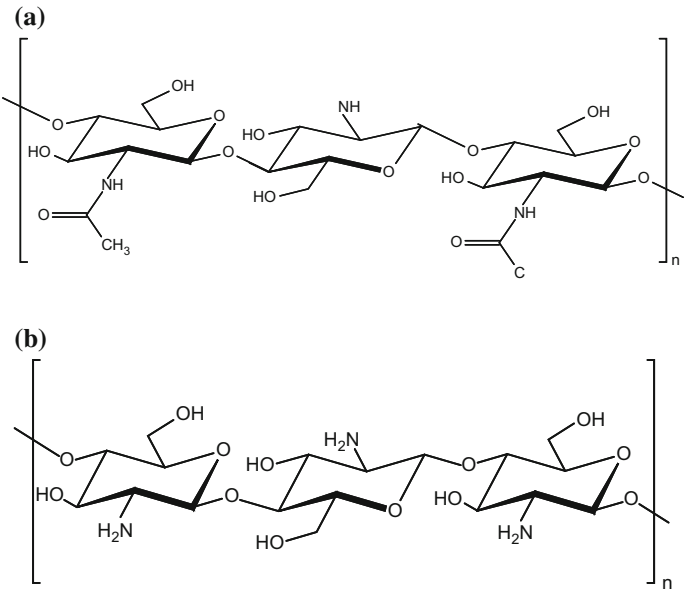

Fig. 16 Structure of chitin (**a**) and chitosan (**b**)

properties such as cationicity, high adsorption capacity, macromolecular structure, abundance, and low price [65, 66].

The chitosan can be dissolved in acid media, cross-linking with, e.g., glutaraldehyde or epichlorohydrin, restores the insolubility features, while maintaining effective adsorption capacity [66, 70]. Preparation of porous cross-linked chitosan microbeads for metal ion adsorption has to take into account control of the pore size [65]. Indeed, a large internal surface area is essential for efficient adsorption capacities. In addition, clogging of the microbeads resulting in high backpressure is prevented by the porous interior. Cross-linked chitosan microbeads show suitable physicochemical properties, but the adsorption capacity is restricted because a number of amino groups participate in the process at the expense of chelation [66].

Recently, there has been a continuing increase in the biopolymer research for various purposes, in particular for multi- applications, since many of these polymers, in addition to being biodegradable, also possess antimicrobial and antioxidant properties [3, 4, 71]. Some of these biopolymers, in particular the chitosan, are also capable of forming nanocomposite films that may be used as coating or packaging for food preservation [4].

1.10 Chitosan Films

In addition, chitosan films have limitations due to their physicochemical characteristics, such as water solubility in dilute acid solution, which limits their use as packing material [3, 4, 66]. Thus, combination of nanomaterias and an antimicrobial/antioxidant compound in chitosan films can be suitable, given its acceptable structural integrity and barrier properties imparted by the nanocomposite matrix.

Recent studies have approved that the incorporation of the nanomaterials into chitosan, which increase the performance of the mechanical properties, functional properties, barrier properties, and water solubility of chitosan films can be achieved [3, 4, 71].

Another disadvantage is that the chitosan films presenting high water vapor permeability, which limits the mechanical performance of chitosan films and its applications. The chitosan films are resistant, but characterized by the limited elongation, which it becomes too inflexible. The antioxidant properties, barrier, mechanical and others factors depend on the film composition, its thickness, and preparation techniques. The incorporation of additional films of chitosan compounds can alter its properties. Consequently, there has been a growing interest in the development of chitosan-based films with certain chemical modifications for the production of functional materials [3, 4, 66, 71].

Methods developed for the chemical modification of chitosan-based films, such as crosslinker (cross-linking polymer) represent effective means to change their properties. In some case (grafting compounds), chitosan is bound to the polymer in order to improve a specific property, and to improve the antioxidant or antimicrobial properties. The method of cross-linking is effective for connecting to other

polymers or different polymer chains of chitosan together. After this process, their properties are very different from those of the original polymer. The cross-linking of the polymer leads to the formation of a continuous three-dimensional covalent network that can allow the diffusion of bioactive material and water and to improve the properties of the polymer [4, 66].

In this topic important methods developed by various authors involving the incorporation of certain polymers and other polysaccharides to improve certain properties of films based on chitosan are reported nanocomposites to diversify their applications.

In connection, Shete et al. [72] reported the synthesis of nanocrystals of magnetite (Fe_3O_4) from ferrous chloride ($FeCl_2$) by alkaline precipitation method in absence of oxidant at low temperature. Then, bare magnetic nanoparticles were coated with chitosan (CS) by ultrasonication. The complete synthesis of Fe_3O_4 nanoparticles and their surface modification with CS is presented in Fig. 17.

Magnetic nanoparticles (MNPs) were studied for their structural, morphological, and magnetic properties. Phase identification and structural analysis were studied by X-ray Diffractometry (XRD). The main characteristic peaks (Fig. 18a) were obtained with the (h k l) values of (2 2 0), (3 1 1), (4 0 0), (4 2 2), and (5 1 1), which correspond to Fe_3O_4 phase. The bright ring patterns of Selected Area Electron Diffraction (SAED) in Fig. 18b indicate polycrystalline nature of the magnetic nanoparticles. The ring pattern corresponds to (2 2 0), (3 1 1), (4 0 0), (4 2 2), and (5 1 1) planes can be clearly seen.

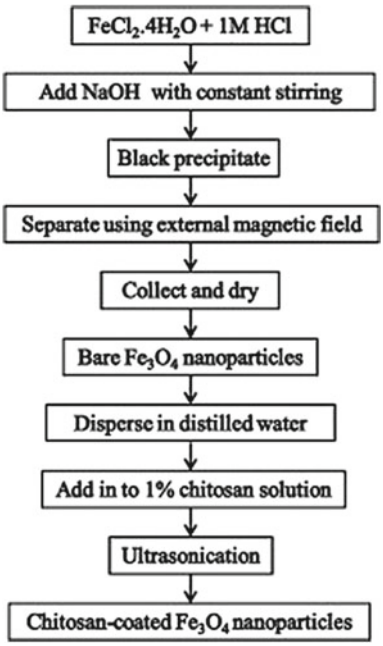

Fig. 17 Flowchart of the procedure for synthesis of Fe_3O_4 magnetic nanoparticles (MNPs) and their surface modification using chitosan (CS). Reprinted with permission [72]. Copy right 2014 Elsevier

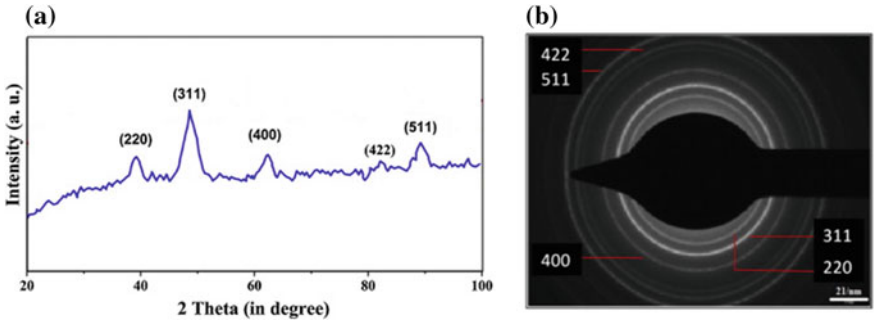

Fig. 18 XRD (**a**) and SAED (**b**) patterns obtained from Fe_3O_4 nanoparticles and their surface modification using chitosan (CS-Fe_3O_4 MNPs). Reprinted with permission [72]. Copy right 2014. Elsevier

Morphology and size were determined using Scanning Electron Microscopy (SEM) and Transmission Electron Microscopy (TEM). SEM image of CS-Fe_3O_4 (Fig. 19a) shows spherical in shape particles agglomerated due to dipole–dipole interaction and they formed small clusters mainly due to your magnetic nature. TEM image (Fig. 19b) shows dispersed particles with 15.1 ± 5.0 nm sizes.

The attachment of CS on the surface of Fe_3O_4, were evaluated by Fourier Transform Infrared (FTIR) Spectroscopy. Thermogravimetric analysis provides a quantitative evidence of the coating of CS on nanoparticles (percentage of CS in the MNPs, 21.3 wt%). The magnetization measurements were performed on a superconducting quantum interference device magnetometer. The CS-Fe_3O_4 MNPs showed superparamagnetic behavior at room temperature, and specific absorption, 118.85 w g^{-1}.

Since the nanocomposites particles will be used for biomedical applications, the detection of biomaterial toxicity has to be addressed. The CS-Fe_3O_4 MNPs showed low cytotoxicity. Induction heating ability of coated particles demonstrated a

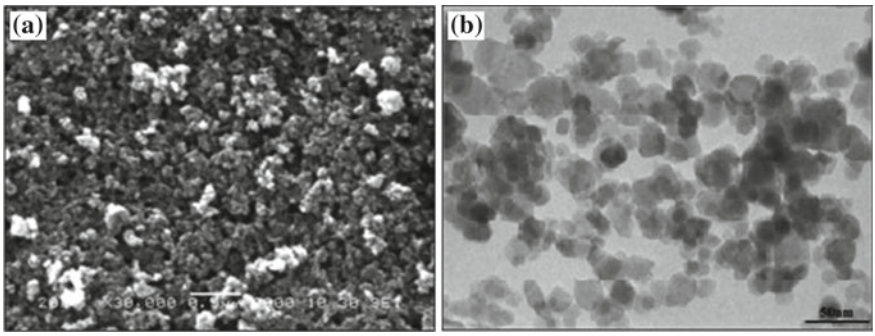

Fig. 19 SEM images (**a**) and TEM images (**b**) of CS-Fe_3O_4 MNPs. Reprinted with permission [72]. Copy right 2014 Elsevier

temperature rise under the application of external applied AC magnetic field. The CS-Fe_3O_4 MNPs were suitable for hyperthermia therapy applications.

Wang et al. [73, 74] used a spin-coating technique to synthesize a nanostructured semiconductor $Zn_xCd_{1-x}S$ in chitosan–alginate nanocomposite films with potential use in bioapplications. A cadmium-zinc-ion-containing CS solution was transferred to a clean quartz substrate, and spin-coated for 30 min, after dried in an oven at 100 °C for 10 min to form a CS layer. The same quartz substrate was covered with a sulfur-ion-containing alginate (AL) solution and spin-coated and dried similarly as the above. $Zn_xCd_{1-x}S$ nanoparticles (NPs) are formed between the CS and AL layers. The preparation cycle was repeated to obtain more $Zn_xCd_{1-x}S$ NPs in the polymer layers.

The $Zn_xCd_{1-x}S$/CS/AL nanocomposite film was characterized by XRD, UV–vis absorption spectroscopy (UV–vis), photoluminescence (PL) spectroscopy, TEM, and atomic force microscopy (AFM). The XRD patterns, UV–vis absorption spectra, and PL spectra demonstrated the formation of cubic $Zn_xCd_{1-x}S$ NPs in the composite films. TEM image (Fig. 20) shows quite small $Zn_xCd_{1-x}S$ NPs are and uniformly distributed in the film (NPs size $\sim$2 nm).

AFM images (Fig. 21) show nanocomposite films with various Zn/Cd molar ratios. The surface morphology of the composite films goes from rough to smooth with increasing Zn/Cd molar ratio, and the phase goes from bump-like shape to particle-like shape with a uniform distribution. The results suggest that the low-sized phase contains more Zn and the large-sized loop-shaped phase contains more Cd due to the radius difference between Zn and Cd ions. When the Zn ratio is larger, the film will be smoother with more low-sized phase.

Chitosan–nanocellulose nanocomposite films were prepared from chitosan (molecular weight of 600–800 kDa), nanocellulose (20–50 nm diameters), and

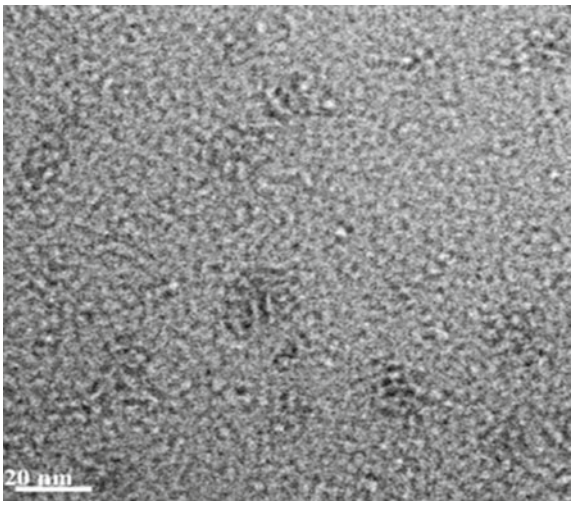

Fig. 20 Typical TEM image for the $Zn_xCd_{1-x}S$/CS/AL composite film with a Zn/Cd molar ratio of 1:1. Reprinted with permission [73, 74]. Copy right 2011 Elsevier

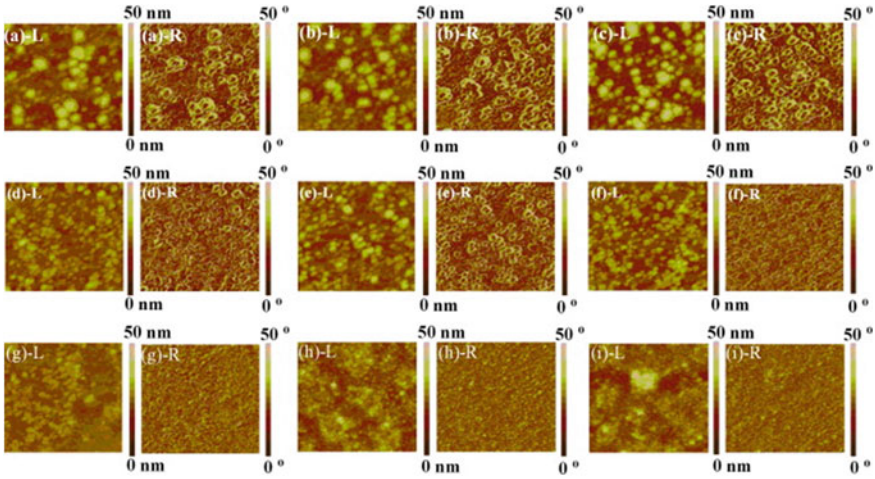

Fig. 21 AFM images of the $Zn_xCd_{1-x}S$/CS/AL nanocomposite films with various Zn/Cd molar ratios. The **a–i** images are for the samples with a Zn/Cd molar ratio of 1:9, 1:4, 2:3, 3:7, 1:1, 7:3, 3:2, 4:1, and 1:9, respectively. For each sample, the *left* image represents the height of the film, and the *right* one represents the phase distribution of the film. Reprinted with permission [73, 74]. Copy right 2014 Elsevier

glycerol under agitation and sonication [75]. The nanocomposites were examined by differential scanning calorimetry and XRD.

Agar disk diffusion test indicated that the nancomposite had inhibitory effects against gram-positive bacteria (*S. aureus*) and gram-negative bacteria (*E. coli* and *S. enteritidis*) through its contact area. Application of chitosan–nanocellulose nanocomposite film as food packaging on the ground meat decreased lactic acid bacteria population up to 3.1 logarithmic cycles (compared with nylon packaged sample) at 25 °C during 6 days of storage.

Youssef et al. [76] investigated the biosynthesis of silver nanoparticles (AgNPs) and gold nanoparticles (AuNPs) by *Bacillus subtilis* bacteria for biodegradable chitosan–silver (CS–Ag) and chitosan–gold (CS–Au) nanocomposites films production. The AuNPs and AgNPs were added to CS (5 % w/w) solution. Then, samples of CS nanocomposite solutions were transferred to flat silicon-coated Petri dishes and left to dry for 24 h, at room temperature and at 35 % relative humidity. CS nanocomposite dried films were unpeeled off manually and stored in the desiccator prior to characterization.

The formation and structural properties of AgNPs, AuNPs, and nanocomposites films were evaluated by UV–vis absorption spectroscopy and XRD, respectively, and their surface morphology properties were investigated by SEM and TEM. SEM images of AgNPs and AuNPs are showed in Fig. 22. The AgNPs are homogenous and smooth round spheres (Fig. 22a) in a 10–25 nm range size, while AuNPs have a cubic structure (Fig. 22b) in a 10–15 nm range size.

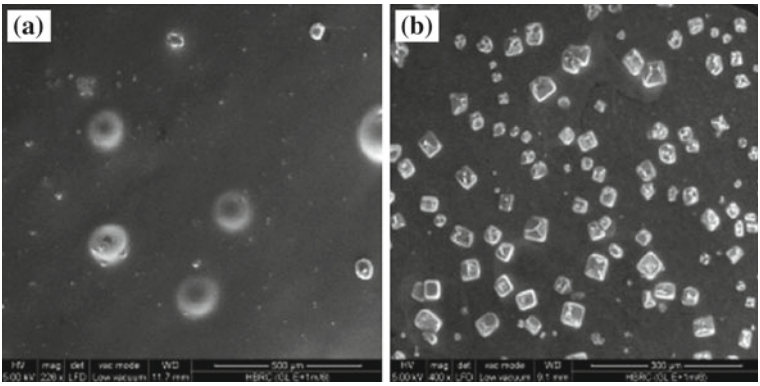

Fig. 22 SEM images of **a** AgNPs and **b** AuNPs prepared by *B. subtilis*. Reprinted with permission [76]. Copy right 2014 Elsevier

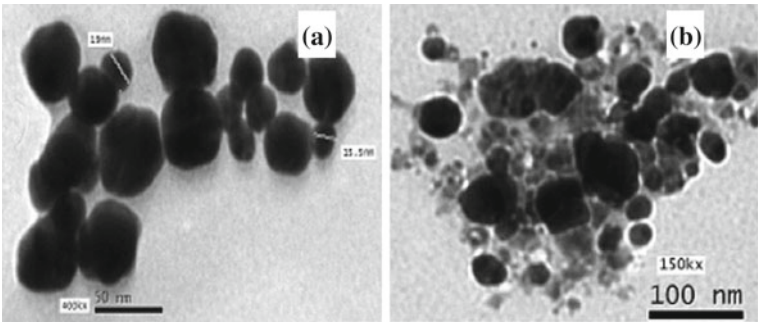

Fig. 23 TEM images of **a** CS–Ag nanocomposites and **b** CS–Au nanocomposites. Reprinted with permission [76]. Copy right 2014 Elsevier

TEM images show the distribution of AgNPs and AuNPs in the CS matrix (Fig. 23a, b, respectively). Both NPs were uniformly dispersed into CS matrix. The sizes of the nanocomposites are restricted to the nano range.

Antimicrobial activity assays of the prepared CS–Ag and CS–Au nanocomposites showed good antimicrobial activity against gram positive (*S. aureus*) and gram negative (*Pseudomonas aerugenosa*) bacteria, yeast (*C. albicans*), and fungi (*A. niger*) (Fig. 24). The zone of inhibition of the CS nanocomposites increased as the concentrations of AgNPs and AuNPs increased in the chitosan matrix (Table 1). These results suggested a potential application of CS–Ag and CS–Au nanocomposites as antimicrobial agents for biomedical, pharmaceutical, biosensor, and edible packaging applications.

Organic–inorganic nanocomposite films based on graphene oxide (GO) and CS were prepared were obtained by sonochemical method [77]. At room temperature, a

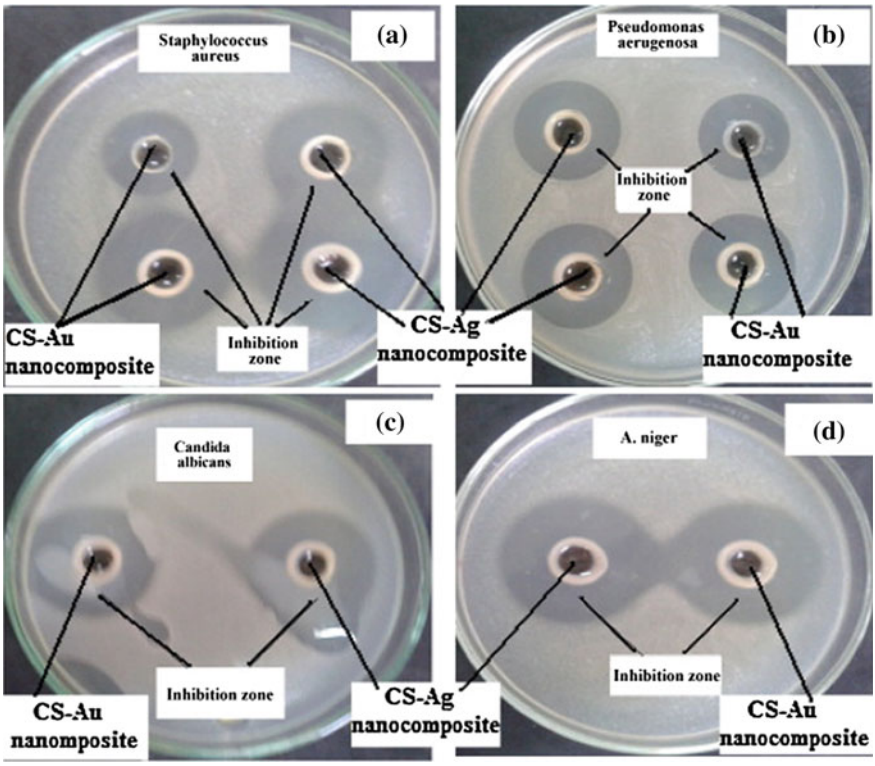

Fig. 24 The antibacterial activity of CS–Au and CS–Ag nanocomposites against **a** gram positive bacteria, **b** gram negative bacteria, **c** yeast, and **d** fungi [76]. Reprinted with permission. Copy right 2014 Elsevier

Table 1 The antimicrobial activity of chitosan as well as CS–Au and CS–Ag nanocomposite films. Reprinted with permission [76]. Copy right 2014 Elsevier

Sample code	Clear zone (Θ mm)			
	S. aureus	*P. aerugenosa*	*C. albicans*	*A. niger*
Chitosan (CS) (% AuNPs)	6	7	6	0
0.5	12	7	8	15
1.0	13	12	14	18
2.0	15	12	13	25
0.5	9	11	12	10
1.0	10	12	12	8
2.0	18	15	19	9

GO (2 % v/v) suspension was added dropwise in a CS (2 % v/v) solutions under stirring. Then, the mixture was sonicated for 1 h and the nanocomposite films were obtained by annealing under vacuum at 60 °C for 24 h.

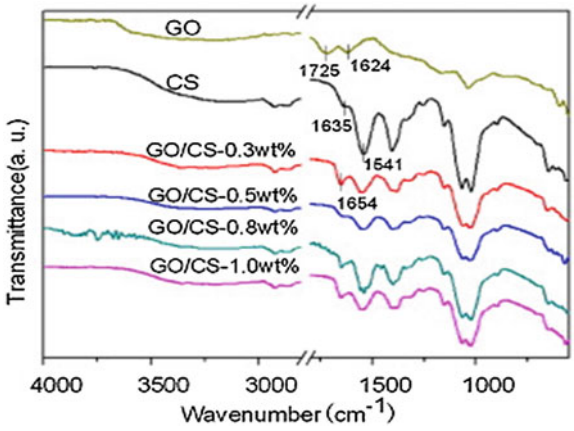

Fig. 25 FTIR spectra of GO, CS, and GO/CS-x wt% (where x is 0.3, 0.5, 0.8 1.0) nanocomposite films. Reprinted with permission [77]. Copy right 2014 Elsevier

The GO/CS nanocomposite films were characterized by SEM, FTIR spectroscopy, Thermogravimetry (TG), and differential scanning calorimetry (DSC). In the infrared spectra of GO/CS composites (Fig. 25), for example, the weak broad peaks in the region of 3000–3500 cm^{-1} (N–H stretching and O–H stretching on CS), the presence of the peak at 1654 cm^{-1} and the absence of peaks at 1635 cm^{-1} (C = O stretch of the carboxylic group related to amide on CS) and at 1725 cm^{-1} (C = O stretch of the carboxylic group on GO) implies an attractive intermolecular interaction between CS and GO.

Electrochemical measurements were evaluated by Cyclic Voltammetry (CV) and others current impedance experiments. CVs of CS and GO/CS composite electrodes (Fig. 26) show a significant increase in redox peak current for GO/CS electrodes, indicating that GO can improve the electroactive surface area of the electrode and catalytic ability.

The characterization of GO/CS nanocomposite films indicates well-dispersed GO nanosheets in the CS matrix. Electrochemical activity of the GO/CS

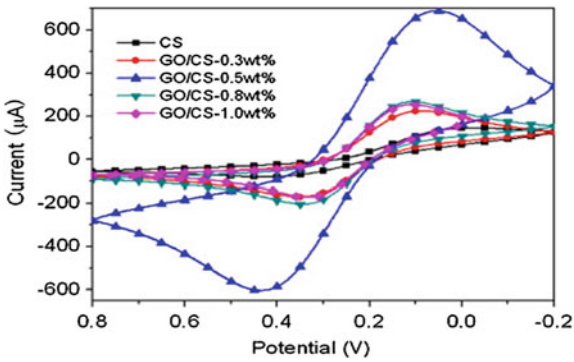

Fig. 26 CVs of CS and GO/CS-x wt% (where x is 0.3, 0.5, 0.8 1.0) electrodes. Reprinted with permission [77]. Copy right 2014 Elsevier

nanocomposite electrode demonstrated its potential application in the fabrication of electrochemical biosensors.

Zhang et al. [78] reported the preparation of electrode by layer-by-layer assembly of hemoglobin (Hb), AuNPs, CS, and graphene (GR) onto glassy carbon electrode (GCE). The Au/GR–CS nanocomposite substrate shows a promotion for the direct electron transfer between hemoglobin and glassy carbon electrode. The ternary nanocomposite modified GCE was constructed by stabilizing GR nanosheets and absorbing AuNPs with the positive charge of amino groups in CS. Figure 27 can been showed the layer-by-layer assembly preparation of nanocomposite electrode and the synergetic interactions between GR, CS, and AuNPs.

The nanocomposite electrodes were characterized by UV–vis spectroscopy, FTIR spectroscopy, SEM, and TEM. The morphology of the modified electrodes showed a homogenous flake structure for the CS-dispersed GR film (Fig. 28a, b). After incorporating AuNPs, the coarse layer structured Au/GR–CS film features a honeycomb surface (Fig. 28c, d). This electrode shows good electrocatalytic performance for the reduction of hydrogen peroxide within a linear range from 2 to 935 μM, a detection limit of 0.35 μM and sensitivity of 347.1 mA cm^{-2} M^{-1}.

Xia et al. [79] proposed a synthesis of Ag-MoS_2/CS nanocomposite and its application as a selective and sensitive electrochemical sensor for the determination of tryptophan (Try). In the synthesis process, graphene-like molybdenum sulfide and silver nanoflakes were directly synthesized on the surface of molybdenum sulfide (MoS_2) films, with CS acted as the stabilizer. This nanocomposite was characterized by TEM and XRD. In the proposed arrangement of the CS chain within the MoS_2 films (Fig. 29), a layer of the CS is intercalated between two layers of MoS_2.

A GCE was covered with Ag-MoS_2/CS nanocomposite film. Electrochemical impedance spectroscopy (EIS), CV, and differential pulse voltammetry (DPV) were employed to evaluate the electrochemical property of Ag-MoS_2/CS toward the oxidation of Try. The possible mechanism for the electrooxidation of tryptophan is proposed in Fig. 30. Under the optimized experimental conditions, the oxidation peak currents are proportional to the concentrations of tryptophan over the range of

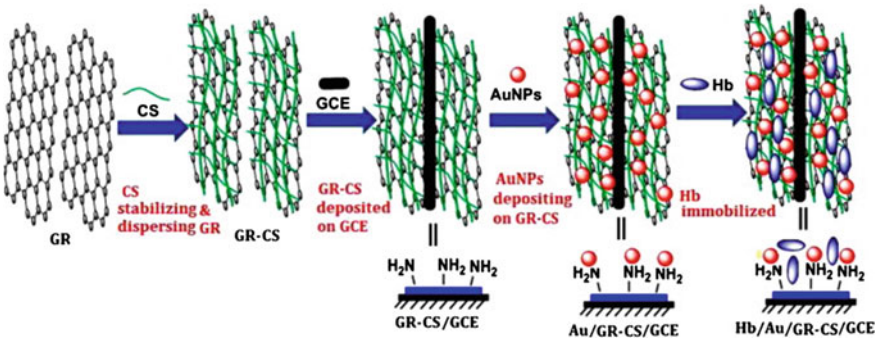

Fig. 27 Layer-by-layer assembly preparation of Hb, AuNPs, CS, and GR onto GCE. Reprinted with permission [78]. Copy right 2014 Elsevier

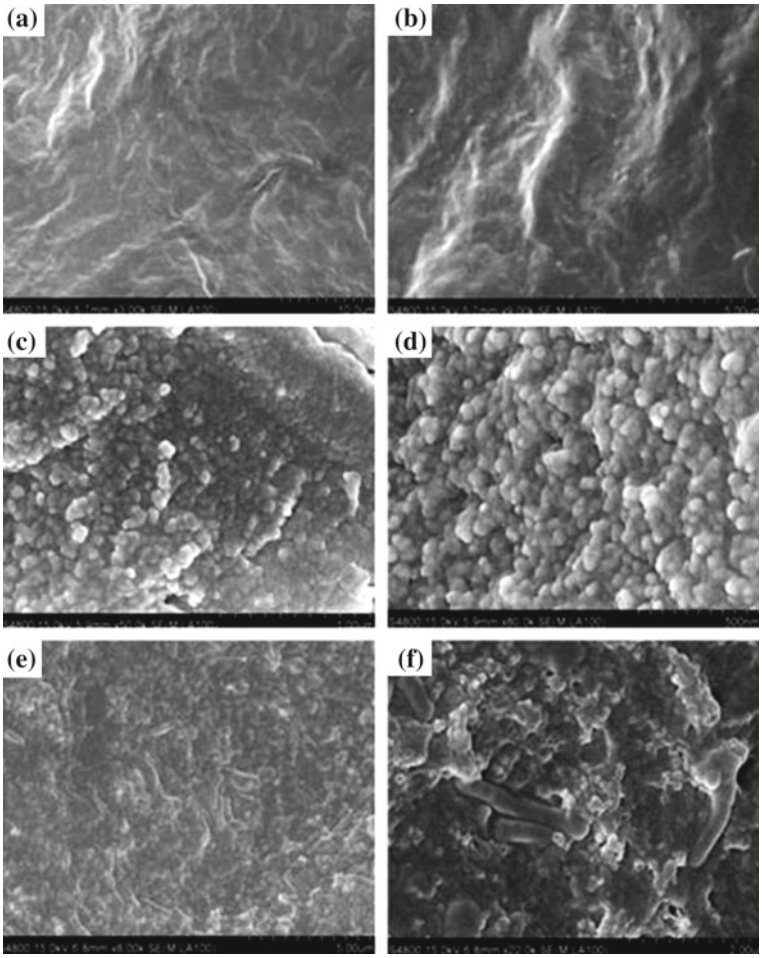

Fig. 28 SEM images of GR–CS **a**, **b**, Au/GR–CS **c**, **d** and Hb/Au/GR–CS **e**, **f** on the GCE. Reprinted with permission [78]. Copy right 2014 Elsevier

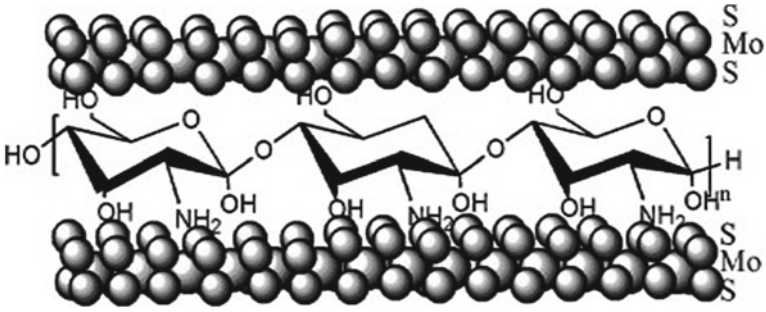

Fig. 29 The structure of proposed lamellar arrangement of MoS_2–chitosan nanocomposites. Reprinted with permission [79]. Copy right 2014 Elsevier

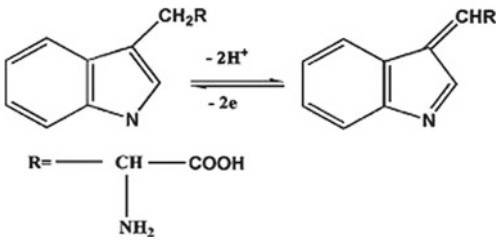

Fig. 30 The proposed oxidation mechanism of tryptophan. Reprinted with permission [79]. Copy right 2014 Elsevier

0.5–120 μM, and the detection limit is 0.05 μM. The proposed electrochemical method is free of interference from other amino acid to other coexisting species.

Seyed Dorraji et al. [80] developed a procedure to synthesize a polyaniline multiwall carbon nanotubes (PAni/MWCNT) nanocomposite by chemical oxidative polymerization on the surface of CS fibers. This Cs/PAni/MWCNT nanocomposite was prepared for potential electrochemical applications.

Morphological characterization of the nanocomposite fibers was performed by SEM. Electrochemical properties were studied by CV, galvanostatic charge/discharge, and EIS. The SEM micrograph of the Cs/PAni/MWCNT nanocomposite fibers (Fig. 31) reveals a highly porous structure can provide an effective diffusion of solvent, protons, and sulfate ions.

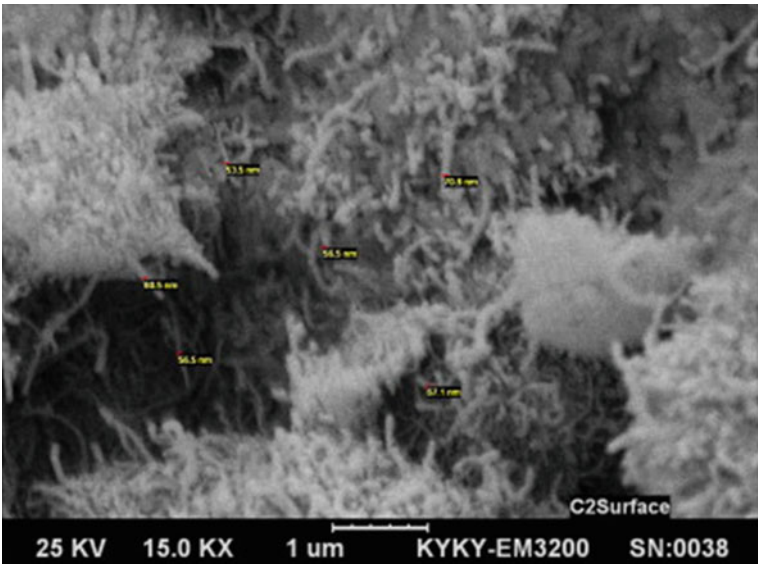

Fig. 31 SEM micrograph of CS/PAni/MWCNT fiber. MWCNTs connected with PAni are observed with typical diameters in the range of 50–70 nm. Reprinted with permission [80]. Copy right 2014 Elsevier

The electrochemical studies showed that nanocomposite fibers have a specific capacitance of 14.48 F cm^{-2} and a specific energy of 0.0013 Wh cm^{-2} corresponding to a specific power of 0.011 W cm^{-2}. These results suggest the potential of the Cs/PAni/MWCNT nanocomposite fibers as electrode material for electrical double-layer capacitors.

Justin and Chen [81] investigated the potential of biodegradable CS–GO nanocomposites for applications in drug delivery. Fluorescein sodium was used to analyze the release rate improvement of therapeutics from nanocomposites due to its dispersibility within aqueous mediums, distinct absorption peaks (between 450 and 500 nm), and similar size to several important drugs such cisplatin (cancer drug), indomethacin (non-steroidal anti-inflammatory), propranolol hydrochloride (beta blocker), and timolol maleate (vasodilator).

The CS nanocomposites containing 2 wt% GO provided the optimal combination of mechanical properties and drug-loading capacity. The drug delivery profiles of the nanocomposite were dependent on the drug loading ratio. The best ratio of drug to GO for a quick and high release of the loaded drug was 0.84:1. The nanocomposite demonstrated pH sensitivity of drug release, releasing 48 % less drug in an acidic medium than in a neutral one.

Characterization of nanocomposites was evaluated by UV-Vis spectroscopy, FTIR spectroscopy, AFM, TEM, laser scattering particle sizing analysis, and XRD analysis. In Fig. 32 TEM micrograph shows the dispersion of graphene oxide nanosheets (black thin lines) within the chitosan matrix.

In others studies, Jeyapragasam and Saraswathi [82] used an acetylcholinesterase (AChE) enzyme immobilized iron oxide/CS nanocomposite film modified GCE as a highly sensitive square wave voltammetric biosensor for the determination of carbofuran pesticide. The Fe_3O_4–CS nanocomposite was prepared by a simple solution mixing process and its formation was confirmed by FTIR spectroscopy. Electrochemical Impedance, SEM, and AFM studies confirmed the effective enzyme immobilization onto the nanocomposite matrix.

The operation of the biosensor is based on inhibition of the AChE. This inhibition is used to amperometric/voltammetric detection of thiocholine, a reaction product of acetylthiochorine chlorate (ATCl) oxidation at a constant potential. As seen in Fig. 33, the ATCl hydrolysis is catalyzed by AchE to thiocholine chloride and acetic acid. At an appropriate voltage, thiocholine chloride is oxidized to dithiocholine. The presence of a pesticide inhibits the AChE activity, and the ATCl conversion is decreased. The anodic oxidation current of thiocholine is inversely proportional to the concentration of pesticide.

Besides Fe_3O_4-CS immobilizates the AChE enzyme onto the nanocomposite, the presence of CS prevents the aggregation of the magnetic nanoparticles and avoids loss of the enzyme molecules by providing a biocompatible microenvironment to maintain the enzyme activity.

The AChE nanocomposite-based biosensor could detect carbofuran as low as 3.6×10^{-9} M, and its practical application was ascertained by the determination of carbofuran from cabbage samples and by comparing the results with those obtained by the standard high-performance liquid chromatography method.

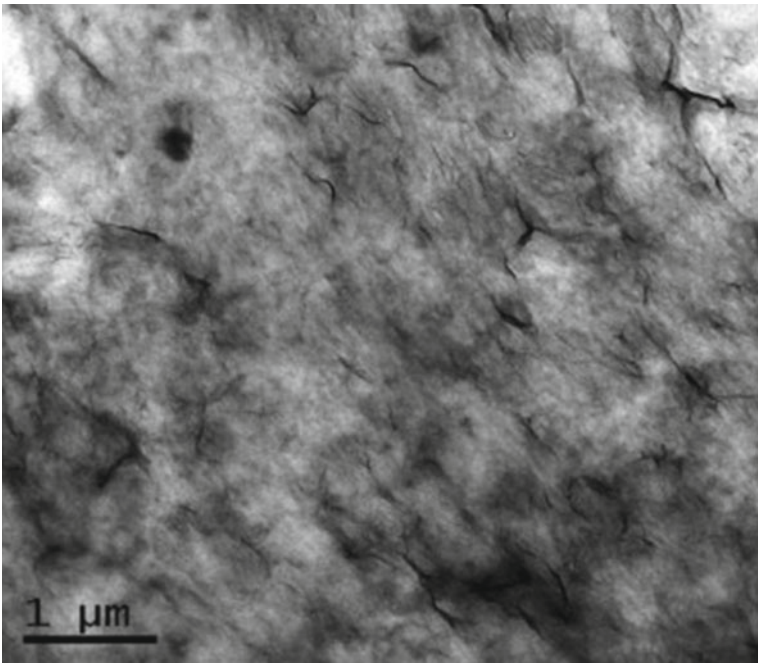

Fig. 32 TEM micrograph of GO/CS nanocomposite. Reprinted with permission [81]. Copy right 2014 Elsevier

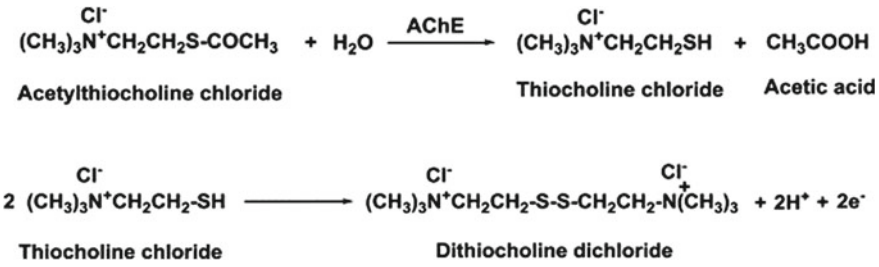

Fig. 33 The principle of the electrochemical AChE biosensor. Reprinted with permission [82]. Copy right 2014 Elsevier

Ferreira et al. [3] reported that a study of chitosan as a renewable polymer to form edible chitosan films allowing the incorporation of functional compounds. The authors investigated the effects in the chitosan films properties after incorporation of grape pomace extracts. In this procedure, 0.15 % of hot water extract (mainly polysaccharides), 0.15 and 0.3 % of chloroform extract (wax), and 0.3 and 0.75 % of *n*-hexane extract (oil) were mixed. The evaluation of the surface morphology revealed that the films with the aqueous extract had the most homogeneous and

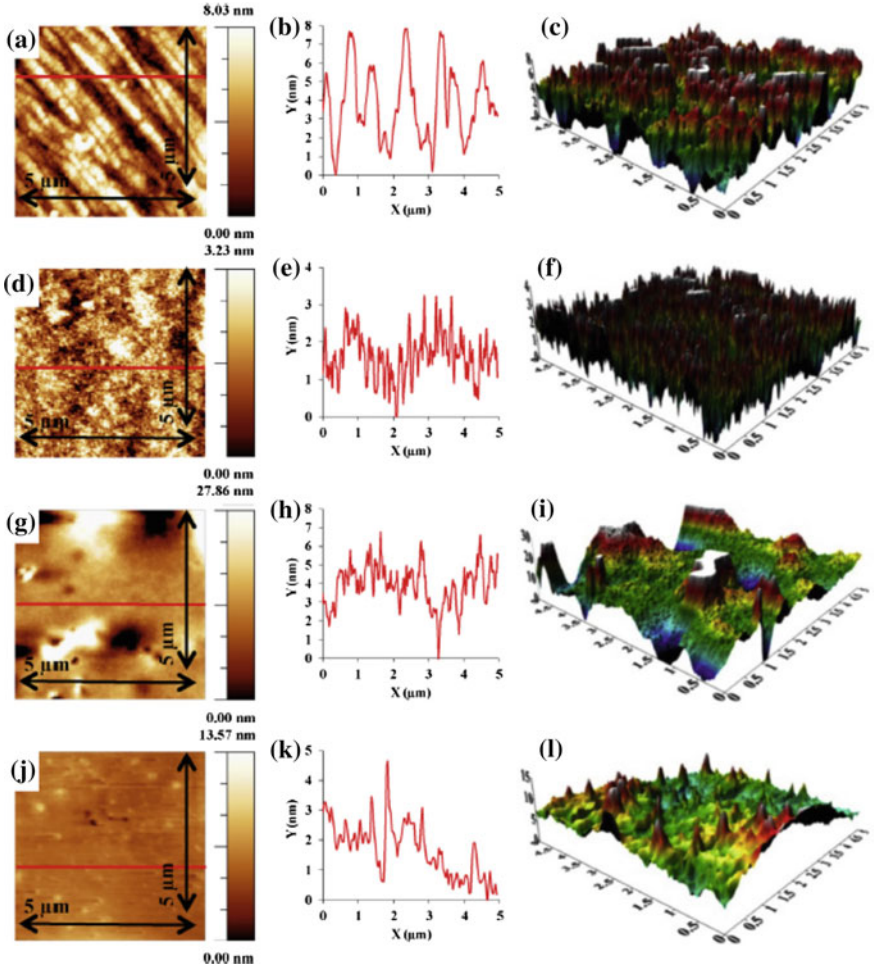

Fig. 34 Surface morphology of the chitosan-based films by AFM. 2D AFM topographic images of **a** Ch film, **d** HWE, **g** W2, and **j** Oil2 (5 × 5 m), where the color scale in the *right side* indicates the respective height values. Profile of the height values along the film in the marked area of 2D AFM topographic images of **b** Ch film, **e** HWE, **h** W2, and **k** Oil2. 3D AFM topographic images of **c** Ch film, **f** HWE, **i** W2, and **l** Oil2. (For interpretation of the references to color in this figure legend, the reader is referred to the web version of this article.). Reprinted with permission [3]. Copy right 2014 Elsevier

smoother topography, Fig. 34, and also suggest that the matrix was not well dispersed in the chitosan film-forming solution. According to the authors, this is probably due to the high molecular weight and hydrophobic character.

The incorporation of higher proportion of oil changed the mechanical properties of the films. According to authors, the chitosan-based films with 0.75 % oil demonstrated a 75 % decrease of solubility in water, due to their hydrophobicity. The

Table 2 mechanical parameters of chitosan—based films. Reprinted with permission [82]. Copy right 2014 Elsevier

	Tensile strength (MPa)	Elongation	Youg's modulus (MPa/%)
Ch	12.61 ± 1.59^{a}	44.24 ± 3.5^{a}	0.20 ± 0.02^{a}
WWE	13.58 ± 1.27^{a}	47.25 ± 4.11^{ab}	0.20 ± 0.02^{ab}
W1	10.99 ± 4.05^{abc}	53.48 ± 12.47^{ab}	0.13 ± 0.01^{c}
W2	9.89 ± 1.59^{b}	49.57 ± 1.79^{bc}	0.13 ± 0.02^{cd}
Oi11	12.34 ± 2.17^{ab}	41.11 ± 3.34^{ad}	0.23 ± 0.02^{b}
Oi12	6.88 ± 0.94^{c}	35.11 ± 1.96^{e}	0.16 ± 0.03^{ad}

Different superscripts letters, in each column, represent values that are significantly (p, 0.05) different (n = 5)

hydrophobic films showed higher antioxidant capacity in organic medium (ABTS and DPPH assay), whereas the most hydrophilic films showed a reducing power assays. According to the authors, the chitosan-based films prepared by incorporation of these grape pomace extracts are promising for food shelf life extension

The different grape pomace extracts were also added to each one of the chitosan solutions in the proportions given in Table 2. This mixture was placed in a water bath at 50 °C with stirring for 10 min for homogenization. This solution was placed in an oven for 18 h at 35 °C for film formation by solvent casting, and a control film was also prepared only with chitosan, no extracts added.

Kurek et al. [4] reported a study about the influence of water vapor conditions on mass transport and barrier properties of chitosan-based films and coatings. They related the relation to surface and structural properties. The parameters, water contact angles, material swelling, polymer degradation temperature, barrier properties, and aroma diffusion coefficients were investigated. The authors concluded that solvent nature and the presence of carvacrol influenced the surface and structural properties and then the barrier performance of activated chitosan films, as well as the plasticization effect of water was more pronounced at high humid environment.

In this study, a chitosan solution was prepared in a 1 % (v/v) aqueous acetic acid, to obtain 2 % (w/v) film solutions (FFS) which were stirred for 2 h at room temperature. Carvacrol (0.5 %, w/v) was homogenized in acid chitosan solution at 24,000 rpm for 10 min to obtain film solutions with an incorporated aroma compound. The films were obtained by evaporation of solvents by drying in a ventilated climatic at 20 °C. The authors also prepared chitosan coated polyethylene films according to methodology described by Sollogoub et al. [83].

Abdollahi et al. [71] reported a study involving a combination of chitosan biopolymer, nanoclay, and rosemary essential oil as a functional bionanocomposite. These materials were evaluated for chemical, microbial, and sensory properties over 16-day storage. The samples were coated with the functional bionanocomposite had the lowest pH and total volatile basic nitrogen. According to authors, the materials coating efficiently retarded lipid oxidation by decreasing peroxide, free fatty acid,

and thiobarbituric acid production in the samples, as well as the coating also reduced total viable and psychrotrophic count of the fillets by the end of storage

Experimental procedure for films preparation was carried out as follows: A solution of chitosan was prepared by placing (20 g of chitosan powder/1000 mL of aqueous acetic acid solution (1 %, v/v) under a magnetic stirring plate (at 90 °C and 1250 rpm for 20 min) and then cooled to room temperature. Clay (3 %, m/m on solid chitosan) was dispersed in 100 mL of 1 % (v/v) aqueous acetic acid solution and vigorously stirred for 24 h. Then 150 mL of chitosan solution was added to the

Table 3 Summary of different types of chitosan nanocomposite films and its applications

Nanocomposites films	Applications	References
Chitosan-Fe_3O_4 nanoparticles	Hyperthermia therapy	[72]
$Zn_xcd_{1-x}s$/chitosan/alginate nanocomposite films	–	[73, 74]
Chitosan–nanocellulose films	Food packaging	[75]
Chitosan–silver and chitosan–gold films	Biomedical, pharmaceutical, biosensor and edible packaging	[76]
Graphene oxide–chitosan films	Electrochemical biosensors	[77]
Hemoglobin/gol/Chitosan/graphene films	Electrochemical biosensor	[78]
Silver-mos_2/chitosan films	Electrochemical biosensor	[79]
Chitosan/polyaniline/multiwall carbon nanotubes films	Electrochemical applications	[80]
Graphene oxide–chitosan films	Drug delivery	[81]
Acetylcholinesterase-Fe_3O_4/chitosan films	Electrochemical biosensor	[82]
Chitosancarbon dots nanocomposite hydrogel film	Biomedical and industrial applications	[84]
B-glucanase/Prussian blue–chitosan film	Electrochemical biosensor	[73, 74]
B-glucanase/gold nanoparticles–chitosan film		
Chitosan/polyethylene oxide-based/chitin nanocrystals fibers	Wound dressing	[85]
Mno_2–chitosan nanocomposite films	Electrochemical energy storage	[86]
Chitosan/olive oil/cellulose nanocrystals films	–	[87]
Chitosan-grafted poly acrylonitrile/silver	–	[88]
Lithium ferrite/chitosan	–	[89]
Chitosan–polyvinyl alcohol/graphene oxide films	–	[90]
Chitosan/clay	–	[91]
Chitosan/montmorillonite	Vitamin package	[92]
pomace extract–chitosan films	Antioxidant and food packaging	[3]
Carvacrol-activated chitosan film.	Antimicrobial	[4]
Chitosan/clay functional bionanocomposite activated with rosemary essential oil	Refrigeration of silver carp fillets	[71]

clay solutions, and the mixture was stirred for 4 h. Then, 0.2 % w/v of essential oil (emulsifier) was added to the mixture and stirred in 40 °C for 30 min. An amount of rosemary essential oil was added to the solution, to reach a final concentration of 1.5 % (v/v) and homogenized at 7000 rpm for 2 min.

The recent progress in the field of environmental friendly biodegradable has increased the interest of researchers in chitosan-based chitosan nanocomposites and the development of new ideas in this field, thus in Table 3 is presented a summary [72–92].

2 Conclusions

The bionanocomposites based on chitosan represent a class of materials that has attracted considerable attention, mainly due to the need to develop environmental friendly materials. Which are produced through the incorporation of a biodegradable matrix and depending on the application, also in a biocompatible matrix. Among the biodegradable matrices of natural origin, the chitosan has high relevance.

The recent progress made in the field of environmental friendly biodegradable polymers and composites has been impressive. The development of nano-chitosan films have been applied in multipurpose fields such as food production, hyperthermia therapy, biomedical, pharmaceutical, biosensor and edible packaging, biomedical and industrial applications, electrochemical biosensor, antioxidant, food packaging, antimicrobial, drug delivery, and adverse effects on biodiversity and other environmental and industrial impacts. In addition, their relatively high production and processing costs have been indicated that the regeneration and reuse studies also are need.

References

1. Thakur VK, Tan EJ, Lin M-F, Lee PS (2011) Polystyrene grafted polyvinylidenefluoride copolymers with high capacitive performance. Polym Chem 2:2000–2009
2. Thakur VK, Singha AS, Kaur I et al (2011) Studies on analysis and characterization of phenolic composites fabricated from lignocellulosic fibres. Polym Polym Compos 19:505–511
3. Ferreira AS, Cláudia N, Alichandra C, Paula F, Colimbra MA (2014) Influence of grape pomace extract incorporation on chitosanfilms properties. Carbohydr Polym 113:490–499
4. Kurek M, Guinault A, Voilley A, Galic K, Debeaufort F (2014) Effect of relative humidity on carvacrol release and permeation properties of chitosan based films and coatings. Food Chem 144:9–17
5. Thakur VK, Singha AS, Thakur MK (2012) Biopolymers based green composites: mechanical, thermal and physico-chemical characterization. J Polym Environ 20:412–421
6. Thakur VK, Ding G, Ma J et al (2012) Hybrid materials and polymer electrolytes for electrochromic device applications. Adv Mater 24:4071–4096
7. Thakur VK, Thakur MK, Gupta RK (2013) Rapid synthesis of graft copolymers from natural cellulose fibers. Carbohydr Polym 98:820–828

8. Thakur VK, Thakur MK, Gupta RK (2013) Graft copolymers from cellulose: synthesis, characterization and evaluation. Carbohydr Polym 97:18–25
9. Thakur VK, Thakur MK (2014) Recent advances in graft copolymerization and applications of chitosan: a review. ACS Sustain Chem Eng 2:2637–2652
10. Dhakal HN, Zhang ZY, Guthrie R, MacMullen J, Bennett N (2013) Development of flax/carbon fibre hybrid composites for enhanced properties. Carbohydr Polym 96:1–8
11. Thakur VK, Thakur MK (2014) Processing and characterization of natural cellulose fibers/thermoset polymer composites. Carbohydr Polym 109:102–117
12. Thakur VK, Thakur MK, Gupta RK (2014) Review: raw natural fiber-based polymer composites. Int J Polym Anal Charact 19:256–271
13. Thakur VK, Thakur MK, Raghavan P, Kessler MR (2014) Progress in green polymer composites from lignin for multifunctional applications: a review. ACS Sustain Chem Eng 2:1072–1092
14. Petzold K, Einfeldt L, Gunther W, Stein A, Klemm D (2001) Regioselective functionalization of starch: synthesis and 1H NMR characterization of 6-O-silylethers. Biomacromolecules 2:965–969
15. He R, Wang XL, Wang YZ, Yang KK, Zeng JB, Ding SD (2006) A study on grafting poly (1,4-dioxan-2-one) onto starch via 2, 4-tolylene diisocyanate. Carbohydr Polym 65:28–34
16. Zobel HF (1988) Molecules to granules: a comprehensive starch review. Starch-Starke 40:44–50
17. Avérous L (2004) Biodegradable multiphase systems based on plasticized starch: A review. J Macromol Sci Polym Rev 231–274
18. Dufresne A, Vignon MR (1998) Improvement of starch film performances using cellulose microfibrils. Macromolecules 31:2693–2696
19. Yu L, Dean K, Li L (2006) Polymer blends and composites from renewable resources. Prog Polym Sci 31:576–602
20. Curvelo AAS, Carvalho AJF, Agnelli JAM (2001) Thermoplastic starch–cellulosic fibers composites: preliminary results. Carbohydr Polym 45:183–188
21. Thakur VK, Singha AS, Misra BN (2011) Graft copolymerization of methyl methacrylate onto cellulosic biofibers. J Appl Polym Sci 122:532–544
22. Thakur VK, Singha AS, Thakur MK (2012) Graft copolymerization of methyl acrylate onto cellulosic biofibers: synthesis, characterization and applications. J Polym Environ 20:164–174
23. Thakur VK, Lin M-F, Tan EJ, Lee PS (2012) Green aqueous modification of fluoropolymers for energy storage applications. J Mater Chem 22:5951–5959
24. Chen L, Qiu X, Xie Z, Hong Z, Sun J, Chen X, Jing X (2006) Poly(l-lactide)/starch blends compatibilized with poly(l-lactide)-g-starch copolymer. Carbohydr Polym 65:75–80
25. Auras R, Harte B, Selke S (2004) An overview of polylactides as packaging materials. Macromol Biosci 4:835–864
26. Carothers WH, Dorough GL, van Natta FJ (1932) Studies of polymerization and ring formation. X. The reversible polymerization of six-membered cyclic esters. J Am Chem Soc 54:761–772
27. Sosnowski S, Gadzinowski M, Slowkowski S (1996) Poly(l, l-lactide) microspheres by ring-opening polymerization. Macromolecules 29:4556–4564
28. Raquez J-M, Habibi Y, Murariu M, Dubois P (2013) Polylactide (PLA)-based nanocomposites. Prog Polym Sci 38:1504–1542
29. Li ZQ, Zhou XD, Pei CH (2010) Synthesis of PLA-co-PGMA copolymer and its application in the surface modification of bacterial cellulose. Int J Polym Mater 59:725–737
30. Lin N, Chen G, Huang J, Dufresne A, Chang PR (2009) Effects of polymer-grafted natural nanocrystals on the structure and mechanical properties of poly (lactic acid): a case of cellulose whisker-graft-polycaprolactone. J Appl Polym Sci 113:3417–3425
31. Goffin AL, Raquez JM, Duquesne E, Siqueira G, Habibi Y, Dufresne A, Dubois P (2011) From interfacial ring-opening polymerization to melt processing of cellulose nanowhisker-filled polylactide-based nanocomposites. Biomacromolecules 12:2456–2465
32. Xanthos M (1992) Reactive extrusion: principles and practice. Hanser Publishers, Oxford University Press, Oxford

33. Gong C, Shi S, Dong P, Kan B, Gou M, Wang X, Li X, Luo F, Zhao X, Wei Y, Qian Z (2009) Synthesis and characterization of PEG-PCL-PEG thermosensitive hydrogel. Int J Pharm 365:89–99
34. Liu CB, Gong CY, Huang MJ, Wang JW, Pan YF, Zhang YD, Li GZ, Gou ML, Wang K, Tu MJ, Wei YQ, Qian ZYJ (2008) Thermoreversible gel–sol behavior of biodegradable PCL-PEG-PCL triblock copolymer in aqueous solutions. J Biomed Mater Res B Appl Biomater 84B:165–175
35. Lu C, Guo S-R, Zhang Y, Yin M (2006) Synthesis and aggregation behavior of four types of different shaped PCL-PEG block copolymers. Polym Int 55:694–700
36. Li Z, Yin H, Zhang Z, Liu KL, Li J (2012) Supramolecular anchoring of DNA polyplexes in cyclodextrin-based polypseudorotaxane hydrogels for sustained gene delivery. Biomacromolecules 13:3162–3172
37. He C, Sun J, Deng C, Zhao T, Deng M, Chen X, Jing X (2004) Study of the synthesis, crystallization, and morphology of Poly(ethylene glycol)−Poly(ε-caprolactone) Diblock copolymers. Biomacromolecules, 5, 2042–2047
38. Li Z, Beng Hoon Tan BH (2014) Towards the development of polycaprolactone based amphiphilic block copolymers: molecular design, self-assembly and biomedical applications. Mater Sci Eng C. (In press). doi: 10.1016/j.msea.2014.06.003. http://www.sciencedirect.com/science/article/pii/S0928493114003658
39. Bertini F, Canetti M, Cacciamani A, Elegir G, Orlandi M, Zoia L (2012) Effect of ligno-derivatives on thermal properties and degradation behavior of poly(3-hydroxybutyrate)-based biocomposites. Polym Degrad Stab 97:1979–1987
40. Stiubianu G, Nistor A, Vlad A, Cazacu M (2011) Modification of water sorption capacity of polydimethylsiloxane based composites by incorporation of lignin. Materiale Plastice 48:289–294
41. Nordström Y, Norberg I, Sjöholm E, Drougge R (2013) A new softening agent for melt spinning of softwood kraft lignin. J Appl Polym Sci 129:1274–1279
42. Thakur VK, Thakur MK, Gupta RK (2013) Synthesis of lignocellulosic polymer with improved chemical resistance through free radical polymerization. Int J Biol Macromol 61:121–126
43. Thakur VK, Thakur MK (2014) Recent trends in hydrogels based on psyllium polysaccharide: a review. J Clean Prod 82:1–15
44. Doherty WOS, Mousavioun P, Fellows CM (2011) Value-adding to cellulosic ethanol: lignin polymers. Ind Crops Prod 33:259–276
45. Nair V, Panigrahy A, Vinu R (2014) Development of novel chitosan–lignin composites for adsorption of dyes and metal ions from wastewater. Chem Eng J 254:491–502
46. Fernandes EM, Aroso IM, Mano JF, Covas JA, Reis RL (2014) Functionalized cork-polymer composites (CPC) by reactive extrusion using suberin and lignin from cork as coupling agents. Compos B Eng 67:371–380
47. Moad G (1999) The synthesis of polyolefin graft copolymers by reactive extrusion. Prog Polym Sci 24:81–142
48. Thakur VK, Thakur MK, Gupta RK (2013) Development of functionalized cellulosic biopolymers by graft copolymerization. Int J Biol Macromol 62:44–51
49. Thakur VK, Thakur MK, Gupta RK (2013) Graft copolymers from natural polymers using free radical polymerization. Int J Polym Anal Charact 18:495–503
50. Ramos LP (2003) The chemistry involved in the steam treatment of lignocellulosic materials. Quim Nova 26:863–871
51. Chaplin M (2010) Water structure and science. http://www.lsbu.ac.uk/water/hycel.html. Accessed Sept 2010
52. Hubble M, Rojas OJ, Lucia LA, Sain M (2008) Cellulosic nanocomposites, review. BioResources 3:929–980
53. Saxena IM, Kudlicka K, Okuda K, Brown RM Jr (1994) Characterization of genes in the cellulose-synthesizing operons (acs operon) of Acterobacter xylinum: implications for cellulose crystallization. J Bacteriol 176(18):5735–5752

54. Dujardin E, Blaseby M, Mann S (2003) Synthesis of mesoporous silica by sol-gel mineralisation of cellulose nanorod nematic suspensions. J Mater Chem 13:696–699
55. Azizi Samir MAS, Alloin F, Sanchez JY, El Kissi N, Dufresne A (2004) Preparation of cellulose whiskers reinforced nanocomposites from an organic medium suspension. Macromolecules 37:1386–1393
56. Azizi Samir MAS, Alloin F, Sanchez JY, Dufresne A (2004) Cross-linked nanocomposite polymer electrolytes reinforced with cellulose whiskers. Macromolecules 37:4839–4844
57. Azizi Samir MAS, Alloin F, Sanchez JY, Dufresne A (2004) Cellulose nanocrystals reinforced poly(oxyethylene). Polymer 45:4149–4157
58. Favier V, Canova GR, Shrivastava SC, Cavaille JY (1997) Mechanical percolation in cellulose whisker nanocomposites. Polym Eng Sci 37:1732–1739
59. Grunert M, Winter WT (2002) Nanocomposites of cellulose acetate butyrate reinforced with cellulose nanocrystals. J Polym Environ 10:27–30
60. McCreight KW, Hoffman DC, Hale WR. Crosslinkable cellulose ester compositions for films for use in optical devices, PCT Int. Appl. 2006-US20123, 2005-648808, 54
61. Heux L, Chauve G, Bonnini C (2000) Nonflocculating and chiral-nematic self-ordering of cellulose microcrystals suspensions in nonpolar solvents. Langmuir 16:8210–8212
62. Yang Q, Pan X, Huang F, Li K (2011) Synthesis and characterization of cellulose fibers grafted with hyperbranched poly(3-methyl-3-oxetanemethanol). Cellulose 18(6):1611–1621
63. Lönnberg H, Fogelström L, Berglund L, Malmström E, Hult A (2008) Surface grafting of microfibrillated cellulose with poly (Îμ-caprolactone)—synthesis and characterization. Eur Polym J 44(9):2991–2997
64. Tran CD, Duri S, Delneri A, Franko M (2013) Chitosan-cellulose composite materials: preparation, characterization and application for removal of microcystin. J Hazard Mater 252–253:355–366
65. Muzzarelli RAA et al (2012) Current views on fungal chitin/chitosan, human chitinases, food preservation, glucans, pectins and inulin: a tribute to Henri Braconnot, precursor of the carbohydrate polymers science, on the chitin bicentennial. Carbohydr Polym 87:995–1012
66. Vakili M, Rafatullaha M, Salamatinia B, Abdullahc, AZ, Ibrahima MH, Tanb KB, Gholami Z, Amouzgar P (2014) Application of chitosan and its derivatives as adsorbents for dye removal from water and wastewater: a review. Carbohydr Polym 113, 115–130
67. Moradi DS, Bahar R, Mashinchian MA, Aberoomand AP (2014) Removal of permethrin pesticide from water by chitosan–zinc oxide nanoparticles composite as an adsorbent. J Saudi Chem Soc 18:348–355
68. Pitakpoolsil W, Hunsom M (2014) Treatment of biodiesel wastewater by adsorption with commercial chitosan flakes: parameter optimization and process kinetics. J Environ Manage 133:284–292
69. Tanhaei B, Ayati A, Lahtinen M, Sillanpa M (2015) Preparation and characterization of a novel chitosan/Al2O3/magnetite nanoparticles composite adsorbent for kinetic, thermodynamic and isotherm studies of Methyl Orange adsorption. Chem Eng J 259:1–10
70. Vieira Rodrigo S, Emerson Meneghetti, Paula Baroni, Eric Guibal, de La Cruz González, Victor M, Alfonso Caballero, Rodríguez-Castellón Enrique, Beppu Marisa M (2014) Chromium removal on chitosan-based sorbents—an EXAFS/XANES investigation of mechanism. Mater Chem Phys 146:412–417
71. Abdollahi M, Rezaei M, Farzi G (2014) Influence of chitosan/clay functional bionanocomposite activated with rosemary essential oil on the shelf life of fresh silver carp. Int J Food Sci Technol 49:811–818
72. Shete PB, Patil RM, Thorat ND, Prasad A, Ningthoujam RS, Ghosh SJ, Pawar SH (2014) Magnetic chitosan nanocomposite for hyperthermia therapy application: preparation, characterization and in vitro experiments. Appl Surf Sci 288:149–157
73. Wang L, Sun Y, Yang X (2014) Fabrication and characterization of ZnxCd1−xS nanoparticles in chitosan alginate nanocomposite films. Ceram Int 40:4869–4873
74. Wang B, Ji X, Zhao H, Wang N, Li X, Ni R, Liu Y (2014) An amperometric β-glucan biosensor based on the immobilization of bi-enzyme on Prussian blue–chitosan and gold nanoparticles–chitosan nanocomposite films. Biosens Bioelectron 55:113–119

75. Dehnad D, Mirzaei H, Emam-Djomeh Z, Jafari S, Dadashi S (2014) Thermal and antimicrobial properties of chitosan–nanocellulose films for extending shelf life of ground meat. Carbohydr Polym 109:148–154
76. Youssef AM, Abdel-Aziz MS, El-Sayed SM (2014) Chitosan nanocomposite films based on Ag-NP and Au-NP biosynthesis by Bacillus Subtilis as packaging materials. Int J Biol Macromol 69:185–191
77. He L, Wang H, Xia G, Sun J, Song R (2014) Chitosan/graphene oxide nanocomposite films with enhanced interfacial interaction and their electrochemical applications. Appl Surf Sci 314:510–515
78. Zhang L, Han G, Liu Y, Tang J, Tang W (2014) Immobilizing haemoglobin on gold/graphene–chitosan nanocomposite as efficient hydrogen peroxide biosensor. Sens Actuators B: Chem 197:164–171
79. Xia X, Zheng Z, Zhang Y, Zhao X, Wang C (2014) Synthesis of Ag-MoS2/chitosan nanocomposite and its application for catalytic oxidation of tryptophan. Sens Actuators B: Chem 192:42–50
80. Seyed Dorraji MS, Ahadzadeh I, Rasoulifard MH (2014) Chitosan/polyaniline/MWCNT nanocomposite fibers as an electrode material for electrical double layer capacitors. Int J Hydrog Energy 39:9350–9355
81. Justin R, Chen B (2014) Characterisation and drug release performance of biodegradable chitosan–graphene oxide nanocomposites. Carbohydr Polym 103:70–80
82. Jeyapragasam T, Saraswathi R (2014) Electrochemical biosensing of carbofuran based on acetylcholinesterase immobilized onto iron oxide–chitosan nanocomposite. Sensors Actuators B Chem 191:681–687
83. Sollogoub C, Guinault A, Bonnebat C, Bennjima M, Akrour L, Fauvarque JF et al (2009) Formation and characterization of crosslinked membranes for alkaline fuel cells. J Membr Sci 335(2009):37–42
84. Konwar A, Gogoi N, Majumdar G, Chowdhury D (2014) Green Chitosan-carbon dots nanocomposite hydrogel film with superior properties. carbohydrate polymers. (in press, Accepted Manuscript)
85. Naseri N, Algan C, Jacobs V, John M, Oksman K, Mathew AP (2014) Electrospun chitosan-based nanocomposite mats reinforced with chitin nanocrystals for wound dressing. Carbohydr Polym 109:7–15
86. Sameh Hassan S, Suzuki M, Ahmed Abd El-Moneim A (2014) Synthesis of MnO2–chitosan nanocomposite by one-step electrodeposition for electrochemical energy storage application. J Power Sources 246:68–73
87. Pereda M, Alain Dufresne A, Mirta I. Arangurena M, Marcovicha NE (2014) Polyelectrolyte films based on chitosan/olive oil and reinforced with cellulose nanocrystals. Carbohydr Polym 101:1018–1026
88. Hebeish AA, Ramadan MA, Montaser AS, Farag AM (2014) Preparation, characterization and antibacterial activity of chitosan-g-poly acrylonitrile/silver nanocomposite. Int J Biol Macromol 68:178–184
89. Srivastava M, Singh J, Mishra RK, Singh MK, Ojha AK, Yashpal M, Sudhanshu S (2014) Novel conducting lithium ferrite/chitosan nanocomposite: synthesis, characterization, magnetic and dielectric properties. Curr Appl Phys 14:980–990
90. Pandele AM, Ionita M, Crica L, Dinescu S, Costache M, Iovu H (2014) Synthesis, characterization, and in vitro studies of graphene oxide/chitosan–polyvinyl alcohol films. Carbohydr Polym 102:813–820
91. Giannakas A, Grigoriadi K, Leontiou A, Barkoula NM, Ladavos A (2014) Preparation, characterization, mechanical and barrier properties investigation of chitosan–clay nanocomposites. Carbohydr Polym 108:103–111
92. Dias MV, Azevedo VM, Borges SV, de Soares NFF, de Fernandes RVB, Marques JJ, Medeiros EAA (2014) Development of chitosan/montmorillonite nanocomposites with encapsulated α-tocopherol. Food Chem 165:323–329

Gold Nanoparticle-Reinforced Eco-friendly Polymer Nanocomposites and Their Applications

Sunanda Sain and Dipa Ray

Abstract Nanocomposites are the most important field of research nowadays. Metal nanoparticles have attracted continuous interest owing to their unusual properties and potential uses in electronics, optics, magnetics, catalysts, and sensors. Green synthesis (for noble metals, such as, gold, silver, platinum, palladium, etc.) and characterization of nanoparticles have emerged as a significant field of nanotechnology. As a well-known noble metal, gold is widely investigated due to its specific impact in the fields of biotechnology and bioscience. Gold nanoparticles (GNP) being the most stable metal nanoparticles have the advantages of (a) easy synthesis, (b) colloidal stability, and (c) ability to be easily conjugated with biological molecules. Gold nanoparticles also present fascinating aspects such as the behavior of the individual particles, size-related electronic, magnetic and optical properties (quantum size effect), and their applications to catalysis and biology. A large number of polymer molecules were selected to decorate the surface of gold nanoparticles in physical or chemical ways for different purposes. Gold nanoparticle-reinforced nanocomposites were prepared using different polymer matrices for different types of applications such as catalytic applications, opto-electronic and magneto-optic applications, biological, medicinal applications, etc.

Keywords Polymer nanocomposites · Gold nanoparticles · Optical properties · Biosensor · Delivery · DNA · Drug delivery

S. Sain
Department of Polymer Science & Technology, University of Calcutta,
700009 Kolkata, India

D. Ray (✉)
Irish Centre for Composites Research (ICOMP), Mechanical,
Aeronautical and Biomedical Engineering Department,
Materials and Surface Science Institute, University of Limerick,
Limerick, Ireland
e-mail: Dipa.Roy@ul.ie

V.K. Thakur and M.K. Thakur (eds.), *Eco-friendly Polymer Nanocomposites*,
Advanced Structured Materials 74, DOI 10.1007/978-81-322-2473-0_17

1 Introduction

Polymers have become an absolute necessity in our daily lives as packaging materials, consumer goods, pharmaceutical and personal care products, dyes, lacquers, and in many other fields. These are also used as the substitute of metallic or ceramic materials [43–45, 54]. Synthetic polymers derived from petroleum resources occupy majority of the market and are detrimental to the environment [46–49]. Recycling of these consumer polymer wastes in bulk is often not a very practical or economical option. On the other hand, biodegradable polymers are mostly derived from natural resources, but their use as consumer products is not always economically favorable. Widely used synthetic polymers like polyolefins and acrylics are not biodegradable. Therefore, recycling and degradation of these polymers is an important issue for environmental protection. In order to reduce the environmental pollution caused by the synthetic polymers, significant efforts are given by the material scientists in recent years to modify the synthetic polymers by combining them with natural fillers, such as, cellulose fibers; soy flour [43–45]. Among these biodegradable materials, renewable resources from agricultural or forestry products create a platform for new industrial products or alternative energy sources. Plant-based fibers are already used in a wide range of products such as, textiles and geotextiles, twines and ropes, special pulps, insulating and padding materials, fleece, felts and nonwoven materials, and recently used as reinforcement for polymers [36, 37]. Though the mechanical properties of plant fibers are much lower than widely used glass fibers, but their low density, the specific properties (property-to-density ratio) like specific strength and stiffness make them comparable to the glass fibers [38]. Plant fibers have proved to be an eco-friendly alternative to conventional reinforcing fibers for composite applications for low to medium strength applications.

Polymer nanocomposites are major growing areas of research which could broaden the application of polymers to the great benefit of different industries [19, 20]. A nanocomposite is a material where one of the components has at least one nanoscopic dimension in around 10^{-9} m. A composite comprises of a resin and a filler or reinforcement, the goal of which is to improve the properties of the resin while reducing the production cost. The type of the reinforcement depends upon the constraints imposed on the designer: high mechanical strength, good thermal stability, cost, resistance to corrosion, etc. The general idea behind the addition of the reinforcing phase is to create a synergy between the various constituents, such that novel properties capable of meeting or exceeding design expectations can be achieved. The properties of nanocomposites rely on a range of variables, like the matrix material, the nanofiller type and loading amount, degree of dispersion, size, shape, orientation and the filler/matrix interactions.

2 Polymer Nanocomposites

Polymer nanocomposites represent a new alternative to conventionally filled polymers. Because of the nanosized fillers, high surface area of the fillers is available to interact with the matrix and results in markedly improved properties when compared to the pure polymers or their traditional microcomposites. These include improved modulus and strength, outstanding barrier properties, improved solvent and heat resistance and decreased flammability. Broadly, nanocomposites can be divided into three types: metal matrix nanocomposites, ceramic matrix nanocomposites, and polymer matrix nanocomposites. Time-dependent properties can also be improved by addition of the nanofillers [29]. The nanofillers can act as molecular bridges between the polymer molecules and help to enhance the mechanical properties. The reinforcing filler can be particles (e.g., minerals), sheets (e.g., exfoliated clay stacks), fibers (e.g., carbon nanofibers and nanotubes or electrospun fibers), fibrils, or whiskers (cellulosic). Ajayan et al. [26] noted chemistry, degree of thermoset cure, polymer chain mobility, polymer chain conformation, and degree of crystallinity can vary significantly and continuously from the interface with the reinforcement into the bulk of the matrix in polymer nanocomposites.

2.1 Natural Polymer-Based Nanocomposites

Recently, an increasing trend is observed in the development of eco-friendly materials derived from biorenewable resources due to rising environmental awareness. These biobased materials with novel properties like biodegradability, acceptable specific strength, low density, recyclability, ease of separation, high toughness, good thermal properties, low health hazards, reduced tool wear, and enhanced energy recovery are used in a various fields especially for the automotive and biomedical applications [55]. Some well-known examples of biopolymers are polysaccharides, such as starch, chitin/chitosan, cellulose, alginate, and carbohydrate polymers, and animal protein-based biopolymers, such as gelatin, wool, silk, and collagen [55]. Cellulose is the most abundant biopolymer present in nature [38]. This structural material is naturally organized as microfibrils which are linked together to form the cellulose fibers. Much of the current research is focused on developing combinations of polymeric and cellulosic fillers, such as, micro- and nanocrystalline cellulose, cellulose nanowhiskers, micro- or nanofibrillated cellulose, etc. in the form of blends, composites, nanocomposites, etc. Favier et al. [10] first reported the preparation of cellulose whisker-based nanocomposites [10]. This was followed by many more studies processing cellulose nanocomposites with various synthetic lattices like copolymer of styrene (35 weight%) with butyl-acrylate (65 weight%) poly(S-co-BuA) [10], poly (β-hydroxyoctanoate) (PHO) [6], polyvinylchloride (PVC) [41], natural rubber [2], polyvinyl acetate (PVAc) [11],

polylactide (PLA) [8], and polymethylmethacrylate (PMMA) [5, 9]. Different nanocomposites based on microfibrillated cellulose or bacterial cellulose have been prepared with petroleum-derived nonbiodegradable polymers such as polyethylene (PE) or polypropylene (PP) and also with biodegradable polymers such as PLA, polyvinyl alcohol (PVOH), starch, polycaprolactone (PCL), and polyhydroxybutyrate (PHB). Thakur et al. [46–49, 51] prepared the graft copolymers from cellulose fibers and methylmethacrylate (MMA) [46, 51]. Thakur et al. [50] also modified the surface properties of natural cellulosic biomass by the graft copolymerization technique [50]. Eco-friendly green nanocomposites were prepared from polymeric resin using lignocellulosic fibers as the reinforcement [52]. Butyl-acrylate (BA)-*g*-*Saccaharum cilliare* fibers were synthesized using a redox initiator via free radical polymerization [53]. Some other studies were reported on *Grewia Optiva* fiber and *Hibiscus sabdariffa* fiber-reinforced phenol-formaldehyde (PF) composites [32–35, 42] and pine needle reinforced urea-formaldehyde composites [30, 31].

3 Nanofillers Used in Polymer Nanocomposites

Apart from cellulosic nanofillers, many other nanofillers such as one-dimensional carbon nanostructures (single- and multiwalled carbon nanotubes), two-dimensional carbon, and inorganic nanomaterials such as graphene platelets, graphene nanoribbon, single and multiwalled graphene oxide nanoribbons, graphene oxide nanoplatelets, molybdenum disulfide nanoplatelets, clays, hydroxyapatite metal nanoparticles are used as reinforcing agents in polymer nanocomposites. Metal nanoparticles have attracted continuous interest owing to their unusual properties and potential uses in electronics, optics, magnetics, catalysts, and sensors. Green synthesis of noble metal nanoparticles such as gold, silver, platinum, palladium, and their characterizations have emerged as a significant field of nanotechnology. As a well-known noble metal, gold is widely investigated due to its specific impact in the fields of biotechnology and bioscience. In this chapter, gold nanoparticle-reinforced eco-friendly polymer nanocomposites will be discussed in details.

4 Gold Nanoparticles (GNPs)

Gold is an important and attractive noble metal for its ancient medicinal and ornamental value and it is the subject of one of the most ancient themes of investigation in science. The emerging nanoscience and nanotechnology research with gold nanoparticles (GNPs) are very interesting and attractive as GNPs are the most stable metal nanoparticles. They present fascinating aspects like multiple assembly types involving materials science, the behavior of the individual particles, size-related electronic, magnetic and optical properties (quantum size effect), and their application to catalysis and biology [22].

Colloidal GNPs are well known since ancient times and are finding use in biological applications [3]. Colloidal gold is a suspension of gold particles (sub-micrometer size) in a fluid, usually water. For particles less than 100 nm, an intense red color and for larger particles, blue or purple color are observed [56]. These colloidal GNPs have applications in different areas, including electron microscopy, electronics, nanotechnology [24], and materials science due to their unique optical, electronic, and molecular-recognition properties. Properties and applications of colloidal GNPs strongly depend upon their size and shape [58], for example, rod-like particles have both transverse and longitudinal absorption peak, and anisotropy of the shape affects their self-assembly [28].

4.1 Synthesis of GNPs

There are various procedures for the preparation of GNPs. Most common method is the reduction method where GNPs are produced by reduction of chloroauric acid (H[$AuCl_4$]). In this method Au^{3+} ions are reduced to neutral gold atoms. With the formation of more and more gold atoms, the solution becomes supersaturated, and gold gradually starts to precipitate in the form of subnanometer particles. The particles formed in this method are fairly uniform in size. To avoid the aggregation effect, some sort of stabilizing agent is added [1]. The methods are discussed below.

(a) *Citrate Reduction*
This method was introduced by Turkevitch in 1951 [4]. In this method, gold salts or derivatives are treated with sodium citrate solution [4]. Citrate ions act here as the reducing agent as well as the capping agent. GNPs formed in this method are around 10–20 nm in size. Yonezawa and Kunitake [57] prepared anionic mercaptoligand-stabilized AuNPs (GNPs) in water using this citrate reduction method, which is schematically shown in Fig. 1.

(b) *Brust-Schiffrin Method*
This method was discovered by Brust and Schiffrin in 1994 [4], and can be used to produce GNPs in organic liquids that are normally not miscible with water (like toluene). It involves the reaction of a chlorauric acid solution with tetraoctylammonium bromide (TOAB) solution in toluene and sodium borohydride ($NaBH_4$) as an anticoagulant and a reducing agent, respectively. The GNPs formed in this method are 2–6 nm in diameter. $NaBH_4$ is used as the reducing agent, and TOAB acts as both the phase transfer catalyst and the stabilizing agent.

(c) *Martin Method*
Martin Method (I): In this method GNPs are produced in water by reducing $HAuCl_4$ with $NaBH_4$. The particles are nearly monodisperse in nature and the diameter can be precisely and reproducibly tunable from 3.2 to 5.2 nm. Even without any other stabilizer like citrate, GNPs are stably dispersed.

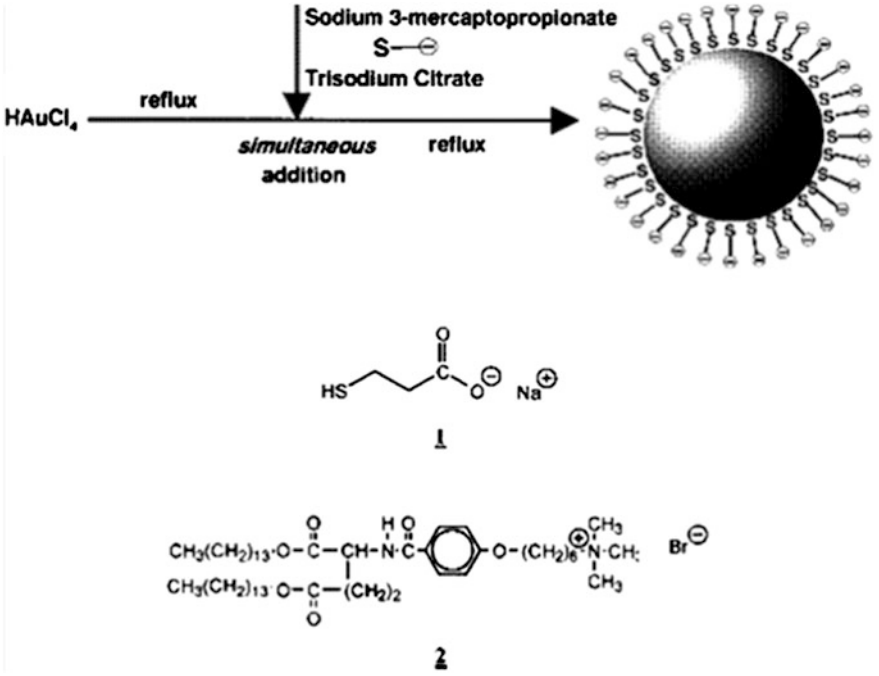

Fig. 1 Preparation of anionic mercaptoligand-stabilized AuNPs in water. Reprinted with permission from [57] Copyright © 1999 Elsevier Science

Martin Method (II): This new synthesis method is simple, cheap, easy-to-adopt, greener, and therefore important for many practical applications. This is a combination of the Turkevich method and the monolayer protection of the Brust method. Here GNPs are coated with a monolayer of 1-dodecanethiol and then phase-transferred to hexane simply by shaking a mixture of water, acetone, and hexane for 30 s.

(d) *Seeding Growth Method*
This is a popular method for the synthesis of GNPs controlling its size distribution ($\sim$10–15 %) in the range of 5–40 nm. Size of GNPs can be manipulated by this method varying the ratio of the seed to metal salt. Using this method, gold nanorods are usually formed [4].

(e) *Physical Methods*
There are other physical methods such as photochemistry, sonochemistry, radiolysis, and thermolysis to synthesize the GNPs. The quality of GNPs can be improved using UV irradiation and with the use of near-IR laser irradiation, the size of thiol stabilized GNPs can be enhanced. Sonochemistry can be used to prepare the GNPs within the pores of silica and radiolysis can be used to control the size of GNPs and to synthesize it in presence of specific radicals.

The thermolysis of $[C_{14}H_{29}\text{-}Me_3N][Au(SC_{12}H_{25})_2]$ at 180 °C for 5 h under N_2 produced alkyl-groups-passivated gold NPs of size 26 nm [4].

Significant efforts have been devoted over the past 40 years to the fabrication of GNPs with monodispersity and controlled size. GNPs with varying core sizes are prepared by the reduction of gold salts in presence of appropriate stabilizing agents that prevent particle agglomeration. Some common synthetic methods of core–shell GNPs are summarized in Table 1.

4.2 Applications of GNPs

(a) *In delivery of molecules into cells*

GNPs have been used for a long time for delivery of molecules into cells. The molecules are adsorbed on the surface of the GNPs and the whole conjugate is introduced into the cells. Introduction into cells can either be forced as in the case of gene guns or achieved naturally by particle ingestion. The molecules eventually detach themselves inside the cells from the gold particles. GNPs are capable of delivering large biomolecules without restricting themselves as carriers of only small molecular drugs. Tunable size and functionality make them a useful scaffold for efficient recognition and delivery of biomolecules. They have shown the success in delivery of peptides, proteins, or nucleic acids like DNA or RNA [13]. Schematic representations of the delivery of molecules by GNPs are shown in Fig. 2 and 3, respectively.

(b) *Labeling applications*

GNPs can be used for labeling applications. Immunostaining was one of the traditional uses of GNPs in biology before the advent of "nanobiotechnology." The molecules/structures on the outer cell surface can be labeled with GNPs which are conjugated with specific antibodies against these molecules/structures [39]. This is shown schematically in Fig. 4.

Albrecht-Buhler has introduced an innovative way of imaging the movement of cells adhering to a substrate. For this purpose, the surface of the substrate is coated with a layer of colloidal GNPs (Fig. 4d). Cells adhering to the substrate incorporate the Au particles. In this way, cells migrating along the substrate leave behind a trail called a "phagokinetic track" in the nanoparticle layer

Table 1 Synthetic methods and capping agents for GNPs of varying core sizes [57]

Synthetic methods	Capping agents	Core size (nm)
Reduction of $AuCl(PPh_3)$ by diborane or sodium borohydride	Phosphine	1–2
Biphasic reduction of $HAuCl_4$ with sodium borohydride in the presence of thiol capping agents	Alkanethiol	1.5–5
Reduction of $HAuCl_4$ by sodium citrate in water	Citrate	10–150

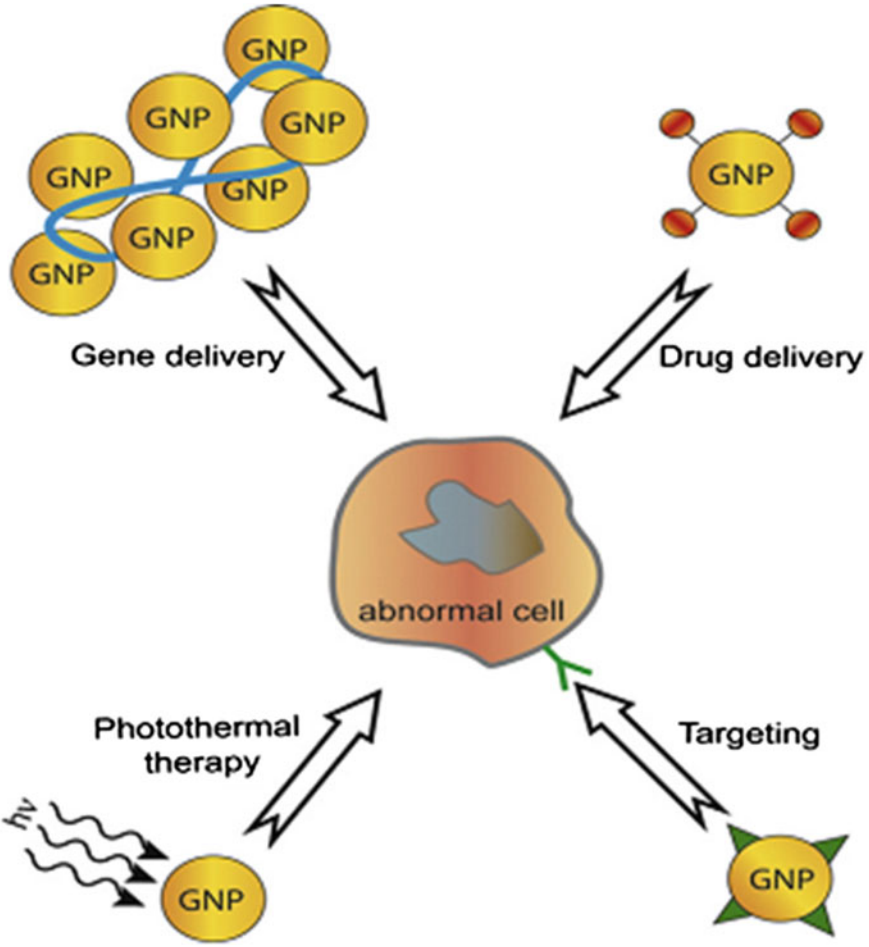

Fig. 2 Applications of GNPs in drug, gene and protein delivery. Reprinted with permission from (Ghosh et al. [13] Copyright © 2008 Elsevier

[39]. Thus a blueprint of the migration pathway of the cell can be obtained through TEM analysis. Many trails can be recorded in parallel on the same substrate and the trails can be imaged ex situ. Thus GNPs can be extensively used as the labels for recording the phagokinetic track.

(c) *Use of GNPs as heat source*

When gold particles absorb light, the free electrons in the gold particles are excited. Excitation at the plasmon resonance frequency causes a collective oscillation of the free electrons. Upon interaction between the electrons and the crystal lattice of the gold particles, the electrons relax and the thermal energy is transferred to the lattice. Subsequently, the heat from the gold particles is dissipated into the surrounding environment. Besides its

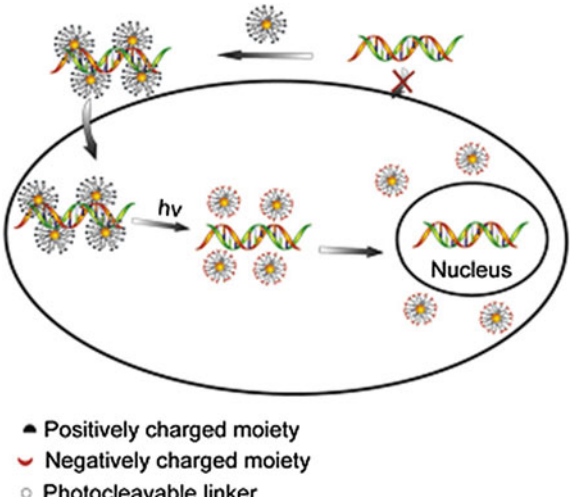

Fig. 3 A schematic illustration for nuclear delivery of DNA using photolabile nanoparticles. Reprinted with permission from [13] Copyright © 2008 Elsevier

combination with imaging techniques, controlled heating of GNPs can be used in several ways for manipulating the surrounding tissues, shown in Fig. 5 [39].

(d) *Use of GNPs as sensors*
GNPs can also be used for sensor applications. These are utilized as sensors to detect the presence of specific analytes and to provide a read out indication of the concentration of the analyte. The presence of the analyte can alter the optical properties of the GNPs which enables utilization of optical read out for sensory purposes. Due to their small size, GNP-based sensors could have an important impact in diagnostics [39]. This is demonstrated in Fig. 6.

5 Polymer/GNP Nanocomposites

GNPs are used as reinforcing agent in polymer nanocomposites. Huang et al. [16] prepared gold–chitosan nanocomposites by adsorbing chitosan molecules onto the GNP surfaces [16]. Recently much attention has been given to chitosan as a potential polysaccharide resource due to its excellent properties such as biocompatibility, biodegradability, nontoxicity, and adsorption properties resulting in many research activities. Chitosan is reported to be a very effective stabilizing agent for GNPs. The GNPs also has an impact on the crystal morphology of chitosan due to the possible nucleating effect of GNPs in chitosan [16].

The polymer molecules can be grafted onto GNPs and this grafting of polymer chains not only enhance the stability of the gold cores immensely, but also functionalize the gold cores by special properties of the outside polymer layers. The

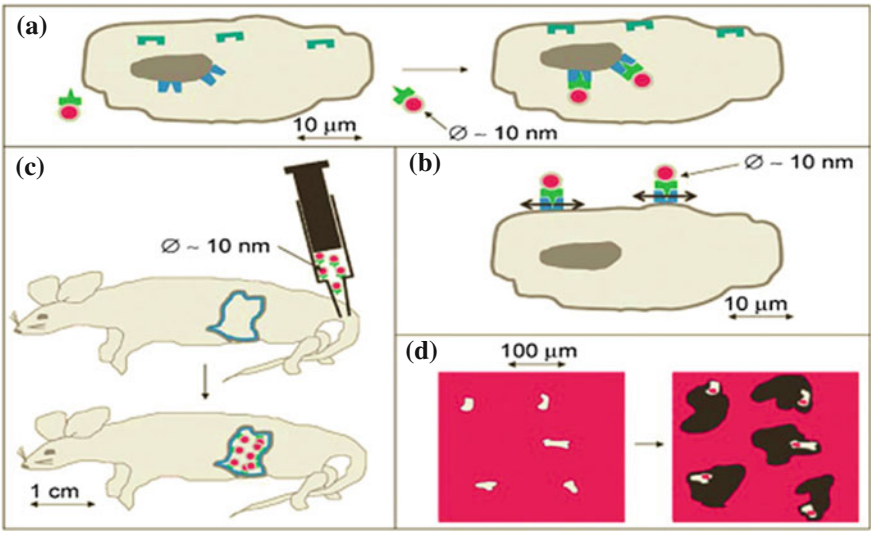

Fig. 4 Labeling with gold nanoparticles. Gold nanoparticles (core in red, stabilizing shell in *gray*) are conjugated with ligands (*green*) which bind to specific receptors (*blue*) but not to other structures (as the receptors shown in *dark green*). **a** Immunostaining: Gold nanoparticles conjugated with ligands against the structures to be labeled are added to fixed and permeabilized cells (shown in *gray*). Guided by molecular recognition they bind to the designated structures which are in this way stained with gold particles. In the image, the particles are conjugated with ligands that bind to receptors on the surface of the nucleus, but not to other receptors, for example, present at the inner cell membrane. **b** Single-particle tracking: Gold nanoparticles conjugated with ligands specific for membrane-bound molecules are added to living cells. In this way, individual membrane-bound molecules are labeled with gold nanoparticles and their diffusion within the cell membrane can be traced via observation of the gold particles. **c** X-ray contrasting: Gold nanoparticles conjugated with ligands that permit specific uptake in target organs are injected into the bloodstream of animals. The organ can then be visualized by X-ray tomography due to the locally enriched gold particles. **d** Phagokinetic tracks: a surface is covered with a layer of gold nanoparticles. When cells (shown in *gray*) are cultured on top of the surface, they ingest the underlying nanoparticles. Upon cellular migration along the surface the cells incorporate, all nanoparticles along their pathway leaving behind an area free of nanoparticles, which is a blueprint of their migration pathway. Images are not drawn to scale and important length scales are indicated in the images [39]. Reprinted with permission from [39]. Copyright © 2008, Royal Society of Chemistry

interactions present between the polymer chains and the GNPs can be of two types: (a) covalent bond formation (this is subdivided into direct synthesis method, "graft-to" strategy and "graft-from" strategy) and (b) physical adsorption method (this is subdivided into hydrophobic interior, nonspecific/coordination adsorption, electrostatic interaction, and so on) [18]. The procedures are schematically shown in Fig. 7.

The different GNP-reinforced polymer nanocomposites reported in literatures are given below in Table 2.

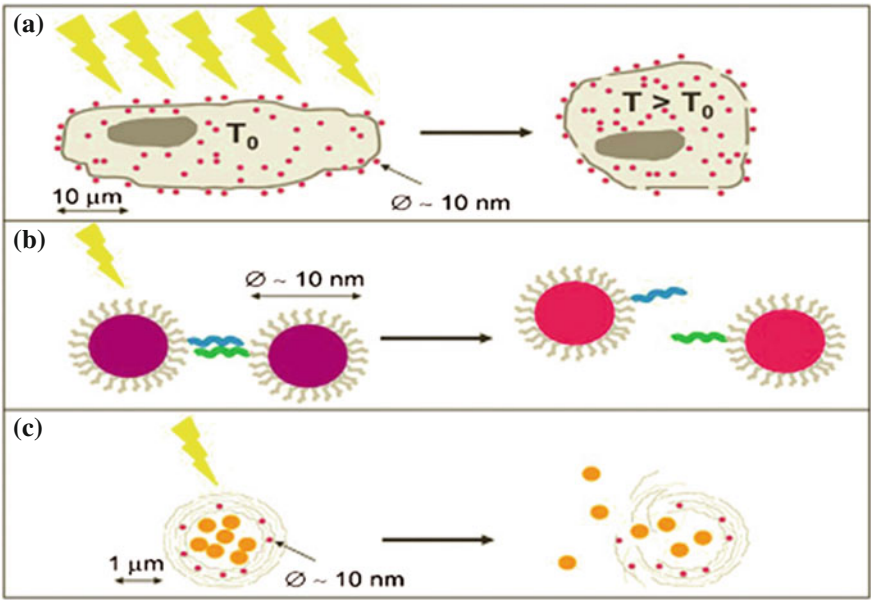

Fig. 5 Heating with gold nanoparticles. Gold particles (core in *red*, stabilizing shell in *gray*) are heated upon absorption of light (shown as *yellow rays*) and mediate the heat to their local environment. **a** Hyperthermia: The temperature inside cells (drawn in *gray*) is raised by illumination of gold particles. A temperature increase of only a few degrees is sufficient to kill cells. **b** Breaking of bonds: When gold nanoparticles (core in *red,* stabilizing shell in *gray*) are conjugated with ligands (shown in *green*) that are specific to receptors (shown in *blue*) which are bound to other gold particles. These two kinds of gold particles get linked to assemblies mediated by receptor–ligand binding. As the distance between the particles in such aggregates is small, their plasmon resonance is shifted to higher wavelengths and the particle solution appears *violet/blue*. Upon illumination, the gold particles get hot and the bonds of the receptor–ligand pairs melt. Therefore, the assemblies are dissolved, the average distance between the particles is increased, and the particle solution appears red. **c** Light-controlled opening of individual polymer capsules (drawn in *gray*) by local heating, mediated by gold nanoparticles. Gold nanoparticles are embedded in the walls of polyelectrolyte capsules. The capsule cavity is loaded with cargo molecules (drawn in *orange*). Upon illumination with light, the heat created by the nanoparticles causes local ruptures in the capsule walls and thus release of the cargo. Reprinted with permission from [39]. Copyright © 2008, Royal Society of Chemistry

6 Polymer/GNP Nanocomposites with Wide Application Potential

6.1 Applications in Light Emitting Diode (LED)

Park et al. [23] reported the fabrication of a blue LED with enhanced environmental and luminescence stability obtained by incorporating 5–10 nm GNPs as the quenchers of the triplet states of poly(9,9'-dioctylfluorene) (PDOF) that lead to

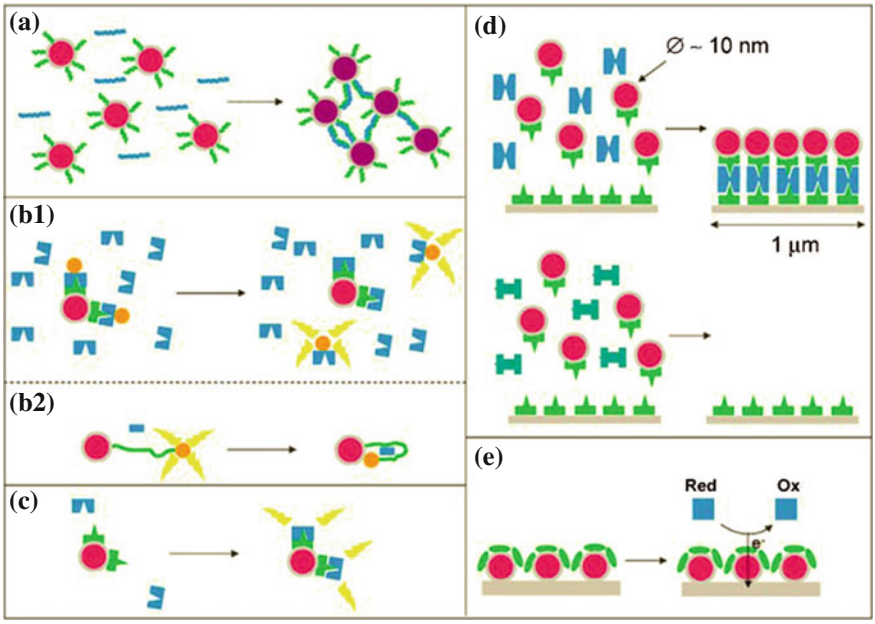

Fig. 6 Sensing with gold nanoparticles. For the specific detection of analytes (shown in *blue*) gold nanoparticles (core in *red*, ligand shell in *gray*) are conjugated with ligands (shown in *green*) that selectively bind to the analyte. **a** Colorimetric assays: Binding of the analyte to the ligands links several particles together to form small aggregates and the *red color* of the colloidal gold solution shifts to *purple/blue*. **b** Quenching of fluorophores: **b1** Gold nanoparticles are conjugated with ligands that specifically bind to the analyte to be detected. The ligands on the nanoparticle surface are then saturated with molecules that bind to the ligands (shown in *blue*) and that have a fluorophore (drawn in *orange*) attached. As the fluorophores are in close proximity to the surface of the gold particles their fluorescence is quenched. The presence of analyte molecules competitively displaces part of the molecules with the fluorophores from the nanoparticle surface. As these fluorophores are no longer in contact with the gold particles their fluorescence (symbolized as *yellow rays*) can be detected. **b2** Fluorophores (drawn in *orange*) are attached via linker molecules (drawn in *green*) to the surface of the gold nanoparticles. Due to the length of the linker, the distance between the fluorophore and the gold nanoparticles is big enough so that no quenching of the fluorophore occurs. Presence of the analyte (drawn in *blue*) changes the conformation of the linker molecules and as the fluorophores are now in close proximity to the gold surface, their fluorescence is quenched. **c** Surface-enhanced Raman scattering: Gold nanoparticles are conjugated to ligand molecules which specifically bind to the analyte to be detected. The analyte (drawn in *blue*) in solution provides only a weak Raman signal. Upon binding of the analyte to the ligands present on the gold surface the analyte comes into close proximity to the gold particles and the Raman signal is dramatically enhanced (as symbolized by the *yellow rays*). **d** Gold stains: Ligands specific to the analyte to be detected are immobilized on a surface and conjugated to gold nanoparticles. Presence of the analyte (drawn in *blue*) causes the binding of the particles to the surface. Other molecules (drawn in *dark green*) do not cause binding of the particles to the surface and thus a washing step removes all gold particles. The presence of the analyte is then quantified by the number of gold particles bound to the surface. **e** Redox reactions: Redox enzymes (drawn in *green*) are conjugated to the surface of gold nanoparticles (core in *red*, ligand shell in *gray*) which are immobilized on top of an electrode (drawn in *gray*). The enzymes oxidize their present substrates (drawn in *blue*) from the reduced form to the oxidized one. The released electrons are transferred via the gold nanoparticles to the electrode, which can be measured as current. Reprinted with permission from [39].

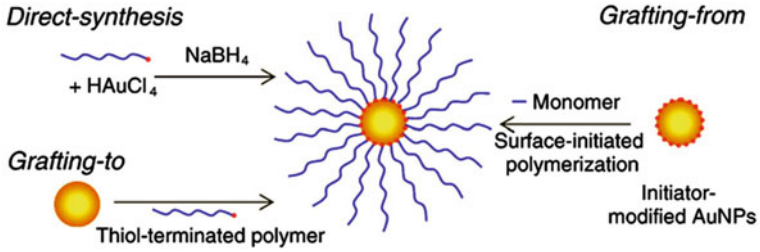

Fig. 7 Schematic representation of polymer chain grafting procedures onto GNPs. Reprinted with permission from [39]. Copyright © 2009, Elsevier

Table 2 Different polymer/GNP nanocomposites reported in the literatures [18]

Polymers used	Synthesis method	Applications
poly(sodium 2-acrylamindo-2-methyl propane sulfonate), poly ((ar-vinylbenzyl)-trimethylammonium chloride), poly(N, N-dimethylacrylamide), poly(3-[2-N-methylacrylamido)-ethyl dimethyl ammonio propane sulfonate-b-N,N-dimethylacrylamide)	Direct	Not done
poly(N-isopropylacrylamide) (PNIPAM) and polystyrene (PS) or poly(methacrylic acid) (PMAA) chains	Direct	Not done
poly (methoxyl oligo(ethylene glycol) methacrylate) (PMOEGMA)	Direct	Salt responsive applications
copolymer of poly(2-(dimethylamino) ethyl methacrylate) (PDMA) and poly (2-(methacryloyloxy) ethyl phosphorylcholine) (PMPC)	"graft-to" method	Biomedical applications
poly(2-(dimethylamino) ethylmethacrylate) (PDMA) and poly (ethylene oxide) (PEO)	"graft-to" method	Not done
thiol-ended poly(ethylene glycol) (PEG)	"graft-to" method	in vivo X-ray computed tomography (CT) imaging
Trithiocarbonate containing poly (acrylic acid) (PAA)	"graft-to" method	Not done
block copolymer of poly(4-vinylpyridine)-b-polystyrene-b-poly (4-vinylpyridine) (PVPb- PS-b-PVP) containing multiple trithiocarbonate	"graft-to" method	pH responsive

(continued)

Table 2 (continued)

Polymers used	Synthesis method	Applications
moieties or with thiol groups as protecting agents		
copolymer of PNIPAM-b-PMOEGMA	"graft-from" method	Thermosensitive
PDMA	"graft-from" method	pH sensitive
Poly (N-isopropylacrylamide)	RAFT	Not done
PS-b-PGA, [PGA: poly(glutamic acid)]	Physical adsorption	Not done
polystyrene-b-poly(acrylic acid) (PS-b-PAA)	Physical adsorption	Not done
diblock copolymer comprising of PNIPAM and poly(N-vinyl-2-pyrrolidone) (PVPRD)	Physical adsorption	Not done
poly(ethylene glycol)-b-poly (4-vinylpyridine)-b-poly (N-isopropylacrylamide) (PEG-b-PVP-b-PNIPAM) triblock copolymer	Physical adsorption	Thermosensitive and pH responsive
Chitosan	By adsorbing chitosan molecules onto the gold nanoparticle surfaces	Not done

polymer oxidation. The fabricated PDOF/gold-nanocomposite-based PLED also exhibited an enhanced quantum efficiency. During the spin-casting of the PDOF/GNP nanocomposite film, the nanoparticles might get attached to the anode and to each other due to strong electrostatic forces; capillary forces then draw the polymer solution around the nanoparticles. The gold nanoparticles modifies the interfacial morphology of the device facilitating the electron injection as well as blocking the hole migration [23].

6.2 Energy Storage Applications

Schmitt et al. [27] reported the preparation of layered nanocomposite films with well-defined layer structure [27]. The schematic representation of the fabrication technique is shown in Fig. 8. A consistent picture of the assembly of the colloidal gold/polyelectrolytes (PE) system and the structures of the resulting multilayer superlattices were obtained from the results of X-ray reflectivity, optical spectroscopy, and various microscopies. The slight differences in colloid packing in the gold monolayer increased the interparticle interactions and a long wavelength band attributed to the plasmon resonance appeared. They also stated that the number of PE interlayers between the gold layers controlled the structural characteristics of the gold/PE multilayer (Fig. 8b). Thus this work lead to rational design of bulk films of

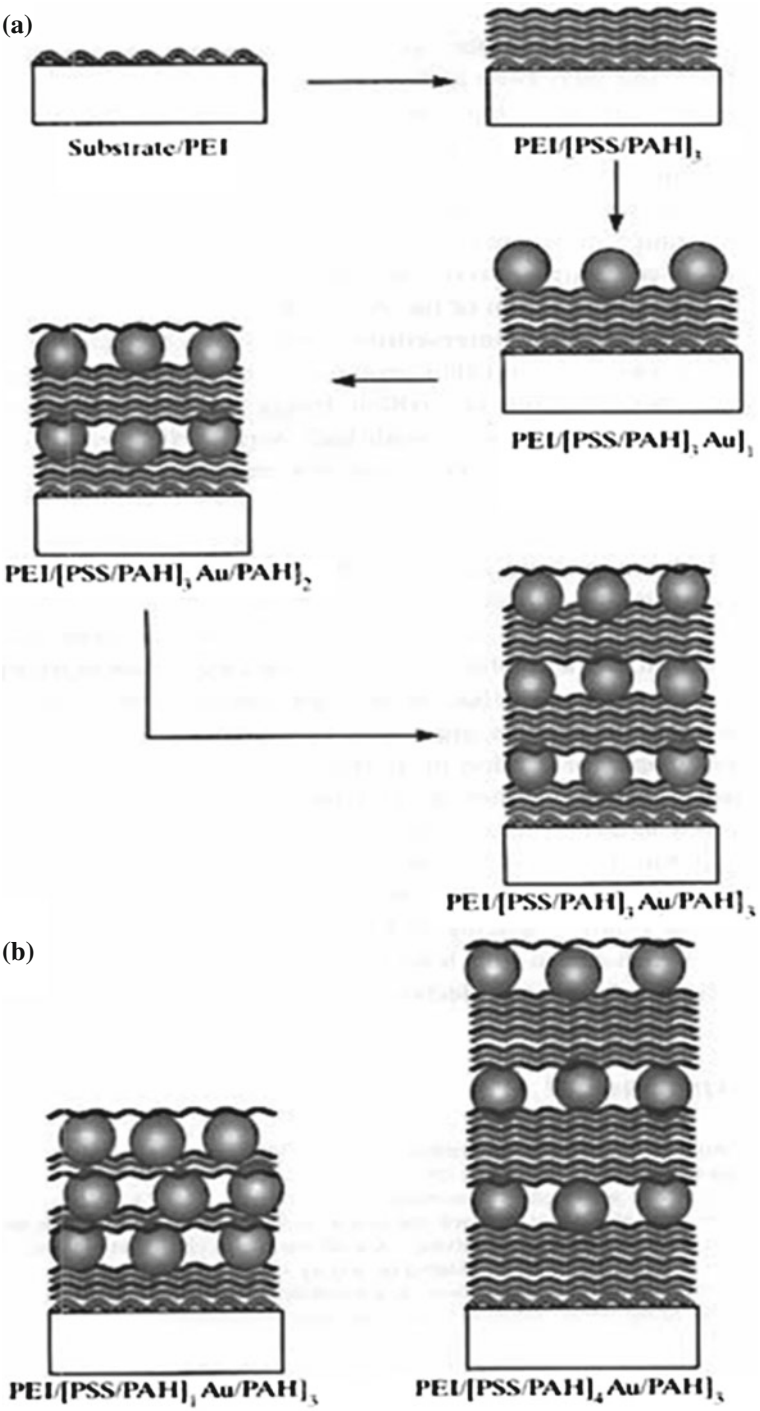
(a)
Substrate/PEI
PEI/[PSS/PAH]3
PEI/[PSS/PAH]3Au]1
PEI/[PSS/PAH]3Au/PAH]2
PEI/[PSS/PAH]3Au/PAH]3
(b)
PEI/[PSS/PAH]1Au/PAH]3
PEI/[PSS/PAH]4Au/PAH]3

◀ **Fig. 8** **a** Process for fabricating colloidal gold/polyelectrolytes (PE) multilayers to a final structure with $m = 3$ and $n = 2$. **b** Schematic representation of increased gold particle layer separation achieved by changing the interlayer spacing from $m = 1$ (*left*) tom = 4 (*right*). On *top* of the PEI layer, PSS is the light-shaded layer and the PAH layer is shaded dark. Note that this drawing is an oversimplification of the actual layer structure. Reprinted with permission from [27]. Copyright © 1997 Verlag GmbH & Co. KGaA, Weinheim

polymer composites containing GNPs having well-defined layer structure and tunable optical, electrical, and other properties and these composites offered the possibility of directional interlayer processes such as photoinduced charge separation for energy storage applications.

6.3 Application as Supporters and Carriers

Li et al. [17] fabricated novel nanocomposites of GNP and poly(4-vinylpyridine) (Au-PVP) through surface-initiated atom-transfer radical polymerization (SI-ATRP) [17]. The fabrication technique is schematically shown in Fig. 9.

The fabricated nanocomposites show pH responsive properties due to the protonation of a pyridyl segment into the pyridinium group which leads to the polymer branches being positively charged. At a low pH (<3.2), the pyridyl ring is protonated and hence the positively charged polymer chains repulse each other by the electrostatic interaction. The polymer layer is loosely swelled; hence, the Au-PVP composite particle displays a comatulid-like nanostructure in 3D AFM images. However, at a relatively high pH (>3.2), the polymer chains shrink and wrap around

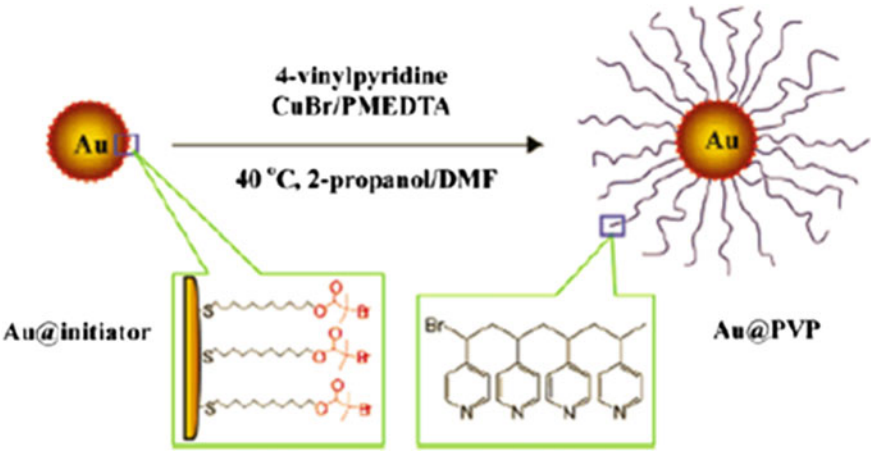

Fig. 9 Schematic fabrication of Au-PVP nanoparticles by SI-ATRP Reprinted with permission from [17]. Copyright © 2007, American Chemical Society

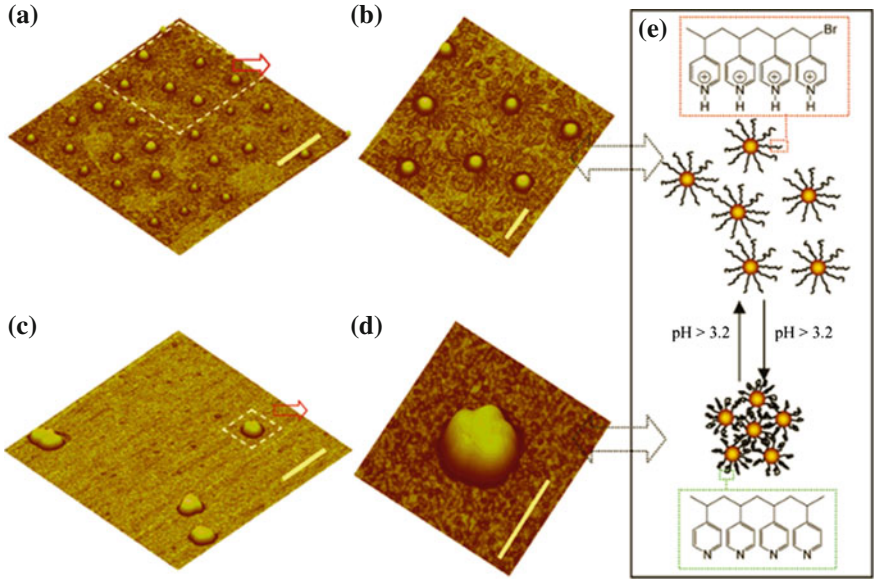

Fig. 10 3D AFM images of Au-PVP nanoparticles (**a**), (**b**) at pH 1.2, and (**c** and **d**) at pH 5.0 with different magnifications. **e** Schematic mechanism illustration of pH response of Au-PVP nanocomposites. Scale bar: 500 nm in panels **a** and **c** and 200 nm in panels **b** and **d**. Reprinted with permission from [17]. Copyright © 2007, American Chemical Society

the GNP surface, which results in the aggregation of GNPs with a thin shrunken polymer layer (Fig. 10).

Such assembled Au-PVP nanoparticles can be considered as an effective coordinating host to the ligand to entrap metal ions by means of pyridyl groups which provide an important basis for various applications. Thus Au-PVP nanocomposites as a smart supporter can entrap transition metal ions by their efficient coordinating segments, and subsequently the metal ions can be reduced in situ to construct novel bimetallic nanocomposites, which are regarded as intelligent catalysts with environmental stimuli activity.

6.4 Optical and Electronic Applications

Srivastava et al. [40] fabricated PMMA/GNP nanocomposites by varying the size of the GNPs over wide range by changing the concentration and molecular weight of the capping agent [40]. They studied the optical properties of the nanocomposite films of various thicknesses with different sizes and volume fractions of GNPs using spectroscopic ellipsometry. Systematic shift in the imaginary part of the dielectric function can be seen with variation in size and fraction of the GNPs. The

thickness of the film also plays a significant role in the tunability of the optical spectra. Systematic variation of the absorption peak, width, and position as a function of fraction of GNPs in PMMA was obtained. This was very useful observation as it indicated the ability to obtain optical coatings with tunable optical properties. They also observed some very interesting behavior of the optical absorption as a function of interfacial morphology. This gave an additional parameter to tune the optical properties of the composites.

6.5 Applications as Diagnostic Probes or Drug Delivery Vehicles

Edwards et al. [7] capped GNPs with stimuli-responsive polymers [7]. They used copolymers of di(ethylene glycol) methyl ether methacrylate (MEO2MA) and poly (ethylene glycol) methyl ether methacrylate (OEGMA) in biphasic water–toluene mixtures.

The schematic representation of fabrication of the nanocomposites is shown in Fig. 11.

They showed that the fraction of GNPs that transferred across the water–toluene interface depended on the chemical composition of the capping polymers and the diameter of the GNPs had little dependency on the ion valency of the salt included in the aqueous phase (Fig. 12).

According to them, these new class of materials might be useful for further developing nanoscale inorganic materials, especially in biophysical interaction with cells and biological barriers embodied within tissues and organs. Their study had implications for the rational design of inorganic NPs as diagnostic probes or drug delivery vehicles targeted for biological interfaces.

6.6 Applications in the Fields of Catalysis and Sensors

Han et al. [15] synthesized uniform and fibrous nanocomposites from poly(2-aminothiophenol) (PATP) and highly dispersed GNPs through a facile templateless one-step method [15]. They showed that diameter of the composite nanofibers could be controlled in the range of 200–80 nm by simply tuning the speed of mechanical stirring during material synthesis. PATP nanotubes can be obtained by removing GNPs embedded in PATP nanofibers, where interiors of PATP nanotubes with continuous or discontinuous nanocavities can be controlled depending on mechanical stirring. PATP/GNP composite nanofibers showed good catalytic activities and reusability toward the reduction of GNP in the presence of $NaBH_4$. In this case, the reaction was catalyzed by smaller nanofibers (80 nm) showing shorter adsorption time and faster reaction rate due to large exposure of gold catalysts on

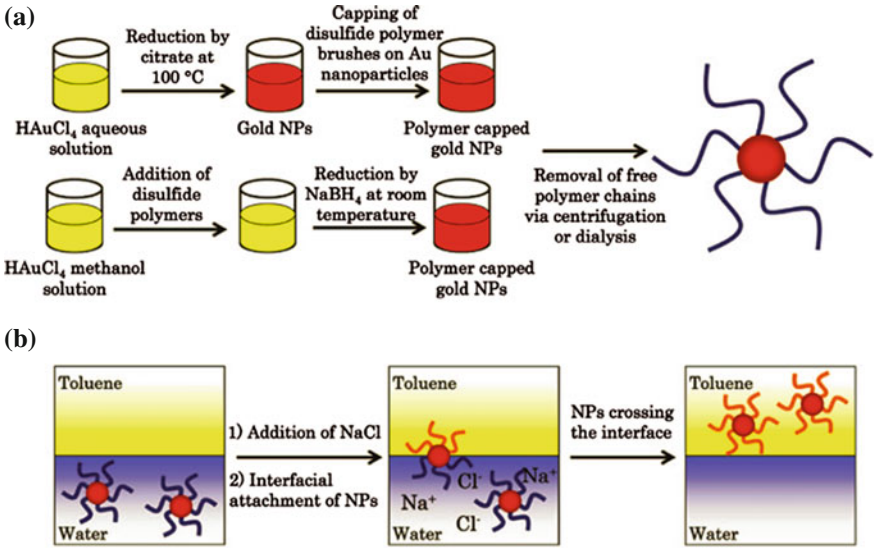

Fig. 11 Schematic diagram illustrating the fabrication of gold NPs protected by copolymers of (MEO2MA) and (OEGMA) and the transfer of the NPs across the water–oil interface. **a** The top row represents the fabrication of gold NPs via the reduction of $HAuCl_4$ using sodium citrate as the stabilizing/reducing agent and subsequent grafting of disulfide-functionalized polymers to the resulting NPs. The bottom row represents the preparation of gold NPs by a one-step reduction of $HAuCl_4$ in the presence of disulfide-functionalized polymer using methanol as solvent. **b** The polymer-protected NPs are then dispersed in water and placed in the presence of a toluene interface. Upon the addition of salt to the aqueous subphase, the polymer-protected gold NPs transfer to the organic phase. Reprinted with permission from [7]. Copyright © 2008, American Chemical Society

fiber surfaces (Fig. 13). This work provided an idea about the shape-controlled synthesis of other nanomaterials by simply introducing mechanical agitation. They said that these PATP/gold nanocomposites had promising applications in the fields of catalysis and sensors.

6.7 Application as Potential Gate Dielectrics in Electronic Industry

Ginzburg et al. [14] utilized spin-casting and ultraviolet (UV) light-induced polymerization to make organic–inorganic nanocomposite thin films using a mixture consisting of polycaprolactone (PCL)-stabilized GNPs and reactive monomer alkoxytitanium triacrylate, and photoinitiator benzophenone, dissolved in *n*-butyl acetate (BuAc) solvent [14]. Resulting nanocomposites were characterized by polarized light optical microscopy, transmission electron microscopy (TEM), and

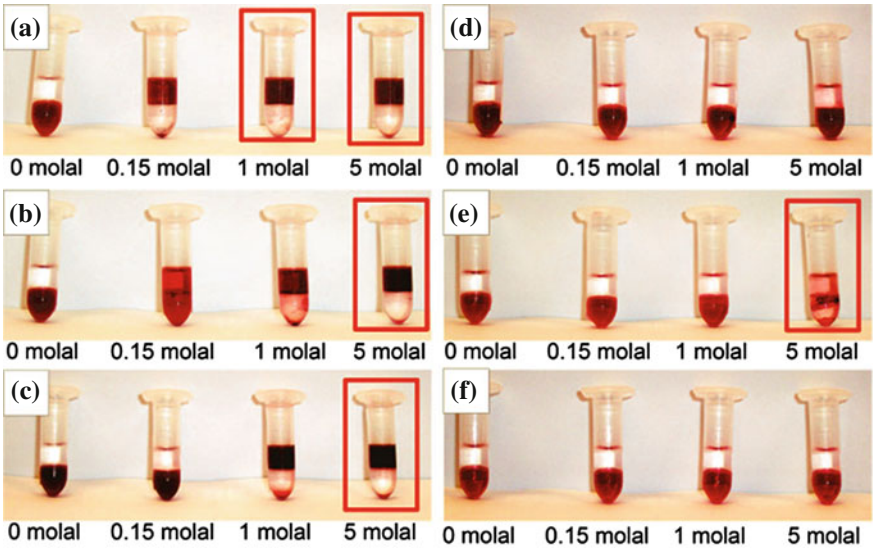

Fig. 12 Optical images of vials containing Au@MEO2MA-*co*-OEGMA NPs initially dispersed in aqueous NaCl solutions after standing those solutions in the presence of a toluene phase for 2 days. Red boxes are placed around vials in which the Au-MEO2MA-*co*-OEGMA NPs were not stable in the aqueous salt solutions. The concentration of NaCl in the aqueous phase is shown below each vial. **a** Au-MEO2MA NPs. **b** Au-MEO2MA-*co*-OEGMA (92-*co*-08) NPs, **c** Au-MEO2MA-*co*-OEGMA (90-*co*-10), **d** Au-OEGMA NPs, **e** Au-PDMAEMA NPs, and **f** Au-PEO NPs. Reprinted with permission from [7]. Copyright © 2008, American Chemical Society

atomic force microscopy (AFM) and a theoretical model was proposed explaining the formation of macro- and microphase-separated structures. The composite film exhibited high electrical capacitance due to the large effective dielectric constant of the metal nanoparticle-rich "nodules," and hence these materials could be used in the electronics industry. From the optical micrographs, numerous "core-shell"-type nodules of different sizes, distributed randomly in the main cross-linked polymer matrix (Fig. 14) and partial dewetting of the film from the substrate were observed. From these observations they opined that the nodules were the result of a complex, "cascading" phase separation process.

Another interesting feature of the film was that the nodules were larger in height than the rest of the film. According to AFM study, the height of a nodule, shown in Fig. 15, was in the order of 4 μm, while the height of the film outside the nodules was only 50–100 nm.

The nodules exhibited very interesting physical properties, most notably very high-dielectric constant combined with reasonably high electrical resistivity. It is expected that such materials hold significant promise for the development of future high-dielectric-constant gate polymers for printed electronics.

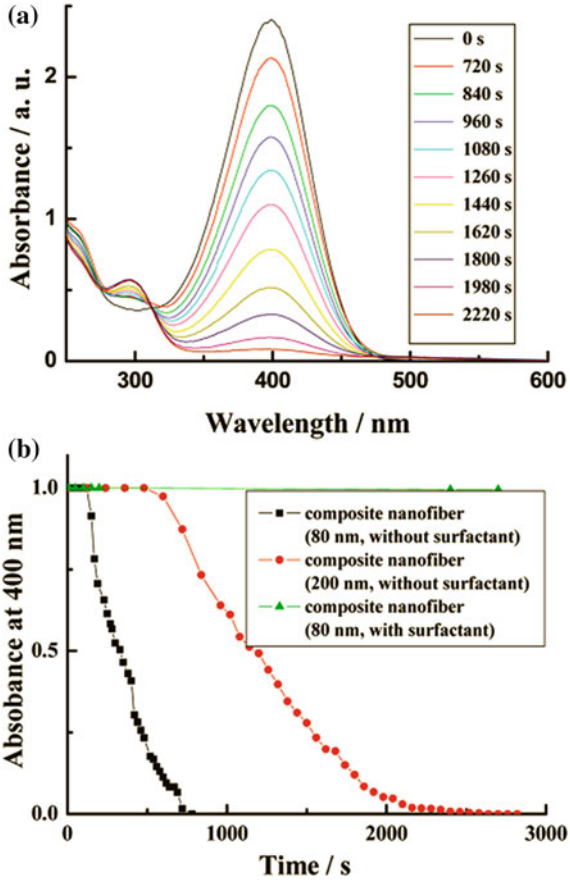

Fig. 13 **a** Successive UV-vis absorbance spectra of the reduction of 4NP by $NaBH_4$ in the presence of PATP/gold nanoparticle composite nanofibers. **b** Normalized absorbance at the peak position for 4NP (400 nm) as a function of time in the presence of PATP/gold nanoparticle composite nanofibers. Reprinted with permission from [15]. Copyright © 2011, American Chemical Society

6.8 *Application as Nonenzymatic Glucose Voltammetric Sensor*

Zhu et al. [60] prepared a nanocomposite gel which comprised of multiwalled carbon nanotubes (MWCNTs)/ionic liquid (IL) and GNPs. GNPs were the cores of this nanocomposite, surrounded by MWCNTs and IL acted as bridges connecting GNPs/MWCNTs with one another with bucky gel as platform for the whole nanocomposite (shown in Fig. 16) [60].

The surface morphology of the nanocomposite was characterized using X-ray photoelectron spectrometer (XPS), scanning electron microscope (SEM), and transmission electron microscope (TEM), respectively. Voltammetry was used to evaluate the electrocatalytic activities of the nanocomposite biosensor toward nonenzymatic glucose oxidation in alkaline media. They showed that the GNPs

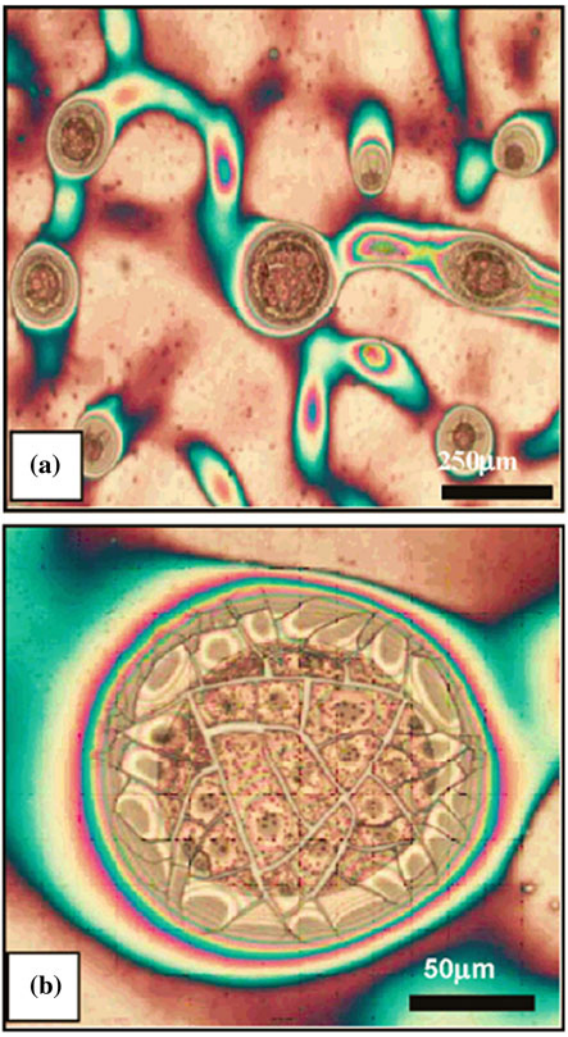

Fig. 14 Cascading macrophase separation and nodule formation in polymer-nanoparticle film. **a** Large-scale polarized light optical micrograph showing phase-separated morphology of the dried film. **b** Magnified image of one nodule showing secondary and tertiary phase separation in its interior. Reprinted with permission from [14]. Copyright © 2006, American Chemical Society

embedded in MWCNTs/IL gel had strong and sensitive voltammetric responses to glucose due to a possible synergistic effect among GNPs, MWCNTs, and IL. Applying the simple and easy approach described in this work, a highly sensitive electrochemical biosensor with higher selectivity could be developed and this also could be used in the determination of glucose in human blood serum with satisfactory result.

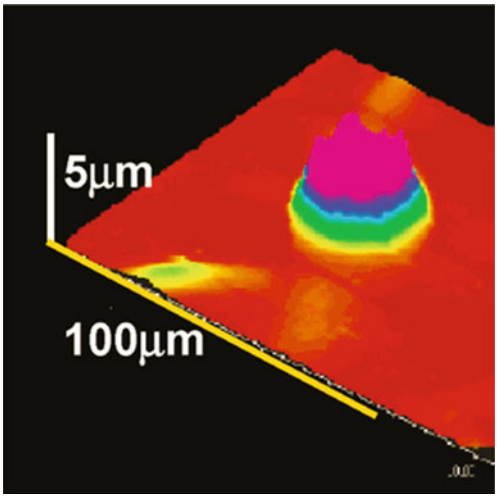

Fig. 15 Atomic force microscope (AFM) image of a dried nodule. Reprinted with permission from [14]. Copyright © 2006, American Chemical Society

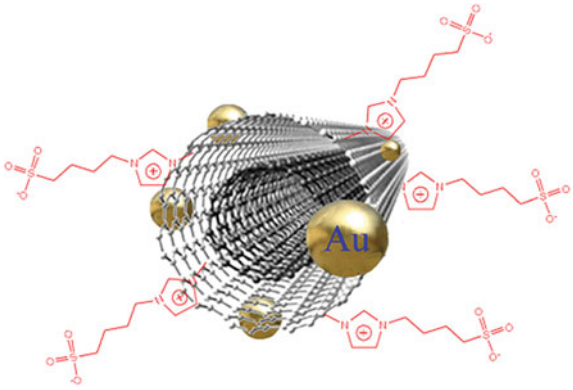

Fig. 16 Schematic illustration of nanocomposite *a* (GNPs/MWCNTs/IL). Reprinted with permission from [60]. Copyright © 2009 Elsevier

6.9 Application as Materials Which Can Engineer Polymers at Relatively Low Temperatures

Liu et al. [21] presented a method for the preparation of spherical gold/poly(methyl methacrylate)(PMMA) hybrid nanocomposites [21]. They observed that large numbers of GNPs were dispersed throughout the PMMA matrix and the diameters and dispersion of the GNPs could be controlled by the polymer concentration (Fig. 17).

They reported that the glass-transition temperature (*T*g) of the gold/PMMA nanocomposite became lower than that of the bulk PMMA polymer (Fig. 18). A nanonetwork structure was formed upon thermal treatment at a temperature around the T_g of the nanocomposites. Based on this observation, the author suggested that

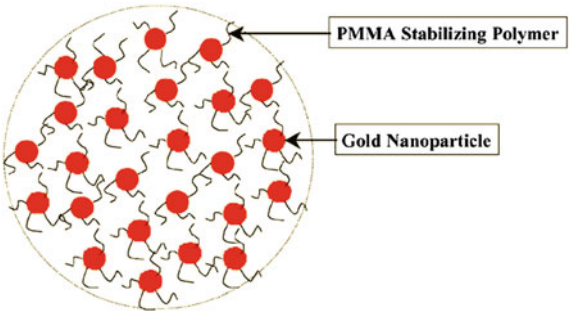

Fig. 17 A schematic diagram of the gold/PMMA nanocomposites. Conditions: 0.83 mM $HAuCl_4$, 35_M PMMA (ca. 5.25 mM with respect to the repeating MMA units), and 0.5 mM $NaBH_4$ in EtOH/H_2O (60:40 (v/v)) at room temperature. Reprinted with permission from [21]. Copyright © 2003 Elsevier

such nanocomposites could be applicable to advance our understanding of methods to engineer polymers by treating them at relatively low temperatures.

6.10 Application in Biosensing

Zhang et al. [59] synthesized novel 1D nanocomposites with adjustable thickness using AuNPs as the reinforcing agent and bacterial cellulose (BC) nanofibers as the biotemplates via one-step method [59]. The BC nanofibers were uniformly coated with AuNPs in aqueous suspension using poly(ethyleneimine) (PEI) as the reducing and linking agent. With the addition of different halides, gold–BC nanocomposites with different gold shell thicknesses were formed, and a possible formation mechanism was proposed in Fig. 19.

The obtained gold–BC nanocomposites offered a promising support for enzyme immobilization and biosensor fabrication. In this work, horseradish peroxidase (HRP) was chosen as the model enzyme to immobilize on the gold–BC bionanocomposite to construct a new H_2O_2 biosensor. HRP was successfully embedded into the nanonetwork structure of the Au–BC nanocomposites with its bioactivity. The electrochemical behavior of the HRP/Au–BC/GCE and Au–BC/GCE in the absence and presence of 5.0 mM of H_2O_2 was investigated by using cyclic voltammetry. The fabricated HRP biosensor allowed the highly sensitive detection of H_2O_2 with a detection limit lower than 1 mM. Thus The Au–BC nanocomposites may find wide applications in bioelectroanalysis and bioelectrocatalysis [3].

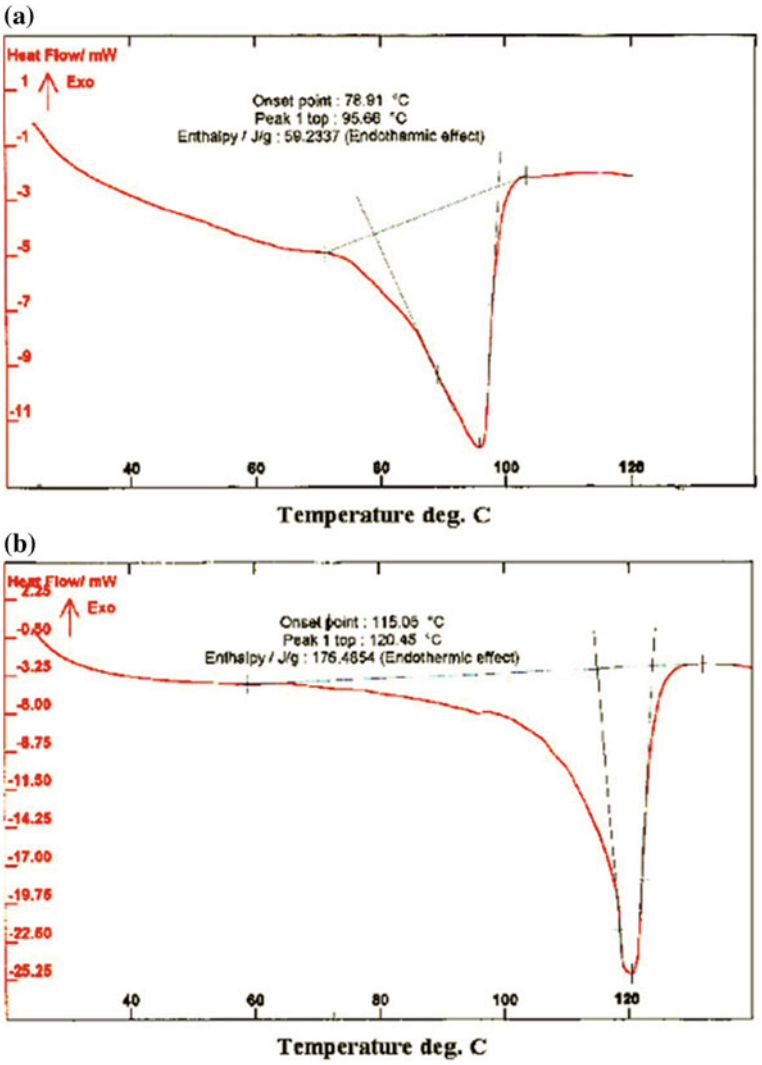

Fig. 18 Glass-transition temperatures of (**a**) gold/PMMA nanocomposites and (**b**) bulk PMMA. Reprinted with permission from [21]. Copyright © 2003 Elsevier

7 Environmental Effects of GNPs

7.1 GNPs in Water

The increasing use of NPs in both industry and research has eased their inclusion into waste water streams. The impact of NPs on water treatment plants and the environment is still unclear. The current studies mainly focus on NP synthesis but

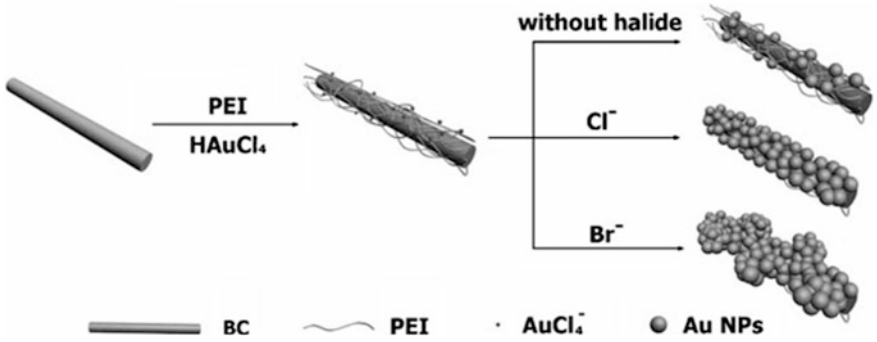

Fig. 19 Schematic illustration of the formation mechanism for Au–BC nanocomposites. Reprinted with permission from [59]. Copyright © 2010 WILEY-VCH Verlag GmbH & Co. KGaA, Weinheim

less so on environmental concerns and toxicity [22]. The GNPs and titanium oxide NPs were found to present zero or low toxicity toward ordinary heterotrophic organisms (OHO), ammonia-oxidating bacteria (AOB), and anaerobic biomass [12]. The effect of such nanoparticles on other toxins already present in the waterways must also be considered and an in-depth research is needed in this area [24]. Also the binding ability of NPs with other organic matter, metals, and contaminants in the water treatment process might lead to undesired consequences [25].

7.2 GNPs in Soil

Generally, NPs reach soil through direct or indirect contact with groundwater. NPs in the soil can help to reduce sequestration of hydrophobic contaminants and help in remediating soil [24]. On the other hand, NPs can adversely affect the respiration rate of the microbes present in the soil. NP contamination can disturb the soil protozoan growth and also affect the growth of fast-growing bacteria. Thus, NP contamination in soil may cause an imbalance between soil and microorganism deteriorating the overall health and function of the soil [25] adversely affecting the plant growth and increase human exposure to NPs. Recent studies revealed that functionalised GNPs could attract certain types of bacteria in soil and on interacting with these bacteria the GNPs may undergo redox reactions [25]. Thus the soil characteristics may get changed significantly on contamination with GNPs.

7.3 GNPs in Air

Airborne NPs impose a danger of human exposure through skin absorption. It is important to study the toxicity and cytotoxicity of airborne NPs and GNPs as these are major areas of research in both biomedical and environmental applications.

8 Prospects for the Future

Gold nanoparticles (GNPs) have been employed in biomedicine since the last decade because of their unique optical, electrical, and photothermal properties. They have been used for various applications like delivery of biomolecules into cells, labeling applications, as heat source and sensors, etc. GNPs are an attractive alternative to traditional organic fluorescent dyes as they can absorb light throughout the visible and NIR spectrum, and they can be nontoxic under certain experimental conditions. A good amount of work has been done with GNPs on in vitro diagnostics and in coming years, it is expected that an intensive research activity will be focused on the in vivo uses of GNPs. These activities will be tied to specific detection, imaging, and therapy for particular target cells (e.g., certain cancers, bacteria). However, the toxicity and side effects of GNPs should also be thoroughly examined before human can be exposed to these materials. In the forthcoming years, an increased collaboration between research scientists in the field of nanoscience and nanotechnology, medicine experts, and medical professionals is likely to occur which will illuminate new fundamental insights into biological systems.

Recently several research works have demonstrated the suitability of GNP-reinforced polymer nanocomposites for diversified applications like light emitting diodes, energy storage applications, as supporters and carriers of transition metal ions which can be reduced in situ to construct novel bimetallic nanocomposites regarded as intelligent catalysts with environmental stimuli activity, optical and electronic applications, as diagnostic probes or drug delivery vehicles in catalysis or as sensors, etc. These diverse ranges of possibilities clearly indicate the importance of GNP-based nanocomposites in the field of science and technology. It is expected that such materials hold significant promise for the development of advanced technologies for future applications.

References

1. Amendola V, Meneghetti M (2009) Laser ablation synthesis in solution and size manipulation of noble metal nanoparticles. Phys Chem Chem Phys 11:3805–3821

2. Bendahou A, Habibi Y, Kaddami H, Dufresne A (2009) physico-chemical characterization of palm from Phoenix Dactylifera-L, preparation of cellulose whiskers and natural rubber-based nanocomposites. J Biobased Mat Bioenerg 3:81–90
3. Cole DH, Shull KR, Baldo P, Rehn L (1999) Dynamic properties of a model polymer/metal nanocomposite: gold particles in Poly(tert-butyl acrylate). Macromolecules 32:771–779
4. Daniel M-C, Astruc D (2004) Gold nanoparticles: assembly, supramolecular chemistry, quantum-size-related properties, and applications toward biology, catalysis, and nanotechnology. Chem Rev 104:293–346
5. Dong H, Strawhecker KE, Snyder JF, Orlicki JA, Reiner RS, Rudie AW (2012) Cellulose nanocrystals as a reinforcing material for electrospun poly(methyl methacrylate) fibers: Formation, properties and nanomechanical characterization. Carbohydr Polym 87:2488–2495
6. Dufresne A, Kellerhals MB, Witholt B (1999) Transcrystallization in Mcl-PHAs/cellulose whiskers composites. Macromolecules 32:7396–7401
7. Edwards EW, Chanana M, Wang D (2008) Capping gold nanoparticles with stimuli-responsive polymers to cross water-oil interfaces: in-depth insight to the trans-interfacial activity of nanoparticles. J Phys Chem C 112:15207–15219
8. Espino-Perez E, Bras J, Ducruet V, Guinault A, Dufresne A, Domenek S (2013) Influence of chemical surface modification of cellulose nanowhiskers on thermal, mechanical, and barrier properties of poly(lactide) based bionanocomposites. Eur Polym J 49:3144–3154
9. Fahma F, Hori N, Iwata T, Takemura A (2013) The morphology and properties of poly(methyl methacrylate)-cellulose nanocomposites prepared by immersion precipitation method. J Appl Polym Sci 128:1563–1568
10. Favier V, Canova GR, Cavaillé JY, Chanzy H, Dufresne A, Gauthier C (1995) Nanocomposite materials from latex and cellulose whiskers. Polym Adv Technol 6:351–355
11. Garcia de Rodriguez NL, Thielemans W, Dufresne A (2006) Sisal cellulose whiskers reinforced polyvinyl acetate nanocomposites. Cellulose 13:261–270
12. Garcia A, Delgado L, Tora JA, Casals E, Gonzalez E, Puntes V, Font X, Carrera J, Sanchez A (2012) Effect of cerium dioxide, titanium dioxide, silver, and gold nanoparticles on the activity of microbial communities intended in wastewater treatment. J Hazard Mater 199–200:64–72
13. Ghosh P, Han G, De M, Kim CK, Rotello VM (2008) Gold nanoparticles in delivery applications. Adv Drug Deliv Rev 60:1307–1315
14. Ginzburg VV, Myers K, Malowinski S, Cieslinski R, Elwell M, Bernius M (2006) High-dielectric-constant self-assembled nodular structures in polymer/gold nanoparticle films. Macromolecules 39:3901–3906
15. Han J, Dai J, Li L, Fang P, Guo R (2011) Highly uniform self-assembled conducting polymer/gold fibrous nanocomposites: additive-free controllable synthesis and application as efficient recyclable catalysts. Langmuir 27:2181–2187
16. Huang H, Yuan Q, Yang X (2005) Morphology study of gold-chitosan nanocomposites. J Colloid Interface Sci 282:26–31
17. Li D, He Q, Cui Y, Li J (2007) Fabrication of pH-responsive nanocomposites of gold nanoparticles/Poly(4-vinylpyridine). Chem Mater 19:412–417
18. Li D, He Q, Li J (2009) Smart core/shell nanocomposites: intelligent polymers modified gold nanoparticles. Adv Colloid Interface Sci 149:28–38
19. Lin M-F, Thakur VK, Tan EJ, Lee PS (2011) Dopant induced hollow BaTiO3 nanostructures for application in high performance capacitors. J Mater Chem 21:16500–16504
20. Lin M-F, Thakur VK, Tan EJ, Lee PS (2011) Surface functionalization of BaTiO3 nanoparticles and improved electrical properties of BaTiO3/polyvinylidene fluoride composite. RSC Adv 1:576–578
21. Liu F-K, Hsieh S-Y, Ko F-H, Chu T-C (2003) Synthesis of gold/poly(methyl methacrylate) hybrid nanocomposites. Colloids Surf A 231:31–38
22. Murphy CJ, Gole AM, Stone JW, Sisco PN, Alkilany AM, Goldsmith EC, Baxter SC (2008) Gold nanoparticles in biology: beyond toxicity to cellular imaging. Acc Chem Res 41:1721–1730

23. Park JH, Lim YT, Park OO, Kim JK, Yu J-W, Kim YC (2004) Polymer/gold nanoparticle nanocomposite light-emitting diodes: enhancement of electroluminescence stability and quantum efficiency of blue-light-emitting polymers. Chem Mater 16:688–692
24. Rao CNR, Kulkarni GU, Thomas PJ, Edwards PP (2000) Metal nanoparticles and their assemblies. Chem Soc Rev 29:27–35
25. Rezic I (2011) Determination of engineered nanoparticles on textiles and in textile wastewaters. TrAC Trends Anal Chem 30:1159–1167
26. Schadler LS (2004) Polymer-based and polymer-filled nanocomposites. In: Ajayan PM, Schadler LS, Braun PV (eds) nanocomposite sciencs and technology. Wiley-VCH, New York, p 153
27. Schmitt J, Decher G, Dressick WJ, Brandow SL, Geer RE, Shashidhar R, Calvert JM (1997) Metal nanoparticle/polymer superlattice films: fabrication and control of layer structure. Adv Mater 9:61–65
28. Sharma V, Park K, Srinivasarao M (2009) Colloidal dispersion of gold nanorods: historical background, optical properties, seed-mediated synthesis, shape separation and self-assembly. Mat Sci Eng R 65:1–38
29. Singh BP, Singh D, Mathur RB, Dhami TL (2008) Influence of surface modified MWCNTs on the mechanical, electrical and thermal properties of polyimide nanocomposites. Nanoscale Res Lett 3:444–453
30. Singha AS, Thakur VK (2008) Effect of fibre loading on urea-formaldehyde matrix based green composites. Iran Polym J 17:861–873
31. Singha AS, Thakur VK (2008) Saccaharum cilliare fiber reinforced polymer composites. E-J Chem 5:782–791
32. Singha AS, Thakur VK (2009) Physical, chemical and mechanical properties of hibiscus sabdariffa fiber/polymer composite. Int J Polym Mater Polym Biomater 58:217–228
33. Singha AS, Thakur VK (2009) Grewia optiva fiber reinforced novel, low cost polymer composites. J Chem 6:71–76
34. Singha AS, Thakur VK (2009) Synthesis, characterization and analysis of hibiscus sabdariffa fibre reinforced polymer matrix based composites. Polym Polym Compos 17:189–194
35. Singha AS, Thakur VK (2009) fabrication and characterization of H. sabdariffa fiber-reinforced green polymer composites. Polym-Plast Technol Eng 48:482–487
36. Singha AS, Thakur VK (2010) Mechanical, morphological, and thermal characterization of compression-molded polymer biocomposites. Int J Polym Anal Charact 15:87–97
37. Singha AS, Thakur VK (2010) Synthesis, characterization and study of pine needles reinforced polymer matrix based composites. J Reinf Plast Compos 29:700–709
38. Siqueira G, Bras J, Dufresne A (2010) Cellulosic bionanocomposites: a review of preparation, properties and applications. Polymers 2:728–765
39. Sperling RA, Rivera Gil P, Zhang F, Zanella M, Parak WJ (2008) Biological applications of gold nanoparticles. Chem Soc Rev 37:1896–1908
40. Srivastava S, Haridas M, Basu JK (2008) Optical properties of polymer nanocomposites. Bull Mater Sci 31:213–217
41. Terech P, Chazeau L, Cavaille JY (1999) A small-angle scattering study of cellulose whiskers in aqueous suspensions. Macromolecules 32:1872–1875
42. Thakur VK, Singha AS (2010) Evaluation of GREWIA OPTIVA fibers as reinforcement in polymer biocomposites. Polym Plast Technol Eng 49:1101–1107
43. Thakur VK, Thakur MK (2014) Processing and characterization of natural cellulose fibers/thermoset polymer composites. Carbohydr Polym 109:102–117
44. Thakur VK, Thakur MK (2014) Recent trends in hydrogels based on psyllium polysaccharide: a review. J Clean Prod 82:1–15
45. Thakur VK, Thakur MK (2014) Recent advances in graft copolymerization and applications of chitosan: a review. ACS Sustainable Chem Eng 2:2637–2652
46. Thakur VK, Singha AS, Misra BN (2011) Graft copolymerization of methyl methacrylate onto cellulosic biofibers. J Appl Polym Sci 122:532–544

47. Thakur VK, Tan EJ, Lin M-F, Lee PS (2011) Polystyrene grafted polyvinylidenefluoride copolymers with high capacitive performance. Polym Chem 2:2000–2009
48. Thakur VK, Tan EJ, Lin M-F, Lee PS (2011) Poly (vinylidene fluoride)-graft-poly (2-hydroxyethyl methacrylate): a novel material for high energy density capacitors. J Mater Chem 21:3751–3759
49. Thakur VK, Singha AS, Kaur I et al (2011) Studies on analysis and characterization of phenolic composites fabricated from lignocellulosic fibres. Polym Polym Compos 19:505–511
50. Thakur VK, Singha AS, Thakur MK (2012) Modification of natural biomass by graft copolymerization. Int J Polym Anal Charact 17:547–555
51. Thakur VK, Singha AS, Thakur MK (2012) Rapid synthesis of MMA grafted pine needles using microwave radiation. Polym Plast Technol Eng 51:1598–1604
52. Thakur VK, Singha AS, Thakur MK (2013) Ecofriendly biocomposites from natural fibers: mechanical and weathering study. Int J Polym Anal Charact 18:64–72
53. Thakur VK, Thakur MK, Singha AS (2013) Free radical-induced graft copolymerization onto natural fibers. Int J Polym Anal Charact 18:430–438
54. Thakur VK, Thakur MK, Gupta RK (2014) Review: raw natural fiber-based polymer composites. Int J Polym Anal Charact 19:256–271
55. Thakur VK, Thakur MK, Raghavan P, Kessler MR (2014) Progress in green polymer composites from lignin for multifunctional applications: a review. ACS Sustainable Chem Eng 2:1072–1092
56. Wessling B (1996) Corrosion prevention with an organic metal (polyaniline): surface ennobling, passivation, corrosion test results. Mater Corros 47:439–445
57. Yonezawa T, Kunitake T (1999) Practical preparation of anionic mercapto ligand-stabilized gold nanoparticles and their immobilization. Colloids Surf A 149:193–199
58. Zeng S, Yong K-T, Roy I, Dinh X-Q, Yu X, Luan F (2011) A review on functionalized gold nanoparticles for biosensing applications. Plasmonics 6:491–506
59. Zhang T, Wang W, Zhang D, Zhang X, Ma Y, Zhou Y, Qi L (2010) Biotemplated synthesis of gold nanoparticle-bacteria cellulose nanofiber nanocomposites and their application in biosensing. Adv Funct Mater 20:1152–1160
60. Zhu H, Lu X, Li M, Shao Y, Zhu Z (2009) Nonenzymatic glucose voltammetric sensor based on gold nanoparticles/carbon nanotubes/ionic liquid nanocomposite. Talanta 79:1446–1453

Structure and Properties of Rubbers With Silica Nanoparticles as Petroleum-Free Fillers

Masayuki Yamaguchi, Vu Anh Doan and Shogo Nobukawa

Abstract Silica nanoparticles, as a petroleum-free eco-friendly material, are being used in the rubber industry instead of carbon blacks. Silica nanoparticles are found to show nucleating ability for the crystallization of butadiene rubber. Furthermore, they show migration behavior from styrene-butadiene rubber to butadiene rubber by Brownian motion, indicating that the interfacial tension with butadiene rubber is lower than that with styrene-butadiene rubber.

Keywords Silica nanoparticle · Rubber · Nucleating ability · Interphase transfer

1 Introduction

The shortage of fossil resources and the increase in the emission of carbon dioxide also affect the research and development in the rubber industry in spite of the huge consumption of natural rubber (NR) as a biomass-derived material [32]. Especially in the tire field, much effort has been carried out to reduce the amount of carbon blacks, because they are produced from fossil resources. One of the most promising candidates for the replacement from carbon blacks will be silica, i.e., silicon dioxide SiO_2, because of the good cost performance. It is usually obtained by mining and purification with pyrogenic process, and known as one of the most abundant materials in the earth crust. The shape is basically spherical with various diameters from nanoscale. Its attractive reinforcing capability has been reported especially for NR [5, 16, 20], and styrene-butadiene rubber (SBR) [30]. Moreover, surface

M. Yamaguchi (✉) · V.A. Doan · S. Nobukawa
School of Materials Science, Japan Advanced Institute of Science and Technology,
923-1292 Asahidai Nomi, Ishikawa, Japan
e-mail: m_yama@jaist.ac.jp

V.A. Doan
School of Textile-Leather and Fashion, Hanoi University of Science and Technology,
1 Dai Co Viet, Hai Ba Trung, Hanoi, Vietnam

V.K. Thakur and M.K. Thakur (eds.), *Eco-friendly Polymer Nanocomposites*,
Advanced Structured Materials 74, DOI 10.1007/978-81-322-2473-0_18

treatment technique is also commercially available, which enables them to be applicable to various rubbers. The replacement provides a new design for various rubber products because of the possibility of cooling.

As similar to carbon blacks, silica particles form higher order structure, which can be characterized by the dibutylphthalate absorption [16]. In general, however, the adsorption of rubber molecules on the surface of silica particles is not stronger than that on carbon blacks, when silica is used without surface treatment. Therefore, more free particles without bound rubber molecules will exist in a rubber. Due to this situation, Brownian motion will play an important role on the distribution state for silica nanoparticles. In particular, it becomes very important in an immiscible blend beyond the glass transition temperature T_g and melting point T_m when the hydrodynamic force is not so strong. In this situation, a large amount of silica nanoparticles will reside in one rubber phase with a small interfacial tension. Furthermore, the interphase transfer may occur during curing process at laminated rubber sheets.

In this chapter, interphase transfer behavior of silica nanoparticles is mentioned using *cis*-1,4-poly(butadiene) (BR) and SBR. Prior to the transfer phenomenon, the nucleating ability of silica particles for BR is mentioned, because silica is known to show the nucleating ability for various crystalline polymers.

2 Nucleating Ability of Silica for Butadiene Rubber

As mentioned in the introduction, silica particles show the nucleating ability for various crystalline polymers such as isotactic and syndiotactic polypropylene (iPP and sPP) [3, 27, 28] polyamide 6 (PA6) [29] poly(propylene oxide) [8] poly(ethylene glycol) [8] isotactic polystyrene [31] and poly(butylene succinate) [4, 26] although the nucleating ability is not so strong as compared with carbon nanofillers and talc. Interestingly, silica is also known to retard the crystallization of poly(vinyl alcohol) [17] and poly(ethylene terephthalate) [36]. Moreover, silica leads to specific crystalline form for some polymorphic polymers such as iPP (β trigonal form) [26, 28] and PA6 (γ hexagonal form) [29].

BR is known as a crystalline polymer which shows monoclinic crystalline form [23]. It has been found that T_m of well-developed crystals is around 0 °C [15, 21] and the heat of fusion for the perfect crystal is 157 J/g [33]. Because of its high molecular weight, i.e., restricted molecular diffusion, the crystalline structure is strongly affected by the processing method [6, 18, 22], as well as the purity and synthesis method [24]. Of course, crosslink points greatly retard the crystallization. The existence of crystalline phase affects the dynamic mechanical properties greatly, which are different from those for a typical rubber. Figure 1 exemplifies the temperature dependence of the dynamic tensile moduli for BR and SBR [13]. Both of them are not crosslinked, leading to the crystallization of BR. In the figure, SBR shows typical dynamic mechanical properties for a rubber in the whole temperature range, whereas BR behaves as a rubbery material only beyond the melting point located around at 0 °C.

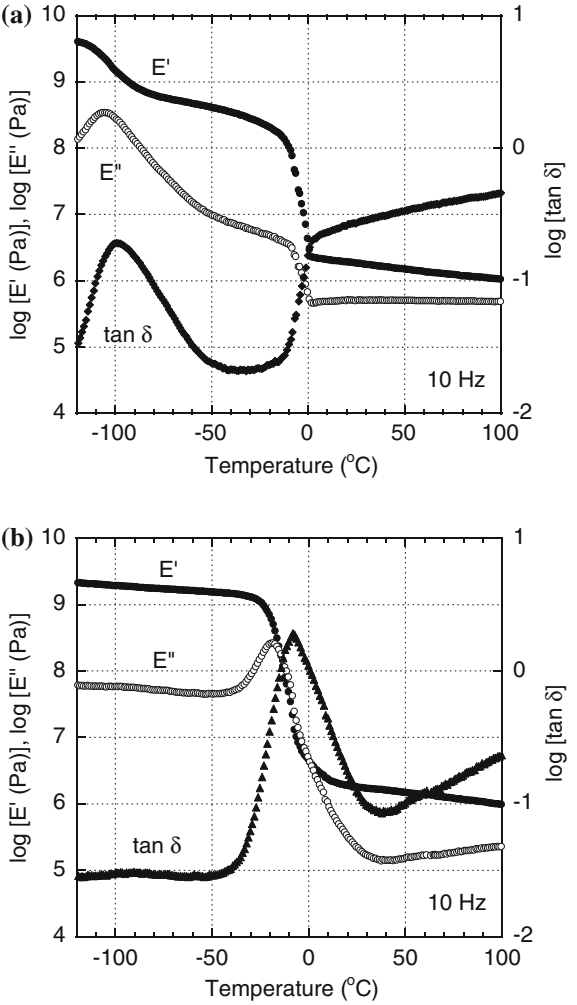

Fig. 1 Temperature dependence of dynamic tensile moduli such as (*closed circles*) storage modulus *E'*, (*open circles*) loss modulus *E''*, and (*closed diamonds*) loss tangent *tan δ* at 10 Hz for **a** pure BR and **b** pure SBR. [13]

The nucleating ability of silica nanoparticles with an average diameter of 16 nm was investigated employing a commercially available BR (94.8 % of *cis*-content and 0.5 % of vinyl fraction) [12]. Figure 2 shows the DSC (differential scanning calorimeter) cooling curves for BR containing various amounts of the silica particles at a cooling rate of 5 °C/min from room temperature. It is clearly shown that the crystallization occurs at higher temperatures for the samples containing the silica particles, indicating that they act as nucleating agents for BR even without surface treatment. The peak temperature of the crystallization exothermic peak is plotted as a function of the silica content in Fig. 3. The nucleating ability is clearly detected even with 0.01 phr, although the effect seems to be saturated beyond 0.5 phr.

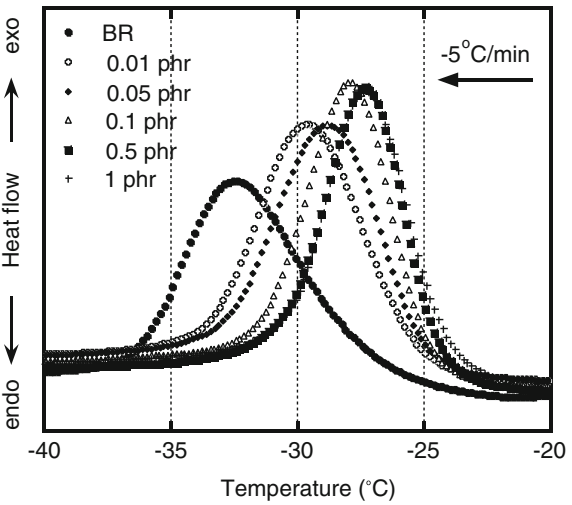

Fig. 2 DSC cooling curves for BR containing various amounts of silica particles. The cooling rate is 5 °C/min. [10]

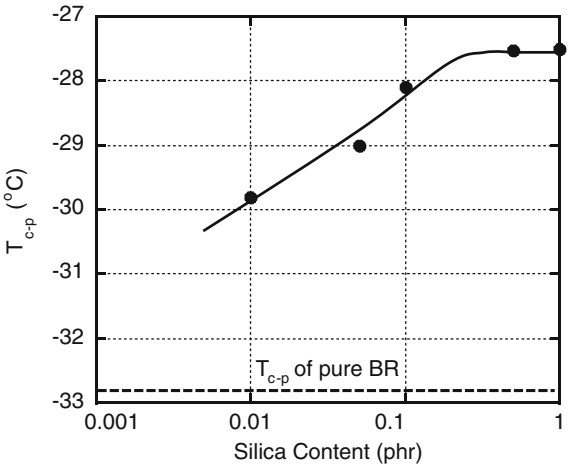

Fig. 3 Peak temperature of the crystallization exothermic peak $T_{c\text{-}p}$ as a function of the silica contents. The dotted line represents $T_{c\text{-}p}$ of pure BR. The values are estimated from Fig. 2

The isothermal crystallization behavior at various crystallization temperatures is shown in Fig. 4 for BR and BR containing 1 phr of the silica particles. The crystallization behavior at various temperatures can be expressed by the classical Avrami equation for both samples, as shown in Fig. 5a. The Avrami equation is given by

$$\log[-\ln(1 - X_{rel})] = n \log t + \log k \tag{1}$$

where k is the parameter to express the overall crystallization rate and n is so-called Avrami index. The relative crystallinity X_{rel} is defined by the following equation.

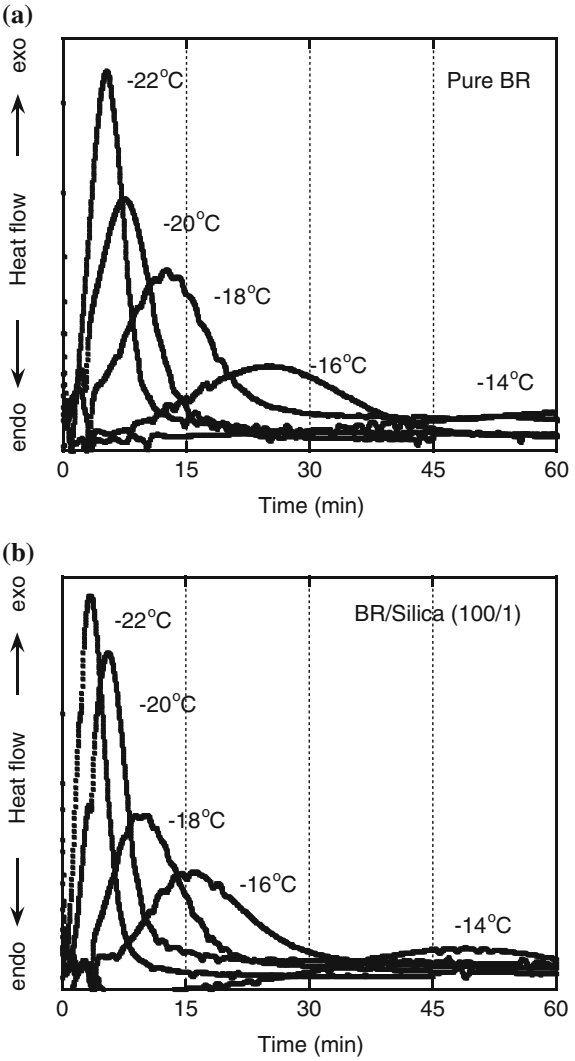

Fig. 4 Isothermal crystallization curves at various crystallization temperatures for **a** pure BR and **b** BR containing 1 phr of silica nanoparticles [10]

$$X_{rel} = \frac{X_t}{X_T} \tag{2}$$

where X_t and X_T are the degree of crystallinity at time t and that at the end of the crystallization.

Although physical meaning of the Avrami equation is known to be obscure these days, the equation is useful, at least, to express the crystallization rate. Since the Avrami index is not so different for all samples in this study, k can be used to compare the crystallization rate, as shown in Fig. 5b. The enhancement of crystallization rate is confirmed in the wide range of crystallization temperatures T_c.

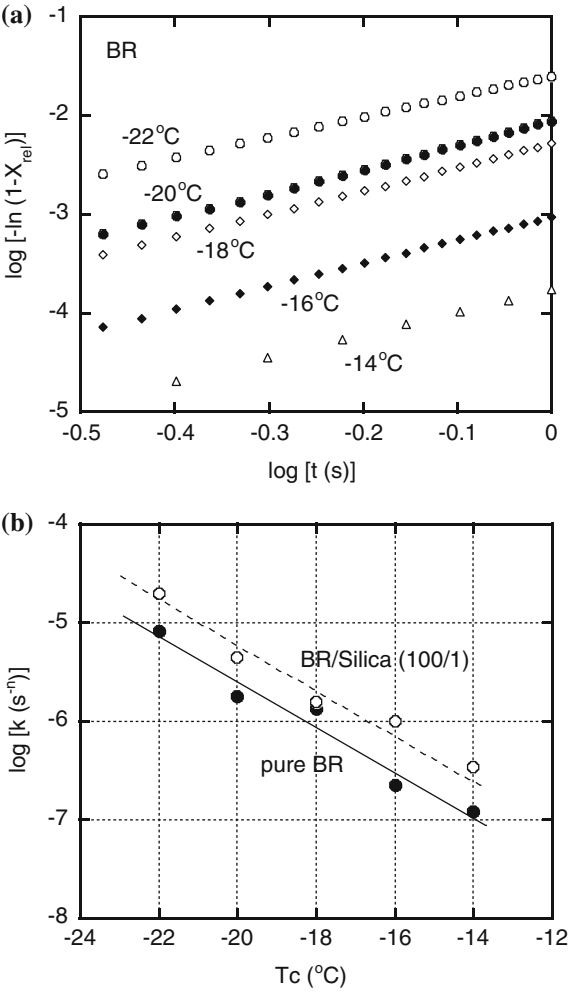

Fig. 5 **a** Avrami plots at various crystallization temperatures for pure BR. **b** Avrami index k at various crystallization temperatures T_c for (*closed*) pure BR and (*open*) BR containing 1 phr of silica nanoparticles

3 Interphase Transfer of Silica Nanoparticles

When the diameter of silica particles is in the order of nanoscale, Brownian motion is expected even in a viscous polymer melt. The diffusion constant of a spherical particle D in a liquid is described by the Stokes-Einstein equation as follows:

$$D = \frac{k_B T}{6\pi\eta_m R} \tag{3}$$

where k_B is the Boltzmann constant, η_m is the viscosity of the medium, and R is the radius of particles.

Therefore, marked Brownian motion is detected for small particles at high temperature, which also leads to low viscosity. The diffusion time t_D for a distance of the radius of a particle is provided by

$$t_D \approx \frac{R^2}{D} = \frac{6\pi\eta_m R^3}{k_B T} \tag{4}$$

In an immiscible blend, the distribution of nanofillers occurs spontaneously by Brownian motion when the experimental time is longer than the diffusion time. Yoon et al. reported that multiwalled carbon nanotudes (MWNTs) with the diameter of 80 nm show marked Brownian motion in a molten polycarbonate (PC) [34]. Because of the Brownian motion, the orientation of MWNTs applied by the processing history, i.e., hydrodynamic force, disappears and becomes random, which greatly affects the electroconductivity due to three-dimensional network structure of MWNTs. Furthermore, MWNTs show the interphase transfer from iPP to PC during annealing procedure of laminated sheets composed of iPP and PC, although no transfer occurs from PC to iPP [35]. This is attributed to the difference in the interfacial tension with MWNT. In other words, the interfacial tension between MWNT and iPP is larger than that between MWNT and PC. Such kinds of interphase transfer occur with an aid of Brownian motion when the size of fillers is in the nanoscale [10]. Interphase transfer, of course, occurs for tackifier, crosslinking agents, and carbon blacks [9, 13].

The interphase transfer of silica nanoparticles was studied using BR and SBR, i.e., the first and second largest consumptions in synthetic rubbers [11]. The temperature dependences of dynamic tensile moduli for the rubbers are shown in Fig. 1. The styrene and vinyl contents in SBR are 27 and 59 %, respectively.

SBR is known to provide good wet skid and traction properties for tires, whereas BR shows low T_g leading to rubbery nature even at low temperature. Therefore, the blend system composed of SBR and BR is one of the most important rubber blends in the tire application, which is currently employed in side wall and tread. It has been clarified that BR and SBR are immiscible pairs [2, 25] although they show good compatibility [14, 19]. Furthermore, the compatibility between them is greatly enhanced by the addition of surface-modified silica particles [1, 7].

Figure 6 shows the procedure for the transfer experiments using laminated sheets composed of BR and SBR, in which only one sheet contains 70 phr of the silica particles. After exposure to annealing at room temperature or 50 °C, the sheets were separated. Then the separated surface was observed by a scanning electron microscope after Pt-Pd coating by using a sputtering machine. It is clearly shown in Fig. 7 that the silica nanoparticles are distributed on the surface of BR, suggesting that they are transferred from SBR to BR. For the sheet produced by compression molding, rigid fillers tend to be covered by viscous fraction, i.e., rubber. Consequently, no particle is detected on the surface by SEM for the original sheet containing the silica particles. This phenomenon can be explained by the existence of a pure SBR layer in the sheet surface. Therefore, the particles on the BR surface must show the diffusion through the surface layer of pure SBR to attach to the pure

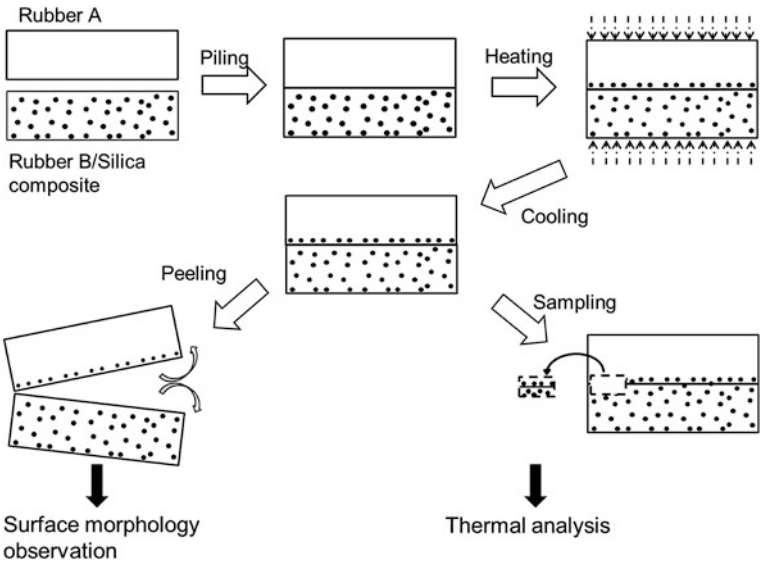

Fig. 6 Schematic illustration of transfer experiments [11]

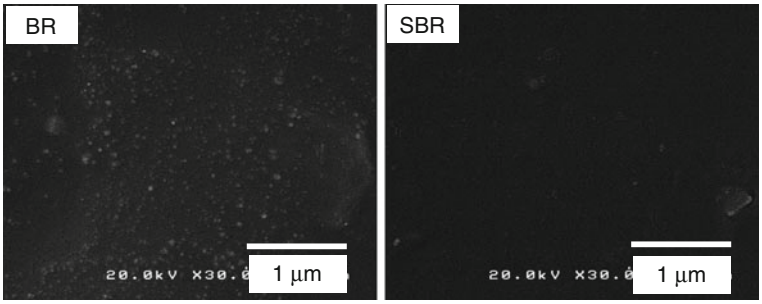

Fig. 7 SEM images of the surface after separation of the laminated sheets. (*left*) BR surface separated from SBR sheet containing silica particles and (*right*) SBR surface separated from BR sheet containing silica nanoparticles [11]

BR sheet. In contrast, no particle is detected on the surface of SBR after separated from the BR sheet containing the silica particles. The asymmetry of the transfer direction is not attributed to the difference in the diffusion time, because the relaxation time of SBR, characterized by the rheological measurements, is found to be significantly longer than that of BR. Therefore, the diffusion time of the silica particles through the surface layer of BR is shorter than that of SBR, assuming the same thickness of the surface layer. The difference in the transfer behavior demonstrates that the silica particles prefer to reside in BR phase rather than SBR. The marked nucleating ability of the silica particles will be attributed to the good compatibility.

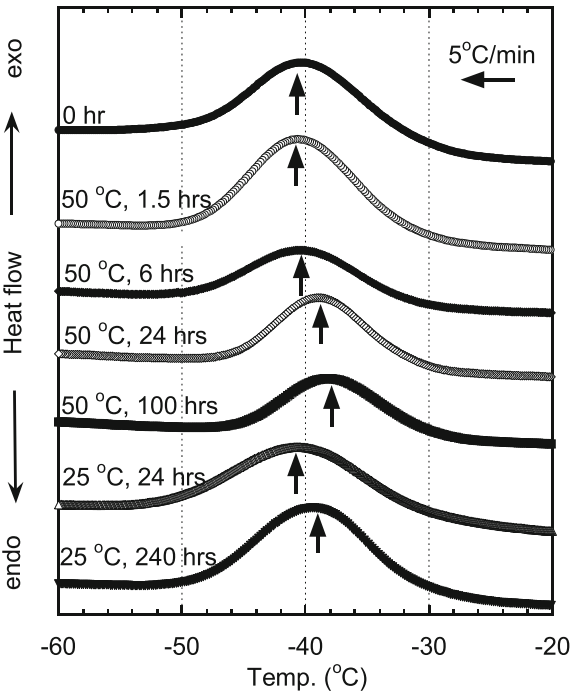

Fig. 8 DSC cooling curves of the BR samples attached to the SBR sheet containing silica nanoparticles after the annealing procedure at various conditions. The cooling rate is 5 °C/min [11]

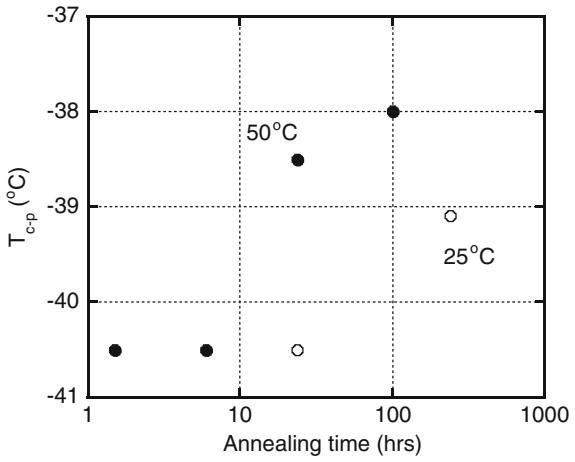

Fig. 9 Peak temperature of the crystallization exothermic peak $T_{c\text{-}p}$ as a function of the annealing time at (*open*) 25 °C and (*closed*) 50 °C. The values are estimated from Fig. 8

Because of the silica transfer, the crystallization temperature of the surface of the BR sheet is enhanced after annealing as shown in Fig. 8. In Fig. 9, the peak temperature of crystallization $T_{c\text{-}p}$ for the BR samples attached to the SBR sheet is plotted against the annealing time at room temperature and 50 °C. The difference in the crystallization temperature between Figs. 2 and 8 is ascribed to the difference in the recipe; the compound used for the transfer experiments contains a process oil. As

shown in the figure, the silica transfer does not take place in a relatively short time. This is reasonable, because the silica particles have to diffuse through the surface layer of SBR to attach to the BR sheet. Moreover, it is confirmed that the exposure to higher temperature accelerates the transfer due to the marked Brownian motion.

Under the flow condition, hydrodynamic force is more important in general to decide the distribution, which is expressed by the Peclet number defined as the following relation.

$$Pe \equiv \frac{\eta_m R^3 \dot{\gamma}}{k_B T} \propto t_D \dot{\gamma}, \tag{5}$$

where $\dot{\gamma}$ is the shear rate. Therefore, the Peclet number can be regarded as a dimensionless shear rate.

When the Peclet number is much larger than 1, Brownian motion is neglected. Therefore, hydrodynamic force decides the morphology of a composite dominantly during mixing procedure at a high shear rate, although the interfacial tension still plays an important role on the distribution of fillers.

In the case of rubber processing, however, crosslinking process is required after mixing of raw materials. Therefore, the silica transfer can take place during the crosslinking process, because no/little hydrodynamic force is applied to the system at the process.

4 Conclusion and Future Perspective

Silica nanoparticles are found to exhibit the nucleating ability for BR, which is saturated beyond 0.5 phr. The nucleating effect is used to characterize the transfer phenomenon of silica nanoparticles from SBR to BR. The silica particles are diffused through the surface layer of SBR and move to BR. As a result, the silica particles are detected by SEM on the BR surface after separated from the SBR sheet containing the silica. In near future, manipulated morphology control including silica nanoparticles will be established to be replaced from rubber blends containing carbon blacks.

Acknowledgments A part of this research was supported by Grant-in-Aid for Scientific Research (B) No. 22350102.

References

1. Anai M, Aizawa S, Ito M (2007) Phase control of BR/SBR by silica particles. J Soft Mater 3:64–69
2. Bar G, Ganter M, Brandsch R, Delineau L (2002) Examination of butadiene/styrene-*co*-butadiene rubber blends by tapping mode atomic force microscopy. Importance of the

indentation depth and reduced tip-sample energy dissipation in tapping mode atomic force microscope study of elastomers. Langmuir 16:5702–5711
3. Bejarano J, Benavente R, Perez E, Wilhelm M, Quijada R, Palza H (2004) Effect of nucleating agents on crystallization and melting behavior and mechanical properties of nucleated syndiotactic poly(propylene). Macromol Mater Eng 289:818–827
4. Bian J, Han L, Wang X, Wen X, Dong L (2010) Nonisothermal crystallization behavior and mechanical properties of poly(butylene succinate)/silica nanocomposites. J Appl Polym Sci 116:902–912
5. Chen Y, Peng Z, Kong LX, Huang MF, Li PW (2011) Dynamics near the filler surface in natural rubber-silica. Polymer 48:1674–1677
6. Cheng TL, Su AC (1995) Spherulites of cis 1,4 polybutadine: molecular weight effect. Polymer 36:73–80
7. Chu W, Chen D (2011) Silica-modified SBR/BR blends. J Appl Polym Sci 120:3695–3700
8. Cole JH, St-Pierre (1978) The role of interfacial energy in the heterogeneous nucleation of polyether crystallization. J Polym Sci Polym Symp 63:205–235
9. Datta S (1999) Elastomer Blends. Polymer Blends, vol 2. Wiley, New York, pp 477–515
10. Doan VA, Nobukawa S, Yamaguchi M (2012) Localization of nanofibers on the polymer surface using interface transfer technique. Compos B 43:1218–1223
11. Doan VA, Nobukawa S, Ohtsubo S, Tada T, Yamaguchi M (2012) Selective migration of silica particles between rubbers. J Polym Res 20:145–150
12. Doan VA, Nobukawa S, Ohtsubo S, Tada T, Yamaguchi M (2013) Crystallization behavior of polybutadiene containing silica particles. J Appl Polym Sci 128:1848–1853
13. Doan VA, Nobukawa S, Ohtsubo S, Tada T, Yamaguchi M (2013) Transfer of tackifier between poly(butadiene) and poly(styrene-co-butadiene). J Mater Sci 48:2046–2052
14. Fujimoto K, Yoshimiya N (1968) Blends of cis-1,4-polybutadiene with natural or styrene butadiene rubber. Rubber Chem Technol 41:669–677
15. Grebowicz J, Aycock W, Wunderlich B (1986) Heat capacity of 1,4-polybutadiene. Polymer 27:575–582
16. Kaewsakul W, Sahakaro K, Dierkes WK, Noordermeer JWM (2013) Optimization of rubber formulation for silica-reinforced natural rubber compounds. Rub Chem Technol 86:313–329
17. Lee J, Lee KJ, Jang J (2008) Effect of silica nanofillers on isothermal crystallization of poly (vinyl alcohol): In-site ATR-FTIR study. Polym Test 27:360–367
18. Lorenzo MLD (2010) Crystallization kinetics of cis-1,4-polybutadiene. J Appl Polym Sci 116:1408–1413
19. Marsh PA, Voet A, Price LD (1967) Electron microscopy of heterogeneous elastomer blends. Rubber Chem Technol 40:359–370
20. Meera AP, Said S, Grohens Y, Thomas S (2009) Nonlinear viscoelastic behavior of silica-filled natural rubber nanocomposites. J Phys Chem C 113:17997–18002
21. Mitchell JC (1963) The melting point of cis-1,4-polybutadiene. J Polym Sci Polym Lett 1:285–288
22. Mitchell JC (1967) Mechanical history effect in the crystallization of cis-1,4 polybutadiene. Polymer 8:369–379
23. Natta G, Corradini P (1956) Crystalline structure of 1,4-cis-polybutadiene and 1,4-cis-polyisoprene. Angew Chem 68:615–616
24. Natta G, Corradini P (1960) The crystal structure of cis 1,4 polybutadiene. Supplemento al Nouvo Cimento 15:111–121
25. Ougizawa T, Inoue T, Kammer HW (1985) UCST and LCST behavior in polymer blends. Macromolecules 18:2089–2092
26. Papageorgiou GZ, Papageorgiou DG, Chrissafis K, Bikiaris D, Will J, Hoppe A, Roether JA, Boccaccini AR (2014) Crystallization and melting behavior of poly(butylene succinate) nanocomposites containing silica-nanotubes and strontium hydroxyapatite nanorods. Ind Eng Chem Res 53:678–692

27. Papageorgiou DG, Vourlias G, Bikiaris D, Chrissafis K (2014) Synergistic effect of functionalized silica nanoparticles and nucleating agent for the improvement of the mechanical properties of propylene/ethylene random copolymer. Macromol Mater Eng 299:707–721
28. Pedrazzoli G, Pegoretti A, Kalaitzidou K (2014) Understanding the effect of silica nanoparticles and exfoliated graphite nanoparticles on the crystallization behavior of isotactic polypropylene. Polym Eng Sci 55:672-680
29. Rafique FZ, Vasanthan N (2014) Crystallization, crystal structure, and isothermal melt crystallization kinetics of novel polyamide 6/SiO_2 nanocomposites prepared using the sol-gel technique. J Phys Chem B 118:9486–9495
30. Sun D, Li X, Zhang Y, Li Y (2011) Effect of modified nano-silica on the reinforcement of styrene butadiene rubber composites. J MAcromol Sci B Phys 50:1810-1821
31. Turturro G, St-Pierre LE (1978) The heterogeneous nucleation of crystallization in isotactic polystyrene. J Colloid Inter Sci 67:349–354
32. Thakur VK, Grewell D, Thunga M, Kessler MR (2014) Novel composites from eco-friendly soy flour/sbs triblock copolymer. Macromol Mater Eng 299:953–958
33. Wunderlich B (1980) Macromolecular physics, vol. 3, Crystal melting, Academic press, New York
34. Yoon H, Okamoto K, Umishita K, Yamaguchi M (2011) Development of conductive network of multi-walled carbon nanotubes in polycarbonate melt. Polym Comp 32:97–102
35. Yoon H, Okamoto K, Yamaguchi M (2009) Carbon nanotube imprinting on a polymer surface. Carbon 47:2840–2846
36. Zheng H, Wu J (2007) Preparation, crystallization, and spinnability of poly(ethylene terephthalate)/silica nanocomposites. J Appl Polym Sci 103:2564–2568

Index

V.K. Thakur and M.K. Thakur (eds.), *Eco-friendly Polymer Nanocomposites*,
Advanced Structured Materials 74, DOI 10.1007/978-81-322-2473-0